

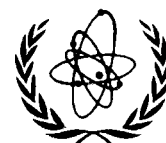


XA9743681 710

IAEA-TECDOC-927

# ***Influence of water chemistry on fuel cladding behaviour***

*Proceedings of a Technical Committee meeting  
held in Řež, Czech Republic, 4–8 October 1993*



INTERNATIONAL ATOMIC ENERGY AGENCY

**IAEA**

February 1997

**VOL 28 No 11**

The IAEA does not normally maintain stocks of reports in this series.  
However, microfiche copies of these reports can be obtained from

INIS Clearinghouse  
International Atomic Energy Agency  
Wagramerstrasse 5  
P.O. Box 100  
A-1400 Vienna, Austria

Orders should be accompanied by prepayment of Austrian Schillings 100,—  
in the form of a cheque or in the form of IAEA microfiche service coupons  
which may be ordered separately from the INIS Clearinghouse.

IAEA-TECDOC-927

# ***Influence of water chemistry on fuel cladding behaviour***

*Proceedings of a Technical Committee meeting  
held in Řež, Czech Republic, 4–8 October 1993*



INTERNATIONAL ATOMIC ENERGY AGENCY

IAEA

The originating Section of this publication in the IAEA was:

Nuclear Fuel Cycle and Materials Section  
International Atomic Energy Agency  
Wagramerstrasse 5  
P.O. Box 100  
A-1400 Vienna, Austria

INFLUENCE OF WATER CHEMISTRY ON FUEL CLADDING BEHAVIOUR  
IAEA, VIENNA, 1997  
IAEA-TECDOC-927  
ISSN 1011-4289

© IAEA, 1997

Printed by the IAEA in Austria  
February 1997

## FOREWORD

Extending fuel burnup is an effective method of improving the economics of water cooled reactors. The fuel used in water reactors consists of uranium dioxide clad with a zirconium based alloy. Cladding corrosion and hydriding are important performance related fuel characteristics and water chemistry, in addition to its effects on circuit contamination, plays a major role in these phenomena, which are, if the conclusions of fuel modelers are confirmed, life limiting parameters. Detailed study to reach a clear understanding of the phenomena involved is the first approach to a solution to the problem. A second approach, which is very promising, is to improve observations on reactors through the development of corrosion monitoring of materials and on-line monitoring of the main water chemistry parameters. A third approach is to examine possible remedies: alternative water chemistry to minimize corrosion and hydriding, even with fuel operated under more severe thermal-hydraulic conditions, and improved cladding material. Internationally, R&D programmes are focussing on these aspects of fuel performance and the Technical Committee meeting held in Řež, Czech Republic, from 4 to 8 October 1993 aimed at reviewing progress made in this area.

The subject of the meeting had been touched upon in several IAEA meetings or co-ordinated research programmes; however, this was the first time that the influence of water chemistry on fuel cladding behaviour was treated as a specific subject.

During this meeting corrosion specialists and water chemists were brought together to promote their synergistic interaction and the timely organization of this meeting in an eastern European country allowed, also for the first time, a comprehensive discussion on WWER water chemistry and Zr-Nb cladding corrosion.

The IAEA wishes to thank all the participants in the meeting for their contributions to this publication, which summarizes experience on cladding corrosion, on the water chemistry used and its monitoring and ongoing research in the field in the participating countries. The IAEA officer responsible for this publication was P. M. Chantoin of the Nuclear Fuel Cycle and Materials Section, Division of Nuclear Power and the Fuel Cycle.

## *EDITORIAL NOTE*

*In preparing this publication for press, staff of the IAEA have made up the pages from the original manuscripts as submitted by the authors. The views expressed do not necessarily reflect those of the governments of the nominating Member States or of the nominating organizations.*

*Throughout the text names of Member States are retained as they were when the text was compiled.*

*The use of particular designations of countries or territories does not imply any judgement by the publisher, the IAEA, as to the legal status of such countries or territories, of their authorities and institutions or of the delimitation of their boundaries.*

*The mention of names of specific companies or products (whether or not indicated as registered) does not imply any intention to infringe proprietary rights, nor should it be construed as an endorsement or recommendation on the part of the IAEA.*

*The authors are responsible for having obtained the necessary permission for the IAEA to reproduce, translate or use material from sources already protected by copyrights.*

## CONTENTS

SUMMARY OF DISCUSSIONS IN THE TECHNICAL COMMITTEE MEETING . . . . .	7
Panel Discussion 1 . . . . .	7
Panel Discussion 2 . . . . .	9
Panel Discussion 3 . . . . .	11
Panel Discussion 4 . . . . .	14
GENERAL CONCLUSIONS AND RECOMMENDATIONS . . . . .	17
PAPERS PRESENTED	
Effect of water chemistry and fuel operation parameters on Zr+1%Nb cladding corrosion . . . . .	23
<i>V.G. Kritsky, N.G. Petrik, I.G. Berezina, V.V. Doilnitsina</i>	
PWR fuel rod corrosion in Japan . . . . .	45
<i>S. Inoue, K. Mori, T. Murata, S. Kobayashi</i>	
Corrosion behaviour of Zircaloy-4 fuel rod cladding in EDF power plants . . . . .	55
<i>H. Romary, D. Deydier</i>	
Parametric tests of the effects of water chemistry impurities on corrosion of Zr-alloys under simulated BWR condition . . . . .	73
<i>S. Shimada, K. Ito, C.C. Lin, B. Cheng, T. Ikeda, M. Oguma, T. Takei, C. Vitanza, T.M. Karlsen</i>	
A new model for the in-reactor corrosion of zirconium alloys . . . . .	91
<i>B. Cox</i>	
Effect of elevated lithium on the waterside corrosion of Zircaloy-4: experimental and predictive studies . . . . .	111
<i>D. Pêcheur A. Giordano, E. Picard, Ph. Billot, Thomazet</i>	
Corrosion of zirconium alloys in nuclear reactors: A model for irradiation induced enhancement by local radiolysis in the porous oxide . . . . .	131
<i>C. Lemaignan, R. Salot</i>	
Growth and characterization of oxide layers on zirconium alloys . . . . .	143
<i>A.J.G. Maroto, R. Bordoni, M. Villegas, M.A. Blesa, A.M. Olmedo, A. Iglesias, G. Rigotti</i>	
Influence of alkali metal hydroxides on corrosion of Zr-based alloys . . . . .	161
<i>Y.H. Jeong, H. Ruhmann, F. Garzarolli</i>	
Modified hot-conditioning of PHT system surfaces of PHWRs . . . . .	193
<i>G. Venkateswaran</i>	
In situ measurement of the effect of LiOH on the stability of Zircaloy-2 surface film in PWR water . . . . .	207
<i>T. Saario, S. Tähtinen</i>	
Oxidizing and hydriding properties of Zr-1Nb cladding material in comparison with Zircalloys . . . . .	227
<i>V. Vrtílková, M. Valach, L. Molin</i>	
Oxidation-induced embrittlement and structural changes of Zircaloy-4 tubing in steam at 700-1000°C . . . . .	253
<i>A.E. Ali, A.G. Hussein, A.A. El-Sayed, S.M. El Raghy, O.A. El Banna</i>	

Application of FEM analytical method for hydrogen migration behaviour in zirconium alloys .....	267
<i>K. Arioka, H. Ohta</i>	
The terminal solid solubility of hydrogen and deuterium in Zr-2.5Nb alloys .....	275
<i>I.G. Ritchie, Z.L. Pan, M.P. Puls</i>	
Corrosion rate transients observed by linear polarization techniques at Zr-1%Nb alloy .....	295
<i>J. Beran, K. Černý</i>	
Sensors for on-line monitoring of water chemistry parameters for NPP's .....	303
<i>P. Aaltonen, K. Mäkelä</i>	
Operational experience of water quality improvement accompanied by monitoring with on-line ion chromatograph .....	315
<i>M. Kobayashi, K. Maeda, H. Hashimoto, T. Ishibe, N. Usui, K. Osumi, K. Ishigure</i>	
In plant corrosion potential monitoring .....	331
<i>B. Rosborg, A. Molander</i>	
Field experience with advanced methods of on-line monitoring of water chemistry and corrosion degradation in nuclear power stations .....	347
<i>B. Stellwag, P. Aaltonen, J. Hickling</i>	
An electrochemical sensor for monitoring oxygen or hydrogen in water .....	381
<i>Leitai Yang, D.R. Morris, D.H. Lister</i>	
Advanced analytical techniques for boiling water reactor chemistry control .....	391
<i>H.P. Alder, E. Schenker</i>	
Control of water chemistry in operating reactors .....	407
<i>R. Riess</i>	
Alternative water chemistry for the primary loop of PWR plants .....	421
<i>N. Henzel</i>	
Water chemistry in WWER reactors .....	433
<i>V.A. Yurmanov, V.A. Mamet, Yu.M. Shestakov, M.M. Amosov</i>	
Some observations on hydrazine and ammonia based chemistries in PWRs .....	455
<i>J. Brunning, P. Cake, A. Harper, H.E. Sims</i>	
Primary water chemistry monitoring from the point of view of radiation build-up .....	465
<i>G.L. Horváth, V. Civin, T. Pintér</i>	
VVER water chemistry related to fuel cladding behaviour .....	473
<i>J. Kysela, M. Zmítko, V. Vrtílková</i>	
Hydrazine-hydrate water regime and operation of fuel elements .....	489
<i>V.I. Pashevitch, D.V. Pashevitch, J. Bogáncs, P. Tilky</i>	
List of Participants .....	497

# SUMMARY OF DISCUSSIONS IN THE TECHNICAL COMMITTEE MEETING

## INTRODUCTION

For the purpose of the meeting water chemistry included the actual practice, the water chemistry monitoring and the on-going research. Corrosion included also hydriding, recent observations made in reactors, modelling and the recent research carried out.

Fifty seven participants representing twenty countries attended the thirty formal presentations and the subsequent discussions. The absence of representation from the United States of America was noted and unanimously regretted by the participants.

The thirty papers presented were split into five sessions covering, Reactor experience, Mechanism and Modelling, Oxidation and hydriding, On-line monitoring of water chemistry and the review of existing and advanced water chemistries.

Four panel discussions including "Corrosion mechanism and Modelling", "Corrosion and Hydriding", "Plant Experience and Loop Experiments", "Water Chemistry, Current Practice and Emerging Solutions" and "On-line Monitoring of Water Chemistry and Corrosion" were organized. The main points of discussion focussed on the optimization of water chemistry, the compatibility of potassium water chemistry with the utilization of Zircaloy 4 or the utilization of zirconium niobium cladding with lithium water chemistry. The effect of the fabrication route and of the cladding composition (Sn content) on the corrosion kinetics, the state of the art and the correlative gaps in cladding corrosion modelling and the recent developments of on-line monitoring of water chemistry together with examination of suitable developments, were also discussed. These discussions are summarized hereafter.

## PANEL DISCUSSION 1

### "Corrosion Mechanism and Modelling"

Chairman: B. Cox (Canada)

The Chairman opened the session by introducing the other members of the Panel. These were Messrs. V.F. Urbanic and B. Rosborg, the Co-chairman of Session 2, and Messrs. Ph. Billot and C. Lemaignan two of the other authors from that session. He then introduced a series of open questions that might be discussed during the session. These were:-

1) Should we be using real oxidation curves in our models.

2) Are we currently using realistic values for:-

Activation Energy for oxidation?

Oxide thermal conductivity?

Thermal hydraulic coefficients?

3) What other subroutines should be incorporated into models:-

Effect of hydride concentration at oxide/metal interface

Effect of Li - is any quantity of Li bad?

Irradiation induced degradation of cladding.

4) How should these components be included in a model?

Additive or multiplicative factors.

5) Radiolysis effects.

The chairman then asked whether there were any further questions that should be added to the list. Mr. Ph. Billot suggested that metal structure factors should be included. The chairman responded that he thought these would automatically be incorporated if real oxidation curves were used rather than the present simplified and stylised kinetics. Mr. V. Polley thought that at least the  $\Sigma A$  parameter (indicator of sensitivity to corrosion) and a frequency factor should be incorporated. However, the  $\Sigma A$  parameter only gives a general indication of oxidation behaviour for different batches of Zircaloy-4, and needs modification for departures from the normal specification even if only to a low tin variant.

Mr. V.G. Kritsky thought that dissolution of zirconia should be one of the factors included, especially where effects of new water chemistry conditions were being investigated. Mr. J. Thomazet thought it was just not possible to have one model that would fit the behaviour of all possible alloys and water chemistry conditions. The chairman responded that he thought it was possible by including sub-routines for all the factors that might influence the corrosion to achieve this, but that for some alloys and some water chemistries some of the sub-routines might be dormant so that a simplification could be made. Mr. V. Polley noted that there was a clear distinction to be made between completely empirical, semi-empirical and mechanistic models. He was not in favour of the first, and opted for the second because he thought the third was too difficult to tackle. The chairman said that even a semi-empirical model should have the correct mechanistic form, it would then be possible to include empirical sub-routines for certain effects until the fundamental constants could be measured. He cited the example of the in-reactor creep and growth model (design equation) for CANDU pressure tubes, where this approach had been very successful in improving the predictions. Mr. V.F. Urbanic supported this argument for a more fundamental approach, since its use would be of value when the development of new alloys was considered. At present the models are unable to predict the behaviour of new alloys.

Mr. A. Maroto pointed out that differences in the pre-transition oxidation kinetics of Zircaloy and Zr-2.5% Nb (cubic and parabolic respectively) may give indications of the respective growth of the inner protective barrier layers. The long term post-transition corrosion rate depends on this. He thought that the parabolic behaviour was much more easily interpreted in physical terms than the cubic kinetics. Mr. V.G. Kritsky noted that a change in kinetics in terms of the solid state physics processes could be understood in terms of changes in the energy levels of the oxide crystals which could be related to impurities, work at his institute studying photo-effects in oxides had been able to measure these energy levels.

Mr. C. Lemaignan noted that it was very important that the effect of radiation damage on the intermetallic should be included. Iron migration and precipitate amorphisation were different processes that interacted with each other. Since amorphisation was possible only at low temperatures there was a feedback loop whereby the increased oxidation rate resulting from intermetallic degradation would raise the oxide-metal interface temperature which in turn could cause recrystallization of the amorphous intermetallic formed early in the irradiation. Mr. V.F. Urbanic commented that because Zr-2.5% Nb was also an alloy that was structurally unstable under irradiation there was a concern about similar effects on its long term corrosion.

Mr. B. Stellwag commented that the problem he had with the discussion so far was that the aim appeared to be to obtain a fundamental understanding, when utilities were interested only in an empirical model that could give day to day predictions of behaviour. The chairman responded that a model could be as empirical or as fundamental as the data allowed, but if it did not have the correct physical form it would be no use for predictions outside the range of the data used to develop it.

Mr. H. Ruhmann observed that all current models started from the very simple observation of a linear post-transition oxidation curve and proceeded to apply various pre-exponential and exponential factors to this, and he thought that this was the correct way to proceed. The chairman responded that all direct measurements of the effect of fast neutron irradiation on zirconium oxidation showed that these effects disappeared at and above 400°C. It would never be possible to predict such a disappearance with a model that only contained multiplicative pre-exponential or exponential factors.

Mr. Ph. Billot noted that the current values for activation energy, oxide thermal conductivity and thermal hydraulic coefficients were based on large numbers of parametric studies from which these constants had been obtained. Mr. H. Ruhmann responded that there were two possible approaches to this, one could either change the factors as a result of a number of parametric experiments, or one could address the problem fundamentally. For him, however, as a chemist changing the activation energy meant changing the rate controlling reaction, and this required justification.

Mr. V. Polley gave the opinion that the main reason why the fundamental approach could not be tackled was that there was not enough money available for such an approach. Mr. D.H. Lister seemed surprised that there was any doubt that it was desirable to move from an empirical to a fundamental understanding of the problem. Mr. V. Polley agreed, but was worried that the present trend was going in the opposite direction; towards purely empirical models.

Mr. C. Lemaignan said that with the drive to even higher burnups there was a pressure to extrapolate outside the limits of the data, and current models were not very extrapolatable. The chairman concluded the session by noting that it was the observation that the early empirical irradiation creep and growth model based on Pickering NGS data could not predict behaviour in the Bruce NGS, which operated at only 10-15 °C higher temperature that forced a move to a more fundamentally based model.

The consensus was that it was important to move towards more fundamentally based models to improve the predictive capability of the current models, and that components addressing the effects of hydride accumulation, lithium, and irradiation degradation of corrosion resistance were required in future models.

## PANEL DISCUSSION 2

"Corrosion and Hydridding: Plant Experience and Loop Experiments"

Chairman: C. Vitanza (Norway)

The intention of this panel was to identify the main issues related to cladding corrosion and hydridding. Of necessity, the discussion was mainly focussed on Western LWRs since the more demanding duty in these reactors poses greater challenges to the fuel than, for instance, in WWER or CANDU reactors.

The current cladding design limit for LWRs is that the hydrogen content should not exceed 500-600 ppm on average, which corresponds to an oxide thickness of ~80-100  $\mu\text{m}$ . It is known, however, that the hydrogen concentration may well exceed the 500-600 ppm limit locally, due to localised temperature gradients. Oxide spalling is observed typically beyond 100  $\mu\text{m}$ , while localised corrosion or hydride pits may lead to cladding perforation beyond thicknesses of ~150  $\mu\text{m}$ . With some exceptions which can be attributed to sporadic deterioration of the water chemistry conditions,

corrosion is not normally a cause of fuel failure. However, the increasing demand for longer cycles, higher outlet coolant temperature and higher burn-ups may raise the cladding oxidation to the performance limit.

The panel observed that cladding corrosion data often exhibit considerable scatter. The data spread is greater at higher exposure. The most important reasons for the data scatter are believed to be the following:

- The oxide thickness versus burn-up plots do not account for the exact power history experienced by each rod. Different core management schemes may result in different power histories and thus in different oxidation behaviour. Calculated powers may also be inaccurate.
- The local thermohydraulic conditions can be different from rod to rod, an effect which is difficult to quantify at present. It was also pointed out that corrosion is often appreciably reduced 10-20 cm upstream of the grids but this cannot be explained in a satisfactory manner.
- Crud deposits and porous oxide layers may develop at higher burn-ups as a combined water chemistry - thermohydraulic effect.
- Different cladding microstructure result in variable corrosion behaviour. It was pointed out that even rods from the same fuel batch may corrode very differently due to temperature gradients in the furnace during annealing.

It was recommended that the data be structured as much as possible in a systematic manner, acknowledging the differences in materials composition/fabrication parameters, thermohydraulics and power history. One possible way of achieving a more consistent picture is to use a predictive model for "linking" the data set and seeing how the measured/predicted ratios behave at increasing burn-up. It was also observed that, while power plant data should remain the reference for real life behaviour, loop data could provide better insights into the mechanisms involved and more understanding of separate effects of individual variables.

The experience with WWER fuel was reviewed, emphasising the fact that the oxide layer at end of service is rather small, typically up to 10  $\mu\text{m}$ . This is based on a considerable data set. It is then apparent that cladding corrosion is not of concern with WWER fuel. The same conclusion applies to CANDU fuel and is due to the lower temperatures and burnups in these plants.

The effect of lithium on PWR fuel clad oxidation was discussed, based both on plant data and on loop test results. A survey has been carried out on those PWRs which have operated with elevated lithium regimes. There were 9 such plants, plus one or two more which had operated with higher than normal lithium for short periods. Data from Ringhals 2,3 and 4 (elevated lithium for five cycles) has not been extensively analyzed in a rigorous manner, taking into account thermohydraulics and exposure conditions but cladding was thought to be unaffected. In Calvert Cliffs 2(1 cycle elevated lithium) oxide thicknesses were normal when plotted versus burn-up. A rigorous analysis of St. Lucie 1 data (1 cycle elevated lithium) published in 1991 has indicated a 15% increase in oxide thicknesses. No analysis had been performed of St. Lucie 2 data (1 cycle elevated lithium). Data from Oconee 1 was presented in 1993 at a Washington Conference showing a possible lithium effect for two of the assemblies analyzed. No lithium effect was observed in several other assemblies which were of lower power. No data have been published from H.B. Robinson (1 cycle elevated lithium), though fuel clad oxide thicknesses were measured. Finally, at this conference, it was shown that increased oxidation of Millstone 3 fuel cannot be concluded.

Although autoclave tests at higher Li content did not reveal an appreciable corrosion increase for Zircaloy-4 coupons up to 30 ppm Li, loop data show that Li is a potential concern in the presence of both heat flux and boiling conditions. This, together with considerations related to corrosion of

components in the primary circuits, has induced utilities to discontinue programmes aimed at operation with Li content beyond 2.2 ppm. The use of KOH as a possible substitute to LiOH is a viable solution from the viewpoint of the cladding corrosion performance, but concerns exist about the compatibility between KOH and stainless steel components in the processes of heating and local boiling such as, in crevices.

Plant data exhibit a trend towards increased corrosion rates at increasing exposure. Many observations were made on the mechanisms causing this burn-up enhancement effect, some related to water chemistry, others not. It was noted that oxide layers tend to become more porous as they grow thicker - a process which may be increased by the presence of lithium in the coolant. This may result in accelerated corrosion. Also the oxide thermal conductivity may become degraded at higher oxide thickness and the metal/oxide interface temperature is increased. Similarly, the formation of crud deposits produces higher corrosion rates. Another important aspect is the fluence-induced dissolution of the cladding alloy precipitate particles, which changes the microstructure of the cladding and consequently its ability to withstand corrosion at high burn-ups. Finally, the presence of an increasing amount of hydrogen in the cladding can produce accelerated corrosion, as shown by a Japanese study conducted with unirradiated specimens. Future loop tests should aim at highlighting the causes of the burn-up enhancement of corrosion and at clarifying the different processes involved. The effect of localised radiation fields on corrosion (via locally enhanced radiolysis) should be also addressed.

The issue of hydrogen migration in the cladding was discussed in one of the papers. Future analytical and/or experimental work should aim at clarifying the effect of pellet gaps and of local spalling on the hydrogen concentration.

As a final remark, the need for an on-line method for measuring the corrosion rate was pointed out. A possible solution, in which a potential drop method can be combined with impedance spectroscopy was outlined. Regardless of the technical solution, it is believed that reliable on-line measurements of corrosion rate during service (in loops) would provide the key to a better understanding of the cladding corrosion mechanisms.

The chairman thanked Messrs. Polley (United Kingdom), Thomazet (France) and Wikmark (Sweden) for their valuable comments and contributions during the discussion.

### PANEL DISCUSSION 3

"Water Chemistry, Current Practice and Emerging Solutions"

Chairman: R. Riess (Germany)

The discussion was opened by recalling the objectives of the WACOLIN-Programme and its objectives.

These were:

- Man-Sievert-Reduction
- Plant Life Extension (PLEX)
- Fuel Life Extension (FLEX)
- General Safety

Because this TCM focused on fuel cladding behaviour it was suggested to emphasize discussions on the question of what can be done with Water Chemistry for Fuel Life Extension (FLEX) and which parameters are most important to influence fuel cladding corrosion.

The discussion was split in two sections according to the basic reactor types, i.e. PWRs and BWRs.

#### A. Pressurized Water Reactors

All parameters that are important for fuel integrity were discussed starting with the parameters shown in the EPRI-Guidelines:

##### Hydrogen:

It was suggested that the hydrogen concentration should be kept in the lower range of the given specification. This suggestion is based on CANDU experience showing that in this range a correlation between the H<sub>2</sub>-uptake and the H<sub>2</sub> concentration in the coolant does exist. However, the effect may flatten off in typical PWR conditions.

A question whether a lower H<sub>2</sub> limit is reasonable was answered by the fact that in PWR conditions an excess of H<sub>2</sub> has to be secured in order to avoid a net decomposition.

Overall it was felt that PWRs should be operated in the lower specification range.

A question regarding improved H<sub>2</sub> measurement techniques did not yield a response.

##### Chloride:

It was stated that this is an important parameter and that it has to be specified.

As well as chloride, other halogenides are believed to be detrimental for the fuel cladding. Any efforts to reduce halogenide concentrations were seen to be beneficial for fuel cladding corrosion resistance.

Several observations in lab-tests were reported on the halogenide (fluoride, chloride impact) on fuel cladding behaviour. An interesting contribution discussed test results on Zircaloy-Iodine interaction. No effect was observed with a few ppm iodine. However, when straining the coupons at room temperature (RT) a protective oxide film could not be formed and cracks were observed in the protective layer. Major incidents with chloride and/or fluoride intrusion in operating stations were not reported.

##### Oxygen:

This parameter had a lower importance because the hydrogen excess ensures that O<sub>2</sub> is below the specified limit.

Dukovany reported a case where greater make-up water volume with higher O<sub>2</sub> concentrations were injected into the reactor coolant. However, after passing the reactor core, the oxygen had been consumed.

##### Lithium:

The interaction of lithium and Zircaloy was discussed throughout the TCM and the panel discussions. For this synthesis it should be noted;

- Lithium should be limited to less than 2.2 or 2 ppm
- The modified B-Li-Chemistry is most favorable
- In case of higher void fractions, higher burnup etc. the use of an alternative pH control agent should be considered, i.e. potassium.

## Parameters outside the existing Guidelines

### Potassium:

Potassium may be less corrosive for Zircaloy than lithium. However, this has to be qualified.

The Zr/Nb fuel cladding and potassium chemistry are highly compatible.

KOH may lead to stress corrosion cracking of reactor components in areas where dry-out by  $\gamma$ -heating can occur.

### Ammonia and nitrogen compounds:

It was mentioned that ammonia and other nitrogen compounds may increase the Zircaloy-4 corrosion. However, this was rejected by several contributions from the audience.

A Russian contribution regarding a comparison of the regular potassium/ammonia and the hydrazine chemistry in operating plants showed that there are controversial data on the benefits of hydrazine (especially on the activity buildup).

A proposal to specify the nitrogen compounds was not supported.

### Organics:

Organics were felt to be big risk for fuel cladding corrosion. Emphasis was given to ion exchange resins that may be injected into the primary system. How to specify and how to control ion exchange intrusion could not be answered during the panel discussion. A suggestion was to use the sulphur content of the coolant as an indicator.

### Silica, Ca, Mg and Al:

This group of substances was mentioned because they can contribute to a zeolite formation and thus can increase fuel cladding corrosion.

It was recalled that these substances are specified in older W-plants and in the Framatome coolant specification.

## B. Boiling Water Reactors

There was much less discussion on parameters in BWRs which are important for fuel cladding integrity. Overall it was felt that IGSCC or IASCC-problems require very stringent specifications and that the fuel cladding corrosion can draw maximum benefit from this circumstance.

There was some discussion on the following parameters:

- Cu specification. This value is specified for the feedwater.
- Importance of SiO<sub>2</sub>.
- pH-value. Specification of this parameter was recommended by Russia, however its necessity was very much questioned by participants.

## PANEL DISCUSSION 4

### "On-Line Monitoring of Water Chemistry and Corrosion"

Chairman: H.P. Alder (Switzerland)

The chairman presented the panel lists: Messrs. P.A. Aaltonen (Finland), B. Rosborg (Sweden), B. Stellway (Germany).

As an introduction the terminology for different kinds of water chemistry monitoring was defined:

OFF-LINE (discontinuous sampling, central laboratory analysis), AT-LINE (discontinuous sampling, analysis by dedicated instrument in the plant), ON-LINE (continuous sampling, analysis in a by-passed flow). In all these cases pressure and temperature are reduced. In a strict sense only IN-LINE (continuous sampling and measurements but with flow disturbance) and NON-INVASIVE (continuous sampling without flow disturbance) techniques are suitable for direct process control which is the ultimate goal. IN-LINE and NON-INVASIVE techniques are often summarized as IN-SITU techniques.

The purpose of monitoring water chemistry for the plant operator is to show:

- that the plant is operating within the technical specifications,
- that measures taken to return from transients to normal operation are effective,
- that no trend exists which may lead to abnormal conditions (early warning).

In a broader sense real time information should lead to a deeper understanding of plant behaviour and improved plant performance:

- to provide data for mathematical modelling,
- to maintain conditions with minimum material corrosion
  - to assure component reliability (Plant life extension or PLEX)
  - to minimize radioactive waste
  - to minimize local radiation dose rates
  - to minimize fuel cladding corrosion to achieve high fuel burnup (Fuel life extension or FLEX).

The subject to be treated was divided into 5 sections as shown in the following overview:

1. **Process control** (temperature, pressure, flow)
2. **Overall water quality** (conductivity, pH)
3. **Water impurities**
  - **Standard procedure** (ion selective electrodes, ion chromatography; atom absorption spectroscopy AAS, inductively coupled plasma mass spectroscopy ICP-MS)
  - **Crud particles** (filtration, particle counter; AAS, ICP-MS, X-ray diffractometry)
  - **Activity** (spectroscopy)

- **Organic carbon** (Ultraviolet-visible-infrared spectroscopy UV-VIS-NFIR; organic carbon analyzer)
- 4. **Corrosion of materials** (corrosion potential, oxygen concentration, hydrogen concentration)
- 5. **Oxide layer on austenites** (impedance spectroscopy, IR-reflection, contact electrical resistance CER; sputtered neutral mass spectroscopy (SNMS), secondary ion mass spectroscopy (SIMS))

1. Process control

Pressure, temperature and flow are measured by IN-LINE or NON-INVASIVE methods. The present state of development is satisfactory.

2. Overall water quality

For the detection of anomalies in water chemistry on IN-LINE conductivity cell up to 300° is developed. This measurement at high temperature however is not very sensitive to impurities in the reactor water.

For IN-LINE measurements of the pH in pressurized water reactors (PWR), yttria stabilized zirconia probes have been applied with success. The determination of absolute pH values is very difficult and the pH cell should rather be used to indicate trends. It can also be imagined that boiling water reactors (BWR) will also operate at higher pH in the future. This may affect the pH-cell design.

3. Water impurities

The standard plant procedure is OFF-LINE (corrosion products), AT-LINE (special measurements), ON-LINE (for BWR conductivity).

Special tools such as filtration IN-LINE by gold membranes and optical light reflection allow the determination of crud particles. These methods are of particular interest to researchers. The determination of the gamma-activity in the reactor water and on the austenitic surfaces is of direct interest to the operator. It can be performed by an NON-INVASIVE technique.

Concerning the organic carbon a direct optical determination seems feasible, provided that a suitable light wave length can be found. This optical method, as well as the crud particle determination, depends on the transparency of the sapphire windows.

4. Corrosion of materials

Electrochemical methods were used with success in plant to determinate the corrosion potential during transients. For these measurements an external reference electrode is sufficient. This method is not yet routine and has to be followed by research staff. The same applies to the hydrogen electrode (Palladium-Silver alloy).

5. Oxide layer on austenites

In principle impedance spectroscopy and contact electrical resistance (CER) should provide information on the corrosion layer on austenites. In both cases the electrical signals have to be translated into physico-chemical processes which is still difficult.

## Summary

Electrochemical methods have been applied with success IN-LINE in plants to monitor steady state operation and transients. Promising techniques are optical and gamma-spectroscopic methods. A general problem is the extrapolation of a result from one sampling location to other locations, in particular the reactor core. For OFF-, AT-, ON-LINE analysis, the question is how can it be guaranteed that sample composition does not change in this long line with pressure and temperature reduction. Not addressed was the question of in-core instrumentation, however such in-situ measurements (e.g. the cladding corrosion rate), a large effort of development is required with a fairly limited prospect of success.

## GENERAL CONCLUSIONS AND RECOMMENDATIONS

J. Kysela, Chairman,  
P. Chantoin, Scientific Secretary

### Main conclusions

#### Actual practice of water chemistry in PWR reactors

From several experiences with "low" and "high" lithium water chemistries, it was concluded that "high" lithium chemistry would increase the Zircaloy-4 corrosion. Modelling performed in France shows an increase of corrosion up to 45% when the lithium concentration jumps from 2.2 ppm to 3.5 ppm. It is also recognized that the lithium (Li) effect is more pronounced in two-phase flow and when the void fraction increases.

Therefore, the recommendation is to use the modified Li-B chemistry with  $\text{Li} \leq 2.2$  ppm (in Germany the limit is set at 2 ppm).

Two other factors have also to be taken into consideration when deciding on water chemistry. On one hand, a constant pH around 7.2 throughout the cycle would probably decrease the activity transport in the primary circuit and therefore the dose rate in the plant. On the other hand, high Li chemistry would increase the risk of stress corrosion cracking of primary circuit components, especially those made of alloy 600.

Several experiments have been conducted on alternative pH controlling agents. It was reported that potassium hydroxide (KOH) has shown good results in both autoclave and loop tests in single or two-phase flow even with high void fraction, the difference of ionic radius between Li and K may be the reason; but there is still a long way to go before being able to operate western PWRs with KOH; extensive tests on corrosion of in-core components working under irradiation would be needed beforehand. It was also reported from Russia (not included in presented papers) that some laboratory tests were showing a higher sensitivity of Zircaloy-4 to hydrogen pick-up when used in WWER chemistry, therefore, behaviour of cladding materials regarding hydrogen pick-up would have to be checked also.

The benefit of zinc addition to decrease the personal dose rate was also discussed.

#### Actual practice of water chemistry in WWER reactors

In WWER reactors potassium water chemistry associated with zirconium 1% Nb cladding shows good results: Low corrosion rate and hydrogen pick-up. Recently, in WWER reactors, a modified water chemistry at pHT 7.0-7.1 was implemented instead of "drifting" pH in the range 6.6-6.9. The result of the application of this new water chemistry was a decrease of personal radiation exposures, however controversy remains over the possible use of ammonia or hydrazine as oxygen scavenger. On one hand it is claimed that the use of hydrazine decreases cladding corrosion and activity transport, on the other hand, some Russian results show that the reactor contamination is higher when hydrazine is used (not in presented papers). A comparison between ammonia and hydrazine has been carried out at the PAKS power plants in Hungary but does not show a significant difference between the two water chemistries from the point of view of dose rates. In this matter there are very few comprehensive results available and further work is needed to clarify the situation (especially fuel examination).

## Effect of low tin content and heat treatment on Zircaloy 4 behaviour

It was recognized that any comparison between "high" and "low" lithium, "high" and "low" tin content or "high" and "low" temperature is somehow impaired by other parameters which seem very sensitive. A wide dispersion of results was obtained, sometimes in the same batch of cladding. Two main parameters were identified as possible culprits:

- Heat treatment during tube fabrication. An improvement of 40% was attributed to optimization of composition and heat treatment, by the French utility.
- Temperature differences in the core.

Further study of the heat treatment will be difficult because the values used in practice are very often commercially classified. The study of temperature differences in a core would require a more sophisticated approach to linear power and thermal-hydraulic modelling.

It was also recognized that low tin alloys were showing improved corrosion behaviour. Although the improvement is sometimes difficult to assess, a figure of 15% benefit in the oxide layer thickness at 50 MWd/kgU was announced by EDF.

## Clad corrosion modelling

Models used up to now are empirical or semi-empirical, their capability to predict the behaviour of a new alloy or the consequence of a moderate increase in temperature (10-15°C) is very limited. The need to go to a more mechanistic understanding of the phenomena involved is therefore apparent.

Two areas have been identified for additional research:

- a) The effect of radiation and energy deposition related to the dissolution and deposition of oxides and hydroxides.
- b) The consideration of real corrosion curves, the study of which would lead to a more mechanistic approach to zirconium alloy corrosion. In this further study, the influence of annealing parameters, alloying elements would have to be studied in more detail.

## On-line monitoring of water chemistry

Many companies are now working on "on-line monitoring of water chemistry". It is agreed that 'On-line' monitoring is the way ahead but is extremely difficult to implement. The potential cost benefit is such that it is very surprising that much more effort is not directed in this area. Several promising methods of measurement are still under development, they are for instance: conductivity, pH, hydrogen, soluble and insoluble impurities, corrosion potential.

During the meeting the benefit of this monitoring for safety, minimization of corrosion or man-sievert reduction was widely discussed. As for any new development, many questions are still open. The most important are:

What measurement to perform?

What kind of sensor to use?

Where to perform the measurement? and

How to extrapolate the measurement results to other locations in the reactor? (modelling).

## Recommendations

*The main developments have been identified as follows:*

### *Water chemistry practice*

- 1) In order to minimize crud, out of core corrosion and activity transport in the primary circuit it is recommended:
  - to use a modified Li-B water chemistry with a pH as close as possible to 7.2 in PWR reactors,
  - to use a modified K-B water chemistry with a  $\text{pH}_T$  7.0-7.1 in WWER reactors.
- 2) Evaluate alternative pH controlling agents, especially potassium hydroxide for PWR applications.
- 3) Further study the influence of zinc on the activity transport.
- 4) Evaluate the behaviour of Zircaloy 4 in WWER water chemistry in normal operation and accident conditions, including the influence of the oxygen scavenger used on corrosion and hydriding (influence of nitrogen and ammonia).
- 5) It is recommended to carry on the comparative study ammonia/hydrazine as oxygen scavenger.

### *Cladding corrosion*

- 6) More observations on cladding corrosion, from power reactors and loops in MTR reactors are needed and an effort has to be made to identify the specific influence of each parameter (temperature, fabrication route, annealing temperature, tin content, alkali concentration ....) on corrosion.
- 7) Special attention has to be given to the in-core assessment of irradiation parameters (linear rate, temperature).

### *Corrosion modelling*

- 8) The effect of radiation and energy deposition on the dissolution and deposition of oxide and hydroxide have to be further studied.
- 9) More mechanistic models of corrosion have to be developed starting from the observed kinetics of corrosion on well characterized cladding.

### *On-line monitoring of water chemistry*

- 10) Further develop the on-line monitoring of water chemistry, appropriate sensors and the correlated modelling. It is considered that the CRP "on-line monitoring of water chemistry" is an important step in this way.

### *Meeting organization*

- 11) In future meetings develop appropriate synergies between research subjects.
- 12) Organize panel discussions in order that specialists can attend the panel of their choice or several of them.

**PAPERS PRESENTED**

**NEXT PAGE(S)  
left BLANK**

## EFFECT OF WATER CHEMISTRY AND FUEL OPERATION PARAMETERS ON Zr + 1% Nb CLADDING CORROSION

V.G. KRITSKY, N.G. PETRIK, I.G. BEREZINA, V.V. DOILNITSINA  
VNIPIET, St. Petersburg,  
Russian Federation

### Abstract

In-pile corrosion of Zr + 1%Nb fuel cladding has been studied. Zr-oxide and hydroxide solubilities at various temperatures and pH values have been calculated and correlations obtained between post-transition corrosion and the solubilities nodular corrosion and fuel operation parameters, as well as between the rate of fuel cladding degradation and water chemistry. Extrapolations of fuel assemblies behaviour to higher burnups have also performed.

### INTRODUCTION

The code for computing the reliability of nuclear fuel operation contains mathematical blocks for estimating the influence of various parameters. These blocks are based on physical and engineering models that correlate the parameters of external attack with fuel cladding behaviour.

This work describes two models of nodular and uniform Zr+1%Nb alloy corrosion LWR environment, produces possible correlation between sequential failures of fuel assemblies observed and the models proposed.

#### 1. DEVELOPMENT OF UNIFORM AND NODULAR CORROSION MODELS AND EQUATIONS.

Corrosion of Zr-alloys is a very complex process that depends on many factors. The initial oxidation stage results in the formation of thin, tightly adhering protective black film.

The oxidation kinetics of this stage obeys parabolic, cubic or logarithmic law in relation to the properties of the protective film. The film is solid zirconium-in-zirconium dioxide solution. It is non-stoichiometric owing to oxygen deficiency. As soon as the oxygen concentration in the film achieves stoichiometry the solid Zr-in-ZrO<sub>2</sub> solution turns into white ZrO<sub>2</sub> which does not possess protective properties. This white porous film grows on the black film, not instead of it. On the corrosion curve this change is marked by "transition". Post transition oxide growth obeys linear law and the oxidation rate becomes practically constant. Currently available models for evaluating the effects of various factors on Zr corrosion take into account the initial (pre-transition) phase and mechanism of solid phase oxidation. The influence of coolant water chemistry cannot be considered in this case.

Under the operating conditions of water reactors the second oxidation stage is most interesting, when oxide growth is accompanied by its dissolution. This stage is described by a diffusion model, where the diffusion regime in pores has a steady-state stationary character. Johnson [1] concluded that the total corrosion gain could be represented by:

$$W = W_T + W_\Phi \quad (1)$$

where  $W_T$  and  $W_\Phi$  - thermal and radiation weight gain components, respectively.

The linear oxidation rate can be written as:

$$v_{\text{uniform}} = \frac{dW}{dt} = k_T + k_\Phi \quad (2)$$

here  $k_T$  and  $k_\Phi$  - thermal and radiation corrosion coefficients, respectively.

### 1.1. Uniform corrosion.

#### 1.1.1. Thermal component of uniform corrosion.

Empirical studies of numerous oxidation reactions have shown that under constant oxygen pressure in the environment the temperature dependence of the oxidation rate can be described by the Arrhenius equation:

$$k_T = k_0 \exp \left( - \frac{Q}{RT} \right) \quad (3)$$

Here  $Q$  - activation energy,  $R$  - gas constant,  $T$  - absolute temperature at the coolant/cladding interface. Experimental values of  $Q$  amount to  $10^4 \pm 10$  kJ/mole (Fig.1) [2].

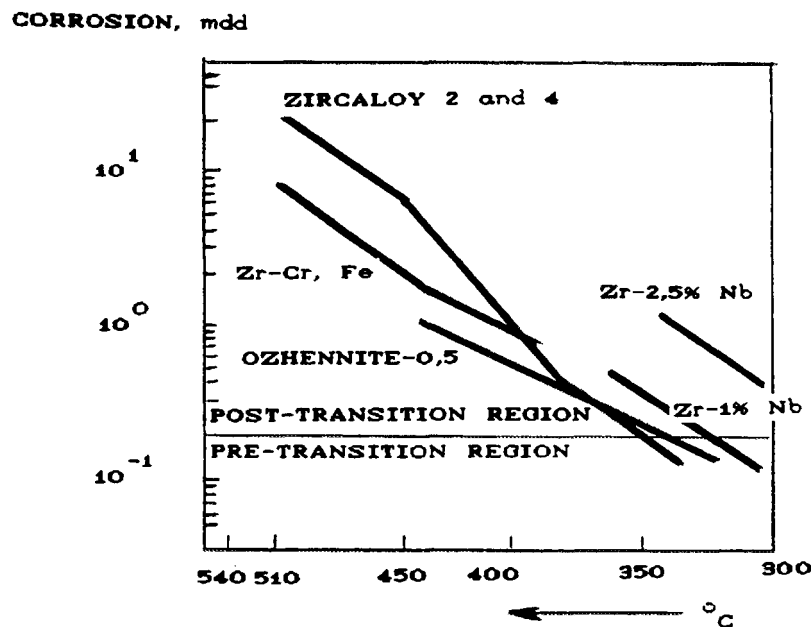


Fig.1. The temperature dependence of the Zr-alloys corrosion rate.

(Videm K. Nuclear Engg. & Design, 33, 170, 1975)

### 1.1.2. Radiation component of uniform corrosion.

The radiation component of uniform corrosion is a function of quite a series of factors [1]:

$$K_{\Phi} = f(\Phi, O_2, T, S, A, M) \quad (4)$$

Here  $\Phi$  - fast neutron fluence,  $O_2$  - oxygen concentration in coolant,  $T$  - temperature,  $S$  - surface condition of alloy,  $M$  - metallurgic state.

The rate of Zr alloy corrosion under reactor irradiation depends on heat flux through fuel cladding coolant chemistry (in addition to  $O_2$ - concentration one should account for the concentrations of hydrogen, ammonia, strong alkalis - LiOH, KOH,  $pH_T$ , etc.) and some other parameters.

The activation energy of radiation corrosion is very small that  $Q_{\Phi} = 0$ .

The concentration of dissolved oxygen is one of the important factors that influences the radiation corrosion. (Fig.2) [3]. It produces strong effect on the stationary concentrations of practically all products of water coolant radiolysis [4]. Oxidizing products of radiolysis participate in corrosion process. Long-lived products with the largest diffusional paths during their life time ( $H_2O_2$  above all) make the maximum contribution into corrosion process. In this case

$$k_{\Phi} = H (H_2O_2)_{st} \quad (5)$$

where  $H$  - adsorption coefficient and  $H_2O_2$  - stationary concentration of  $H_2O_2$  that depends on radiation intensity, chemical composition of water, vapour content etc.

WEIGHT GAIN,

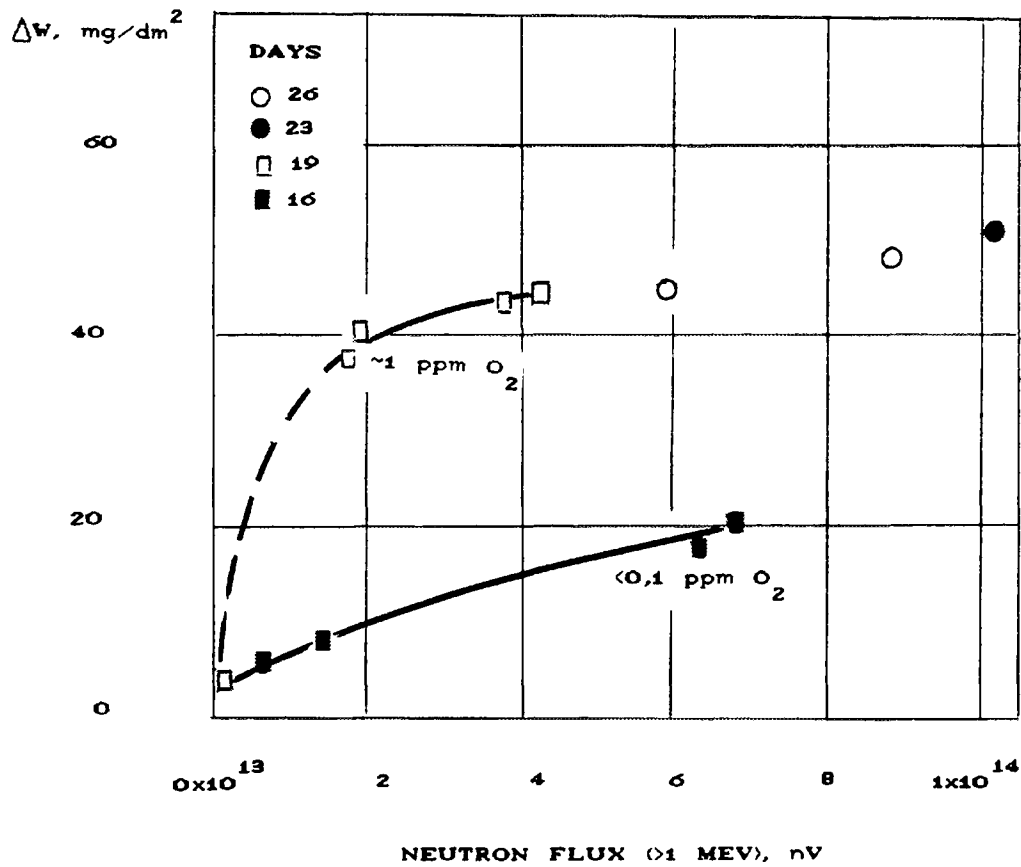


Fig.2. Effect of neutron flux on the oxidation of Zircaloy-2 in high ( $\sim 1 \text{ ppm}$ ) and low ( $< 0.1 \text{ ppm}$ ) oxygen water (in the ETR G-7 loop). [8]

In the case of two-phase flow (BWR conditions) solving the material balance equation for the products of radiolysis by applying the stationary concentrations method and simplified radiolysis scheme results in the integral expression:

$$(\text{H}_2\text{O}_2)_{st} = R B \Phi^n \left( 1 + \left( \frac{k_G^{\text{H}_2}}{p} - 1 \right) \alpha \right) \quad (6)$$

Here: R, B - constants;

$\Phi$  - fast neutrons fluence,  $n = 0,5 - 1$ ;

$K_G^{H_2}$  - Henry constant;

p - pressure;

$\alpha$  - mass vapour content ( $\alpha = 0...1$ ).

For BWRs  $\frac{K_G^{H_2}}{p} \alpha \gg 1$  and Eq. 5 takes the form:

$$k_{\Phi}^{BWR} = N \frac{K_G^{H_2}}{p} \Phi^n \alpha \quad (7)$$

where N - constant.

In the case of single-phase flow (PWRs) the material balance equation has another solution. According to [5] for single-phase water flow under irradiation

$$[H_2O_2]_{st} \approx \frac{1}{5} ([H_2O_2]_0 + 2[O_2]_0 - [H_2]_0) \quad (8)$$

where  $[H_2O_2]_0$ ,  $[O_2]_0$  and  $[H_2]_0$  - initial concentration of  $H_2O_2$ ,  $O_2$  and  $H_2$  in the coolant at the inlet to the core. Calculations result in very low values of  $[H_2O_2]_{st}$ , hence, as a first approximation for PWRs, one can assume that

$$k_{\Phi}^{PWR} \approx 0.$$

Thus, the thermal component (Eq. 3) is common to the corrosion equation (Eq. 2) for BWR and PWR alike.

Next we shall consider the correlation between  $K_T$  and water coolant chemistry.

1.2. Relationship between equilibrium oxide solubility and thermal component of corrosion.

At the linear kinetics the thickness of the corrosion reaction zone remains constant and no accumulation of the corrosion products occurs there. In this situation the diffusion stage of corrosion products removal becomes limiting. At this regime the concentration of corrosion products,  $m_x$  in every point,  $(x)$ , is independent on time, i.e.

$$\frac{\partial m_x}{\partial t} = 0 \quad (9)$$

The concentration gradient is constant, if the diffusion coefficient is independent on the concentration, and since no accumulation of substance at some level occurs, at a steady-state regime, general flow (i.e. oxidation rate  $\frac{\partial S}{\partial t}$  mole/s) through equipotential surface can be written as:

$$\frac{dS}{dt} = D_e \frac{\Delta m}{V l} S_q = K_s, \text{ and } K_s \approx K_T \quad (10)$$

where  $D_e$  - water diffusion coefficient,  $m^2/s$ ;

$\Delta m$  - concentration gradient, mole/kg;

$V$  - specific volume of oxide ( $ZrO_2$ ),  $m^3/kg$ ;

$l$  - reduced distance between the cell faces, that have the concentration constant in time;

$S_q$  - unit surface area,  $m^2$ ;

$K_T$  - from Eg. 3.

In the boundary case, when  $\Delta m$  is maximum, it is equal to the equilibrium gross concentration products in solution ( $m_c$ ). Comparing the contributions of charged zirconium products, formed in the solution (first of all  $Zr(OH)_3^+$  and  $Zr(OH)_5^-$ ) to the gross concentration of  $ZrO_2$  shows that the right side of Eq.10 can be written as the sum of the constant  $C = \frac{S}{V l}$  and the variable.

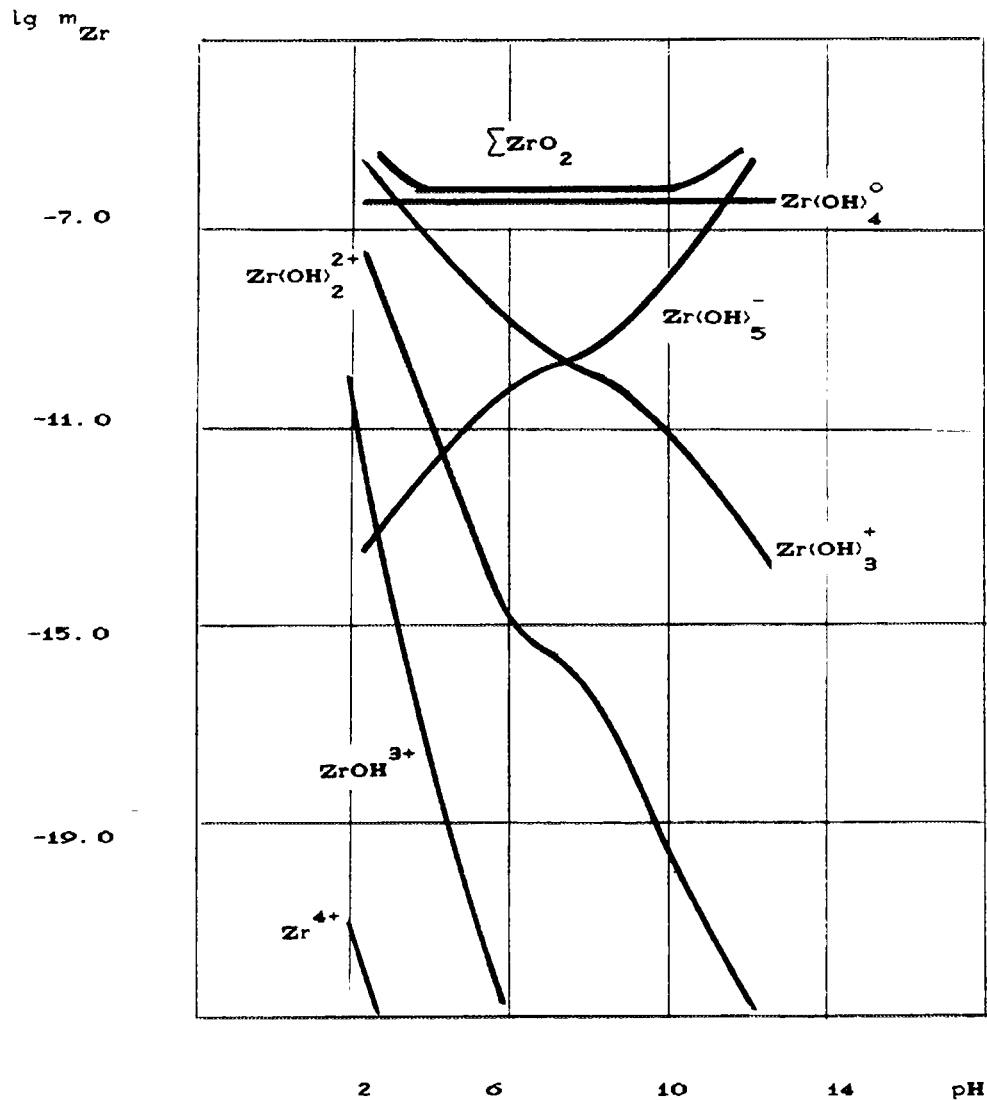


Fig.3. The calculated solubilities of zirconium corrosion products in PWR conditions. [6]

Taking the logarithm of Eq.10 gives:

$$\lg K_T = \lg\left(\frac{dS}{dt}\right) = \lg(\Sigma m_c) + \lg D_e + \lg C, \quad (11)$$

where  $\Sigma m_c$  - sum of concentrations prevailing in solution at given thermodynamic conditions of ions, mole/kg.

It is well known, that the solubility is dependent on T, pH and the concentrations of salts and impurities in solution. The

## CORROSION RATE

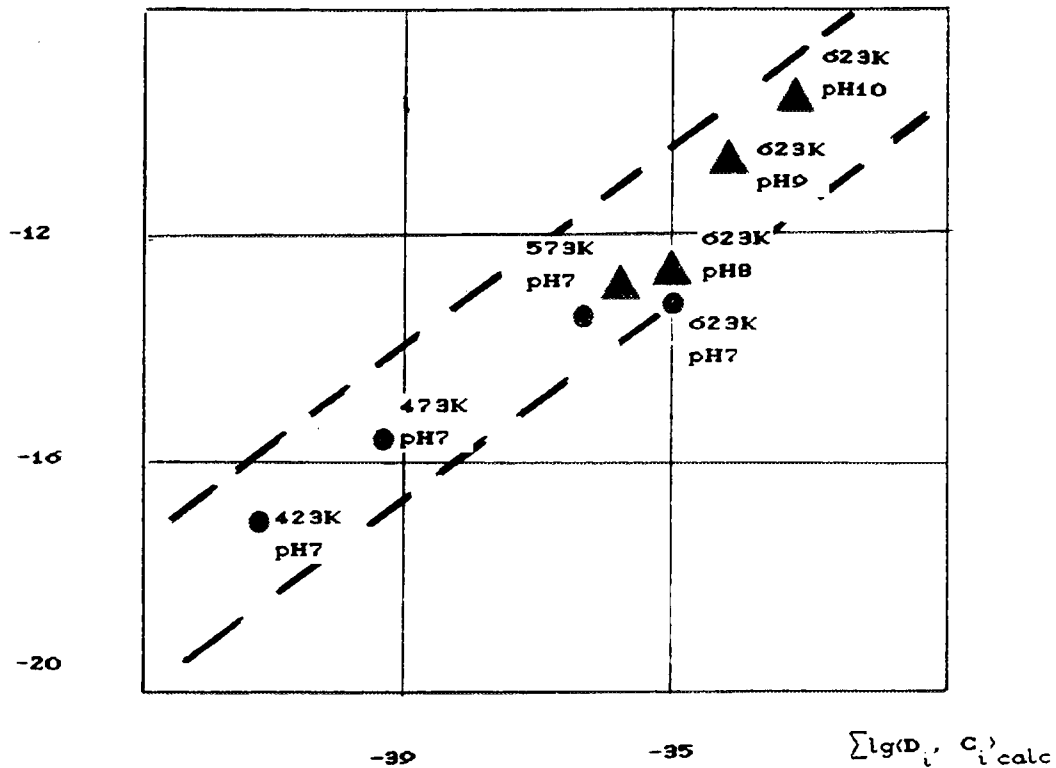


Fig.4. The correlation between calculated and experimental data in view of temperature and pH changes.

solubility was determined [6] for the systems: zirconium corrosion products ( $ZrO_2$ ,  $Zr(OH)_4$ ) - water ( $H_2O$ ) - corrective additives (HCl, KOH) over the temperature range of 298-623 K and the correlation between the solubility and Zr alloys corrosion rate analyzed. Fig.3 shows the calculated solubilities of zirconium products in PWR conditions.

Fig.4 shows the correlation between calculated with Eq.11 and experimental data [7,8] in view of temperature and pH changes. Similar correlations have been obtained for Fe- and Cu-based alloys [9,10].

### 1.3. Nodular corrosion.

By analogy with Eq.2 for uniform corrosion the linear kinetics equation for nodular corrosion can take the form:

$$v^{loc} = k_T^{loc} + k_{\Phi}^{loc} \quad (12)$$

#### 1.3.1. Thermal component of nodular corrosion.

The thermal component is most frequently described on the base of CILC-effect. The physical meaning of this effect consist in the temperature growth on the external surface of fuel cladding due to the deposition of corrosion products [11]. From this standpoint in accordance with Eq.3. we can write:

$$k_T^{loc} = k_0 \exp \left( - \frac{Q}{R(T + \Delta T)} \right) \quad (13)$$

where  $\Delta T$  - growth of cladding temperature under corrosion deposits layer.

$$\Delta T = \bar{q}_S \frac{\bar{\Delta\delta}}{\lambda} = \bar{q}_S \frac{K}{\lambda} \bar{C} \quad (14)$$

where  $\bar{q}_S$  - average heat flux across fuel cladding, MW/m<sup>2</sup>;

$\bar{\Delta\delta}$  - average thickness of corrosion deposits layer, m;

$\lambda$  - conductivity coefficient for corrosion deposits layer;

$K$  - coefficient of corrosion products distribution in zone [11];

$\bar{C}$  - average concentration of corrosion products in coolant.

Then Eq.13 takes the form:

$$k^{loc} = k_0 \exp \left[ - \frac{Q}{R \left( T + \bar{q}_S \frac{K}{\lambda} \bar{C} \right)} \right] \quad (15)$$

### 1.3.2. Radiation component of nodular corrosion.

The model that describes the radiation component of nodular corrosion, combines several factors that exert simultaneous effect on nodule formation, namely, boiling, radiation, coolant, impurities, local change of heat flux. It is also assumed that it is local boiling that provokes the nodular corrosion.

The physical meaning of the model lies in the fact that in the place of local boiling the vapour content exceeds the mean value and takes the form:

$$\alpha^{loc} = \bar{\alpha} + \Delta\alpha \quad (16)$$

where  $\alpha^{loc}$  - local vapour content;

$\bar{\alpha}$  - average vapour content.

Hence, Eq. 7 can be written as:

$$k_{\Phi}^{loc} = N \frac{K_G^{H_2}}{p} \Phi^n (\bar{\alpha} + \Delta\alpha) \quad (17)$$

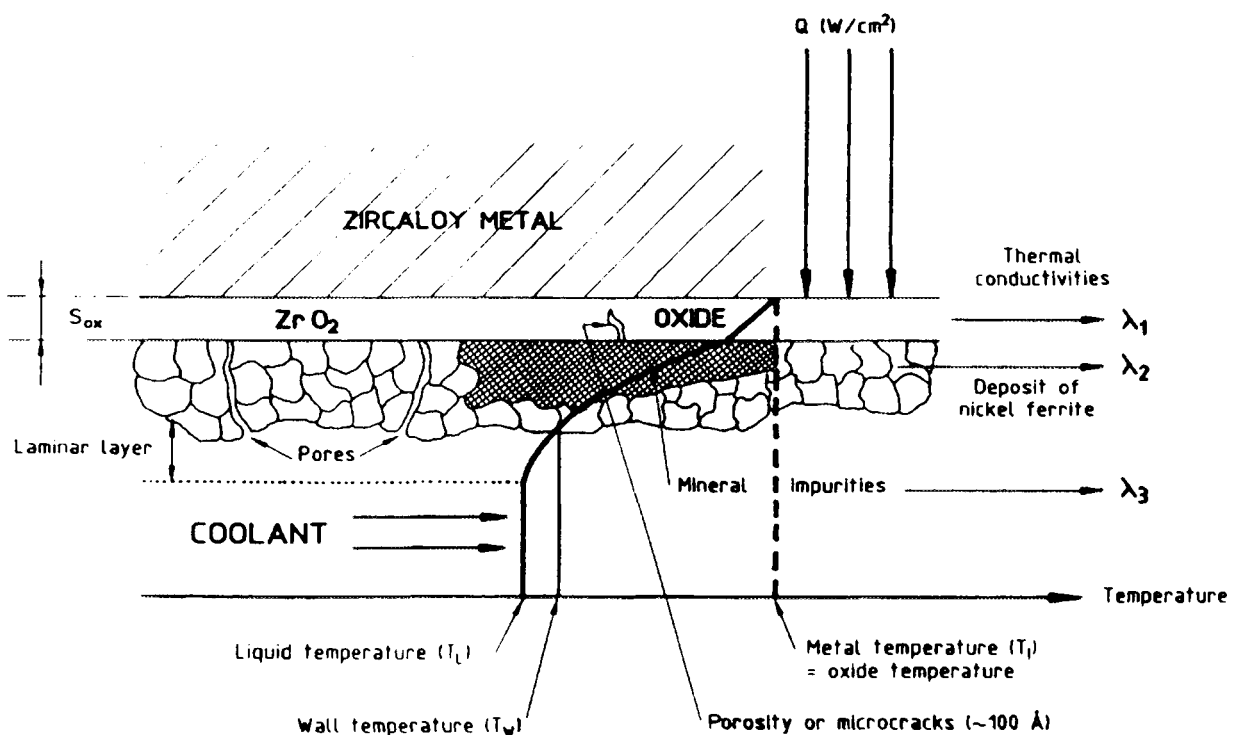
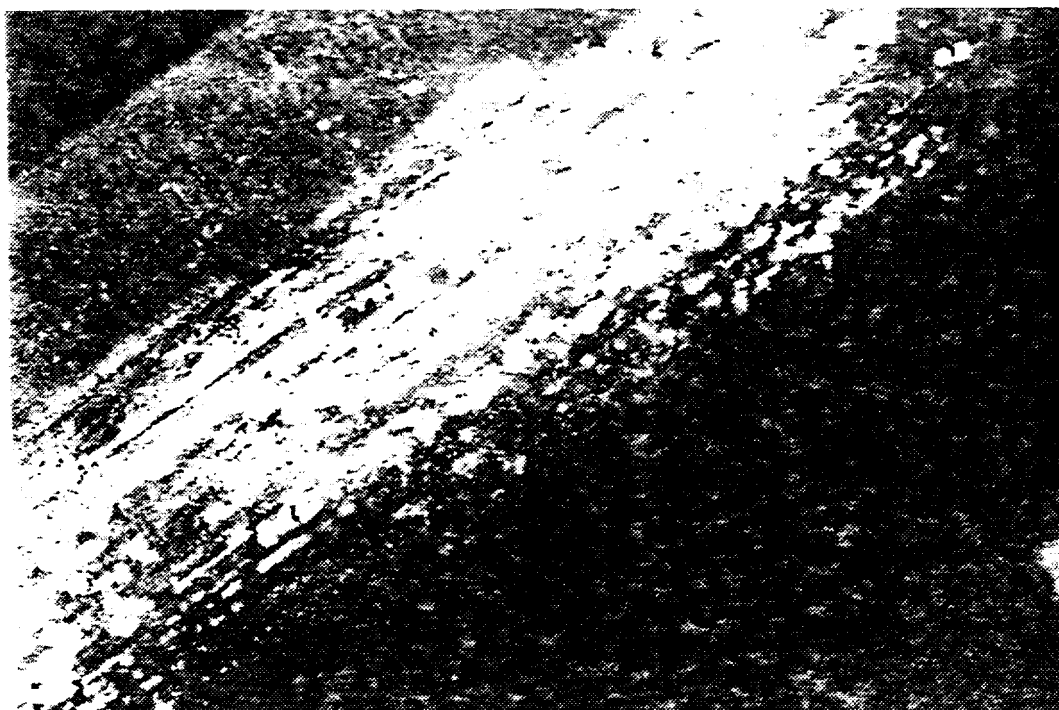


Fig.5. Corrosion under a thermal gradient. [2]



a)



b)

Fig.6. a) Chimneys in crud.  
b) Scraping with white deposit.[2]

To determine  $\Delta\alpha$  one should consider a situation when the distribution of corrosion deposits over the fuel surface is either irregular or there are areas, that differ widely in thickness (Fig.5). At the deposits/cladding interface heat flux "bypasses" deposits areas with high thermal resistance, spreads through cladding metal with low thermal resistance, and then goes into coolant across open areas of fuel cladding (or zones with much thinner oxide film) (Fig.6). Excess heat flux at the "near-interface" (boundary) layer creates a region of increased vapour content, i.e. a region of local boiling.

After some simplifications solving the thermal balance equation for local heat flux through the boundary layer of corrosion deposits results in the expression:

$$q_S^{loc} = \bar{q}_S + \Delta q = \bar{q}_S \left[ 1 + \frac{1}{\pi D} \sqrt{\frac{\Delta\bar{\delta} a \lambda_a}{\lambda_c}} \right] \quad (18)$$

where  $\bar{q}_S$  - average heat flow across fuel cladding,

$a$  - cladding thickness,

$D$  - cladding diameter,

$\lambda_a$  and  $\lambda_c$  - coefficients of thermal conductivity for zirconium and corrosion deposits, respectively,

$\Delta\bar{\delta} = K\bar{c}$  - thickness of corrosion deposits layer.

The vapour content  $\alpha$  relates to the heat flux as

$$\alpha = \frac{q_s S}{r_b G} \quad (19)$$

where  $S$  - heat transfer area,  $m^2$ ,

$r_b$  - heat of vaporization, MJ/kg,

$G$  - coolant flow rate, kg/s.

Hence

$$\alpha^{loc} = \bar{\alpha} + \Delta\alpha = (\bar{q}_s + \Delta q) \frac{s}{r_b G} \quad (20)$$

Substituting into Eq.17 results in

$$k_{\Phi}^{loc} = N \frac{K_G^{H_2}}{p} \Phi^n \bar{\alpha} \left( 1 + \frac{1}{\pi D} \sqrt{\frac{a \lambda_a K}{\lambda_c} \bar{C}} \right);$$

$$k_{\Phi}^{loc} = N \frac{K_G^{H_2}}{p} \Phi^n \bar{\alpha} (1 + M \sqrt{\bar{C}}) \quad (21)$$

where  $M = \frac{1}{\pi D} \sqrt{\frac{a \lambda_a K}{\lambda_c}}$ ,  $\bar{\alpha}$  - average vapour content,

$\bar{C}$  - average concentration of corrosion products in coolant.

Fig.7 shows the relationship between  $k_{\Phi}$  and  $\alpha\%$ .

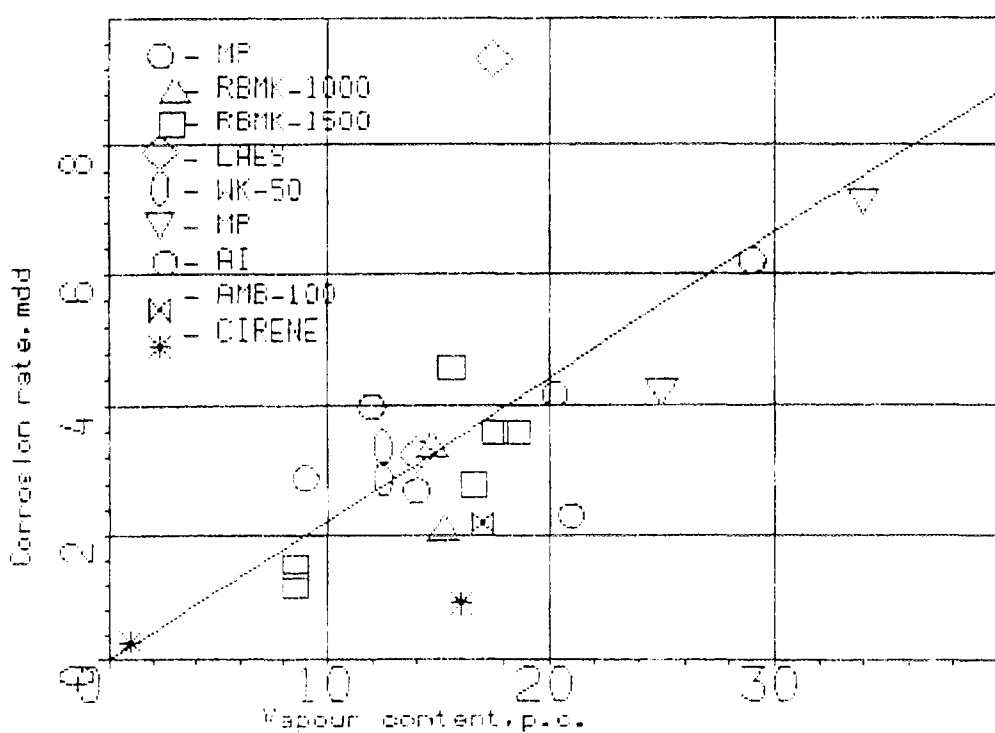


Fig. 7. The vapour content influence on linear Zr-alloy corrosion in various AEI environment

In the end the general equation of nodular corrosion kinetics takes the form:

$$v_{BWR}^{loc} = k_T^{loc} + k_{\Phi}^{loc} = k_0 \exp\left[-\frac{Q}{R(T + \bar{q}_S \frac{K}{\lambda_c} \bar{C})}\right] + N \frac{k_G^{H_2}}{p} \Phi^n \bar{\alpha} (1 + M \sqrt{\bar{C}}) \quad (22)$$

for BWR, and

$$v_{PWR}^{loc} = k_0 \exp\left[-\frac{Q}{R(T + \bar{q}_S \frac{K}{\lambda_c} \bar{C})}\right] \quad (23)$$

for PWR.

Our studies have shown that the local deposition of fairly thick layers of products of corrosion or other origin may result in overheating as great as 30 - 70 °C and local boiling. In these cases nodular corrosion under PWR conditions can be described by the equations for BWR.

## 2. NODULAR CORROSION OF Zr + 1% Nb FUEL CLADDING AND FUEL FAILURE INTENSITY IN LWRs - EXPERIMENTAL RESULTS.

The applicability of the foregoing equations for describing experimental data has been assessed by the use of correlation analysis for the case of nodular corrosion of Zr + 1% Nb fuel cladding under irradiation in research, and LWR power reactors<sup>1</sup>.

---

1

Corrosion data were kindly put at our disposal by professor Bibilashvili Yu.K. and Nikulina A.V., Scientific Research Institute of Inorganic Materials, Moscow.

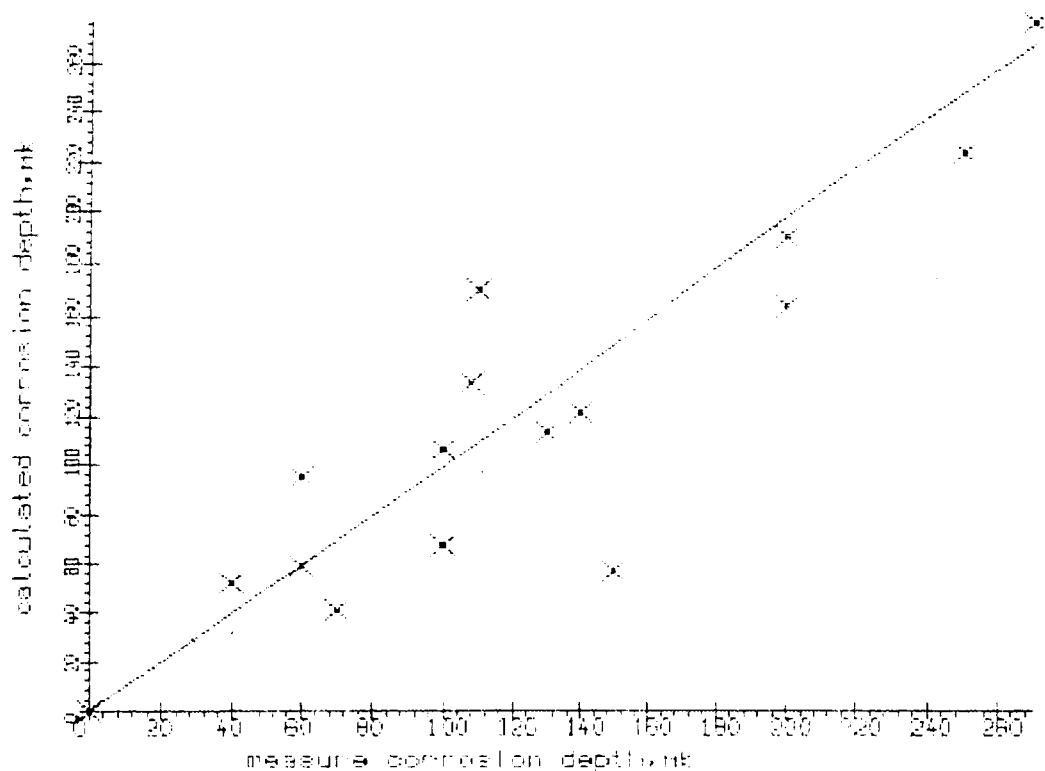


**Fig. 8. Correlation between calculated and measured nodular corrosion depth for BWR**

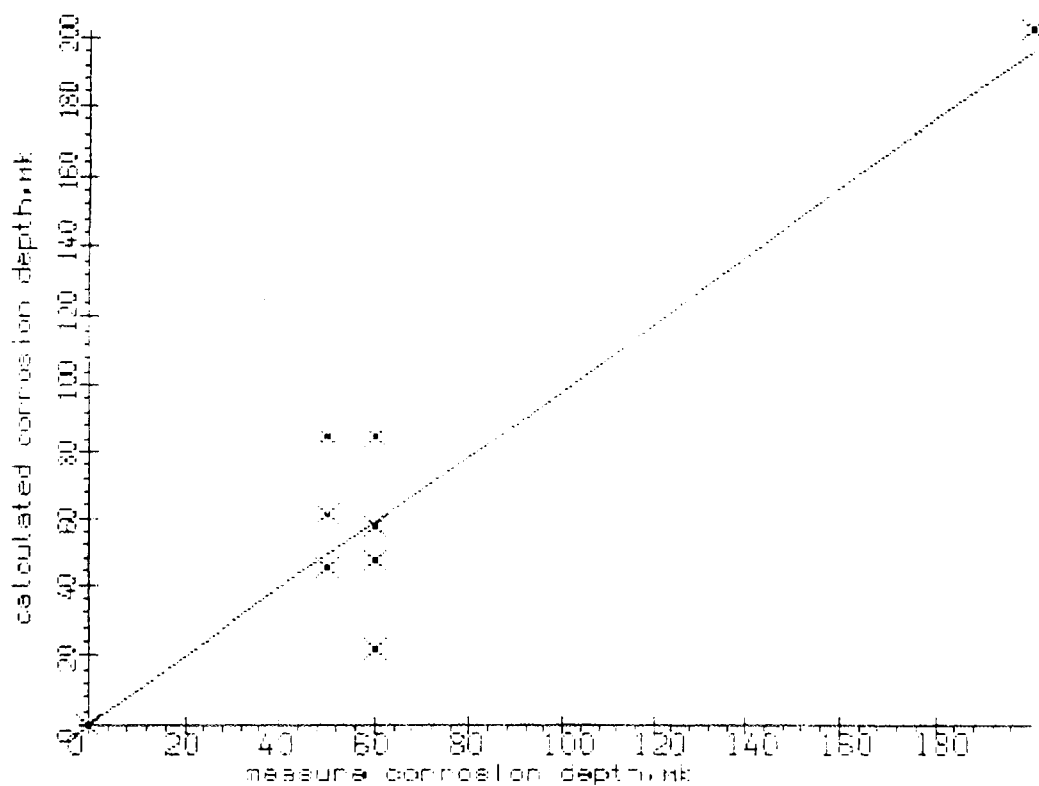


**Fig. 9. Correlation between calculated and measured nodular corrosion depth for BWR**

The data mass incorporates: time of experiment, fast neutron fluence, fuel burn-up, heat flux, average vapour content, nodular corrosion depth. In some cases in the absence of heat flux data  $\bar{q}_s$  was replaced by  $\bar{B}/\tau$ , where  $B$  - average burn-up, Mwt/kg U and  $\tau$  - time.

From Figs 8 and 9 it follows that theory agrees well with the experiment. That fact lends strong support to the applicability of the above models and equations for the description of fuel cladding corrosion. If we install hydraulic component, agrees will better.

For BWR the radiation component prevails in 50% and the thermal component in 20% of the data mass. In the rest cases both

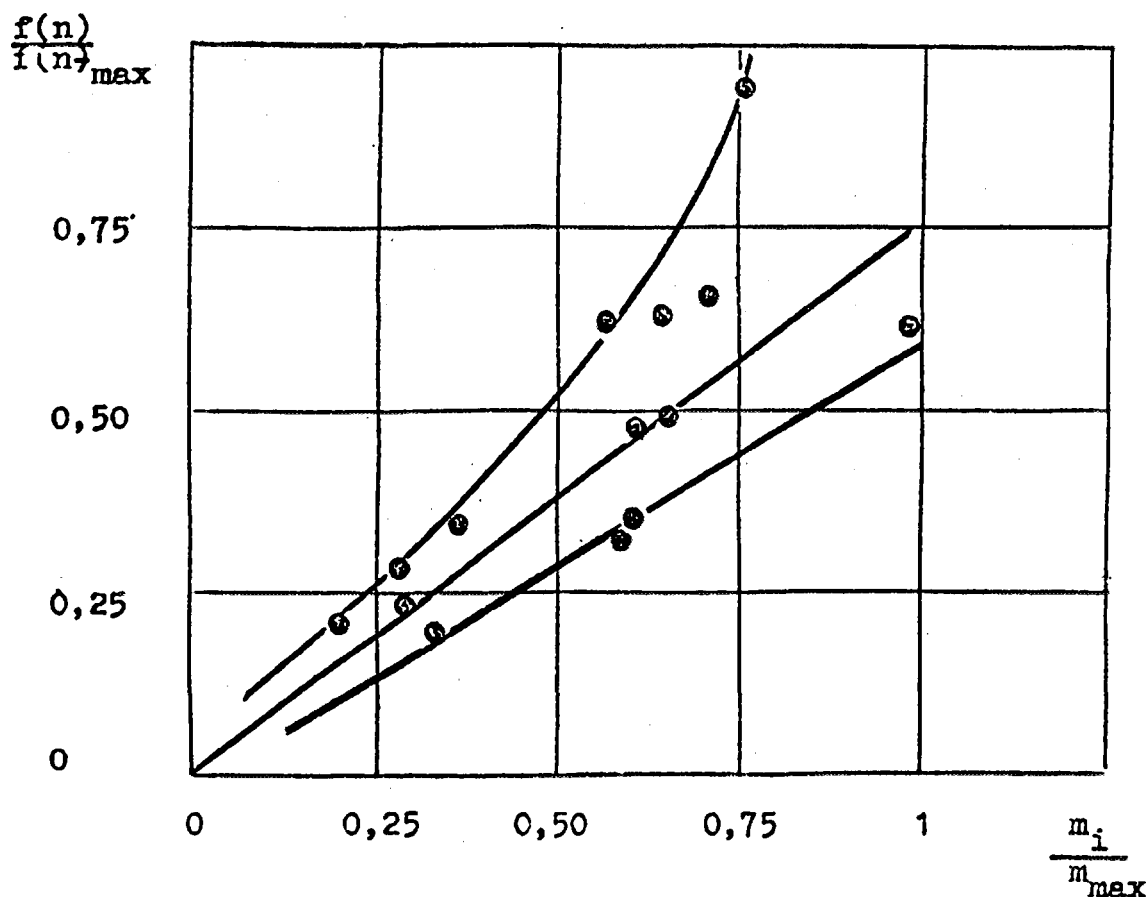


Fig. 10. Fuel cladding failure probability  $f(n)$  as function of total input to RBMK reactor

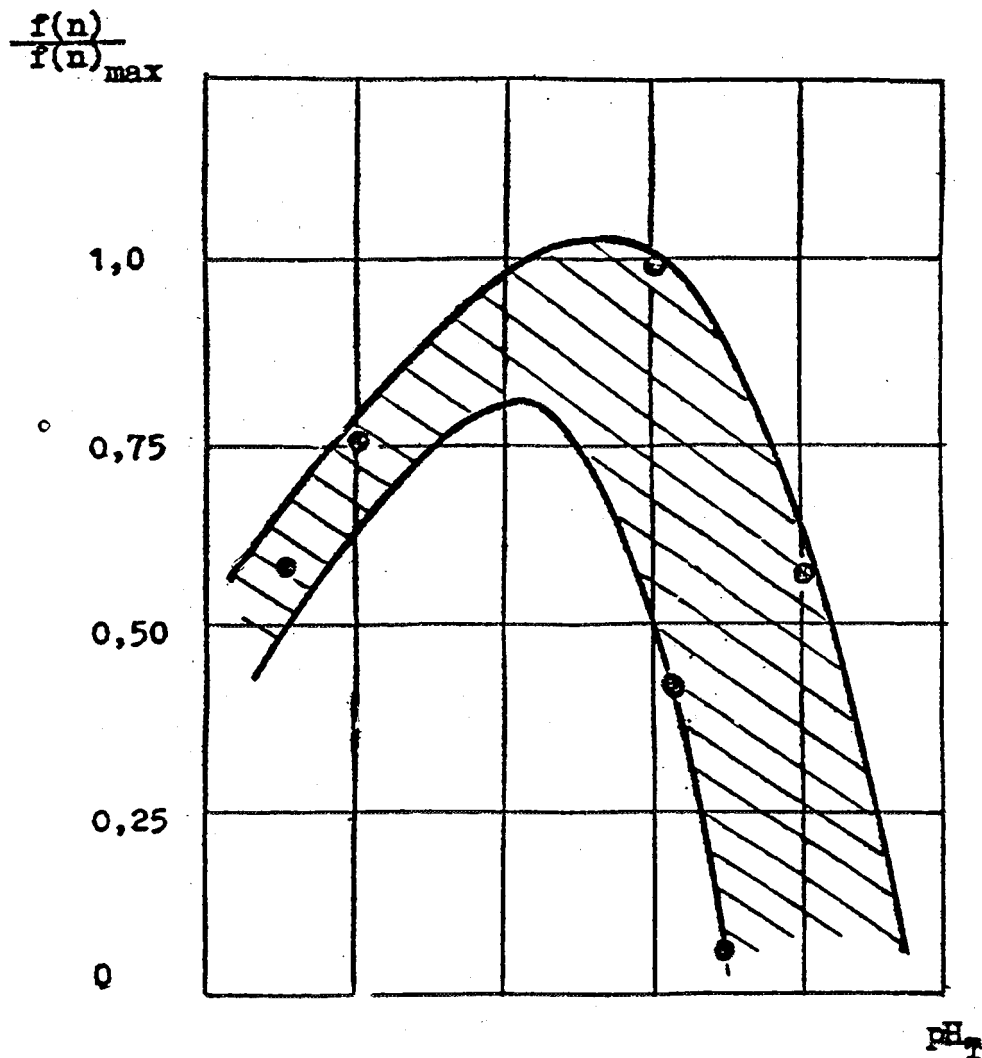


Fig. 11.  $f(n)$  as function of  $pH_T$  for primary circuit of WWER

components are close in their magnitude. As it follows from Eq.22 and 23  $C_{Fe}$  also plays an important role.

Hence, one would expect a correlation exists between the failed fuel quantity and that of CPs entering the core (with the feed water in BWRs or accumulated in the primary circuit in PWRs) [11].

Fig.10 shows a number of fuel assemblies discharged from four RBMK-1000 units during 5 years, plotted as function of the CP quantity transported to the reactor. The data are normalized on the maximum value in the data set.

It is known [12] that the precipitation rates of CPs in PWRs depend on  $C_{cp}$  and  $\Delta Fe(pH_T)$

$$\frac{d\delta}{d\tau} = K_d C_{cp} + K_{d-d} [Fe(T_1) - Fe(T_2)] - R_d \delta, \quad (24)$$

where  $\delta$  - surface concentration of particles;

$K_d$  - deposition coefficient;

$K_{d-d}$  - diassolution-deposition coefficient;

$Fe(T)$  - iron solubility at T;

$T_1$  - coolant temperature;

$T_2$  - surface temperature;

$R_d$  - deposit release coefficient.

$C$  and  $\Delta Fe(T)$  are functions of  $pH_T$ . It follows, therefore, that  $\delta(T)$  is a complex nonlinear function of  $pH_T$ . Fig.11 shows a plot of  $f(n)$  against  $pH_T$ , obtained from the data averaged over the 5-year operation of 7 WWER-1000 units.

It follows from Figs 10 and 11, that optimal water chemistry control results in the decrease of  $f(\Delta\tau)$ . At some power units the intensity of fuel failure can be reduced at least by a factor of two.

## CONCLUSION

1. On the base of a multiplicative model formulae have been developed that describe the influence of physical parameters on Zr alloy corrosion. A choice has been made of LWR and chemical parameters, that influence the uniform and nodular corrosion of Zr alloys and can be measured during WPP operations. The parameters have been incorporated into a models for calculating the reliability of fuel operation. The formulae have been tested by operation results on Zr + 1%Nb alloy corrosion under WWER and

RBMK conditions. The effects of water chemistry, as well as the temperature and radiation components of corrosion kinetics were also assessed.

2. A model has been developed to justify the correlation between the solubility of oxide film under the influence of water chemistry parameters and zirconium corrosion under PWR conditions.

3. Fuel failure intensity at NPPs with WWERs and RBMKs has been shown to depend on coolant quality namely on the growth of Fe-oxide deposits and local vaporization. At some power units optimal water quality control can reduce the fuel failure intensity at least by half.

#### REFERENCES

1. Johnson A.B., Jr. A review of corrosion phenomena on zirconium alloys, niobium, titanium, inconel, stainless steel and nickel plate under irradiation.- Reviews on Coatings and Corrosion, Vol.1, No4, 1975, Tel-Aviv, Israel, Freund Publishing House Ltd.-P.300-366.
2. Corrosion of Zirconium alloys in nuclear power plants. IAEA, Vienna, 1993. IAEA-TECDOC 684.
3. Cox B. Oxidation of Zirconium and its Alloys. Advances in Corrosion Science and Technology, 1976, Vol.5, P.278-291.
4. Burns w.C., Moore P.B. Water radiolysis and its effect upon in-reactor Zircaloy corrosion.- Radiation Effects, 1976, Vol.30, P.233-242.

5. Бяков В.М., Ничипоров Ф.Г. Радиоллиз воды в ядерных реакторах. - М.: Энергоатомиздат, 1990, с.176.
6. Крицкий А.В. Растворимость продуктов коррозии циркония и хрома в водных растворах при 298-623 К. Автореферат диссертации на соискание ученой степени кандидата химических наук. С.-Петербург, 1992.
7. T.D.Pyecha, G.M.Bain, W.A.McInteer, C.H.Pham External cladding corrosion of B&W-designed PWR fuel rods through burnups of 50 GWD/MTU. IAEA Technical Committee on External Cladding Corrosion in Water Power Reactors. GEN-CADARACHE, France - 14-18 October 1985.
8. Cox B. An assessment of irradiation corrosion mechanisms for zirconium alloys in high temperature water.- Materials presented for IAEA CS on Influence of Radiation on Corrosion of Structural Materials (IAEA, Vienna, Austria, June & December 1989).
9. Зарембо В.И., Крицкий В.Г. О принципиальной зависимости коррозии-эрозии углеродистых сталей в водных контурах энергетических установок от термодинамических факторов равновесия. ЖТХ.- 1988. N4, с.781-785.
10. Коррозия и накипеобразование на меди в системах охлаждения АЭС/ В.Г.Крицкий, П.С.Стяжкин, .В.Ивашов//Вопросы атомной науки и техники. Сер.Ядерная техника и технология.- 1990, вып.3, с.9.
11. Kritskij V.G. Influence of water chemistry regimes on fuel cladding failure in LWRs.- Mater. of Techn. Comm. Meet. on Fuel Failure in Normal Operation of Water Reactors: Experiments, Mechanisms and Management. 26-29 May 1992, Dimitrovgrad, Russia.
12. Коэн П. Технология воды энергетических реакторов. Перев. с англ. М.:Атомиздат, 1973, с.328.



## **PWR FUEL ROD CORROSION IN JAPAN**

S. INOUE

Kansai Electric Power Co., Inc.

K. MORI, K. MURATA, S. KOBAYASHI

Nuclear Fuel Industries, Ltd

Osaka, Japan

### **Abstract**

Many particular appearance were observed on the fuel rod surfaces during fuel inspection at reactor outage in 1991. The appearances looked like small black circular nodules. The size was approximately 1 mm. This kind of appearances were found on fuel rods of which burnup exceeded approximately 30 GWd/t and at the second or third spans of the fuel assembly from the top. In order to clarify the cause, PIE was performed.

The black nodules were confirmed to be oxide film spalling by visual inspection.

Maximum oxide film thickness was 70  $\mu\text{m}$  and spalling was observed where oxide thickness exceeded 40 or 50  $\mu\text{m}$ . Oxide film thickness was greater than expected.

Many small pores were found in the oxide film when the oxide film had become thicker. Many circumferential cracks were also found in the film. It was speculated that these cracks caused the spalling of the oxide film.

Hydride precipitates were mainly orientated circumferentially. Dense hydrides were observed near the outer rim of the cladding. No concentrated hydrides were observed near the spalling area. Maximum hydrogen content was 315 ppm.

It was confirmed that the results of tensile test showed no significant effects by corrosion.

The mechanism of accelerated corrosion was studied in detail. Water chemistry during irradiation was examined. Lithium content was maintained below 2.2 ppm. pH value was kept between 6.9 and 7.2. There were no anomalies in water chemistry during reactor operation. Cladding fabrication record clarified that heat treatment parameter was smaller than the optimum value.

In Japan, heat treatment of the cladding was already optimized by improved fabrication process. Also chemical composition optimization of the cladding, such as low Tin and high Silicon content, was adopted for high burnup fuel. These

remedies has already reduced fuel cladding corrosion and we believe we have solved this problem.

## 2. Fuel rod

Three fuel rods were withdrawn from 17X17 fuel assembly that was irradiated 2 cycles and transported to Hot cell Facility. Burnup of the rods are 35,000 – 35,400 MWd/t. fuel rods are 3,852 mm long and its diameter is 9.5 mm. Japanese 17X17 fuel has 9 grids.

## 3. Post Irradiation Examination

### 3.1 Visual Examination

Many spallings were found between 2000 mm and 3200 mm from bottom of fuel rod. Spallings are circular and its diameter is 0.5 mm – 2.0 mm (Fig. 1). White homogeneous oxide covered between 1000 mm and 3300 mm from bottom of fuel rod. Other anomalies were not found.

### 3.2 Oxide film thickness and diameter measurement

Oxide film thickness was measured by Eddy Current Test (ECT). Maximum oxide film thickness is 70  $\mu\text{m}$ . spalling area is correspond to thick (>40–50  $\mu\text{m}$ ) oxide film. These area is also shown in ECT charts as many dips (Fig. 2). Diameter of fuel rod was determined by creep down and oxide film thickness. Fig. 3 shows axial diameter change and corrected diameter. Corrected diameter was calculated by the relation :

$$\text{corrected diameter} = \text{measured diameter} - \text{oxide film thickness} \times 0.85$$

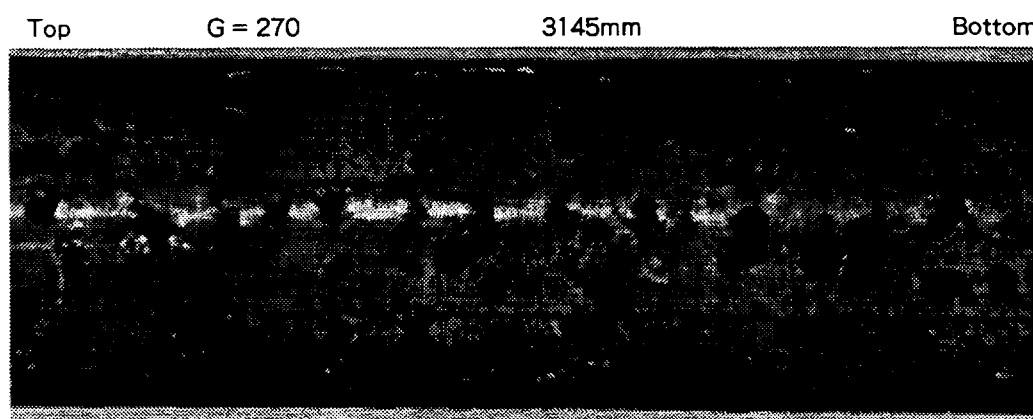


Fig. 1 Spalled Cladding (Oxide Thickness : 55  $\mu\text{m}$ )

oxide thickness ( microns )

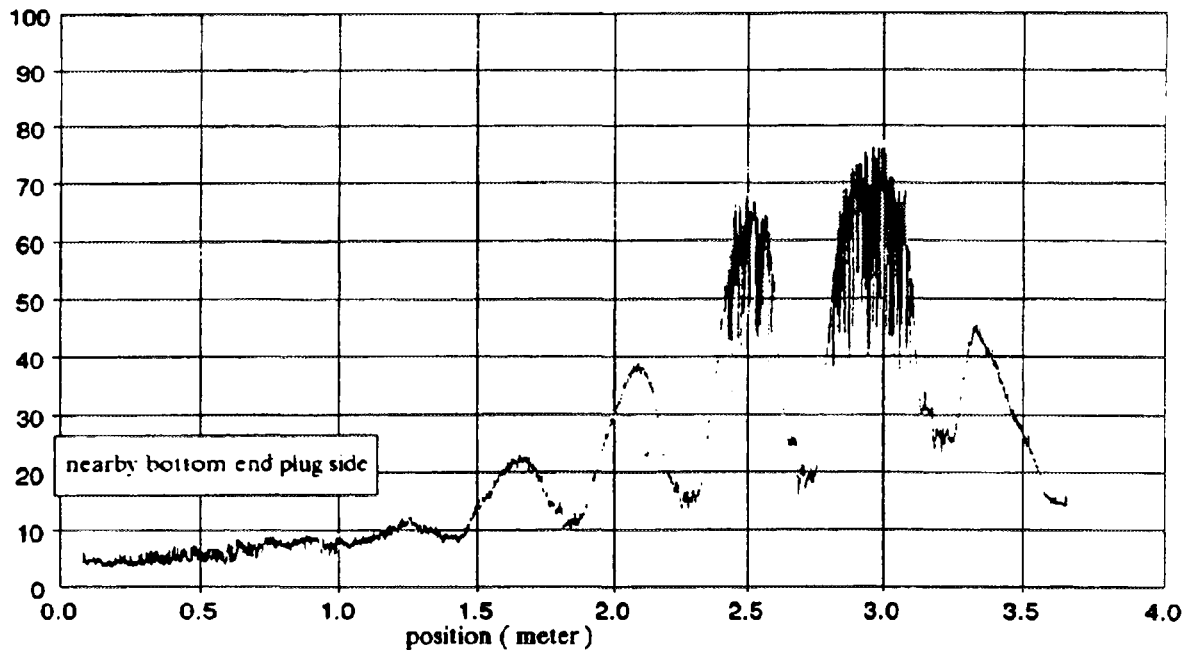


Fig. 2 Result of Oxide Thickness Measurement

average diameter ( mm )

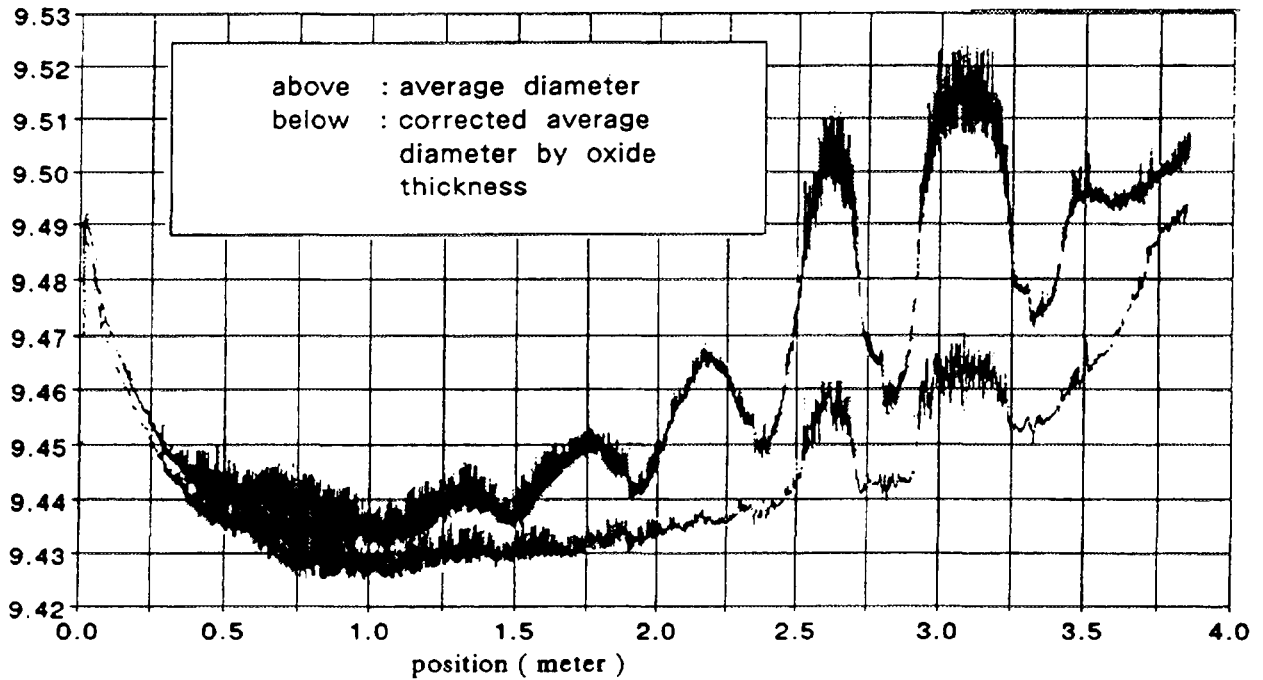


Fig. 3 Result of Diameter Measurement

As a result of correction, diameter of lower part was almost flat. But diameter at spalling area is larger than the diameter at the other area. It suggests that oxide at spalling area is low density or contains gaps or pores.

### 3.3 Metallography

Fuel rods were cut at maximum oxide position and cross sections were observed (Fig. 4). Oxide film contains many small pores and circumferential cracks. According to the observation on the borderline of oxide and spalled part, crack in oxide and surface of spalled part are continuous. It was speculated that these cracks caused the spalling of the oxide film.

The oxide film under the spalled part looks like the other oxide film. No abnormal corrosion occurred under the spalled part.

Hydride precipitates basically circumferential (Fig. 5). Most precipitated hydride were observed near the surface of cladding. No concentration of hydride was observed, even just under the spalling oxide. Maximum hydrogen content is 315 ppm at spalled area.

Small metallic particles were observed in oxide film close to cladding. These metallic particles are observed by SEM and EPMA. The result shows these metallic particles are Zircaloy (Fig. 6).

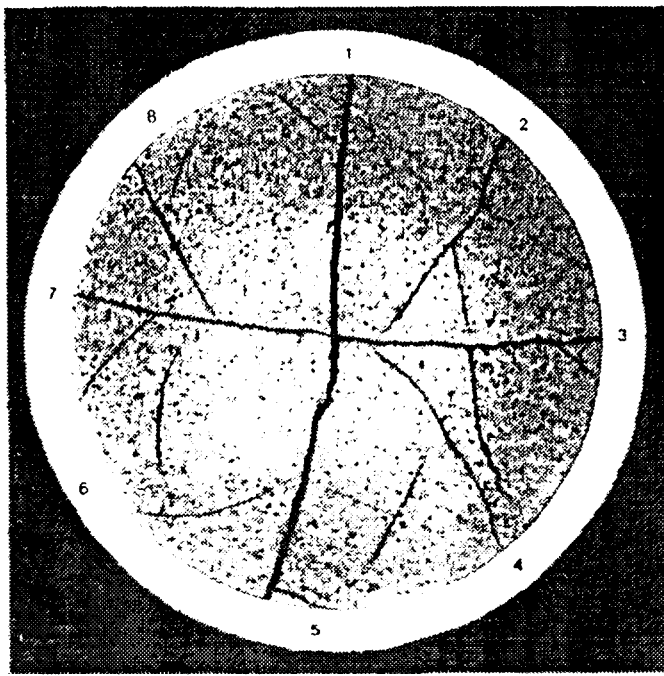
### 3.4 Tensile test

Tensile tests were performed under the condition of room temperature and 385°C (Table 1). Tensile test specimens were prepared double wing shape. In case of 385°C, the samples at spalled area show slightly lower 0.2% yield strength than the sample at non spalled area. But 0.2% yield strength is greater than 500 MPa and enough for fuel performance.

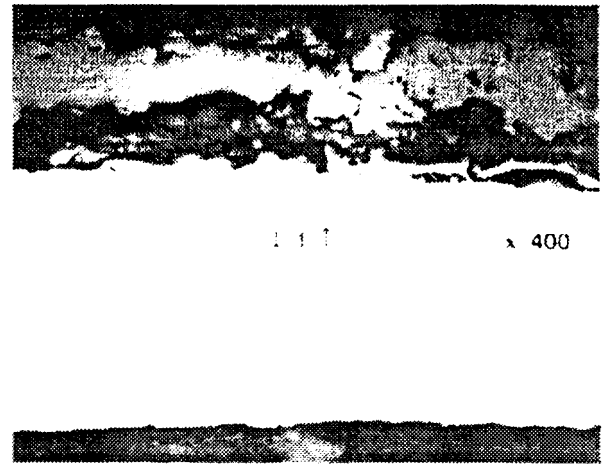
## 4. Discussion

After we found such a particular surface on the fuel rods, characterization data of the fuel cladding and water chemistry during irradiation were investigated. Tin content, Silicon content and heat treatment are important items for corrosion. Tin content was center value of specification (1.52%).  $\Sigma Ai$  was low ( $0.9 \times 10^{-18}$ ). Silicon content was 80 ppm.

On the other hand, lithium content was maintained below 2.2 ppm, and pH value was kept between 6.9 and 7.2. There were no anomalies in water chemistry during reactor operation.



x 10



1 1 ↑

x 400



1 5 ↑

x 400



1 2 ↑

x 400



M

1 6 ↑

x 400



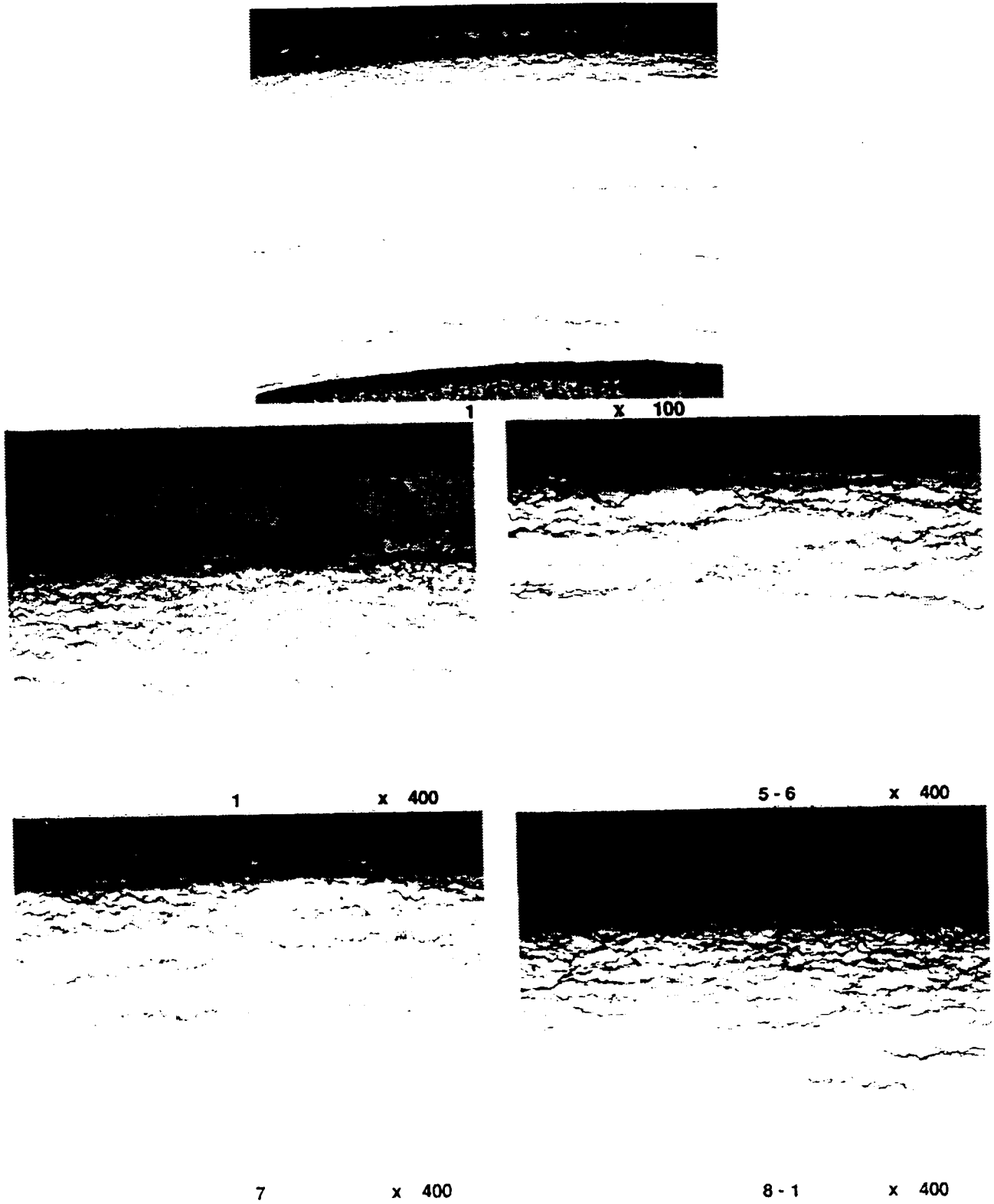
1 3 ↑

x 400



M: Metallic particle

Fig. 4 Metallography at Maximum oxide position (as polished)



\* Each number correspond to Fig. 4

Fig. 5 Metallography at Maximum oxide position (etched)



Backscattered electron image

× 800

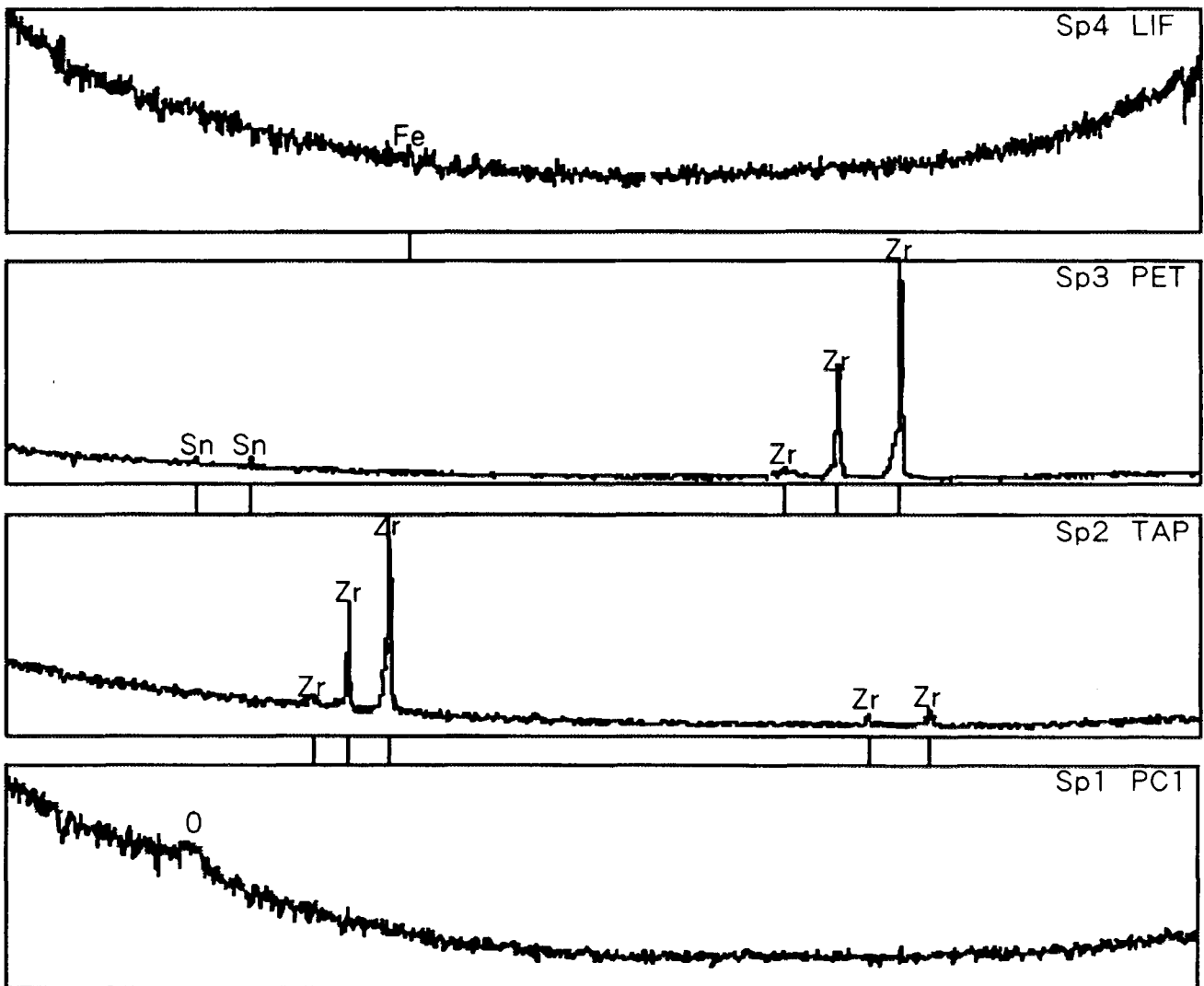


Fig. 6 EPMA results on metallic particle

TABLE 1. TENSILE TEST RESULTS

Rod No.	SPAN	Specimen Location <sup>(1)</sup> (mm)	Test Temperature (°C)	Oxide Thickness (mm)	0.2 % Yield strength (MPa)	Ultimate Tensile strength (MPa)	Total Elongation <sup>(2)</sup> (%)
1	2	3071	385	0.062	491	604	13 – 14
	3	2621	385	0.055	527	646	14 – 15
	4	2214	R.T	0.036	741	979	14 – 15
2	2	3069	385	0.060	514	624	10 – 19
	3	2623	R.T	0.051	668	950	11 – (3)
	4	2203	385	0.037	546	686	19 – 19
3	2	3073	385	0.052	517	637	17 – 18
	3	2621	R.T	0.045	624	938	14 – 16
	4	2210	385	0.035	543	674	18 – 20

R.T. : Room Temperature

(1) At the middle of the specimen

(2) Value on 1st wing – value on 2nd wing

(3) Only one wing tested

We performed on-site oxide film thickness measurement also. At this time, we used two different type of cladding, due to different tube shell maker. one is the same as the cladding that we used at this work. The another is higher  $\Sigma\text{Ai}$  ( $3 \times 10^{-18}$ ) and lower Si content (<30ppm). Two type of claddings show same corrosion behavior, such as oxide thickness and surface condition.

As there were no anomalies in water chemistries and two type of cladding show same corrosion behavior, we conclude that both heat treatment and Si content affect corrosion behavior.

Based on the PIE results, mechanical properties of spalled cladding nearly equal to normal one.

## 5. Conclusion

We performed hot cell PIE for spalled claddings. The results show that these claddings has thick oxide but these mechanical performance is enough for usual operation.

For better performance, we change the heat treatment of cladding and Si specification of Si content. These change will be solve the problem up to the burnup limitation of 48 GWd/t.

## ACKNOWLEDGEMENTS

This study was performed as a joint project between 5 PWR utilities and Nuclear Fuel Industries. The authors wish to thank the engineers from the 5 utilities for their cooperation and help, and also to express our thanks to the EDF people who performed the PIE works.



## **CORROSION BEHAVIOUR OF ZIRCALOY 4 FUEL ROD CLADDING IN EDF POWER PLANTS**

**H. ROMARY, D. DEYDIER**  
EDF, Direction de l'Equipement SEPTEN,  
Villeurbanne, France

### **Abstract**

Since the beginning of the French nuclear program, a surveillance of fuel has been carried out in order to evaluate the fuel behaviour under irradiation. Until now, nuclear fuels provided by suppliers have met EDF requirements concerning fuel behaviour and reliability. But, the need to minimise the costs and to increase the flexibility of the power plants led EDF to the definition of new targets : optimisation of the core management and fuel cycle economy. The fuel behaviour experience shows that some of these new requirements cannot be fully fulfilled by the present standard fuel due to some technological limits. Particularly, burnup enhancement is limited by the oxidation and the hydriding of the Zircaloy 4 fuel rod cladding. Also, fuel suppliers and EDF need to have a better knowledge of the Zy-4 cladding behaviour in order to define the existing margins and the limiting factor. For this reason, in-reactor fuel characterisation programs have been set up by fuel suppliers and EDF for a few years. This paper presents the mains results and conclusions of EDF experience on Zy-4 in-reactor corrosion behaviour. Data obtained from oxide layer of zirconia thickness measurements show that corrosion performance of Zy-4 fuel rod cladding, as irradiated until now in EDF reactors, is satisfactory but not sufficient to meet the future needs. The fuel suppliers propose in order to improve the corrosion resistance of fuel rod cladding, low tin Zy-4 cladding and then optimised Zy-4 cladding. Irradiation of these claddings are on going. The available corrosion data show the better in-reactor corrosion resistance of optimised Zy-4 fuel rod cladding compared to the standard Zy-4 cladding. The scheduled fuel surveillance program will confirm if the optimised Zy-4 fuel rod cladding will meet the requirements for the future high burnup and high flexibility fuel.

### **1. INTRODUCTION**

Since the beginning of the French nuclear program, a surveillance of fuel has been carried out in order to evaluate the fuel behaviour under irradiation. Until now, nuclear fuels provided by suppliers have met EDF requirements concerning fuel behaviour and reliability. But, the need to minimise the costs and to increase the flexibility of the power plants led EDF to the definition of new targets :

- optimisation of the core management (frequency control, load follow) in response of the grid needs,
- fuel cycle economy such as increasing the discharge burnup (60 GWd/tU).

These requirements cannot be fully fulfilled by the present standard fuel due to some technological limits. Particularly, burnup enhancement is limited by the oxidation and the hydriding of Zy-4 fuel rod cladding. Fuel suppliers and EDF also need to have a better knowledge of the Zy-4 cladding behaviour in order to define the existing margins and the limiting factors. This last point is very important to determine a way to improve the Zy-4 behaviour particularly the corrosion performance. For this reason, in-reactor fuel characterisation programs have been set up by fuel suppliers and EDF for a few years, in particularly for new fuel, for high discharge burnup and load follow operations conditions. These programs include pre-characterisation of unirradiated claddings, poolside and hot cell oxide layer of zirconia and hydrogen pickup measurements. In addition analytical tests are sometimes performed in order to explain some particular trends in reactor and to compare the performance of several standard and improved Zy-4 cladding irradiated in EDF reactors. The term "new fuels" covers the assemblies with major design changes compared to the assemblies provided previously and the first assemblies delivered by new suppliers. The purpose of this article is to present the main conclusions of EDF experience on Zy-4 fuel rod cladding corrosion.

## 2. EDF EXPERIENCE ON Zy-4 CORROSION BEHAVIOUR AND HYDRIDING

The main part of the corrosion data has been obtained on 900 MWe assemblies. During the qualification program of 1300 MWe fuel oxide layer measurements have been carried out and these results are presented further in this article. The corrosion data consist mainly on poolside oxide layer measurements and on hot cell examinations performed on extracted rods.

Poolside oxide thicknesses are measured until now on the peripheral rods of the assemblies, by the fuel suppliers and, recently also by EDF. These measurements are performed with equipment using an eddy current probe. In hot cell, the oxide layer is measured on metallographic cross sections of cladding samples at different levels and also by eddy current examination along the fuel rod. The EC examination gives access to the axial and circumferential evolution of the oxide layer. The determination of the hydrogen concentration is carried out by mass spectrometry on clad samples, after vacuum extraction at high temperature : thus, the measured concentration is the hydrogen contained in the cladding and in the oxide layer.

The oxide layer measurements on irradiated fuel are for the fuel suppliers and EDF the best way of evaluating the cladding corrosion behaviour under irradiation compared to autoclave tests and loop tests. Indeed, the isothermal autoclaves corrosion tests can sometimes lead to results in total contradiction with the Zy-4 fuel rod cladding corrosion behaviour observed in reactors. The loop tests seem to reproduce in a more reliable way the in-reactor behaviour.

Before a more detailed analysis of EDF experience feedback, we present in table I the principal thermal-hydraulic characteristics of EDF 900 and 1300 MWe power plants. This table shows that for the 1300 MWe reactors the coolant inlet temperature has been dropped due to corrosion problem on the steam generators.

The experience feedback on claddings irradiated in EDF 900 and 1300 MWe power plants is illustrated by figure 1. The main observations on the Zy-4 fuel rod cladding behaviour concern :

### Oxide layer thickness and profile

- The in-reactor corrosion rate of Zy-4 cladding fuel rods increases with the oxide layer thickness and so with the burnup. In the same way, the thicknesses scatter increases with the thickness and with the burnup. This observation is illustrated by figure 2. An estimation of the standard Zy-4 cladding corrosion average growth and scatter between cycles is given in table II.
- An oxide layer higher than 100 microns, threshold considered by EDF, were measured after 4 cycles (approximately 44 GWd/tU) and sometimes even after 3 cycles (approximately 33 GWd/tU). A few of assemblies could not be reloaded for a fourth cycle due to this high corrosion rate.
- A typical example of axial corrosion profile after 3 cycles obtained by eddy current in hot cell is presented shown on figure 3. The oxide thickness increases along the fuel rod from the bottom to the top of the assembly. This profile is explained by the metal / oxide temperature evolution which increases from the bottom to the top of the rod with a maximum at the sixth span for the 900 MWe fuel and the seventh - eighth for 1300 MWe fuel. At the grid location areas, a thinner oxide thickness is observed. This thinner oxide layer results from the lower cladding temperature due to the better coolant conditions when coolant flow passes through the grids.
- The oxide layer measurements performed on metallographic cross sections confirm the oxide thickness levels recorded on site. However, these hot cell values are in general quite lower than the poolside thicknesses. The metallographic hot cell data are presented on figure 4. Moreover, these metallographies reveal an oxide layer on the internal face of the cladding. The internal oxide can reach a thickness of about 8 - 10 microns at high burnup.

TABLE I : THERMALHYDRAULIC CHARACTERISTICS IN EDF REACTORS

	900 MWe Reactors	1300 MWe Reactors	
		Before Temperature Decrease	After Temperature Decrease
Coolant flow in core (m3/hr)	61710	92340	89965
Average Temperature (°C)	304.6	310.7	306.5
Inlet Temperature (°C)	289.3	293.7	289.3
Outlet Temperature (°C)	325.3	327.7	323.7

TABLE II: EVOLUTION OF OXIDE LAYER THICKNESSES AND SCATTER BETWEEN CYCLES

	Average increase per cycle	Scatter per cycle
cycle 1	8 microns	< 10 microns
cycle 2	10 microns	> 10 microns
cycle 3	15 microns	30 microns
cycle 4	33 microns	40 microns
cycle 5	40 microns	70 microns

TABLE III : REACTOR COOLANT CHEMISTRY 900 and 1300 MWe

	BOC	EOC
pH	7.0	
Li (ppm)	2.2 - 2.0	0.7
B (ppm)	1200	0
O2 (ppb)	2 - 5 ( Maximum 10 )	
H2 (ml(STP)/kg water)	25 - 50 25 - 35 in practice	5

TABLE IV : CLADDING'S CHEMISTRY AND CUMULATIVE ANNEALING FACTOR

CLADDING		CHEMISTRY					Annealing Parameter
Origin		%Sn	%Fe	%Cr	O (ppm)	C (ppm)	ΣA
A1	standard	1.58	0.22	0.11	1320	120	1.1 E-17
A2	standard	1.56	0.21	0.11	1260	130	1.6 E-17
B1	standard	1.42	0.21	0.10	1280	140	1.4 E-17
B2	Improved ΣA	1.45	0.20	0.11	1260	130	3.0 E-17
B3	Optimised (Chemistry-ΣA)	1.28	0.21	0.11	1320	130	3.0 E-17

## Visual appearance of the oxide layer

- Up to a thickness of 70-80 microns, the oxide layer formed on the cladding grows quite homogeneously. At higher thicknesses the phenomenon of desquamation occurs : the oxide layer may start delaminating which induce blisters. Then parts of these blisters may spall off. This phenomenon is often noticed on the span where the oxidation is highest. The measurements carried out on high burnup fuel rods (until 55 GWd/tU) show that most of the rods are affected by this phenomenon. Presence of desquamation has been sometimes observed on lower span levels. But, generalised desquamation has not been observed until now. Examples of a fifth cycle fuel rod cladding appearance are shown in figure 5 : small circular blisters of oxide have spalled off. Figure 6 shows a delaminated oxide layer on a fourth cycle cladding sample : the layer of zirconia reached 44 microns.

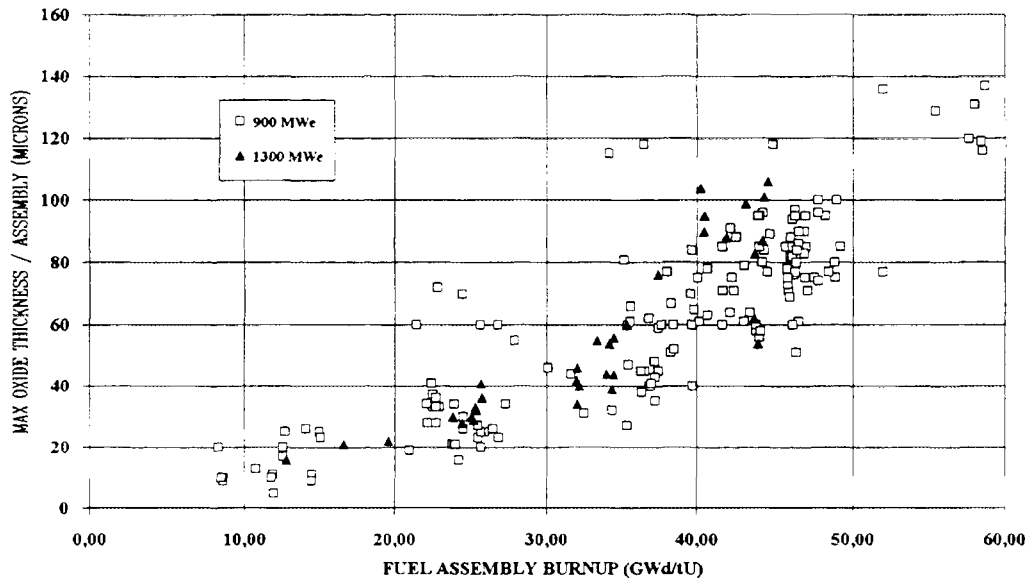


FIGURE 1 : EDF CORROSION EXPERIENCE ON 900 AND 1300 MWe PWR REACTORS (On site Measurements)

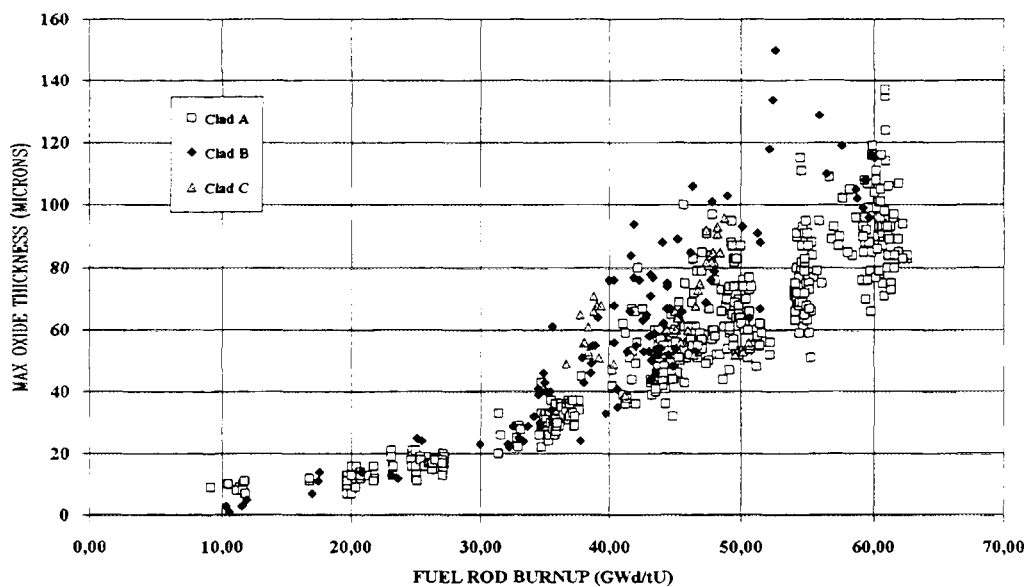


FIGURE 2 : CORROSION EXPERIENCE ON 900 MWe PWR REACTORS COMPARISON OF THREE CLADDINGS (On site measurements)

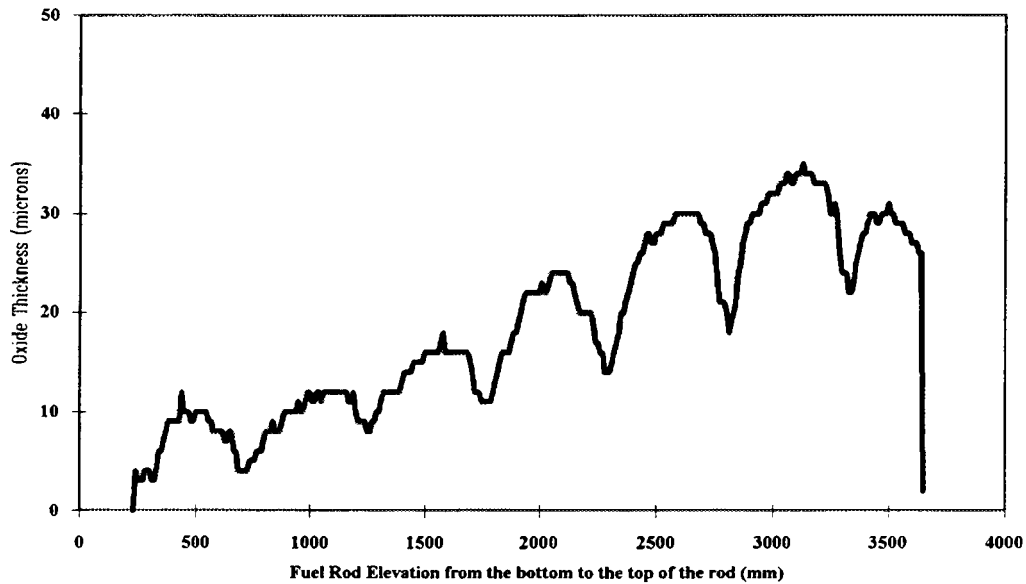


FIGURE 3 : TYPICAL WATERSIDE CORROSION AXIAL PROFILE (after 3 cycles of irradiation)

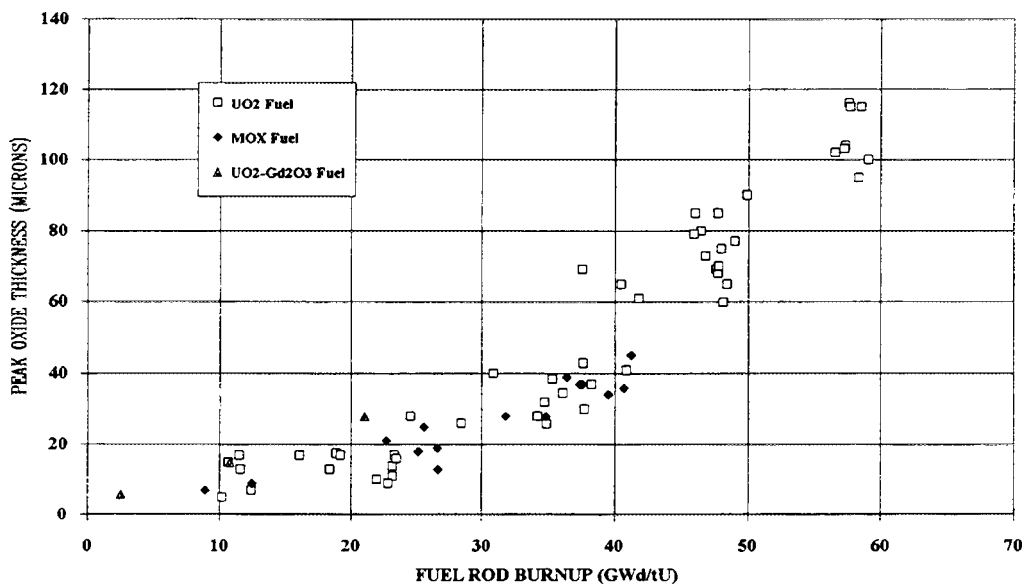


FIGURE 4 : HOT CELL MEASUREMENTS OF OXIDE THICKNESS LAYER [COMPARISON OF DIFFERENT FUELS]

- Care must be taken in the analysis of oxide thicknesses measured in zones affected by desquamation because an over estimation of thicknesses can be done. Figure 9 shows an oxide thickness analysis on fifth cycle irradiated rods : this analysis distinguishes the rods which are or are not affected by desquamation.

#### Hydriding

- The preferential orientation of the hydrides is circumferential. Hydriding increases with the burnup and the oxide layer thickness. The precipitation of the hydrides is more important in the waterside of the cladding. A typical hydride morphology obtained after four cycles of irradiation (about 44 GWd/tU) is shown on figure 6.

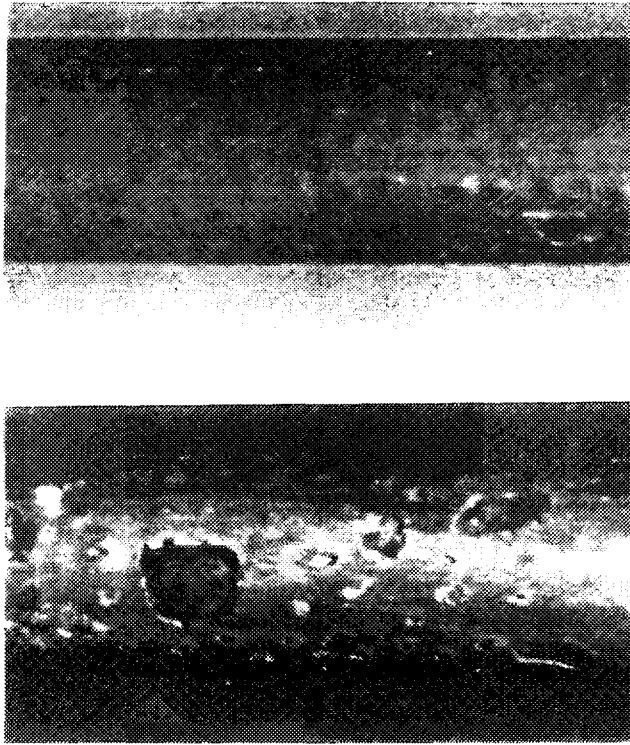
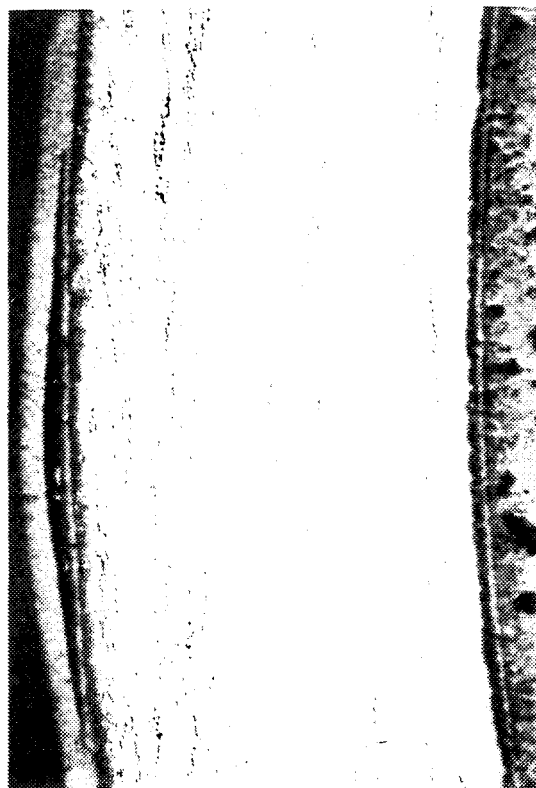


FIGURE 5 : PHOTOGRAPHY OF TYPICAL HIGH BURNUP CLADDING



↑  
Delamination of the Oxide Layer

200 μm

FIGURE 6 : MICROPHOTOGRAPHY OF TYPICAL DELAMINATED OXIDE LAYER

- On high burnup fuel rods which showed spallation, quite different behaviours have been observed [1] :
  - an intensive migration of the hydrides in the spalled area which was the coldest part of the cladding. A typical view of this behaviour is shown on figure 7.
  - or a new oxide layer grows on the spalled area and the hydrides had emptied this zone. The mechanism of this behaviour shown on figure 8 is not yet fully explained.
- Measurements of hydrogen concentration, presented on figure 10, show that about 20% of the hydrogen produced by the Zy-4 oxidation reaction are absorbed by the cladding. Table V gives examples of hydrogen concentrations versus irradiation.

#### Corrosion behaviour comparison between different kinds of cladding

- Significant differences in the corrosion performance of Zy-4 fuel rod claddings have been observed. Figure 2 presents the corrosion evolution of three standard Zy-4 claddings supplied by different manufacturers. These three tubes were manufactured according product specifications issued from ASTM B353 and quite equivalent. These cladding tubes were made from Zy-4 materials whose the chemistries were fairly closed and with process outlines having some main differences (ingot melting, quenching conditions, cold pilger steps, intermediate anneals, final heat treatment, surface finish). Thus corrosion behaviour difference between these claddings is explained by the differences more on the thermomechanical processes than on the chemical compositions. Very high corrosion rates were observed for some particular Zy-4 standard claddings (see figure 11). Oxide layer thicknesses of about 70 and 115 microns were measured in a fuel assemblies whose burnup were respectively 22.80 and 34.20 GWd/tU. This bad behaviour has been mainly explained by the thermomechanical process characterised by an annealing cumulative factor lower than  $2 \text{ E-18}$  which is quite low compared to the other claddings.

Many factors are known to influence the corrosion behaviour of the Zy-4 fuel rod. The main factors listed by many authors [2 for example] are the followings :

- external conditions with the cladding, i.e. operating conditions ; fluence, hydraulic flow, coolant temperature, coolant chemistry, exposure time, etc.
- the cladding feature, i.e. alloy chemical composition, metallurgical structure, surface finish, annealing heat treatments, etc.

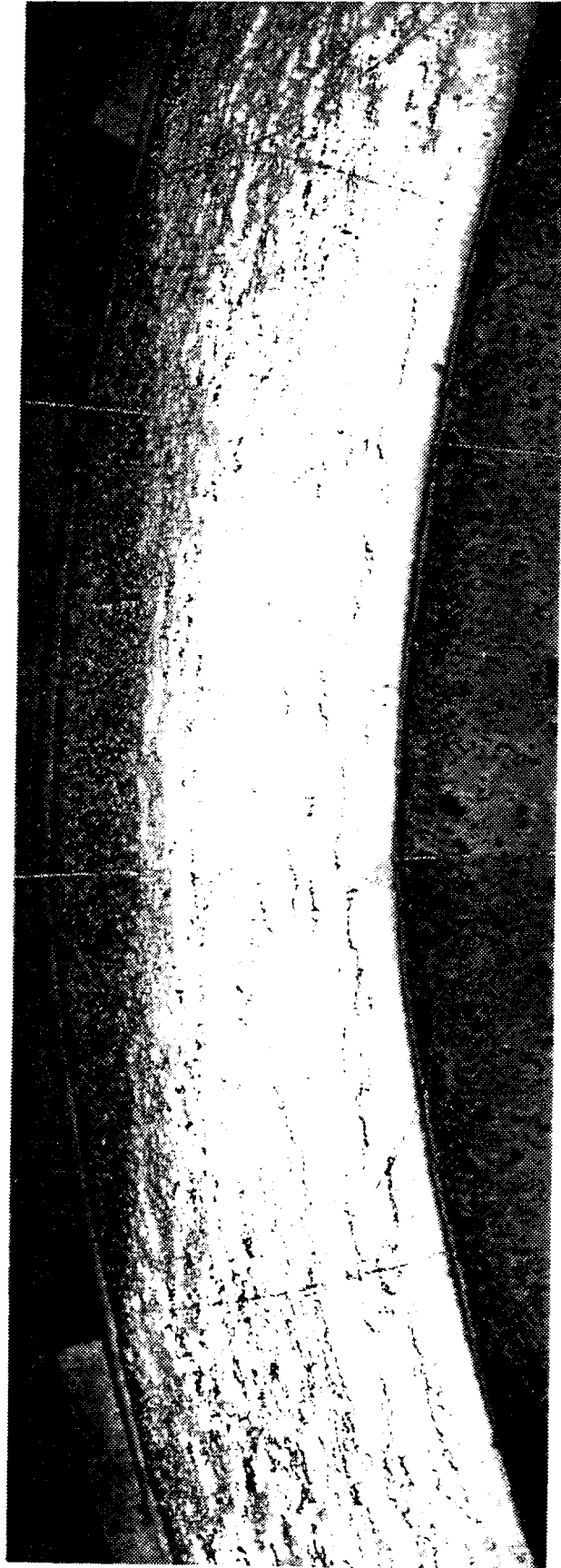
We will show below in this paper for some of these factors if their effects were noticed on all the claddings irradiated in the EDF nuclear power plants.

### 3. INFLUENCE OF REACTOR CONDITIONS

#### 3.1. Coolant Chemistry

The coolant chemical specification which is presented in table III and figure 12 has been applied to the EDF power plants since 1981. This specification consists of maintaining a pH  $300^{\circ}\text{C}$  higher than 6,9 all along the cycle . This pH is sufficient for avoiding the problem of deposit on fuel rods. This assertion has been confirmed by visual inspections and examinations of crud's samples performed during fuel surveillance. The deposits observed on cladding are in general negligible : their thicknesses estimated by comparison of oxide thickness before and after brushing do not exceed 2 microns and are lower than the measuring accuracy.

In order to reduce the contamination of the primary circuit, EDF has experimented a modified chemical specification into 6 reactors. This modified specification (see figure 13) consists by increasing pH $300^{\circ}\text{C}$  to 7,2 and by retaining a new evolution of the lithium concentration. No difference in Zy-4 fuel cladding corrosion behaviour due to the change of chemical specification has been noticed.



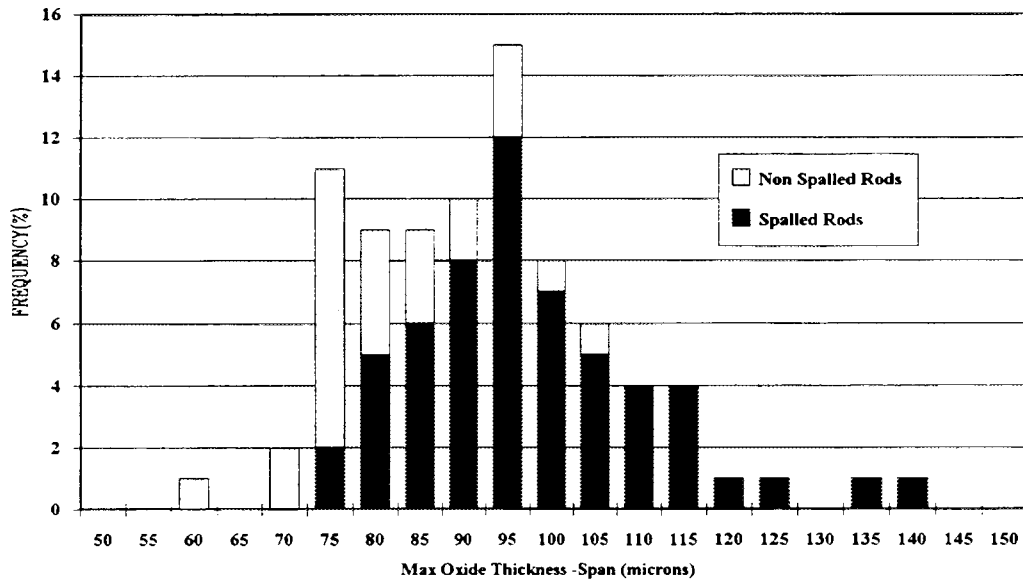
200 μm

**FIGURE 7 : MICROPHOTOGRAPHY OF TYPICAL SPALLED CLADDING  
with spalled off area and over concentration of hydrides [1]**



200 μm

**FIGURE 8 : MICROPHOTOGRAPHY OF TYPICAL SPALLED CLADDING  
with a new oxide layer on the desquamed area [1]**



Number of Rods = 102 - Number of spalled Rods = 83

FIGURE 9 : COMPARISON OF OXIDE THICKNESS FOR NON SPALLED AND SPALLED RODS

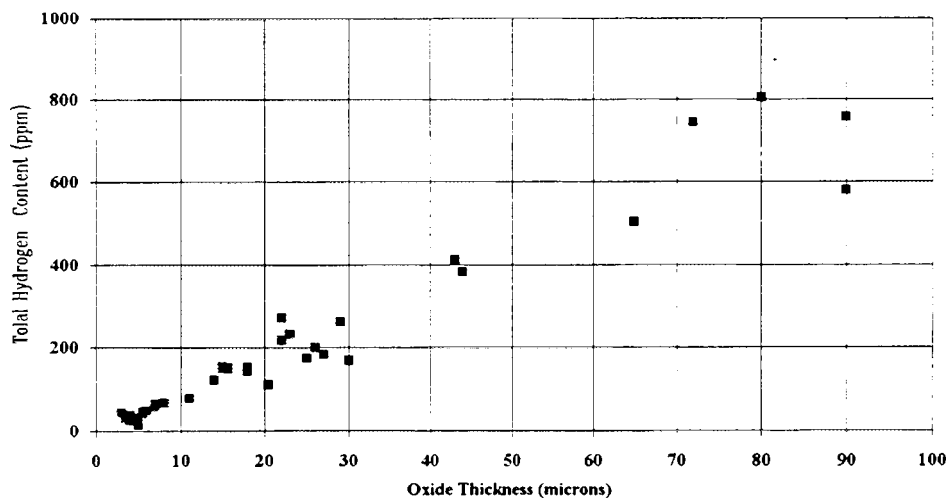
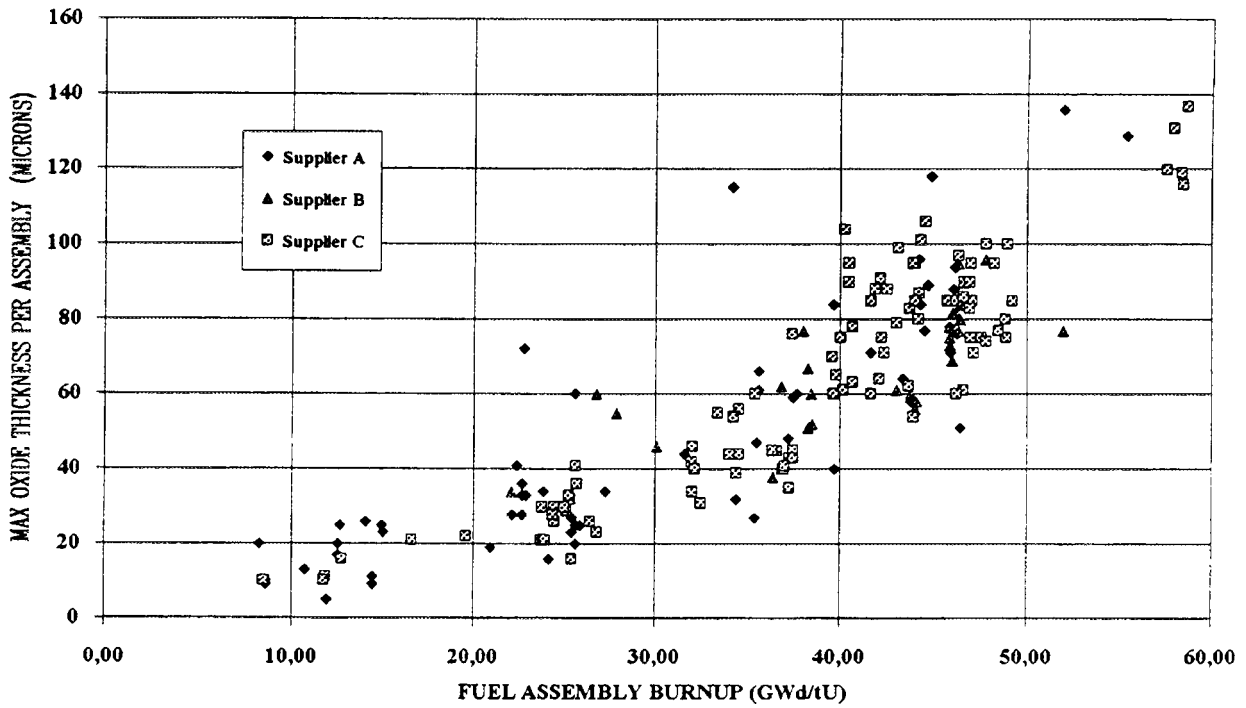


FIGURE 10 : TOTAL HYDROGEN CONTENT ON IRRADIATED CLADDINGS

During experimental program on fuel behaviour on 900 MWe reactor operating under load follow conditions, primary coolant chemistry and its additives were followed accurately. The aims of this analysis are to establish, if necessary, relations between oxide thickness, crud chemical analysis and reactor operating conditions, and to determine if load-following has an influence on reactor coolant chemistry. The evolution of boron, lithium and hydrogen in the primary coolant follows the chemical specification and no anomalies were pointed out and no disturbance were observed due to load follow operations.

### 3.2. Reactor and Coolant Temperature Effect

A qualification program of fuel including poolside oxide layer measurements was carried out at the beginning of the 1300 MWe power plants. The corrosion data have shown a higher corrosion rate than usually observed in the 900 MWe reactors and also, a stronger corrosion acceleration from the third cycle (33 GWd/tU). The average oxide thickness growth was about 50 microns during the fourth cycle and the maximum thicknesses were higher than 100 microns. A



**FIGURE 11 : EDF CORROSION EXPERIENCE ON PWR REACTORS**  
**Comparison of different claddings supplies**

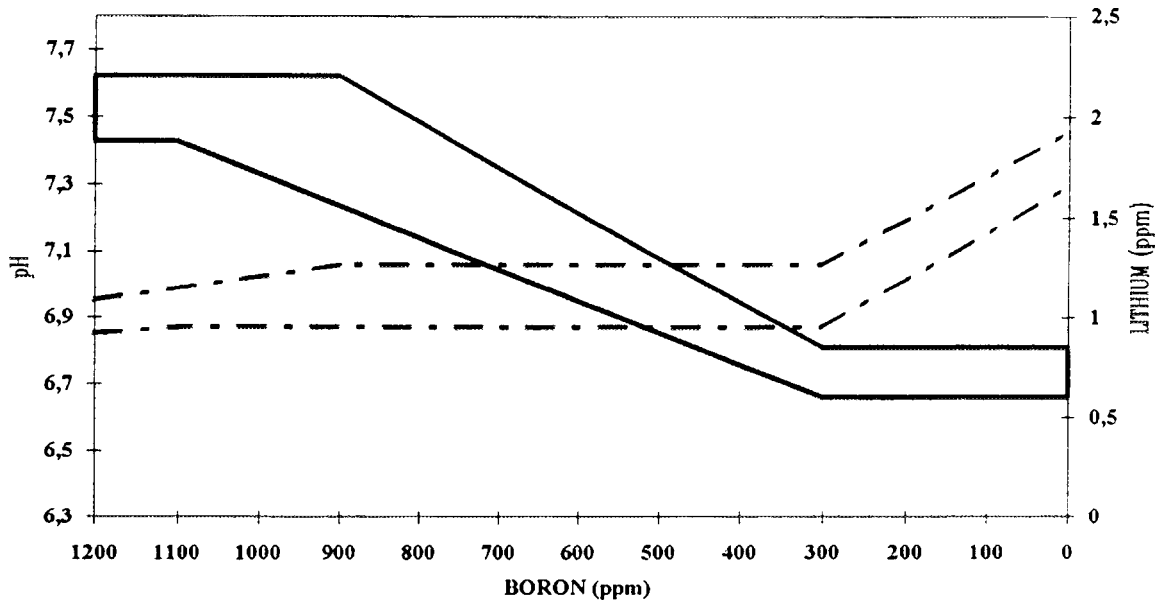


**FIGURE 12 : EDF Lithium - Boron Co-ordinated Chemistry and Calculated pH (300°C)**

comparison between oxide layer thickness measurements in 900 and 1300 MWe reactors is presented on figure 14. This comparison points out the influence of the more penalising conditions of the 1300 MWe reactors on the fuel rod corrosion. The inlet temperature of the coolant was 310.7°C.

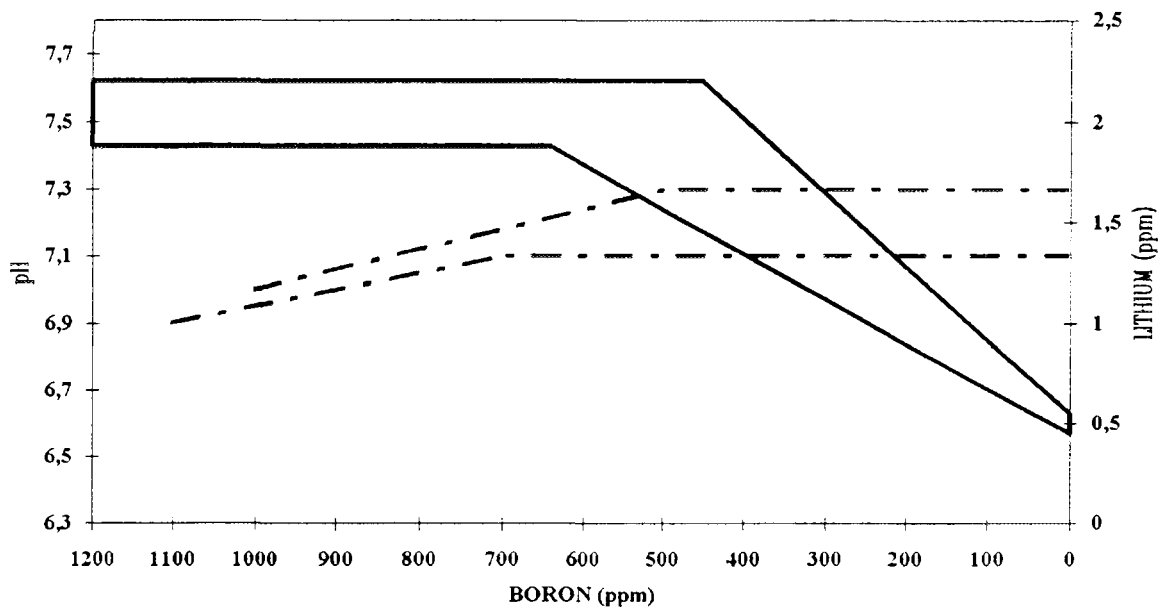


FIGURE 13 : EDF Lithium - Boron Modified Chemistry and Calculated pH (300°C)

TABLE V : HYDROGEN CONTENT VERSUS BURNUP

Span	Average Burnup (GWd/tU)	Average Hydrogen Content (ppm)
5	13.1	26
6	12.8	37
5	23.8	69
6	23.6	79
5	41.1	252
6	40.8	122

The coolant inlet temperature was decreased to 306.5°C because of corrosion problem occurred in the steam generators. The effect of this lower temperature was noticed on assemblies which carried out their fourth irradiation cycle after the temperature drop. The oxide thickness measurements after this fourth cycle are quite comparable with 900 MWe results. A reduction of the oxide thickness scatter was also observed. These results are illustrated on figures 14 and 15.

### 3.3. Load Following Operation

In order to evaluate fuel performance during load following, oxide thickness measurements have been carried out on characterised assemblies during four cycles of irradiation. Oxide layer measurements on these assemblies did not lead to show an appreciable difference on corrosion behaviour between cycled and non cycled rods. The comparisons of poolside and hot cell oxide measurements on cycled and non cycled rods are presented respectively on figures 16 and 17.

### 3.4. Fuel Types

Several types of fuels have been irradiated in EDF power plants : UO<sub>2</sub> fuel, MOX fuel and Gd<sub>2</sub>O<sub>3</sub> enriched UO<sub>2</sub> fuel. Oxide thickness measurements on poolside and in hot cell have not shown any difference on UO<sub>2</sub> and MOX cladding corrosion behaviour. Oxide layer

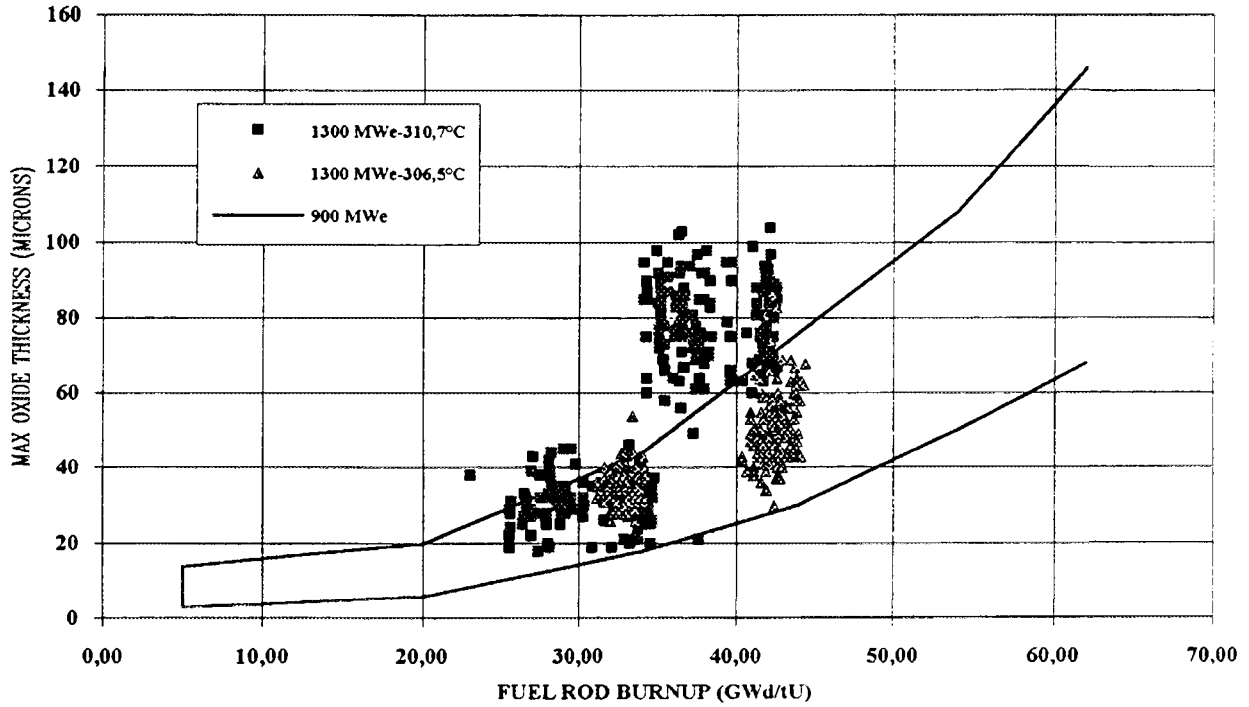


FIGURE 14 : CORROSION EXPERIENCE IN 1300 MWe REACTORS - EFFECT OF COOLANT TEMPERATURE

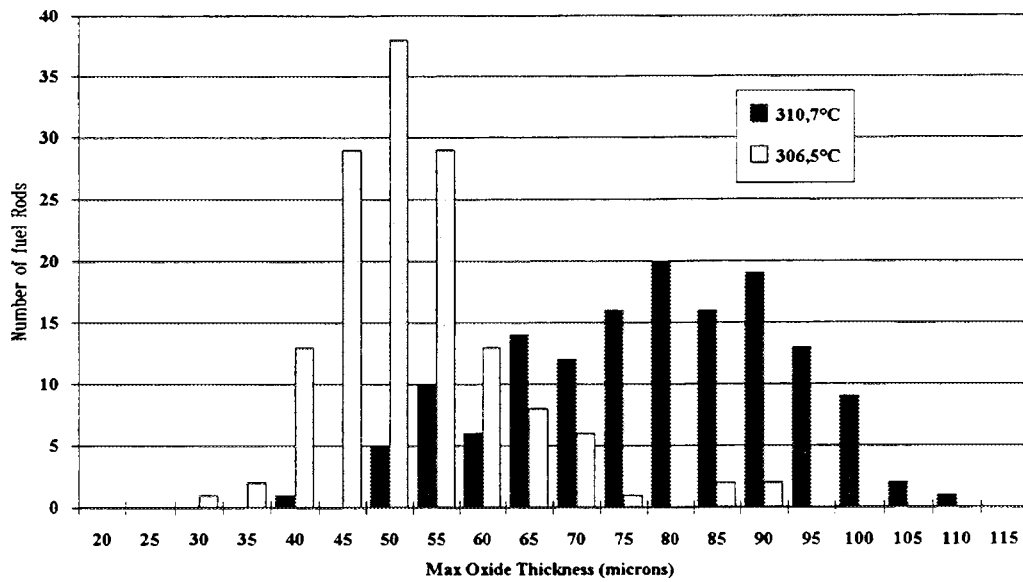


FIGURE 15 : COMPARISON OF OXIDE THICKNESS SCATTER FOR TWO COOLANT INLET TEMPERATURES

measurements on metallographies are presented at the figure 4. Concerning the UO<sub>2</sub>-Gd<sub>2</sub>O<sub>3</sub> fuel, the number of oxide thickness measurements available is insufficient to find a reliable trend.

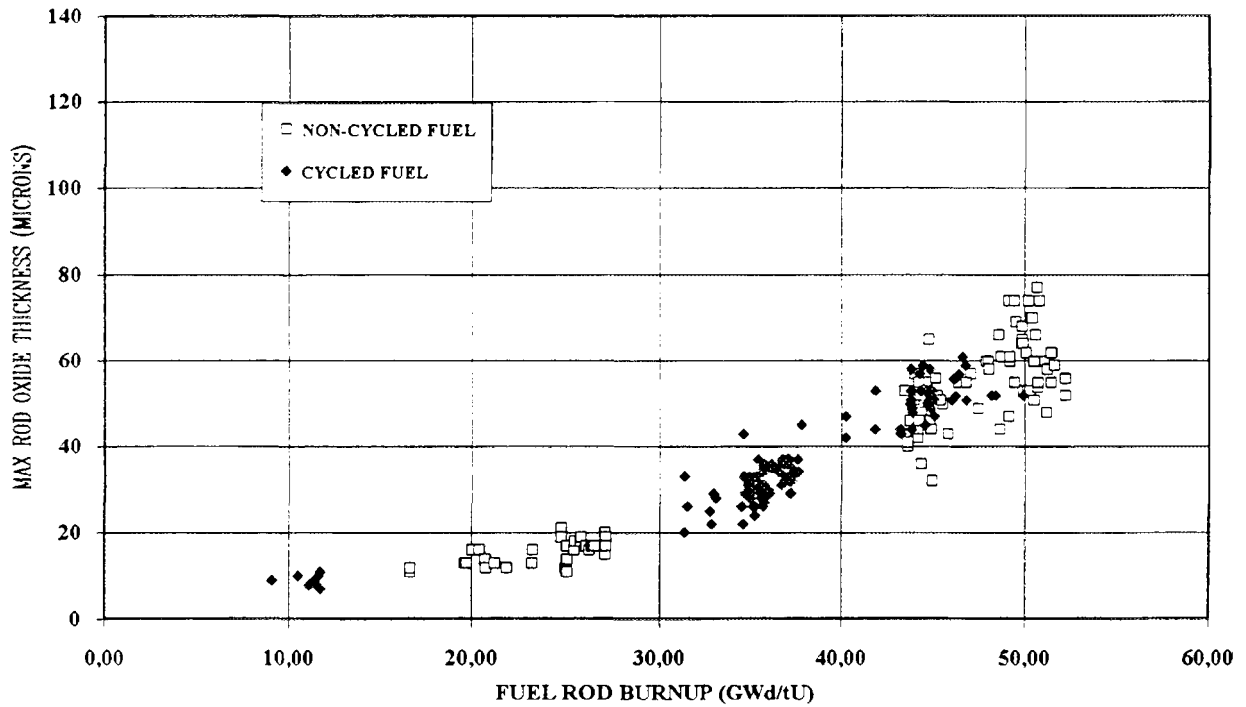


FIGURE 16 : COMPARISON OF CORROSION BEHAVIOUR FOR BASE AND LOAD FOLLOWING CONDITIONS (On Site Measurements)

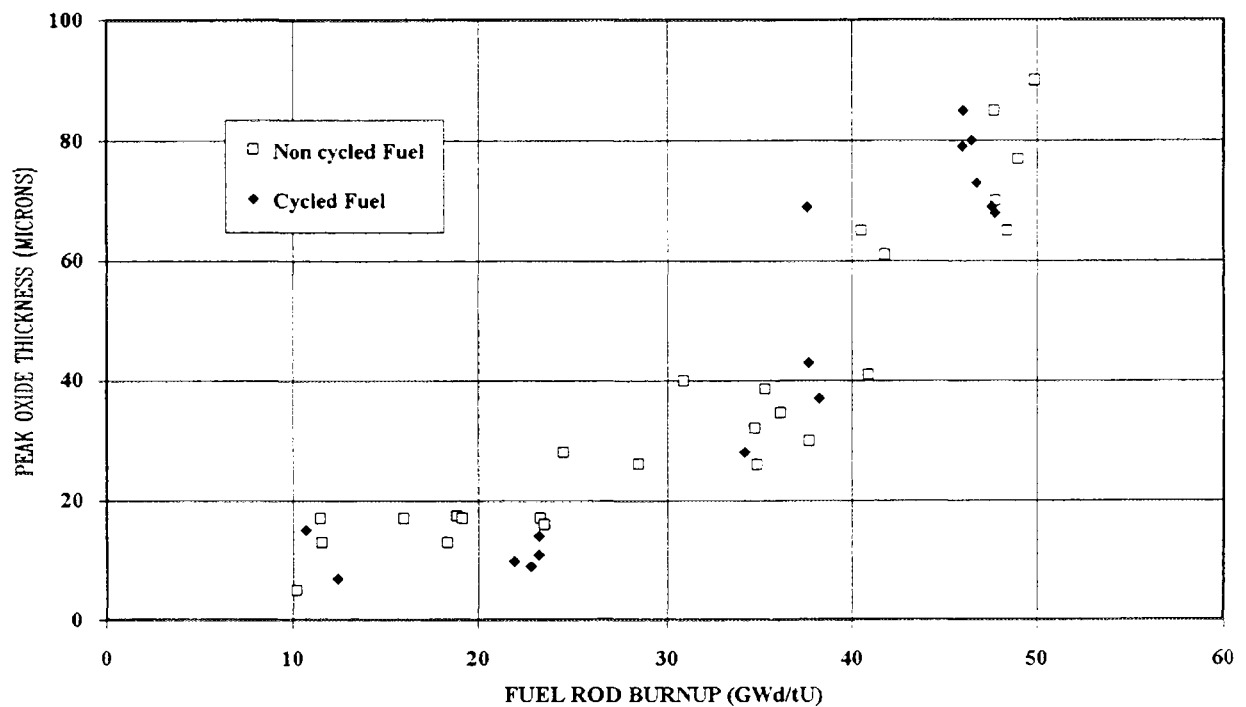


FIGURE 17 : COMPARISON OF CORROSION BEHAVIOUR FOR BASE AND LOAD FOLLOWING CONDITIONS (Hot Cell Measurements)

## 4. INFLUENCE OF Zy-4 CLADDING CHARACTERISTICS

### 4.1. Tin Content

For several years, the use of low tin level within the specification range has been considered as one way to improve corrosion performance of Zy-4 cladding. Many studies have showed the influence on the Zy-4 corrosion resistance of the content variation of the various alloy elements within the specified range [3,4,5]. It was clearly established that a low tin content has a beneficial effect for the Zy-4 cladding corrosion resistance. This has been confirmed by EDF feedback on low tin claddings. The corrosion behaviour of two lots (1,45%Sn and 1,28%Sn) made according the same process and irradiated in the same reactor is compared on figure 18 : a benefit for an irradiation of about 44 GWd/tU can be estimated at 10%.

Concerning the effect of other alloys or impurities elements (Si, Fe, Cr, etc.), it's difficult from the available in reactor experience feedback to do a reliable analysis of their influence.

### 4.2. Influence of Heat Treatment

The in-reactor corrosion susceptibility of Zy-4 fuel rod cladding is dependent on the thermomechanical process performed after the beta quenching. Longer annealing times and/or higher annealing temperature in the alpha range lead in general to better corrosion performance. These annealing conditions have an effect on the growth of the particle size. The influence of the precipitates size on the corrosion resistance has been clearly shown [6]. The cumulative annealing factor (CAP) which characterises the couple time / temperature of annealing heat treatments after beta quenching has been defined by STEINBERG and Al [7]. Several studies [5,8,9,10] have established a correlation between the corrosion resistance of the Zy-4 cladding and the CAP.

The improvement of in-reactor corrosion resistance due to the increase of the CAP has been observed on EDF reactors. This observation is illustrated by figure 19. Claddings lots called A and B made by different manufacturers have exhibited a better in-reactor corrosion resistance when their CAP increases. The CAP of these lots are given in table IV. The claddings lots A and B were irradiated on two different reactors. However the comparison between cladding lots can be made only if the manufacturing processes until beta quenching are identical, which is not the case of the lots A and B. It should be noted that for B2 cladding lot, the improvement consists on the CAP and on the controlled chemical composition : so the improved corrosion resistance of this cladding is explained by the simultaneous effect of the chemical composition and the manufacturing process.

### 4.3. Optimised Cladding

Improvements are made by the tubes suppliers to the manufacturing processes in order to provide cladding lots presenting more homogeneous characteristics : the smaller characteristics variation between lots and within lots should induce a better cladding behaviour like corrosion resistance. These improvements should reduce the oxide thickness scatter observed for high burnup. So, the suppliers propose now an optimised Zy-4 fuel rod cladding : this optimisation results in a judicious choice of the chemical composition (low tin, high Si, etc.) and in a more controlled manufacturing conditions. These controlled manufacturing conditions are characterised by a specific CAP range. Fuel suppliers propose optimised Zy-4 fuel rod claddings which are now under irradiation. The available oxide thickness measurements on these optimised claddings show a better in-reactor corrosion behaviour than Standard Zy-4 claddings. However the in-reactor experience isn't, at the moment, sufficient to evaluate the real benefit on the corrosion resistance due to the use of the optimised Zy-4 claddings. Thus, the behaviour comparison of the standard B1 and optimised B3 claddings shows for a burnup rate of 55 GWd/tU a gain of about 30 microns (30% approximately) (see figure 19). The fuel surveillance program scheduled on these claddings which will be generalised would confirm in the next future their better corrosion resistance and demonstrate if the optimised claddings can fully satisfy the EDF requirements on the future high burnup and high flexibility fuel.

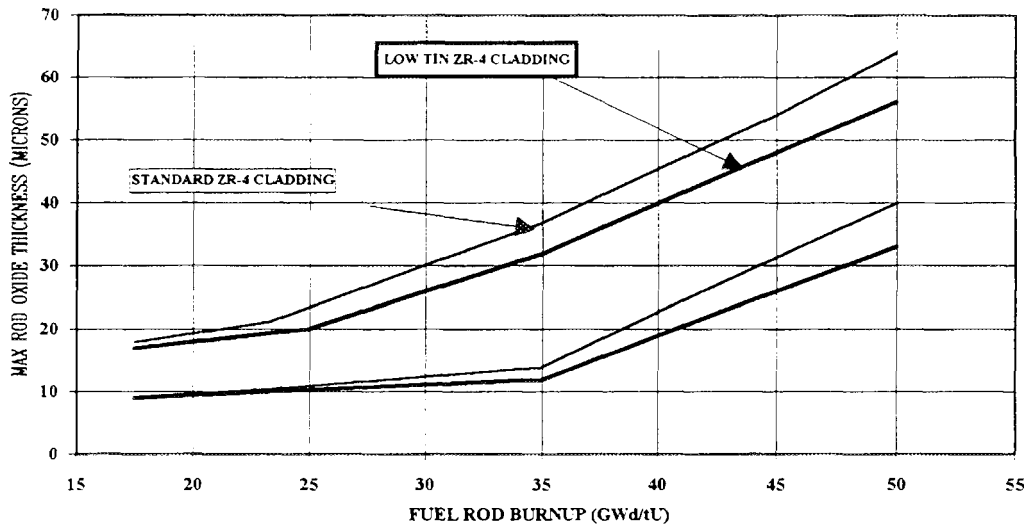


FIGURE 18 : EFFECT OF TIN CONTENT ON CORROSION BEHAVIOUR

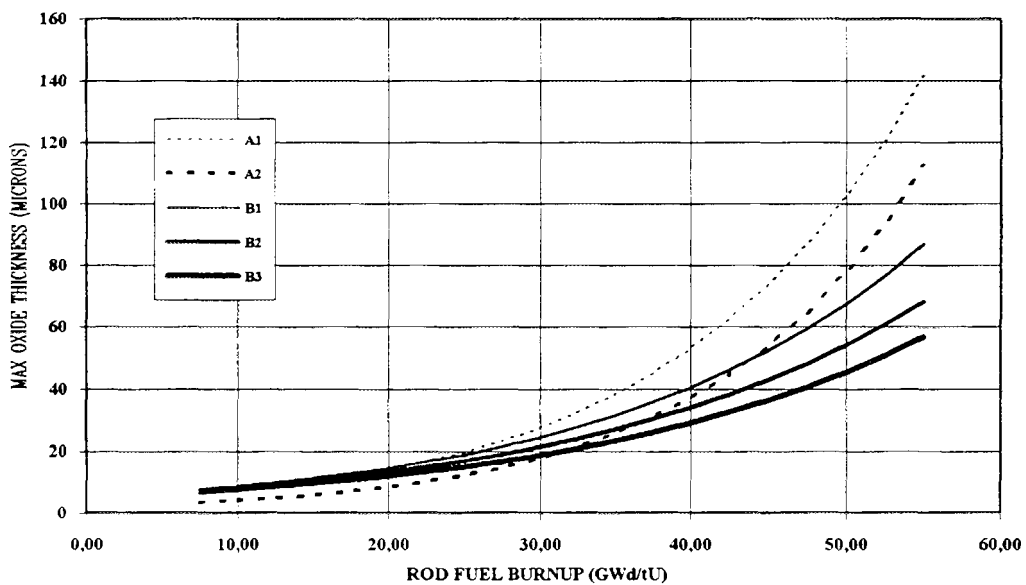


FIGURE 19 : CORROSION BEHAVIOUR OF STANDARD, IMPROVED AND OPTIMISED ZY-4 CLADDINGS

#### 4.4. Future Cladding

Many fuel suppliers think that the optimisation of the Zy-4 material are nearly reached its limits. To reach higher levels of performance, other technological solutions are already developed or under development by the suppliers : new materials (massive or duplex cladding) proposed by fuel designers are or will be soon irradiated in EDF reactors. The aim of these experimental programs is to get a better knowledge on the performance of these materials in particular on corrosion and to contribute to the development of the future high burnup assemblies (until 60 GWd/tU).

#### CONCLUSION

The EDF experience shows that the overall corrosion behaviour of Zy-4 fuel rod cladding has been satisfactory. However, oxidation and hydriding of the standard Zy-4 fuel rod cladding are limiting factors of the operation of fuel in EDF reactors. This cladding should not be able to reach

high burnup and allow better fuel flexibility. Although low tin Zy-4 claddings show a better corrosion resistance under irradiation than standard Zy-4 claddings, this improvement is not sufficient. All suppliers propose now an optimised Zy-4 cladding which is characterised by an optimised chemical composition and an improved manufacturing process. The first in-reactor experience on these optimised claddings confirms the better corrosion performance observed during autoclave tests. The fuel surveillance of these optimised claddings will show the existing margins and the limiting factors. Many suppliers think that the Zircaloy 4 fuel rod cladding material has reached its optimisation limits and study more advanced technological solutions in response to utilities needs.

## REFERENCES

- [1] GUEDENEY P. § AI, AÑS "International Topical Meeting LWR Fuel Performance", Avignon FRANCE, April 21-24, 1991
- [2] IAEA-TECDOC-684 (January 1993)
- [3] EUKEN C. § AI, ASTM STP 1023 (1989) 43
- [4] WEIDINGER H. § AL, ASTM STP 939 (1987) 364
- [5] ANDERSSON T. § AL, IAEA-SM-288/59
- [6] GARZAROLLI F. § AI, IAEA-SM-288/24
- [7] STEINBERG E. § AI, ASTM STP 824 (1984) 106
- [8] CHARQUET D. § AI, ASTM STP 939 (1987) 431
- [9] GARZAROLLI F. § AI, ASTM STP 1023 (1989) 202
- [10] THORVALDSSON T. § AI, ASTM STP 1023 (1989) 128



**PARAMETRIC TESTS OF THE EFFECTS OF WATER  
CHEMISTRY IMPURITIES ON CORROSION OF  
Zr-ALLOYS UNDER SIMULATED BWR CONDITION**

S. SHIMADA, K. ITO  
Nippon Nuclear Fuel Development Co.,  
Japan

C.C. LIN  
GE Nuclear Energy, USA

B. CHENG  
Electric Power Research Institute, USA

T. IKEDA  
Toshiba Corporation, Japan

M. OGUMA  
Hitachi, Ltd, Japan

T. TAKEI  
Tokyo Electric Power Company, Japan

C. VITANZA, T.M. KARLSEN  
OECD Halden Reactor Project,  
Norway

**Abstract**

The Halden BWR corrosion test loop was constructed to evaluate the impact of water chemistry variables, heat flux and boiling condition on corrosion performance of Zr-alloys in a simulated BWR environment. The loop consists of two in-core rigs, one for testing fuel rod segments and the other for evaluating water chemistry variables utilizing four miniautoclaves. Ten coupon specimens are enclosed in each miniautoclave. The Zr-alloys for the test include Zircaloy-2 having different nodular corrosion resistance and five new alloys. The first and second of the six irradiation tests planned in this program were completed. Post-irradiation examination of those test specimens have shown that the test loop is capable of producing nodular corrosion on the fuel rod cladding tested under the reference chemistry condition. The miniautoclave tests showed that nodular corrosion could be formed without flux and boiling under some water chemistry conditions and the new alloys, generally, had higher corrosion resistance than the Zircaloy in high oxygen environments.

## 1. INTRODUCTION

Although ex-reactor tests<sup>(1)-(3)</sup> have been developed to evaluate Zircaloy corrosion, those tests were qualified only as a screening tool for ranking the relative corrosion resistance of different lots of Zircaloy for in-reactor applications. Because the tests use superheated steam as the test medium, it is not possible to employ those tests to evaluate the effects of impurities in reactor water on Zircaloy corrosivity which has been regarded to be important to fuel performance in BWRs<sup>(4)(5)</sup>. An irradiation experiment was thus initiated to investigate the effect of water chemistry impurities and other operational variables on the corrosion performance of Zircaloy and new Zr-alloys under simulated BWR conditions.

## 2. TEST PROCEDURE

A light water corrosion loop was designed and constructed to simulate the fast and thermal neutron fluxes as well as the thermohydraulic conditions of typical BWRs in the boiling heavy water reactor (HBWR) at Halden. The conditions of the test loop are summarized in Table 1. The in-core test sections or rigs can accommodate a fuel rod segment of approximately 1 m or four miniautoclaves in which Zr-alloy samples can be tested under different water chemistry conditions.

Table 1 Specification for BWR Corrosion Loop  
(Reference Test Conditions)

Temperature	288 °C
Pressure	7 MPa
Neutron Flux(E>1MeV)	$5-8 \times 10^{13} \text{ n/cm}^2/\text{s}$
Flow Velocity	~2m/s
Water Purity	
- Conductivity	0.1-0.3 $\mu\text{S/cm}$
- pH(Room temperature)	6.5-7.5
- Silicates	<100 ppb
- Chlorides	< 20 ppb
- Total Metallic Ions (Cu)	< 15 ppb (< 5 ppb)
- Total Organics(As Carbon)	<100 ppb
- Oxygen	200-300 ppb
- Hydrogen	< 25 ppb

## 2.1 Loop Design

The test facility is a twin-rig recirculating loop as shown in the schematic flow diagram in Fig.1. After water is preheated to ~280 °C, it enters the fuel segment rig where boiling takes place. The loop water continues to circulate through the miniautoclave rig. The flow velocity past the surface of the fuel rod near the bottom is ~2 m/s. A portion(10%) of the loop water is cleaned through an ion exchange loop before returning to the main loop. Water samples can be taken at the inlet and outlet ports of the fuel rod rig as shown in Fig.1. The samples are analyzed for conductivity, cation and anion concentrations, oxygen, hydrogen, and pH.

The configuration of the in-core rig containing a fuel rod is also shown in Fig.1. The test fuel rod of 1 m long is surrounded by 12 booster rods segments of the PWR type with ~20 wt% U<sup>235</sup> enrichment. The length of the booster rods (fueled section) is 80 cm. Light water enters the rig from the top through the space between the flow channel tube and the downcomer tube then turns upward through the gap between the test fuel rod and the flow channel tube.

The fuel rod rig and fuel rod for the first test are schematically shown in Fig.2. The first test rod was designed to produce bulk boiling at about 35 cm from the rod bottom. Below the location of onset of bulk boiling, nucleate boiling will occur.

A schematic of the miniautoclave setup is also shown in Fig.2. The four miniautoclaves are constructed of Zircaloy-2 tube fabricated from a heat treated tubeshell. The length of each miniautoclave is 124 mm with an outer diameter of 14.3 mm and a wall thickness of 0.5 mm. Each miniautoclave contains 10 coupon specimens prepared from Zircaloy -2 and other Zr-alloys. The dimension of the coupon specimen from a tube is approximately 23 mm long with an arc of 135° out of an 11 mm OD tube. The pressure in the miniautoclaves is kept about 10 MPa in order to avoid the boiling. All four miniautoclaves have separate inlet and outlet lines made of stainless steel tubes. The inlet water lines are connected to feed water tanks. The water flowrate is about 5-7 ml/min.

## 2.2 Test Variables

Test variables include (1) fuel cladding material, fuel pellet design and water chemistry for the fuel rod test and (2) alloy process and alloy

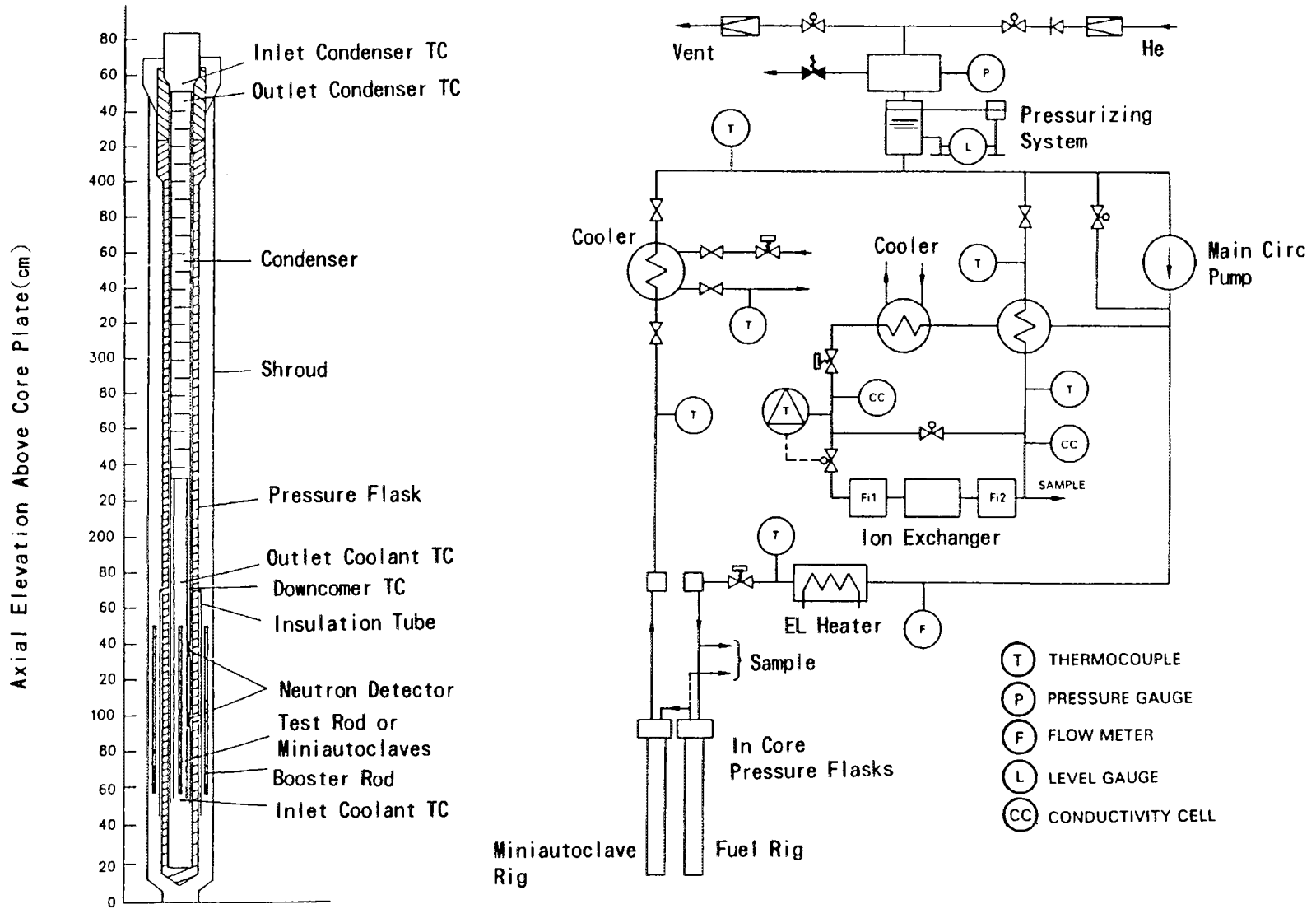


Fig.1 BWR Corrosion Loop Flow Sheet and In-Core Rig Configuration

chemistry and water chemistry impurity in the miniautoclave test. The water purity specified in Table 1 is used for the first and second fuel rod tests.

### 2.2.1 Fuel Rod Segment

The Zircaloy-2 cladding for the first and second tests was selected from a lot of barrier cladding tubes which exhibited a low to medium degree of nodular corrosion susceptibility, i.e., about  $\leq 10$  % nodular oxide in the ex-reactor two-step steam test<sup>(1)</sup>. The outside diameter of the cladding is 12.33 mm, the inside diameter, 10.567 mm. The first segment was fabricated using  $UO_2$  pellets having enrichment in the range of 4-4.5 wt%  $U^{235}$ . The total length of the pellet stack for the first test was about 80 cm(Fig.2).

### 2.2.2 Miniautoclave Samples

All four miniautoclaves contain the same alloy matrix: four Zircaloy-2 specimens(Alloys A, B, C, and D) having different degrees of resistance to nodular corrosion performance and five new alloys. Alloy A is a Zr-lined cladding fabricated using an in-process heat treated(IPHT) sequence(i.e.,  $\beta$ -quenched at an intermediate reduction stage). The alloy chemistry of Alloy A is that of the controlled chemistry type. Alloy B was fabricated from a heat treated tubeshell as a reference. Alloy C is a Zr-lined tube from the same lot as the fuel cladding tube used to construct the fuel cladding segments. Alloy D is a high nodular corrosion susceptible tube fabricated from a non-heat treated tubeshell produced in about 1980. Alloys B, C, and D are all from normal chemistry ingots.

The new alloys include three alloys modified from Zircaloy-2 by (1) increasing the Fe content(Alloy E), (2) increasing the Fe and Ni contents(Alloy F), (3) adding Nb(Alloy G). The other two alloys are Zr containing Sn, Nb and Mo(Alloy H) and Zr containing Nb and Bi(Alloy I and J). Sample identification numbers were stamped on the specimens. Prior to the surface finish operation, 100  $\mu m$  of the inner surfaces of Alloys A and C were removed mechanically to remove the Zr-liner. Subsequently, Alloys A and C, as well as Alloy D were etched for 2 to 3 minutes to produce a lustrous surface.

### 2.2.3 Miniautoclave Water Chemistry Matrix

In this program, six consecutive irradiation tests have been planned with each having four miniautoclaves. The water chemistry that are being evaluated include: oxygen, Cu added as nitrate or sulfate, Zn added as nitrate or sulfate, nitrogen, chromate, hydrogen, etc. The four test conditions for the first test are shown in Fig. 2. The standard condition of 250 ppb  $O_2$  and 25 ppb  $H_2$  is based on the water chemistry measured at recirculating lines of many BWRs. The high oxygen condition was to test the effect of oxygen. The  $Cu(NO_3)_2$  and  $Zn(NO_3)_2$  conditions were to evaluate the effects of  $Cu^{+2}$  and  $Zn^{+2}$ , and  $NO_3^-$ . The concentrations of  $Cu^{+2}$  and  $Zn^{+2}$  were 300 and 100 ppb, respectively. The nitrate compounds were selected to study the effect of  $NO_3^-$ .

The miniautoclave water chemistries (i.e.,  $O_2$  and  $H_2$  contents, pH, conductivity, ionic(added) concentration, and other impurities) were measured on grab samples using ion chromatography and, in some cases, atomic absorption techniques for the inlet and outlet water.

## 3. TEST RESULTS AND DISCUSSION

The first test was performed for 153 days within the 196-day period from June 28, 1990 to January 11, 1991.

### 3.1 Irradiation Test

#### 3.1.1 Irradiation Parameters

The irradiation parameters were either directly measured or calculated from measured parameters. Table 2 tabulates the measured steady state values. The system, nucleonic, and thermohydraulic parameters in the first test have, overall, met the specification and design limits.

The axial profiles of the thermal neutron flux within the test zone showed that the neutron flux peaking factor was <10%. The void fraction at the outlet portion of the fuel rod rig was about 50%.

Table 2 Summary of Nucleonic and Thermohydraulic Conditions for the First Test

	Fuel Rig	Miniautoclave rig
Coolant Temperature, °C		
Inlet	282-284	283-285
Outlet	286-287	282
Specimen		285-287
Pressure, MPa	7.4-7.5	Same
(In the miniautoclave)	-	(9.5-10 MPa)
Flow Velocity, m/s	1.8-2.0	Same
(In the miniautoclave)		(~0.1 mm/s)
Onset of Bulk Boiling, cm	23-40	-
Fuel Rod Rating, kW/m	20-23	-
Average Fast Flux		
n/cm <sup>2</sup> /s	5-5.8X10 <sup>13</sup>	5.6-6.2X10 <sup>13</sup>
γ Flux, W/g	1.3-1.4	1.4-1.6

### 3.1.2 Water Chemistry Data

#### (a) Loop Water Chemistry

Table 3 summarizes the range of the measured value. The oxygen and hydrogen contents at the inlet were measured in the range of 250-330 ppb and ~10 ppb respectively.

Among the metallic impurities, Ni<sup>+2</sup> was the only species which showed a significant concentration, ranging from 2 to 20 ppb during the first 30 days and gradually decreasing to 2-6 ppb afterwards. As for the anionic impurities, NO<sub>2</sub><sup>-</sup> was barely detected. SO<sub>4</sub><sup>-2</sup>, NO<sub>3</sub><sup>-</sup>, Cl<sup>-</sup>, and F<sup>-</sup> were measured in the range of 5-10 ppb during the first 30 days, and all decreased to less than 2 ppb afterwards. The main anionic species was CrO<sub>4</sub><sup>-2</sup>. The high Ni<sup>+2</sup> concentration during the first 30 days and the high CrO<sub>4</sub><sup>-2</sup> concentration throughout the test might be attributed to corrosion of the stainless steel and Inconel components in the loop system.

Table 3 Summary of Loop Water Chemistry Condition for the First Test

Item	Measured Values <sup>†</sup>
Conductivity ( $\mu\text{S}/\text{cm}$ )	0.12 - 0.20
Oxygen(ppb)	250 - 330
Hydrogen(ppb)	~10
Cationic Impurities	
Fe, Co, Zn, Cu	<5 ppb
Ni	2 - 20 ppb(1-30 days) 2 - 6 ppb(> 30 days)
Anionic Impurities	
NO <sub>2</sub>	< 2 ppb
NO <sub>3</sub> , F ,Cl , SO <sub>4</sub>	<10 ppb(1-30 days) < 2 ppb(> 30 days)
CrO <sub>4</sub>	15 -40 ppb

※ Water sampled at a location near inlet of the fuel rod rig.

(b) Miniautoclave Water Chemistry Data

The inlet water to the four miniautoclaves was prepared according to the compositions shown in Fig.2. Table 4 is a summary of the measured inlet and outlet water chemistry data in the four miniautoclaves.

Miniautoclave A had 240-310 ppb O<sub>2</sub> and 18-34 ppb H<sub>2</sub> in the inlet water, and no chemical impurity addition. The oxygen was depleted and only <10ppb was measured in the outlet water. The hydrogen content did not show significant change.

Miniautoclave B had oxygen addition of 250-290 ppb and hydrogen of 21-30 ppb. Cu was added as Cu(NO<sub>3</sub>)<sub>2</sub> at a concentration of 200-400 ppb Cu<sup>+2</sup>. The weight concentration of NO<sub>3</sub><sup>-</sup> was 400-800 ppb. In the outlet water, the Cu content decreased to 40-120 ppb, and NO<sub>3</sub><sup>-</sup>, to 200-350 ppb. In the meantime, the O<sub>2</sub> and H<sub>2</sub> were significantly increased to 350-400 and 82-96 ppb, respectively. The data from this test suggest that some Cu was deposited in the test line, and some NO<sub>3</sub><sup>-</sup> was reduced to NO<sub>2</sub><sup>-</sup> even in the presence of excess oxygen. It is possible that other lower oxidation state nitrogen compounds might also exist in the effluent water. The reason for

Table 4 Summary of Major Chemistry Results of Miniautoclave Test  
(in ppb)

Test Condition	Inlet	Outlet	Net Change
MAC A: Standard			
O <sub>2</sub>	240-310	1- 7	-(240-300)
H <sub>2</sub>	18- 34	26-54(?)	Unchanged
MAC B: Cu(NO <sub>3</sub> ) <sub>2</sub>			
O <sub>2</sub>	250-290	350-400	+100
H <sub>2</sub>	21- 30	80- 96	+66
Cu	200-400	40-120	-(150-300)
NO <sub>3</sub> <sup>-</sup>	400-800	200-350	-(200-500)
NO <sub>2</sub> <sup>-</sup>	0	100-200	+(100-200)
MAC C: High O <sub>2</sub>			
O <sub>2</sub>	780-850	310-430	-450
H <sub>2</sub>	0	5- 50(?)	+(5-50)
Fe	< 3	100-200	+(100-200)
MAC D: Zn(NO <sub>3</sub> ) <sub>2</sub>			
O <sub>2</sub>	250-310	4- 15	-(240-300)
H <sub>2</sub>	20- 34	~27	Unchanged
Zn	90-120	50-120	-(20-30)
NO <sub>3</sub> <sup>-</sup>	160-250	0- 30	-(160-220)
NO <sub>2</sub> <sup>-</sup>	0	0- 20	Increase
Preliminary results(second test)			
CuSO <sub>4</sub>			
O <sub>2</sub>	700-800	400-600	-(200-300)
H <sub>2</sub>	0	3- 46	+(3-46)
Cu	300	50	-250
SO <sub>4</sub> <sup>-2</sup>	400	400	Unchanged

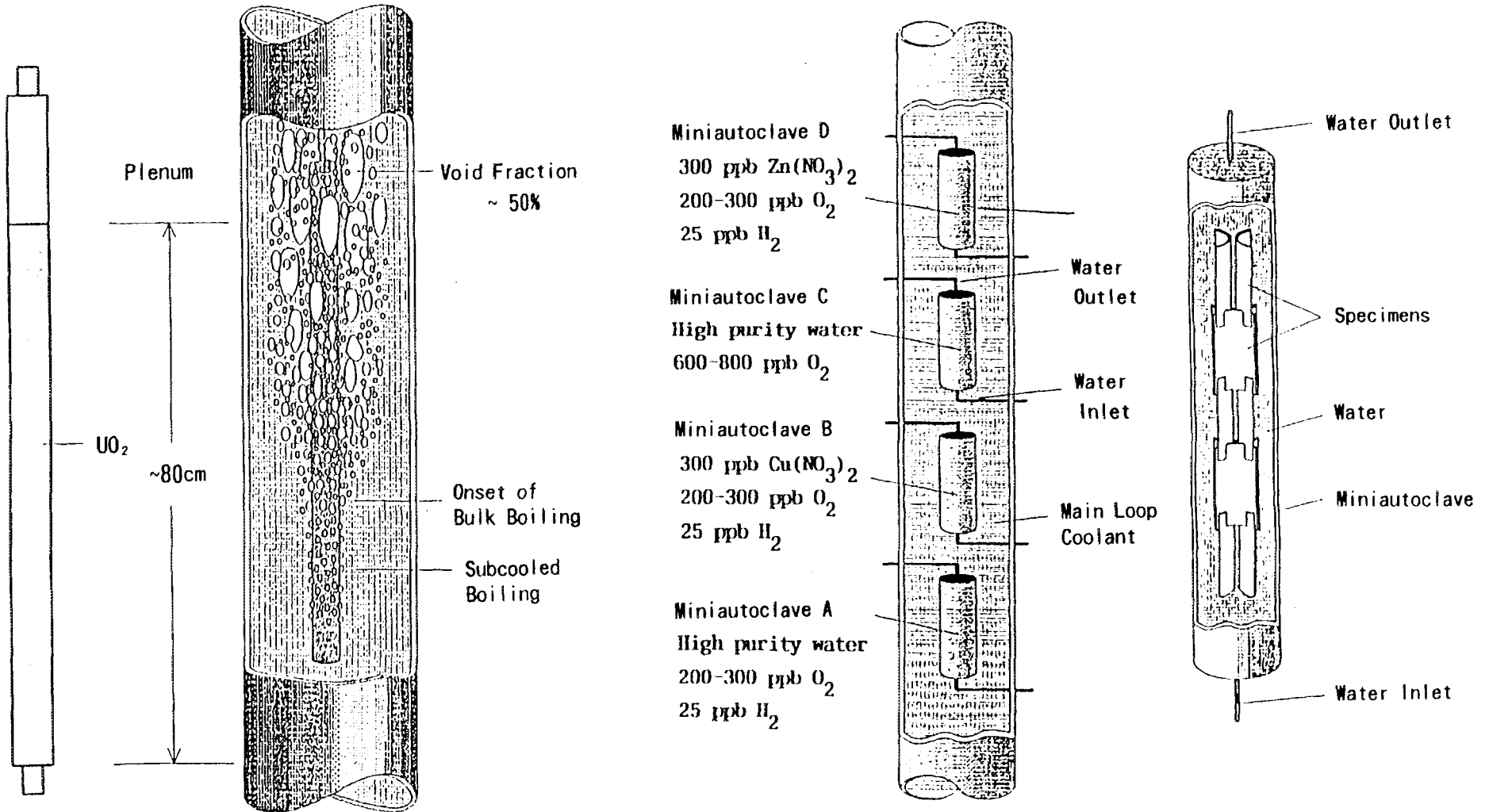


Fig.2 Schematic of Fuel Rod and Miniautoclaves

the large increase in  $O_2$  and  $H_2$  in the outlet water is not clear. It was thought that Cu caused poisoning of the recombination reaction of oxygen and hydrogen ions, thus promoting the production of  $O_2$  and  $H_2$ . However, the preliminary results from the second test using  $CuSO_4$  did not show a similar large increase in  $O_2$  and  $H_2$  in the outlet water as shown in Table 4. Explanation of these observations require analyses of radiation water chemistry in the future.

Miniautoclave C had 780-800 ppb  $O_2$  and no  $H_2$  in the inlet water. The oxygen content was reduced to 310-430 ppb in the outlet water. Some hydrogen in the range of 5-50 ppb was also detected in the outlet water.

Miniautoclave D contained the same amount of  $O_2$  and  $H_2$  as the standard test(miniautoclave A) in the inlet water. The  $Zn^{+2}$  and  $NO_3^-$  contents were 90-120 and 160-250 ppb, respectively. The majority of added  $Zn^{+2}$  passed through the water line and the miniautoclave, as 50-120 ppb Zn was detected in the outlet water. Essentially, all the added  $O_2$  and  $NO_3^-$  were depleted and only <15 and <30 ppb were detected, respectively. Unlike the  $Cu(NO_3)_2$  test of miniautoclave B, very little  $NO_2^-$  (<20 ppb) was detected in the outlet water. Thus, in this test condition, the end product of the reduction of  $NO_3^-$  may be  $N_2$ ,  $NH_3$ , and/or  $NH_4^+$ , which were not measured in this study.

## 3.2 POST-IRRADIATION EXAMINATION

### 3.2.1 Fuel Rod Segment

#### (a) Non-destructive examination

Visual observation of the cladding surface did not reveal unusual feature. Eddy current oxide thickness measurements were performed along the entire rod length at azimuthal orientations of 60° apart. The oxide thickness traces are shown in Fig.3. There was little azimuthal variation in the oxide thickness.

#### (b) Destructive examination

Cross-section metallography was performed on cladding specimens at the elevation of the 11, 22, 41, 51, 65, and 84 cm. Nodular oxide was found on all samples. Isolated and coalesced nodules can be seen in the range of

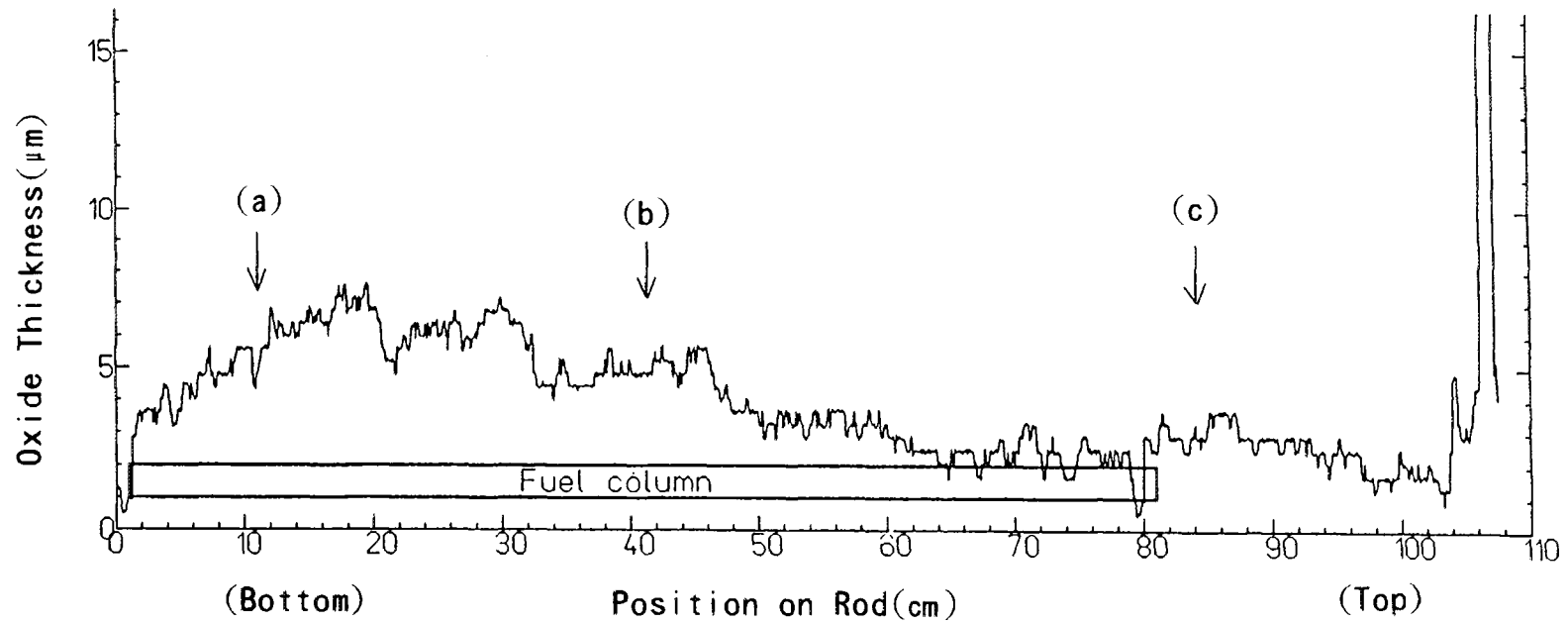
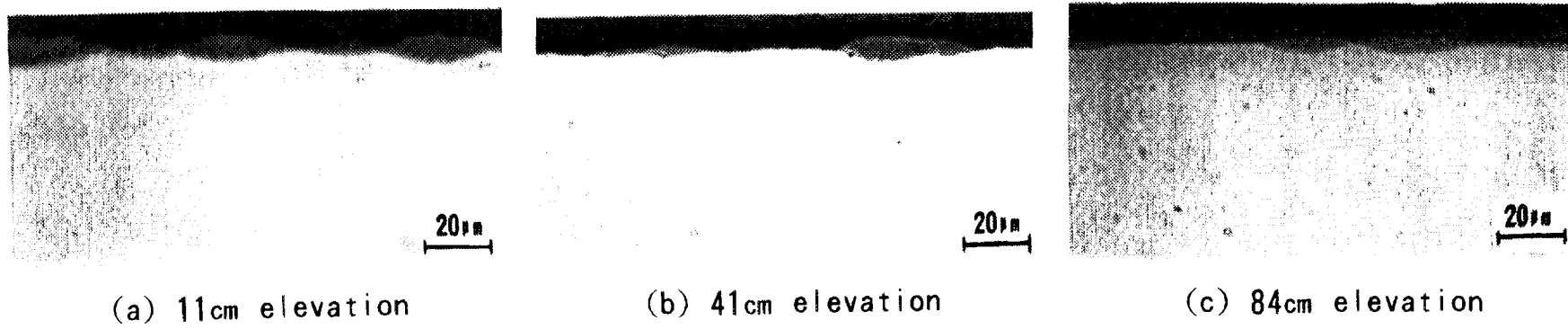


Fig.3 Oxide Thickness on Fuel Rod(angle 0°) and Surface Oxide at the 11, 41, and 84 cm Elevations

5-12  $\mu\text{m}$  at the 11 cm elevation. At the 22 and 41 cm elevations, which were close to the onset of boiling positions, nodules of 5-12  $\mu\text{m}$  were found. At the 51 and 65 cm elevations, which were in the saturation boiling region, several nodules with the maximum thickness of 6  $\mu\text{m}$  were observed. A few oxide nodules of 5-10  $\mu\text{m}$  appeared in the plenum region at the 84 cm elevation. The uniform oxide at all elevations was found to be 1-2  $\mu\text{m}$ . Figure 3 also shows examples of the surface oxide at the elevation of 11, 41, and 84 cm. The hydride contents estimated from metallographic observation in the fuel cladding were all <30 ppm.

The surface morphology and chemistry were analyzed using a scanning electron microscope (SEM) and an electron probe microscope (EPMA). The crud deposition on the fuel rod surface is generally light, and there was no evidence of the reddish iron oxide deposit ( $\text{Fe}_2\text{O}_3$ ).

### 3.2.2 Miniautoclave Samples

#### (a) Non-destructive examination

The miniautoclave coupon specimens were visually inspected and weight measured at Halden. Examples of the visual appearance of the Alloy D in the four miniautoclaves can be seen in Fig.4. The visual inspection indicated that the high  $\text{O}_2$  test was most aggressive and caused nodules on the outer surfaces of Alloys B, C, D, and H. The Weight gain data of the coupon specimens in the four miniautoclaves suggested that the high  $\text{O}_2$  test was the most corrosive condition for all specimens.

#### (b) Destructive examination

The detailed corrosion behavior for all coupon specimens were characterized by metallographic observation. Some of the photographs are shown in Fig.4 for Alloy D. All of the test results are summarized in table 5. The table indicates that the high  $\text{O}_2$  and  $\text{Zn}(\text{NO}_3)_2$  test conditions are corrosive to some Zircaloy specimens. The preliminary results for the  $\text{CuSO}_4$  test were also included in the Table. All coupon specimens exhibited good corrosion resistance in both the  $\text{Cu}(\text{NO}_3)_2$  and  $\text{CuSO}_4$  tests, although the water chemistry behavior differed between the two conditions as can be seen in Table 4. The results suggested that Cu might have improve corrosion resistance of Zr alloys in the miniautoclave test condition.

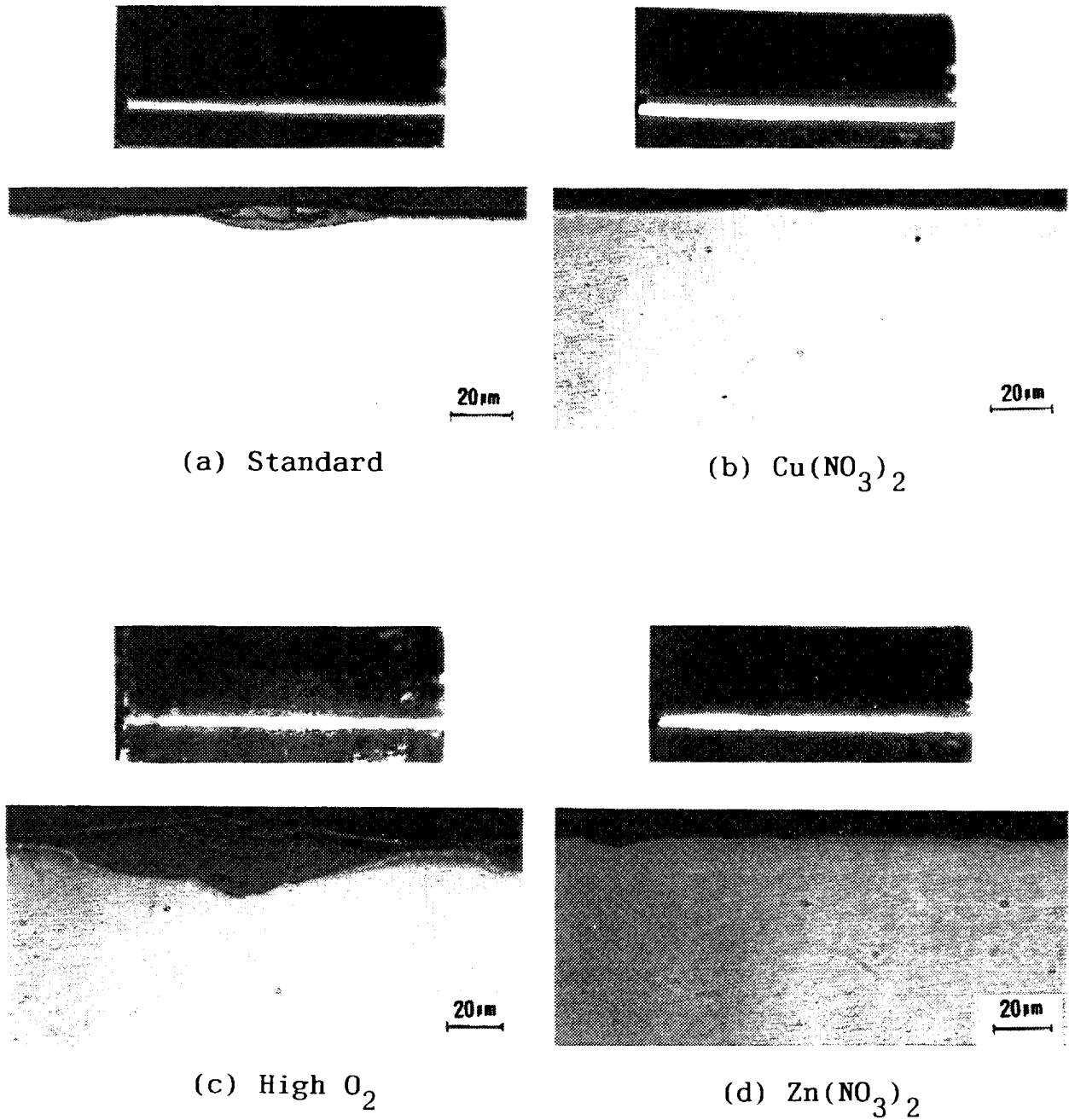


Fig.4 Visual Appearance and Surface Oxide of the Alloy D Coupon Specimens Tested in the Miniautoclaves

With respect to the Zircaloy-2 specimens, the ranking of the corrosion resistance of the specimens tested in this program is as predicted from ex-reactor MAT test results, which are shown in Table 5.

SEM observations and EPMA analyses were performed on the outer surfaces of all coupon specimens. The SEM observations are consistent with the metallographic results. The EPMA analyses showed that major deposits

Table 5 Summary of Miniautoclave Test Results

Alloy	Water Chemistry	Standard	High O <sub>2</sub>	Zn(NO <sub>3</sub> ) <sub>2</sub>	Cu(NO <sub>3</sub> ) <sub>2</sub>	CuSO <sub>4</sub>	Ex-Reactor(MAT)
	(O <sub>2</sub> )	(~250ppb)	(~750ppb)	(~250ppb)	(~250ppb)	(~750ppb)	Corrosion (% Nodular)
Zry-2	A(IPHT)	×	×	○ 5, (3)	×	×	0
	B(TSHT)	×	○20, (3)	○ 5, 30%	×	×	0
	C(Rod Ref.)	×	○ 5, 70%	○12, 10%	×	×	2-5
	D(No HT)	○12, 40%	○29, 20%	○ 6, 30%	×	×	80-100
New Alloy	E(Zry-2+Fe)	×	×	×	×	×	0
	F(Zry-2+Fe, Ni)	×	×	×	×	×	0
	G(Zry-2+Nb)	×	×	×	×	×	0
	H(Zr+Sn, Nb, Mo)	×	○12, 50%	×	×	×	0
	I(Zr+Nb, Bi)	×	×	×	×	×	0

× : Uniform Oxide (1-2 μm)

○ : Nodular Oxide (Max. Thickness in μm), (Coverage Ratio in %, or Number of Nodule)

on the specimen surfaces were oxides of Fe, Cr, and Ni for the standard and high O<sub>2</sub> test, and considerable amounts of Cu and Zn oxides deposited in the Cu(NO<sub>3</sub>)<sub>2</sub> and Zn(NO<sub>3</sub>)<sub>2</sub> tests, respectively. Especially in the Zn(NO<sub>3</sub>)<sub>2</sub> test, many species of impurities were also detected.

#### 4. CONCLUSION

From the first test, the following conclusions could be derived:

- (1) The fuel rod test results indicate that the Halden BWR corrosion loop can simulate the typical nodular corrosion found in BWRs.
- (2) Zircaloy nodular corrosion can occur on the fuel rod surface in the oxidizing loop water without the presence of chemical impurities, such as Cu, Zn, etc.
- (3) The maximum nodular oxide thickness of ~12 μm appeared at around the onset of boiling region in the fuel rod.
- (4) The coupon specimen test showed that nodular corrosion could be formed without heat flux and boiling.
- (5) Oxygen addition to the environment not only increased the nodular corrosion susceptibility, but also increased the oxide growth rate.
- (6) Zn as nitrate produced nodular corrosion on many Zircaloy-2 specimens.
- (7) The ranking of the corrosion resistance of the Zircaloy-2 specimens tested in this program is as predicted from ex-reactor nodular corrosion test results.
- (8) The new alloys, generally, have high corrosion resistance in the high oxygen environment.
- (9) Cu as nitrate and sulfate suppressed nodular corrosion on all Zr-alloys.

The miniautoclave tests provided valuable information on radiation chemistry. One example is the different instability of NO<sub>3</sub><sup>-</sup> in the Cu(NO<sub>3</sub>)<sub>2</sub> and Zn(NO<sub>3</sub>)<sub>2</sub> tests, and another, the net change in O<sub>2</sub> contents between the inlet and outlet water in the Cu(NO<sub>3</sub>)<sub>2</sub> and CuSO<sub>4</sub> tests. Further study to evaluate the water chemistry conditions in the miniautoclaves is in progress using the same loop system.

#### ACKNOWLEDGEMENTS

This study was performed as a cooperative work with the Tokyo Electric Power Co., Inc., the Tohoku Electric Power Co., Inc., the Chubu Electric Power Co., Inc., the Chugoku Electric Power Co., Inc., and the

Japan Atomic Power Company. The authors would like to their thanks to those members.

### REFERENCES

- (1) B. Cheng, H. A. Levin, R. B. Adamson, M. O. Marlowe, and V. L. Monroe, "Development of a Sensitivity and Reproducible Steam Test for Zircaloy Nodular Corrosion", ASTM STP-939, p.257(1987).
- (2) B. Cheng, and R. B. Adamson, "Mechanistic Studies of Zircaloy Nodular Corrosion", *ibid.*, p.387.
- (3) K. Ogata, Y. Mishima, et al., "A Systematic Survey of the Factors Affecting Nodular Corrosion", ASTM STP-1023, p.291(1989).
- (4) M. O. Marlowe, J. S. Armijo, B. Cheng, and R. B. Adamson, Proceedings, Topical Meeting on Light Water Reactor Fuel Performance, Orlando, Florida, ANS, p.3(1985).
- (5) Y. Hayashi, T. Matsumoto, et al., "Fuel Failure at Hamaoka Unit 1", presented at IAEA Technical Committee Meeting, Dimitrovgrad, Russian Federatim, May 26-29, 1992.



## **A NEW MODEL FOR THE IN-REACTOR CORROSION OF ZIRCONIUM ALLOYS**

**B. COX**

Centre for Nuclear Engineering,  
University of Toronto,  
Ontario, Canada

### **Abstract**

Previous models for the in-reactor corrosion of zirconium alloys have assumed that the mechanism is a completely solid-state diffusion process, determined by the growth and breakdown of the protective oxide film. In-reactor kinetics have been related to out-reactor kinetics with the oxide-metal interface temperature calculated from effects of heat flux. Recent experimental results have suggested that oxide dissolution and reprecipitation may be a major process leading to the formation of thick porous oxide films in-reactor. The model described here is based on the dissolution of primary recoil tracks in the oxide as the primary process distinguishing in-reactor from out-reactor corrosion. The consequences of such a model would be a very different microscopic morphology of in-reactor and out-reactor thick films, a significant irradiation effect on non-heat transfer surfaces, and a change in the kinetics of the overall process. This model should be equally applicable to PWR and BWR water chemistries because of the amphoteric nature of  $ZrO_2$ , and the effects of LiOH should operate by an essentially identical mechanism. A reciprocal rate equation should fit these processes and with additive terms seems capable of accommodating all water chemistry effects, except for discontinuous processes such as nodular corrosion.

### **1. Introduction**

The oxidation of zirconium alloys in high temperature aqueous environments is usually considered to be controlled by the growth and breakdown of a protective surface oxide film dictated entirely by solid state processes[1,2]. The out-reactor oxidation kinetics proceed in two stages; a pretransition period where kinetics are close to cubic or quartic and the oxide film is protective, and a post-transition period after the breakdown of this protective film where the kinetics are approximately linear, although in detail they may

consist of a number of cycles, and may slowly accelerate over long periods of time[3-5]. In laboratory autoclave tests the oxidation kinetics of the Zircalloys are relatively independent of water chemistry, and only additions of high concentrations of lithium hydroxide result in any major increase in the corrosion rate[6-14].

Studies of the effects of irradiation on the oxidation kinetics have generally shown a small increase in pre-transition kinetics and a reduction in the time to transition for studies performed in dry gaseous (low pressure steam or carbon dioxide) environments[12]. Early experiments in high temperature water in-reactor have tended not to confirm these observations[13], and clear evidence for an accelerating effect of irradiation was absent until after the transition point. Most of the recent in-reactor studies have been based on the subsequent measurement of oxide thickness by either metallography or eddy current techniques, neither of which are very accurate at low oxide thicknesses. As a result the establishment of an irradiation effect on the pretransition kinetics in water reactors had to await the development of more accurate methods for oxide thickness measurements[14].

The extent of the accelerating effect of irradiation was apparently strongly dependent on the reactor water chemistry. In loop tests and in Boiling Water Reactor (BWR) environments, where radiolysis of the water results in the presence of excess oxygen in solution, a severe self-propagating localised breakdown of the protective oxide film led to the formation of oxide nodules, which in the worst cases could lead to through wall oxidation of the cladding. Nodular corrosion could also be severe on non-heat transfer surfaces such as fuel channels[15-22]. The precise mechanisms leading to nodular corrosion remain unknown, but a practical mitigation of the problem has been achieved by careful beta-quenching and other fabrication treatments of the cladding[23-24]. As a result of this, examination of BWR fuel cladding showing essentially no nodular corrosion has shown that the growth of the uniform black oxide film in BWR water chemistry is very similar to the growth rate of uniform oxides in PWRs. Thus, the effect of water chemistry seems only to be significant in initiating nodules in susceptible cladding batches[25,26].

In Pressurised Water Reactor (PWR) environments[27-32], where additions of dissolved hydrogen inhibit water radiolysis, oxide breakdown appears to be relatively uniform and the thick porous films formed at high burnups vary in thickness along the length of the fuel pin, and azimuthally around it at any particular elevation, but are uniform on a local scale. Modelling of PWR oxidation is relatively easier than for BWR oxides because of the general uniformity of the behaviour. The many models for PWR corrosion have generally started from a simplified two-stage out-reactor kinetic model. By applying a thermal hydraulic model for the fuel assembly using an estimated thermal conductivity for the oxide film, and the heat flux calculated from the reactor physics data, an iterative calculation of the oxide-metal interface temperature can then be carried out as a function of burn-up and an estimate of the oxide thickness as a function of time made assuming an activation energy for the corrosion process[33-37]. A comparison of the results of such a model with the in-reactor observations is then made and a multiplicative factor applied to accommodate differences between calculation and observation. Such factors are regarded as irradiation enhancement factors and appear relevant only to specific reactors when observed[33]. In other instances[34] no apparent effect of irradiation is claimed. This dichotomy of results is permitted to some extent by a lack of accurate knowledge of the various thermal-hydraulics constants, oxide thermal conductivities and activation energies that are used.

In practice, these models have difficulty in simultaneously predicting, with the same input parameters, both the minima in oxide thicknesses at grid spacers and the maxima seen in the adjacent intergrid spans; or the oxide thicknesses seen on fuel cladding at any given elevation and that seen on guide tubes or grids (non-heat transfer) at the same elevation in the same bundle[34]. Present models do not predict the rather large azimuthal variations in oxide thickness that are seen. Recent attempts (presented at the EPRI-PWR Fuel Corrosion Workshop, Washington, DC, July 1993) to make these models fit better have continued to use multiplicative enhancement factors, even though additive irradiation effects may be more realistic[38,39]. They have now incorporated sub-routines to allow for LiOH concentration, the long-term acceleration in the oxidation kinetics, and potential effects of hydride precipitation. However, in many instances, there

is no room for these additional factors because thermal-hydraulic factors have been able to account for virtually all of the oxide growth. In a recent paper it was shown that this situation may arise because the activation energies for corrosion that are used are too high[40]. It is proposed here that a complete departure from such in-reactor models should be adopted.

## **2. A Revised Corrosion Mechanism**

Recent results have suggested that in aqueous solutions under irradiation a major change in our ideas about the corrosion process should be adopted. In studies in 0.1-1.0 mol. lithium hydroxide solutions, it has now been clearly demonstrated that dissolution and reprecipitation of  $ZrO_2$  is the primary mechanism leading to acceleration of the oxidation rate[41-43]. This dissolution process apparently results from the preferential dissolution of tetragonal or cubic  $ZrO_2$  crystallites in the oxide film, and (because of their small volume fraction) leads to the development of open porosity wherever an interconnected path of these phases is present in the oxide. The dissolved oxide reprecipitates mainly on the specimen surface as monoclinic  $ZrO_2$  that does not represent a diffusion barrier. Evidence for some crystallite boundary dissolution in solutions with 70ppm lithium has recently been reported[44].

Earlier work had shown that photodissolution of anodic oxides was possible even at room temperature if high applied electrical fields were present[45]. Again, pores were developed in the oxide films, and it is tempting to assume that preferential dissolution of tetragonal or cubic  $ZrO_2$  crystallites was again the mechanism. This could not be demonstrated in this instance because good Laser Raman spectra could not be obtained from such thin oxide films. These observations, however, provided an explanation for the growth of thick porous interference colour oxide films at low temperatures on Zircaloy growth specimens in the ATR reactor[45]. In this instance, there was no externally applied electrical field. It was possible that an internal field could be generated in the oxide from emission of Compton electrons in the high gamma field, but an alternative mechanism whereby primary knock-on damage tracks in the oxide from fast-neutron collisions were preferentially dissolved could not be eliminated.

In order to test the generality of this dissolution and reprecipitation process, specimens were examined from short in-reactor loop tests that had shown weight gains less than that expected from the time, temperature and out-reactor pre-transition kinetics[46], and from experiments in low power density uranyl sulphate tests in-reactor where small increases in weight gain (compared with out-reactor tests) were observed[47]. In both instances porosity was seen in the oxides. Thus, generation of porosity by  $ZrO_2$  dissolution and reprecipitation seems to be evident in all in-reactor tests where such evidence has been sought. The preferential dissolution of recoil damage spikes seems a strong possibility for a micromechanism in such cases, and the amphoteric nature of  $ZrO_2$  means that such dissolution should be possible whatever the pH of the reactor water.

Other early work would support such a mechanism. Evidence for a radiation induced transformation of monoclinic to cubic  $ZrO_2$  was obtained by several investigators[49-50]. Although in most instances this could be explained by the stabilising effects of impurities present in the material[51-52], from the corrosion standpoint this would not matter. If the passage of a primary knock-on spike produced a column of cubic  $ZrO_2$  it could be argued that this would preferentially dissolve, although merely disordering the same volume of material might be expected to have a similar effect. In retrospect, it is interesting to note that attempts to find cubic  $ZrO_2$  in the oxides of relatively thick oxide films formed in uranyl sulphate solution[47] were unsuccessful. At that time it was concluded that this was evidence that the irradiation induced phase transformation did not occur during in-reactor corrosion; however, the explanation that it did occur, but that the cubic material preferentially dissolved and reprecipitated as monoclinic  $ZrO_2$  was not considered, although a dissolution mechanism was proposed and subsequently dropped at this time. Nevertheless, it now appears that the preferential dissolution of local regions of the oxide (whether or not these are transformed to cubic  $ZrO_2$  under irradiation) seems to be a regularly observable phenomenon in radiation experiments in aqueous solutions.

Before moving on to examine the details of such a model we must ask whether there is any contribution of dissolution processes to the corrosion mechanism in high

purity water in the laboratory. No detectable effect of LiOH concentration on the oxidation kinetics is seen until solutions of  $\sim 0.01$  mol. are employed. Thus, if there is any dissolution of  $ZrO_2$  in pH7 water, it must be exceedingly small and may be restricted to dissolution of oxide crystallite boundaries as reported for oxides grown in 0.01 mol. LiOH[44]. However, this does not mean that it is making zero contribution to the kinetics. In general, corrosion tests in water and dry steam at the same temperature and on identical samples have not been reported for long post-transition experiments so that a direct comparison of conditions where dissolution is possible and not possible cannot be made. Short tests in steam and water have not shown any clear differences[55]. Oxidation of identical specimens in 633K water and 673K steam tests, however, generally show lower exponents for the post-transition kinetics in 673K steam and, occasionally, the actual weight gains at long times are almost identical[40]. This may be an indication that dissolution of  $ZrO_2$  tends to enlarge the pores and cracks developed at the rate transition in 633K water, but not in 673K steam. These effects also suggest that the use of a single activation energy for the oxidation process at all post-transition oxide thicknesses may be inappropriate.

### 3. The New Model

The basis of this model is that in-reactor the laboratory oxidation kinetics are modified by the cumulative generation of porosity resulting from the preferential dissolution of primary knock-on spikes induced by fast-neutron collisions with either hydrogen atoms in the water molecules at the oxide environment interface, with oxygen atoms within the oxide or in the water, or with zirconium atoms in the oxide or the metal. In general, we will assume that a damage spike that does not intersect the oxide-environment interface will not dissolve, although if it remains as a persistent area of damage or cubic  $ZrO_2$  there is a possibility that it might contribute when the oxide between it and the original oxide-environment interface becomes porous (Fig. 1). Damage spikes that do not dissolve will contribute to the small increase in diffusion controlled oxidation such as is seen in dry gaseous atmospheres[12].

In order to perform a direct numerical calculation of the corrosion rate predicted by this model, an estimate of the following quantities would be needed:-

- The number and dimensions of damage spikes resulting from various fast-neutron knock-on events.
- The rate of dissolution of such spikes as a function of temperature and water chemistry.
- The extent of any limitation to flow through the pores generated by dissolving these spikes as a result of reprecipitation of the dissolved material.
- The relative effect of individual pores on the local oxidation rate as a function of their size and closeness of approach to the oxide/metal interface.
- The effect of undissolved damage spikes, which do not intersect a free surface, on the diffusion controlled growth rate of any remaining barrier oxide layer.

Many of these quantities cannot be estimated, although sources of data such as those on the temperature and concentration dependence of the oxidation in LiOH solutions

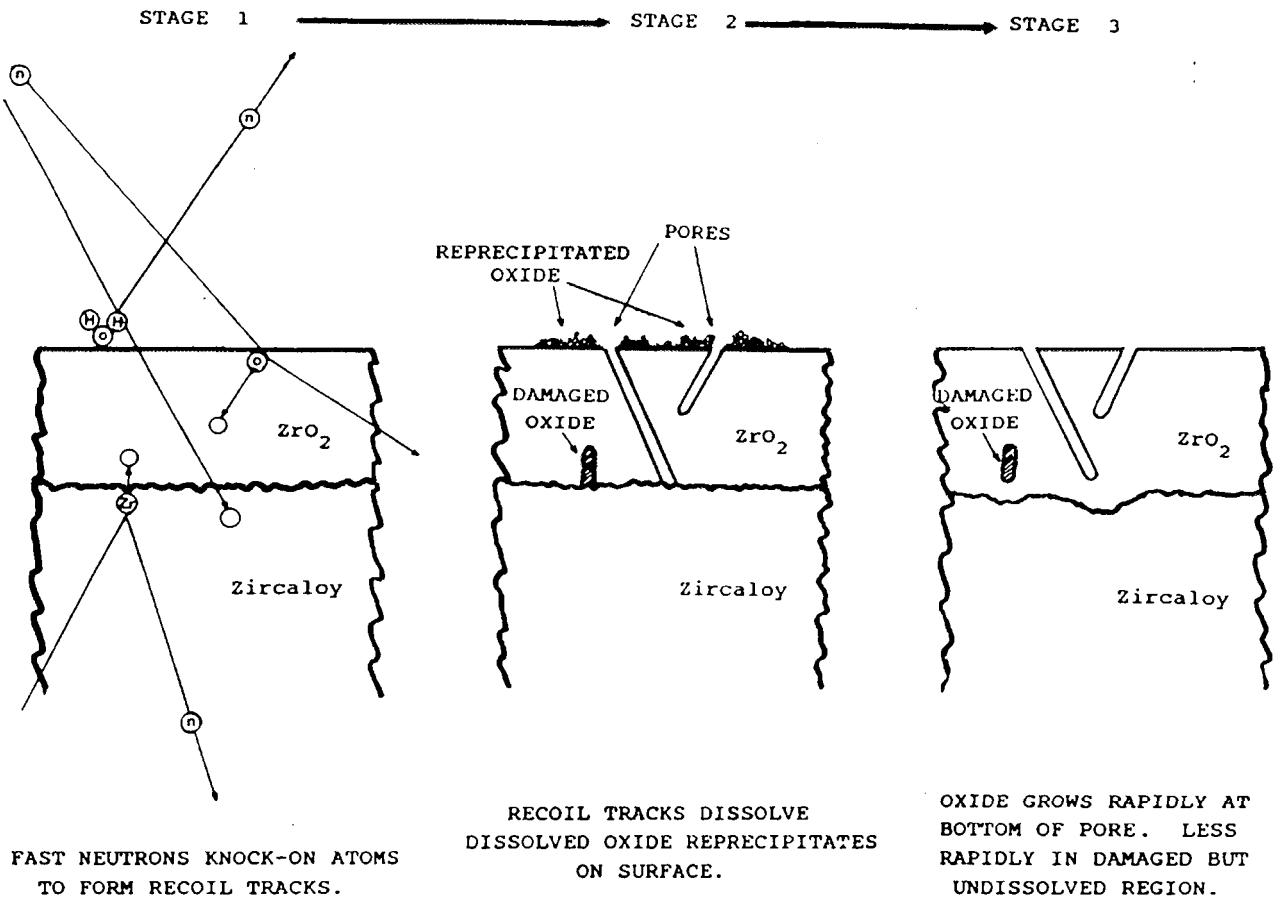


FIG. 1. Schematic diagram of irradiation corrosion mechanism.

may help because of the similarity of the proposed micromechanisms in the two situations. However, a model that was developed for the corrosion in uranyl sulphate solutions provides a framework for constructing the model proposed here[56].

The original hypothesis for the effect of irradiation on Zircaloy corrosion assumed that fast neutron or fission fragment damage spikes provided easy diffusion paths in the protective oxide film (or the barrier oxide layer during post-transition corrosion). A combination of irradiation and thermal annealing of these spikes provided a time-dependent recovery mechanism[57]. With the advantage of recent experimental evidence this would need modifying so that the easy diffusion path is now the dissolved, or partially dissolved, damage spike and the recovery process is the regrowth of a thicker barrier oxide at the base of the pore created by the dissolution process (Fig. 1). The form of the oxidation rate dependence should remain the same as that developed for the original hypothesis. Thus, we would expect to obtain a reciprocal rate/fast neutron flux equation of the form

$$\frac{1}{R} = \frac{K_1}{K_2\phi + R_x} + \frac{K_3}{R_y} \quad (1)$$

- Where
- R is the measured corrosion rate in-reactor
  - R<sub>x</sub> is the post-transition corrosion rate at the calculated metal-oxide interface temperature, for metal with the appropriate irradiation induced structure (R<sub>x</sub> will be fluence dependent)
  - R<sub>y</sub> is the rate of growth of oxide at the base of a pore that develops through to the oxide-metal interface (R<sub>y</sub> is the oxide free initial reaction rate of the metal)
  - K<sub>1</sub>,K<sub>2</sub> will be material dependent constants
  - K<sub>3</sub> is a constant that modifies R<sub>y</sub> because pores will only penetrate to the oxide-metal interface over a small fraction of the area, and may not penetrate right to the interface
  - φ is the fast neutron flux

This form of equation can be derived from the proposed in-reactor corrosion mechanism in the following way:

1. The oxidation rate in-reactor is postulated to be directly proportional to the number of "active" pores (N) present in the oxide film at any particular time. Thus

$$R = aN \quad (2)$$

2. If it is assumed that the recoil damage spikes dissolve rapidly compared with the rate of regrowth of oxide, then their formation rate will be proportional to the fast neutron flux. The effect of these pores will be eliminated when oxide has regrown at the bottom of them to a thickness equal to or greater than the normal barrier oxide thickness during post-transition oxidation. To a first approximation this regrowth can be assumed to be linear with time and proportional to the number of pores present. A second effect here will be the direct effect of irradiation on the diffusion controlled processes involved in this oxide regrowth. Previous evidence suggests that this should be an additive effect to the thermal process[38,39]. Thus the number of "active" pores (N) is given by

$$dN/dt = k_0a\phi - k_1N - k_2aN\phi \quad (3)$$

where  $k_0, k_1$  and  $k_2$  are constants associated with the production of pores, and their elimination by thermal and irradiation induced phenomena respectively.

3. During irradiation the number of active pores will reach a steady state condition such that

$$N_s = \frac{k_0a\phi}{k_1+k_2a\phi} = \frac{R_s}{a} \quad (4)$$

This can be rewritten to give the steady state in-reactor corrosion rate

$$\frac{1}{R_s} = \frac{k_1}{k_0a\phi} + \frac{k_2}{ak_0} \quad (5)$$

The first term in this equation represents the acceleration caused by irradiation, but will not reduce to the normal out-reactor corrosion rate at zero flux unless a further additive term is included. The second term is the oxide regrowth rate at the oxide-metal interface at the bottom of a pore. At infinite fast neutron flux this reaches a limiting value equal to the reaction rate of a bare zirconium alloy surface. The final equation then becomes

$$\frac{1}{R_s} = \frac{K_1}{K_2\phi + R_x} + \frac{K_3}{R_y} \quad \text{as noted above (with constants changed)}$$

$R_s$  and  $R$  will be equivalent for steady irradiation at a constant fast neutron flux.

For transients, however, there will be a difference that will be time dependent.

The form of the fast neutron flux dependence derived from the equation is very similar to that extracted by Garzarolli et al.[33] from their in-reactor data (Fig. 2).

## **4. Effects of Water Chemistry**

### **4.1 EFFECT OF RADIOLYSIS**

As presented here the in-reactor growth rate of uniform oxide shows no dependence on the water chemistry. Since the micromechanism involved is the dissolution of a recoil damage spike to create a pore, and since zirconia is an amphoteric oxide, we would not expect much difference in either pore formation or elimination rates whatever the effective pH of the reactor coolant. This is supported by the hydrothermal dissolution experiments of Somiya et al.[58] who found similar dissolution behaviour for  $ZrO_2$  in both concentrated acid and concentrated alkali solutions. P(H)WR coolants are usually on the alkaline side of neutral because of LiOH additions, whereas BWR coolant is effectively slightly acid of neutral pH because of the effects of radiolysis. To a first approximation, therefore, we would not expect to see much difference between in-reactor corrosion rates in P(H)WR and BWR coolants.

In practice this is the case. For Zircalloys heat treated to eliminate susceptibility to nodular corrosion the uniform oxide growth rates in BWRs are close to those expected for a PWR when allowance is made for the lower temperatures in BWRs[26]. Some data for material not showing nodular corrosion in BWRs are plotted in Fig. 3 in comparison with typical PWR data. Thus, the unique effect of the radiolytic species and other aspects of BWR water chemistry is only to produce nodular corrosion in susceptible batches of Zircaloy, and does not affect the uniform oxide growth. This model does not address the question of the mechanism of nodular corrosion, and in practice we are no nearer to an understanding of this phenomenon than we have ever been, despite the large number of mechanisms that have been proposed.

### **4.2 EFFECT OF LiOH**

The mechanism by which LiOH influences the corrosion rates of zirconium alloys appears to be formally identical to that proposed for the direct effect of fast neutron flux,

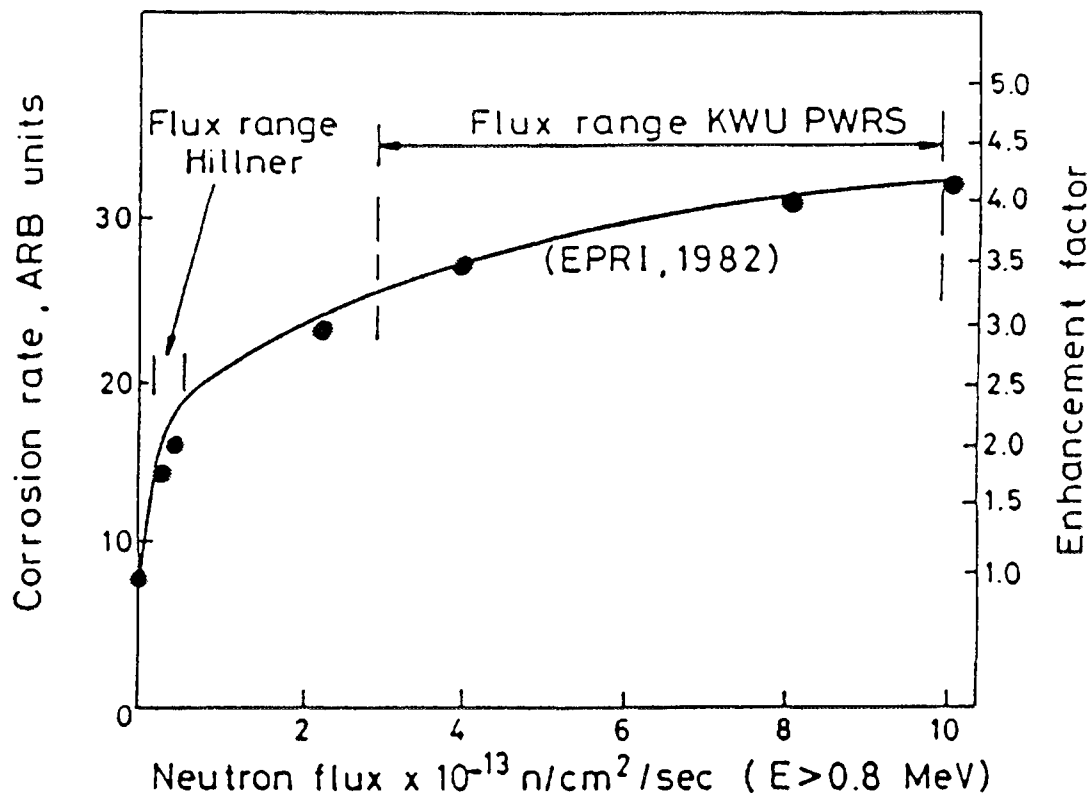


FIG. 2. Comparison of effect of neutron flux from KWU data with shape of dependency predicted by the new model.

namely, local dissolution at preferred sites in the oxide[41,42]. Recent work on the effect of transient exposures to high concentrations of LiOH[43] shows that the immediate effect is to rapidly change the depth of penetration of the porosity, without any large immediate change in weight gain (Fig. 4). After the chemistry transient the oxide grows rapidly to re-establish the normal protective oxide thickness, when the oxidation rate returns to its previous value (Fig. 5). Under these conditions, the dissolution takes place very rapidly compared with the rate of oxide regrowth, as was postulated above for the dissolution of recoil damage spikes during neutron irradiation.

Once the oxidation rate has returned to its normal value an increment in oxide thickness has been added as a result of the transient, when compared with the oxide thickness that would have been present at this time if no chemistry transient had been introduced (Fig. 5). Thus, the integrated effect of LiOH additions on the oxidation rate may be represented by an equation of the same form as that used to model effects of fast neutron flux. If this is the case then the data for effects of LiOH at various concentrations and temperatures, obtained from the literature, should appear as a series of straight lines

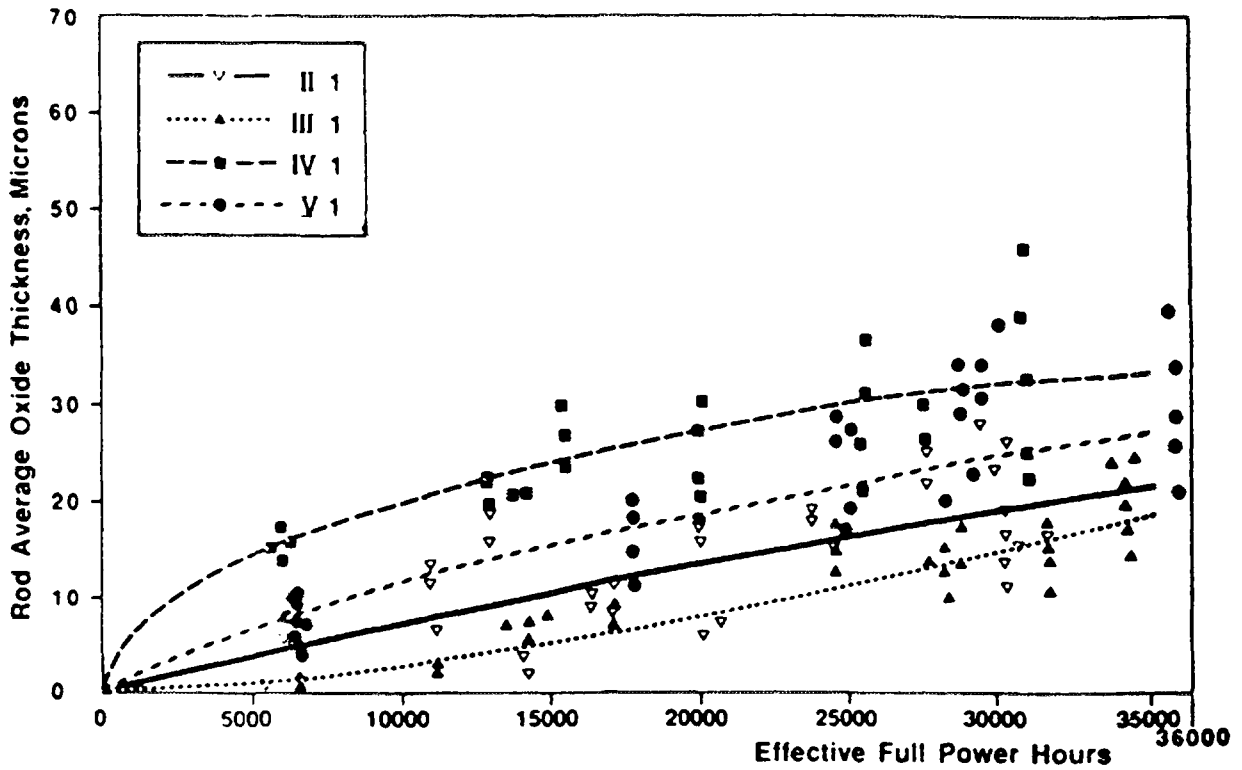


FIG. 3. Comparison of uniform oxide growth in BWRs and PWRs.

(a) Rod average oxide thickness versus EFPH in Ringhals 1, Barseback 1, Oskarshamn 1, Oskarshamn 2 and Forsmark 1[26].

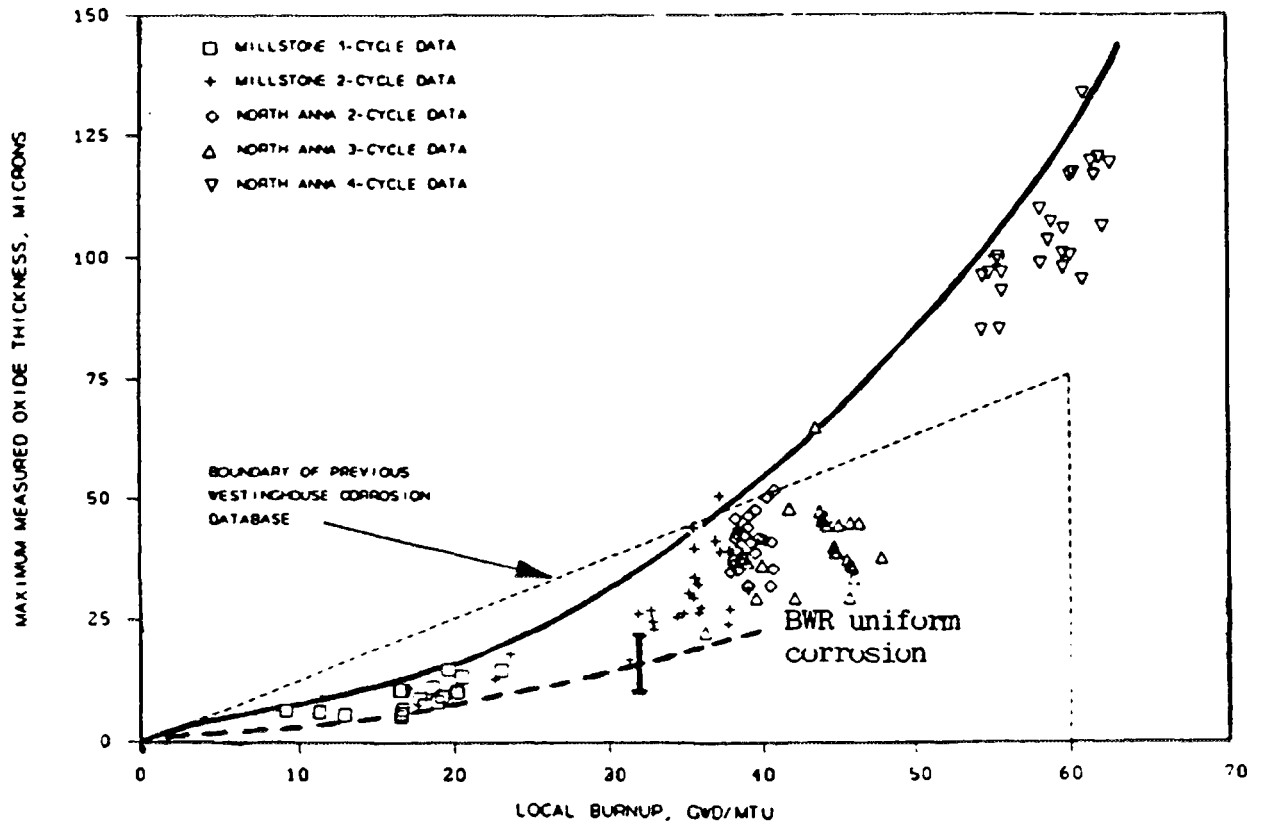


FIG. 3. Comparison of uniform oxide growth in BWRs and PWRs.

(b) Maximum measured oxide thickness vs. local burnup in Millstone and North Anna[32]

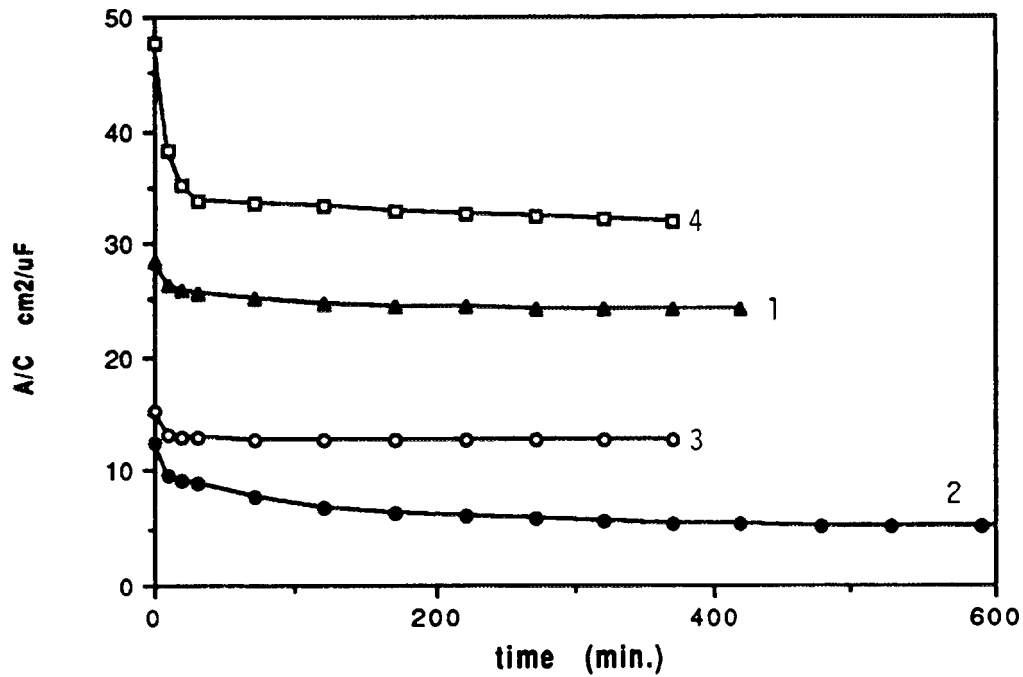


FIG. 4. Changes in pore depth following an LiOH transient[43]

- (1) Superficial porosity formed in original oxide in 0.1 mol. LiOH, 25d.
- (2) Effect of 1 day exposure to 1.0 mol. LiOH.
- (3) Regrowth of barrier oxide after 3 days in 0.1 mol. LiOH.
- (4) Continued regrowth after 7d. Initial impedance thickness is now higher because total oxide is thicker.

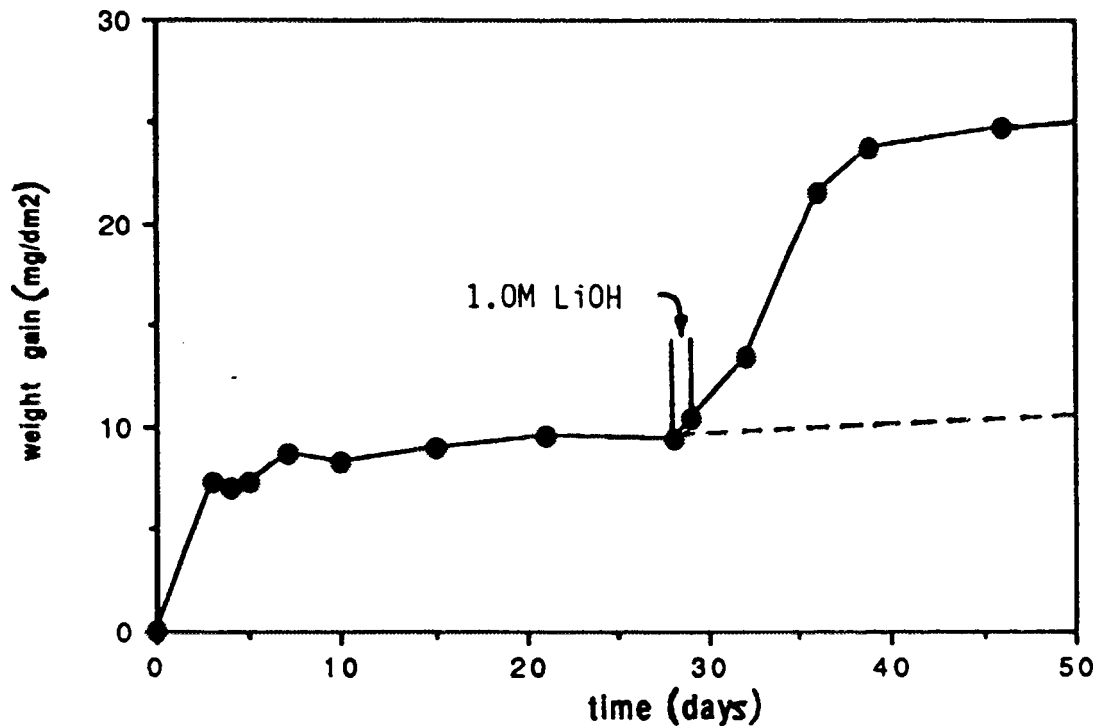


FIG. 5. Transient induced in an oxidation curve in 0.1 mol. LiOH solution at 573K by one day exposure to a 1.0 mol. solution at the same temperature[43].

on reciprocal rate versus reciprocal LiOH concentration plot. It can be seen (Fig. 6) that the literature data do fit such a model quite closely.

Thus, the effect of LiOH additions on in-reactor corrosion can probably be modelled by an additional reciprocal term in equation 1. Since there is no evidence for any interaction between the effects of fast neutron irradiation and effects of LiOH this term should probably be incorporated as a separate additive term. A further algorithm would be needed to calculate the actual concentration of LiOH in a porous oxide as a function of heat flux and the corrosion reaction[37].

Thus we obtain a composite equation of the form

$$\frac{1}{R} = \frac{K_1}{K_2\phi + R_x + R_{Li}} + \frac{K_3}{R_y} \quad (6)$$

Where  $R_x = C_1 D_0 R_0 \exp^{-Q/RT}$

and  $\frac{1}{R_{Li}} = \frac{K_4}{[LiOH]_{ox}}$

$C_1$  is a proportionality constant that reflects the change in post-transition oxidation rate for specimens pre-irradiated to a fast neutron fluence  $D_0$ .

$K_4$  is a constant derived from Fig. 6, and the calculated LiOH concentration at the bottoms of pores in a thick oxide must be used.

Evidence shows that there will probably be LiOH concentration effects that result from both the effect of heat flux and the concentrating effects of the corrosion reaction itself in the absence of heat flux[59]. Since in this model the LiOH merely acts to dissolve the oxide locally, and this oxide reprecipitates as a hydrated oxide on the cladding surface (or other surfaces), there is no necessity for any prior Li incorporation in the oxide film in order to see the effect. The LiOH causing the effect would be expected to be readily leachable, and any Li incorporated in the reprecipitated oxide during this reprecipitation process would be a consequence of the mechanism and not a cause of the effect. Any apparent effect of Li implantation in the oxide would be evident only if it affected the proportion of tetragonal  $ZrO_2$  in the oxide, and might actually be merely a damage effect caused by the implantation itself[60].

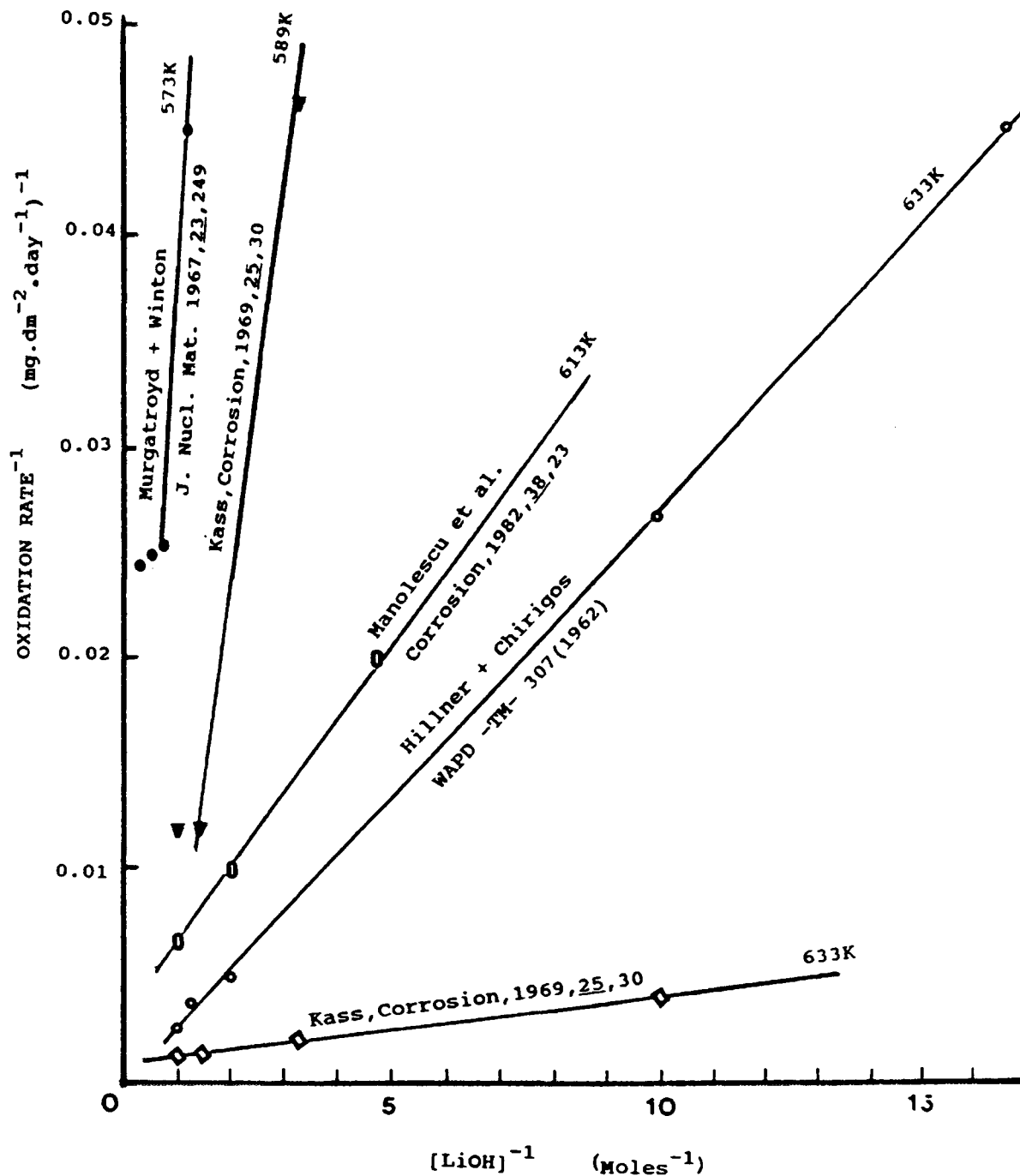


FIG. 6. Reciprocal rate plot of the literature data for the effect of lithium hydroxide on Zircaloy corrosion.

## 5. Conclusions

It has been shown that models based on the use of multiplicative irradiation factors and out-reactor kinetics do not give a good fit for both heat transfer and non-heat transfer surfaces in-reactor. A new model based on a micromechanistic process whereby recoil damage tracks from fast neutron recoils are rapidly dissolved to form pores which are then

eliminated by regrowth of additional oxide is proposed. It is shown that it can give a good fit to results for effects of fast neutron irradiation. It is also demonstrated that increases in corrosion rates resulting from LiOH concentration effects can be incorporated using an analogous mechanism where LiOH also dissolves the oxide locally to generate pores. LiOH effects can be incorporated in the same model by an additional additive term. This model predicts that uniform corrosion of Zircalloys should be little affected by reactor water chemistry. This is in line with observations on Zircaloy fuel cladding heat treated to eliminate nodular corrosion.

### REFERENCES

- [1] COX, B., *Advances in Corrosion Science and Technology*, M. G. Fontana and R. W. Staehle, Eds., Vol. 5, Plenum, N.Y. (1976), 177.
- [2] "Corrosion of Zirconium Alloys in Nuclear Power Plants", International Atomic Energy Agency, Vienna, IAEA-TECDOC-684, (Jan. 1993).
- [3] GRIGGS, B., MAFFEI, H.P., SHANNON, D.W., *Electrochem. Soc.*, 109, (1962), 665.
- [4] KASS, S., *Corrosion*, 23, (1967), 374.
- [5] PETERS, H.R., ASTM-STP-824, (1984), 507-518.
- [6] CORIOU, H., GRALL, L., MEUNIER, J., PELRAS, M., WILLERMOZ, J., *J. Nucl. Mater.*, 7, (1962), 320.
- [7] HILLNER, E., CHIRIGOS, J., "The Effect of Lithium Hydroxide and Related Solutions on the Corrosion Rate of Zircaloy-2 in 680°F Water", U.S. Report, WAPD-TM-307, Bettis Atomic Power Lab. (1967).
- [8] MURGATROYD, R.A., WINTON, J., *J. Nucl. Mater.*, 23, (1967), 249.
- [9] KASS, S., *Corrosion*, 25, (1969), 30.
- [10] MacDONALD, S.G., SABOL, G.P., SHEPPARD, K.D., ASTM-STP-824, (1984), 519-530.
- [11] MANOLESCU, A.V., MAYER, P., SIMPSON, C.J., *Corrosion*, 38, (1982), 23.
- [12] COX, B., *J. Nucl. Mater.*, 28, (1968), 1.

- [13] HILLNER, E., ASTM-STP-754, (1982), 450-478.
- [14] RAMASUBRAMANIAN, N., "Corrosion and Hydriding of Zircaloy-4 Fuel Cladding in a CANDU Fuel Channel", Proc. EPRI-PWR Fuel Corrosion Workshop, Washington, DC, July 28-30, 1993 (to be published).
- [15] IRVIN, J.E., Electrochem. Tech., 4, (1966), 240.
- [16] JOHNSON, A.B., JR., "Aqueous Corrosion and Hydriding of Zirconium Alloys in Nuclear Reactor Environments", Proc. 4th Int. Cong. on Metallic Corrosion, Amsterdam, National Association of Corrosion Engineers, (1972), 168-177.
- [17] JOHNSON, A.B. JR., "A Review of Corrosion Phenomena on Zirconium Alloys, Niobium, Titanium, Inconel, Stainless Steel and Nickel Plate under Irradiation", Revs. on Coatings and Corrosion, Ed. J. Yahalom, Vol. 4, Freund, Tel Aviv, (1975), 299.
- [18] JOHNSON, A.B., JR., "Zirconium Alloy Oxidation and Hydriding Under Irradiation: Review of Pacific Northwest Laboratory's Test Program Results", U.S. Report EPRI-NP-5132, Electric Power Research Inst. (1987).
- [19] NELSON, R.C., "The Corrosion of Zircaloy-2 Fuel Element Cladding in a Boiling Water Reactor", Proc. USAEC Symp./ in Zirconium Alloy Development, Pleasanton, CA, 1962, U.S. Report GEAP-4089, Vol. 2, #17, General Electric Co.
- [20] TROWSE, F.W., SUMERLING, R., GARLICK, A., ASTM-STP-633 (1977), 236-257.
- [21] SUMERLING, R., GARLICK, A., STUTTARD, A., HARTOG, J.M., TROWSE, F.W., SIMS, P., ASTM-STP-681 (1979), 107-121.
- [22] COX, B., "Mechanistic Understanding of Nodular Corrosion", U.S. Report EPRI-NP-6944-D, Electric Power Research Institute (1990).
- [23] CHENG, B., ADAMSON, R.B., ASTM-STP-939 (1987), 387-416.
- [24] GARZAROLLI, F., STEHLE, H., STEINBERG, E., WEIDINGER, H., ASTM-STP-939 (1987), 417-430.
- [25] RUDLING, P., LUNDBLAD-VANNESJO, K., VESTERLUND, G., MASSIH, A.R., ASTM-STP-939 (1987), 292-306.

- [26] RUDLING, P., MACHIELS, A.J., ASTM-STP-1023 (1989), 315-333.
- [27] GARZAROLLI, F., JORDE, D., MANZEL, R., PARRY, G.W., SMERD, P.G., "Review of PWR Fuel Rod Waterside Corrosion Behaviour", U.S. Report EPRI-NP-1472, Electric Power Research Inst. (1980).
- [28] DALGAARD, S.B., "Long-Term Corrosion and Hydriding of Zircaloy-4 Fuel Clad in Commercial Pressurized Water Reactors with Forced Convective Heat Transfer", Presented at Electrochem. Soc., Spring Meeting, Washington, DC (1976).
- [29] DICKSON, I.K., EVANS, H.E., JONES, K.W., J. Nucl. Mater., 80, (1979), 223.
- [30] SMALLEY, W.R., "Saxton Core II AND III, Fuel Performance Evaluation, Part I - Materials", U.S. Report WCAP-3385-56 AND 57, Westinghouse Electric Co. (1971 AND 1974).
- [31] MELEHAN, J.B., KUNISHI, H., SMALLEY, W.R., BALFOUR, M.G., de STEFANO, J., PERRY, W.R., "Interim Report, Trojan Cycle 3 Fuel Performance", U.S. Report WCAP-9963, Westinghouse Electric Co. (1981).
- [32] SABOL, G.P., LEACH, W.J., WEINER, R.A., MILLER, R.S., "Corrosion Modelling and ZIRLO Performance Update", Paper presented at EPRI-PWR Fuel Corrosion Workshop, Washington, DC, USA, 28-30 July 1993, Electric Power Research Institute (to be published).
- [33] GARZAROLLI, F., JUNG, W., SCHOENFELD, H., GARDE, A.M., PARRY, G.W., SMERD, P.G., "Waterside Corrosion of Zircaloy Fuel Rods", U.S. Report, EPRI-NP-2789, Electric Power Research Institute (1982).
- [34] KAISER, R.S., MILLER, R.S., MOON, J.E., PISANO, N.A., "Westinghouse High Burnup Experience at Farley 1 and Point Beach 2", Proc. ANS Topical Meeting on LWR Fuel Performance, Williamsburg, VA, (April 1988), 119-124, American Nuclear Society.
- [35] CLAYTON, J.C., FISCHER, R.L., "Corrosion and Hydriding of Zircaloy Fuel Rod Cladding in 633K Water and Reactor Environments", Proc. ANS Topical

Meeting on Light Water Reactor Fuel Performance", Orlando, FL, (April 1985), Paper 3-1, American Nuclear Society.

- [36] ALMARSHAD, A.I.A., KLEIN, A.C., *J. Nucl. Mater.*, 183, (1991), 186.
- [37] BILLOT, Ph., GIORDANO, A., *ASTM-STP-1132* (1991), 539-565.
- [38] COX, B., "Assessment of PWR Waterside Corrosion Models and Data", U.S. Report EPRI-NP-4287, Electric Power Research Inst., (1985).
- [39] COX, B., "Assessment of In-Reactoer Corrosion Models and Data for Zircalloys in Water", *Proc. 2nd Int. Symp. on Environmental Degradation of Materials in Nuclear Systems - Water Reactors*", Monterey, CA, (Sept. 1985), Amer. Nuclear Soc.
- [40] COX, B., "Modelling the Corrosion of Zirconium Alloys in Nuclear Reactors Cooled by High Temperature Water", *Proc. NATO Adv. Res. Workshop on Modelling Aqueous Corrosion*, RNEC Manadon, U.K., (Sept. 1993), (to be published).
- [41] COX, B., WONG, Y-M., *ASTM-STP-1132* (1991), 643-662.
- [42] COX, B., WU, C., *J. Nucl. Mater.*, 199, (1993), 272.
- [43] COX, B., WU, C., *J. Nucl. Mater.*, to be published.
- [44] BEIE, H.J., MITWALSKY, A., GARZAROLLI, F., RUHMANN, H., SELL, H.F., "Examinations on the Corrosion Mechanism of Zirconium Alloys", Presented at 10th Int. Symp. on Zirconium in the Nuclear Industry, Baltimore, MD, (June 1993), *ASTM-STP*-to be published.
- [45] COX, B., FIDLERIS, V., *ASTM-STP-1023* (1989), 245-265.
- [46] COX, B., "AECL Experiments on the Corrosion of Zirconium Alloys Under Irradiation", *Canadian Report AECL-2257*, Atomic Energy of Canada Ltd., (1965).
- [47] COX, B., ALCOCK, K., DERRICK, F.W., *J. Electrochem. Soc.*, 108, (1961), 129.
- [48] JOHNSON, J.R., *Trans. Met. Soc. AIME*, 212, (1958), 13.
- [49] WITTELS, M.C., SHERRILL, F.A., *J. Appl. Phys.*, 27, (1956), 643.
- [50] WITTELS, M.C., SHERRILL, F.A., *Phys. Rev. Lett.*, 3, (1959), 176.

- [51] ADAM, J., COX, B., J. Nucl. En. (A), 11, (1951), 31.
- [52] ADAM, J., COX, B., Phys. Rev. Lett., 3, (1959), 543.
- [53] ADAM, J., COX, B., J. Nucl. En. (A/B), 17, (1963), 435.
- [54] JENKS, G.H., "Effects of Irradiation on the Corrosion of Zircaloy-2", U.S. Report, ORNL-CF-57-9-11, Oak Ridge National Laboratory (1957).
- [55] COX, B., YAMAGUCHI, Y., J. Nucl. Mater., to be published.
- [56] JENKS, G.H., ASTM-STP-378 (1964), 41-57.
- [57] JENKS, G.H., "Review and Correlation of In-Pile Zircaloy-2 Corrosion Data and a Model for the Effect of Irradiation", U.S. Report ORNL-3039, Oak Ridge National Lab. (1961).
- [58] SOMIYA, S., "Hydrothermal Reactions for Materials Science and Engineering", Elsevier Applied Science, NY, (1989).
- [59] CAUSEY, A., URBANIC, V.F., COLEMAN, C.E., J. Nucl. Mater., 71, (1977) 25.
- [60] BILLOT, Ph., BESLU, P., ROBIN, J.C., "Consequences of Lithium Incorporation in Oxide Films Due to Irradiation Effect", Proc. ANS Topical Meeting on Fuel for the 90's", Avignon, France, Vol. 2, (1991), 757-769, American Nuclear Society /European Nuclear Society.



**EFFECT OF ELEVATED LITHIUM ON THE WATERSIDE  
CORROSION OF ZIRCALOY-4:  
EXPERIMENTAL AND PREDICTIVE STUDIES**

D. PÊCHEUR, A. GIORDANO, E. PICARD, Ph. BILLOT  
Commissariat à l'Energie Atomique, Cadarache

J. THOMAZET  
FRAMATOME, Nuclear Fuel Division, Lyon

France

**Abstract**

Lithium and boron content in the coolant are known to influence the oxidation behaviour of the fuel cladding. Since new PWR operating conditions could consist in an increase of the lithium and the boron concentration in the coolant early in the cycle, a specific study has been conducted to analyze and to predict the effect of such new water chemistry conditions on the oxidation kinetics of the Zircaloy-4 material. Experimental studies have been performed in out-of-pile loop tests, under one and two phase flow heat transfer in various water chemistry conditions ( $0 \leq \text{Li} \leq 350$  ppm,  $0 \leq \text{B} \leq 1000$  ppm,  $0 \leq \text{K} \leq 56$  ppm). A simulation of the effect of elevated lithium on the corrosion has been made using the semi-empirical COCHISE corrosion code.

Under one phase flow heat transfer conditions, the addition of lithium hydroxide in the coolant increases the oxidation rate, essentially in the post-transition regime for low lithium levels ( $\leq 75$  ppm) and immediately in the pre-transition phase for very high lithium level (350 ppm). Under two phase flow heat transfer, an enhancement of the corrosion is observed in the area of the rod submitted to boiling. Based on the out-of-pile loop test performed in presence of KOH instead of LiOH, such an enhancement of the corrosion appears to be due to a lithium enrichment in the oxide layer induced by boiling and not to a pH effect.

The simulation of the increase of lithium content in the coolant from 2.2 to 3.5 ppm leads to an enhancement in corrosion rates which becomes only significant at high burn up. This predictive result of elevated lithium effect on corrosion is then compared with oxidation data derived from reactors operating under an elevated lithium regime.

## **1. Introduction**

The new types of fuel management (extended cycle up to 18 months, higher burn up) will bring to think over new primary coolant chemistry (for example, an increase of the boron content in the coolant). Nevertheless, to maintain the pH<sub>300</sub> of the primary coolant between the recommended values of 7.2 and 7.4, it will be necessary to increase the lithium content in the fluid above 2.2 ppm, typically to 3.5 ppm. Moreover, another current trend to improve the performance of PWRs is to increase the water temperature. This trend towards high thermal efficiency can lead to boiling over a small fraction of the fuel rods and can increase the concentration of lithium hydroxide and boric acid at their surfaces. Such increases of lithium and boron in coolant and at the surface of the fuel rods are known to have consequences in cladding corrosion [1-4]. So, before operating such new conditions in reactor (longer cycle, higher burn up and coolant temperature), it is necessary to complete these previous studies and, particularly, to predict the effect of an increase in lithium content in the coolant on the corrosion performance of the fuel cladding.

In this work, the corrosion behaviour of the Zircaloy-4 cladding is investigated in out-of-pile loop tests, under one and two phase flow heat transfer, with various water chemistries. After reporting experimental results, the effect of lithium and boron on corrosion is analyzed and modelled empirically. A corrosion code based on these experimental results is then developed and used to predict the impact on corrosion of increasing lithium content in the primary coolant from 2.2 to 3.5 ppm. The result of this simulation is then compared with in reactor oxidation data.

## **2. Experimental procedure and corrosion model**

### **2.1. Out-of-pile loop corrosion tests**

The material tested in the experimental program is standard Zircaloy-4 cladding tubing in a stress relieved state. It is oxidized in out-of-pile loop tests simulating the PWRs operating conditions except the neutron flux. Boiling regimes of the primary fluid are obtained for higher temperature and power levels. The parameter used to characterize the boiling phenomenon is the void fraction ( $\alpha$ ). It is

Tab.1 . Thermalhydraulic and chemical conditions of the oxidation tests performed in out-of-pile loops.

Corrosion Tests	Li (ppm)	B (ppm)	K (ppm)	pH300	Flux (W/cm <sup>2</sup> )	T <sub>wall</sub> (°C)	P (bars)	Void fraction (%)	Time (EPFD)
C12	10	1000	0	7.7	103	344	150	<35	50
C13	0	1000	56	7.7	103	344	150	<35	50
CX1	5	650	0	7.5	100	347	154	<30	171
CIR	2.2	650	0	7.2	100	347	154	<3	368
RE1	40	0	0	9.1	100	363	190	<3	31
RE2	75	0	0	9.3	100	363	190	<3	13
RE5	350	0	0	9.8	100	363	190	<3	11

defined as the percentage of surface occupied by the vapor phase in the section of the hot channel and calculated using the CEA thermalhydraulic code FLICA. In this work,  $\alpha$  is ranging between 0 (no boiling) and 40% (high boiling rates). The corrosion behaviour of the Zircaloy-4 tubing is studied under various lithium and boron concentrations in the primary fluid, in the range of 0 to 350 ppm for lithium and 0 to 1000 ppm for boron. An additional out-of-pile loop corrosion test is performed in equivalent coolant pH but in presence of KOH instead of LiOH to separate pH and cations ( $\text{Li}^+$ ,  $\text{K}^+$ ) effects. The average thermal/hydraulic and chemical parameters of these oxidation tests are presented in Table 1. The thicknesses of the oxide layer grown on the fuel rods are measured by the eddy current technique.

## 2.2. Corrosion model (COCHISE code)

The corrosion data measured from the out-of-pile loop tests are used to develop a semi-empirical corrosion growth code (COCHISE). In this model, the Zircaloy-4 oxidation kinetics are represented by Arrhenius type laws such as  $D=D_0 \exp(-Q/RT)$ . The two stages of the corrosion kinetics, in the pre- and post-transition regimes which are characterized respectively by cubic and linear oxidation rates [5], are then described as follows :

In the pre-transition regime : 
$$\frac{dS^3}{dt} = K_{pre} \exp \frac{-Q_{pre}}{R \cdot T_i}$$

In the post-transition regime : 
$$\frac{dS}{dt} = K_{post} \exp \frac{-Q_{post}}{R \cdot T_i}$$

$$T_i = T_w + \frac{\phi \cdot S}{\lambda}$$

where S = oxide thickness

K = frequency factor in the pre- and post-transition regimes

Q = activation energy in the pre- and post-transition regimes

T<sub>i</sub> = metal-oxide interface temperature

T<sub>w</sub> = wall temperature

φ = heat flux

λ = oxide thermal conductivity

The COCHISE code and, particularly, the means to determine the frequency factors and the activation energies through experimental corrosion data have been extensively described previously [6]. This corrosion code is then used to predict the corrosion behaviour of the Zircaloy-4 cladding in out-of-pile and in reactor conditions.

### 3. Experimental results : Lithium effect under two phase flow heat transfer

The axial profile of oxidation measured on the cladding corroded during the C12 CIRENE corrosion test is presented in Fig.1 as a function of the void fraction. The main result consists in an acceleration of the corrosion kinetics in the part of the fuel rod submitted to boiling conditions (i.e. high void fraction). As observed in this figure, the corrosion rates increase with the void fraction. This phenomenon is characterized by an oxidation enhancement factor (F<sub>α</sub>) described as followed :

$$F\alpha = \frac{S_\alpha}{S_0} \quad \text{where} \quad S\alpha = \text{oxide thickness measured in the area of boiling}$$

S<sub>0</sub> = oxide thickness measured in the area of one phase flow heat transfer conditions (at the same wall temperature).

CIRENE P=150 bars  
(50 EFPD)  $0 < \alpha < 35\%$

(B) = 1000 ppm  
(Li) = 10 ppm  
pH300 = 7.7

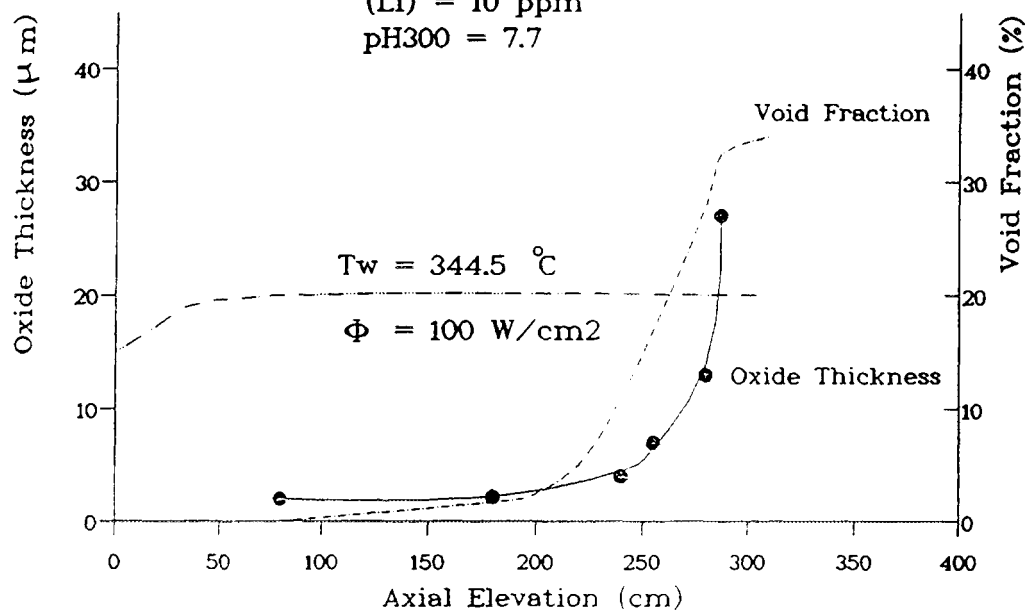


Fig.1 . Oxide thicknesses grown on the cladding during the C12 corrosion loop test versus void fraction : axial oxidation profile.

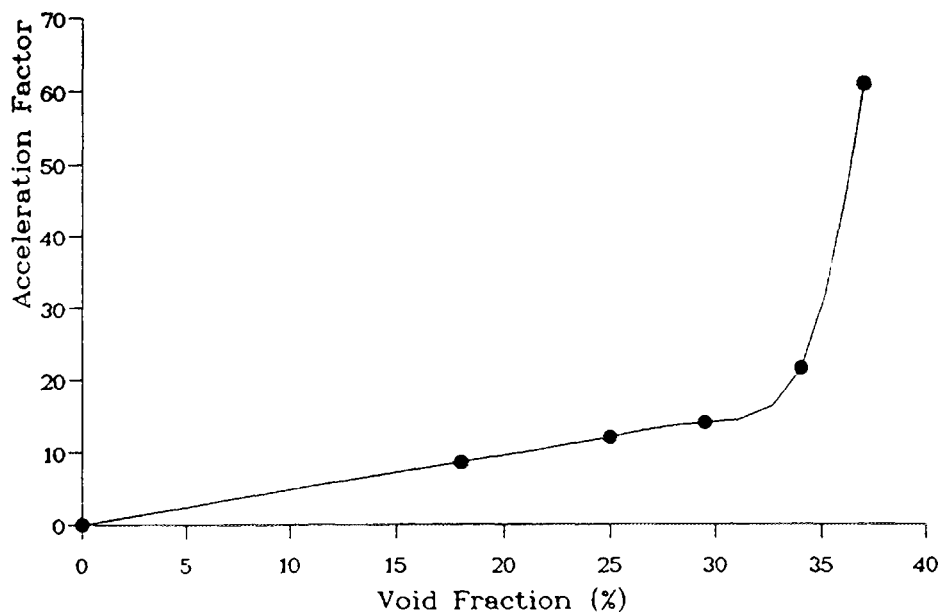


Fig.2 . Factor of oxidation enhancement of a fresh tube versus void fraction. Tube oxidized during the C12 corrosion loop test.

■ — LI-CONCENTRATION IN THE OXIDE FILM  
 ● — CALCULATED AVERAGE VOID FRACTION PROFILE

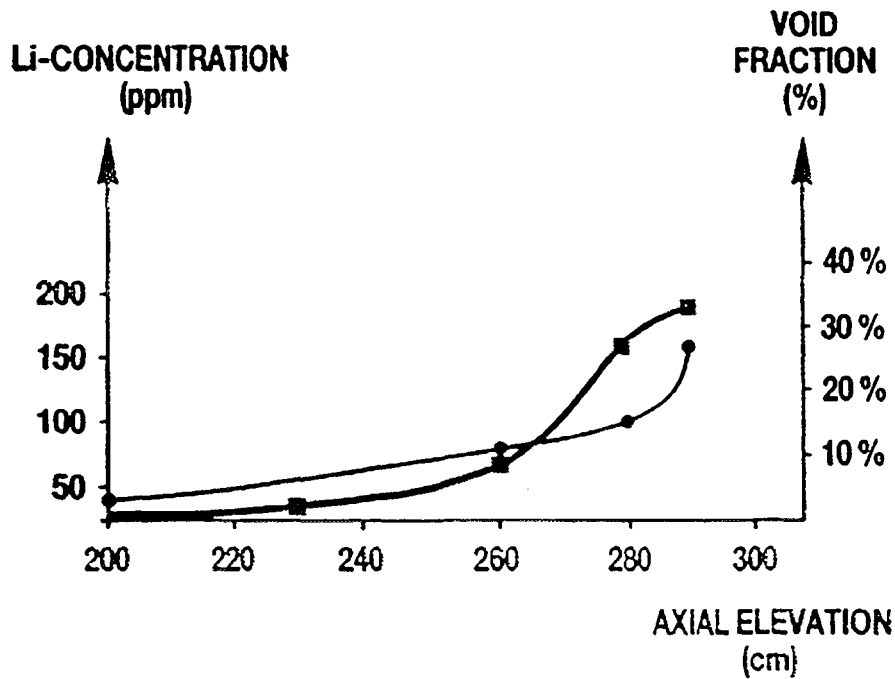


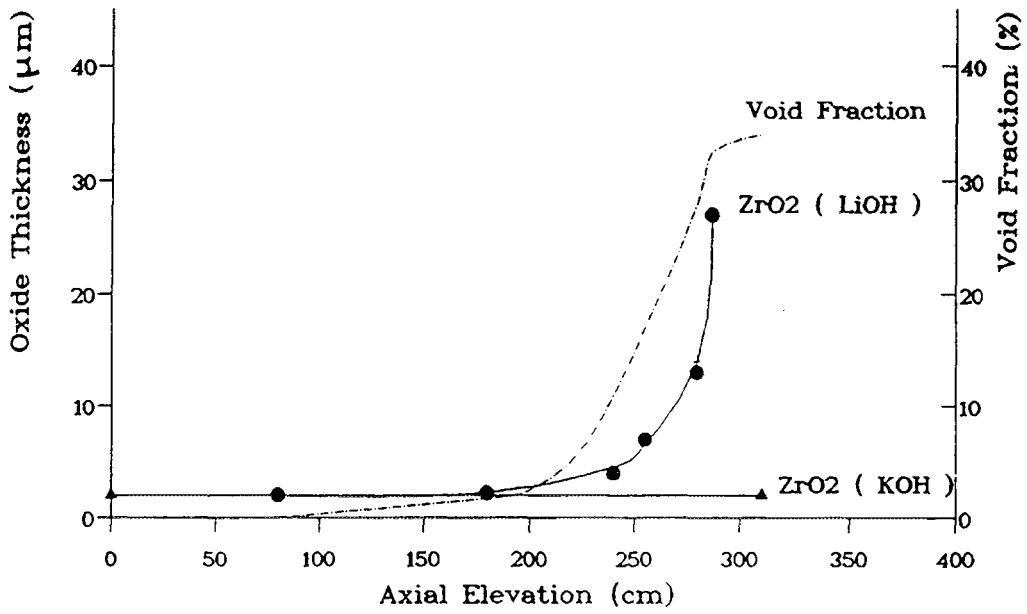
Fig.3 . Lithium concentration in the oxide layer grown during the C12 corrosion loop test versus the void fraction.

This factor increases gradually from 1 to 20 up to a void fraction of 34% and then increases strongly for upper void fraction (Fig.2).

After measuring oxide thicknesses, a lithium concentration profile has been determined in the oxide layer by atomic absorption as a function of void fraction. The results of these analysis are presented in Fig.3. They show that the lithium concentration in the oxide layer increases with the void fraction, from a few ppm for low void fraction ( $\alpha < 3\%$ ) to more than 150 ppm for higher void fraction ( $\alpha \approx 30\%$ ). This indicates therefore that, on the one hand, the boiling conditions induce a lithium enrichment in the oxide layer and, on the other hand, the acceleration in corrosion kinetics is related to this lithium enrichment .

However, if the acceleration in corrosion kinetics can be induced by a lithium enrichment in the oxide layer due to boiling conditions, a local increase in coolant pH can also be involved. In order to check the particular lithium effect, the above

a



b

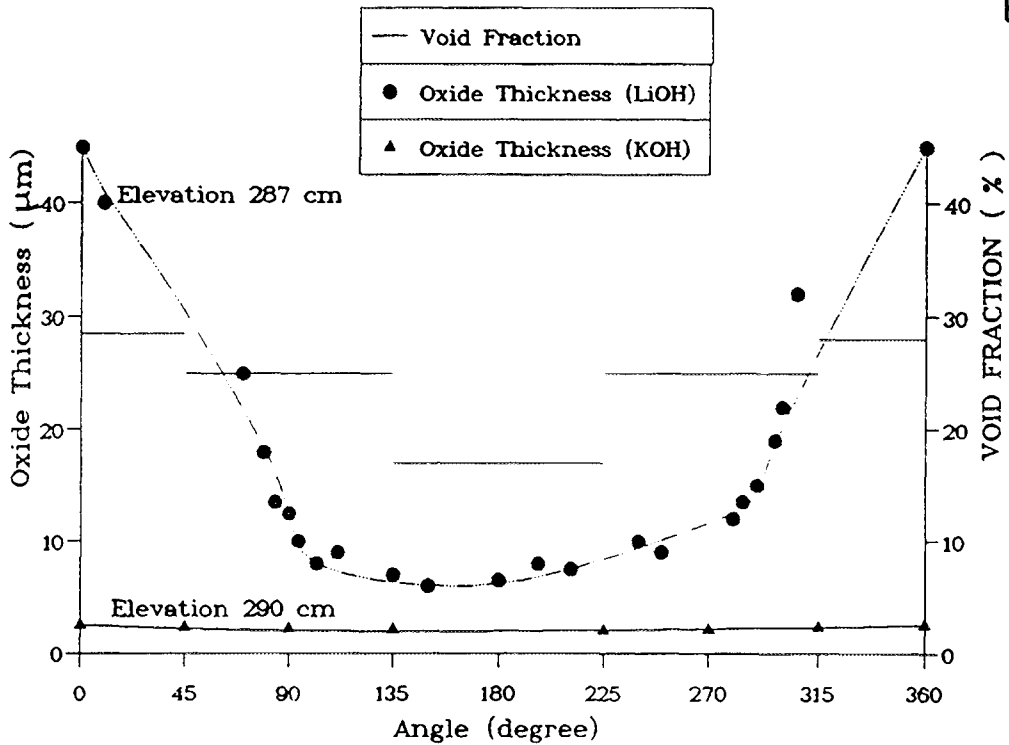


Fig.4 . Comparison between the oxide thicknesses grown on the cladding in LiOH environment (C12 test) and those grown in KOH environment (C13 test), versus the void fraction : a) axial and b) azimuthal oxidation profile.

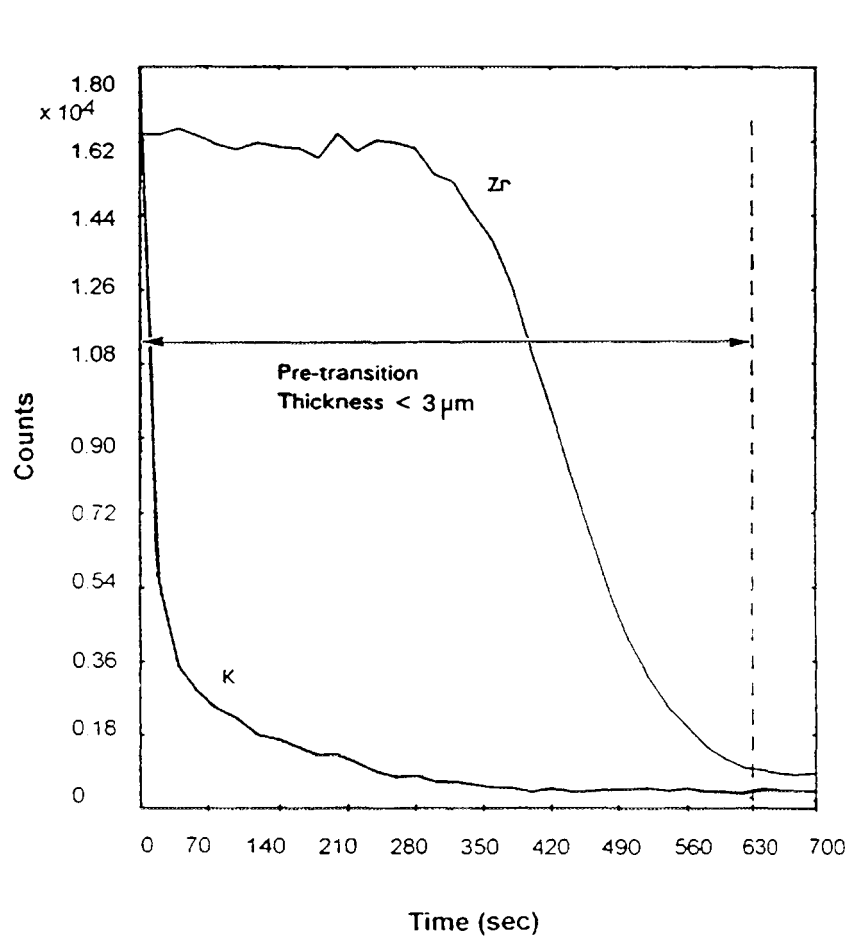
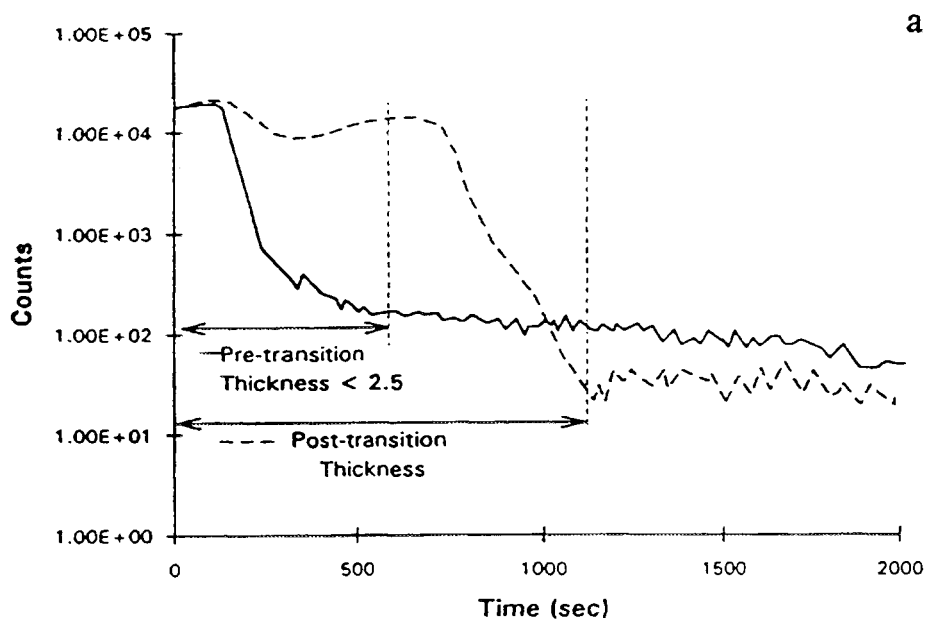


Fig.5 . Profile of lithium (a) and potassium (b) in oxide layers grown in LiOH and KOH environments, respectively.

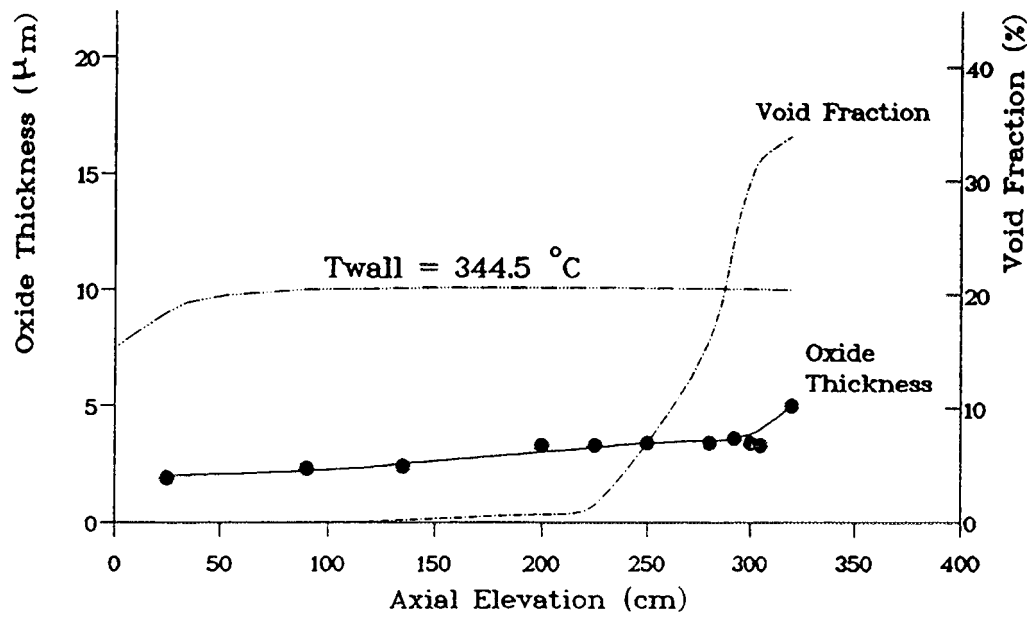


Fig.6 . Axial oxidation profile of pre-oxidized cladding versus void fraction. Tube oxidized during the C12 corrosion loop test.

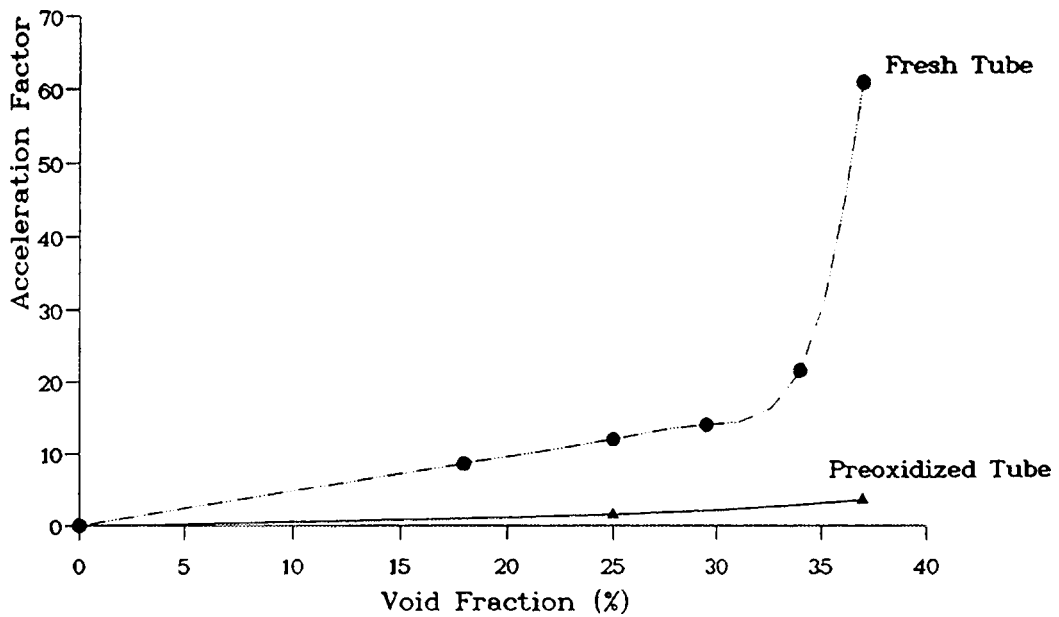


Fig.7 . Comparison between the factor of oxidation enhancement of a fresh tube and of a pre-oxidized one versus the void fraction. Tubing oxidized during the C12 corrosion loop test.

results have been compared with those obtained in the C13 CIRENE corrosion loop test which has been performed at the same coolant pH but in presence of KOH instead of LiOH. As presented in Fig. 4a and 4b, the oxide thicknesses obtained during this test (with KOH) remain constant along the rod (about 2  $\mu\text{m}$  thickness) and are independent of the void fraction for both axial and azimuthal oxidation profiles. So, in opposition to the corrosion test performed using LiOH, no enhancement of the corrosion rates are observed with potassium hydroxide, even in the area of very high void fraction ( $\alpha = 35\%$ ). In addition to these oxidation kinetics considerations, SIMS analysis have been conducted on oxide layers grown in LiOH and KOH environments. They reveal a lithium enrichment in the pre-transition oxide layer grown in the presence of LiOH (Fig.5a) while no significant trace of potassium is observed in the one grown in the presence of KOH (Fig.5b). This result can be related to the difference in the potassium and lithium ionic radius which are equal to 1.33 Å and 0.78 Å, respectively. The analysis of the post-transition oxide layer grown in LiOH environment shows an uniform lithium distribution in the external porous oxide layer.

The C12 corrosion test has also been performed in order to study the behaviour of a pre-oxidized cladding. Before this oxidation test, an oxide layer of about 3  $\mu\text{m}$  thickness had been developed on this tube for 128 EPFD under one-phase flow heat transfer conditions with a lithium and boron content in the coolant equal to 2.2 and 1000 ppm, respectively. During the C12 corrosion test (Li=10 ppm,  $\alpha_{\text{max}}=35\%$ ), no significant accelerated corrosion is observed on this pre-oxidized fuel rod, even in the area of very high void fraction (Fig.6), while, as reported above, fresh tubing exhibited high accelerated corrosion rates. In the case of the corrosion of pre-oxidized cladding, the enhancement factor of oxidation never goes beyond 3 (at  $\alpha=35\%$ ) compared to 60 for fresh tubing (Fig.7). This singular behaviour of the pre-oxidized tube with respect to the fresh one can be related to the presence of the oxide film of 3  $\mu\text{m}$  thickness, grown in low aggressive conditions (2.2 ppm of lithium, in liquid phase) prior to the corrosion test performed in more aggressive conditions (10 ppm of lithium, boiling conditions). This pre-transition oxide layer formed

appears therefore to keep a protective effect with regard to more aggressive conditions.

#### 4. Modeling results

##### 4.1. Lithium and boron effect under one phase flow heat transfer

In the COCHISE code, the influence of lithium and boron content on the oxidation kinetics is taken into account based on the experimental program conducted in out-of-pile corrosion tests under various chemistry conditions.

*Lithium effect* : From out-of-pile loop test performed under one phase flow heat transfer, it is observed that the increase of lithium content in the coolant increases the oxidation rates of the Zircaloy-4 cladding. This result is valid in presence or not of boron and is consistent with those previously reported by Kass [1], Hillner [2] and Mc Donald [3]. In absence of boric acid, at low lithium levels ( $\leq 75$  ppm), this corrosion enhancement occurs essentially during the post-transition phase while, at very high lithium level (350 ppm), no pre-transition phase is observed. These results are consistent with those of Evans [7] who has shown that, in the absence of boron, oxidation rates are enhanced in the post-transition phase for lithium levels  $\geq 7$  ppm while, in the pre-transition regime, they are increased only for very high lithium levels ( $\geq 420$  ppm). The analysis of these results have led to the development of correlations between the lithium content and the two following parameters : the frequency factors (K) and the activation energies (Q). The lithium effect is then expressed as follows :

$$Q_{pre} = 16950 + 23 [Li]$$

$$Q_{post} = 17860 + 20.4 [Li]$$

For  $Li < 5$  ppm :

$$\ln K_{pre} = -2.19204 + 0.11962 [Li]$$

$$\ln K_{post} = 15.75685 + 0.17819 [Li]$$

For  $5 < \text{Li} < 350$  ppm :

$$\text{Ln } K_{\text{pre}} = -1.81964 + 4.5142 \cdot 10^{-2} [\text{Li}]$$

$$\text{Ln } K_{\text{post}} = 16.44013 + 4.1535 \cdot 10^{-2} [\text{Li}]$$

*Boron effect* : The boron effect is taken into account from experimental results obtained from standard Zircaloy-4 tubing oxidized in static autoclave with two different boron contents, typically 0 and 650 ppm (Tab.2). The main result is that, for a lithium content in the coolant equal to 1.5 ppm, the increase of boron content from 0 to 650 ppm leads to a decrease of the oxidation rate close to 35%. Moreover, according to other unpublished results obtained from out-of-pile loop tests and at boron content ranging between 200 and 1000 ppm, this boron effect does not appear to depend on the boron level. Therefore, the boron effect on the oxidation kinetics is expressed in the corrosion code in the form of a multiplicative coefficient which can be applied to the frequency factors as follows :

$$B = 0 \quad : F_{\text{boron}} = 1$$

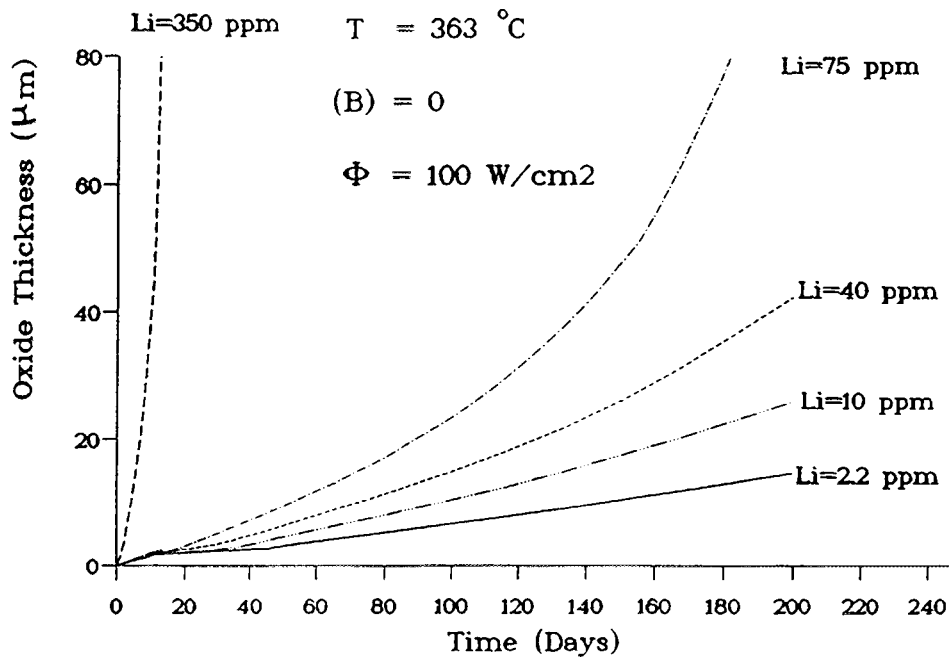
$$200 \leq B \leq 1000 \text{ ppm} \quad : F_{\text{boron}} = 0.64 \text{ (for } \text{Li} \leq 70 \text{ ppm).}$$

Using this semi-empirical correlations, oxidation kinetics under one phase flow heat transfer conditions have been calculated for several lithium and boron concentrations in the coolant and are presented in Fig.8.

Tab.2 . Effect of boron content on the oxidation rate of Zircaloy-4 tubing oxidized in static autoclave.

[Li] (ppm)	[B] (ppm)	pH300	Oxidation rate at 360°C mg/dm <sup>2</sup> /day
0	0	5.7	0.5 [3]
1.5	0	7.7	0.55 [3]
1.5	650	7	0.35

a



b

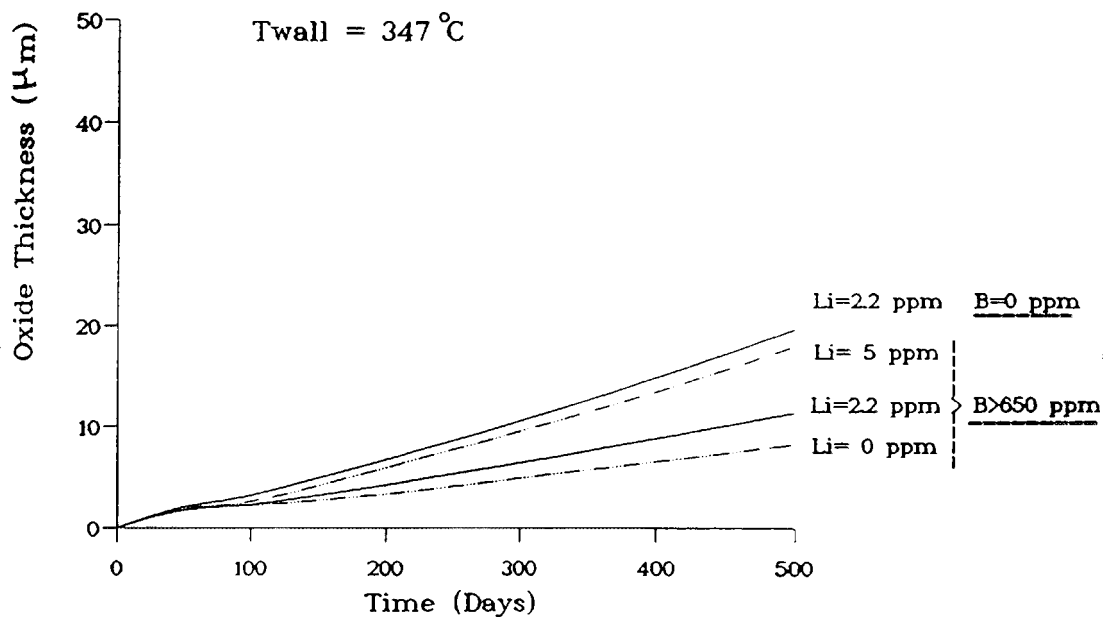
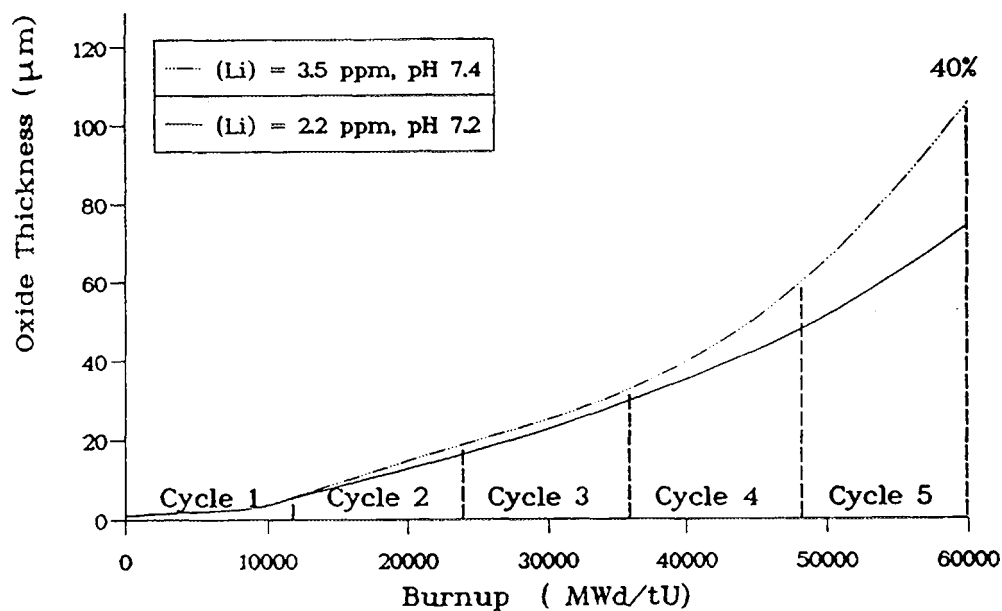


Fig.8 . Effect of lithium and boron contents on the oxidation kinetics of Zircaloy-4 materials oxidized in out-of-pile oxidation loop under one phase flow heat transfer : a) without boron in the coolant, b) with boron.

a

17x17 - 12 month-cycle



b

17x17 - 18 month-cycle

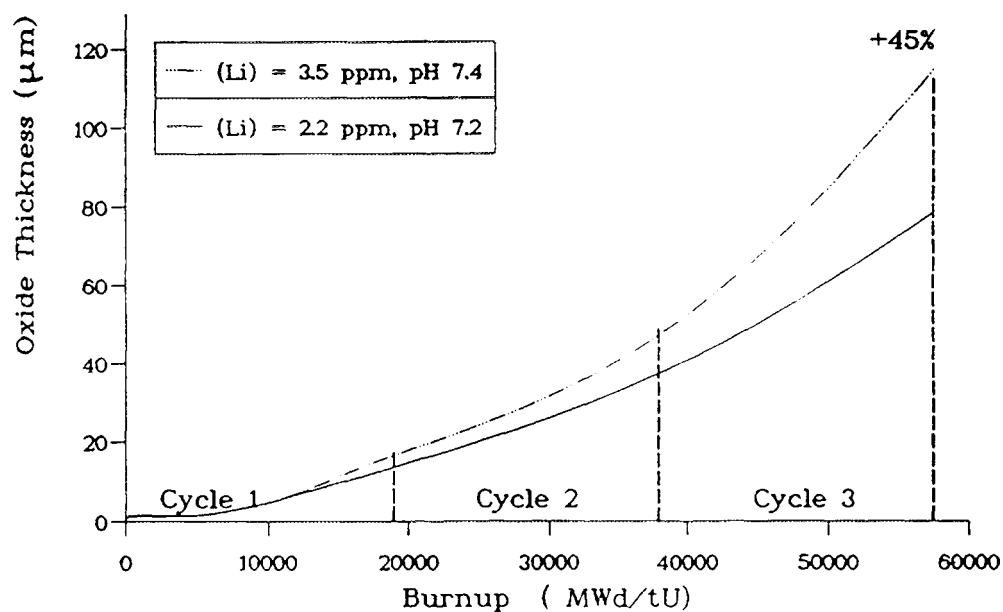


Fig.9 . Effect of an increase in lithium content from 2.2 ppm to 3.5 ppm on the oxidation kinetics of fuel cladding. Prediction calculated by the COCHISE code for two types of fuel management : a) 12 month-cycles, b) 18 month-cycles.

## 4.2 Prediction of in reactor corrosion under elevated lithium conditions

The corrosion model extended to varied chemistry conditions from out-of-pile results is now used to predict the corrosion kinetics of Zircaloy-4 cladding in pressurized water reactors. However, as the model is based on out-of-pile corrosion data (i.e. without neutron flux), an additional enhanced factor has been taken into account to simulate the irradiation effect on the corrosion kinetics. This coefficient, determined by the comparison of out-of-pile loop and PWRs corrosion data, is close to 3 (in the post-transition regime). Previous work [8] has shown that this corrosion code provides satisfactory results of in-reactor corrosion behaviour, the oxide thicknesses measured in several commercial reactors being close to those predicted by the code.

In this work, this corrosion model is used to predict the effect of increasing the lithium content in primary coolant from 2.2 to 3.5 ppm (i.e. new trends of operating conditions) on the fuel cladding corrosion. Predictions are made for two types of fuel management :

- 12 month cycles up to a final Burn up of 60 GWd/tU (Fig.9a).
- 18 month cycles up to a final Burn up of 50 GWd/tU (Fig.9b).

In both cases, the increase of lithium from 2.2 to 3.5 ppm leads to an enhancement of external corrosion. However, this enhancement of corrosion rates can be considered significant only beyond a critical burn-up, which is close to 50 GWd/tU for 12 month-cycle reactor and to 40 GWd/tU for a 18 month-cycle one.

## **5. Discussion**

### 5.1 Effect of lithium on corrosion under two phase flow heat transfer

From out-of-pile loop test performed under two phase flow heat transfer conditions with lithium hydroxide in the coolant, it is shown that the corrosion rates of the Zircaloy-4 material increase in the area of the rod submitted to boiling conditions. Some PWRs data reveal that these phenomena can occur in the hottest channels of some PWRs reactors. However, as observed from the C13 out-of-pile loop test, in the same coolant pH and boiling conditions, such an enhancement of

the corrosion rates does not occur in presence of KOH instead of LiOH. We can then assume that the accelerated corrosion kinetics observed in the fuel rods area of high void fraction is essentially due to a lithium effect. Moreover, since it is related to a local lithium enrichment in the oxide layer, the enhancement of corrosion occurring under boiling conditions must involve two phenomena : a lithium enrichment in the oxide layer induced by boiling and a chemical effect of lithium on the oxidation process. Therefore, in order to simulate the corrosion kinetics of the Zircaloy-4 material under two phase flow heat transfer (boiling at the surface of the cladding or within the porosity of the oxide), the lithium enrichment in the oxide layer is assessed in the COCHISE corrosion code. The determination of the lithium enrichment factor, which depends on the thermalhydraulic conditions and on the characteristics of the oxide layer (porosity), is currently under progress using experimental oxidation data and theoretical studies. One mechanism involving the porosity of the oxide layer has been proposed elsewhere [9] to interpret such a lithium enrichment in the oxide layer induced by boiling.

## 5.2 Effect of elevated lithium on corrosion : comparison between predictions and in-reactor oxide data

The simulation of the effect of elevated lithium on fuel cladding corrosion leads to an increase in corrosion kinetics which is getting significant for burn up upper than 50 GWd/tU for 12 month cycle reactor and than 40 GWd/tU for 18 month cycle one. To valid this result, the oxidation data derived from several reactors operating under elevated lithium regime (Ringhals-3 [10,11], Millstone-3 [10], St Lucie-1 [10] and Reactor A) are analyzed and compared with COCHISE code prediction (Table 3).

After four cycle (three of which being operated at elevated lithium corresponding to  $\Delta_{\text{burn up}}$  equal to 33.8 GWd/tU), the Ringhals-3 oxide data do not show any significant enhancement in corrosion rates. This result confirms the predictions presented in Fig.9a where no significant corrosion enhancement is expected for such a burn up. At St Lucie-1 and Millstone-3 after burn ups equal to

Tab.3 . Effect of elevated lithium on the fuel cladding corrosion : comparison between in reactor oxidation data derived from Ringhals-3, Millstone-3, St Lucie-1 and reactor A [10,11] and prediction.

TYPE OF PWRs	OPERATING CONDITIONS			CYCLE AT ELEVATED LITHIUM		ACCELERATED CORROSION	
	cycle	length	chemistry conditions	number	Burn up	Measured	Calculated
Ringhals-3	1	12 months	Li = 0.7 ppm	3	33 GWd/tU	No	No
	2 - 3 - 4	12 months	Li = 3.2 - 3.5 ppm until pH 7.4				
Millstone-3	1	12 months	coordinated pH 6.9 chemistry	1	20 GWd/tU	Yes	<15%
	2	18 months	Li = 3.2 - 3.5 ppm until pH 7.4				
St Lucie-1	1 - 2	18 months	coordinated pH 6.9 chemistry	1	20 GWd/tU	<15%	<15%
	3	18 months	Li = 3.2 - 3.5 ppm until pH 7.4				
Reactor A	1	18 months	Li = 3.2 - 3.5 ppm until pH 7.4	1	18 GWd/tU	No	No
	2	12 months	Li = 3.2 - 3.5 ppm until pH 7.4	2	32 GWd/tU	<15%	20%
	3	12 months	Li = 3.2 - 3.5 ppm until pH 7.4	3	44 GWd/tU	>30%	25%

about 43 and 40 GWd/tU respectively, the corrosion rates appear to be, on average, somewhat higher than expected when compared with other experiences under standard coordinated water chemistry. Recent results derived from the Reactor A show that no significant elevated lithium effect on the corrosion is observed after a burn up equal to 32 GWd/tU while, at higher burnup ( 44.7 GWd/tU), an increase in the oxide thickness of 10  $\mu\text{m}$  is shown.

If the enhancement in corrosion rates observed at Millstone, St Lucie and Reactor A are related to elevated lithium concentration, some other causes (material effect, crud deposition...) could also be involved. Nevertheless, it seems to appear that an increase in corrosion rates of the fuel cladding can be calculated or measured only when a critical burn-up is reached. However, more in-reactor oxidation data and at higher burn-up (50-60 GWd/tU) are needed to confirm these predictions and, especially, the value of the critical burn up.

### 5.3 Effect of elevated lithium on the activity level of the primary circuit

In order to reduce the contamination of primary circuits by corrosion products and hence to decrease dose rates, PWR operation with high coolant pH is now recommended in France. This result is based on simulations using computers codes [12], loop tests [13] and PWRs data. In France, where pH<sub>300</sub> was up to now maintained at 7.0, circuit contamination was controlled in 6 EDF PWR reactors with a pH<sub>300</sub> of the primary coolant maintained at 7.2 throughout the cycle. After a few cycles, a first evaluation reveals that the effect of pH increase on PWR contamination is not very significant and less than predicted by loop tests and theoretical studies [14]. Therefore, if the effect of elevated lithium on the dose rates reduction cannot be considered as a good argument to increase the lithium content in the fluid from 2.2 to 3.5 ppm, coordinated chemistry based on a lithium level of 2.2 ppm at the beginning of longer cycles of 18 months can lead to a significant increase in the contamination of the primary circuits.

## 6. Conclusion

The corrosion studies performed in out-of-pile loop tests under various chemical conditions, in one and two phase flow heat transfer, lead to the main conclusions :

- Under one phase flow heat transfer conditions, the addition of lithium hydroxide in the coolant increases the oxidation rate, specially in the post-transition phase.
- Under two phase flow heat transfer conditions and in presence of LiOH, an enhancement of the corrosion kinetics is observed in the area of the rod submitted to boiling, while such a phenomenon is not observed in KOH environment (at the same pH).
- The enhancement of the corrosion kinetics occurring under lithium and two phase flow heat transfer appears to be due to a lithium enrichment in the porosity of the oxide films formed.

The predictive study of the effect of increasing lithium content from 2.2 ppm to 3.5 ppm on the fuel corrosion, based on a semi-empirical corrosion code (COCHISE), shows that elevated lithium conditions do not increase significantly the corrosion rates at low burn-up. However, when the fuel burn-ups reach a critical value, typically about 50 GWd/tU for 12 month fuel cycles, and 40 GWd/tU for 18 month fuel cycles, a noticeable enhancement of the corrosion rates can be expected in presence of elevated lithium. These predictions are in a good agreement with the in-reactor oxidation data derived from Ringhals-3, Millstone-3, St Lucie-1, Reactor A.

## REFERENCES

- [1] Kass, S., Corrosion, Vol.25, N°1, Jan. 1969, p.30.
- [2] Hillner, E. and Chirigos, J.N., WAPD-TM-307, Westinghouse Electric Corp., Bettis Atomic Laboratory, Pittsburgh, Pa., Aug. 1962.
- [3] Mc Donald, S.G., Sabol, G.P., Sheppard, K.D., in Zirconium in the Nuclear Industry, Sixth International Symposium, ASTM STP 824, American Society for Testing and Materials, Philadelphia, 1984, p.519.

- [4] Bramwell, I.L., Parsons, P.D., Tice, D.R., in *Zirconium in the Nuclear Industry*, Ninth International Symposium, ASTM STP 1132, American Society for Testing and Materials, Philadelphia, 1991, p.628.
- [5] Hillner, E., in *Zirconium in the Nuclear Industry*, Third International Symposium, ASTM STP 633, American Society for Testing and Materials, Philadelphia, 1977, p.211.
- [6] Billot, Ph., Beslu, P., Giordano, A., Thomazet, J., in *Zirconium in the Nuclear Industry*, Eighth International Symposium, ASTM STP 1023, American Society for Testing and Materials, Philadelphia, 1989, p.165.
- [7] Evans, H.E., Bale, M.G., A review of the NFIR-I Zircaloy corrosion projects : vol.2, evaluation of the corrosion data. EPRI report, NP-7320-D, 1991.
- [8] Billot, Ph., Giordano, A., in *Zirconium in the Nuclear Industry*, Ninth International Symposium, ASTM STP 1132, American Society for Testing and Materials, Philadelphia, 1991, p.539.
- [9] Billot, Ph., Robin, J.C., Giordano, A., Peybernès, J., Thomazet, J., Amanrich, H., in *Zirconium in the Nuclear Industry*, Tenth International Symposium, American Society for Testing and Materials, Philadelphia, 1993, in press.
- [10] Polley, M.V., Evans, H.E., Review of effect of lithium on PWR fuel cladding corrosion, *Water Chemistry of Nuclear Reactor Systems*, BNES, Bournemouth, 1992, p.61.
- [11] Polley, M.V., Evans, H.E., Andersson, P.O., Larsson J., Effect of Lithium Hydroxide on Zircaloy Corrosion in the Ringhals-3 PWR Plant, EPRI report TR61003899, 1992.
- [12] Beslu, P et al., Pactole, to Predict Activation of Corrosion Products in PWRs. *Water Chemistry of Reactor System*, BNES, London 1978.
- [13] Billot, Ph et al. Zircaloy Corrosion properties under LWR Coolant Conditions. EPRI NP 7562D.
- [14] Anthoni, S. et al, Effect of pH of Primary Coolant PWR Contamination, *Water Chemistry of Nuclear Reactor Systems*, BNES, Bournemouth, 1992, p.9.

# **CORROSION OF ZIRCONIUM ALLOYS IN NUCLEAR REACTORS: A MODEL FOR IRRADIATION INDUCED ENHANCEMENT BY LOCAL RADIOLYSIS IN THE POROUS OXIDE**

C. LEMAIGNAN, R. SALOT  
CEA/DRN/DTP, CENG-SECC,  
Grenoble, France

## **Abstract**

An analysis has been undertaken of the various cases of local enhancement of corrosion rate of zirconium alloys under irradiation. It is observed that in most cases a strong emission of energetic  $\beta^-$  is present leading to a local energy deposition rate higher than the core average. This suggests that the local transient radiolytic oxidising species produced in the coolant by the  $\beta^-$  particles could contribute to corrosion enhancement, by increasing the local corrosion potential.

This process is applicable to the local enhanced corrosion found in front of stainless steels structural parts, due to the contribution of Mn, and in front of Pt inserts or Cu-rich crud. It explains also the irradiation corrosion enhancement of Cu-Zr alloys.

Enhanced corrosion around neutron absorbing material is explained similarly by pair production from conversion of high energy capture photons in the cladding, leading to energetic electrons. The same process was found to be active with other highly ionising species like  $\alpha$  from Ni-rich alloys and fission products in homogeneous reactors.

Due to the changes induced by the irradiation intensity on the concentration of the radiolytic species, the coolant chemistry, that controls the boundary conditions for oxide growth, has to be analysed with respect to the local value of the energy deposition rate. An analysis has been undertaken which shows that, in a porous media, the water is exposed to a higher intensity than bulk water. This leads to a higher concentration of oxidising radiolytic species at the root of the cracks of the porous oxide, and increases the corrosion rate under irradiation.

This mechanism, deduced from the explanation proposed for localised irradiation enhanced corrosion, can be extended to the whole reactor core, where the general enhancement of Zr alloys corrosion under irradiation could be attributed to the general radiolysis in the porous zirconia.

## **1. INTRODUCTION**

It is usually observed that the corrosion rate of Zr alloys used as fuel cladding or as structural materials exceed, in nuclear reactors, the value measured in the different out of reactor devices developed for corrosion testing of those alloys [1]. Indeed, the corrosion rates deduced from autoclave tests have to be multiplied by an irradiation enhancement factor of 2 to 4 to fit the corrosion layer thicknesses observed in power plants [2, 3]. In addition, several cases of local higher enhancement have been reported in the literature.

A strong correlation between all the cases of local enhancement of corrosion rate under irradiation and the presence of a local emission of energetic electrons has been presented earlier and will be briefly outlined [4]. In addition, the porous nature of the external layer of the oxide leads to a strong increase of the energy deposition rate in the water of the pores, compared to the one in the bulk of coolant. The enhanced radiolysis induced in the vicinity of a  $ZrO_2$ -water wall is quantified, and it will be shown that it supports in more details the model of irradiation enhancement of corrosion by the local radiolysis in the pores of the zirconia layer.

## 2. CORROSION ENHANCEMENT OF ZIRCONIUM ALLOYS UNDER IRRADIATION

Numerous case of local enhancement, under irradiation, of corrosion rates of Zr alloys have been reported in the past and have been reviewed in detail in [1, 4]. The different cases can be gathered in a few main classes:

- local enhancement in front of :
  - stainless steel parts (Fig. 1 a)
  - particular metallic alloys (Pt), placed as voluntary inserts
- very high corrosion rate of some specific alloys under development (Zr Cu-1%), which showed favourable behaviour out of reactor [5]. High corrosion rate under high copper content cruds [2].
- local enhancement in the case of Gd bearing fuel rods (Fig. 1b). This was particularly easy to observe in the case of zebra type fuel pellet stacks - Gd bearing and pure  $\text{UO}_2$  [2].

### 2.1 $\beta^-$ decay

In all these cases, a detail analysis of the radioactive behaviour of all the structural materials contributing the radiation environment has been undertaken. A particular attention has been given to the source of possible local increase of irradiation effects. It was found that a common parameter is a major contribution of the local  $\beta^-$  flux to the energy deposition rate (EDR) in the surroundings. Indeed, all the situations have shown a specific material having an activable isotope, with a decay by high energy  $\beta^-$ . This is the case of  $^{55}\text{Mn}$  in stainless steels,  $^{198}\text{Pt}$  in the case of Pt inserts,  $^{65}\text{Cu}$  in the case of Cu rich alloys or cruds. The energies of the electrons emitted by the activated nuclei are always high ( $E_e > 1.5 \text{ MeV}$ ), allowing them to have a range of a few millimetres in water.

A computation has been performed of the intensities of the flux for the various geometric cases found in the literature, with a general procedure taking into account the following considerations :

- Activation cross sections for thermal neutrons were considered [6, 7], and, due to the short lifetime of the activated species, radioactive equilibrium was assumed.
- Due to the distribution of the energies of the  $\beta^-$  electrons, their recoil distances were computed for their most frequent emission energy (i.e. one third of the maximum energy).

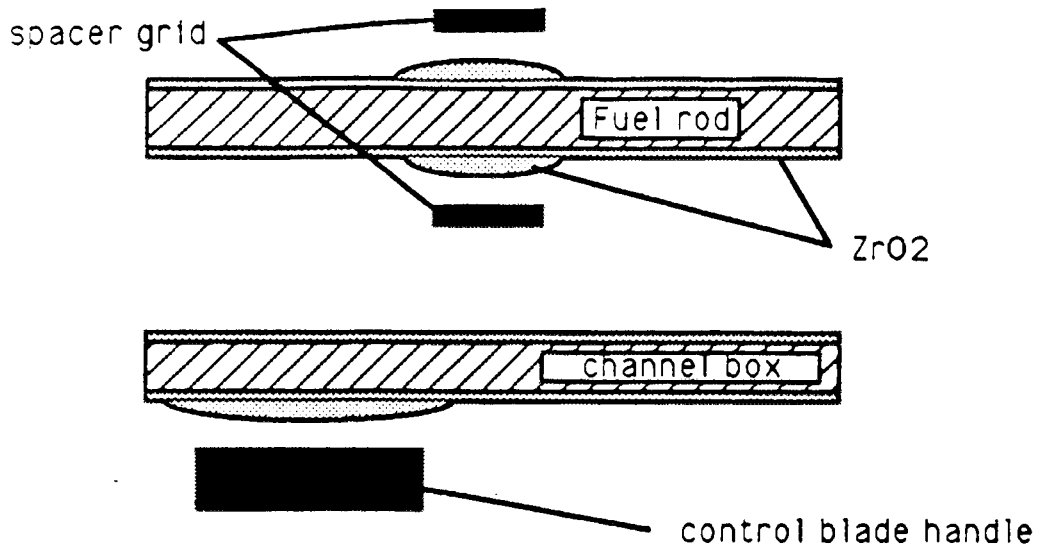


Figure 1.a : Locally-enhanced corrosion in front of stainless steel structural parts

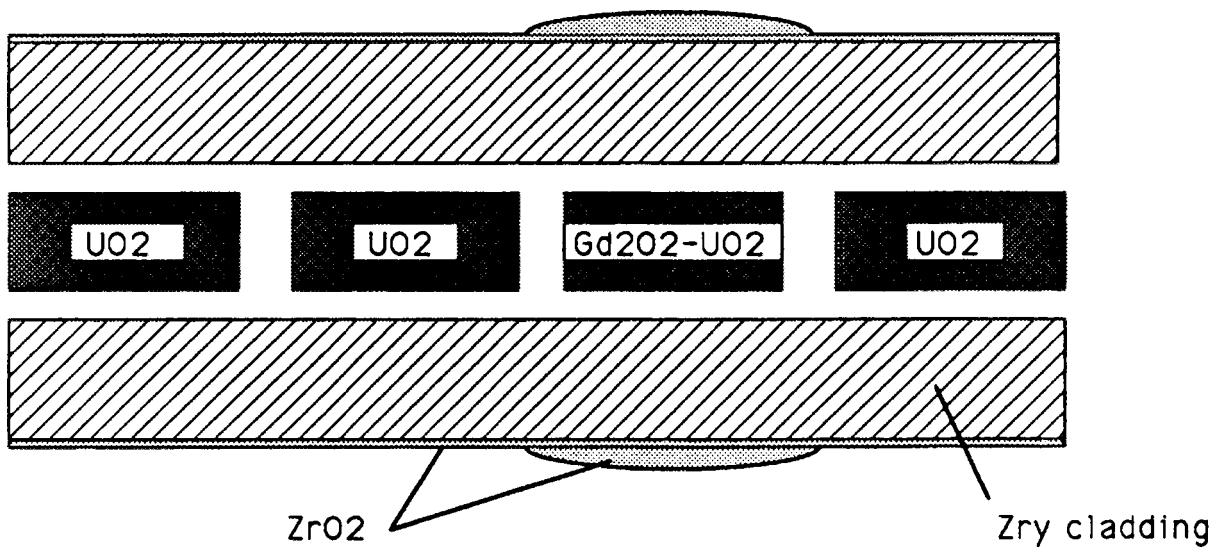


Figure 1.b : Enhanced corrosion in front of Gd-doped fuel pellets

- The number of  $\beta^-$  electrons, of a given energy released by the activated atoms, were weighed according to the probabilities of the various decay schemes.
- For each decay scheme, the volume of material considered for  $\beta^-$  emission out of the material was evaluated using a thickness corresponding to the recoil distance, or, if smaller, to the maximum thickness of the material available in the reactor (e.g. CuO type crud : 50  $\mu\text{m}$  [2]).
- The flux of  $\beta^-$  particles produced by the activated metal was calculated as one quarter of those produced in this zone, due to the classical geometrical considerations of recoil [8].
- In the case of various isotopes involved for one chemical species, all the contributions were summed unless some were marginal compared to the others, and, for an alloy, the contributions of all the components were weighed according to the chemical composition.
- The energy deposition rates were obtained as the average value over the stopping range using standard cross section for interaction of electrons with mater [9] and a straggling factor of  $\pi^2$  for the low energy end of the electron path.

The results are given in table 1. It clearly shows that the energy deposition rates in the vicinity of the said materials is high compared to the deposition due to the general  $\gamma$  irradiation due. This later is induced by all the  $\gamma$  created during fission and radioactive decay, a typical value in the BWR being  $10^{18} \text{ eV.cm}^{-3}.\text{s}^{-1}$ .

In PWR, boron is added as neutron absorbing element. Its interaction with neutrons leads to the creation of lithium and 0.7 MeV  $\alpha$  particles. As  $\alpha$  is a highly ionising specy, it contributes to the general phenomenon of radiolysis. First calculations indicate that the resulting energy deposition rate in PWR is about  $2.10^{19} \text{ eV.cm}^{-3}.\text{s}^{-1}$ . This high value could explain why no local effect is observed in this kind of reactor.

## 2.2 Pair production from capture $\gamma$

For the case of Gd bearing fuel rods, a cascade of nuclear reactions has to be considered : the first step is the capture of a neutron by the absorbing isotopes of Gd; this capture is associated with the emission of a very high energy  $\gamma$  photon. This photon, itself, is transformed, by pair production, as an electron plus an anti-electron. These two particles are shearing the remaining energy after mass production. Thus a flux of electrons is created in the surrounding environment.

Table 1 : Energy deposition rate due to  $\beta$ - emitted by material activated in the core  
(normalized to a thermal neutron flux of  $2.10^{13}$  n.cm<sup>-2</sup>.s<sup>-1</sup>)

Material	Chemical species/isotope	Natural concentration	Activation cross section (barns)	$\beta$ energy (MeV)	Recoil distance in metal (mm)	Material comp.	$\beta$ flux from material (cm <sup>-2</sup> .s <sup>-1</sup> )	Recoil distance in water (mm)	Energy deposition rate (eV.cm <sup>-3</sup> .s <sup>-1</sup> )
Stainless steel	Cr 24 54	0.03	0.38	2.8	0.65	0.17	9.81E+08	4.88	8.71E+17
	Mn 25 55	1.00	13.22	2.86	0.67	0.005	2.78E+10	4.99	2.47E+19
	Fe 26 58	0.00	1.01	0.46	0.04	0.68	5.43E+07	0.30	4.82E+16
	Ni 28 64	0.01	1.52	2.1	0.48	0.12	5.01E+08	3.62	4.45E+17
	Mo 42 98	0.24	0.51	1.23	0.27	0.02	2.81E+08	2.05	2.50E+17
Platinum insert	Pt 78 196	0.25	0.87	0.67	0.02	1	4.41E+09	0.51	3.91E+18
	Pt 78 198	0.07	3.9	1.69	0.13	1	2.23E+10	2.88	1.98E+19
Copper cruds	Cu 29 65	0.31	1,8	2.6	0.51	0.5	1.22E+11	4.52	1.09E+20
Zr alloys	Zr 40 94	0.17	0.076	0.38	0.04	0.98	2.12E+08	0.23	1.89E+17
	Zr 40 96	0.03	0.053	1.91	0.50	0.98	3.52E+08	3.28	3.13E+17
	Sn 50 120	0.33	0.14	0.38	0.04	0.015	7.97E+06	0.23	7.08E+15
	Nb 41 93	1.00	1.4	1.3	0.34	0.025	2.50E+06	2.18	2.22E+15
	Cu 29 65	0.31	1.8	2.6	0.51	0.025	2.70E+09	4.52	2.40E+18

In the case of those neutron absorbing materials, the same type of computation has been performed in detail: Starting from a typical BWR neutron flux, the absorption rate is obtained from the cross section. In fact, the Gd acts as a black material and any entering neutron gives rise to a capture. The spectrum of the capture  $\gamma$  emission is known accurately [10] and the total flux is easily obtained. In the case of gadolinium a important emission occurs at 6.5 MeV. The types of interactions of those high energy  $\gamma$ 's are strongly dependant on the material atomic number. In the case of zirconia, the process having the highest cross section is pair production [11]. It leads to the creation of an electron of initial kinetic energy of 3.65 MeV, since at this energy of a photon, the energy remaining after the creation of the two masses of the  $e^+$  and  $e^-$ , is evenly shared between those two particles [12]. Thus the flux of capture  $\gamma$  leads to a net production of energetic electrons from the cladding.

The result of this computation is given in table 2 for various type of absorbing materials, and is compared with the contribution that could come from the other  $\gamma$  in the core. A strong enhancement of the  $e^-$  flux is indeed seen in the case of a Gd bearing absorbing fuel rod.

Table 2 : Energy deposition rate due to the  $\beta^-$  obtained by the conversion of gamma into  $\beta^- / \beta^+$

Species	Reaction	Cross section (barn)	Nb of $\gamma$ $E > 5$ MeV per capt.	Flux of $\gamma$ $E > 5$ MeV ( $\text{cm}^{-2} \cdot \text{s}^{-1}$ )	$\gamma$ energy (MeV)	Pair prod. cross section (barn)	Flux of $\beta$ from fuel rod ( $\text{cm}^{-2} \cdot \text{s}^{-1}$ )	Energy of the created $\beta$ (MeV)	Energy deposition rate ( $\text{eV} \cdot \text{cm}^{-3} \cdot \text{s}^{-1}$ )
				from fuel rod					
Gd	capture	46000	0.3	3.0E+13	8.5	2.9	2.70E+11	3.65	2.43E+19
Hf	capture	105	0.12	7.4E+10	7.6	2.6	5.97E+08	3.2	5.37E+16
238 U	capture	3.7							
235 U	fission	570	0.04	1.6E+10	5.5	1.9	2.90E+07	2.15	2.61E+15
	FP	570							
				from material					
SS (Mn)	capture	13.2	0.5	2.3E+10	7.25	2.55	1.86E+08	3.025	1.67E+16
Cu crud	capture	3.8	0.7	5.7E+10	7.9	2.7	3.83E+07	3.35	3.45E+15
Pt insert	capture	8.1	0.15	4.5E+10	7.9	2.7	5.04E+07	3.35	4.54E+15

A typical energy spectrum of the electrons leaving a Gd doped burnable poison fuel rod, was found to be very similar to the case of the  $\beta^-$  decay and the energy deposition rate due to the electrons leaving the fuel rod, originated from pair production is given in Fig. 2: Close to the surface, the local energy deposition rate have a value of  $6 \cdot 10^{19} \text{ eV} \cdot \text{cm}^{-3} \cdot \text{sec}^{-1}$ , and decreases smoothly to vanish at 3-4 mm.

The effect of this high intensity of local irradiation is a major change in local chemistry at the roots of the pores, increasing the oxygen potential at the outer part of the dense zirconia layer, i. e. at the location of boundary condition for oxide growth.

### 3. ENERGY DEPOSITION RATE IN A POROUS MEDIUM

The specific aspect of the corrosion mechanism of the zirconium alloys is the occurrence of a transition of the corrosion rate after a few microns of zirconia. This transition is connected to a change in the crystallographic form of the zirconia. At the beginning of oxide growth, the zirconia is mainly tetragonal, while after the

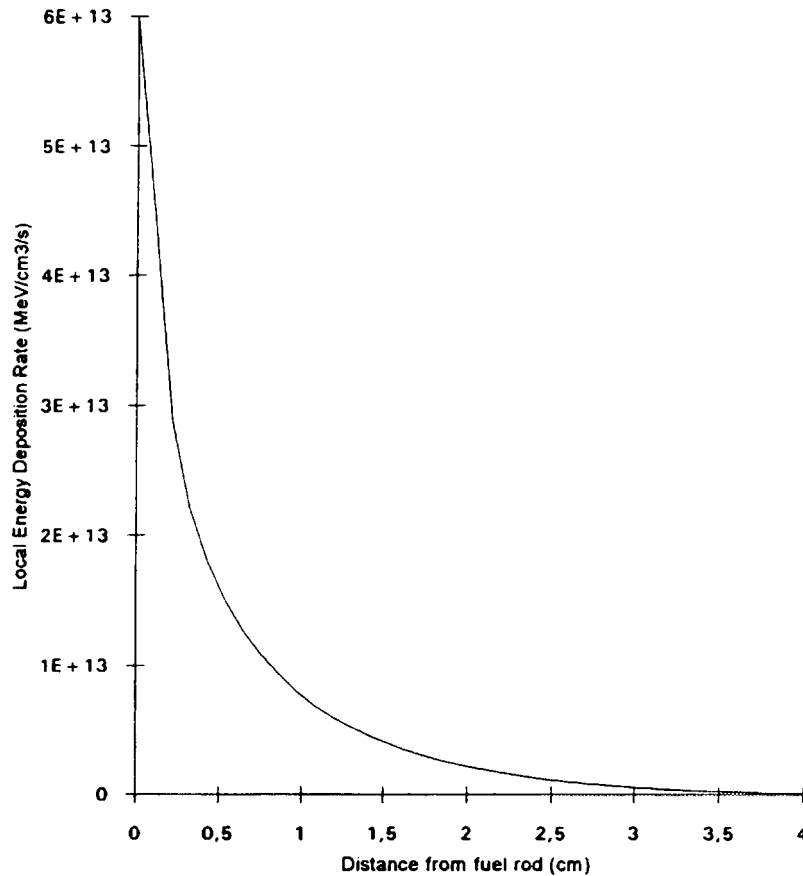


Figure 2 : Energy deposition rate in front of a Gd bearing fuel rod  
(EDR average =  $2.4 \cdot 10^{13} \text{ MeV} \cdot \text{cm}^{-3} \cdot \text{s}^{-1}$ , cf. table 2)

transition it is composed of an inner dense oxide layer mainly tetragonal and an outer oxide layer essentially monoclinic [13]. This transformation is of martensitic type and, in an ionic crystallographic structure, will develop internal porosity due to strain incompatibility between the surrounding grains. Electron microscopy examinations have confirmed the presence of this open porosity and it has been shown to have a typical gap size of a few nanometers [1, 14].

In order to analyse the intensity of the irradiation effect, it is necessary to compute the energy deposition rate due to the irradiation in the specific environment considered, i.e. in a porous medium. In that case the value of the EDR is not the same as for bulk materials. For the case to be considered, we will analyse the EDR due to a PWR's  $\gamma$  spectrum, in hot pressurised water in the pores of the zirconia, compared to bulk water under the same  $\gamma$  flux.

The PWR's  $\gamma$  spectrum has been analysed in detail for the purpose of  $\gamma$  heating knowledge and shielding. A typical spectrum was grouped in three energy groups, having the following ranges : 0, 0.25, 0.9 MeV and above, referred as 0.1, 0.5 and

Table 3 : Surface enhancement of EDR

PWR $\gamma$ spectrum		Interaction cross section				Induced electron spectrum at the interface			
		ZrO <sub>2</sub>		H <sub>2</sub> O		from ZrO <sub>2</sub>		from H <sub>2</sub> O	
Energy (MeV)	normalized intensity	Photo. (barns)	Compton (barns)	Photo. (barns)	Compton (barns)	Energy (MeV)	electron per $\gamma$ photon	Energy (MeV)	electron per $\gamma$ photon
0,1	6	104,2	10,7	0,08	0,16	0,05	$2,0 \cdot 10^{-3}$	0,05	$4,1 \cdot 10^{-4}$
0,5	3,7	1,15	0,47	0	0,01	0,07	$3,1 \cdot 10^{-2}$	0,07	$1,6 \cdot 10^{-4}$
1,5	1	0,11	0,05	0	0	0,25	$5,1 \cdot 10^{-4}$	0,25	$1,6 \cdot 10^{-4}$
						0,47	$2,9 \cdot 10^{-3}$	0,47	0
						0,75	$6,8 \cdot 10^{-5}$	0,75	0
						1,47	$3,4 \cdot 10^{-4}$	1,47	0
<b>Ratio of the EDR in porous zirconia and in the bulk of water</b>									
52									

1.5 MeV in the following tables. In each group, the cross section for different photon interactions (photoelectric, Compton and pair production) were computed for water and zirconia (mass average over H, O and Zr). Each of those interaction give rise to the release of an electron having the following energies:

Photoelectric  $E_e = E_\gamma - E_K$

Compton  $E_e = E_\gamma / 2$

Pair production  $E_e = (E_\gamma - 2.m c_0^2) / 2$

The flux of electrons and their energies can thus be computed in the two media (zirconia and water) considered as bulk and are presented in table 3. The EDR in bulk material is the integral of those net spectra. In order to compute the behaviour in the porous zirconia, the range of the electrons, deduced from their energies, leads to the flux and energies of the electrons allowed to leave the zirconia at a water interface. Computing the EDR due to this flux of electrons, a 50-fold increase is

obtained due to the presence of the zirconia. Hence, it is clear that the irradiation effects, like radiolysis of the water, is very different for water away from the structural materials and for the water located in a confined medium, surrounded by a dense material. This remark, developed for the specific case of porous zirconia, could easily be extended to any similar case, like the behaviour of water in crack of sharp notch. This is to be connected to irradiation enhanced SCC of stainless steel.

#### 4. WATER RADIOLYSIS UNDER VARIABLE EDR CONDITIONS

The interaction of irradiation particles (neutron, gamma,  $\beta^-$ ) with the coolant water leads to the formation of radiolytic oxidizing species, that are assumed to be responsible for the large increase in corrosion rate of Zr alloys in reactor, compared to similar out of reactor conditions.

The water radiolysis in the reactor core has been analyzed in great details with the objective of knowing the steady state concentration of the radiolytic species during irradiation and their possible effect upon the zirconium corrosion rate [15]. The main process of radiolysis is an instantaneous decomposition of the water molecules by interaction with the electrons in spurs (small volume of high interaction along the path of the electron), giving birth to metastable species that recombine in a variety of possible ways. The complexity of the recombination reactions can be illustrated by the large number (35 to 40) of reactions to be considered, each with its own rate. The concentrations of the intermediate and final products depend strongly on irradiation rate and initial conditions and therefore, local changes in irradiation intensity lead to drastic changes in the concentrations of radiolytic species. Some species are obtained for very short times as intermediate steps to long-lived species [16]. Computer programs are thus used for the computation of the evolution of those species versus initial chemical and irradiation conditions [17].

We have used the Macksima-chemist code developed by AECL [18] to analyse the effect of the intensity of the EDR on the radiolytic species concentration. As expected from the complex interactions between the various chemical ions and molecules, the concentration of oxidizing species is not a linear function of the EDR and in the case of hydrogenated water, a higher EDR leads to a much higher oxidizing environment as presented in Fig. 3. For instance, the 50-fold increase described above, leads to a factor 30 for  $[H_2O_2]$  or 300 for  $[HO_2]$ , while there is almost no change in reducing compounds  $[H^+, H_2, H]$ .

The corrosion rate is controlled by the flux of oxygen ions through the dense protective oxide layer. This flux is proportional to the gradient in oxygen potential across this layer. A change in boundary conditions, mainly the oxygen potential in the water at the roots of the pores, will lead to a corresponding increase in corrosion

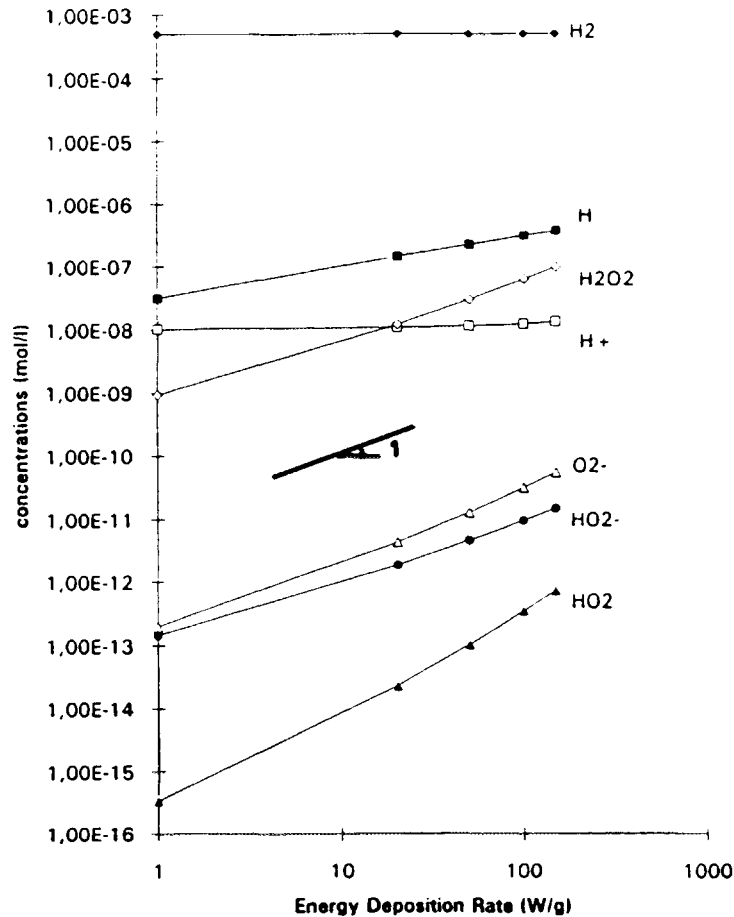


Figure 3 : Radiolytic species concentration versus local Energy Deposition Rate at  $10^{-1}$  s.

rate. In addition, the surfaces of the pores will act as sinks for the oxidizing species, giving rise to a higher flux of oxygen than what could be deduced only from the equilibrium concentration of species obtained by recombination. Indeed, due to the rate constant of each recombination reaction, the oxidizing products like  $O_2^-$  are available at much higher concentration ( $10^{-6}$  molar) for short time (a few microseconds) just after radiolysis. Due to the diffusion time necessary for crossing the pore thickness, those species will interact with the surface of zirconia before recombining with the other radiolytic species.

## 5. CONCLUSIONS

By an analysis of the various cases of local enhancement of corrosion rate of zirconium alloys under irradiation, the local transient radiolytic species produced in the coolant by energetic  $\beta^-$  particles are proposed to give an important contribution to this phenomenon. In that way, local enhanced corrosion under irradiation is explained in front of stainless steels structural parts, due to the contribution of Mn,

in front of Pt inserts and Cu-rich crud. It explains also the high corrosion rate under irradiation of Zr-1%Cu alloy.

Enhanced corrosion around neutron absorbing material is explained similarly by pair production from high energy capture photons, leading to energetic electrons.

The local energy deposition rate at the interface zirconia / water has been evaluated in the case of porous oxide. The 50-fold increase compared to a bulk environment leads to a much higher concentration of radiolytic species in the pores. Moreover, the high surface to volume ratio within the pores is supposed to favour the interaction of these species with the oxide at the expense of the recombination process. This would lead to a net flux of oxygen in the zirconia. Thus, the same mechanism as for locally-enhanced corrosion is proposed as a contribution to the general enhancement of Zircaloy corrosion under irradiation.

In reactor environment, irradiation has also an effect on the cladding. Thus, the microstructural evolutions induced by irradiation in Zircaloy contribute to change continuously the conditions of formation of the oxide. Furthermore, the irradiation appears clearly to affect the crystallographic nature of the oxide and its growth within the oxide layer. It seems also to enhance the diffusion of iron in the oxide, contributing locally to the stabilisation of tetragonal zirconia.

These two approaches appear to be the main mechanisms by which the irradiation contributes to the corrosion enhancement in nuclear reactors.

In PWR's, the contribution of  $\alpha$  particles from the boron leads to a more general behaviour, and less local effects are expected.

## REFERENCES

- [1] Corrosion of zirconium alloys in nuclear power plants, IAEA-TECDOC-684, Jan. 93.
- [2] M. O. Marlowe, J.S. Armijo, B. Cheng and R.B. Adamson, Proc. ANS Topical Meeting on Light Water Reactor Fuel Performance, Orlando, FL, April 21-24, 1985, Vol. 1 p. 3-73.
- [3] F. Garzarolli, R. P. Bodmer, H. Stehle and S. Trapp-Pritsching, Proc. ANS Topical Meeting on Light Water Reactor Fuel Performance, Orlando, FL, April 21-24, 1985, Vol. 1 p. 3-55.
- [4] C. Lemaignan, J. of Nucl. Mater. 187(1992) 122-130.

- [5] C. Fizzotti and L. Castaldelli, Proc. IAEA Spec. Meet. on Infl. Power React. Wat. Chem. on Fuel Clad. Reliab. , San Miniato, Italy (1981), IWGFPT-11, AIEA, Vienna, 1982 pp. 57-73.
- [6] R. Pannetier, Vade-Mecum du technicien nucléaire, T.2, S.C.F. du Basset, Massy, France, 1980.
- [7] W. E. Alley and R. M. Lessler, Nuclear Data Tables, 11 (1973) 621-826.
- [8] D. R. Olander, Fundamental Aspects of Nuclear Reactor Fuel Elements, TID 26711 P1, 1976, p. 293.
- [9] O.S. Oen, ORNL 4897 (1973).
- [10] Reactor Physics Constants, ANL 5800, 1963, p.630-632.  
G. A. Bartholomew, L. V. Groshev et al. , Nuclear Data, A3 (1967) 367-650; A5 (1968) 1-242; A5 (1969) 243-431.
- [11] E. Storm and H. I. Israel, Nuclear Data Tables A7, (1970) 565-681.
- [12] L. Feru and P. Jaskula, DEA, INPG (1992).
- [13] J. Godlewski, J. P. Gros, M. Lambertin, J. F. Wadier and H. Weidinger (1991), 9th. Inter. conf. Zr in Nucl. Ind., Kobe, Japan, ASTM-STP 1132, pp. 416-436.
- [14] X. Iltis and F. Lefebvre, unpublished results.
- [15] W. G. Burns and P. B. Moore, Radiat. Eff. 30 (1976) 233.
- [16] S. Lukac, Radiat. Phys. Chem. 158 (1988) 240-252.
- [17] G. V. Buxton and A. J. Elliot, Proc. JIAF Int. Conf. on Water Chemistry in Nuclear Power Plant, Fukui City, Japan, April 22-25, 1991, pp. 283-289.
- [18] M. B. Carver, D. V. Hanley and K. R. Chaplin, Maksima-Chemist, AECL 6413 (1979).

## **GROWTH AND CHARACTERIZATION OF OXIDE LAYERS ON ZIRCONIUM ALLOYS**

A.J.G. MAROTO, R. BORDONI, M. VILLEGAS,  
M.A. BLESA, A.M. OLMEDO, A. IGLESIAS, G. RIGOTTI  
Comisión Nacional de Energía Atómica,  
Buenos Aires, Argentina

### **Abstract**

**Corrosion behaviour in aqueous media at high temperature of zirconium alloys has been extensively studied in order to elucidate the corrosion mechanism and kinetics. The characterization of the morphology and microstructure of these oxides through the different stages of oxide growth may contribute to understand their corrosion mechanism.**

**Argentina has initiated a research program to correlate long term in and out-reactor corrosion of these alloys. This paper reports a comparative study of out of pile oxidation of Zr-2.5Nb and Zry-4, which are structural materials of in-core components of nuclear power plants. Kinetic data at different temperatures and microstructural characterization of the oxide films are presented.**

### **1.- INTRODUCTION**

**Short term corrosion tests, in and out of pile, are not enough by themselves to predict the corrosion behaviour of zirconium alloys. Complementary results are given by long term corrosion data, either from out of pile autoclave testing or gathered from in-reactor components as coolant channels or pressure tubes. The corrosion mechanism of zirconium alloys is still not well understood; the characterization of the oxide microstructure and morphology through the different stages of oxide growth, a detailed study of the corresponding changes in the metal/oxide interface, specially those of the thin, dense layer identified at the interface, are some of the most important aspects that may contribute to understand their corrosion mechanism.**

**Argentina has initiated a research program to correlate long term in and out-reactor corrosion of Zr-base alloys considering all these aspects. The present paper describes the results gathered in the out of pile test program for a range of temperatures between 265 and 435 °C and exposure times up to 6000 hs and 1500 days.**

## 2.- Microstructure and composition of the alloys

Samples of Zr-2.5Nb were machined from pressure tube material which is extruded at 820-850 °C, cold-worked 20-30 %, then stress relieved in steam 24 h at 400 °C. A batch of samples was heat treated at 500 °C for 10 h (TT) before oxidation. Samples of Zry-4 came from fully recrystallized sheet. The chemical composition of both alloys is given in Table I.

The microstructure of Zry-4 has the typical equiaxed grains of a fully annealed material. For Zr-2.5Nb, the microstructure consists of elongated  $\alpha$ -Zr grains of approximately 35  $\mu\text{m}$  length in the axial direction, 7  $\mu\text{m}$  width and 0.2 to 0.7  $\mu\text{m}$  thickness surrounded by a grain-boundary network of the  $\beta$ -Zr phase with about 20% Nb.

TABLE I

CHEMICAL COMPOSITION OF THE ALLOYS

	Nb	Sn	Fe	Cr	Fe+Cr	O	C	Si
	%	%	%	%	%	ppm	ppm	ppm
Zr-2.5Nb	2.5	-	0.04	<0.06	-	1080	185	50
Zry-4	-	1.45	0.21	0.1	0.31	970	45	46

## 3.- CORROSION KINETICS

Tests were carried out in the autoclaves located out of core in Embalse NPP (265 and 305°C, pH<sub>25°C</sub>=10.2-10.8, hydrogen content 3 - 10 c.c./kg D<sub>2</sub>O). Complementary, accelerated tests were done in static autoclaves at 350 °C simulating primary coolant (pH 10.4 (lithiated) water with hydrogen overpressure) and at 400 and 435 °C in degassed steam at high pressure (105 bar).

Corrosion data in steam at 435 °C, Fig. 1, show a cyclic behaviour for Zry-4. The kinetic law followed in these cycles is expressed by  $W^3 = K_{pr} t$ , the second cycle starts in the transition after 500 h at an oxide thickness of 3.2  $\mu\text{m}$  and it lasts until 1350 h reaching 6.4  $\mu\text{m}$  of oxide thickness. One single value of  $K_{pr}$  suffices to describe the first two cycles once the correction for the dense oxide thickness has been made. The cyclic nature of this stage is afterwards annealed out. The post-transition corrosion rate, 1,08 +/- 0.02 mg/dm<sup>2</sup>.d, can be described using the same  $K_{pr}$  value and a constant dense oxide thickness of circa 0.6  $\mu\text{m}$ . No

## CORROSION KINETICS 435 °C

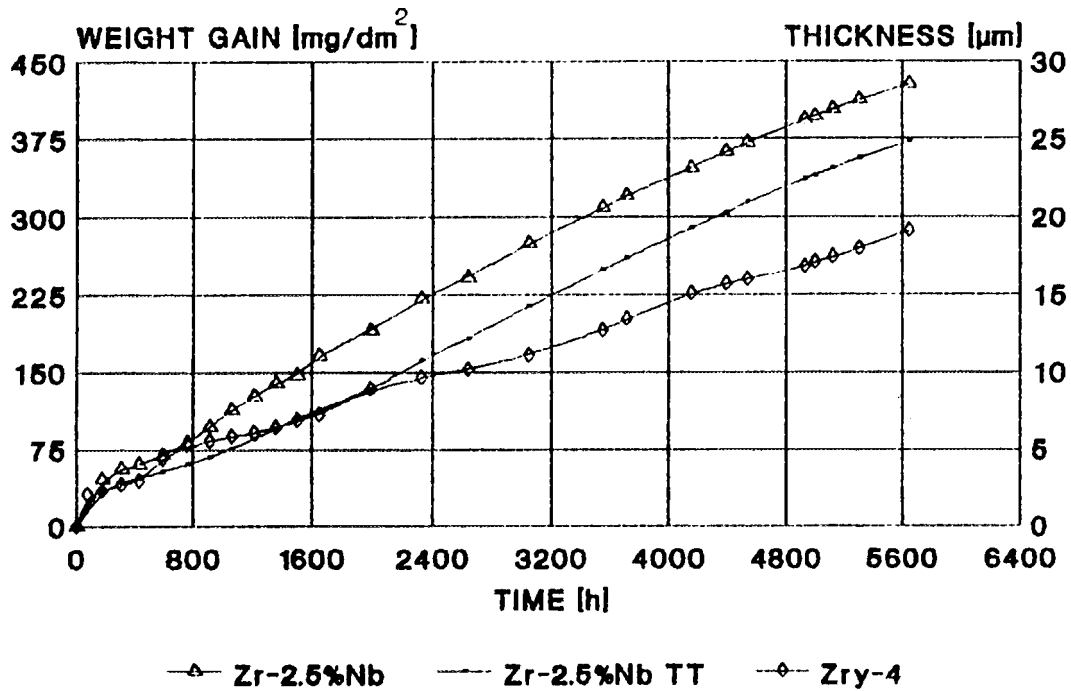


Fig. 1 . Corrosion kinetics of Zry-4 and Zr-2.5Nb at 435 °C

## CORROSION RATE 435 °C

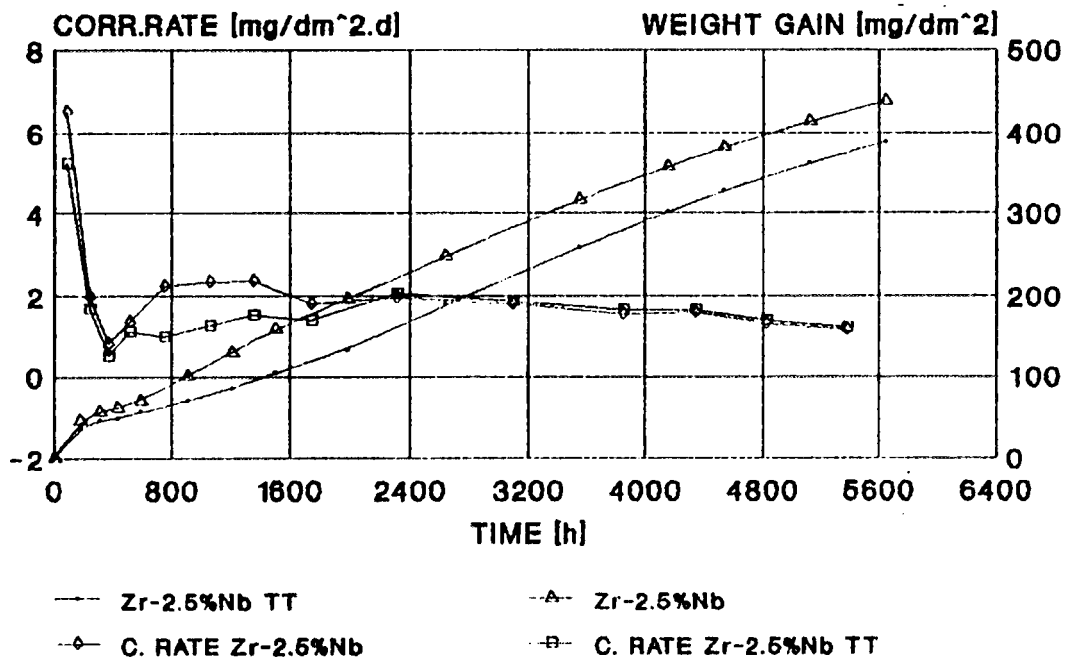


Fig. 2 . Corrosion rate of Zr-2.5Nb at 435 °C

increase in the post-transition corrosion rate was found up to a weight-gain of 280 mg/dm<sup>2</sup>, as was reported previously in the literature [1,2].

Zr-2.5Nb, either heat-treated (TT) or not, follows a two-stage oxidation kinetics. A parabolic pre-transition rate and a linear post-transition one. The transition point is about 600 h of exposure for both batches at an oxide thickness of 3.6 μm (TT) and 4.6 μm respectively. Although both lots show a deviation from the paralinear kinetics this is far less pronounced than the cyclic nature of the Zry-4 oxidation [3].

The heat treatment improves the corrosion resistance of Zr-2.5Nb. This is related to the microstructure of the alloy. During the heat treatment not only the β-Zr phase decomposes but also small β-Nb precipitates are formed within the alpha grains [4,5]. The corrosion rates of both lots superimposed to their oxidation kinetics at 435 °C are given in Fig. 2. During the first 2000 hs of the test the heat treated material has a lower corrosion rate. From then on, both corrosion rates are equal. Microstructural changes are induced on the material without heat treatment by the temperature of the test so that both lots have the same response after a certain lapse of time.

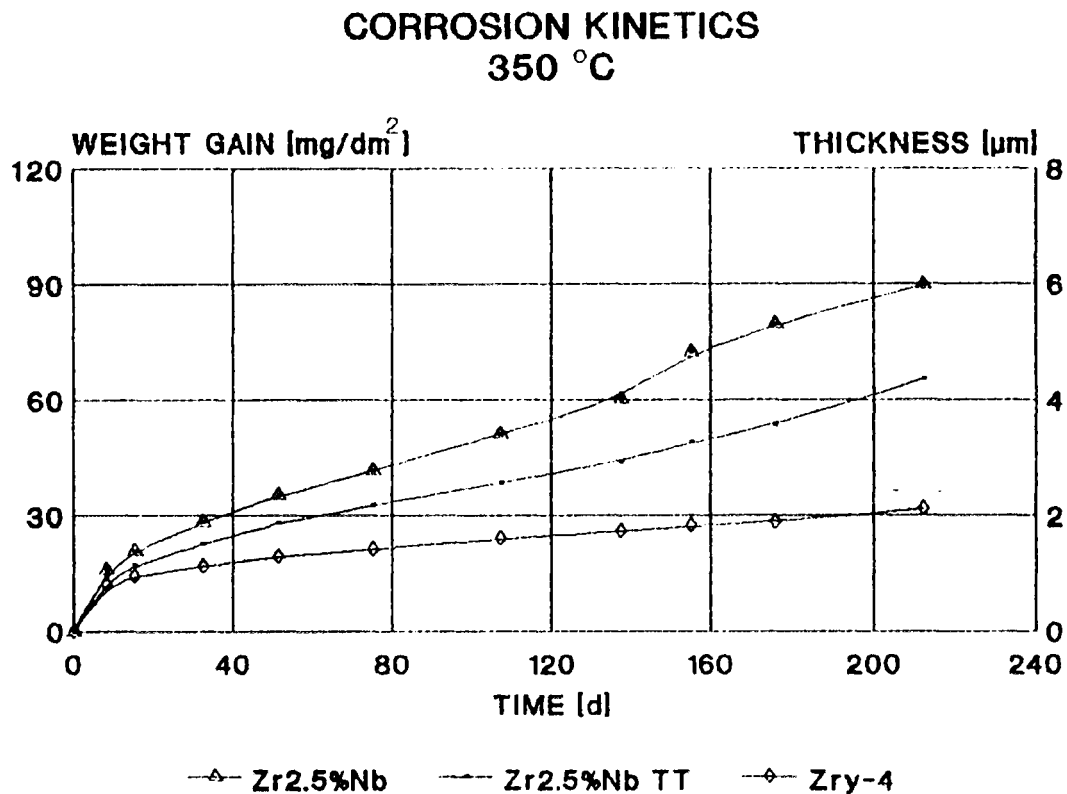
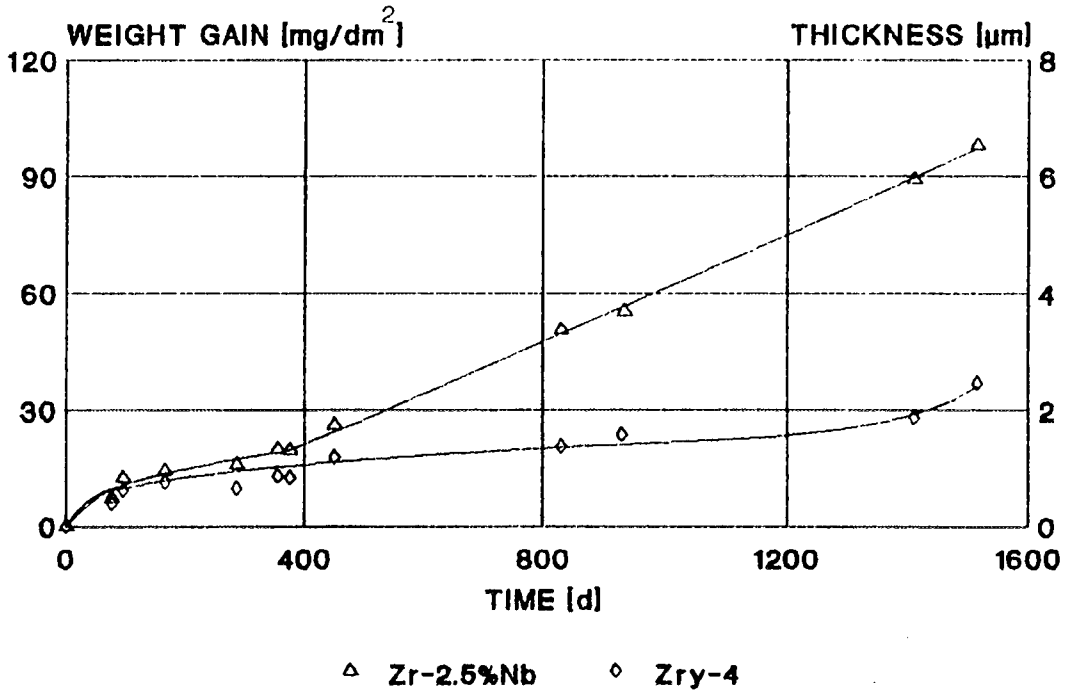
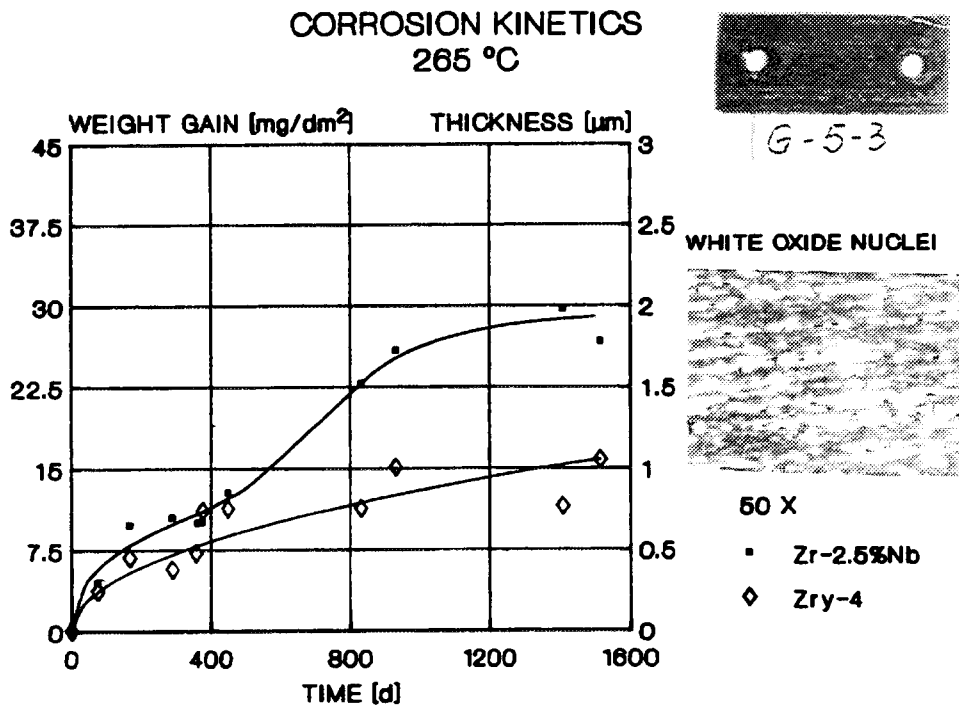


Fig. 3 . Corrosion kinetics of Zry-4 and Zr-2.5Nb at 350 °C

## CORROSION KINETICS 305 °C



**Fig. 4 . Corrosion kinetics of Zry-4 and Zr-2.5Nb at 305 °C**



**Fig. 5 . Corrosion kinetics of Zry-4 and Zr-2.5Nb at 265 °C**

Results at 350 °C, Fig. 3, indicate that after 210 days of exposure Zry-4 has not reached the transition point. This can be partially attributed to the chemical composition of the material tested as has been already reported [6]. Zr-2.5Nb samples, with and without heat treatment, increase their corrosion rate after 180 and 140 days respectively with the same trend observed at 435 °C.

Fig. 4 and 5 correspond to the kinetic data gathered at 305 and 265 °C from the samples inserted in the autoclaves of the primary circuit of Embalse NGS. Zr-2.5Nb maintains the trend found at higher temperatures with a transition point about 400 days in both cases. The post-transition rate is 0.067 mg/dm<sup>2</sup> d (1.6 µm/y) at 305 °C. The formation of white oxide nuclei is seen at 265 °C from the transition point on and these nuclei grow with increasing exposure, Fig. 5. After 1000 days of oxidation the spalling of white oxide spots can balance the weight-gain of the samples. The Zry-4 samples in the hot leg seem to have reached the post-transition after 1400 days exposure while those in the cold leg are in the pre-transition period.

At all temperatures, the corrosion rate of the Zry-4 tested is lower than that of Zr-2.5Nb. The improvement in corrosion resistance of heat treated pressure tube material of Zr-2.5Nb shows clear evidence of the susceptibility of this alloy to heat ageing treatments. The time to transition of Zr-2.5Nb is always shorter than for Zry-4, save at 435 °C. The difference in transition points increases when the temperature decreases. This should also be related to the microstructural changes induced by the temperature of the exposure, more relevant the higher the temperature is, thus improving the corrosion resistance of Zr-2.5Nb.

#### 4.- ACTIVATION ENERGY OF PRETRANSITION STAGE

The pretransition rate constants of Zry-4 and Zr-2.5Nb were calculated at the different temperatures, assuming that Zry-4 has a cubic pretransition kinetics and Zr-2.5Nb a quadratic one as reported in the literature [3,7-9]. The Arrhenius plot for both materials are in Fig. 6 and 7. From the slope of the graphs the activation energy results 35800±1500 [cals/mol] for Zry-4 and 31400±3800 [cals/mol] for Zr-2.5Nb. Garzarolli et al [7] have estimated 32289 [cals/mol] for Zry-4.

#### 5.- MICROSTRUCTURE

##### 5.1.- IMPEDANCE MEASUREMENTS

AC impedance measurements were done in a 1M H<sub>2</sub>SO<sub>4</sub> electrolyte solution that permeates pores and cracks in the oxide layer thus partially

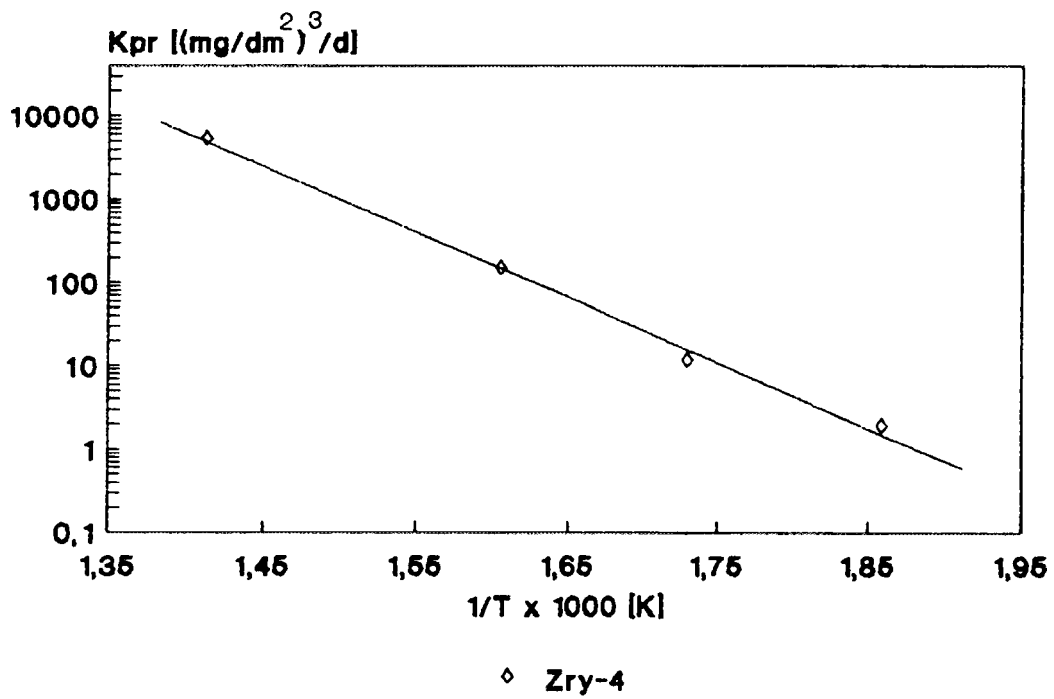


**Fig. 6 . Arrhenius plot of pretransition rate constant for Zry-4**

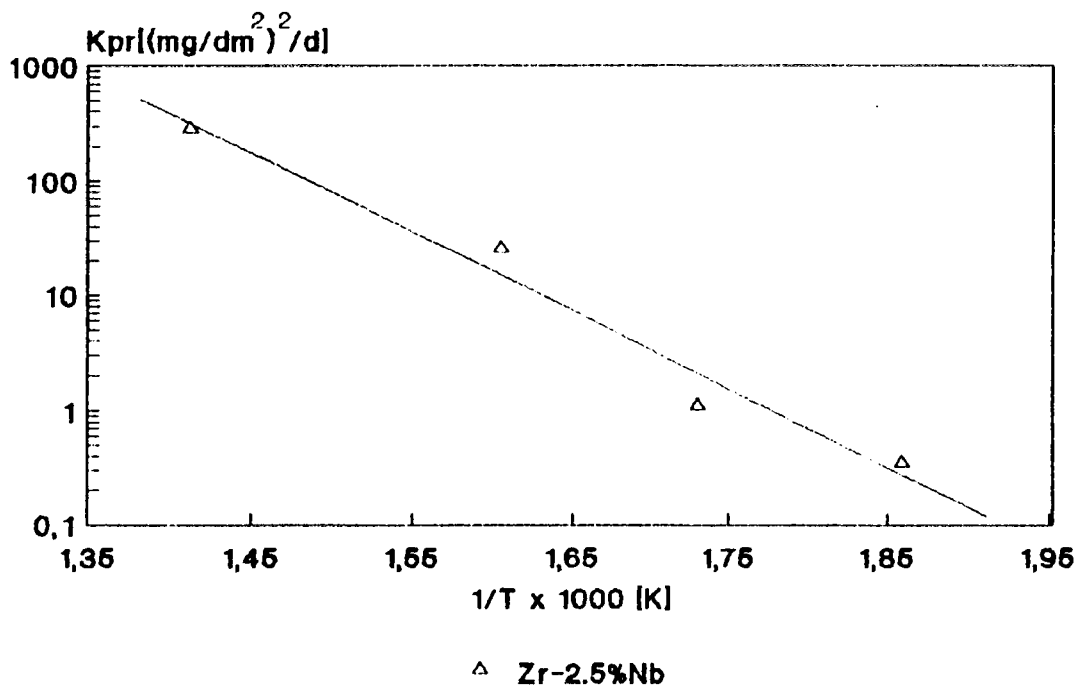


**Fig. 7 . Arrhenius plot of pretransition rate constant for Zr-2.5Nb**

### Zry-4

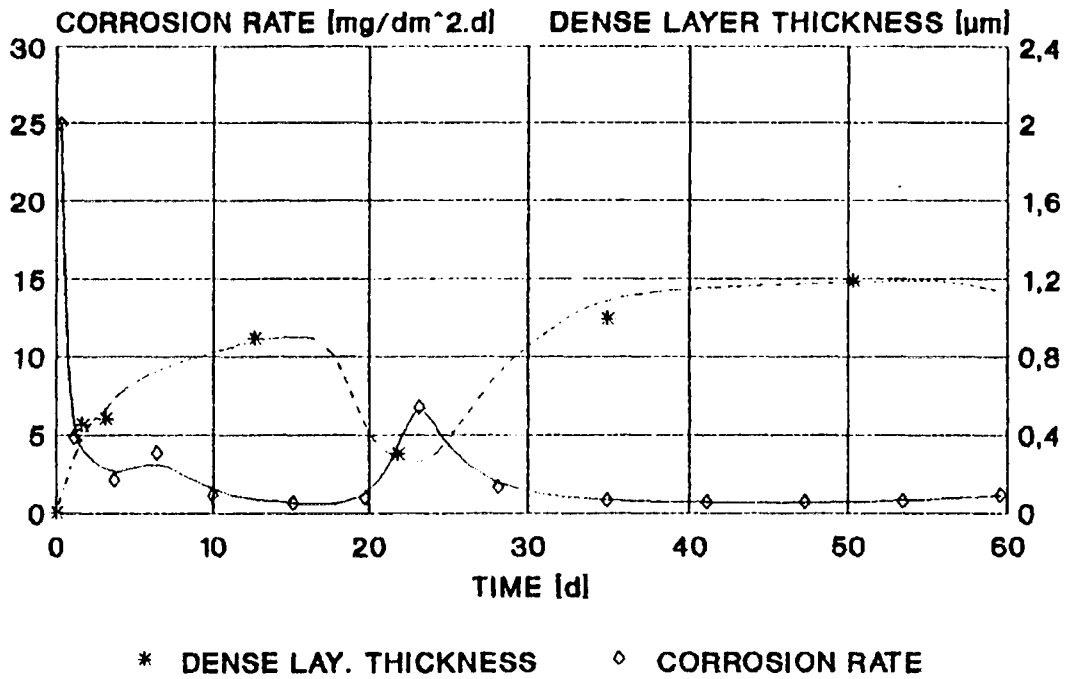


**Fig. 8 . Dense layer thickness and corrosion rate of Zry-4 vs time of exposure**

### Zr-2.5%Nb

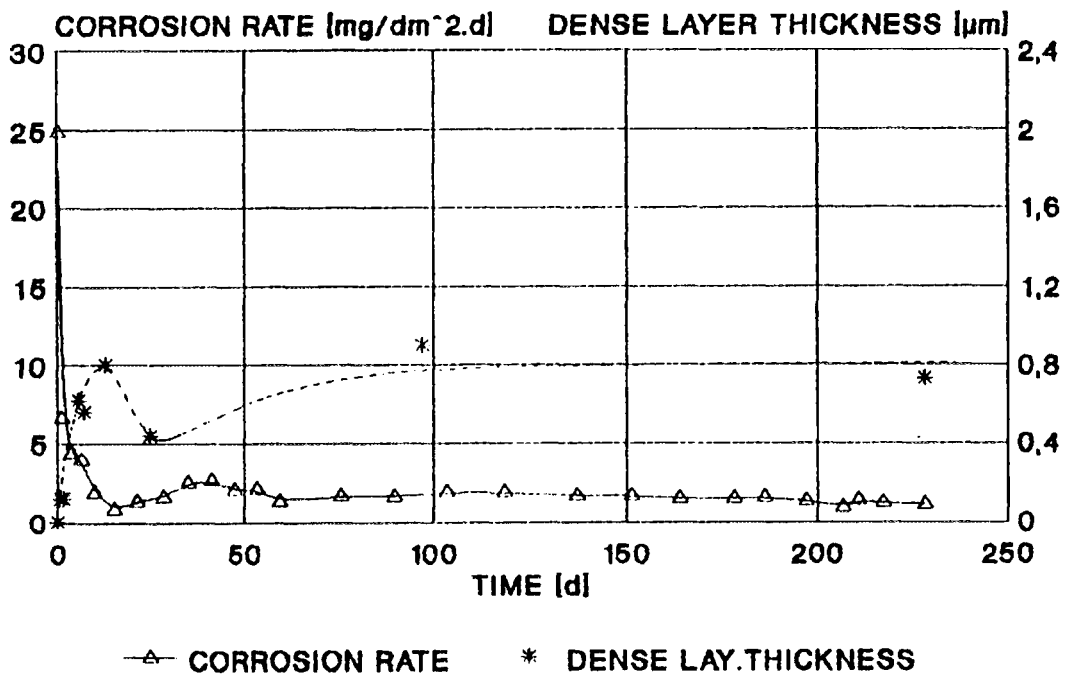


**Fig. 9 . Dense layer thickness and corrosion rate of Zr-2.5Nb vs time of exposure**

short-circuiting the isolating film. An equivalent oxide thickness was calculated from the capacitance measured by the formula [10]

$$d (\mu\text{m}) = 19.47 / C (\text{nF/cm}^2)$$

The oxide layer is formed by two layers with different features, the external one permeated, either through pores or cracks, and the internal layer, dense and impervious. Fig. 8 presents the corrosion rate and the average thickness of the dense oxide film for Zry-4 at 435 °C vs time of exposure. During the first cycle the oxide inner layer grows and the corrosion rate decreases accordingly, at the transition point when the thickness of this layer decreases the corrosion rate increases and towards the end of the second cycle the thickness of the dense layer is increasing once again.

The pattern followed by Zr-2.5Nb is shown in Fig. 9. The dense layer grows up to the transition point and from then on has a near constant value. The thickness of the dense layer measured for Zry-4 is greater than that corresponding to Zr-2.5Nb in agreement with the lower corrosion rate found for Zry-4.

## 5.2.- X-RAY ANALYSIS

X-ray analysis of the oxide films was performed without removing the oxide layer from the samples. The X-ray intensities indicate a significant texture of the oxides. Not only the (111)<sub>m</sub> reflection is very weak in the oxides of both alloys but the same is found for the  $\alpha$ -Zr reflection peak (100) corresponding to the base materials. The X-ray diffractograms from the oxides contain the peaks of the monoclinic zirconia and a broad weak peak at an interplanar spacing of around 0.295 nm attributed to the (111) planes of tetragonal zirconia.

Although the oxide formed had mainly the monoclinic structure a fraction of the tetragonal phase that varied with the oxide layer thickness was also measured. Tetragonal zirconia is not stable at this temperature, contrary to the monoclinic phase stable at all temperatures below 1170 °C, but the tetragonal phase is stabilized by stresses and/or impurities [11,12] and very large compressive stresses are produced in the oxide films in the vicinity of the oxide-metal interface [13].

The amount of tetragonal phase calculated from X-ray diffraction data gives the average concentration on the whole scale. A semiquantitative volume fraction of tetragonal zirconia was calculated using the Garvie and Nicholson formula [14]

$$(\% \text{ZrO}_2)_t = I(111)_t / [I(111)_t + I(111)_m + I(1\bar{1}\bar{1})_m]$$

Fig. 10 shows the volume fraction of tetragonal zirconia at different oxide thicknesses of both alloys. A decrease of the tetragonal fraction is

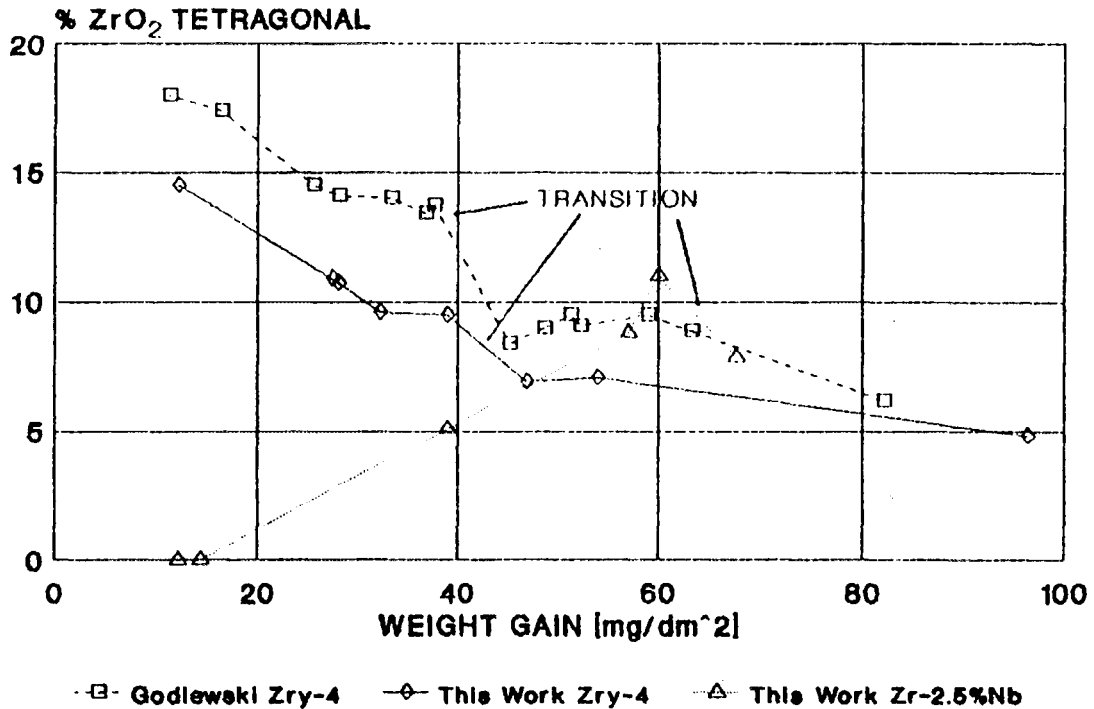


**Fig. 10 . Evolution of tetragonal zirconia volume fraction vs weight-gain of Zry-4 and Zr-2.5Nb samples**

observed around the onset of transition. The tetragonal zirconia was not found in oxide films of Zr-2.5Nb below 1  $\mu\text{m}$ .

The average crystallite size of each film is calculated with the Scherrer expression for the intrinsic broadening with appropriate corrections for instrumental broadening. The effect of line broadening and displacement produced by the stresses existing in the oxide layer was not considered. The oxide crystallite size for Zry-4 varies from 14.0 to 19.7 nm in oxides of 0.8 to 3.6  $\mu\text{m}$  while in Zr-2.5Nb ranges from 10.7 to 22.4 nm in oxide films of 0.7 to 4.5  $\mu\text{m}$ .

The sequence of formation amorphous ZrO<sub>2</sub> --> tetragonal ZrO<sub>2</sub> --> monoclinic ZrO<sub>2</sub> has been postulated to occur both in the course of the oxidation of zirconium alloys [15] and in the formation of ZrO<sub>2</sub> by hydrolysis of Zr(IV) aqueous solutions [16]. Although the starting materials are very different, the nature of the phases reflects in both cases the structural constraints in the evolution to the final stable monoclinic variety. The tetragonal phase is formed in the present case through a topotactic process that is heavily influenced by the metal faces undergoing oxidation. The lower interfacial energies contribute to its stabilization but are not the causative factor. In agreement, the tetragonal phase contents do not always decrease monotonously upon increasing oxide thickness, as evidenced in Fig. 10 for Zr-2.5Nb.

## 6.- OXIDE TOPOGRAPHY

Optical examination with polarized dark field illumination of the Zry-4 oxides detects bright spots that grow along with the film thickness. These bright regions are indicating zones with either pores or micro-cracks. SEM examinations confirm the existence of micro-cracks along the grain boundaries. Both features are shown in Fig. 11.

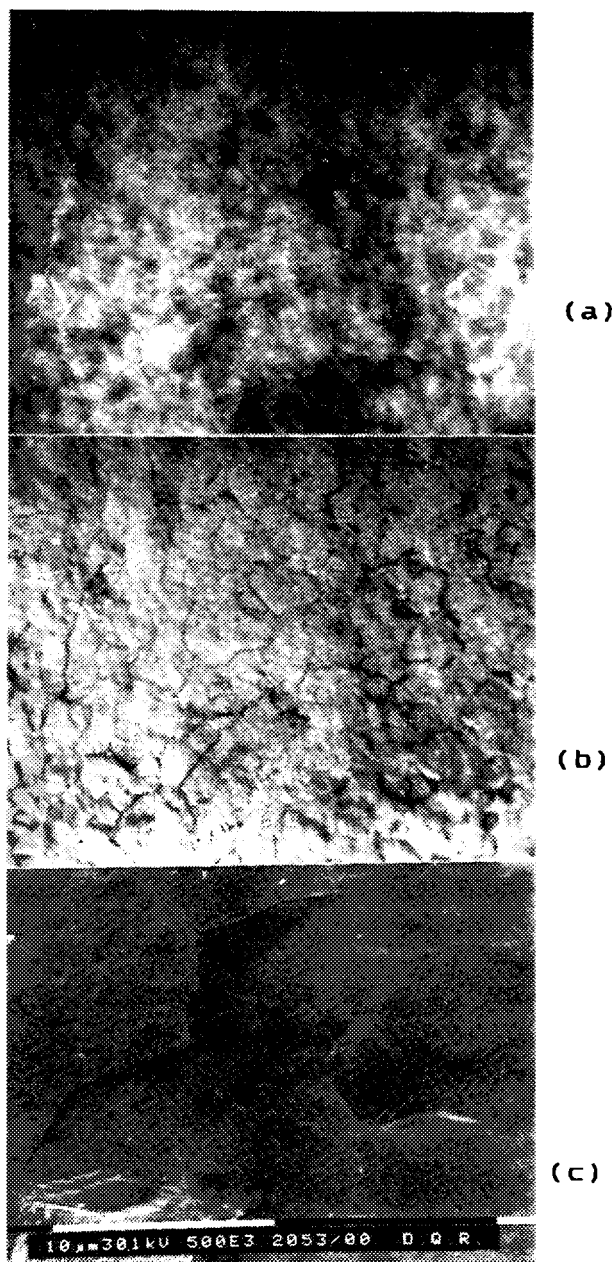


**Fig. 11 . Zry-4, oxide thickness 15  $\mu\text{m}$ . a) Optical microscopy, polarized dark field illumination, b) optical microscopy, bright field, c) SEM micrograph. a) and b) 33  $\mu\text{m}$  \_\_\_\_\_**

The growth of the oxide on the base metal gives birth to tensile stresses on the metal and compressive stresses on the oxide. These stresses, that reach a maximum value before transition and then decrease [13,17] starting to grow once again in the second cycle [13], induce the development of microcracks in the oxide layer at the transition zone. These microcracks are related to the relaxation of stresses, the phase transformation of tetragonal zirconia and the decrease in thickness of the dense impervious layer found by X-Ray diffraction and impedance measurements. The wide bright zones on Fig. 11 appear once the oxide is thick enough and the stresses on its surface are sufficiently low [11].

A similar behaviour could be expected for Zr-2.5Nb in the transition since the tetragonal phase decreases and the thickness of the dense layer diminishes. Still, there is a difference up to a 1  $\mu\text{m}$  thick oxide since no tetragonal phase was detected and the dense layer is thinner. This might be a consequence of micro-cracks developed at an early stage of oxidation [18,19] that have partially relaxed the stresses hindering the stabilization of the tetragonal phase and caused the parabolic rate law of growth of the oxide.

## 7.- METAL/OXIDE INTERFACE

SEM analysis of the metal-oxide interface shows changes as long as the oxide grows. For 1  $\mu\text{m}$  thick oxide of Zry-4 the oxide grows substrate-oriented since the corrosion rate depends on the orientation of the grains, Fig. 12. From 5  $\mu\text{m}$  on, the grain boundaries are almost lost and protrusions zones that penetrate deeper into the metal are formed. At a thickness of 20  $\mu\text{m}$  these protrusions zones are a common feature, Fig. 13.

The existence of areas with and without protrusions indicates a differential growth of the oxide into the metal so that the development of microcracks and the formation of the inner dense layer will be simultaneous giving thus a constant corrosion rate [6,15,20].

For 1  $\mu\text{m}$  thick oxide of Zr-2.5Nb the metal/oxide interface shows ridges of oxide, coincident with the filaments of the  $\beta$ -Zr phase of the base material that grow deeper into the substrate due to the higher corrosion rate of this phase [5,21-24], Fig. 14. As the oxide grows the ridges become wider and deeper and coalescence starts in different zones. The width increase is 0.2, 1 and 1.5  $\mu\text{m}$  as the oxide ranges through 1, 5 and 30  $\mu\text{m}$  thickness.

Within the  $\alpha$ -phase, at 5  $\mu\text{m}$  thick oxide, bigger oxide particles are surrounded by clusters of very small crystallites from the ridges, Fig. 15. At 8  $\mu\text{m}$  thickness, ridges and areas with crystals in-between are still evident in the interface. Once the oxide reaches 12  $\mu\text{m}$ , the coalescence of the ridges provides an array of coarse ridges and holes all over the interface, presumably the holes represent areas of a lower corrosion rate.

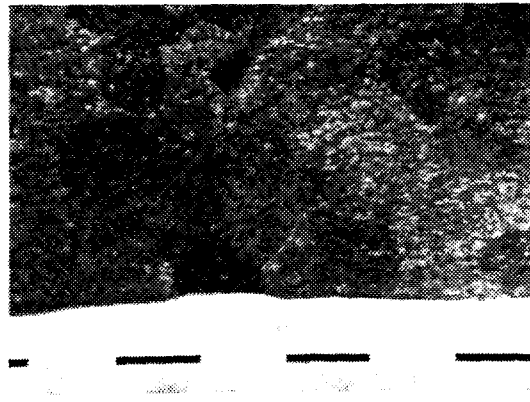


**Fig. 12 . Zry-4,oxide/metal interface. 1 μm thick oxide.**

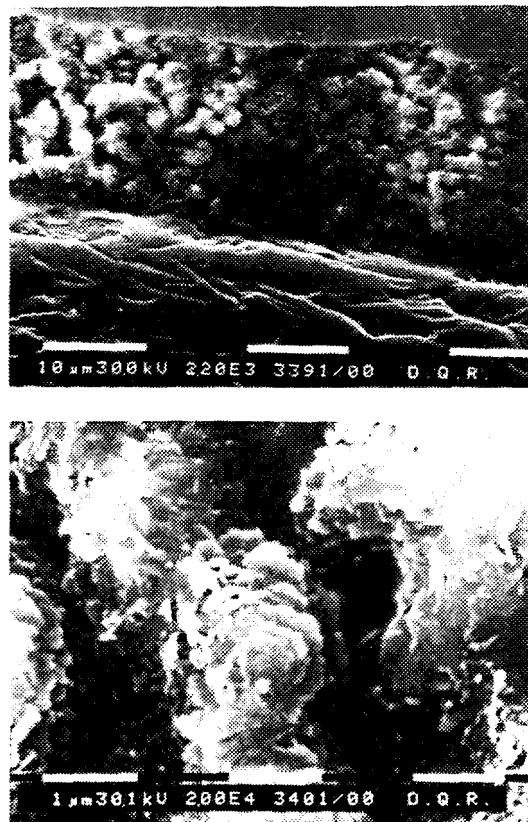


**Fig. 13 . Zry-4,oxide/metal interface. At a thickness of 20 μm protrusions zones are a common feature**



**Fig. 14 . Zr-2.5Nb, oxide/metal interface, 1 μm thick oxide.**

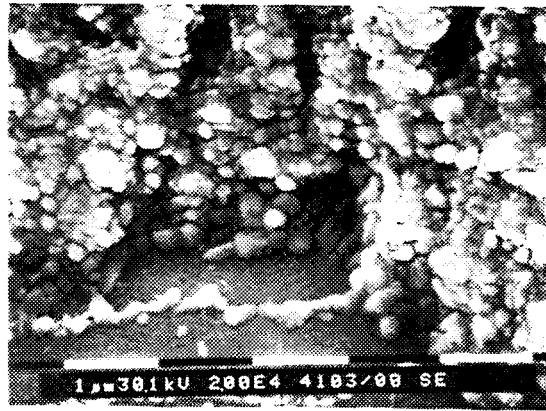


**Fig. 15 . Zr-2.5Nb, oxide/metal interface, 5 μm thick oxide.**

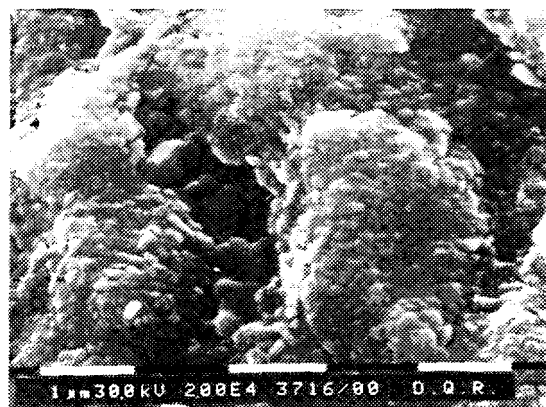


**Fig. 16 . Zr-2.5Nb, oxide/metal interface, 30 μm thick oxide.**

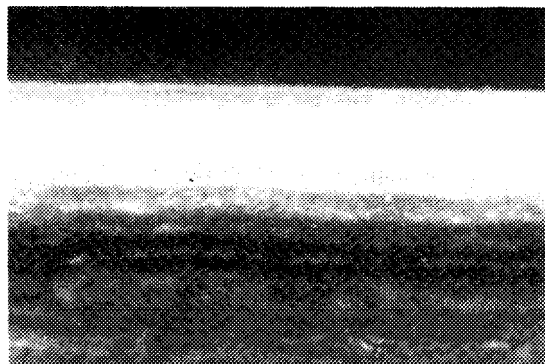


**Fig. 17 . Zr-2.5Nb, polarized dark field illumination showing the multilayered structure of the oxide. \_\_\_\_ 9  $\mu$ m.**

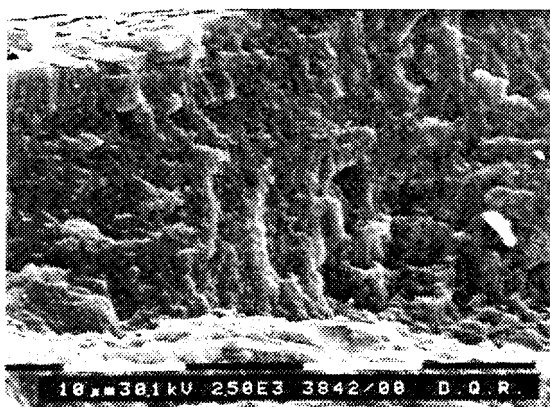


**Fig. 18 . Zr-2.5Nb, SEM analysis of a fractured oxide**

The ridges are formed by clusters of crystallites of around 0.2  $\mu$ m. At a 30  $\mu$ m thickness of the oxide two well defined microstructures are detected. Areas of ridges that have grown in width and depth, still formed by clusters, and areas in between with lower corrosion rate were well-defined crystals around 300 and 400 nm are found, Fig. 16. The same features are seen in the interface of a 25  $\mu$ m thick oxide in the Zr-2.5Nb alloy heat treated.

The results indicate a preferential growth of the oxide since the ridges generated by the  $\beta$ -phase in the oxide grow as the oxide thickness increases. Once a coalescence stage is reached (5  $\mu$ m oxide) areas of oxide that penetrate deeper into the metal are established and the average growth of the oxide results from localized areas with different corrosion rates. If the formation of the microcracks and the growth of the inner layer are thus shifted the cyclic stage observed for Zry-4 cannot be detected. Nevertheless, optical microscopic examination, with bright field

and polarized dark field illumination have shown that the oxide layers exhibit a multi-layered structure as has been found for Zry-4 [20,25] and is also confirmed by SEM analysis of a fractured oxide, Figs. 17 and 18.

## 8.- CONCLUSIONS

- The corrosion rate of Zr-2.5Nb is higher than that of Zry-4 for the alloys that were tested.
- Zry-4 presents a cyclic oxidation kinetics while Zr-2.5Nb shows a two-stage behaviour.
- Heat treatments modify significantly the corrosion rate of Zr-2.5Nb. This affects the pressure tube material even during the corrosion tests, depending on the temperature of the exposure.
- Single Kpr value could be used to describe the corrosion rate of Zr-4.
- The activation energies during the pretransition stage indicate that Zry-4 is slightly more dependant on the temperature.
- The transition is a consequence of the abrupt decrease of the thickness of the dense inner layer that is due to the extensive development of microcracks induced by the high stresses which are in turn partially relaxed during the transition.
- Analysis of the films during the pretransition stage shows a volume fraction of tetragonal zirconia phase between 10 and 15 %, mainly transformed into the monoclinic phase after the transition point, as a consequence of stress relaxation.
- Metal-oxide interfaces of both alloys show different features. The ridges arising in Zr-2.5Nb and their growth could explain the absence of the cyclic oxidation stage found in Zry-4 on account of the higher corrosion rate of the  $\beta$ -phase. The end of the cyclic stage in Zry-4 is probably related to the zones of protrusions once they are extensively developed.

## REFERENCES

- [1] GRAHAM, R.A., EUCKEN, C.M., Ninth Int. Symp. on Zirconium in the Nuclear Industry, Kobe, Japan, (1991).
- [2] SABOL, G.P., KILP, G.R., BALFOUR, M.G., ROBERTS, E., Eight Int. Symp. on Zirconium in the Nuclear Industry, ASTM STP 1023 (1989) p. 227.
- [3] COX, B., J. Nucl. Mat., vol. 148,(1987) p. 332.
- [4] URBANIC, V.F., WARR, B.D., MANOLESCU, A., CHOW, C.K., SHANAHAN, M.W., Eight Int. Symp. on Zirconium in the Nuclear Industry, ASTM STP 1023, (1989), p. 20.
- [5] URBANIC, V.F., GILBERT, R.W., IAEA Tech. Committee Meeting on Fundamental Aspects of Corrosion of Zirconium-Base Alloys, Portland, Oregon, USA, (1989) p. 262.
- [6] BORDONI, R., BLESÁ, M.A., IGLESIAS, A.M., MAROTO, A.J.G. , OLMEDO, A.M., RIGOTTI, G., VILLEGAS, M., Tenth Int. Symp. on Zirconium in the Nuclear Industry, Baltimore, USA (1993).
- [7] GARZAROLLI, F., JUNG, W., SCHOENFELD, H., GARDE, A.M., PARRY, G.W., SMERD, P.G., EPRI NP-2789, (1982).

- [8] HILLNER, E., Zirconium in the Nuclear Industry, ASTM STP 633, (1977) p. 211.
- [9] URBANIC, V.F., COX, B., FIELD, G.J., Seventh Int. Symp. on Zirconium in the Nuclear Industry, ASTM STP 939, (1987) p. 189.
- [10] ROSECRANS, P.M., Sixth Int. Symp. on Zirconium in the Nuclear Industry, ASTM STP 824, (1984) p. 531.
- [11] ROY, C., DAVID, G., J. Nucl. Mat., vol. 37, (1970) p.71.
- [12] DAVID, G., GESHER, R., ROY, C., J. Nucl. Mat., vol. 38, (1971) p. 329.
- [13] GODLEWSKI, J., Tenth Int. Symp. on Zirconium in the Nuclear Industry, Baltimore, USA (1993).
- [14] GARVIE, R.C., NICHOLSON, P.S., J. Am. Ceram. Soc., vol. 55-6, (1972) p. 303.
- [15] GARZAROLLI, F., SEIDEL, H., TRICOT, R., GROS, J.P., Ninth Int. Symp. on Zirconium in the Nuclear Industry, ASTM STP 1132, (1991) p. 395.
- [16] BLESÁ, A.M., MAROTO, A.J.G., PASSAGGIO, S.I., FIGLIOLIA, N.E., RIGOTTI, G., J. Mat. Science, vol. 20, (1985) p. 4601.
- [17] BRADHURST, D.H., HEUER, P.M., J. Nucl. Mat., vol. 37, (1970) p. 35.
- [18] COX, B., AECL-5610, (1976)
- [19] BORDONI, R., MAROTO, A.J.G., VILLEGAS, M., GELDSTEIN, M.C., OLMEDO, A.M., Seminar on Zirconium Alloys: Structure, Mechanical Properties and Post-Irradiation Changes, Hydrogen Impact on Properties of Alloys. Moscow, Russia, 1991.
- [20] BRYNER, J.S., J. Nucl. Mat. vol. 82, (1979) p. 84.
- [21] WARR, B.D., RASILE, E.M., BRENNENSTUHL, A.M., IAEA Tech. Committee Meeting on Fundamental Aspects of Corrosion of Zirconium-Base Alloys, Portland, Oregon, USA (1989).
- [22] WARR, B.D., ELMOSELHI, M.B., RASILE, E.M., BRENNENSTUHL, A.M., Fuel Channel Technology Seminar, Alliston, Ontario, Canada (1989).
- [23] URBANIC, V.F., CHOUBEY, R., CHOW, C.K., Ninth Int. Sym. on Zirconium in Nuclear Industry, Kobe, Japan (1990).
- [24] URBANIC, V.F., CHAN, P.K., KHATAMIAN, D., WOOD, O.T., Tenth Int. Symp. on Zirconium in the Nuclear Industry, Baltimore, U.S.A. (1993).
- [25] STEHLE, H., GARZAROLLI, F., GARDE, A.M., SMERD, P.G., Sixth Int. Symp. on Zirconium in the Nuclear Industry, ASTM STP 824, p. 483 (1984).



## **INFLUENCE OF ALKALI METAL HYDROXIDES ON CORROSION OF Zr-BASED ALLOYS**

Y.H. JEONG

Korea Atomic Energy Research Institute,  
Dae Jun, Republic of Korea

H. RUHMANN, F. GARZAROLLI

Siemens-KWU, Power Generation Group,  
Erlangen, Germany

### **Abstract**

In this study the influence of group-1 alkali hydroxides on different zirconium based alloys has been evaluated. The experiments have been carried out in small stainless steel autoclaves at 350 °C in pressurized 17 MPa water, with in low (0.32 mmol), medium (4.3 mmol) and high (31.5 mmol) equimolar concentrations of Li-, Na-, K-, Rb- and Cs-Hydroxides. Two types of alloys have been investigated: Zr-Sn-(Transition metal) and Zr-Sn-Nb-(Transition metal). The corrosion behavior was evaluated from weight gain measurements. From the experiments the cation could be identified as the responsible species for zirconium alloy corrosion in alkalized water. The radius of the cation governs the corrosion behavior in the pre accelerated region of zircaloy corrosion. Incorporation of alkali cations into the zirconium oxide lattice is probably the mechanism which allows the corrosion enhancement for Li and Na and the significantly lower effect for the other bases. Nb containing alloys show lower corrosion resistance than alloys from the Zr-Sn-TRM system in all alkali solutions. Both types of alloys corrode significantly more in LiOH and NaOH than in the other alkali environments. Lowest corrosive aggressiveness has been found for CsOH followed by KOH. Concluding from the corrosion behavior in the different alkali environments and taking into account the tendency to promote accelerated corrosion, CsOH and KOH are possible alternate alkalis for PWR application.

## INTRODUCTION

In order to maintain low corrosion and activation of corrosion products in pressurized light water reactors the primary water has to be pH controlled. This is performed usually by the addition of alkalizers such as lithium hydroxide or potassium hydroxide to the coolant. Under certain operation conditions with high operational temperatures locally increased void levels have to be anticipated. In out of pile loop experiments performed under heat flux conditions and in the presence of lithium hydroxide, enhanced corrosion of zircaloy cladding has been reported [1]. Even isothermal experiments performed in autoclaves in water under high pressure showed that lithium hydroxide is detrimental to the corrosion resistance of zircaloy.

Several studies using concentrations between 0.1 and 3 mol of LiOH in aqueous solutions have been performed in the past [2, 3, 4, 5, 6]. Only few results are available from literature which include different alkalizers like sodium-, potassium- or other hydroxides from group I or II of the periodic table. Coriou et al. [7] investigated the influence of LiOH, NaOH, KOH and NH<sub>3</sub> upon the corrosion in the temperature range of 330 to 370 °C. They found the highest effect on corrosion rate for LiOH and no effect for NH<sub>3</sub>. The threshold concentration for acceleration of corrosion was reported as 3 mmol for LiOH [14].

In the corrosive solution, in principle, either the cation or the OH-anion can induce enhanced corrosion. Some experimental results have been reported which should allow one to determine on the responsible ionic species for the enhanced LiOH corrosion. Hillner [4] reported no or only a slight increase of the corrosion for 1 molar Lithium nitrate (pH = 7.8). Perkins and Bush [8] measured a significant decrease in the aggressiveness of the LiOH solutions if OH is converted to carbonate by exposure to air (pH decreased from 12.4 to 10.3). Furthermore, the addition of boric acid reduces the pH of the alkali solution and

also the corrosion aggressiveness [9, 10]. All these results can be interpreted that both the metal cation and the OH anion should have a significant effect on Zry corrosion in caustic solutions. No systematic study has been performed to decide this question or to investigate the influence of different alkali metals.

Mechanistic models have been suggested in the literature to explain the accelerating effect of LiOH [11]. The substitutional incorporation of Li<sup>+</sup> into the growing zirconium oxide would cause an increased anion vacancy concentration which allows an accelerated charge transfer through the metal oxide interface and therefore enhanced corrosion. As pointed out recently by Cox [15] this incorporation model needs significant effects on corrosion in the pretransition oxide if it should be valid.

A second mechanism which influences the morphology of the corrosion layer was addressed by Garzarolli et al. [12] to a modified crystal growth mechanism (crystallization of oxide) induced by alkalizers like LiOH. The influence the formation and conversion of primary growing tetragonal oxide nuclei to the monoclinic modification. As a result more equiaxed oxide grains than columnar structures are developed. Finally both mechanistic aspects are used by Ramasubramanian [11] who also indicated non dissociated LiOH as a responsible factor for the development of fast growing porous oxide layers on zirconium alloys.

Increased concentrations of Li in porous oxide structures under non isothermal, boiling conditions are responsible for the enhanced alkali induced corrosion of Zry (known as hideout [10]). This phenomenon suggests the diffusion of solute species in porous structures as a driving mechanism. Diffusion in aqueous solutions is governed by the radius of the solvated ion (under otherwise constant conditions). In the sequence of the group-I alkali cations Li<sup>+</sup> has the largest radius in opposition to Li<sup>+</sup> in the crystal lattice (see Tab. 1). Therefore, if

Tab.1 Properties of Group-I alkali metals.

Metal	At.No	At.Wt %	Cryst. Struct.	Density (g/cm <sup>3</sup> )	At.Radius (pm)	Ion Radius pm (Coord.)	Ion Radius solv. (pm)	Ion Cond. 25 C (cm <sup>2</sup> /ohm mol)	M.P (C°)	B.P (C°)
Li	3	6.94	BCC	0.53	152	76 (6)	340	38.7	186	1342
Na	11	23	BCC	0.968	185.8	102 (6)	276	50.1	97.7	881
K	19	39.1	BCC	0.86	227.2	151 (8)	232	73.5	63.6	756
Rb	37	85.5	BCC	1.52	247.5	161 (8)	228	77.8	39	686
Cs	55	133	BCC	1.89	265.5	174 (8)	228	77.2	28.45	678
Zr					159	72 (8)				
NH <sub>4</sub>						150 (6)		73.6		

an increased concentration of alkali is induced by a diffusion process in solution filled pores, the effect should be more pronounced for NaOH to CsOH in comparison to LiOH.

This study was performed without focusing on the mechanistic aspects of accelerated corrosion in alkalized environments. It was carried out in order to check the potential for alternate alkalizers in nuclear power plants. The influence of group-1 alkali hydroxides on two different types of zirconium based alloys was the objective of the investigation. Nevertheless, the study was designed in a way not to exclude mechanistic observations.

## **EXPERIMENTAL PROCEDURES**

Critical evaluation of the literature shows a significant ambiguity between cation or anion influence on Zry corrosion in alkaline solutions. Therefore, a comparative experiment which should allow one to decide on the influence of the metallic ionic species must be performed at equimolar concentrations keeping the OH concentration constant. Experiments comparing effects in solutions with equal mass percentages (ppm) of hydroxides mean that different numbers of molecules are present in the reactive environment and therefore difficult to evaluate with respect to the active species. The range of applied concentrations in this study was chosen to cover the pure water condition (or at least the range of concentrations applied in PWRs (app. 2 ppm Li) up to concentrations above the threshold value reported for accelerated corrosion (30 ppm for LiOH) but avoiding concentrations which level out alloy composition sensitivities by being overly aggressive or bare the risk of crud deposition from the autoclave materials (1 mol of LiOH as reported by Ref.[15]).

The concentrations of Li-, Na-, K-, Rb-, and Cs-hydroxides selected for this study were 0.32 mmol, 4.3 mmol and 31.5 mmol, where 0.32 mmol (2.2 ppm Li) represents the standard concentration for lithium in the primary PWR coolant and 35.2 mmol (220 ppm Li) is above the threshold for accelerated corrosion for LiOH. The solutions were prepared from commercially available salts of analytical grade except for RbOH for which only a solution was available. Hydrates and noted impurities (carbonates) have been considered. Nevertheless, as can be seen from Table 2, some deviations from the intended equimolarity were revealed by chemical analysis of the solutions especially for RbOH and CsOH. The cation and anion concentrations have been analyzed independently. With the exception of RbOH, the cation- and anion concentrations are in fairly good agreement (accuracy of the OH determination +/- 5 %). The Rb solution contained obviously much more carbonate than indicated. Identical stock solutions

Tab.2 Results of the chemical analysis of the used alkali solutions.

Alkali-Hydroxide	c(M <sup>+</sup> ) ppm	Molarity of M <sup>+</sup> , mmol			c(OH <sup>-</sup> ) ppm	Molarity of OH <sup>-</sup> , mmol		
		Calculated	Measured	Dev.%		Calculated	Measured	Dev.%
LiOH	2.2	0.32	0.29	-9.4	5.3	0.31	0.3	-3.2
NaOH	7.2	0.32	0.29	-9.4	5.3	0.31	0.33	6.5
KOH	12	0.32	0.28	-12.5	5.3	0.31	0.35	12.9
RbOH	27	0.32	0.42	31.3	5.3	0.31	0.38	22.6
CsOH	42	0.32	0.38	18.8	5.3	0.31	0.4	29.0
LiOH	30	4.3	4.22	-1.9	73	4.3	4.3	0.0
NaOH	99	4.3	4.5	4.7	73	4.3	4.4	2.3
KOH	169	4.3	4.6	7.0	73	4.3	4.5	4.7
RbOH	369	4.3	5.6	30.2	73	4.3	4.8	11.6
CsOH	574	4.3	4.7	9.3	73	4.3	4.8	11.6
LiOH	220	31.5	31.7	0.6	535	31.5	32.5	3.2
NaOH	724	31.5	32.9	4.4	535	31.5	32.5	3.2
KOH	1231	31.5	32.6	3.5	535	31.5	34	7.9
RbOH	2692	31.5	44.9	42.5	535	31.5	35.5	12.7
CsOH	4186	31.5	33.8	7.3	535	31.5	34	7.9

were used for the corrosion experiments taking especially care not to expose them to CO<sub>2</sub> from the atmosphere to avoid changes in composition.

Corrosion tests have been carried out in small 100 ml static autoclaves at 350°C and 17 MPa. In order not to complicate the experiments, the temperature has been chosen far away from the critical temperature of water (374 °C). All samples were carefully kept submerged in the water during exposure. No special inert gas purging has been applied prior to closing the autoclaves. In comparable experiments no influence of remaining air was reported by Perkins [8]. Measurements of pH of the used solutions were performed. If pH values are compared before and after the 35 day run (Table 3) no significant differences for the higher alkali concentrations (4.3 mmol and 32.5 mmol solutions) can be observed. Only

Tab.3 Summary of pH measurements before and after the autoclave tests.

Alkali-Hydroxide	Molarity (mmol)	Cal.pH at 25°C	Measured pH at 25°C		
			Before Test	After 35d run	Diff.
LiOH	0.315	10.5	8.5	7	-1.5
	4.32	11.6	11.4	10.6	-0.8
	31.5	12.5	12.2	12.1	-0.1
NaOH	0.315	10.5	10	7.5	-2.5
	4.32	11.6	11.4	11	-0.4
	31.5	12.5	12.2	12.2	0
KOH	0.315	10.5	10.4	7.9	-2.5
	4.32	11.6	11.4	11.2	-0.2
	31.5	12.5	12.3	12.2	-0.1
RbOH	0.315	10.5	10	9.6	-0.4
	4.32	11.6	11.5	11.3	-0.2
	31.5	12.5	12.4	12.4	0
CsOH	0.315	10.5	10	7.8	-2.2
	4.32	11.6	11.5	11.2	-0.3
	31.5	12.5	12.4	12.4	0

Tab. 4 Composition of the test materials.

Alloy Type	Mark	Nb (%)	Sn (%)	Transition Metals* (TRM)
Zr-Sn-(TRM)	A-1	-	1,4	0,33
Group A	A-2	-	1,1	0,6
	A-3	-	0,8	0,8
Zr-Sn-Nb-(TRM)	B-1	0,3	0,8	0,5
Group B	B-2	0,8	0,8	0,3
	B-3	1.0	-	0,87

the low concentration 0.3 mmol Li-, Na-, K-, and Cs-alkali solutions lost their OH concentration during the run of the experiment.

Tested materials:

Two groups of Zr based materials were investigated. Table 4 gives the chemical composition of the alloys used for the corrosion test. The samples are grouped into

Group A : Zr-Sn-(Transition Metal) type

Group B : Zr-Sn-Nb-(Transition Metal) type.

The main interest was addressed to the influence of niobium under the experimental conditions. The samples were used in form of small (area app. 3 cm<sup>2</sup>) flat material coupons or cladding tube segments (A1 and B3). The condition of the materials was mainly fully recrystallized. All samples have been pickled prior to testing. Corrosion behavior was evaluated from the weight gain. The oxides formed in various alkali hydroxides were investigated by metallography and some of them characterized by SEM.

### 3. RESULTS

#### 3.1. Influence of alloy composition under different alkali environments.

The weight gains measured for the different alloys up to 150 day exposures under various alkali environments are compiled in Table 5. Fig.1 to 5 show graphical presentations of the findings for the materials in low concentration (0.31 mmol, top diagram) medium concentration (4.3 mmol, middle diagram) and high concentration (32.5 mmol, bottom diagram) of Li-, Na-, K-, Rb- and Cs-hydroxide solutions, respectively.

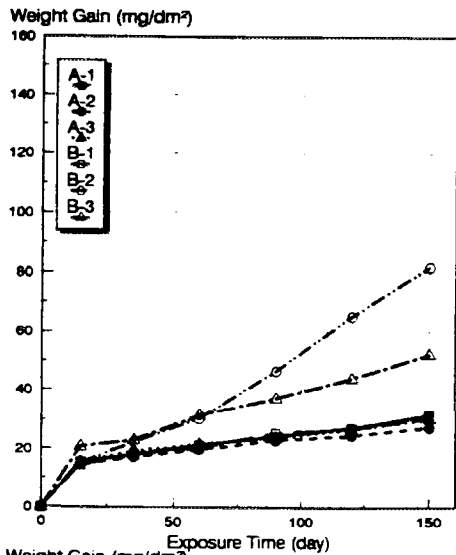
Low concentration behavior:

As shown in Fig.1 to 5 in the LiOH test, group A alloys had low weight gains (around 30 mg/dm<sup>2</sup>) in the pre-transition region after 150 day exposure time without any significant acceleration of corrosion rate. However the Nb-containing alloys (group B) exhibits generally higher corrosion rate than group A alloys if the Nb concentration is above 0.3 % (B2 and B3). The low Nb B1 alloy behaves very similar to Zr-Sn-(TRM) materials. The corrosion behavior in low concentration of NaOH, KOH and CsOH solution (Fig.2, 3 and 5) is not very different from that in LiOH. In RbOH solution (Fig.4) group B alloys showed somewhat higher weight gains and corrosion rates than in other alkali solutions. This result may be induced by the deviations in the Rb concentrations in solution. As can be seen from the data of chemical analysis (Table 2), the difference between cation and anion concentration is high for the RbOH solution. This higher corrosion in Rb is also visible at higher alkali concentrations and is not eliminated by correction to the nominal concentration what would point to a higher sensitivity of Nb alloys to Rb<sup>+</sup>. The carbonate concentration has not been

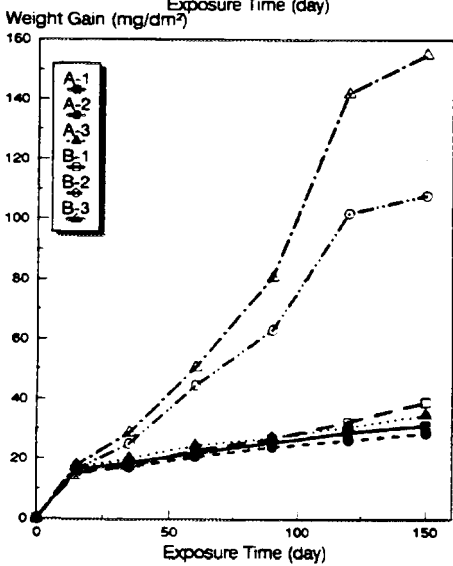
Tab. 5 Corrosion Results.

Alloy	conc. MOH (mmol)	Exposure (day)	Weight Gain (mg/dm <sup>2</sup> )				
			LiOH	NaOH	KOH	RbOH	CsOH
A1	0,315	90	24,1	24,1	25,1	28,8	26,2
		120	26,9	27,0	27,3	31,5	29,6
		150	31,1	29,2	28,9	32,4	31,2
	4,3	90	25,5	24,3	23,7	30,3	25,4
		120	29,0	27,3	27,1	36,1	28,4
		150	31,2	28,0	27,4	39,4	29,9
	31,5	90	182,0	28,1	25,0	29,7	25,6
		120	630,0	30,8	28,1	31,1	28,0
		150	906,0	47,0	31,0	34,2	29,4
A2	0,315	90	22,7	22,3	22,3	25,6	25,0
		120	24,3	24,5	25,3	27,5	25,8
		150	27,0	27,7	26,3	28,8	27,8
	4,3	90	24,1	23,6	22,5	26,5	21,7
		120	26,3	26,8	25,5	32,2	24,0
		150	28,7	27,6	24,9	35,8	25,4
	31,5	90	40,2	27,2	23,5	24,6	21,6
		120	109,0	28,0	26,3	28,0	24,0
		150	237,0	29,4	27,6	28,6	25,0
A3	0,315	90	23,3	23,8	23,6	26,1	28,1
		120	26,1	25,5	26,2	29,0	28,6
		150	29,9	28,4	26,3	30,1	31,7
	4,3	90	27,2	29,6	23,8	29,0	23,6
		120	30,7	31,8	26,2	35,5	26,8
		150	34,9	33,0	26,7	38,4	28,2
	31,5	90	565,0	29,6	27,5	26,9	24,3
		120	1130,0	30,5	29,5	28,7	26,8
		150	1548,0	31,7	29,9	30,7	28,3
B1	0,315	90	25,1	22,9	23,4	26,6	26,7
		120	26,4	25,9	27,1	31,4	28,3
		150	30,2	29,5	29,1	34,2	32,0
	4,3	90	26,7	24,0	22,8	31,0	23,2
		120	32,4	26,7	27,3	40,0	26,5
		150	39,1	28,5	27,5	45,9	28,6
	31,5	90	1307,0	27,5	26,2	27,9	23,5
		120	1992,0	29,7	29,4	31,6	26,3
		150	2462,0	32,8	31,2	34,1	28,1
B2	0,315	90	46,3	57,4	65,4	87,0	66,2
		120	65,1	71,6	84,0	111,0	83,0
		150	81,7	84,6	96,2	132,0	96,7
	4,3	90	63,1	47,6	42,8	75,7	32,0
		120	102,0	67,6	57,2	108,0	38,0
		150	108,0	89,4	71,2	130,0	44,1
	31,5	90	235,0	46,9	49,2	52,1	38,4
		120	919,0	52,3	56,8	61,1	42,7
		150	1499,0	61,8	64,2	71,3	47,8
B3	0,315	90	37,1	38,4	43,0	72,1	41,4
		120	43,7	47,7	52,7	98,1	51,9
		150	51,9	62,6	65,0	128,0	65,2
	4,3	90	80,8	49,5	46,5	97,0	36,3
		120	140,0	72,9	57,0	138,0	41,6
		150	155,0	93,0	119,0	188,0	46,7
	31,5	90	3203,0	-1478,0	-322,0	-245,0	-26,0
		120	4300,0	-2400,0	-550,0	-480,0	-185,0
		150	4600,0	-2974,0	-713,0	-632,0	-315,0

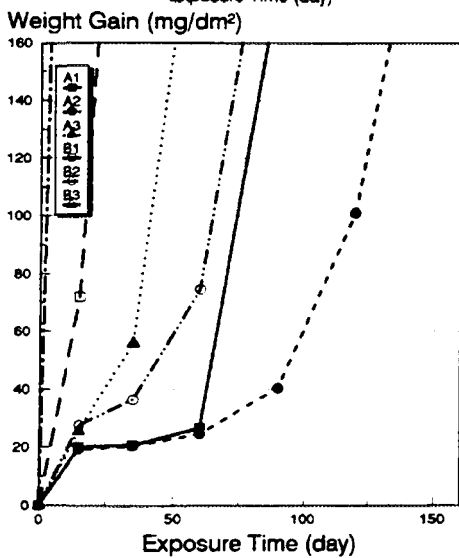
Negative values indicate spalling.



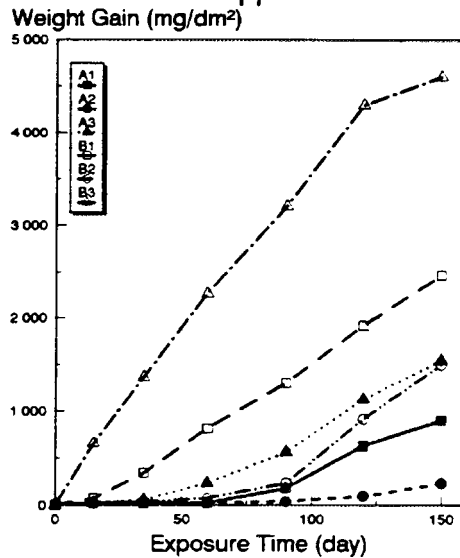
0.32 mmol LiOH  
2.2 ppm Li



4.3 mmol LiOH  
30 ppm Li

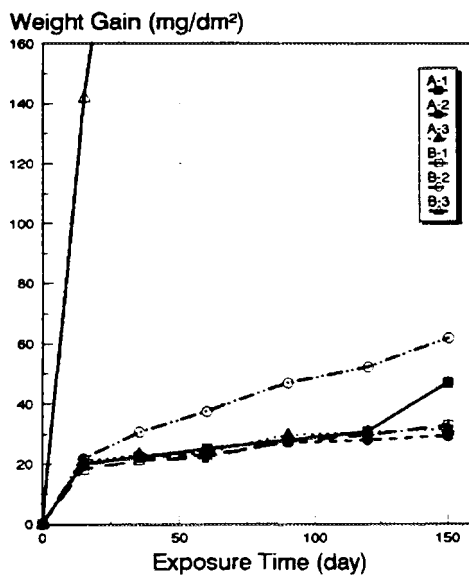
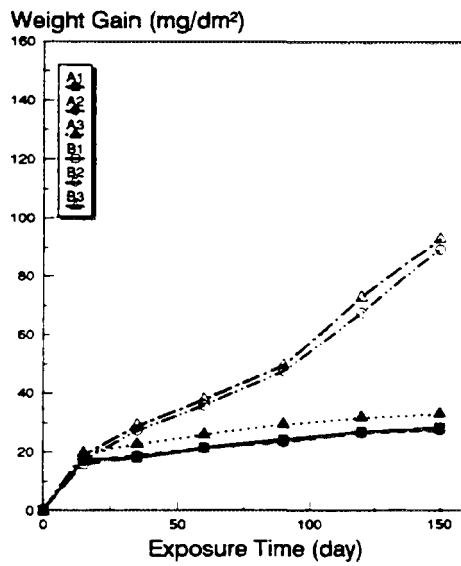
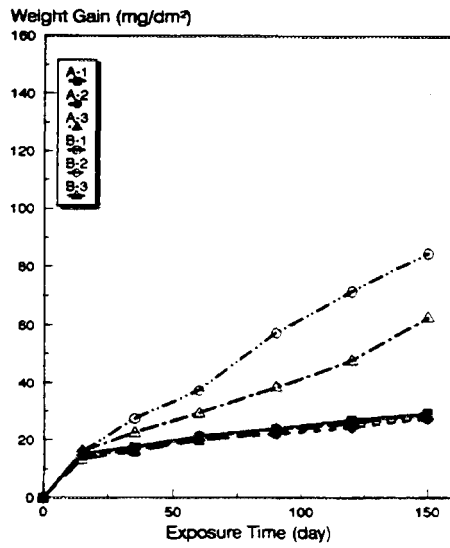


31.5 mmol LiOH  
220 ppm Li



WGLJ

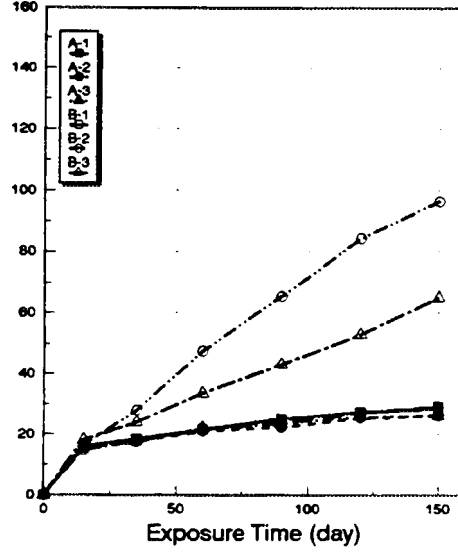
Fig. 1 Corrosion of different Zr alloys in LiOH. Test conditions: 350 °C, 17 MPa. Weight gain vs. exposure time



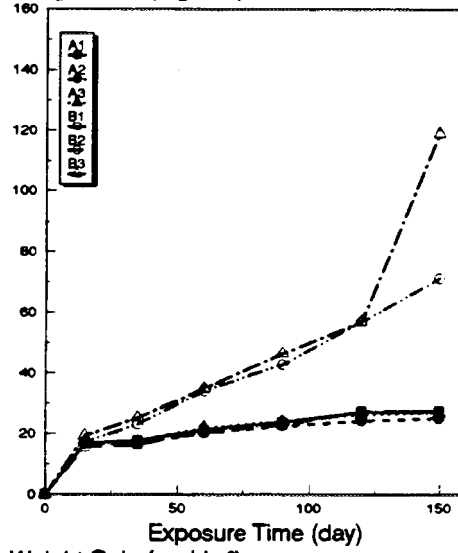
WQNA

Fig. 2 Corrosion of different Zr alloys in NaOH. Test conditions: 350 °C, 17 MPa. Weight gain vs. exposure time

Weight Gain (mg/dm<sup>2</sup>)



Weight Gain (mg/dm<sup>2</sup>)



Weight Gain (mg/dm<sup>2</sup>)

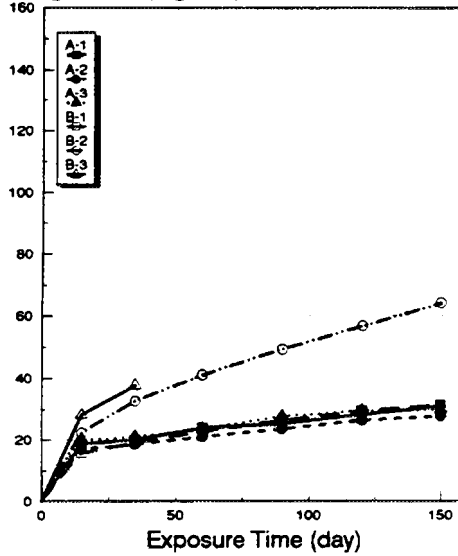


Fig. 3 Corrosion of different Zr alloys in KOH. Test conditions: 350 °C, 17 MPa. Weight gain vs. exposure time

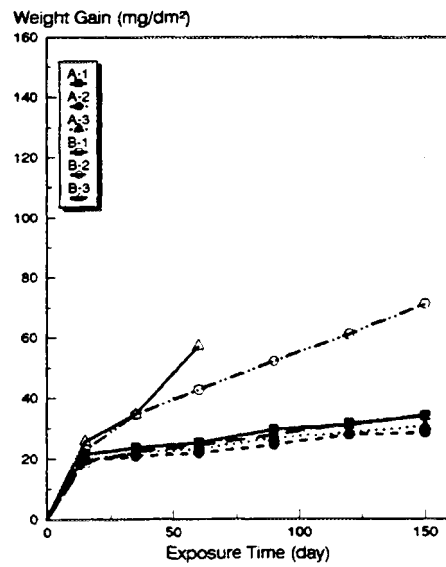
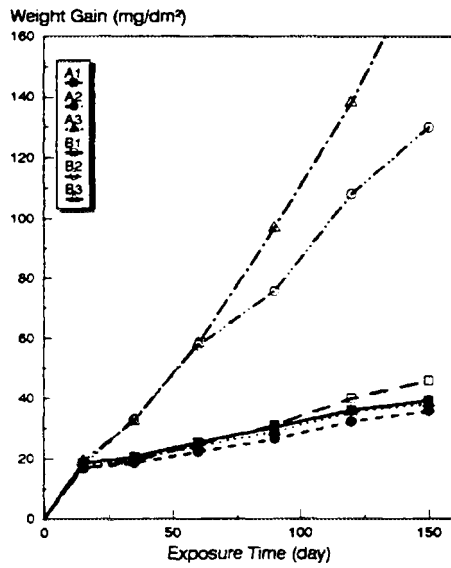
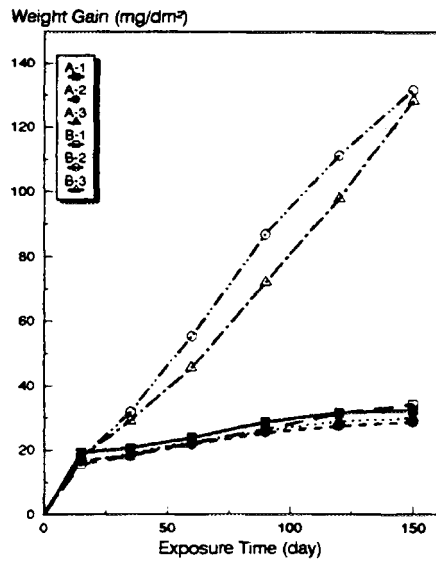


Fig. 4 Corrosion of different Zr alloys in RbOH. Test conditions: 350 °C, 17 MPa. Weight gain vs. exposure time

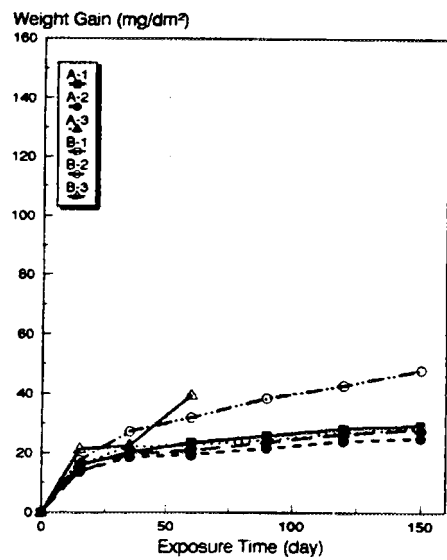
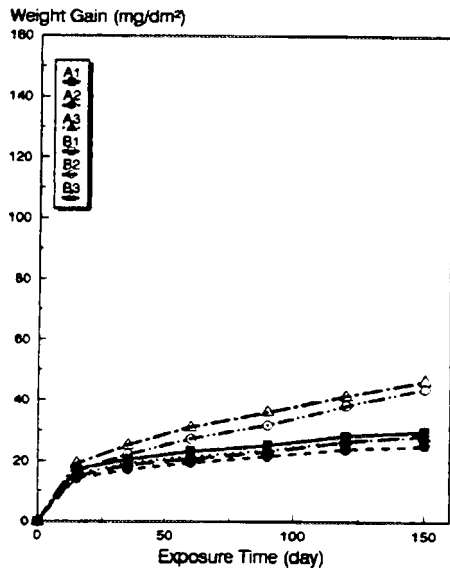
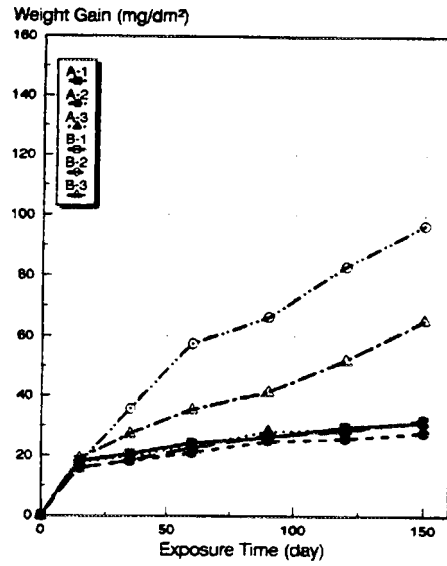


Fig. 5 Corrosion of different Zr alloys in CsOH. Test conditions: 350 °C, 17 MPa. Weight gain vs. exposure time

determined but may be responsible for the effect. A detrimental influence of carbonate anions on the corrosion of Nb alloys was reported by Ref. [16].

#### Medium concentration behavior:

The middle diagrams of Fig.1 to 5 show the corrosion behaviors of the test materials under medium concentrations (4.3 mmol) of Li-, Na-, K-, Rb- and Cs-hydroxides, respectively. The ranking between group A and B materials keeps similar. B3 within group B alloys now shows the highest weight gains of all tested materials. B3 alloy is the only material which shows in 4.3 mmol KOH an onset to post transition accelerated corrosion. Corrosion in 4.3 mmol Rb solution (Fig. 4 middle) is characterized by somewhat higher corrosion rates for B2 and B3 materials comparable to the behavior in LiOH. The group A samples show minor, but significant variations in weight gains what will be analyzed in detail later.

#### High concentration behavior:

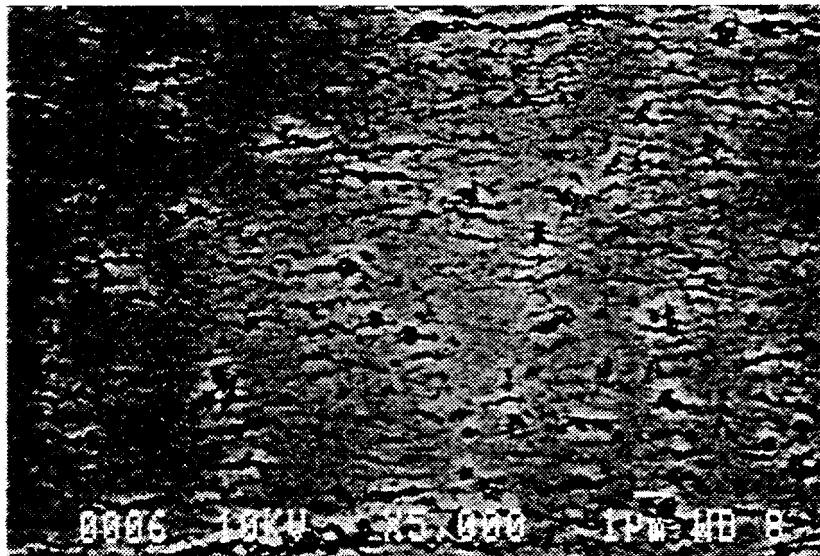
The lower diagrams in Fig.1 to 5 present corrosion results in high concentration (31.5 mmol) alkali hydroxides. In LiOH all samples show enhanced or accelerated corrosion after 150 day exposure. The onset of acceleration and the corrosion rate depends significantly on alloy composition as can be seen in the diagram with extended weight gain scale in Fig. 5. The decrease of the corrosion rate of B-3 alloy after 120 day may be caused by oxide spalling. Generally group A alloys behave better than group B alloys. A2 alloy among the all samples tested has the best corrosion resistance in high concentration LiOH solution .

The high concentration behavior of the materials in Na, K, Rb and Cs solutions are very similar. Weight gains keep below 50 mg/dm<sup>2</sup> for group A

alloys. A1 alloy in 32.5 mmol NaOH may be starting starting to experience corrosion enhancement. From the group B alloys B3 experienced spalling in all alkali solutions except LiOH. On B3 corrosion layers grown in Na, K, Rb and Cs solution spalled off at low weight gains and short exposure times. The reason for this observation is found in different morphologies of the corrosion layers formed in LiOH in comparison to the other alkali solutions. This was confirmed by a SEM investigation comparing LiOH and NaOH grown corrosion layers of sample B3 as shown in Fig. 7. The back scatter electron images show cross sections of sample B3 approximately at the same distance from the metal oxide interface at the same magnification. Both oxides are structured by horizontal pores but in the case of the NaOH grown corrosion layer coarser grains and extensive separation of layers is visible.

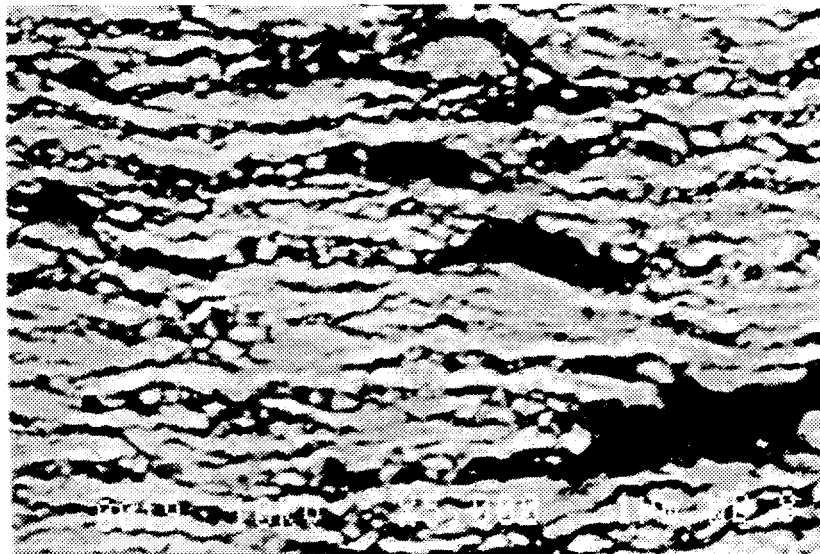
### 3.2 Influence of the different hydroxides on corrosion

The influence of the different alkali hydroxides on one alloy representing group A and group B will be discussed in this section. For this reason in Fig. 8 and Fig. 9 weight gains obtained in the different alkali environments after 90, 120 and 150 day exposure are plotted. The values are linearly corrected according to the deviations from the target concentrations of the alkali solutions revealed by chemical analysis (Table 2). The x-scale represents the alkali hydroxide by the cation radius of the alkali metal (see Table 1). The ion radii used for the plots are those for the highest coordination (6 in the case of Li and Na, 8 for K to Cs). This is reasonable due to the fact that if an alkali cation is incorporated into the zirconia lattice substituting a zirconium  $4^+$  cation it would be surrounded by 8 oxide anions in the cubic modification fluorite lattice). In the monoclinic modification  $Zr^{4+}$  is surrounded by 7 nearest oxygen neighbours as determined by structure



LiOH

Magnification: V = 5000 : 1



NaOH  
(spalled)

Magnification: V = 5000 : 1

Test Conditions: 350 °C, 17 MPa, Alkali Concentration 31.5 mmol, Exposure 90 d.

Fig. 6 Microstructure of corrosion layers of sample B3 in LiOH and NaOH.  
SEM investigation (back scatter electron mode) .

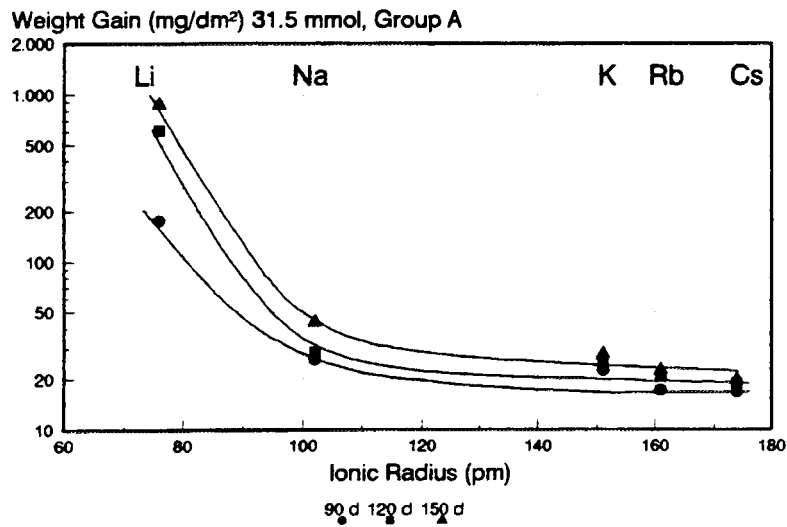
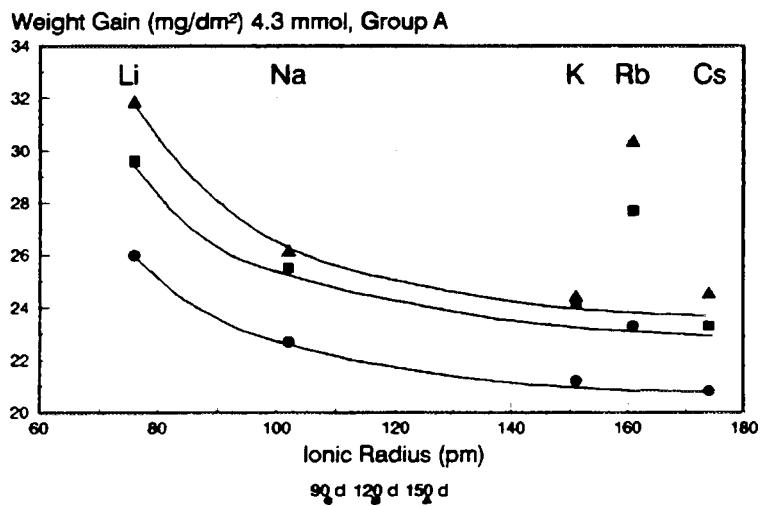
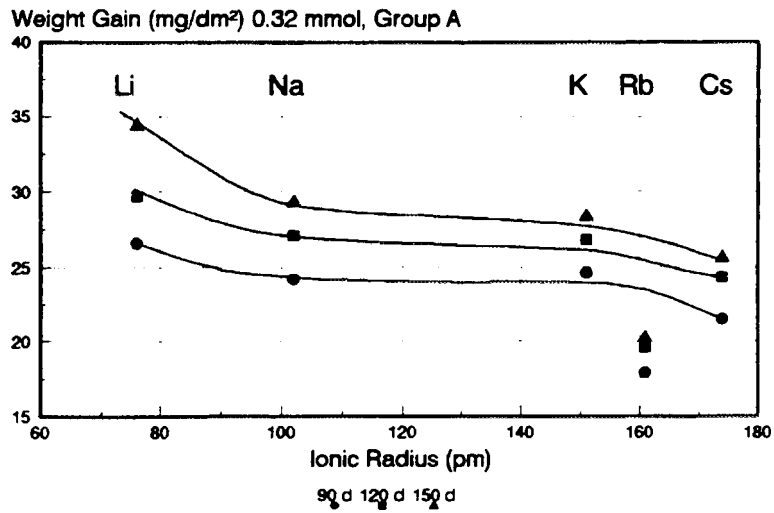


Fig. 7 Comparison of the corrosion behavior of group A materials (Zr-Sn-TRM) in different alkali hydroxide environments.

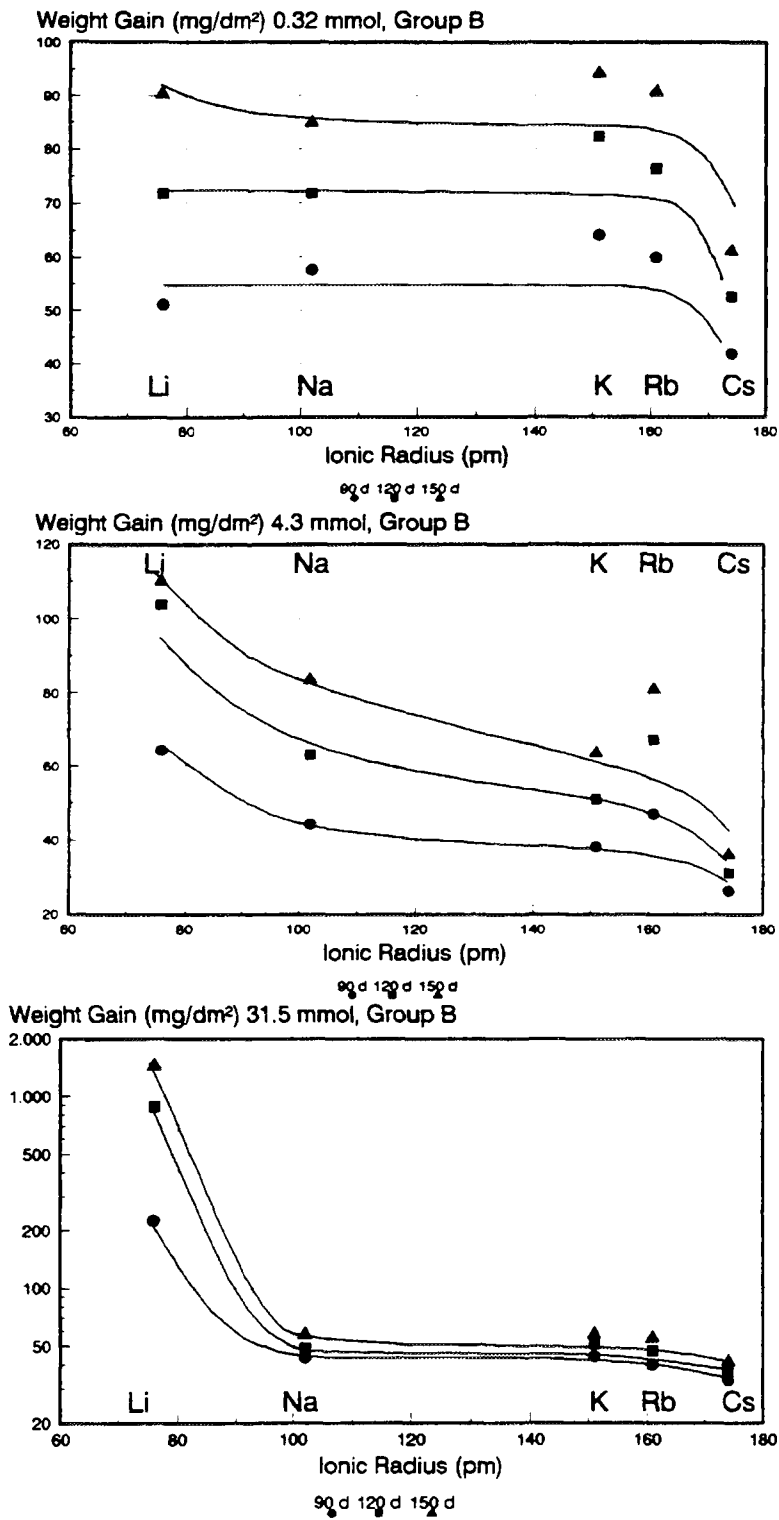


Fig. 8 Comparison of the corrosion behavior of group B materials (Zr-Sn-Nb-TRM) in different alkali hydroxide environments.

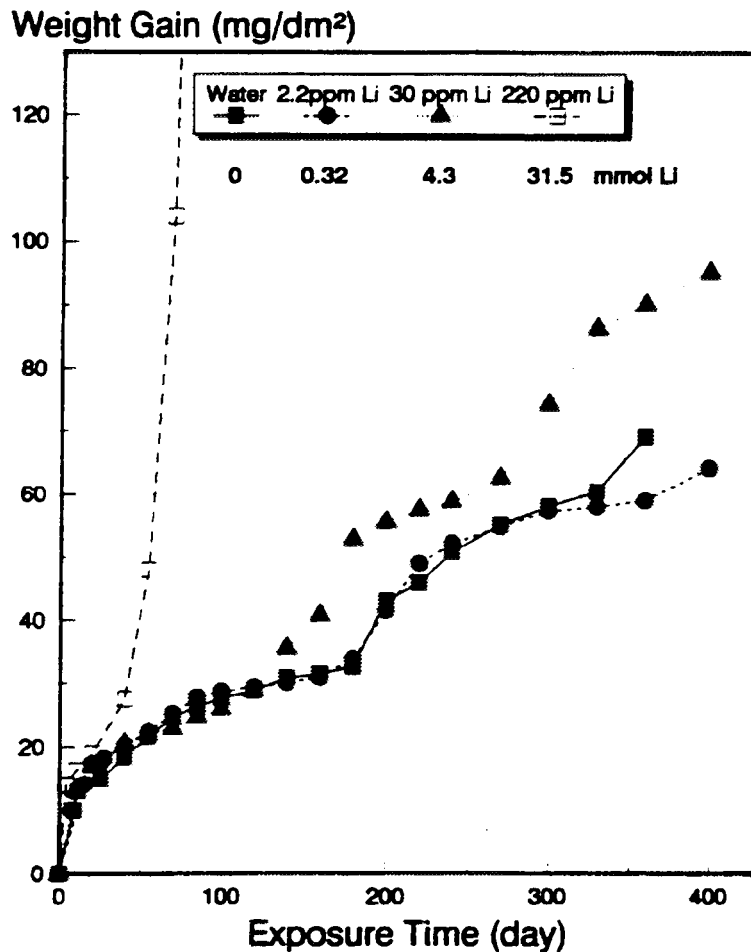


Fig. 9 Long term corrosion behavior of sample A1 in LiOH solutions of different concentrations. Test conditions: 350 °C, 17 MPa water.

analysis [17]. The figures compile weight gain data for the three hydroxide concentrations applied in this study.

On the first glance the general tendency observed is a more or less continuous decrease of weight gain with increasing ion radius of the alkali metal. No big alloy depending differences in this behaviour can be seen between group A (represented by A1 alloy) and group B materials (represented by B2 alloy) except of the range of weight gains covered. The Rb data at low and medium concentration do not follow the general trend. This may indicate additional influencing ionic species in these solutions.

### 3.3 Influence of alkali hydroxide concentration

The corrosion results reported in Fig. 1 to 5 showed a strong dependency of corrosion on the concentration of the applied solution. Especially, the point of onset for enhanced corrosion depends on concentration. The effect of accelerated corrosion in LiOH has been reported earlier and was recently reconfirmed [13]. In Fig. 10 and 11 long term exposure results are shown for sample A1 and A2, respectively. Two different regions can be distinguished in the weight gain curves: An enhanced corrosion significant for Li concentrations above 4.3 mmol (30 ppm) and accelerated corrosion for Li concentrations above 31.5 mmol (220 ppm). The onset of enhanced

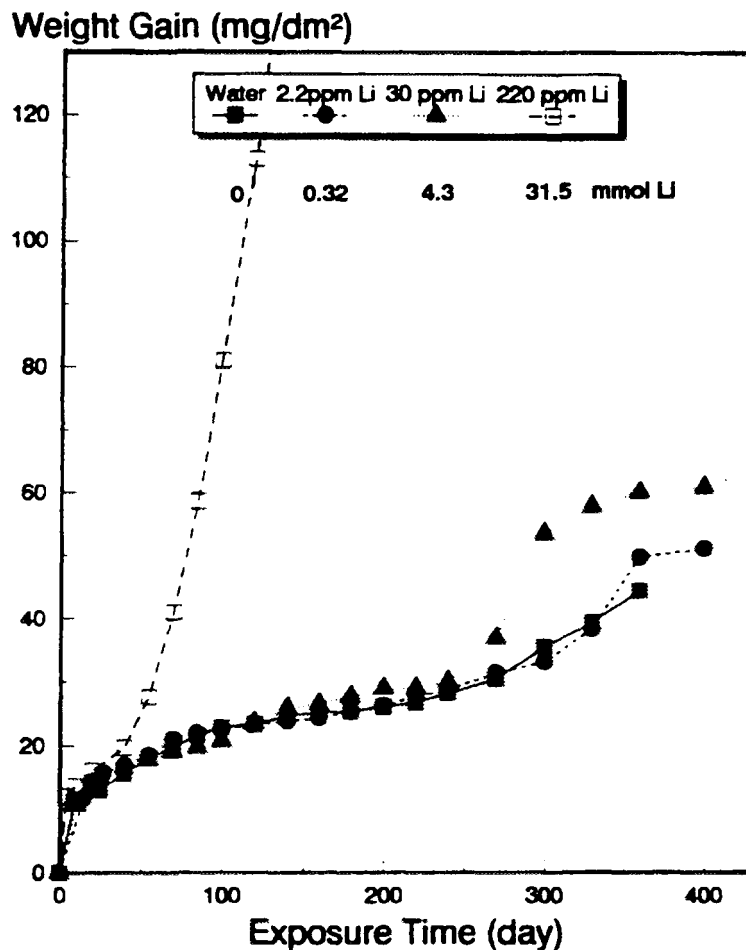


Fig. 10 Long term corrosion behavior of sample A2 in LiOH solutions of different concentrations. Test conditions: 350 °C, 17 MPa water.

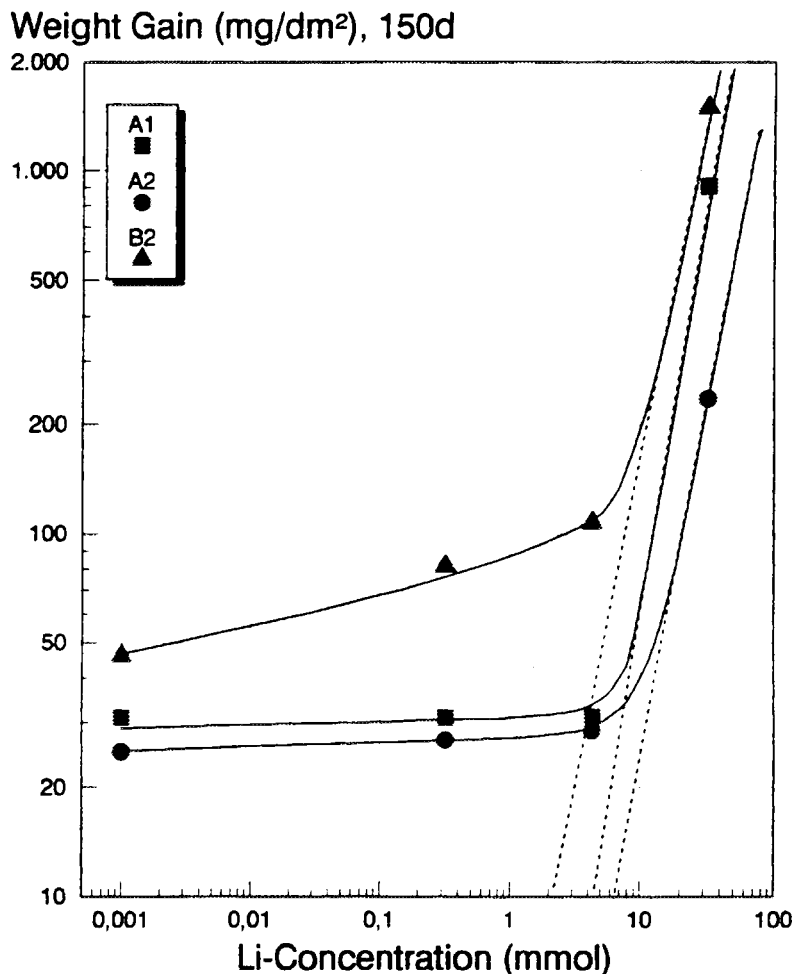


Fig. 11 Variation of weight gain as function of Li-content. Test conditions: 350 °C, 17 MPa water.

corrosion (which corresponds to the first transition in water tests) is sensitive to the alloy composition. Obviously the weight gain at this point is not strongly influenced and increases more or less constantly with increasing Li concentration. Even for Li enhanced corrosion at 32.5 mmol, differences in the corrosion rate for the different materials are still visible. But it should be noted that experiments with even higher alkali concentration showed an increasing lost of differentiation with respect to alloy composition. The onset of Li induced increased corrosion can be deduced from Fig. 11. For sample A1 and A2 extrapolation gives values around 10 mmol (70 ppm Li); for alloy B2 with poor corrosion behavior a value below 10 mmol is obtained. These values for the onset of an Li

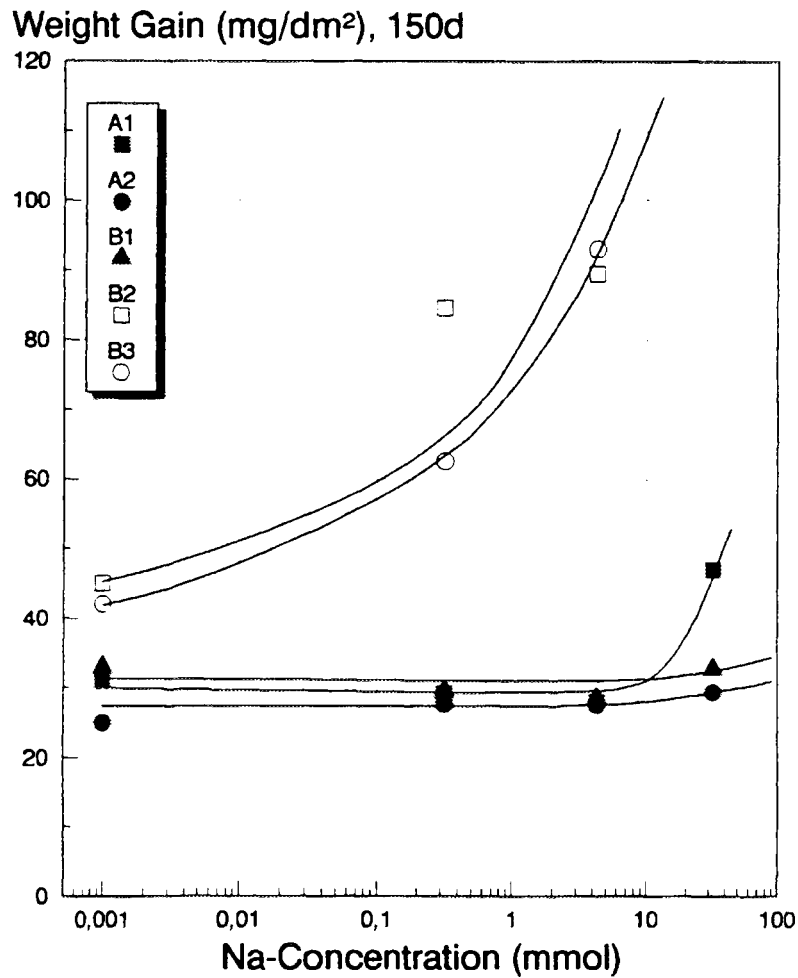


Fig. 12 Variation of weight gain as function of Na-content. Test conditions: 350 °C, 17 MPa water.

induced enhanced corrosion are somewhat lower but within the range of values reported by other authors [4, 9, 14].

Different behavior is found for corrosion in the other solutions. From group A materials only A1 showed an increase of corrosion at the highest NaOH concentration applied in the test (Fig. 13). For the other alloys or solutions no enhanced corrosion can be observed. The behavior of niobium alloys (group B samples) is different. B1 behaves like Group A materials without increase of corrosion. B3 and B2 corrosion is enhanced in NaOH already at lowest concentrations. At the highest alkali concentration B2 exhibits a decrease of weight gain in all solutions except LiOH.

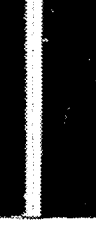
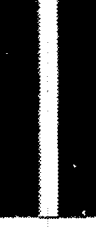
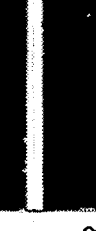
LiOH						
	WG(mg/dm <sup>2</sup> )	182	40.2	565	1307	235
NaOH						
	WG(mg/dm <sup>2</sup> )	28.1	27.2	29.6	27.5	46.9
KOH						
	WG(mg/dm <sup>2</sup> )	25.0	23.5	27.5	26.2	49.2
RbOH						
	WG(mg/dm <sup>2</sup> )	29.7	24.6	26.9	27.9	52.1
CsOH						
	WG(mg/dm <sup>2</sup> )	25.6	21.6	24.3	23.5	38.4
	A1	A2	A3	B1	B2	B3

Fig. 13 Surface appearance of samples exposed to 31.5 mmol alkali hydroxide solutions for 90 days. Test condition: 350 °C, 170 MPa water.

### 3.4 Visual Appearance and Microstructures of oxides

Fig. 13 shows the surface appearance of the samples exposed to 31.5 mmol alkali hydroxides for 90 day at 350°C. The oxides formed in LiOH solution show a different surface appearance depending on alloy composition. Black oxide is found for A-2, gray oxide for B-3, B-1 and A-1, and nodular oxide for A-1 and B-2. In other alkali solutions (Na, K, Rb and Cs hydroxides) most alloys showed the black oxide only sample B-3 appears gray or white with spalling of oxide. This results are consistent to the variation of weight gain shown in Fig.1 to Fig. 5.

## 4. DISCUSSION

### 4.1 Influence of alloy composition

The results presented show a significant difference in the behavior of Zr-Sn-(Transition Metals, TRM) and Zr-Nb-(TRM) alloys. In group B, alloys containing Nb below 0.3 % are comparable in their corrosion resistance to Zr-Sn-(TRM) materials. Under the test conditions, Nb containing alloys showed a significantly higher corrosion rate in all alkali solutions.

Accelerated corrosion occurred in LiOH and for the samples with low corrosion resistance also in NaOH, KOH, and RbOH. The corrosion behavior of the high Nb alloy in RbOH is comparable to that in LiOH, but the structures of the corrosion layers developed are different. No tendency toward spalling is observed only for LiOH grown oxides in contrast to all other alkali environments.

Zr-Sn-(TRM)-alloys show accelerated corrosion only in LiOH and for one material (A1) just beginning after 120 day exposure in NaOH. In all other

alkali solutions no acceleration is observed. The weight gains developed up to 150 days are below 50 mg/dm<sup>2</sup>. A detailed analysis shows dependencies in different alkali hydroxides which can be understood by Zr substitution in the oxide lattice of these pre transition oxides. In LiOH a remarkable differentiation for the different alloy compositions is visible at concentrations above 4.3 mmol up to 31.5 mmol.

Comparing the tendency to undergo accelerated corrosion for different materials in different alkali solutions NaOH would be not the first choice as a substitute alkali due to acceleration found for niobium alloys. Lowest corrosion enhancement is observed for CsOH. From this study we would not recommend to use RbOH but KOH seems to be a good compromise, far away from the pronounced LiOH effect and nearly as good as CsOH with respect to the tendency to induce accelerated corrosion.

#### 4.2 Mechanistic aspects

The weight gain results clearly show two distinct regions of alkali induced corrosion of zirconium alloys: a pre transition region with minor but significant effects of enhanced corrosion in different environments and a region of accelerated corrosion. Both phenomena may be but are not necessarily governed by the same corrosion mechanism. The incorporation and substitution of Zr in the dense growing zirconium oxide was suggested by Hillner and Chirigos [4] in their solid solution model for an increased number of anion vacancies which enhance the O<sup>2-</sup> defects and lead to higher corrosion rates by an increased anion conductivity. This incorporation into the zirconium oxide lattice is highly dependent on the radius of the cation for substitution into the host lattice. If we compare the ion radii for the different alkali cations to the radius of Zr<sup>4+</sup> (72 pm) one can

easily see that only  $\text{Li}^+$  has an comparable size (see Table 1). The tendency for incorporation should significantly decrease if Li is changed to Na to Cs with their larger ionic radii. If there is a correlation between corrosion and cation substitution in the oxide, this can be observed in the enhanced weight gains obtained under equimolar alkali hydroxide conditions in the region prior to accelerated corrosion. The diagrams presented in Fig. 8 and 9 clearly show this dependency. If we plot the measured weight gains obtained in 4.5 mmol solutions versus the inverse radius of the incorporated cation, as has been done in Fig. 14 for group A and Fig. 15 for group B materials (excluding the RbOH data), a linear relation is obtained especially for the 90 day exposure data. The validity of this relation points to a radius dependent conductivity in the zirconium oxide. The same plot performed with the data at higher alkali concentrations shows a non linear dependency. This can be understood

Weight Gain ( $\text{mg}/\text{dm}^2$ ) 4.3 mmol, Group A

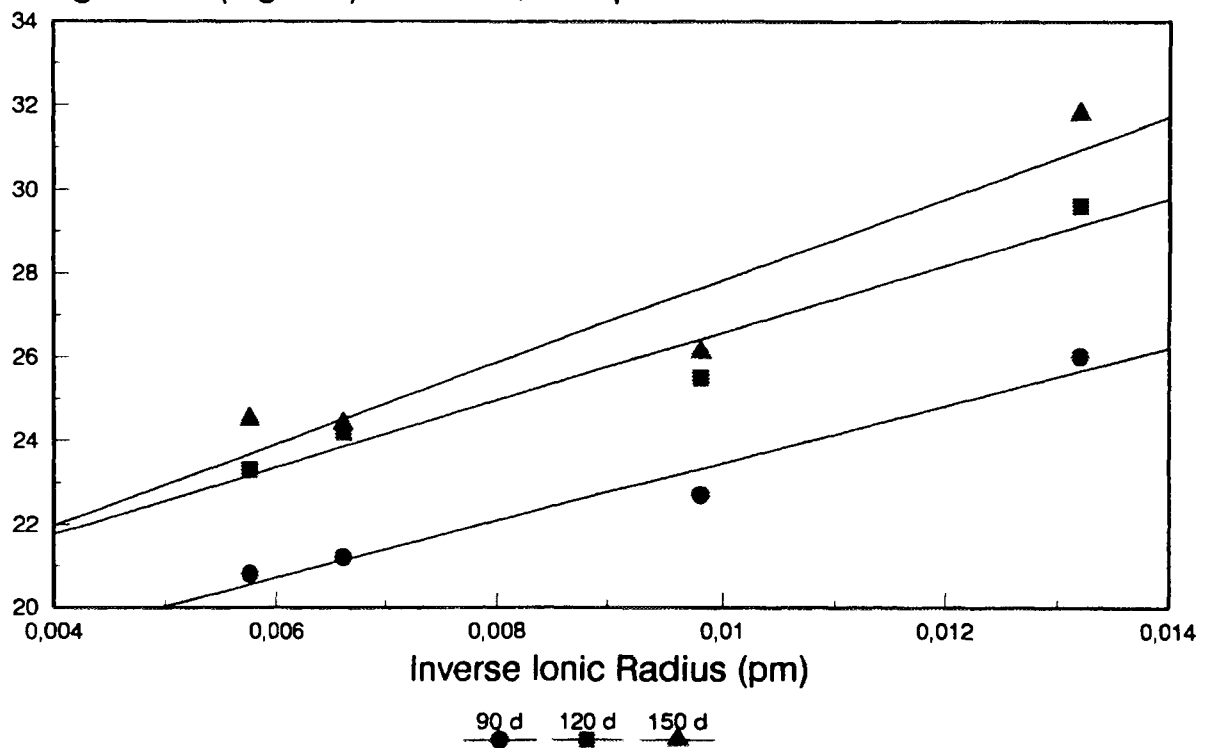


Fig. 14 Weight gain of group A material vs. inverse ion radii for different alkali hydroxide cations.

Weight Gain (mg/dm<sup>2</sup>) 4.3 mmol, Group B

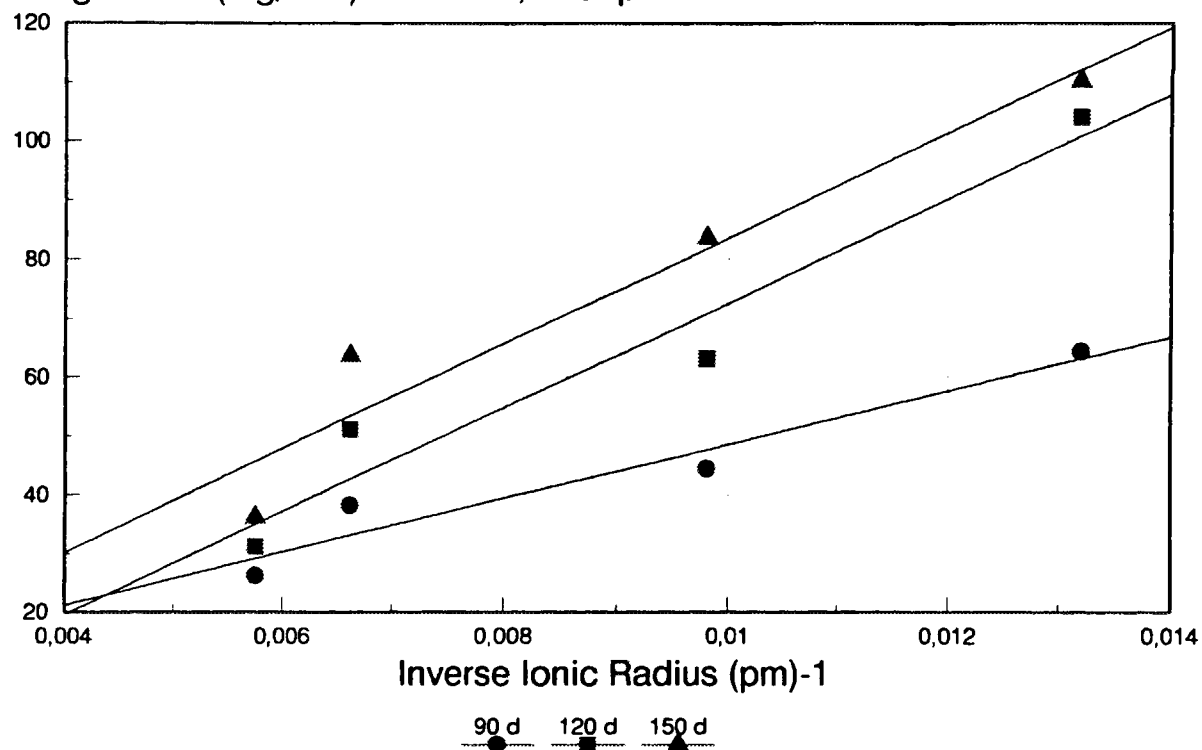


Fig. 15 Weight gain of group B material vs. inverse ion radii for different alkali hydroxide cations.

due to the fact that under these concentrations accelerated corrosion occurs for some of the materials in LiOH which can not be understood by ion substitution in the dense oxide. This accelerated corrosion phenomenon obviously is not governed by a substitutional effect. Probably crystal growth effects like nucleation and recrystallization and the development of porous structures may be influenced by the different environments. Whether the cation or the anion is responsible for this crystal growth effect is not yet answered. But this question may be solved by tests with prolonged exposure times under higher molar concentrations of the alkali hydroxides than applied in this study.

## 5. CONCLUSION

From the results presented in this study we draw the following conclusions:

1. From the experiments performed under equimolar conditions for the group-I-alkali hydroxides, the cation could be identified as the responsible species for zirconium alloy corrosion in alkalized water.
2. The radius of the cation governs the corrosion behavior in the pre accelerated region of zircaloy corrosion. Incorporation of alkali cations into the zirconium oxide lattice is probably the mechanism which allows the corrosion enhancement for Li and Na and the significant lower effect for the other bases.
3. Nb containing alloys show lower corrosion resistance than alloys from the Zr-Sn-TRM system in all alkali solutions. Both types of alloys corrode significantly more in LiOH and NaOH than in the other alkali environments. Lowest corrosive aggressiveness has been found for CsOH followed by KOH.
4. Concluding from the corrosion behavior in the different alkali environments and taking into account the tendency to promote accelerated corrosion, CsOH and KOH are possible alternate alkali for PWR application.

## REFERENCES

- [1] Billot, Ph., Beslu, P., Giordano, A. and Thomazet, ASTM STP 1023, pp.165-184.

- [2] Kass, S. , Corrosion , Vol. 25, No. 1, 1969, pp. 30-46.
  
- [3] Murgatroyd, R. A. and Winton, J. Journal of Nuclear Materials, Vol 23, 1967, pp. 249-256.
  
- [4] Hillner, E. and Chirigos J. N., Bettis Atomic Power Laboratory, Report WAPD-TM-307 (1962).
  
- [5] McDonald, S.G., Sabol, G. P. and Sheppard, K. D., ASTM-STP 824 (1984), p. 519.
  
- [6] Andrako, A. M. and Fisch, H. A., Knolls Atomic Power Laboratory, KAPL-2000-19.
  
- [7] Coriou, H., Grall, L., Meunier, J. Pelras, M. and Willermoz, H., Journal of Nuclear Materials, Vol. 7, 1962, pp. 320-327.
  
- [8] Perkins, R. A. and Bush, R., ASTM-STP 1132, 1991, pp. 595-612.
  
- [9] Garzarolli, F. , Pohlmeier J., Trapp-Pritsching, S. and Weidinger, H. G., Proc. IAEA Tech. Comm. on Fundamental Aspects of Corrosion..., Portland 1989, WGFPT/34, p. 34.
  
- [10] Bramwell, I. L., Parsons, P. D. and Tice, D. R., ASTM-STP 1132, pp. 628-642.
  
- [11] Ramasubramanian, N., Precoanin, N. and Ling, V.C., ASTM-STP 1023, pp. 187-201.

- [12] Garzarolli, F., Seidel, H. Tricot, R. and Gros, J. P., ASTM-STP 1132, pp. 395-415.
- [13] Ramasubramanian, N., Balakrishnan, P. V. Preprint of a paper presented at the 10th International Conference on Zirconium in the Nuclear Industry, Baltimore 1993.
- [14] Garzarolli, F. and Holzer, R. Nucl. Energy, 31, 1992, pp. 65-85.
- [15] Cox, B. and Chenguang, W. Journal of Nucl. Mat., 199, 1993, pp. 272-284.
- [16] Rosenfeld, I. L., Olbrownikow, J. P. and Szudarikowa, A. A. IAEA Meeting on Corrosion of Reactor Materials, Salzburg, June 1962.
- [17] McCullough, J. D. and Trueblood, K. N., Acta Cryst., 12, 1959, p. 507.

**MODIFIED HOT-CONDITIONING OF PHT SYSTEM SURFACES OF PHWRs**

G. VENKATESWARAN

Bhabha Atomic Research Centre,  
Trombay, Bombay, India**Abstract**

The increased awareness on the importance of controlling activity transport and radiation buildup on out-of-core surfaces of water cooled nuclear reactors is leading to a host of measures both from chemistry as well as engineering sides being undertaken. Passivation of the surfaces of structural materials is one such. Pressurised Heavy Water Reactors of CANDU design use large surface area of carbon steel alloy in the Primary Heat Transport System. Hot-conditioning of the PHT system with deoxygenated light water at temperatures  $\approx 473 - 523$  K during commissioning stage is done to form a protective magnetite film on the surfaces of carbon steel essentially to guard this material from corrosion during the intervening period between initial commissioning and first fuel loading and achieving nuclear heat. However, a need is felt to improve the quality of this magnetite film and control the crud release so that the twin objectives of controlling the corrosion of carbon steel and reducing a possible deposition of corrosion products on surfaces of fuel clad could be achieved. Laboratory static autoclave investigations have been carried out on the formation of protective magnetite film on carbon steel at 473 K, pH 10 (pH at 298 K) deoxygenated aqueous solutions of chelants like HEDTA, DTPA, NTA apart from EDTA. Additionally, influence of AVT chemicals like hydrazine, cyclohexylamine, morpholine and additives like glucose, boric acid has been studied. The data have been compared with the standard procedure of hot-

conditioning namely with simple LiOH. It is found that chelants increase the base metal loss but the oxide formed is more protective than the one formed under simple LiOH treatment. The efficiency of passivation is greatly enhanced by hydrazine and boric acid while it is adversely affected by glucose. AVT chemicals acts as effective corrosion inhibitors.

1. Introduction : Passivation of carbon steel alloy which is used as out-of-core piping material in the primary heat transport (PHT) system of PHWRs is done essentially to protect this material from corrosion during the intervening period between initial commissioning of the system and first fuel loading with subsequent achieving of nuclear heat. However, with increasing awareness on the importance of controlling activity transport and radiation field buildup, this passivation treatment is recognised as an important commissioning activity not only from corrosion point of view but also from reducing the deposition of corrosion products on the fuel clad surfaces. Usually, the pre-conditioning is done in deoxygenated, pH 10 (pH @298 K) LiOH solutions at as high achievable temperatures as possible typically in the range 473-523 K - the lower temperatures around 473 K being more readily realisable than the higher ones - for periods ranging from 5 to 15 days, the lower duration for a higher temperature and vice versa. Much of the work reported in literature in improving the quality of magnetite film formed on carbon steel with respect to better adherence and reduced porosity is centered around the use of EDTA at temperatures  $\geq 523$  K.[1-4] However, it has been shown that at  $\approx 473$  K EDTA itself is not beneficial compared to LiOH treatment.[5-6]. It was therefore considered attractive to investigate the effects of other chelating agents

like 2-hydroxyethyl ethylene diamine triacetic acid (HEDTA), diethylene triamine pentaacetic acid (DTPA) and nitrilo acetic acid (NTA).

Though literature data exists on the beneficial effects of  $\approx 200$  mg/kg of hydrazine in the passivation behaviour of carbon steel at temperatures 423 - 523 K in terms of reduced base metal loss and corrosion release rate, the protectivity of the coating in terms of its polarization behaviour is not reported.[7-8] It has also been mentioned in literature that passivation of carbon steel in presence of EDTA + AVT chemicals (AVT - All Volatile Treatment - employing 100 mg/kg hydrazine and pH adjusted to 9.5 with ammonia) at 563 K for 68 days, developed thicker coatings than simple AVT without EDTA.[1] Based on these conditions it was suggested that  $Fe_3O_4$  formed under EDTA/AVT was more protective than the one obtained only with AVT. However, the role of morpholine (MOR) and cyclohexylamine (CHA), which are also widely used as AVT chemicals in the secondary system of PHWRs/PWRs, on the high temperature passivation of carbon steel is not reported and has been investigated in this work. For comparison purposes, the effect of additives like glucose [9,10] and boric acid [9] which are known to be good stimulant and inhibitor respectively for the near room temperature of  $Fe(OH)_2$  have also been investigated. As a base line reference, the role of above additives namely chelants, AVT chemicals, glucose and boric acid has been compared with the "no-additive" case which is simply passivation obtained under simple LiOH treatment.

2. Experimental: A static 1 l pre-conditioned stainless steel autoclave was employed for the studies. Deoxygenated ( $\approx 10$   $\mu\text{g}/\text{kg}$ ) demineralised water was used for preparing the various formulations. Circular specimens of  $\approx 15$  mm diameter and 1.25 mm

thickness were cut from ASTM A 106 Grade B Carbon steel plates of the composition (wt %) 0.3C - 0.23Si - 0.77Mn - <0.01P - 0.0245S - bal Fe. A 350 mg/kg concentration was chosen for the various additives considered in this study. In the experiments with chelants (initial pH adjusted to 10 at 298 K with NaOH) an initial thermal treatment was given to the specimens by maintaining the solution temperature at 393 K for 24 h before reaching 473 K. This was done to enable the formation of metal-ligand complexes for the subsequent decomposition at higher temperatures. Gravimetry on the exposed specimens was performed to evaluate the total oxide build-up, adherent oxide thickness, base metal loss and % adherency. The oxide coating formed under LiOH was tested for the presence of Li. The autoclave solutions at the end of the experiments were analysed for soluble and insoluble iron, free additive concentration and pH. The oxide structure on the coated specimens was established using X-ray diffraction studies and the protectivity of the oxide films was assessed at room temperature by electrochemical measurements.

3. Results: Table-I shows the gravimetric data obtained with the carbon steel coupons. Base metal loss in each of the three

Table-I  
Weight change data in presence and absence of additives

Additive	Base metal loss (mgdm <sup>-2</sup> )	Total oxide buildup (mgdm <sup>-2</sup> )	Adherent oxide (mgdm <sup>-2</sup> )	%adhe- rency (average)
Boric acid	13.1±3.5	12.3±4.5	9.0±2.3	72.6
Hydrazine	25.1±3.1	25.9±3.1	24.3±2.9	94.0
Cyclohexylamine	48.0±5.2	41.7±6.2	31.4±4.2	75.4
Morpholine	63.2±6.4	41.9±5.5	30.4±4.3	72.6
LiOH (blank)	82.9±4.3	60.8±2.8	45.5±3.6	74.9
Glucose	194.1±7.9	61.1±4.8	54.9±5.1	89.7
HEDTA	173.9±4.3	53.0±1.8	44.7±1.2	84.4
DTPA	209.0±4.5	58.6±4.8	44.9±3.3	76.6
NTA	323.3±6.2	65.7±2.1	53.4±3.2	81.3

chelants was very high following the order: NTA > DTPA > HEDTA > LiOH, But the levels of total oxide build-up and adherent oxide buildup are quite comparable. In the case of AVT chemicals, boric acid and glucose, base metal loss follows the order: glucose > LiOH > MOR > CHA > hydrazine > boric acid. Thus effective inhibition of corrosion process is seen under boric acid and hydrazine conditions. The total and adherent oxide buildup follows the order: boric acid < hydrazine < CHA  $\approx$  MOR < LiOH < Glucose. The % adherency is seen to be more than 70 in all cases. X-ray diffraction (XRD) studies showed the presence of crystalline oxide layer on the surface having an inverse spinel structure viz., magnetite and did not reveal the peaks due to  $\alpha$ -Fe<sub>2</sub>O<sub>3</sub>. With respect to the weight of the adherent oxide coating observed on the specimens treated in presence of LiOH, the Li content was determined to be 0.2% (w/w). This works out to  $\approx$ 10% (w/w) LiFe<sub>5</sub>O<sub>8</sub> if all the Li is assumed to be present as  $\beta$ -LiFe<sub>5</sub>O<sub>8</sub>.

Table-II shows the data from analyses of the autoclave solutions at the end of the experiments. End of run pH shows a decrease in all cases except under hydrazine case which could be explained by thermal decomposition/consumption of additive in the corrosion process. Even in the case of hydrazine, a slight increase in pH noticed could be explained by its thermal decomposition to ammonia viz.,  $3\text{N}_2\text{H}_4 \rightarrow 4\text{NH}_3 + \text{N}_2$ . End of run [NH<sub>3</sub>] is 126 mg/kg against an expected 150 mg/kg, the difference could be explained by slight leaks from the autoclave. In the case of glucose, pH after the run has decreased by nearly 6 units which is due to the thermal decomposition of glucose to various aliphatic acids viz., lactic acid, glycollic acid, acetic acid, formic acid, dihydroxy butyric acid etc.[11] An increased concentration of soluble Fe with all the chelants is seen when

Table-II  
Results of analyses of autoclave solutions for different additives

Additive	Initial pH	Final pH	Soluble Fe (mg/kg) <sup>a</sup>	Insoluble Fe (mg/kg) <sup>a</sup>	Fe deposited on stringer	Free additive concentration(mg/kg)
LiOH	10	9.5	0.17	30.8	6.6	-
HEDTA	10	7.9	Fe-X <sup>+</sup> : 1.8	47.0	45.6	< 5
			Fe-HEDTA: 7.1			
DTPA	10	8.0	Fe-X <sup>+</sup> : 2.8	45.5	60.0	< 5
			Fe-DTPA: 7.7			
NTA	10	8.0	17.8	183.4	75.5	206
Boric acid	10	9.9	0.1	2.4	0.8	350
N <sub>2</sub> H <sub>4</sub>	10.3	10.5	0.6	3.3	1.2	6.5
CHA	11.3	10.9	0.1	8.6	6.0	330
MOR	10.3	9.8	0.2	23.0	7.3	316
Glucose	10.0	4.2	15.3	151.5	16.3	35

<sup>a</sup> The values are normalised to 1 dm<sup>2</sup> surface area of specimens  
<sup>+</sup> Complexes with decomposition products of the ligands

compared with the LiOH case. The soluble iron observed with NTA is higher than that observed with the other two chelants and also considerable amount of free NTA is observed at the end of run while end of run HEDTA and DTPA are negligible. In the case of AVT chemicals and other additives the soluble iron is very low except in the case of glucose. Insoluble iron is the highest under NTA condition while that in the case of HEDTA and DTPA are quite similar but higher than that obtained with LiOH. In the case of AVT chemicals and other additives the insoluble Fe showed a similar behaviour as under the base metal loss.

The variation of open-circuit-potential (OCP) in pH 10 (@298 K) deoxygenated(Argon saturated) LiOH medium of the oxide coated surfaces(OCS) and plain carbon steel is shown in Fig.1. Table-III shows the steady state OCPs and the corrosion potential

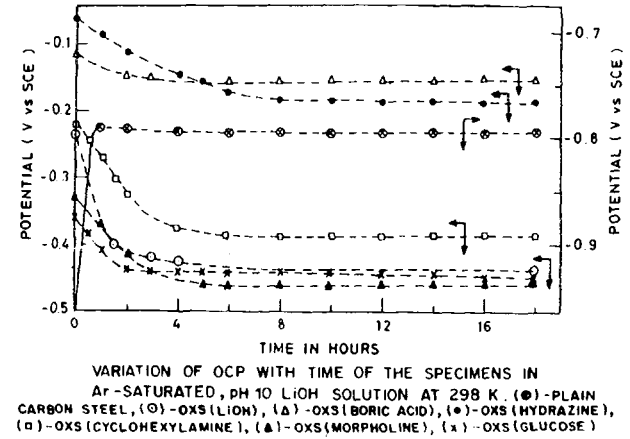
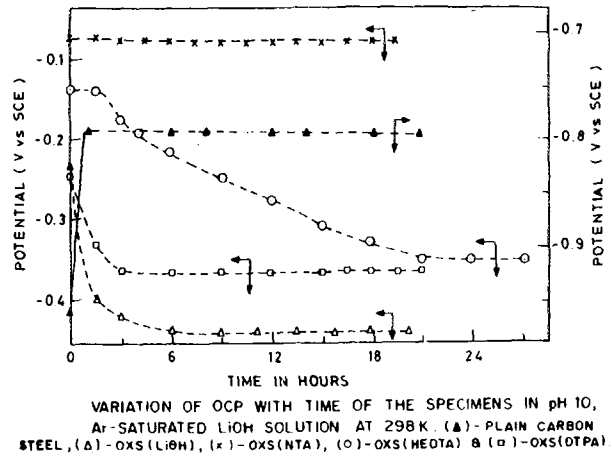


Fig.1

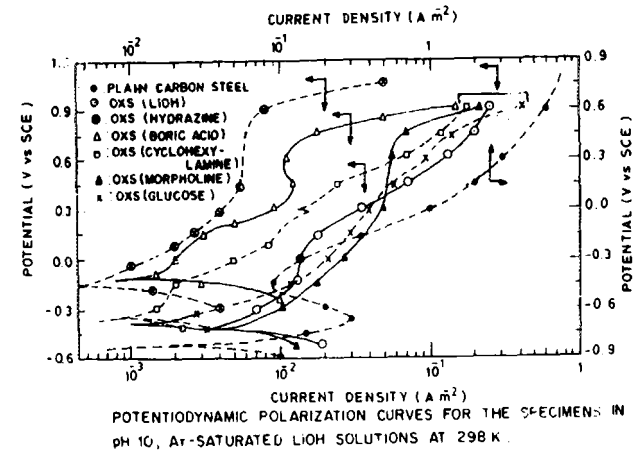
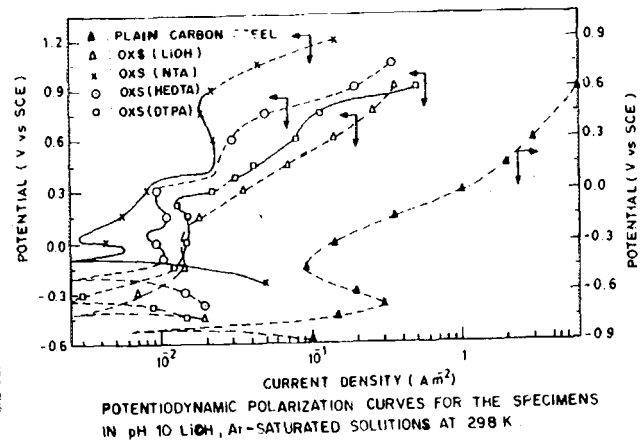
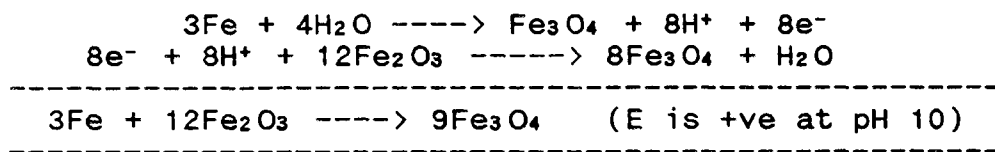


Fig.2

( $E_{corr}$ ) values derived from these measurements. The initial as well as the steady state OCPs for all OCS(additives) fall in the  $Fe_2O_3$  region of the Pourbaix diagram. Thus the electrochemical potential values show a surface oxidation behaviour while XRD studies have shown the bulk oxide to be magnetite. The general shift of OCPs to more active values indicates the attack of base metal through the pores present in the oxide and the oxidation of the base metal being accounted by the reduction of  $Fe_2O_3$  to  $Fe_3O_4$ :



In general all the oxide coated specimens exhibit more noble  $E_{corr}$  as compared to plain (uncoated) specimen. Among the coated specimens while OCS(NTA), OCS(boric acid) and OCS( $N_2H_4$ ) have shown much nobler corrosion potentials as compared to others. OCS(NTA) looks to be very protective by showing little shift from its initial OCP value. Fig.2 shows the cathodic and

Table-III  
Data derived from electrochemical measurements

Specimen description	Steady state OCP <sup>a</sup> (V vs SCE)	Corrosion potential <sup>b</sup> $E_{corr}$ (V vs SCE)
Carbon steel (blank)	-0.795	-0.820
OCS(LiOH)	-0.440	-0.420
OCS(HEDTA)	-0.349	-0.200
OCS(DTPA)	-0.359	-0.340
OCS(NTA)	-0.076	-0.105
OCS(boric acid)	-0.153	-0.120
OCS( $N_2H_4$ )	-0.186	-0.160
OCS(CHA)	-0.385	-0.360
OCS(MOR)	-0.460	-0.410
OCS(Glucose)	-0.446	-0.390

Table-IV  
pHs at temperature of solutions of various additives

Additive employed	Initial pH(298K)/corresponding pH(473K)	Computed pH at 473 K (based on measured concentration of the additive or measured pH at 298 K at the end of the experiment)*	Computed/measured end of experiment pH at 298 K based on measured concentration of additive at the end of experiment
Boric acid	10.0/7.3	7.2	10/9.9
Hydrazine	10.3/7.6	7.6	10.3/10.5
CHA	11.3/8.6	8.0	10.8/10.9
MOR	10.3/7.6	7.3	10.0/9.8
LiOH	10.0/7.3	6.8	9.5/9.5

\* The values of pH at 473 K given in this column since they have been computed from the additive concentration left in the autoclave solution or pH at 298 K at the end of the experiment, these pH values would be a minimum pH that the specimens would have seen at 473 K.

anodic polarisation curves constructed in pH 10 deoxygenated medium at 298 K with a scan rate of 0.0005 V/s. In general  $E_{corr}$  values determined from polarisation curves fairly agree with the observed steady state OCPs. Comparing the anodic currents obtained at different applied potentials, the specimens can be arranged in the order of their increasing passive character : Plain carbon steel < OCS(glucose)  $\approx$  OCS(MOR)  $\approx$  OCS(LiOH) < OCS(CHA)  $\approx$  OCS(DTPA) < OCS(HEDTA) < OCS(boric acid) < OCS(N<sub>2</sub>H<sub>4</sub>) < OCS(NTA).

4. Discussion: a) Chelants: The beneficial role of chelants during passivation can be explained in terms of formation and subsequent decomposition of Fe-chelants to give a solution precipitated magnetite layer providing improved coverage of the surface of the alloy. The stability constants ( $\log_{10}K$  at 298 K) of complexes of Fe<sup>2+</sup> with DTPA(H<sub>5</sub>A), HEDTA(H<sub>3</sub>AOH) and NTA(H<sub>3</sub>A) are 21.5(FeAOH<sup>4-</sup>), 17.2(Fe(AOH)OH<sup>2-</sup>), <12(FeAOH<sup>2-</sup>) respectively. At higher temperatures K values will change but there is no reason to

believe that their magnitudes will drastically alter. Such complex formation results in the release of  $H^+$  ions resulting in lowering of pH observed at the end of the experiments. A 350 mg/kg of chelant employed corresponds to 0.89, 1.26 and 1.83 mmol/kg concentration of DTPA, HEDTA and NTA respectively. The expected base metal corrosion would therefore be  $NTA > HEDTA > DTPA$ . At 473 K thermal decomposition of chelate and chelant can begin. However, decomposition of NTA at 473 K is much lower ( $t_{\frac{1}{2}} \approx 1000$  h) than that of HEDTA and DTPA ( $t_{\frac{1}{2}} \approx 2$  h). Thus from thermal decomposition of chelate and chelant angle one expects the order of base metal loss to be:  $NTA > DTPA > HEDTA$ . From the initial concentration of chelant, the amount of Fe that would be complexed is calculated to be 70.4, 49.7 and 102.2 mg/kg for HEDTA, DTPA and NTA respectively. This corresponds to base metal losses of 79.2, 55.9 and 114.9 mg/dm<sup>2</sup> respectively, but values of base metal loss actually obtained are much higher. This can only be explained by pronounced lowering of pH of the medium as well as by the free additive left at the end of the experiment. Hence under chelant conditions, a combined situation of complex formation and pH controlled corrosion exists.

Bloom et al., [12] have attributed the disappearance of LiOH from the solution in the oxide coating studies on mild steel at 589 K to a reaction of the type  $5Fe_3O_4 + 3LiOH + H_2O \rightarrow 3LiFe_5O_8 + 5/2H_2$ . At LiOH concentration of < 1% , a diminishing effect on [LiOH] has also been observed. In the present study the decrease in pH measured in LiOH experiments and the observation of Li in the oxide coating could point to such incorporation of Li in the oxide. From the protectivity point of view, the chelants can better passivate the surfaces than LiOH. This is achieved, however, with a great amount of base metal loss and

crud release which are undesirable effects for any passivation treatment. In the case of EDTA treatment of carbon steel at 473 K under similar experimental conditions, not only high base metal loss and crud release are encountered during the process, but also the oxide film is found to be less protective than the one formed under simple LiOH condition. The beneficial effect of EDTA treatment is realised only at higher temperatures ( $\geq 523$  K). In this way the chelants used in the present study offer a better protective film on the carbon steel surface than the one obtained with EDTA or LiOH treatments. However, from an overall assessment of passivation treatment, taking into account the base metal loss, crud release and protectivity of the coating, the simple LiOH treatment appears to be a better option than chelant treatments.

b) AVT chemicals and other additives: The pH effect alone (Table-IV) except in the case of glucose cannot explain the observed base metal losses with these additives and protection offered is probably due to the specific interaction of these additives with the base metal/oxide surfaces. The presence of borate ion in solution in the pores of the oxide coating thus suppressing the solubility of iron in the pores and restricting its diffusion could be the cause for the low base metal attack observed with this additive. This is due to the fact that the solution method of oxide film growth involves diffusion through the porous oxide predominantly via the solution present in the pores as the solid state diffusion is very slow at 473 K. Though the adherent film thickness observed is much less as compared to that obtained under LiOH and other additives, the film is seen to be highly protective in terms of decreased charge carrying capacity as shown by the polarization studies.

Adsorption of bifunctional base like  $N_2H_4$  and amines such as cyclohexylamine/morpholine on plain carbon steel or oxide coated surfaces is known to be responsible for reducing the corrosion rate of this material under ambient conditions.[13] Such an adsorption mechanism could result in polarising the dissolution reaction of iron. The results of the present study have shown in terms of reduced base metal losses observed in presence of hydrazine, cyclohexylamine and morpholine as compared to the base metal loss observed with LiOH that these additives act as corrosion inhibitors even at 473 K. In hot-conditioning with  $N_2H_4$ , significant amounts of  $NH_3$  is generated which can be better adsorbed on the surface as compared to the amines. Base metal loss obtained in the hydrazine case is found to be much less than that observed with CHA and MOR thereby confirming its better inhibiting action. Between CHA and MOR base metal loss in presence of CHA is less than that with MOR which conforms to the better inhibiting efficiency of CHA over MOR reported in literature.[14]

**6. Conclusions:** A comparative impact of complexing and non-complexing additives on the passivation of carbon steel at 473 K has been evaluated in terms of base metal loss, corrosion product release and the protectivity of the oxide coatings. The additives can be arranged in the following order with respect to base metal loss: boric acid < hydrazine < cyclohexylamine < morpholine < LiOH < HEDTA < glucose < DTPA < NTA. The protectivity of the oxide film grown in presence of these additives can be classified in the order: NTA > hydrazine > boric acid > HEDTA > cyclohexylamine  $\approx$  DTPA > LiOH  $\approx$  morpholine  $\approx$  glucose. Thus passivation in presence of hydrazine or boric acid seems to be the best for carbon steel at 473 K.

## REFERENCES

- [1] TVEDT, T.J., S.L.WALLACE, Power,131 (1987) 25.
- [2] MARGULOVA, T., BURSUK, L., TEVLIN, S., BOGATYREVA, S., TRSOKIN, V., Proc. Int. Conf. "High temperature, high pressure electrochemistry in aqueous solutions", organised by Central Electricity Authority, NACE and University of Surrey, Surrey (1973) 241.
- [3] SARUP, S., VENKATESWARAN, G., VENKATESWARLU, K.S., Proc. Nat. Symp. "Nuclear Science and Engineering", organised by Department of Atomic Energy, Bombay, (1973) paper OE-8.
- [4] GADIYAR, H.S., ELAYATHU, N.S.D., Corrosion(NACE), 36(6) (1980) 306.
- [5] VENKATESWARAN, G., VENKATESWARLU, K.S., Corrosion(NACE), 44(11) (1988) 818.
- [6] JOSHI, P.S., VENKATESWARAN, G., VENKATESWARLU, K.S., Corrosion(NACE), 48(6) (1992) 501.
- [7] ELAYATHU, N.S.D., CHAUHAN, P.K., GADIYAR, H.S., Proc. Topical Meeting on "Water Chemistry in Nuclear Power Stations", organised by Department of Atomic Energy, BARC, Bombay, (1981), 233.
- [8] CHAUHAN, P.K., ELAYATHU, N.S.D., GADIYAR, H.S., Proc. 8th Int. Cong. on Metallic Corrosion, Frankfurt(Germany), (1981),236.
- [9] ZINKUN, Z., RONGCHUA, L., SHUXIN, W., YUANFU, X., SHOUREN,Q., KEXUE TONGBAO, (1984), 1091.
- [10]SCHRAUZER, G.N., GUTH, T.D., J.Am.Chem.Soc., 98, (1976),3508.
- [11]POPOFF, T., THENDER, O., Carbohyd Res., 48 (1976) 13.
- [12]BLOOM, M.C., KRULFELD, M., FRASER, W.A., Corrosion(NACE), 38, (11982), 104.

[13]UNITSUGU, K., ARAMAKI, Proc. 5th Int. Conf. on Metallic  
Corrosion, Tokyo(Japan),(1972), 549.

[14]BAVARIAN, B., MOCCARI, A., MaCDONALD, D.D., Corrosion(NACE),  
38, (1982), 104.

## IN SITU MEASUREMENT OF THE EFFECT OF LIOH ON THE STABILITY OF ZIRCALOY-2 SURFACE FILM IN PWR WATER

T. SAARIO, S. TÄHTINEN  
Technical Research Centre,  
Espoo, Finland

*Presented by P.A. Aaltonen*

### **Abstract**

Surface films on the metals play a major role in corrosion assisted cracking. A new method called Contact Electric Resistance (CER) method has been recently developed for in situ measurement of the electric resistance of surface films in high temperature and high pressure environments. The technique has been used to determine in situ the electric resistance of films on metals when in contact with water and dissolved anions, during formation and destruction of oxides and hydrides and during electroplating of metals. Electric resistance data can be measured with a frequency of the order of one hertz, which makes it possible to investigate in situ the kinetics of surface film related processes which are dependent on the environment, temperature, pH and electrochemical potential.

This paper present the results of the CER investigation on the effects of LiOH on the stability of Zircaloy-2 surface film in water with 2000 ppm  $H_3BO_3$ . At 300°C the LiOH concentrations higher than  $10^{-2}$  M (roughly 70 ppm of  $Li^+$ ) were found to markedly reduce the electric resistance of the Zircaloy-2 surface film during a test period of less than two hours. The decrease of the film resistance is very abrupt, possibly indicating a phase transformation. Moreover, the advantages of the CER technique over the other competing techniques which rely on the measurement of current are discussed.

## 1. INTRODUCTION

The current trends in nuclear power generation are towards plant life extension and extended fuel burnup. At the same time there is an interest to increase the coolant inlet temperature and an apparent need to reduce the activity buildup and resulting radiation fields by controlling the coolant chemistry. This leads to a situation where better predictability of corrosion behavior of the core materials is needed. In PWRs the contemporary operation practice is to keep the coolant pH value between 6.9 and 7.4 during the cycle. The pH value is controlled by adjusting lithium hydroxide and boric acid concentrations of the coolant. The upper limit of the Li concentration in the lower pH range is specified as 2 ppm and in the upper pH range the lithium concentration is limited to 3.5 ppm. Although the increase of the lithium concentration has a beneficial effect on transport of corrosion products and resulting radiation buildup, lithium is known to enhance the stress corrosion cracking of Inconel 600 steam generator tubes and the corrosion of Zircaloy fuel cladding rods. The plant experience has also demonstrated that the oxide on fuel cladding tubes is thicker than expected when using elevated lithium concentrations [1, 2]. Due to hideout effects and the current tendency to increase the lithium content in primary coolant the local enrichment of lithium may result in concentrations well above the actual bulk content. Therefore, there is a potential risk that the corrosion rate of Zircaloys is strikingly enhanced.

During an initial phase corrosion of Zircaloys follows a cubic or parabolic time relation during which the oxide growth rate is rather low. However, after a transition to approximately linear kinetics the oxide growth rate increases to a

much higher level. Experimental observations have shown that high LiOH concentrations result in a reduction of the time to transition and to an increased post transition oxidation rate as can be seen in Fig. 1. The post transition corrosion rate is nearly linear upon exposure time at high LiOH concentrations. Growth of the oxide layer of Zircalloys depends also on coolant chemistry, e.g. on the specific cations and anions, pH and temperature of the coolant. Salts of lithium, e.g. such as lithium carbonate, nitrate or sulfate or hydroxides of sodium, potassium or ammonium have been shown to enhance the corrosion of Zircalloys less than lithium hydroxide [3, 4]. Accelerated corrosion has been observed in laboratory tests only in lithium hydroxide solutions at a pH greater than about 12. Corrosion rate of Zircalloys is also greatly enhanced at temperatures above 360°C compared to more relevant operation temperatures of around 320°C [4, 5].

The reported corrosion rates of Zircalloys in solutions containing both lithium hydroxide and boric acid are much lower than the corrosion rates in the same lithium concentration but without addition of boric acid. It has been suggested that there exists a threshold boron concentration which inhibits the LiOH induced corrosion. This threshold is likely to be dependent on lithium concentration and temperature. In fact, the threshold has been found to exist at about 10 ppm boron in 200 ppm lithium solution at temperature of 360°C. The beneficial effect of boron is suggested to be related to a reduced pickup of lithium by the oxide or simply to a pH effect [6, 7].

The detailed mechanism of how lithium hydroxide increases the corrosion of Zircalloys is controversial. The behavior has been explained by a mechanism in which Li ion is incorporated into substitutional solid solution in the zirconium oxide

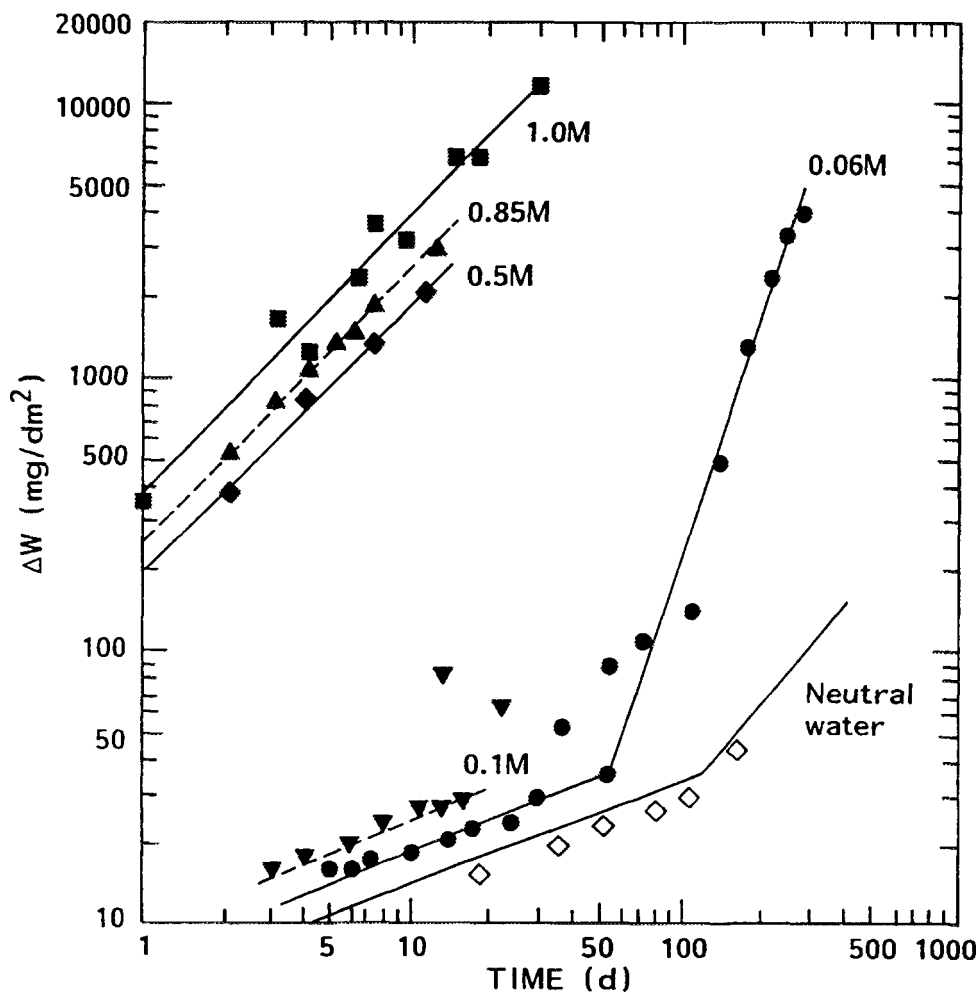


Fig. 1. Zircaloy oxide thickness ( $\Delta W$ , weight gain) as a function of the Li concentration and time (autoclave tests). The LiOH concentrations and room temperature pH values are, respectively: 0.06M LiOH, pH 12.8; 0.1M LiOH, pH 13.1; 0.5M LiOH, pH 13.6; 0.85M LiOH, pH 13.8; 1.0M LiOH, pH 14.0 [8].

causing a large increase in the anion defect concentration and hence an increase in oxygen diffusion rate through the oxide film [8]. Another hypothesis postulates that lithium hydroxide influences the recrystallization processes in the oxide and hence results in more rapid transition from tetragonal to monoclinic oxide phase which further affects the nucleation of pores and cracks in the oxide films [7]. A third hypothesis postulates that the accelerated corrosion in concentrated solutions is caused by the participation of the undissociated lithium hydroxide and hydroxyl

ions in reactions at anion vacancies of the zirconium oxide to produce -OLi groups. These -OLi groups in turn retard the recrystallization and growth of the zirconium oxide and thus maintain either a diffusion path for oxygen or generate porosity in the oxide by further reacting to form soluble lithium oxide [9]. Also a simple chemical dissolution and reprecipitation process has been proposed to explain the local degradation and formation of porosity in pretransition oxides [10].

## 2. EXPERIMENTAL

The Contact Electric Resistance (CER) method [11] enables an accurate measurement of electric resistance between two periodically contacted specimens. The measurement system is shown in Fig. 2a. There are two frames on top of the autoclave head 1. The first frame 2 supports the step motor 3 with the pull rod 4 passing into autoclave through the sealing 5. The other frame 6 supports the rigid spring 7. This spring consists of an immobile lower part and a mobile upper part. Insulating specimen holders 8 and 9 are fastened to the rigid spring by screws. Connecting wires 10 passing through the autoclave head are connected to the external resistance element  $R_2$  and to the double bridge (Fig. 3a). The rigid spring 7 is cyclically loaded by the step motor 3 through the soft spring 11. Such a loading system eliminates the effects of friction and the high internal autoclave pressure on the deformation of both springs and the replacement of contacting surfaces of the samples. Calibration of the system has shown that each step of the step motor moves the contacting surfaces about  $10^{-9}$  m. The reproducibility of the movement of the step motor is better than one tenth of a step. Thus, the reproducibility of the contact situation is estimated to be better than  $10^{-10}$  m.

All components of the CER autoclave unit were made of stainless steel AISI 316, except for the specimen holders (Fig. 2b) and the rigid spring, which were made of oxidized zirconium. Measurement cables were silver soldered into the specimens and the joint areas were covered with several layers of PTFE-tape.

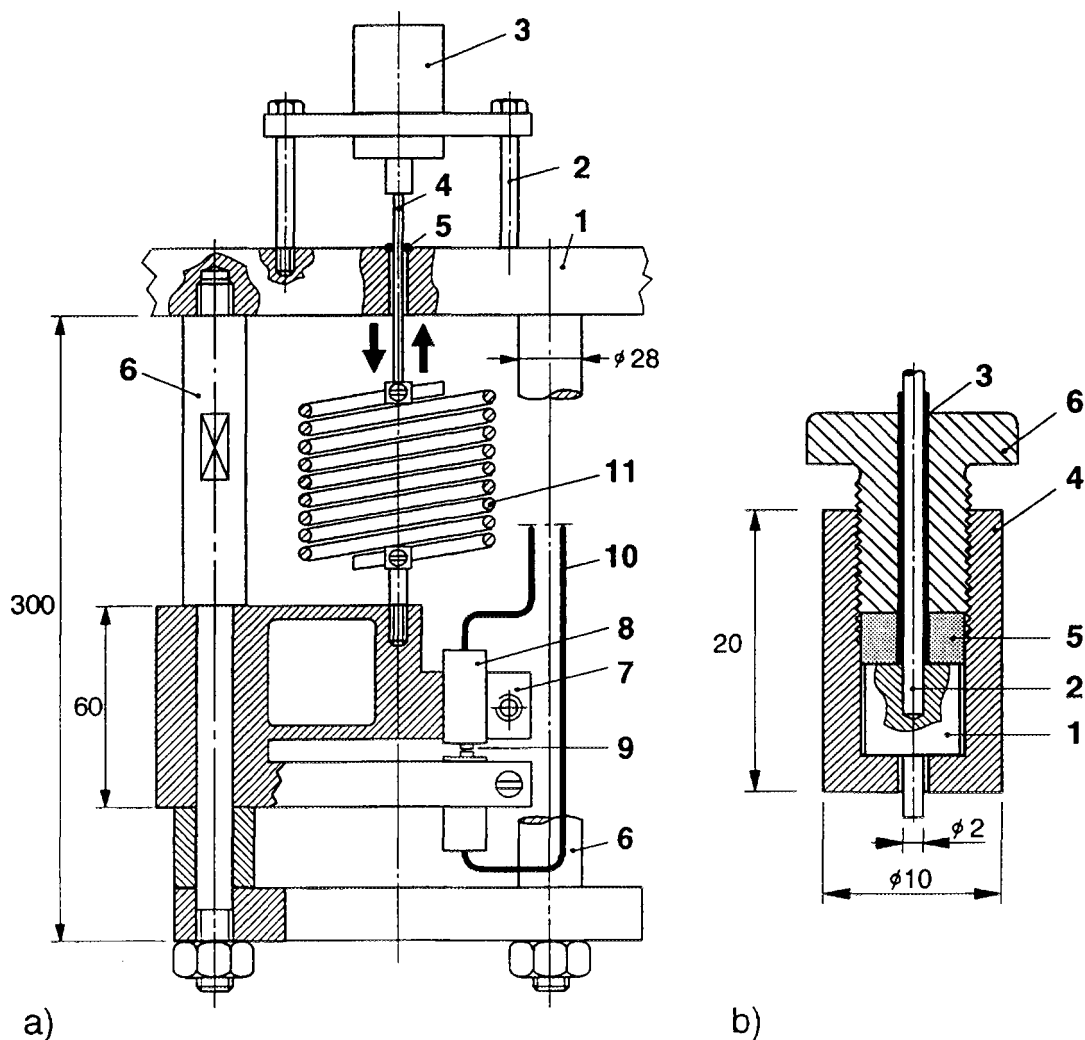


Fig. 2. Scheme for measurement of the surface film resistance at high temperatures and pressures (a). [1] autoclave head, [2] supporting frame, [3] step motor, [4] pull rod, [5] seal, [6] supporting frame, [7] stiff spring, [8] specimen holder, [9] specimen, [10] connecting wires, [11] soft spring. Specimen holder with fixed specimen (b). [1] specimen, [2] silver connecting wire, [3] insulation, [4] Zr holder, [5] Zr ring, [6] Zr screw.

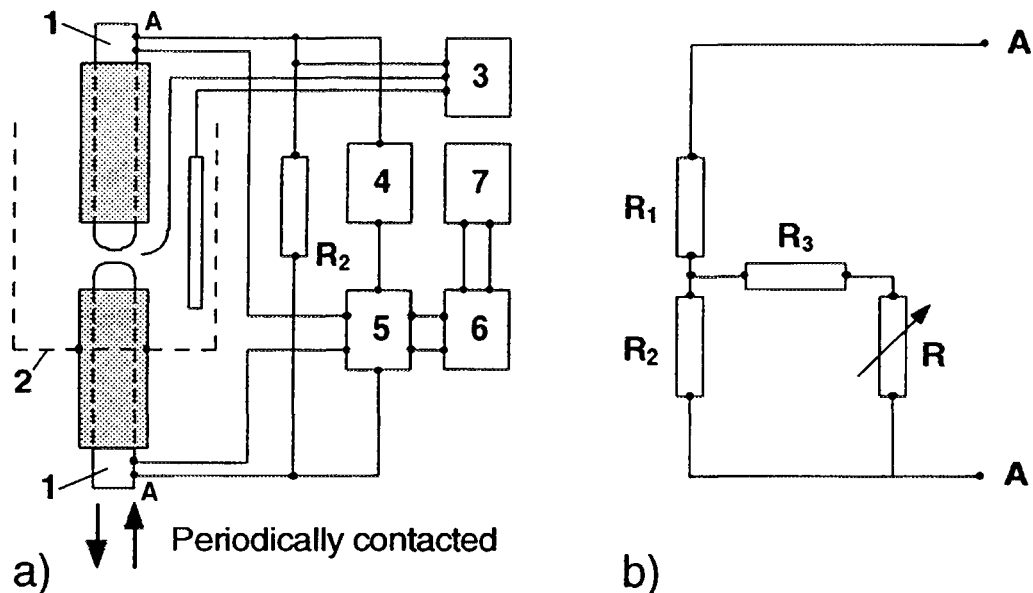


Fig. 3. Scheme of the Contact Electric Resistance (CER) measurement system (a) and the electrical analog of the measurement system (b). [1] Sample, [2] electrochemical cell, [3] potentiostat Wenking Model LB 81 M, [4] direct current source Hewlett Packard 6033A, [5] double bridge P329, [6] dc amplifier Yokogawa 3131, [7] recorder Yokogawa LR 4220.  $R_2$  is an external resistance element,  $R_1$  is the resistance of the measurement wires,  $R_3$  is the resistance of the connecting wires between the contacting surfaces and the resistance element  $R_2$ . The resistance of the successive chain metal-film-electrolyte-film-metal, the contact resistance, is designated  $R$ .

The CER measurement system is shown schematically in Fig. 3a and the electrical analogue of the measurement system in Fig. 3b. The points AA indicate the points of current supply and switching in of the double bridge.  $R_1$  is the resistance of the measurement wires,  $R_2$  is an external resistance element and  $R_3$  is equal to the electric resistance of the connecting wires between the two contacting surfaces and the resistance element,  $R_2$ . The resistance of the successive metal-film-electrolyte-film-metal system, the contact resistance, is designated  $R$ .

The contact resistance has been found to be independent of the ionic electrolyte conductivity, at the level of sensitivity of the technique. When the specimens are not in contact the measured resistance  $R$  is equal to  $R_1 + R_2$ . When the specimens are in contact the measured resistance is equal to  $R_1 + R_2 \cdot (R_3 + R) / (R_2 + R_3 + R)$ . The variation of the electric resistance,  $\Delta R$ , during each contacting cycle is determined by the equation {1} and the contact resistance  $R$  by the equation {2}:

$$\Delta R = R_2^2 / (R_2 + R_3 + R) , \quad \{1\}$$

$$R = R_2^2 / \Delta R - R_2 - R_3 . \quad \{2\}$$

The choice of the resistance element  $R_2$  depends on the materials under investigation, and the resistance is typically in the range 0.05 - 500 m $\Omega$ . A rule of thumb in choosing the magnitude of  $R_2$  is that the larger the free energy of formation of the oxide under investigation, the higher resistance is required. In the case of Zircaloy the value of  $R_2$  has usually been 300 m $\Omega$ . The resistance of the contacting wires,  $R_3$ , is constant during the experiment and normally less than 100 m $\Omega$ .

In the case of Zircaloy-2 the electric resistance of its surface film (oxide) is among the highest investigated so far by the CER-technique. The maximum measurement capacity of the CER technique depends mainly on the value of  $R_2$ . Increase of  $R_2$  increases the maximum resistance measurement capacity, but introduces a large error in the electrochemical potential of the sample, due to the voltage drop generated by the direct current passing through the  $R_2$  resistance element ( $\Delta E = I \cdot R_2$ ). For this purpose the technique was modified so that one of

the two contacting specimens was replaced by a similar sample made of pure Iridium. Iridium does not form an oxide film in the electrochemical potential range in which Zircaloy-2 studies were performed. Adsorption of anions on Iridium does occur, but the resistance increase due to this was found to be negligible in comparison with the resistance measured for Zircaloy-2. Use of Iridium as the other electrode gives a possibility to increase the measurement capacity by about three orders of magnitude.

All tests were carried out in static autoclaves made of AISI 316 stainless steel. The electrolytes used were prepared from ion purified water and reagent grade chemicals. Nitrogen gas was used to remove oxygen from solution before starting the test. Electrochemical potential was measured with an external 0.1 M Ag/AgCl reference electrode and with a Pd hydrogen electrode. The Pd hydrogen electrode consists of a Pd electrode which is electrochemically hydrogenated so that the potential of the electrode is always at the hydrogen reduction/oxidation potential. In systems where pH is known and stable it is very convenient to use this type of electrode because there is no need to correct various junction potentials. The LiOH was injected directly into the autoclave using a liquid chromatography pump.

Specimens with a 2 mm in diameter contact surfaces were machined from a rod ( $\varnothing$  13 mm) of Zircaloy-2. Before starting the tests the contact surfaces were polished and the oxide was removed by sand paper immediately after the specimens had been assembled into the specimen holders and fastened to the rigid spring. After polishing the contact surfaces were rinsed with ion pure water. After autoclave tests specimen surfaces were studied by scanning electron microscopy (SEM) and secondary ion mass spectroscopy (SIMS).

### 3. RESULTS

The measured surface film resistance of a Zircaloy-2 sample in water containing 2000 ppm  $H_3BO_3$  and a total of 93 ppm Li during 35 hours exposure is shown in Fig. 4. The initial film resistance before the first lithium hydroxide injection showed a constant value of 100 Ohm. The first two small amounts (3.5 ppm and the additional 8 ppm Li) did not cause any change in the resistance, within the time allowed. After the last lithium hydroxide injection (81 ppm Li) the measured film resistance increased first and seemed to stabilize at a value of about 500 Ohm. The first indication of the resistance breakdown occurred after about 4 hours from the injection, followed by a slow increase of the resistance. The second considerable breakdown in film resistance occurred after about 10 hours

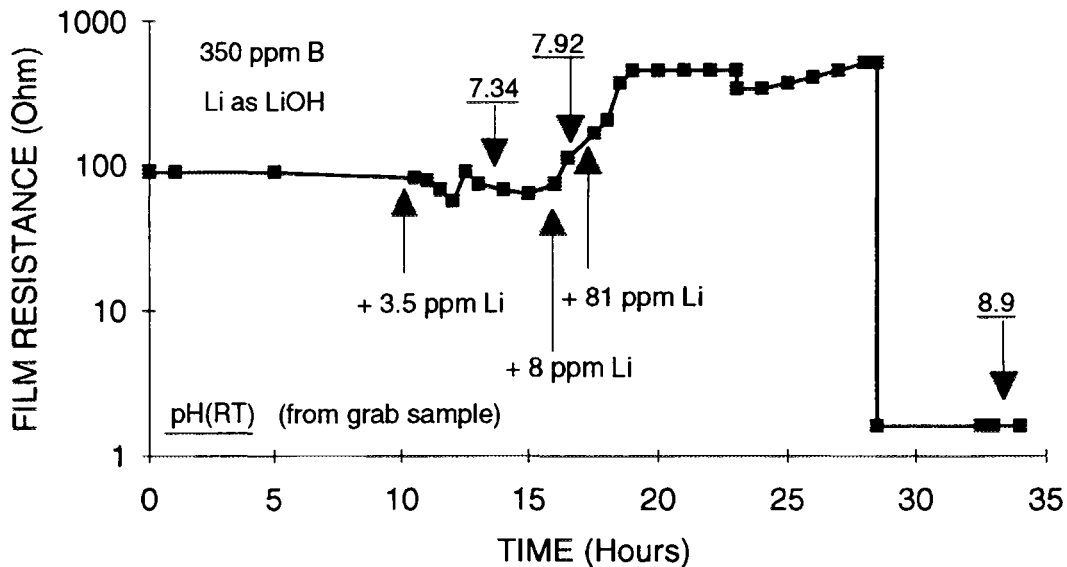


Fig. 4. Surface film electric resistance of Zircaloy 2 specimen in ion purified water with 350 ppm B as  $H_3BO_3$  and a total of 93 ppm Li as LiOH at temperature of 300°C. The pH of the electrolyte was checked after each addition of LiOH by taking a grab sample. The moments of taking the grab sample as well as the measured room temperature pH are marked in the figure.

from the LiOH injection. The measured film resistance decreased from a value of about 500 Ohm to a value below 1 Ohm, and remained thereafter at this low level. In both cases the breakdown occurred within less than twenty seconds, which was the measurement frequency used. After the resistance had remained at the low level for about six hours, the test was stopped, the autoclave cooled down and the specimen surface investigated by SEM and SIMS.

Figure 5 shows the appearance of the specimen surface. There are local areas of corrosion attack and areas where the oxide seems to be more dense with reprecipitated crystallites on the surface. The corresponding SIMS analysis on corroded surface indicated an oxide thickness of about 0.2 microns as shown in Fig. 6. No evidence of lithium or hydrogen enrichment in the oxide layer was observed.

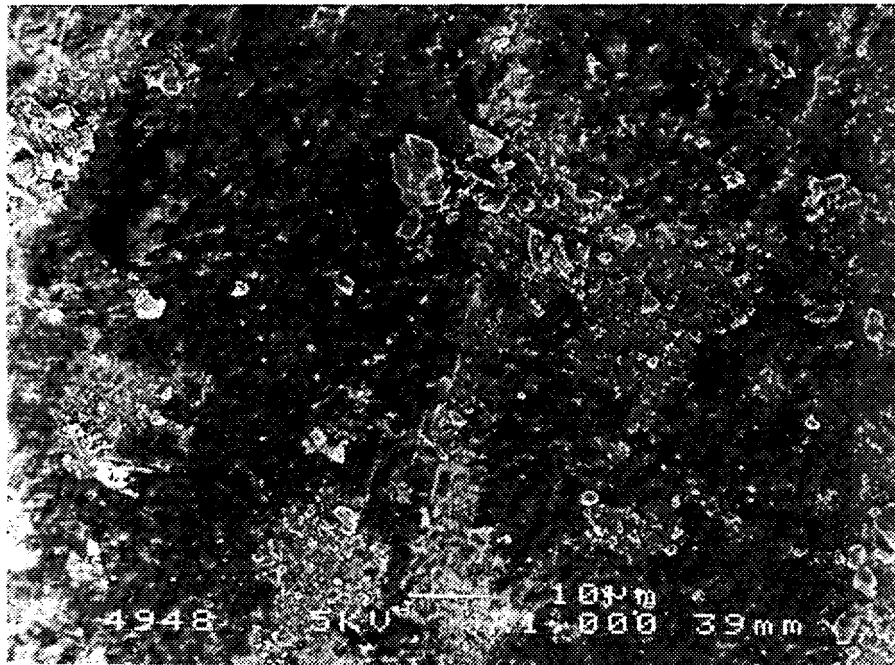


Fig. 5. Surface appearance of Zircaloy 2 specimen after about 35 hours testing in ion purified water with 350 ppm B as  $H_3BO_3$  and 93 ppm Li as LiOH at temperature of 300°C.

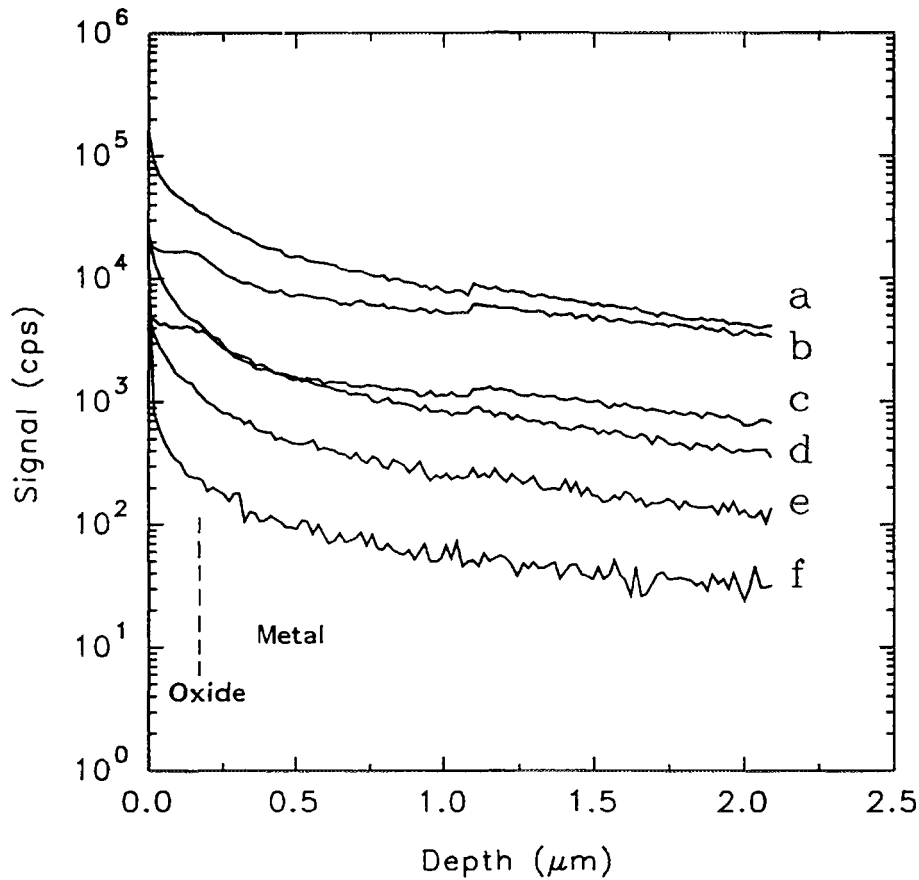


Fig. 6. SIMS depth profiles of Zircaloy 2 specimen after about 35 hours testing in ion purified water with 350 ppm B as  $\text{H}_3\text{BO}_3$  and 93 ppm Li as LiOH at temperature of  $300^\circ\text{C}$ . a)  $^7\text{Li}$ , b)  $^{96}\text{Zr}$ , c)  $^{16}\text{O}$ , d)  $^{11}\text{B}$ , e)  $^{56}\text{Fe}$  and f)  $^1\text{H}$ .

The surface film resistance at different lithium hydroxide concentrations is shown in Fig. 7. Each measuring point represents a resistance value measured after about two hours after the injection of the lithium hydroxide. The resistance of the oxide was constant at low lithium hydroxide concentrations but a decrease in oxide resistance was observed at about 110 ppm added lithium. At the level of 700 ppm lithium in the solution the oxide resistance decreased from an initial value of about 30 Ohms to about 2 Ohms. In all cases decrease of the resistance occurred abruptly.

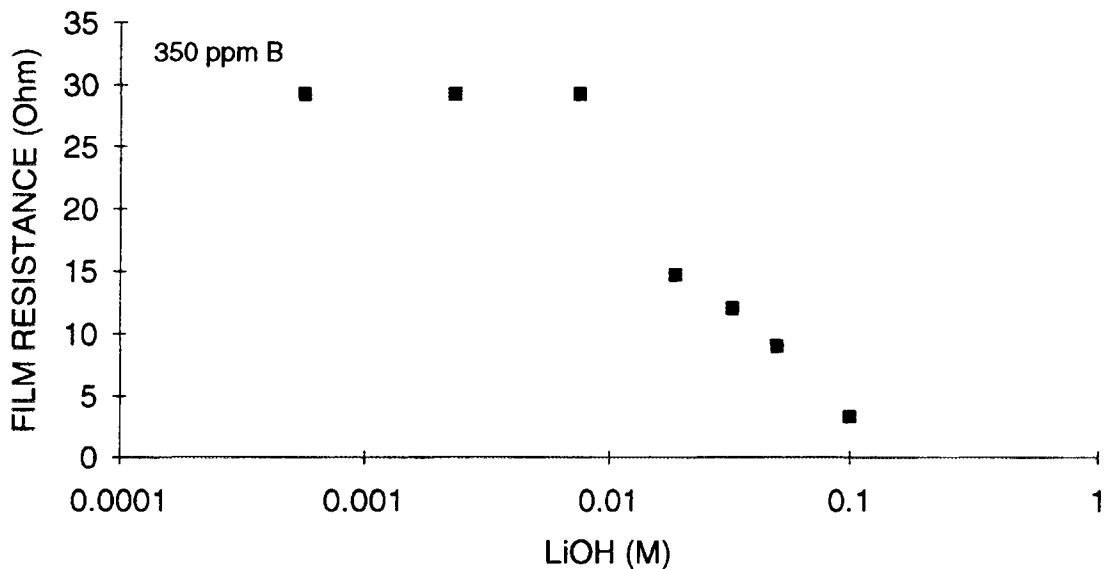


Fig. 7. Surface film electric resistance of Zircaloy 2 specimen as a function of LiOH concentrations. Ion purified water with 350 ppm B as  $H_3BO_3$  at temperature of  $300^\circ C$  where Li was added as LiOH by injection pump. Each data point represents a measurement period of not more than two hours.

#### 4. DISCUSSION

Based on various Zircaloy weight gain measurements, there is a threshold lithium hydroxide concentration above which there is no transition from low growth rate to high growth rate. This threshold level has been found to be between 0.1 and 0.5 M LiOH (Fig. 1). When the lithium hydroxide concentration exceeds this level, the weight gain rate has been found to be very high immediately from the start of the test. The CER measurements shown in Fig. 7 indicate that the surface film resistance of Zircaloy-2 starts to decrease when the LiOH concentration exceeds the level of about  $10^{-2}$  M. At the level of 0.5 M LiOH the surface film resistance approaches to zero, which indicates that there is active corrosion taking place. Comparison of Figs. 1 and 7 shows that the time for the transition

measured by weight gain has the same dependency on LiOH concentration as the surface film resistance measured by the CER technique. However, because of the much higher sensitivity of the CER technique in comparison with the weight gain technique the time required for testing is several orders of magnitude lower, in favor of the CER technique. It is expected that the weight gain depends on the rates of the electrochemical processes involved. Thus it is not surprising that there is a good correlation between film resistance, which governs the rate of the electrochemical processes, and the weight gain rate.

The relative decrease of the film resistance measured in this investigation, i.e. two orders of magnitude, is in the same range that has been earlier found by a.c. impedance techniques [12, 13]. The observed decrease in surface film resistance is also in accordance with the increase in conductivity due to lithium hydroxide found in electrochemical polarization measurements [14].

The observed abrupt decrease in resistance after an incubation period, during which the resistance remained almost constant, seems to indicate a phase transformation rather than a diffusion limited process as the mechanism of degradation. The transformation in question could be oxide recrystallization or a transition from tetragonal to monoclinic structure, hydride precipitation or a possible reactions between zirconium and lithium. There is a lack of data on specific resistance values of different forms of zirconium oxides. However, monoclinic oxide is generally considered to be more porous and to have a higher conductivity in comparison with a tetragonal oxide structure. Electrical conductivity of zirconium hydride has been reported to be even higher than that of metallic zirconium [15].

In highly reducing environments, such as PWR primary water and BWR water with hydrogen water chemistry, the hydrogen oxidation-reduction reaction is the major electrochemical reaction taking place on the metal surfaces. This reaction, with a high exchange current density, relate the corrosion potential with the potential of the reversible hydrogen electrode as schematically shown in Fig. 8. Any electrochemical measurement of metal based on the current measurement and carried out close to its corrosion potential is dominated by the current generated in hydrogen reduction/oxidation reaction. However, the CER technique, which is

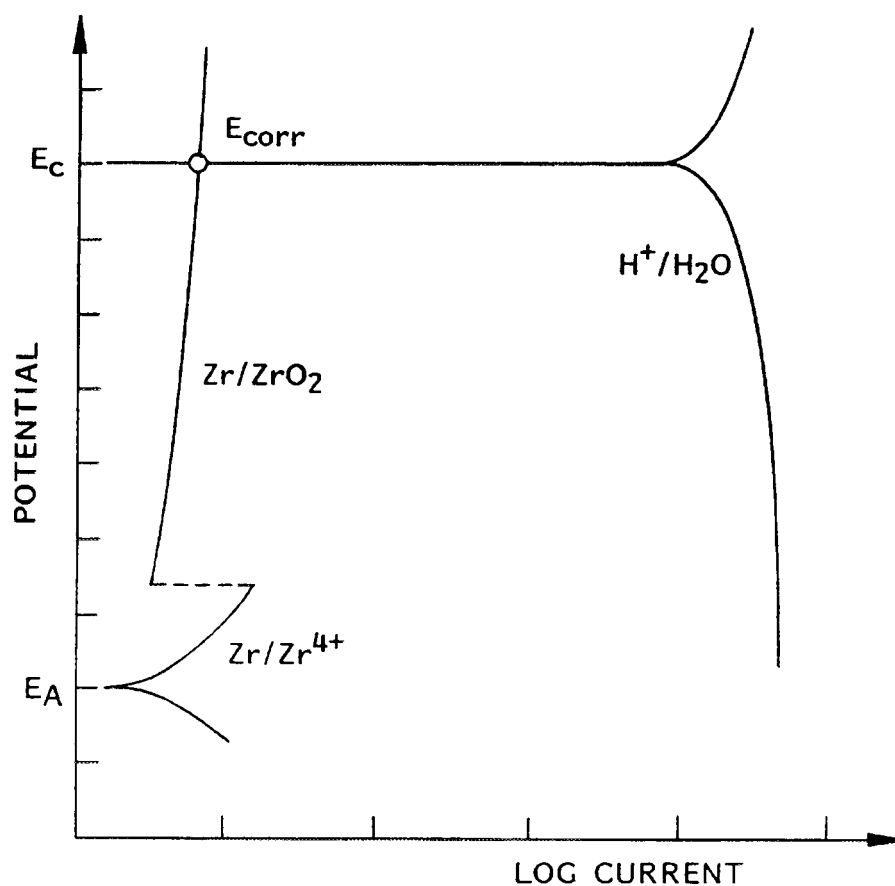


Fig. 8. Schematic potential versus log current curves showing how the corrosion potential of metals is fixed to the hydrogen reduction/oxidation equilibrium potential in reducing environments.  $E_A$  and  $E_C$  denote the equilibrium potentials of the anodic and the cathodic reactions, respectively.

based on direct measurement of the contact electric resistance of the surface film, can be reliably applied even in these reducing environments.

## 5. CONCLUSIONS

Surface film resistance measurements of Zircaloy-2 samples showed that LiOH in excess of about 70 ppm ( $10^{-2}$  M) in pure water with 2000 ppm  $H_3BO_3$  at 300 °C decreases dramatically the electric resistance of the surface film. The observed decrease in film resistance occurred abruptly, within 20 seconds, after an incubation period which depends on the concentration of LiOH.

The extremely fast kinetics of the decrease in the surface film resistance indicates that the mechanism of degradation of zirconium oxide in LWR environments containing lithium hydroxide is controlled by a phase transformation rather than a diffusion limited process.

The trends of oxide growth kinetics in LiOH solutions found in long term weight gain tests are similar to the trends in the surface film resistance measured with the CER technique in this work.

Due to the high sensitivity of the CER measurement technique to detect the changes in the surface film properties, the time required for corrosion testing of Zircalloys can be decreased by several orders of magnitude in comparison with the common weight gain tests.

## ACKNOWLEDGEMENTS

This work was funded by the OECD Halden Reactor Project. Additional financing by the Academy of Finland is acknowledged.

## REFERENCES

- [1] INTERNATIONAL ATOMIC ENERGY AGENCY, Coolant Technology of Water Cooled Reactors: An Overview, Technical Report Series No. 347, Vienna, Austria (1993).
  
- [2] SHANN, S., VAN SWAM, L., MARTIN, L., Effects of Coolant Li Concentration on PWR Cladding Waterside Corrosion, Proc. of International Topical Meeting on LWR Fuel Performance, Avignon, April 21 - 24, European Nuclear Society (1991), 742-748.
  
- [3] MCDONALD, S.G., SABOL, G.P., SHEPPARD, K.D., Effect of Lithium Hydroxide on the Corrosion Behavior of Zircaloy-4, Zirconium in the Nuclear Industry: Sixth International Symposium, ASTM-STP 824, Eds. Franklin, D., Adamson, R., American Society for Testing and Materials, Philadelphia (1984), 519-530.
  
- [4] CORIOU, H., GRALL, L., MEUNIER, J., PELRAS, M., VILLERMOZ, H., Corrosion du Zircaloy Dans Divers Milieux Alcalins A Haute Temperature, Journal of Nuclear Materials 7 (1962) 320-327.

- [5] PERKINS, R., BUSCH R., Corrosion of Zircalloys in Presence of LiOH, Zirconium in the Nuclear Industry: Ninth International Symposium, ASTM-STP 1132, Eds. Eucken, C. M. & Garde, A. M., American Society for Testing and Materials, Philadelphia (1991), 595-612.
- [6] BRAMWELL, I., PARSONS, P., TICE, D., Corrosion of Zircaloy-4 PWR Fuel Cladding in Lithiated and Borated Water Environments, Zirconium in the Nuclear Industry: Ninth International Symposium, ASTM-STP 1132, Eds. Eucken, C. M. & Garde, A. M., American Society for Testing and Materials, Philadelphia (1991), 628-642.
- [7] GARZAROLLI, F., POHLMAYER, J., TRAPP-PRITSCHING, S., WEIDINGER, H., Influence of Various Additions to Water on Zircaloy 4 Corrosion in Autoclave Tests at 350°C, Fundamental Aspects of Corrosion on Zirconium Base Alloys in Water Reactor Environments, IAEA Technical Committee Meeting, IWGFPT/34, International Atomic Energy Agency, Vienna (1990), 65-72.
- [8] HILLNER, E., CHIRIGOS, J., The Effect of Lithium Hydroxide and Related Solutions on the Corrosion Rate of Zircaloy 2 in 680F Water, Report WAPD-TM-307, Bettis Atomic Power Lab. W. Mifflin, PA (1967).
- [9] RAMASUBRAMANIAN, N., Lithium Uptake and the Corrosion of Zirconium Alloys in Aqueous Lithium Hydroxide Solutions, Zirconium in the Nuclear Industry: Ninth International Symposium, ASTM-STP 1132,

Eds. Eucken, C. M. & Garde, A. M., American Society for Testing and Materials, Philadelphia (1991), 613-627.

- [10] COX, B., WU, C., Dissolution of Zirconium Oxide in 300°C LiOH, Journal of Nuclear Materials 199 (1993) 272-284.
  
- [11] SAARIO, T., MARICHEV, V., A New Contact Electric Resistance Technique for In-Situ Measurement of the Electric Resistance of Surface Films on Metals in Electrolytes at High Temperatures and Pressures, International Corrosion Congress '93, Houston, Texas, 19 - 24 September, 1993, Paper No 134.
  
- [12] COX, B., A Porosimeter for Determining the Sizes of Flaws in Zirconia or Other Insulating Films "In Situ", Journal of Nuclear Materials 27 (1968), 1-11. Wanklyn, J. & Silvester, D., A Study of Corrosion Films on Zirconium and Its Alloys by Impedance Measurements, Journal of the Electrochemical Society 105 (1958) 647-654.
  
- [13] INAGAKI, M., HIROTA, M., Electrical Resistivity of Zirconium Oxide Film Formed in 288°C Water Containing Various Impurities, Water Chemistry '91, ed. Ishigure, K., Japan Atomic Industrial Forum, Inc. (JAIF), Fukui City, Japan (1991).
  
- [14] INTERNATIONAL ATOMIC ENERGY AGENCY, Corrosion of Zirconium Alloys in Nuclear Power Plants, IAEA-TECDOG-684, Vienna, Austria (1993).

- [15] BICKEL, P., BERLINCOURT, T., Optical Mode Scattering Contribution to Electrical Resistivity in Zirconium Hydride, *Physical Reviews* 119 (1960) 1603-1610.



# **OXIDING AND HYDRIDING PROPERTIES OF Zr-1Nb CLADDING MATERIAL IN COMPARISON WITH ZIRCALOYS**

V. VRTÍLKOVÁ  
Nuclear Fuel Institute, Zbraslav

M. VALACH  
Nuclear Research Institute, Řež plc

L. MOLIN  
Nuclear Fuel Institute, Zbraslav

Czech Republic

## **Abstract**

This paper presents an overview of experimental research related to the Zr-1Nb corrosion behaviour in water and steam environment performed in the Czech Republic. Presented work is focused on the differences between Zr1Nb and Zircaloy corrosion performance. The effects of steam pressure, temperature transients and preoxidation are discussed.

## **1. INTRODUCTION**

In this paper, our experience in the field of the Zr1Nb cladding tube corrosion in an inactive environment is described emphasizing some differences in the corrosion behaviour of Zr1Nb and Zry-4 alloys.

The research works were aimed at the kinetics of corrosion (oxidation) and hydriding in water and steam environments up to 1400°C. Moreover, the effect of the KOH, H<sub>3</sub>BO<sub>3</sub> and LiOH additions on the corrosion kinetics in water, preoxidation, vapour pressure and short-time superheatings on the oxidation process in steam was examined.

In the experiments, reactor grade Zr1Nb (former USSR) and Zry-4 (SANDVIK Co.) cladding tubes were used.

## **2. PRESENTATION OF THE EXPERIMENTAL RESULTS**

### **2.1. Zr1Nb corrosion in water**

During the long-term corrosion tests ( ~ 30 000. h), a black and adhesive oxide formed and no break of the kinetic curves was found (300 and 350°C test temperature).

Experiments performed recently in water with additions of boric acid (4 g/l) and potassium hydroxide (11 mg/l) confirmed the non-existence of a break of corrosion curves. The corrosion deposits of by-products from the autoclave (iron oxides, copper) on the oxide surface are very small. The results are illustrated in Fig.1 [1]. As seen in Fig.1, the corrosion rate in higher pH water was slightly lower. At the same time, the alloy absorbed, in the first phase, slightly more hydrogen, ~ 13% from that formed in theory during the corrosion process compared to < 10% hydrogen absorbed by the alloy in pure water. Having achieved the oxide thickness of ~ 1.5 μm, the hydrogen quantity absorbed by the alloy did not practically increase.

At present, we concentrate at corrosion tests in water containing LiOH and H<sub>3</sub>BO<sub>3</sub>. Previous tests confirmed a higher sensitivity of the Zr1Nb alloy to the LiOH addition compared to Zry-4, see Fig.2 and a corrosion rate moderating effect of boric acid. [2]

## **2.2 Zr1Nb corrosion in high pressure steam**

The corrosion tests of Zr1Nb are performed in 10 MPa steam and 350 - 600°C temperature range. In dependence on the temperature and oxidation time, a black, bright and adhesive oxide forms, changing to a grey, light brown and, eventually, to a white stoichiometric oxide.

The corrosion layer is, in the initial stage, thin and nonuniform, later uniform and, if oxide is not black, cracks perpendicular to the oxide-metal interface develop.

The oxidation kinetics are controlled initially in temperatures less than 450°C by the cubic law followed by a parabolic law and break of corrosion curves, the further corrosion course being nearly linear. The results are documented in Fig.3. [1]

The temperature dependence of the corrosion rate may be expressed by the following relations:

for the calculation of the mass increment, ΔG<sub>p</sub>, in the parabolic part of the oxidation curve, it is:

$$\Delta G_p = 2.336 \times 10^6 \times \exp\left(-\frac{8385}{T}\right) \times t^{0.5} \quad (1)$$

for the calculation of the mass increment, ΔG<sub>L</sub>, in the linear part of the oxidation curve, it is:

$$\Delta G_L = 5.945 \times 10^8 \times \exp\left(-\frac{13193.6}{T}\right) \times t^{0.84} \quad (2)$$

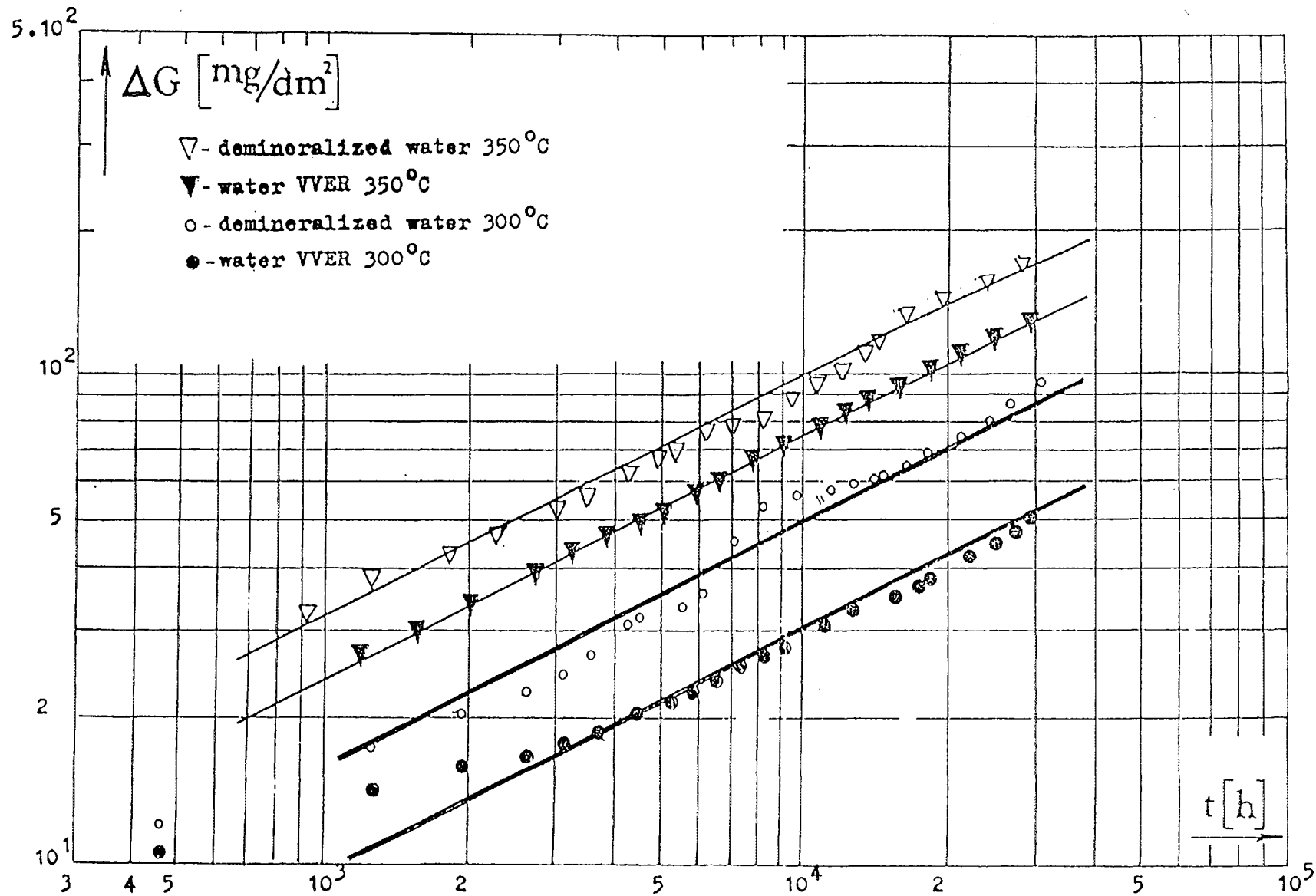


Fig.1. Corrosion kinetics of Zr1Nb alloy in water at 300 and 350°C.

the break of the kinetic curves occurring at an increment,  $\Delta G_B$ :

$$\Delta G_B = 660.9 \times \exp\left(\frac{1304.7}{T}\right) \quad (3)$$

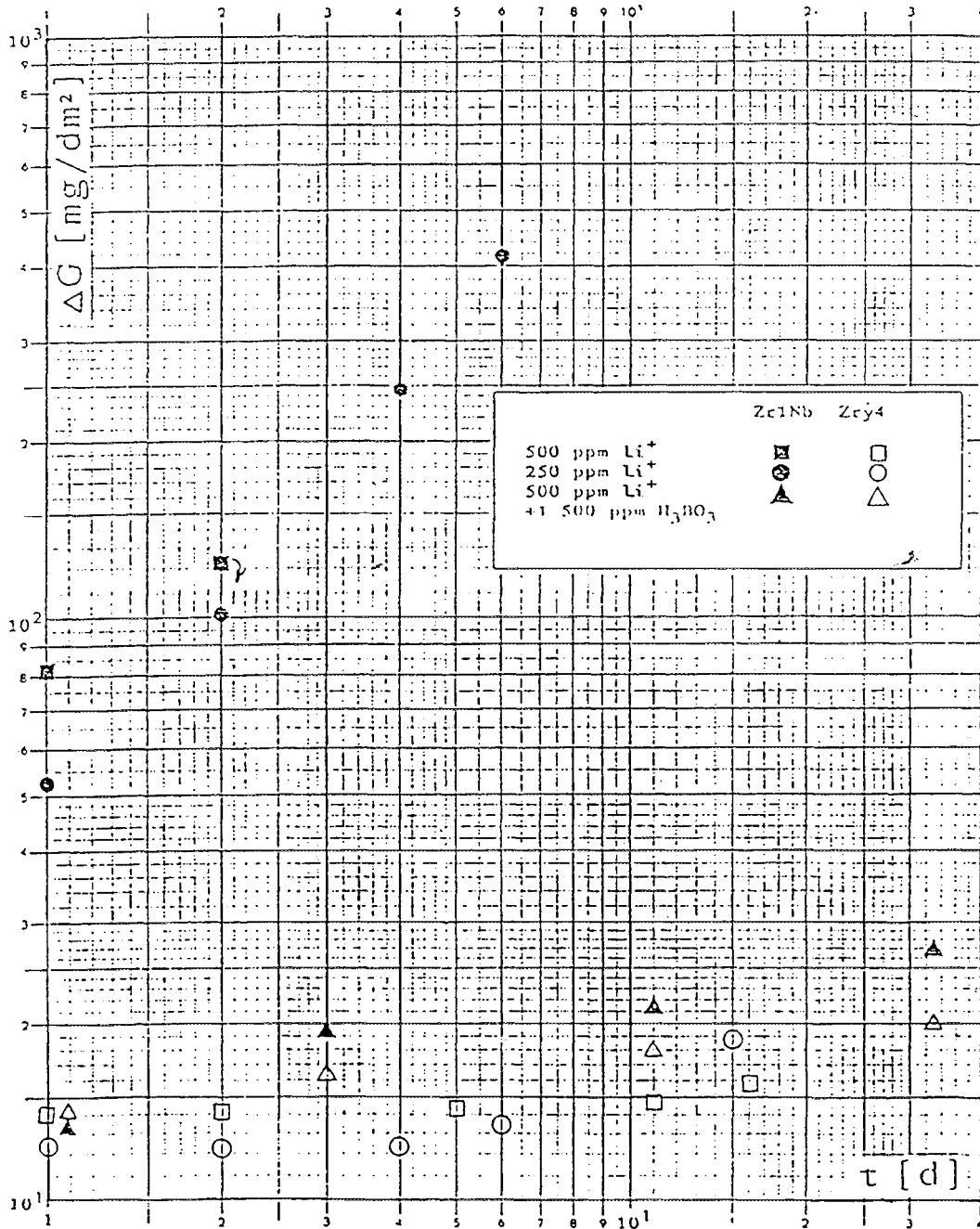


Fig.2. Corrosion kinetics of Zr1Nb and Zry-4 alloys in water at 350°C with additions of:

- a) 500 ppm of  $\text{Li}^+$ ,
- b) 250 ppm of  $\text{Li}^+$ ,
- c) 500 ppm of  $\text{Li}^+$  and 1500 ppm of  $\text{H}_3\text{BO}_3$ .

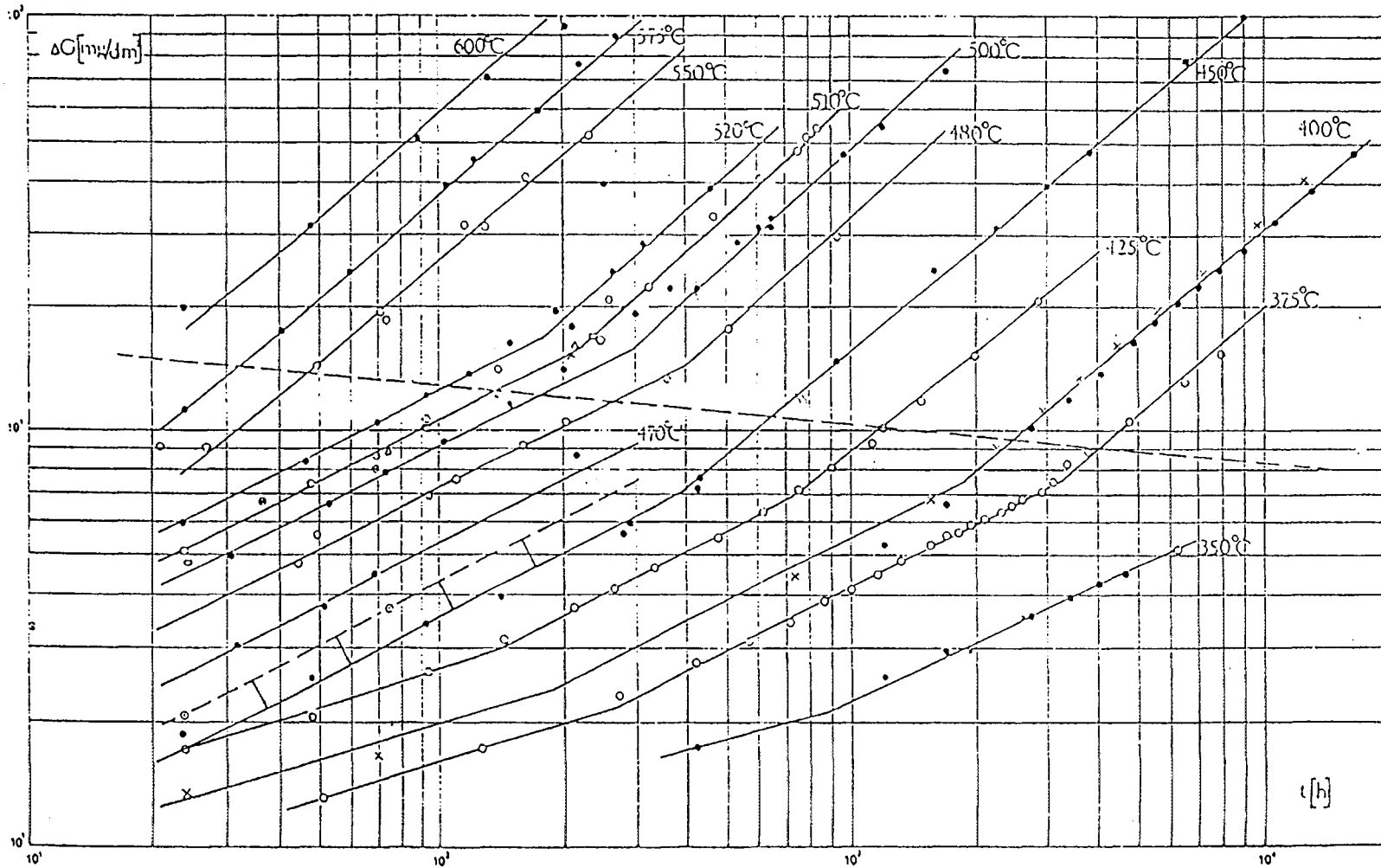


Fig.3. Corrosion kinetics of Zr1Nb alloy in steam at the temperature range 350 - 600°C.

where the mass increment,  $\Delta G$ , is given in  $\text{mg}/\text{dm}^2$  and the temperature,  $T$  in  $\text{K}$ , the exposure time  $t$  is being given in days (see Fig.4).

At 500 and 600°C, the influence of the vapour pressure (0.1, 7, 14 MPa) was examined. The increase of the vapour pressure from 0.1 to 14 MPa resulted in an increase of the corrosion rate corresponding approximately to a 10°C higher temperature.

The hydrogen content of the alloy increases with the exposure time. The maximum hydrogen content of this alloy was observed in the linear oxidation range between 400 and 450°C, i.e.  $\sim 50\%$  of the theoretical quantity of hydrogen released during the oxidation process. At higher temperatures, the percentages of hydrogen absorbed drop to values less than 30%.

The calculation of the mass increment based on the relations (1) and (2) to be used in transient conditions was verified by the transient experiment illustrated in Fig.5. In the end of the experiment, the measured value,  $\Delta G_{\text{exp}} = 835.6 \text{ mg}/\text{dm}^2$ , and calculated value  $\Delta G = 894.2 \text{ mg}/\text{dm}^2$  with hydrogen content = 1630 ppm can be compared.

The preoxidation did not affect substantially the mass increments for the further isotherm, however, the effect of preoxidation on the hydrogen content of the alloy was more evident, especially in the case of the oxide being in a pretransient stage. Figures 6,7 documents the character of hydrides during the transient experiment:

- exposure starting at 300°C in water,
- exposure starting at 350°C.

Fig. 7 shows the difference between the isothermal exposure and after the preoxidation at 300°C ( $\sim 21$  d).

It should be noted that in any environment, temperature and vapour pressure no so-called nodular corrosion was observed.

For the isotherms selected, the Zry-2 and Zry-4 alloys were used as reference samples. The results obtained correspond to the data published (see Fig.8) and, especially at 550°C, there was a destruction of samples for the exposure  $< 24$  h. [3]

Short-time overheatings (3, 5, 10, 25 and 60 s) for temperatures from 600 to 1050°C of the Zr1Nb samples preoxidized in steam 350°C ( $\sim 40 \text{ mg}/\text{dm}^2$ ) showed a very little influence on the further oxidation process in steam 350°C up to the overheat temperature of 700°C. At higher overheatings from 700°C the mass increments were lower than the values presupposed. For the overheat temperatures  $\geq 900^\circ\text{C}$ , the samples were grey and, after a further exposure at 350°C, oxide began to spall. [1]

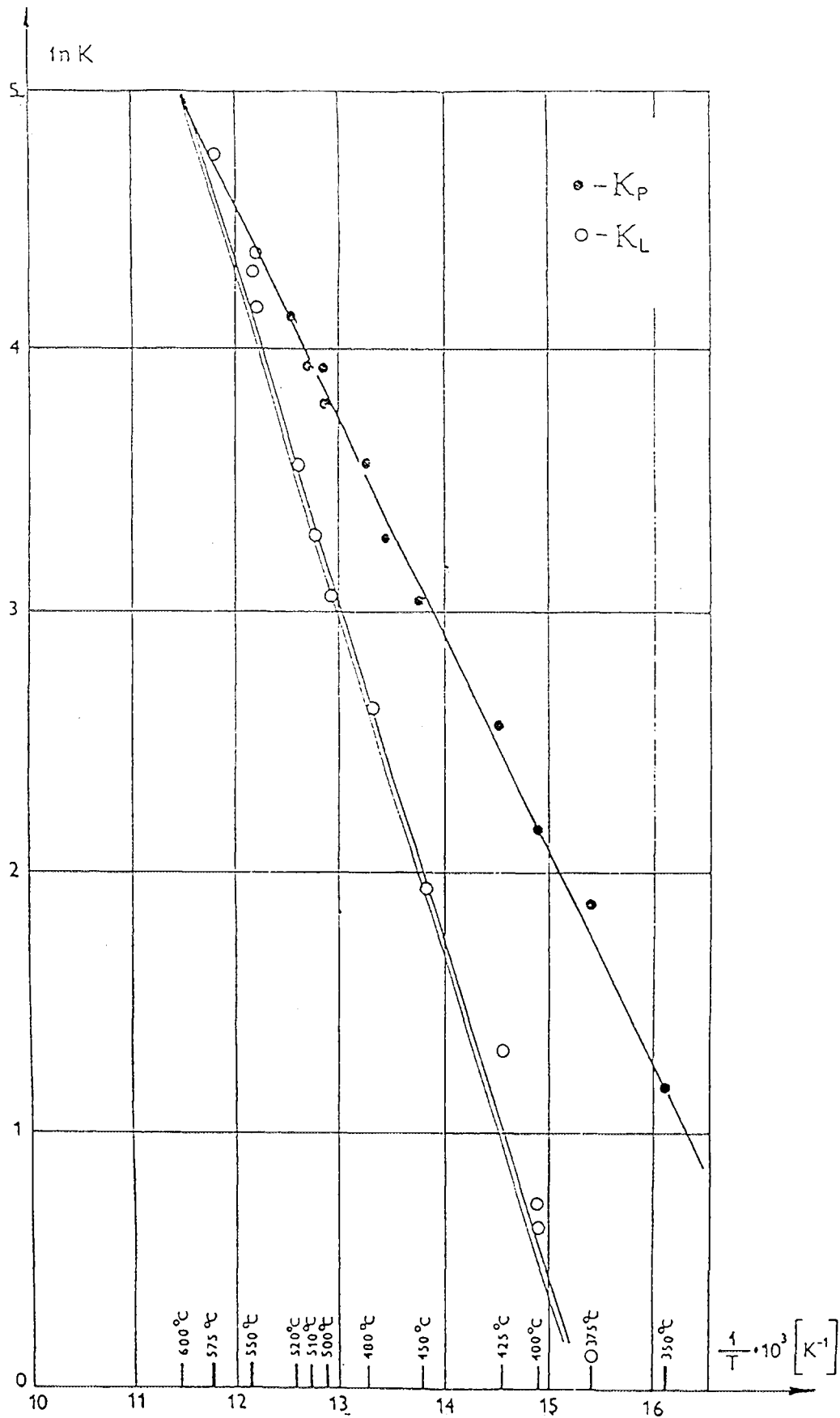


Fig.4. Dependence of  $\ln K_P$  and  $\ln K_L$  on  $1/T$  for Zr1Nb alloy.

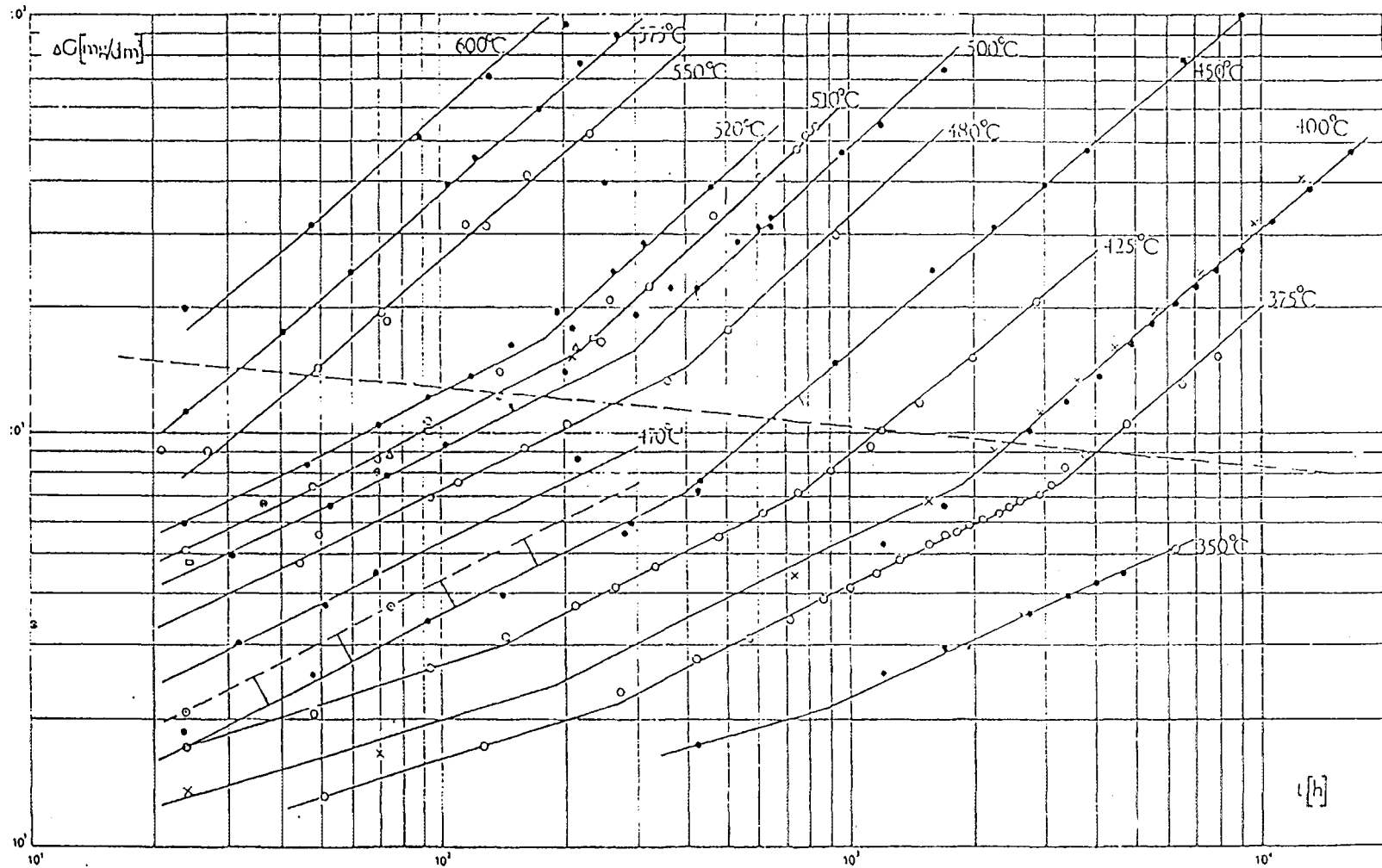


Fig.5. Transient experiment course with  $\Delta G$  measured and calculated comparison.

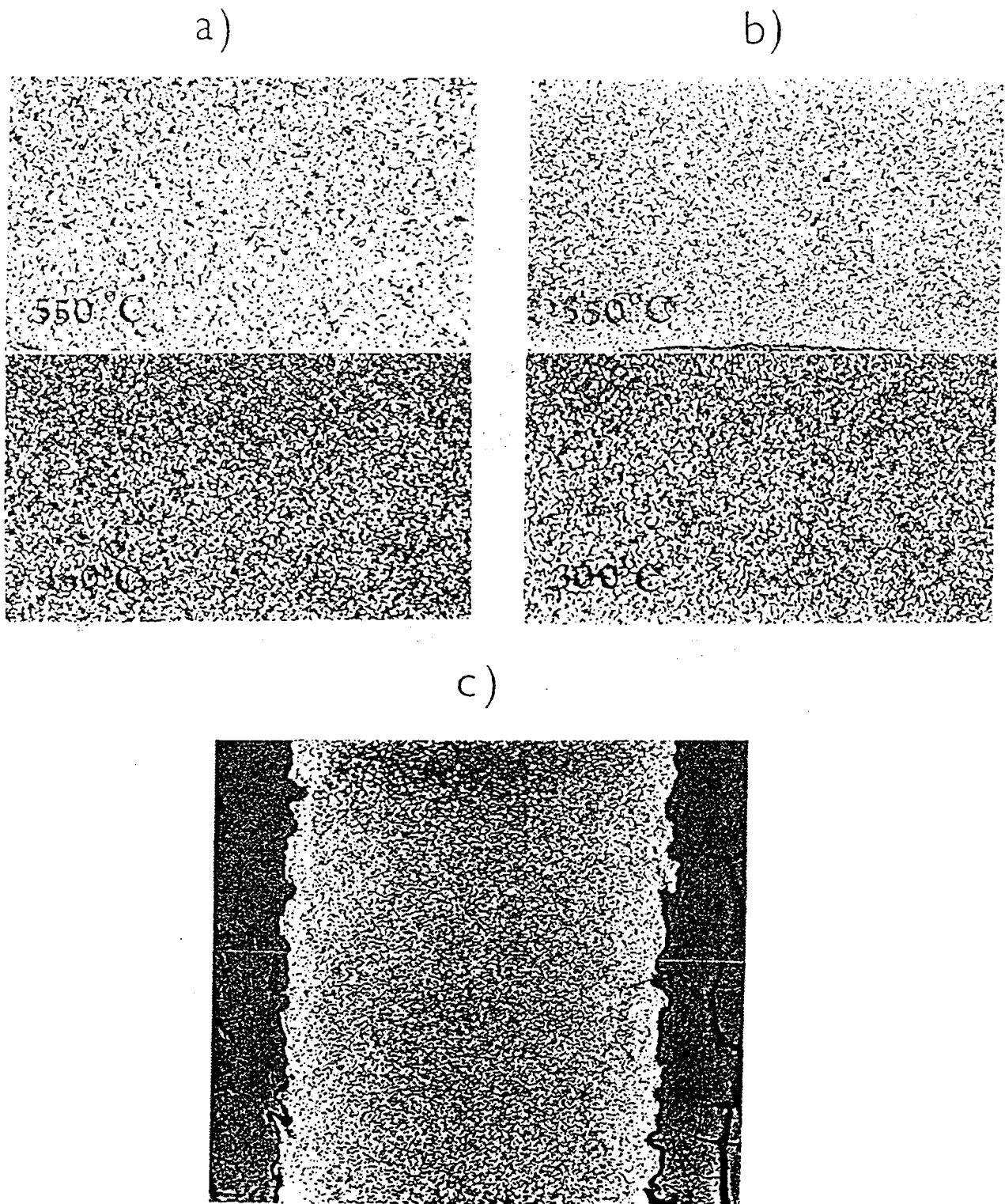


Fig.6. Character of hydrides in various phases of the transient experiment:

- a) samples initially exposed in water at 300°C,
- b) samples initially exposed in water at 350°C  
(Magnified 100x),
- c) tube wall crosssection (Zr1Nb) after experiment  
(Magnified 50x).

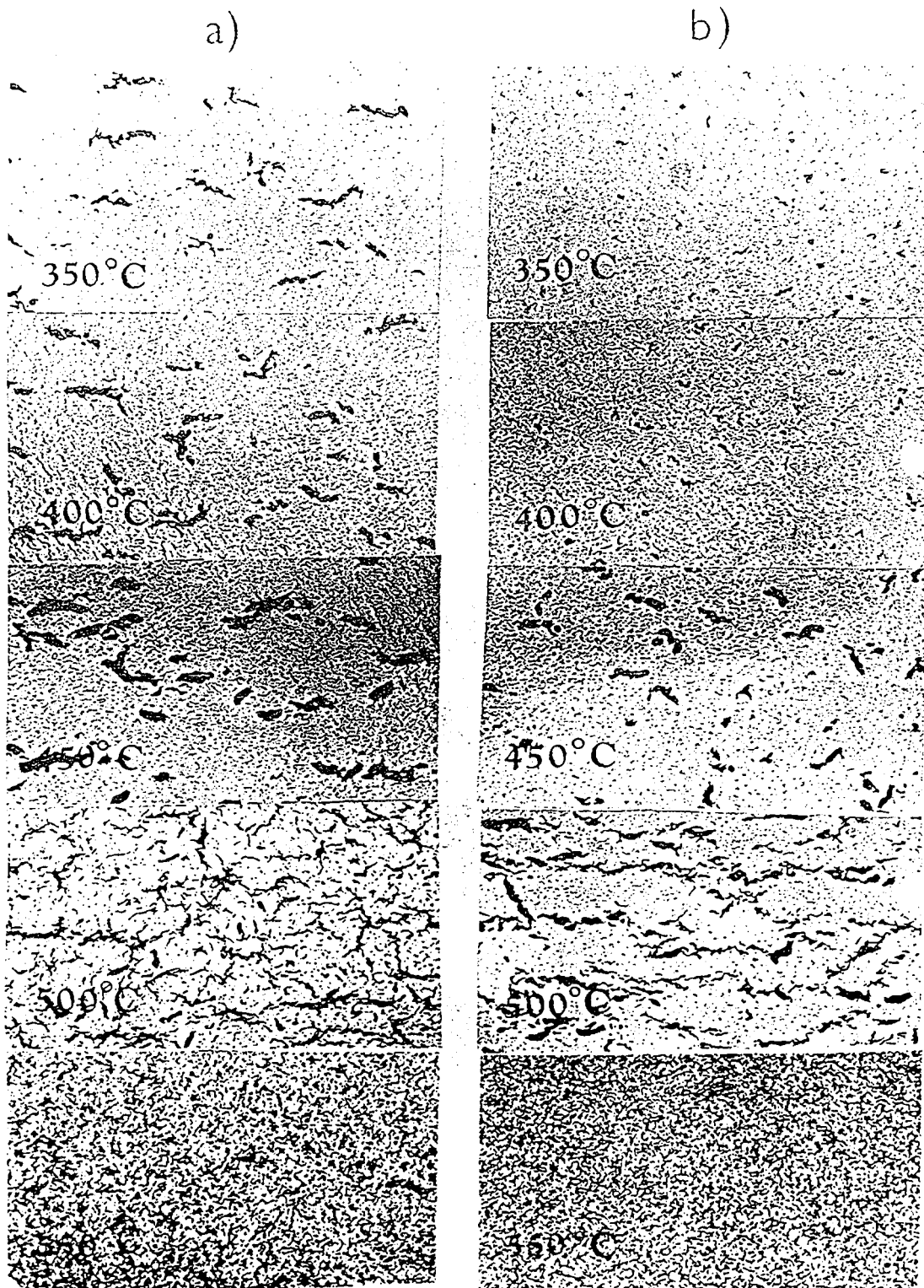


Fig.7. Demonstration of the preoxidation influence on the hydrides character.

Preoxidation performed in water at 300°C temperature with exposure time 21 days.

a) samples without preoxidation,

b) preoxidized samples

(Magnitude 1:100).

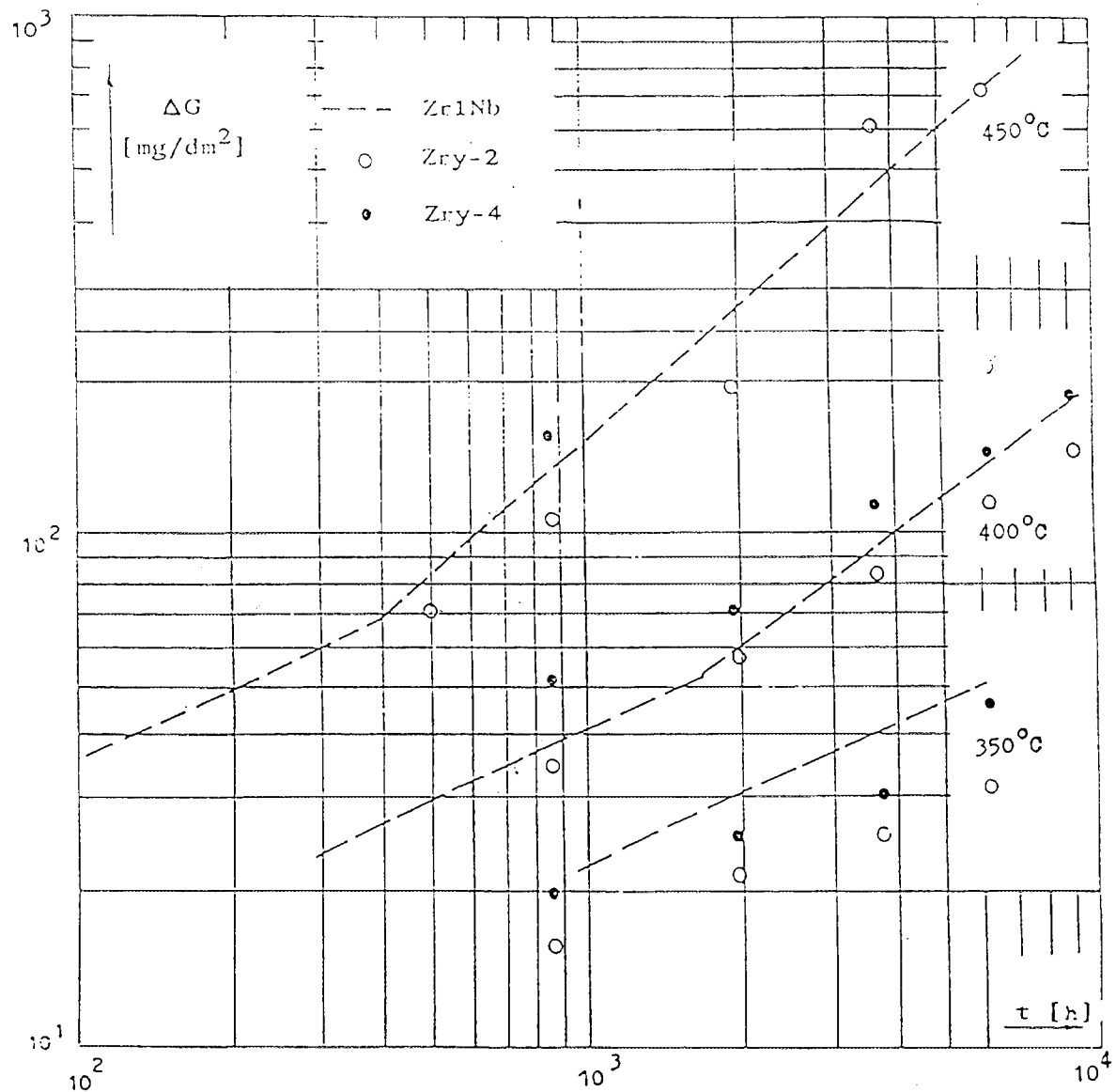


Fig.8. Oxidation kinetics of Zr-alloys in steam 10 MPa.

The relations (1) and (2) may be used to calculate the mass increment,  $\Delta G$ , in accordance with the experiment. However, it is not valid for overheating temperature greater than 700°C.

### **2.3. Conclusions for the low temperature region**

To conclude chapters 2.1 and 2.2 it may be stated that, in contrast to the Zry-4 alloy, the Zr1Nb alloy does not show any break on the corrosion curves in a water medium (up to 350°C). The alloy contains less hydrogen and exhibits a higher corrosion resistance in steam media under a high pressure and a lower susceptibility to nodular corrosion. On the contrary,

it shows a higher susceptibility to the corrosion acceleration due to LiOH and, in temperature transients to the  $\beta$ -Zr temperature range, oxide formed in the  $\alpha$ -Zr range spalls.

## **2.4. Zr1Nb high temperature oxidation**

All experimental methods used up to the present were verified on the Zry-4 alloy (SANDVIK Co.) and for the whole experimental program, the specimens were prepared from reactor cladding tubes. In several experiments, the Zry-4 specimens were tested in parallel for comparison.

The influence of temperature ( $\leq 1450^\circ\text{C}$ ), exposure time, vapour pressure ( $\leq 10$  MPa), preoxidation at  $350^\circ\text{C}$  on the mass increment, oxide thickness,  $\alpha\text{Zr(O)}$  thickness and the hydrogen content absorbed by the alloy were studied in the high-temperature range.

The results of high temperature oxidation kinetics were verified using transient experiment.

### **2.4.1. $\alpha$ temperature region**

On the base of gained results it followed, that in the temperature range of  $\alpha\text{Zr}$  existence ( $\leq 750^\circ\text{C}$ ) the oxidation kinetics exhibits, initially, a parabolic character (black oxide), followed by a break and the further course is controlled approximately by the linear law (light oxide, oxide cracks being perpendicular to the oxide-metal interface).

In this temperature range, the vapour pressure increases slightly the corrosion rate. [Fig.9] [4]. In the case of a black oxide was observed hydrogen content in the alloy was determined low ( $< 30$  ppm). For the steady state, the hydrogen content was measured less than 20% of the theoretical quantity [5]. The specimen preoxidation shows little influence on the corrosion rate [6].

The axial deformation of the specimen due to the Pilling-Bedworth ratio depends on the mass increment only (depending neither on the specimen temperature nor the oxidation stage).

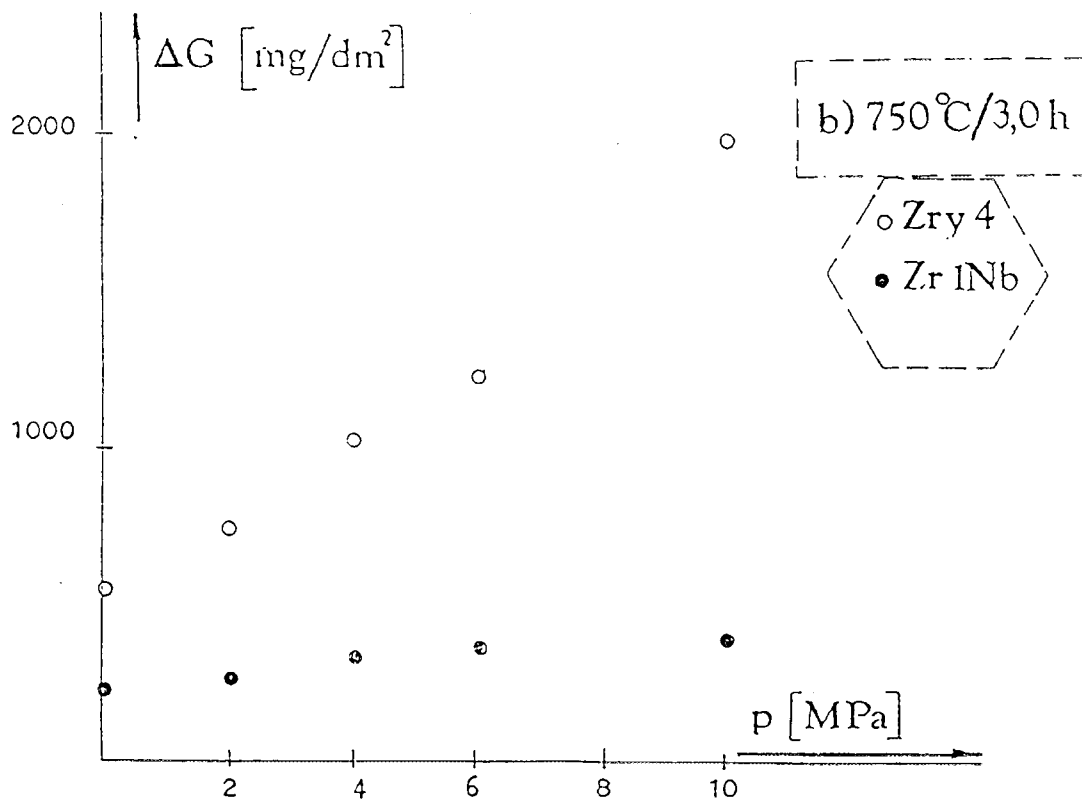
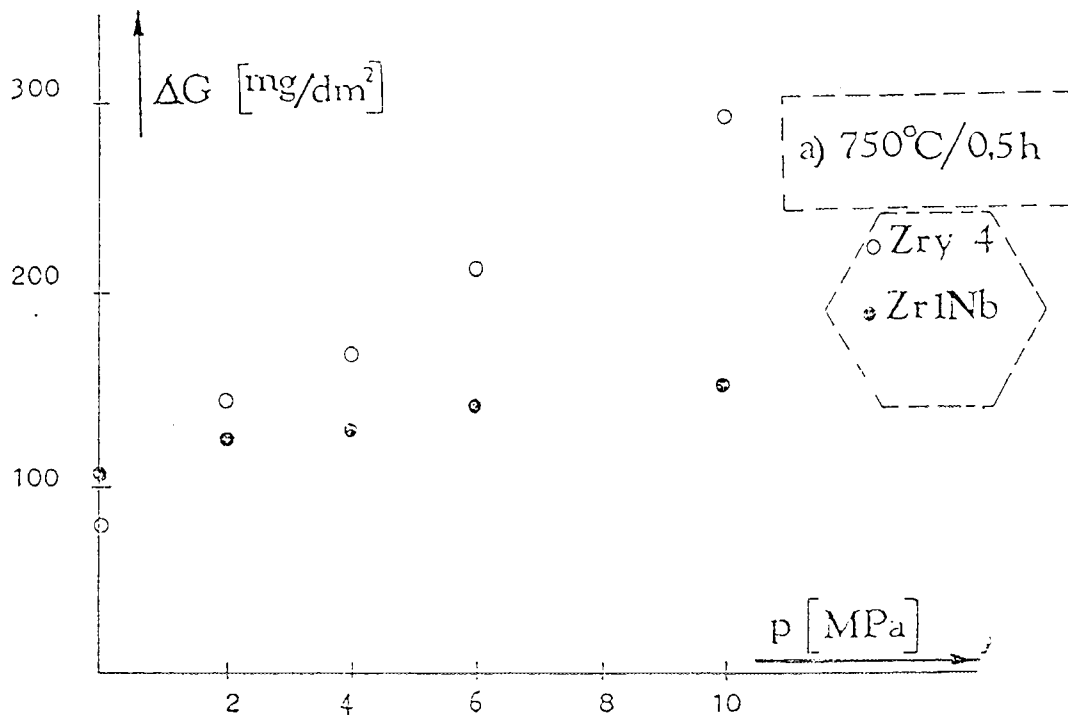


Fig.9. Dependence of the weight gains of Zr1Nb and Zry-4 alloys on steam pressure at 750°C.

### 2.4.2. $\alpha+\beta$ temperature region

In the temperature range of the ( $\alpha+\beta$ ) Zr existence, the oxidation exhibits a parabolic course only. There was no break on the kinetic curves. Initially, the oxide was black, later light and spalling. The parallel cracks to the oxide-metal interface were characteristic for the corrosion layer. In the steady state, the hydrogen content in the alloy was < 40% of the total quantity released during the steam oxidation.

The effect of vapour pressure (4.0 MPa) on the oxidation kinetics was very significant. At a test temperature 800°C and exposure time greater than  $\sim 1.5$  h or at higher temperature and time less than 0.1 h mass increments  $\sim 2000$  mg/dm<sup>2</sup> were measured.

During the further exposure regular oxidation kinetics was measured [Fig.10].

The specimen axial deformation in this temperature range depended not only on the mass increment but also on the test temperature.

### 2.4.3. $\beta$ temperature region

At temperatures up to the 1000°C, the oxidation kinetics show a parabolic character. Only in the first oxidation phase was a black oxide observed, the mass increments were lower. Along with the parabolic kinetics, there was a light oxide spalling in large lumps and the hydrogen content of these specimens ranged from 1000 to 2000 ppm. The hydrogen content of the alloy was not connected with the oxide thickness like at the temperatures  $\leq 950^\circ\text{C}$ . There was a saturation to a certain value connected with the temperature (At the temperature 1000°C, the maximum hydrogen content was 2000 ppm approximately, at 1200°C < 1000 ppm).

On metallographic specimens, a columnar oxide character could be observed along with a  $\alpha\text{Zr(O)}$  layer being very irregular and consisting of acicular formations [Fig.11]. The preoxidation ( $\sim 40$  mg/dm<sup>2</sup> at 350°C) affects markedly the oxidation in steam 0.1 MPa and the hydrogen absorption by the alloy in the initial stage (0.5 - 1 h). The same effect of preoxidation was observed for the temperature greater than 1000°C [Fig.12].

The axial deformation of specimens versus the mass increment was approximately 7x lower than that of the specimens exposed to the temperatures < 750°C and  $\geq 1150^\circ\text{C}$ , independent of the temperature.

On the specimens exposed to steam at 1450°C, metallic Zr in the oxide was observed suggesting a decrease of the tetragonal to cubic transformation temperature due to Nb.

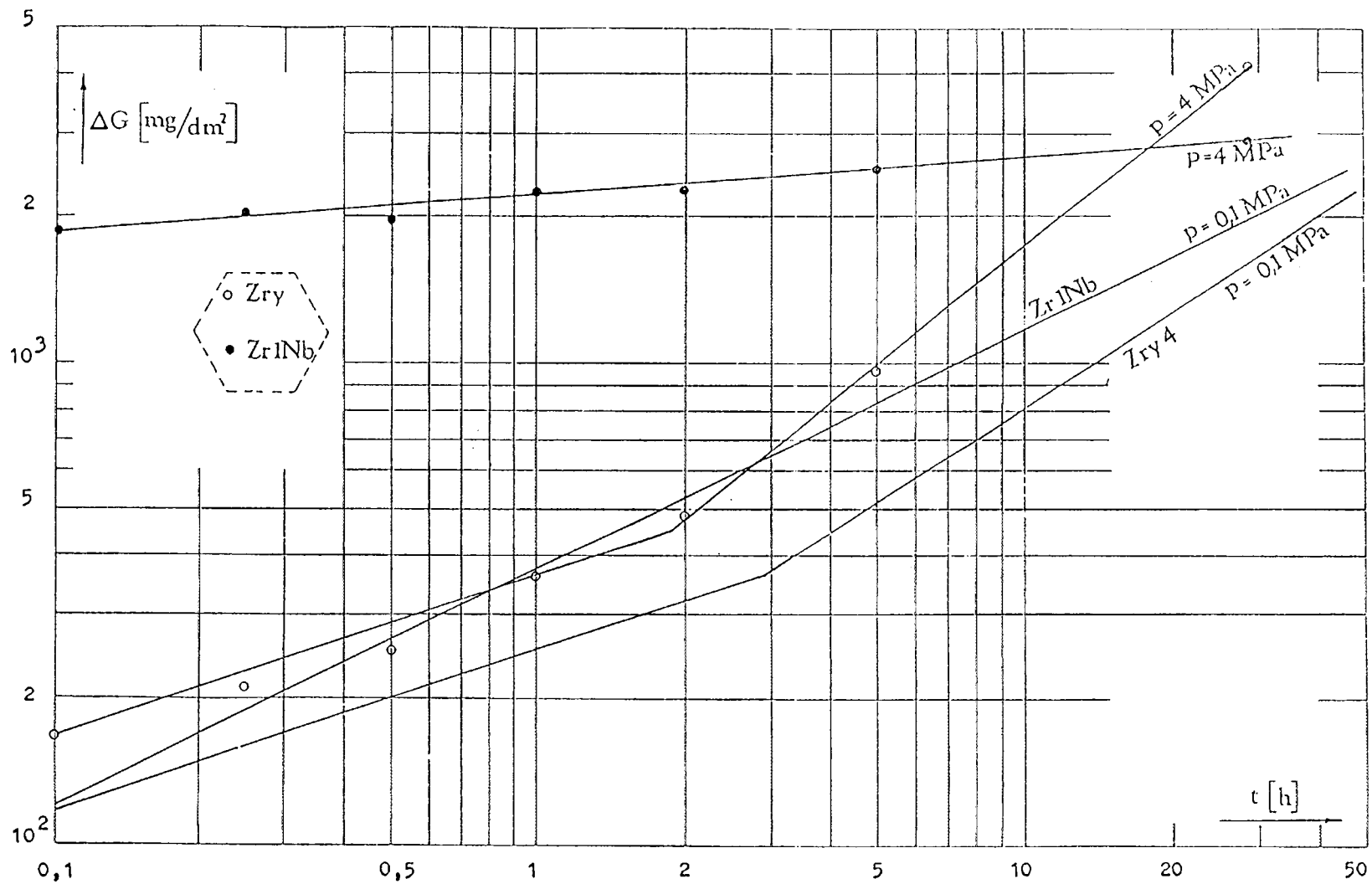
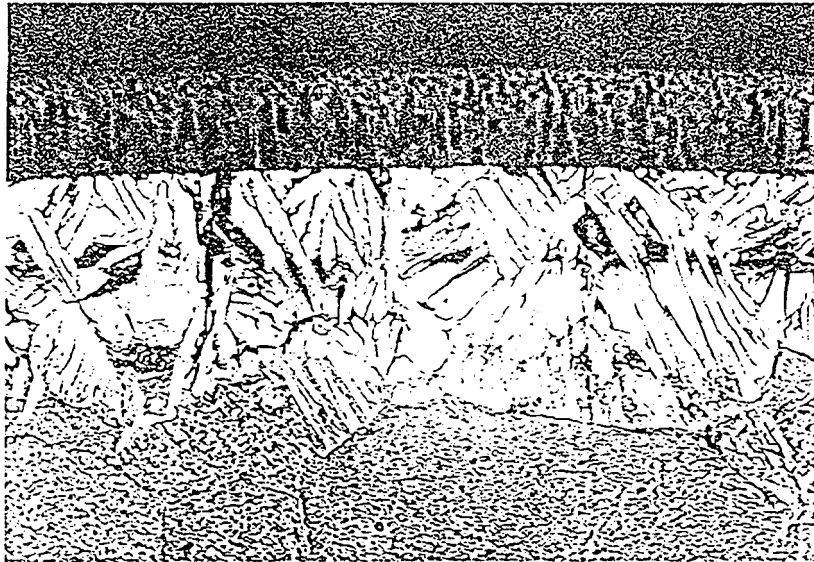
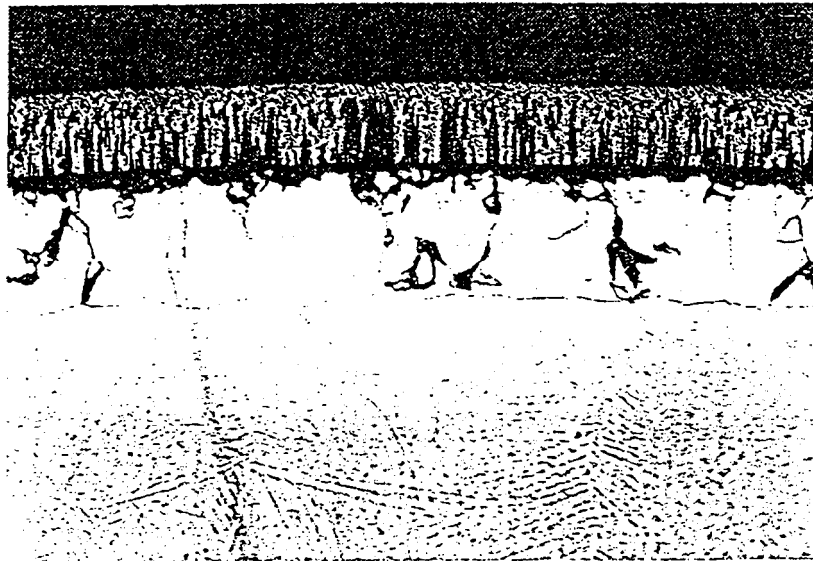


Fig. 10. Influence of steam pressure on the oxidation kinetics of Zr1Nb and Zry-4 alloys at temperature 850°C.



Zr1Nb



Zry4

Fig.11. Character of the oxide and  $\alpha$ Zr(O) layers at 1200°C after heat up rate 12°C/min.  
(Magnified 25x)

- a) Zr1Nb alloy,
- b) Zry-4 alloy.

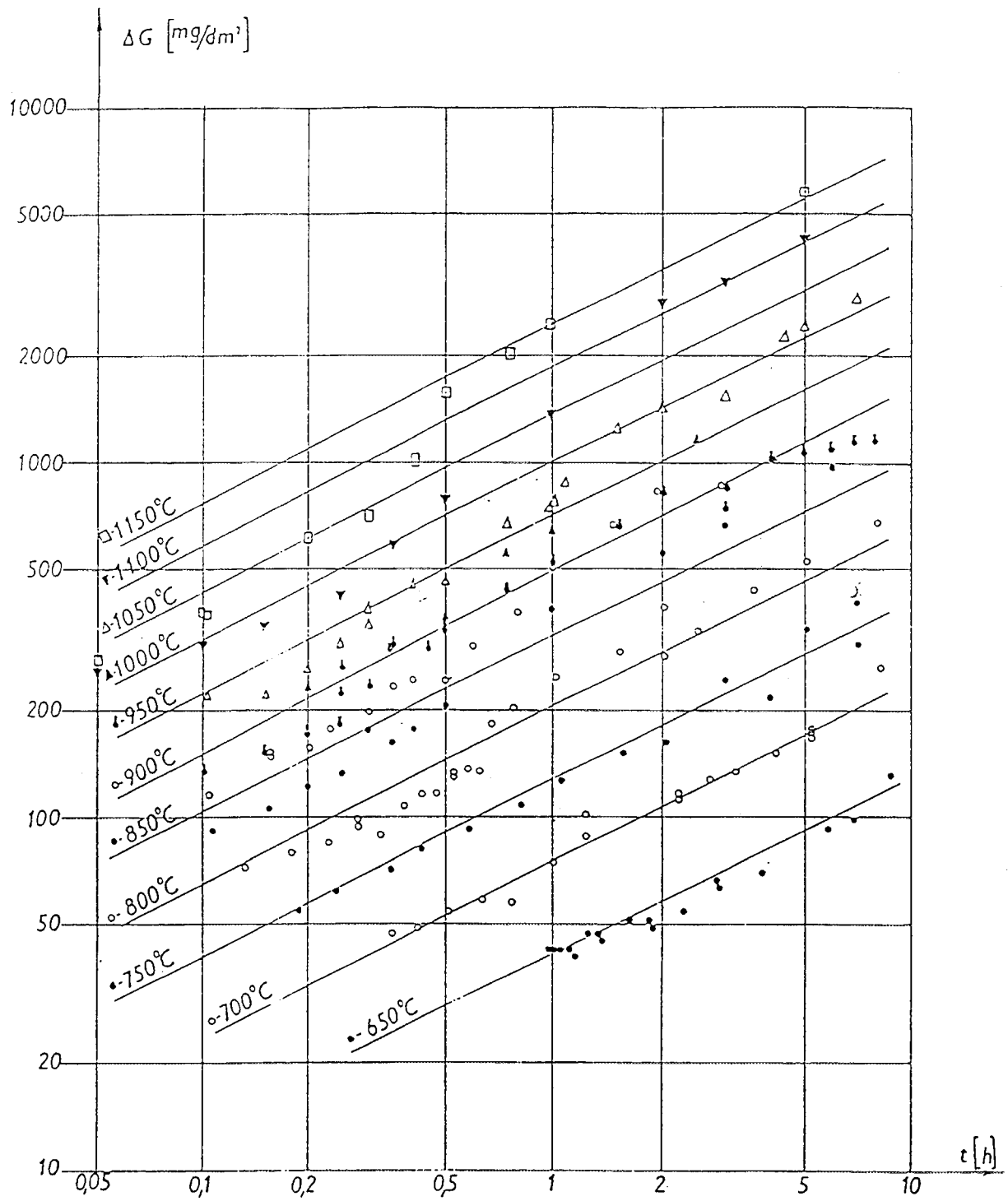


Fig.12. Oxidation kinetics of Zr1Nb alloy in steam for preoxidized samples in steam at 350°C and  $\Delta G \sim 40 \text{ mg/dm}^2$ .

#### 2.4.4. Proposed correlations

The results of the Zr1Nb alloy high temperature oxidation kinetics may be summarized as follows:

- a) for the calculation of the mass increment,  $\Delta G$ :

$$\Delta G = 7.49 \times 10^3 \times \exp \frac{-10713}{T} \times t^{0.5} \quad (4)$$

- b) for the calculation of the oxide thickness,  $X_{ZrO_2}$ :

$$X_{ZrO_2} = 1.77 \times 10^3 \times \exp \frac{-9691}{T} \times t^{0.5} \quad (5)$$

- c) for the calculation of the  $\alpha Zr(O)$  thickness,  $X_{\alpha ZrO}$ :

$$X_{\alpha ZrO} = 2.88 \times 10^5 \times \exp \frac{-15981}{T} \times t^{0.5} \quad (6)$$

where  $\Delta G$  is given in  $g/m^2$ , and  $X$  in  $\mu m$ .  $T$  indicates the temperature in K and  $t$  the exposure time in seconds [Fig.13] [7, 8].

#### 2.4.5 Transient experiment

The results mentioned are consistent with those reported by Böhmert et al [9, 10]. These authors participated also in the evaluation of the transient experiment performed in NFI Zbraslav aimed at examining the possibility of using the above mentioned relations in the computer codes.

The course of the transient experiment can be described by the temperature hold up at  $600^\circ C$  for a 6 min, than increase at a rate of  $12^\circ C/min$  up to  $1200^\circ C$ , which was followed by a 1 min hold up at  $1200^\circ C$  and by a cooling at a rate of  $15^\circ C/min$  up to  $750^\circ C$ . Having reached the exposure determined, the specimens were removed from the temperature range and quenched in ice water. The development of the Zr1Nb and Zry-4 alloy structure is documented on the Fig.14, 15.

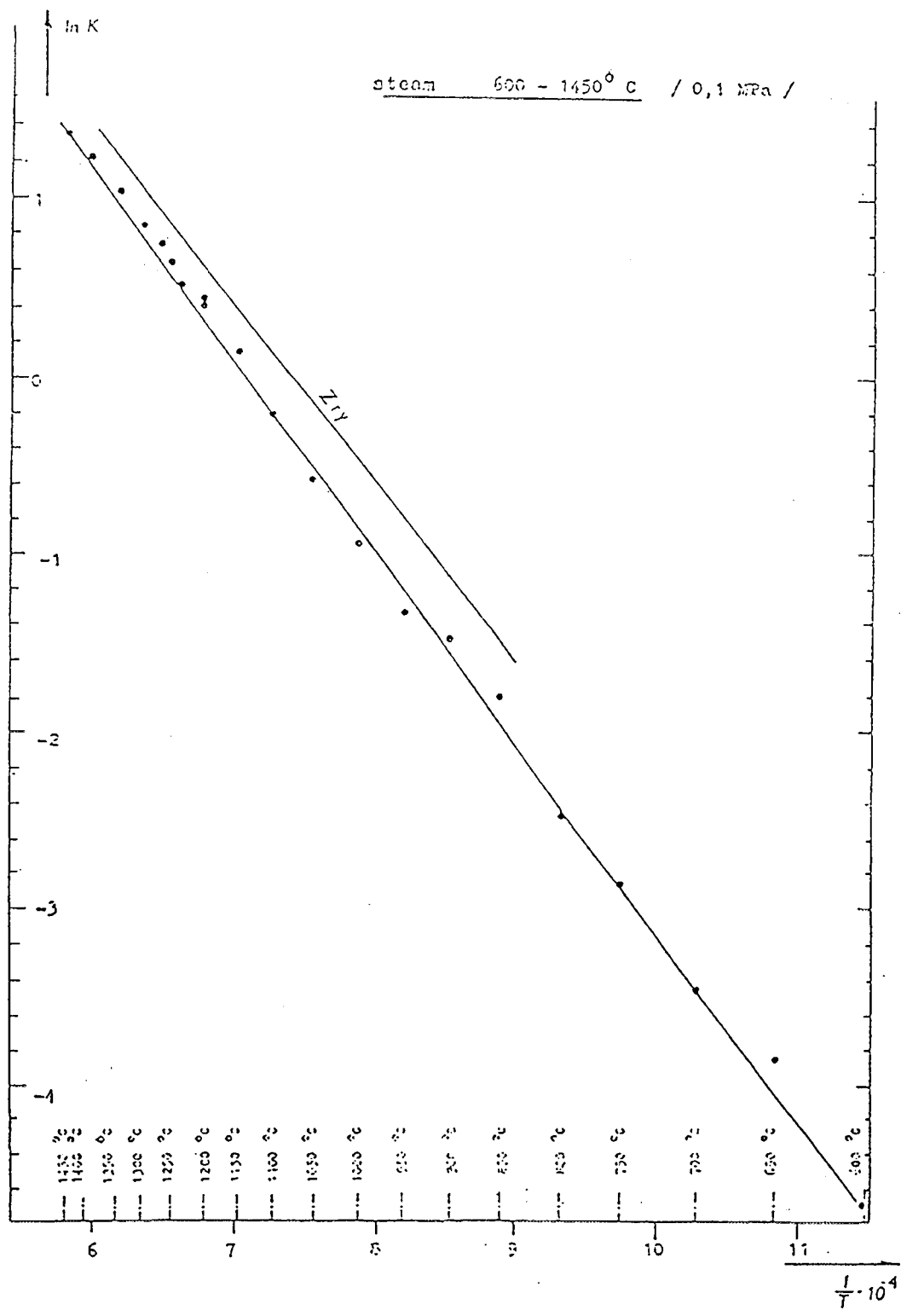


Fig. 13. Dependence of ln K on 1/T for Zr1Nb alloy at the temperature range 600 - 1450°C in steam 0.1 MPa.



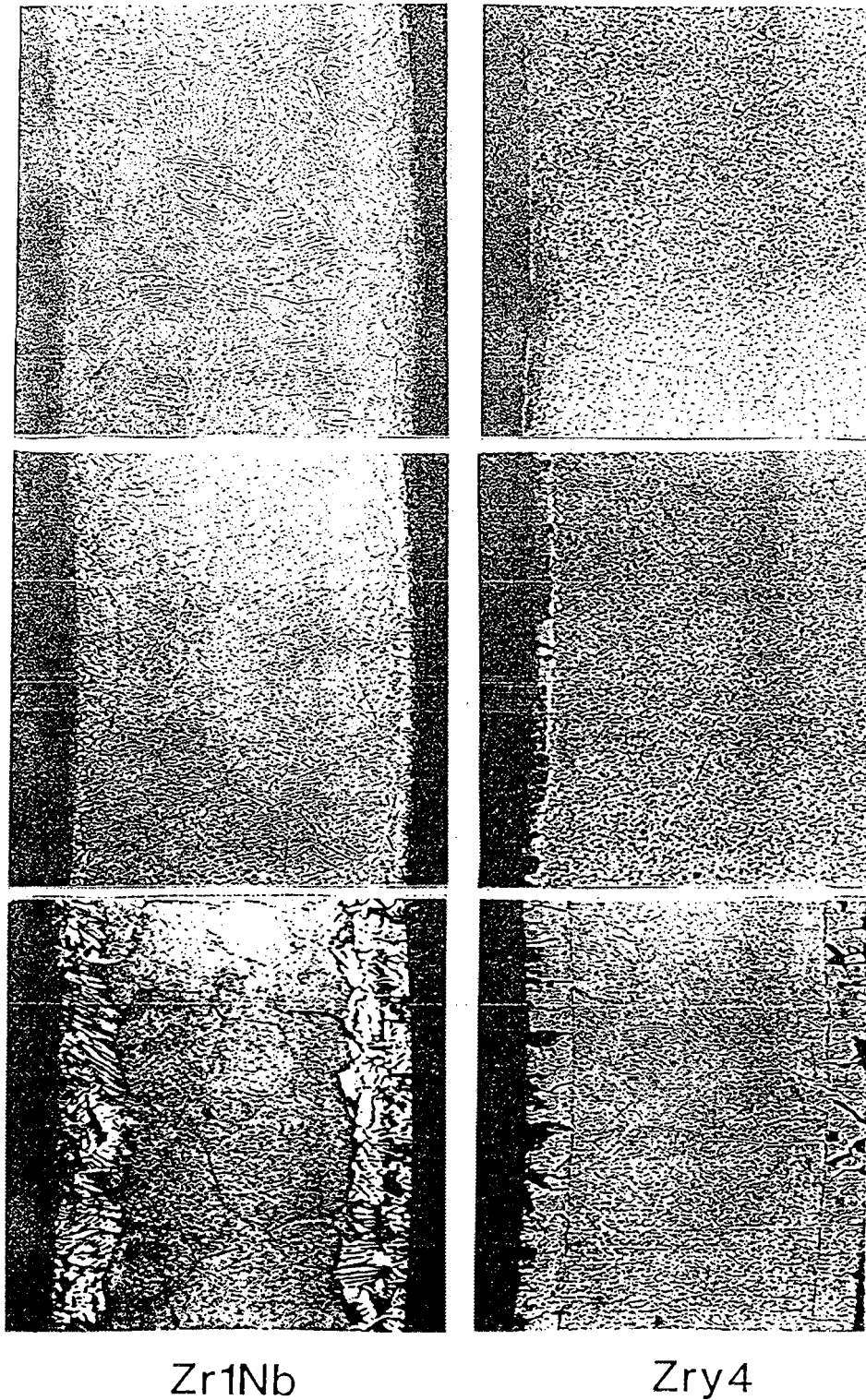


Fig.15. Morphology of Zr1Nb and Zry samples in various phases of the transient experiment:

- a) after 57 min. (1200°C),
- b) after 67 min. (1050°C),
- c) after 87 min. (750°C).

The Zry-4 specimens exhibited a black and bright oxide during the whole experiment while the Zr1Nb specimens, having achieved the temperature  $\sim 800^{\circ}\text{C}$ , were light with oxide spalling in larger lumps. The results show the calculation to be conservative. according to the relations 1, 2 and 3 to be conservative [11].

## **2.5 Conclusions for the high temperature region**

When summarizing the results on the Zr1Nb alloy with respect to the Zry-4 alloy, we may state the Zr1Nb alloy corrosion rate to be slightly lower, a thinner oxide forms and more oxide dissolves in the alloy. The  $\alpha\text{Zr(O)}$  thickness is increased and the oxygen content in the  $\beta$ -phase higher (based on a microhardness test).

In contrast to the Zry-4, oxide is in light colour and tends to spall the outer layer even if the kinetics are controlled by the parabolic law. Owing to the failure of the outer oxide layer, the hydrogen content in the alloy are several orders of magnitude higher (1000 - 2000 ppm).

The effect of the vapour pressure on the Zry-4 corrosion rate up to the temperature  $750^{\circ}\text{C}$  is higher than for Zr1Nb alloy.

For the Zr1Nb alloy in the temperature range  $\alpha+\beta$  Zr existence the influence of vapour pressure is very strong especially in the initial stage (up to the exposure time  $\sim 0.1$  hour). The mass increment  $\sim 2000 \text{ mg/dm}^2$  during this initial stage was observed.

The explanation of this phenomenon as well as that of oxide spalling are related to the  $\alpha\text{Zr} \rightarrow \beta\text{Zr}$  transformation and the stress relaxation at the oxide-metal interface, respectively. Due to the different Zr and  $\text{ZrO}_2$  molar volume, a stress forms at the oxide-metal interface. This stress is relaxed in both oxide and metal and this result also to the axial deformation of the specimen. The constant of proportionality between the axial deformation and the mass increment for a tube with the 0.71 mm thick wall for the temperatures less than  $750^{\circ}\text{C}$  ( $\alpha\text{Zr}$ ) is approximately 7x higher than for higher temperatures. Owing to the modification of mechanical properties of the alloy and the way of relaxation during the  $\alpha\text{Zr}$  to  $\beta\text{Zr}$  transformation accompanied by a monoclinic-to-tetragonal oxide transformation there is a separation of the oxide formed under the conditions of the  $\alpha\text{Zr}$  existence from the oxide forming at higher temperatures. If we prevented the oxide from forming at the temperatures of the  $\alpha\text{Zr}$  existence, e.g. by heating the specimen in an inert atmosphere, the oxide produced would be black, bright and adhesive, the hydrogen content of the alloy would be low ( $\sim 10$  ppm), the oxidation kinetics would show a parabolic character from the very

beginning of the oxidation as observed with the Zry-4 alloy. Another way of preventing the formation of a non-adhesive light oxide is to pressurize the specimens or to use thin-wall tubes.

### 3. CONCLUSIONS

Based on our experience on corrosion behaviour of Zr1Nb alloy (cladding tubes for fuel elements) we can conclude:

1. Zr1Nb oxidation kinetics in the initial stage shows a parabolic character. This is possibly caused by the oxygen diffusion through the oxide lattice. Zry oxidation kinetics in the initial stage shows a cubic character and the oxygen diffusion occurs preferably along the oxide grain boundaries [12]. This conclusion is valid up to the temperature 1000°C.
2. At the temperature range of  $\beta$ -Zr existence, the ratio of oxygen forming oxide to the oxygen dissolved in the alloy is shifted, as compared with Zry-4, to the benefit of oxygen dissolved in the alloy. This is consistent with the finding that the phase boundaries in the pseudobinary phase diagram of Zr1Nb-O are shifted to higher oxygen concentration [13].
3. In the steam environment and the temperature range of the  $\alpha$ -Zr existence, there is a low sensitivity of the corrosion rate to the vapour pressure. Formation of nodular oxide was not observed.
4. Oxide formed in the temperature range of the  $\alpha$ -Zr existence exhibits protective properties, especially in the initial oxidation phase for the temperatures greater than 950°C.

At the same time, this oxide tends to spall separating from oxide formed after a temperature transient  $\alpha$ - $\beta$ . Even if the oxidation course shows a parabolic character, the outer oxide surface is white and hydrogen generated during the steam-Zr alloy reaction is absorbed in a considerable quantity (  $\sim$  1000 ppm) by the alloy. Consequently and due to a higher content of hydrogen dissolved in the alloy the specimen brittleness increases.

Based on the out of pile experimental results and information published in the open literature for the standard PWR and WWER coolant environment it is possible to state that both alloys have comparable properties. Further research work should be mainly directed to the more precise determination of the oxygen and lithium influence on the Zr1Nb alloy

behaviour. Presented results in the high temperature region support our opinion [14], that in the case of Zr1Nb alloy further experimental and theoretical research should more realistically determine safety margins in safety criteria for the fuel element damage under LB LOCA.

## REFERENCES

- [ 1 ] VRTÍLKOVÁ,V., RANSORFOVÁ,B., HAMOUZ,V., MOLIN,L.: Corrosion of Zr1Nb cladding tubes II. Report NFI 597, 1985 (in Czech).
- [ 2 ] VRTÍLKOVÁ,V., MOLIN,L.: Influence of additions in the coolant on the Zr1Nb cladding. Report NFI 720, 1992 (in Czech).
- [ 3 ] VRTÍLKOVÁ,V., MOLIN,L.: Oxidation kinetics of Zr-alloys in steam under high pressure. Report NFI 700, 1990 (in Russian).
- [ 4 ] VRTÍLKOVÁ,V., MOLIN,L.: Influence of steam pressure on oxidation kinetics of Zr-alloys in the temperature range 600 - 900°C. Report NFI 712, 1991 (in Czech).
- [ 5 ] VRTÍLKOVÁ,V., MOLIN,L.: High temperature oxidation of Zr1Nb cladding tubes I. Report NFI 599, 1986 (in Czech).
- [ 6 ] VRTÍLKOVÁ,V., MOLIN,L.: Influence of the preoxidation at 350°C on the high temperature oxidation of Zr1Nb cladding tubes. Report NFI 632, 1988 (in Czech).
- [ 7 ] VRTÍLKOVÁ,V.: Statistical evaluation of the oxidation equations. Report NFI 631, 1988 (in Czech).
- [ 8 ] VRTÍLKOVÁ,V., MOLIN,L.: Oxidation kinetics of Zr1Nb cladding tube in steam at 0.1 MPa pressure and temperatures 1200 - 1400°C. Report NFI 673, 1989 (in Czech).
- [ 9 ] BÖHMERT,J., DIETRICH,M., LINEK,J.: "Research of High-temperature oxidation in Steam of Zr1Nb alloy .....". Report ZfK Rossendorf, 1990 (in German).

- [10] BÖHMERT, J. et al: Final Report - "Safety of fuel elements", ZfK Rossendorf, 1990 (in German).
- [11] VRTÍLKOVÁ, V., MOLIN, L.: Oxidation kinetics of Zr1Nb claddings tube in the transient conditions. Report NFI 698, 1990 (in Czech).
- [12] ZAJMOVSKIJ, A.S., NIKULINA, A.V., REŠETNIKOV, N.G.: "Cirkonievye splavy v atomoy energetike", Energoizdat, Moscow 1981.
- [13] BÖHMERT, J.: Draft Report ZfK, 1990, private communication.
- [14] VALACH, M.: Proposal for the legislative measures related to the safety criteria and fuel damage under accident conditions. Report NRI 9850-T, January 1993; private communication.

**NEXT PAGE(S)  
left BLANK**



## OXIDATION-INDUCED EMBRITTLEMENT AND STRUCTURAL CHANGES OF ZIRCALOY-4 TUBING IN STEAM AT 700 - 1000 °C

A.E. ALI, A.G. HUSSEIN, A.A. EL-SAYED  
Atomic Energy Authority

S.M. EL RAGHY  
Faculty of Engineering, Cairo University

O.A. EL BANNA  
Atomic Energy Authority

Cairo, Egypt

### Abstract

The oxidation-induced embrittlement and structural changes of Zircaloy-4 (KWU-Type) tubing was investigated under light water reactors (LWR) Loss-of-Coolant. Accident conditions (LOCA) in the temperature range 700-1000°C. The effect of hydrogen addition to steam was also investigated in the temperature range 800-1000°C.

The oxidation-induced embrittlement was found to be a function of both temperature and time. Fractography investigation of oxidized tubing showed a typical brittle fracture in the stabilized-alpha zone. The microhardness measurements revealed that the alpha-Zr is harder than that near the mid-wall position. The oxidation-induced embrittlement at 900°C was found to be higher than at 1000°C. The results also indicated that the addition of 5% by volume hydrogen to steam resulted in an increase in the degree of embrittlement.

### 1. INTRODUCTION

The oxidation behaviour of Zircaloy-4 cladding tube material in steam is an extremely important factor to be considered in the safety analysis of LOCA and Severe Fuel Damage (SFD) accidents. The oxidized cladding tube wall consumption determines cladding embrittlement and influences fuel-clad interaction [1-8]. The lack of enough data for the high temperature reaction kinetics of Zircaloy and steam and the experimental difficulties associated with accurately determining the reaction rates were the main reasons for proposing the conservative Baker-Just (BJ) correlation[1] to calculate the Zircaloy-steam oxidation and the

equivalent cladding reacted (ECR). However an extensive amount of work has been performed afterwards on the oxidation of Zircalloys in steam at high temperatures. Some examples, of numerous publications addressing the embrittlement criteria (associated with oxide formation and oxygen-containing sub-surface layers) under LOCA conditions can be cited [9-13].

This work presents the results of Zircaloy-4 tubing oxidized in flowing steam under isothermal conditions at 700 to 1000°C. The results presented in this paper specifically address the oxidation-induced embrittlement of Zircaloy-4 cladding tubes.

## 2. EXPERIMENTAL

Zircaloy-4 KWU-type tubing (10.75 mm OD, 0.725 mm thick, 10 mm long specimens) of standard composition (Table I) were used for the investigation. After degreasing and pickling in a mixture of hydrofluoric acid, nitric acid and water the specimens were oxidized in an open, non-pressurized loop under a steam flow rate of 520 mg/cm<sup>2</sup> min. The effect of hydrogen addition (5% by volume of the steam) was also investigated. Oxidation time ranged between several minutes and few hours depending on temperature.

Fractographic investigation and microhardness measurements were made across the thickness of the oxidized tube. Microhardness testing (using SHIMATZU-V) was performed using 300 g load for 10 seconds. The microhardness indentation was done at various locations making sure that the distance between each two successive indentations is greater than 4 times the indentation diameter.

**Table I** : Chemical Analysis of Zircaloy-4 KWU-Tubing

Material	Sn	Fe	Cr	O	Zr
Zircaloy-4	1.35-1.47	0.19-0.21	0.09-0.10	0.12	98.1-98.25

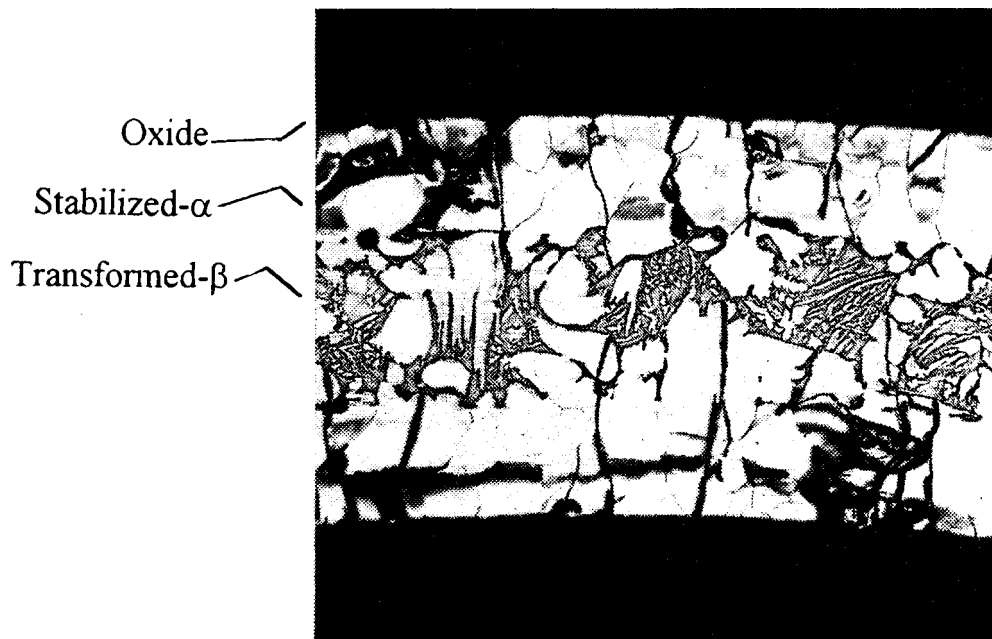


Fig. 1. Zircaloy-4 Tubing oxidized at 1345°C for the typical LOCA duration (x100).

### 3. RESULTS

The microhardness measurements taken across oxidized tubing are shown in Figures 2-7 and tables II and III. A hardness gradient exists across the tube wall, with the material nearest to the metal-oxide (M/O) interface being harder than that near the center of the tubing. The results indicated that the microhardness increases with both temperature and time. The degree of embrittlement for specimens oxidized for short durations (10 to 30 min) were high only near the metal-oxide interface through a small thickness layer (about 50  $\mu\text{m}$ ) at 900 and 1000°C. The thickness of the brittle layer was found to increase with time at all test temperatures. The embrittlement was found to be higher at 900 than at 1000°C. The results also indicated an enhancing effect of hydrogen to embrittlement. It is noted that the microhardness results were not precisely symmetric around the mid-wall position of the tube thickness, particularly for cases of high temperature and long durations of oxidation. Metallographic examinations substantiated that, revealing that the outside oxide film thickness is slightly greater than the inner side film thickness.

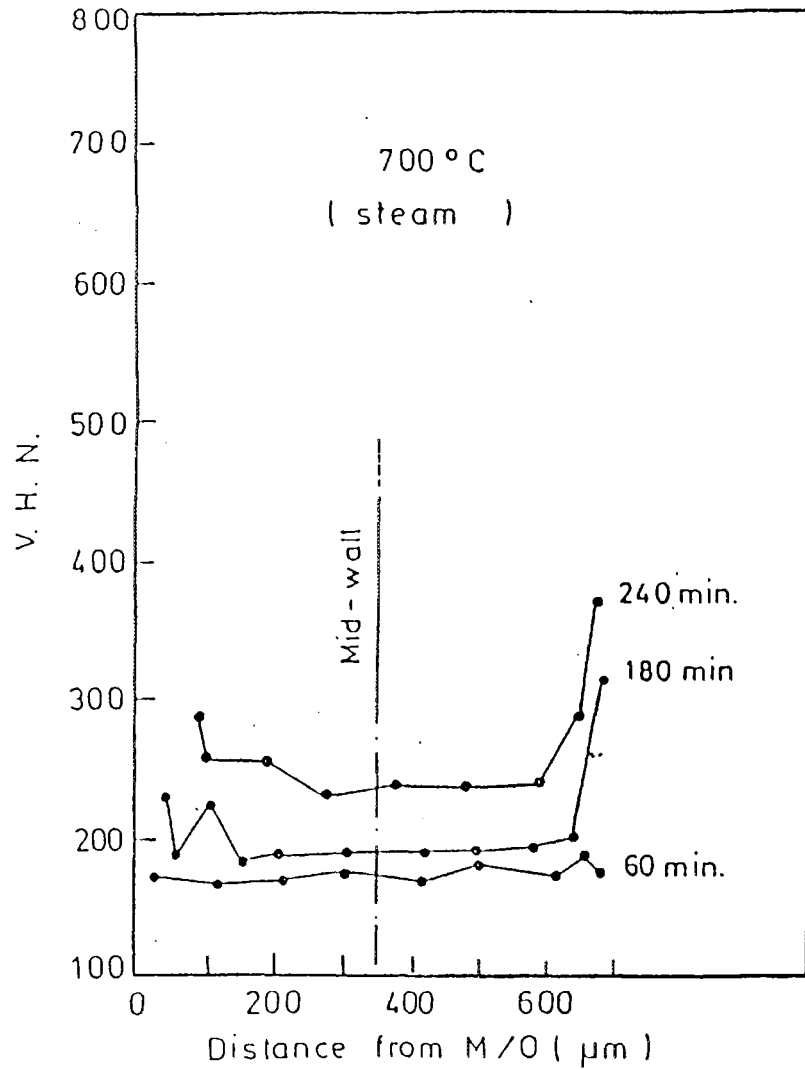


Fig. 2. Variation of microhardness with distance from metal/oxide interface (700°C).

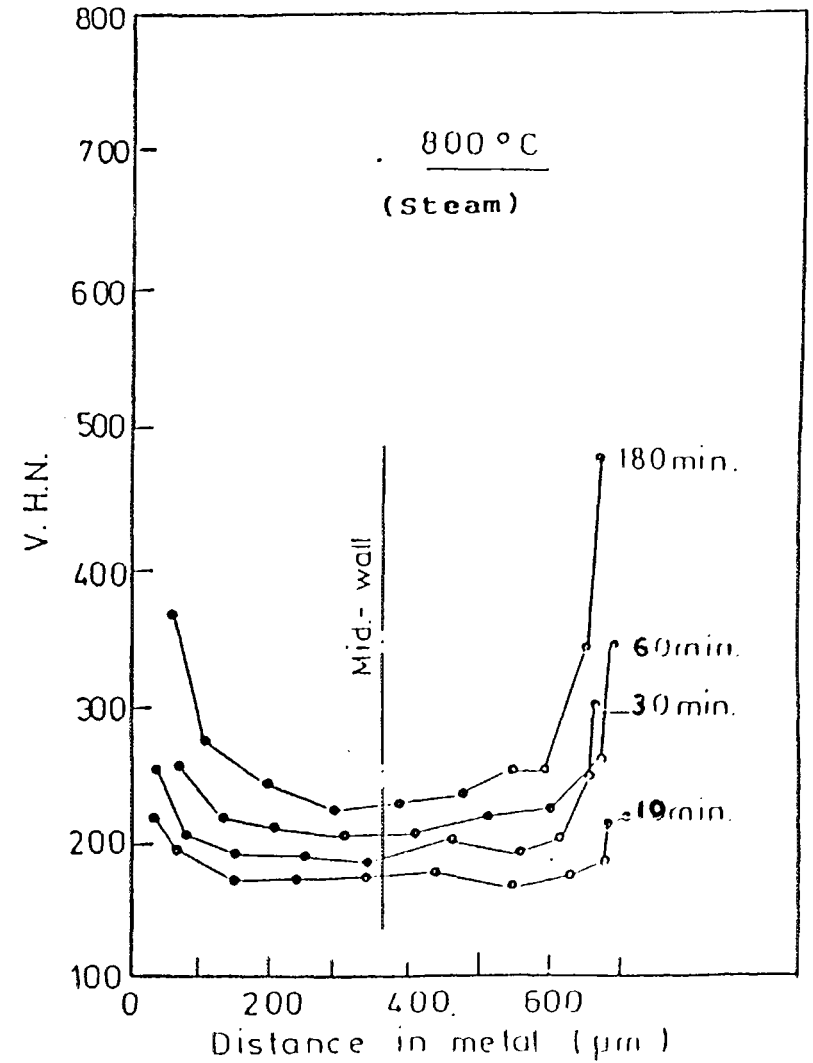


Fig. 3. Variation of microhardness at 800°C.

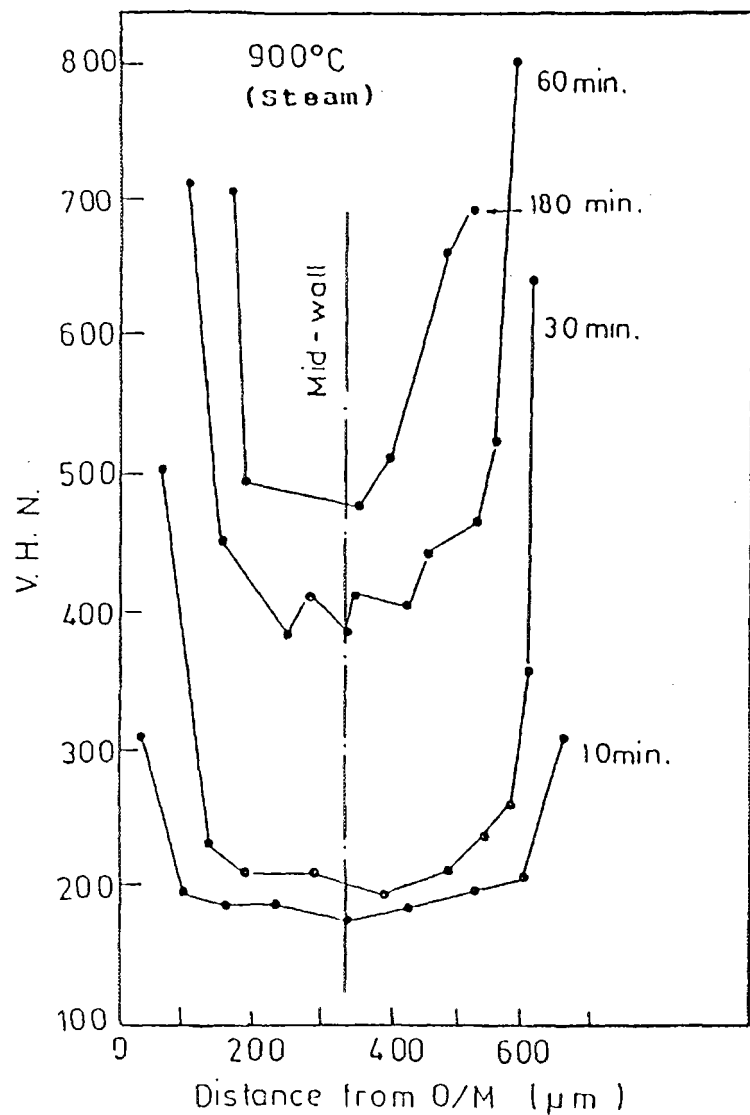


Fig. 4. Variation of microhardness at 900°C.

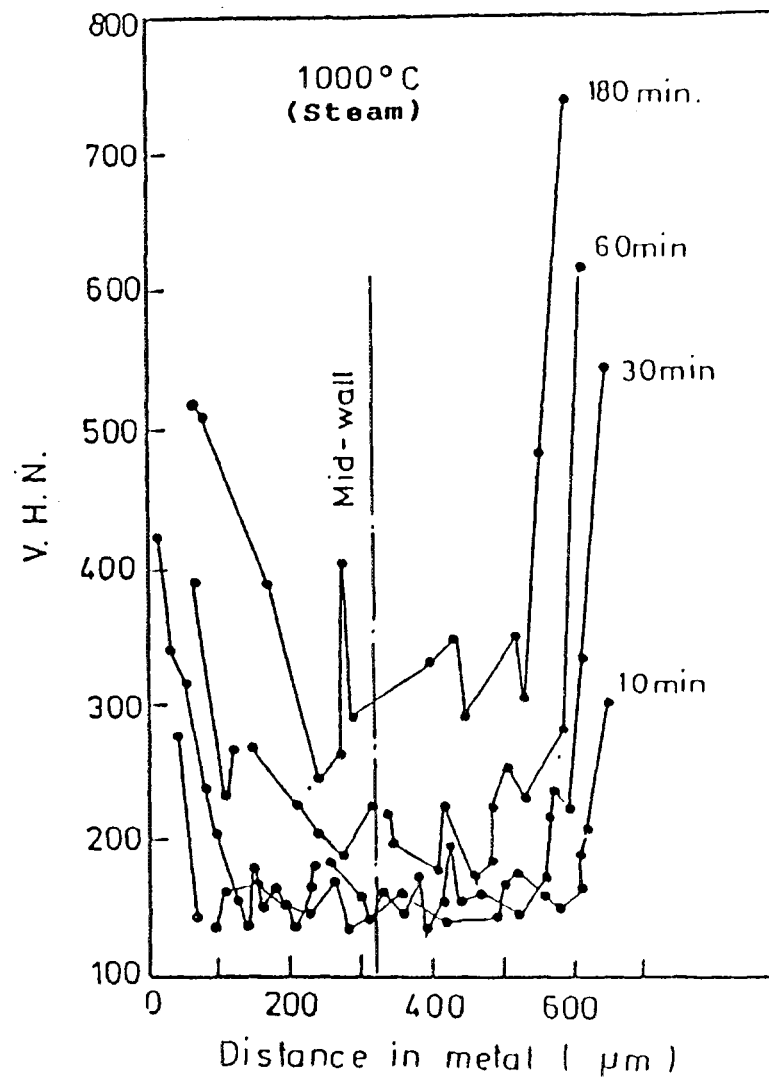


Fig. 5. Variation of microhardness at 1000°C.

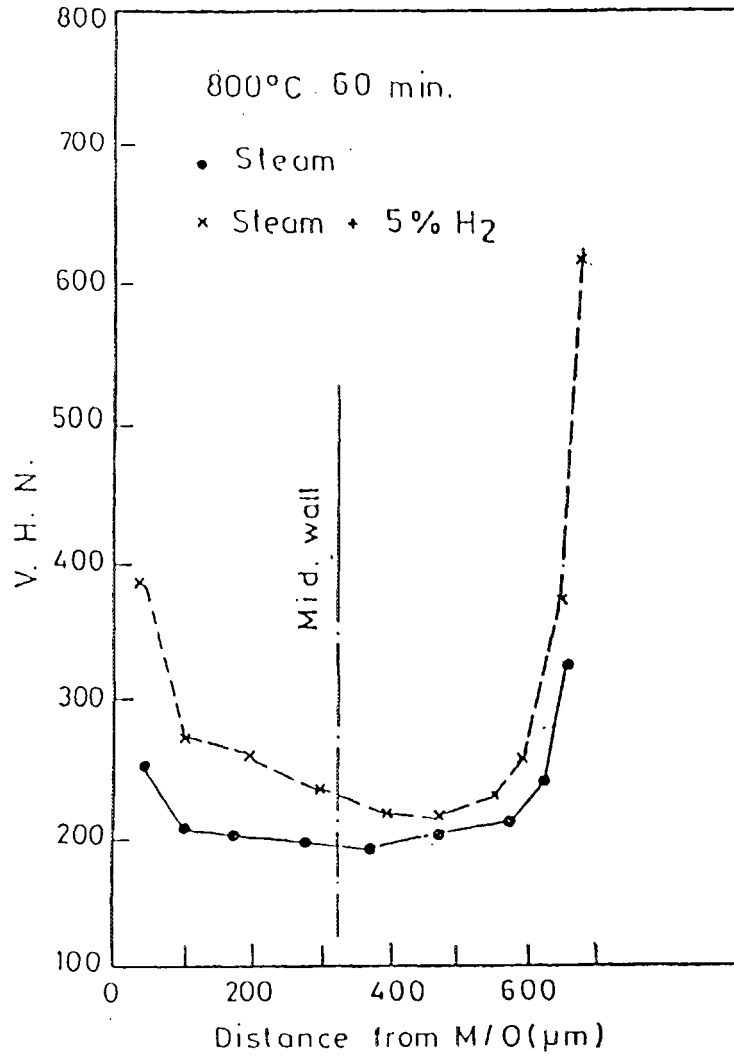


Fig. 6. Variation of microhardness for steam and hydrogen mixture at 800°C.

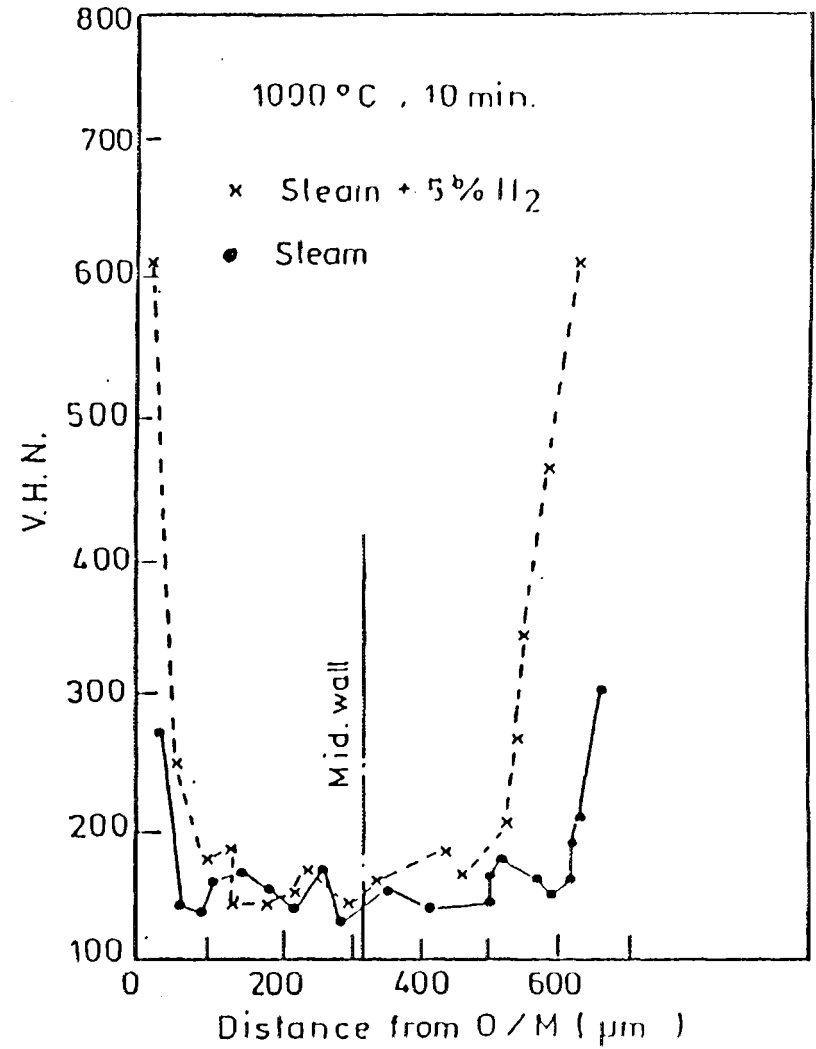


Fig. 7. Variation of microhardness at 1000°C and 10 min. for steam and steam+H<sub>2</sub>.

**Table II :** Vicker Hardenss Number (V.H.N) at the inner and the outer surface oxide/metal interface, and the mid-wall position of the tube for oxidation times 1/2 and 1 hr. in steam +5% H mixture.

Time						
	1/2 hr			1 hr		
Temp.	inner	outer	mid	inner	outer	mid
800°C	320	580	220	400	620	260
900°C	550	820	320	700	720	350
1000°C	350	500	200	---	---	---

**Table III :** Vicker Hardenss Number (V.H.N) at the inner and the outer surface oxide/metal interface of the tube, and in the mid-wall position for oxidation times 1/2, 1 and 3 hrs. in pure steam.

Time									
	1/2 hr			1 hr			3 hr		
Temp.	inner	outer	mid	inner	outer	mid	inner	outer	mid
700°C	200	200	100	180	190	180	230	320	200
800°C	240	290	200	250	330	200	350	480	230
850°C	---	---	---	550	650	350	---	---	---
900°C	510	650	210	800	900	400	700	1060	600
1000°C	350	550	150	400	600	200	500	740	320

The results also indicated that the addition of 5% by volume hydrogen to steam resulted in an increase in the degree of embrittlement.

The microstructural features of the oxidized Zircoloy-4 tubings are shown in Fig. 1. The outermost layer is  $ZrO_2$ . Adjacent to the oxide is a layer of  $\alpha$ -Zr (O) (stabilized-alpha) overlying a transformed  $\beta$ -Zr matrix.

Fractography investigation of the oxidized tubing reveals the brittle fracture of the tubing wall which is mostly stabilized  $\alpha$ -Zr (O) (Fig. 8). Figure 9 reveals a severe crack extending from the oxide through the underlying metal.

#### 4. DISCUSSION

The oxidation-induced embrittlement of Zircaloy tubings, as indicated by the microhardness and structural measurements, was shown to increase with increasing time and temperature of oxidation. The results also indicated the enhancing effect of hydrogen addition to steam on the oxidation-induced embrittlement. It has been shown earlier [8] that when Zircaloy-4 tubings are oxidized in air at 850°C and 1000°C for a typical LOCA duration (5 min.), the amount of ductility exhausted increases from 14% at 850°C to 95% at 1000°C.

The present results as well as previous work [6, 8] reveal the dependence of the degree embrittlement on the amount of

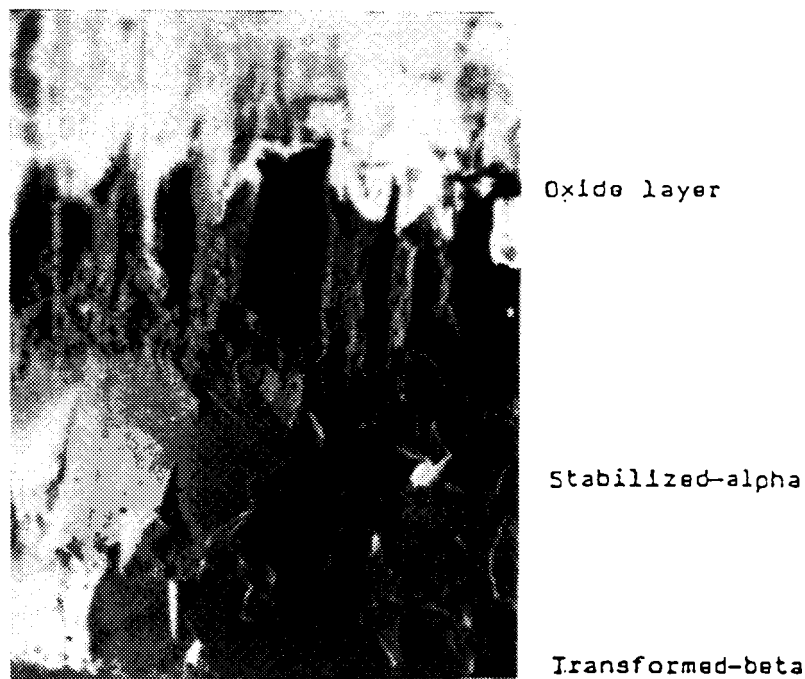


Fig. 8. Scanning electron microscopy (SEM) fractograph of Zircaloy-4 tubing oxidized at 1200°C under transient conditions for the typical LOCA duration (300 sec.) (x150).

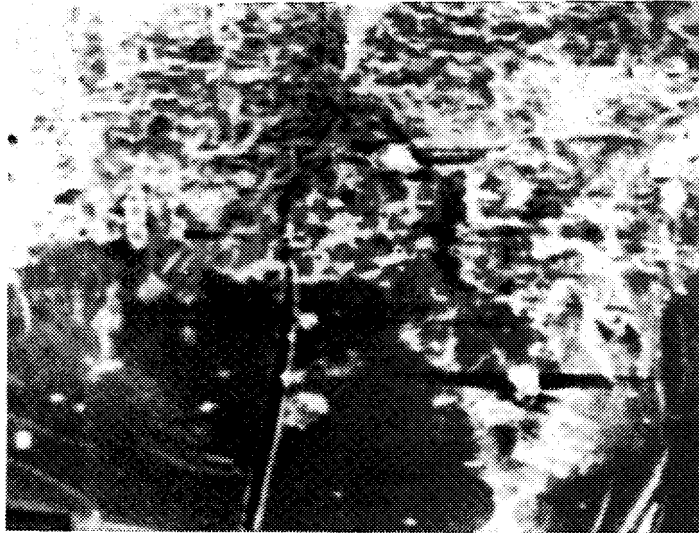


Fig. 9. SEM fractograph of Zircaloy-4 oxidized at 1300°C under transient conditions for the typical LOCA duration, showing a severe crack extending from oxide through the metal. (X 650).

oxidation. The ductility of Zircaloy is a direct function of its oxygen content which is a function of temperature and time. The results indicated that temperature is more effective in promoting embrittlement; in agreement with the results of Hobson and Rittenhouse [14].

Fracture surface investigation of the oxidized Zircaloy-4 tubings, by scanning electron microscopy (SEM), reveals the severe brittle fracture within the stabilized-alpha phase width. The results of this work and those of others [6, 15, 16] indicate that the metallurgical characteristics of the oxidized Zircaloy, generally, consist of an outer layer of  $ZrO_2$ , a central layer of oxygen-stabilized alpha Zircaloy and a base of transformed beta phase. Microhardness measurements revealed that  $\alpha$ -Zircaloy material is extremely hard and that  $\beta$ -Zircaloy region exhibits an increase in hardness, with that material nearest to the  $\alpha$ -phase being harder than that near the center of the tube.

The increasing amount of the stabilized-alpha phase with both temperature and time in addition to the increased

thickness of the oxide would be responsible for the enhancing effect of both temperature and time on the degree of embrittlement. The comprehensive microstructural investigation performed by Aly [6] for Zircaloy-4 tubings oxidized in steam reveals the enhancing effect of oxidation on both oxide and stabilized  $\alpha$ -phases. The results of this work are also in agreement with those of Hobson and Rittenhouse [14] and others [5] indicating that the increasing degree of embrittlement with oxidation could be explained in terms of the increasing thickness of the combined  $ZrO_2/\alpha$ -Zircaloy layer.

The increase in oxygen content of zirconium is known to increase the hardness of the material and modify other relevant mechanical properties. Treco [17] reported that the extensive hardening effect of oxygen might be due in part to the lattice distortion accompanying its introduction and possibly the preferred positions may inhibit the normal slip processes of the zirconium hexagonal lattice during plastic deformation.

The change in the metallurgical characteristics of Zircaloy tubing due to oxidation has been considered by many investigators to play the predominant role in determining its ductility [5, 14, 15]. These investigators pointed out that the lower the value of the ratio of the transformed- $\beta$  thickness to the total thickness of the cladding the lower would be the ductility.

Due to the importance of oxygen embrittlement, as one of the modes of cladding failure, several embrittlement criteria have been proposed and are now in use in the USA [11-13, 18]. Based on the fraction of the cladding wall thickness which is beta phase, Scatena [19] suggested an embrittlement criterion which states that the material is considered embrittled if the fraction of the remaining beta-phase thickness to the original unoxidized wall thickness is  $\leq 0.5$ . Pawel [20] considered the cladding embrittled if the oxygen content of the  $\beta$ -phase exceeded 95 percent of the saturation level. The presently used acceptance

criteria specify that the oxide thickness which would result if all the oxygen uptake produced  $ZrO_2$  (Called "equivalent cladding reacted") must not exceed 17% of the original cladding wall thickness [18].

The enhancing effect of hydrogen on the oxidation-induced embrittlement could be attributed to the hydride formation as well as the hydrogen effect on the oxide growth mechanism. The results are in agreement with those of Leistikow et al. [21] and Eklom [22].

## 5. CONCLUSION

The oxidation induced embrittlement of Zircaloy-4 tubings is a function of both temperature and time. The embrittlement is related to the detrimental effect of oxygen on both the mechanical and structural characteristics of Zircaloy tubing. Fractography investigation of oxidized tubings revealed severe embrittlement indicated by a typical brittle fracture of the stabilized- $\alpha$  zone of the oxidized tubing.

## REFERENCES

- [1] BAKER, L; JUST, L.C.: Studies of Metal-Water Reactions at High Temperatures. III Experimental and Theoretical Studies of the Zirconium-Water Reaction. ANL-6548 (1962).
- [2] CATCHCART, J.V. et al. : Zirconium Metal-Water Oxidation Kinetics. IV. Reaction Rate Studies. ORNL/NUREG-17 (1977).
- [3] BIEDERMAN, R.R. et al. : A Study of Zircaloy-Steam Oxidation Reaction Kinetics, EPRI NP-734 (1978).
- [4] BROWN, A.F.; HEALEY, T. : The Kinetics of Total Oxygen Uptake in Steam-Oxidized Zircaloy-2 Between 1000-1400°C. RD/B/ N4117 (1977).

- [5] KAWASAKI, S.; FURUTA, T.; SUZUKI, M. : Oxidation of Zircaloy-4 under High Temperature Steam Atmosphere and its Effect on Ductility of Cladding, J. Nucl. Sc. Technol. **15** (1978) 589.
- [6] ALY,A.E. : Oxidation of Zircaloy-4 Tubing in steam at 1350-1600°C, KFK 3358 (1982).
- [7] LEISTIKOW,S.; SCHANZ,G.; BERG,H.Y.; ALI,A.E.: Comprehensive Presentation of Extended Zircaloy-4-Steam Oxidation Results 600-1600°C. Proc. OECD/NEA-CSNI/IAEA Spec. Meeting on "Water Reactor Fuel Safety and Fission Product Release in Off-Normal and Accident Conditions". Riso (Denmark) May 16-20, 1983, IAEA Summary Report. IWGFPT/16 (1983) 188.
- [8] ALI, A.E. : Oxidation Behaviour of Zircaloy cladding Tubes at Elevated Temperatures, Ph. D. Thesis, Cairo University (1980).
- [9] HIROSHI, U.; FURUTA, T. : Embrittlement of Zircaloy-4 due to Oxidation in Environment of Stagnant Steam, J. Nucl. Sci. Technol., **19** (1982) 158.
- [10] FURUTA, T.; KAWASAKI, S. : Estimation of Conservatism of Present Embrittlement Criteria for Zircaloy Fuel Cladding under LOCA, 6 International Conference on Zirconium in the Nuclear industry, Vancouver (Canada) 28 June-1 July 1982 Published in : Zirconium in the Nuclear Industry (Franklin, D.G. Ed.) ASTM (1984) 734.
- [11] WILLIFORD, R.E. : Safety Margins in Zircaloy Oxidation and Embrittlement Criteria For Emergency Core Cooling System Acceptance, Nucl. Technol. **74** (1986) 333.
- [12] ERBACHER, F.J.; LEISTIKOW, S.: A Review of Zircaloy Cladding Behaviour in Loss of Coolant Accidents, KFK Rept. 3973 (1985).

- [13] CHUNG, H.M.; KASSNER, F.F. : Embrittlement Criteria for Zircaloy Fuel Cladding Applicable to Accident Situations in Light Water Reactors, Summary Rept. ANL -79-48 (1980).
- [14] HOBSON, D.O.; RITTENHOUSE, P.L. : ORNL-4758 (1972).
- [15] YUREK,G.J.; CATHCART,J.V.; PAWEL,R.E.: Microstructures of Scales Formed on Zircaloy-4 in Steam at Elevated Temperatures, Oxidn of Metals **10** (1976) 255.
- [16] BENNEK-KAMMERICHS, B.; FRANZ, J.; LEISTIKOW, S.; SCHANZ, G.: Experiments on the Morphology an Kinetic Consequencies of Defect Scale Formation During Zircaloy-4-Steam High Temperature Oxidation, KFK 3052 (1980).
- [17] TRECO, R.M.: Trans. AIME-45 (1953) 872.
- [18] Code of Federal Regulations CFR, 10 CFR 50.46. Acceptance Criteria for Emergency Core Cooling Systems for Light Water Nuclear Power Reactors (1983).
- [19] SCANTA, C.J.: BNES Conf., London, Oct. (1973).
- [20] PAWEL,R.E; et al.: Diffusion of Oxygen in Beta Zircaloy and the High Temperature Zircaloy-Steam Reaction, ASTM-STP-633 (1977) 119.
- [21] SHANZ, G.; LEISTIKOW, S.: Oxygen and Hydrogen Uptake of Zircaloy-4 under LWR Accident Conditions, KFK Rept. (1985).
- [22] EKLOM, L.R.: The Effect of Hydrides on the Growth of Zirconia, Mytroeping (SWEDEN), Studsrik Energitek Unik AB (1982) 62.

## **APPLICATION OF FEM ANALYTICAL METHOD FOR HYDROGEN MIGRATION BEHAVIOUR IN ZIRCONIUM ALLOYS**

K. ARIOKA, H. OHTA  
Takasago Research and Development Center,  
Mitsubishi Heavy Industries Ltd,  
Hyogo-ken, Japan

### **Abstract**

It is well recognized that the hydriding behaviors of Zirconium alloys are very significant problems as a safety issues.

Also, it is well known that the diffusion of hydrogen in Zirconium alloys are affected not only by concentration but also temperature gradient.

But in actual component, especially heat transfer tube such as fuel rod, we can not avoid the temperature gradient in some degree.

So, it is very useful to develop the computer code which can analyze the hydrogen diffusion and precipitation behaviors under temperature gradient as a function of the structure of fuel rod.

For this objective, we have developed the computer code for hydrogen migration behavior using FEM analytical methods. So, following items are presented and discussed.

- Analytical method and conditions
- Correration between the computed and test results
- Application to designing studies

### **1. Objective**

It is well known that the diffusion of hydrogen in Zirconium alloy are affected not only by concentration but also temperature gradient.

And, the hydriding behaviours are very significant problems as a safety issues.

But in actual component, especially such as fuel rod of nuclear power plants, we can not avoid temperature gradient in some degree.

So, it is very useful to develop computer code which can analyze the hydrogen diffusion and precipitation behaviours under temperature gradient as a function of the structure of fuel rod.

For these background, we have developed computer code for hydrogen migration behavior using Finite Element Metod.

## 2. Analytical Method

Following equation were used for our computer code

$$\partial C / \partial t = \nabla D (\nabla C + (C \cdot Q^* / RT^2) \nabla T) + \Sigma F$$

ここで,  $C$  ; Hydrogen concentration (mol/cm<sup>3</sup>)

$t$  ; time (sec)

$D$  ; Diffusion coefficient of Hydrogen (cm<sup>2</sup>/sec)

$Q^*$  ; Heat of transport (cal/mol)

$R$  ; gas constant (cal/dey)

$T$  ; temperature (° K)

$\Sigma F$  ; Hydrogen permeation rate from surface (mol/cm<sup>2</sup> · sec)

$F_1$  ; Permeation rate of dissolved hydrogen in reactor coolant water

$F_2$  ; Permeation rate of hydrogen due to corrosion

This equation were solved under following conditions.

- (1) We ignore the change of diffusion coefficient due to the precipitation of hydride.
- (2) We treated that heat of transport is not temperature dependent.
- (3) Precipitation of hydride were occurred when the hydrogen concentration exceed its saturated concentration
- (4) We considered that the chemical composition of hydride are ZrH<sub>1.6</sub>.

In order words, the maximum concentration of hydrogen in the alloys are around  $1.7 \times 10^4$  ppm.

Under above condition, two dimentional computer code were developed.

## 3. Results and Discussion

### 3.1 Diffusion coefficient and heat of transport

- (1) Diffusion coefficient of hydrogen in Zr alloys.

Following data have been presented on Zr alloys.

$$D_H^{(1)} = 4.15 \times 10^{-3} \exp [-9470/RT] \quad (\text{cm}^2/\text{sec})$$

$$D_H^{(2)} = 7.73 \times 10^{-3} \exp [-10830/RT] \quad (\text{cm}^2/\text{sec})$$

- (2) Heat of transport

Heat of transport of Zr alloys are shown in Table 1.

- (3) Hydrogen solubility

Hydrogen solubility in Zirconium alloy are available in literatures and shown in Table 2.

**Table 1 Data for the heat of transport of Zr alloys**

Alloy	Temperature range (°C)	Q* (cal/mol)
Zr (crystal bar) <sup>(3)</sup>	300 – 500	5800 – 6000
Zry-2 <sup>(3)</sup>	300 – 500	4700 – 6100
Zry-2 + 0.6%Y <sup>(3)</sup>	300 – 494	5700 – 5800
Zry-2.6%Nb <sup>(3)</sup>	300 – 497	3300 – 5900
Zry-2.5%Hf <sup>(4)</sup>	300 – 640	5800 – 6000
Zry-2 <sup>(5)</sup>	300 – 620	4200

**Table 2 Hydrogen solubility in Zr alloys**

Material	Temperature range (°C)	Solubility (ppm)
Zry-2 <sup>(6)</sup>	260 – 525	$1.15 \times 10^5 \exp [8260/RT]$
Zr <sup>(6)</sup>	260 – 525	$1.18 \times 10^5 \exp [8720/RT]$
Zr <sup>(7)</sup>	100 – 398	$1.3 \times 10^5 \exp [10670/RT]$
Zr <sup>(7)</sup>	100 – 398	$1.15 \times 10^5 \exp [7730/RT]$
Zry-2 <sup>(8)</sup>	231 – 359	$1.10 \times 10^5 \exp [7630/RT]$
Zry-2 <sup>(8)</sup>	163 – 290	$1.03 \times 10^5 \exp [6020/RT]$
Zry-4 <sup>(8)</sup>	233 – 441	$1.15 \times 10^5 \exp [8360/RT]$
Zry-4 <sup>(8)</sup>	188 – 372	$1.14 \times 10^5 \exp [7700/RT]$

So, we have checked the influence of these physical constants to the computed results.

The results were shown in Fig.1. We can understand that there are no so significant impact to the computed results.

Then, we have used following values in our computer code as diffusion coefficients, heat of transport, and hydrogen solubility.

$$D = 7.73 \times 10^{-3} \exp [-10830/RT] \text{ (cm}^2\text{/sec)}$$

$$Q^* = 5500 \text{ (cal/mol)}$$

$$S = 6.66 \times 10^4 \exp [-7200/RT] \text{ (ppm)}$$

### 3.2 Correlation between test and computed results

To check the accuracy of the computed results, we have examined the correlation between test and computed results.

The results were shown in Fig.2~ Fig.4.

Good correlation were observed.

### 3.3 Application to the designing studies

As well known, there are axial temperature gradient at the bottom portion of fuel rod. So, to study the effect of the fuel structure, analytical studies have been carried out. In this analysis, hydrogen pick up from surface due to corrosion of

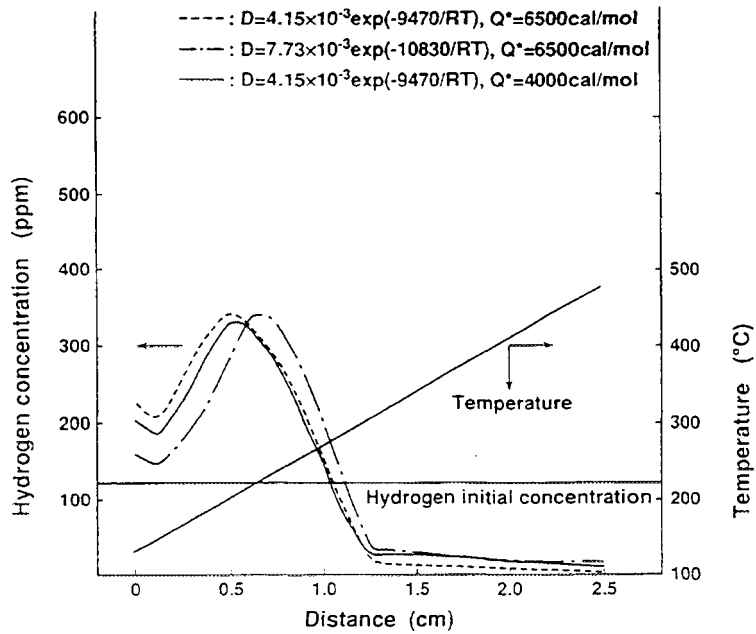


Fig.1 Influence of the physical constants (diffusion coefficients and heat of transport) to the computed results after 34days

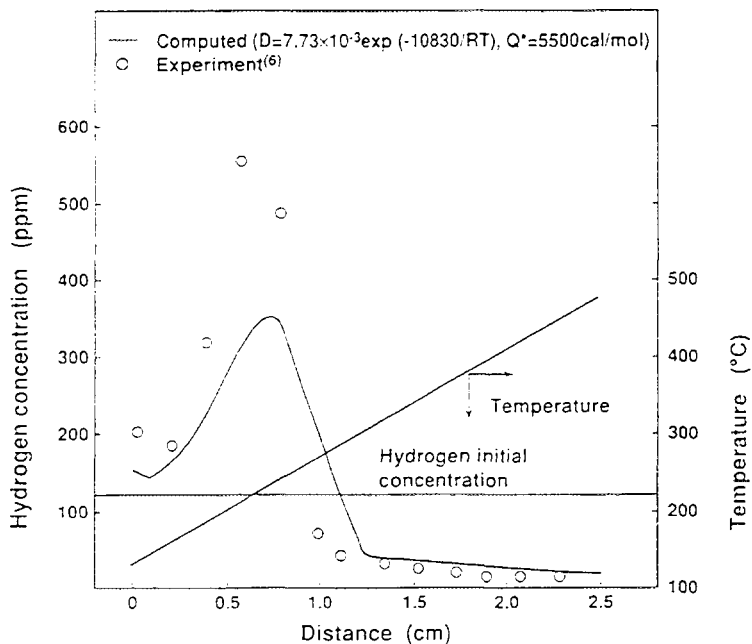


Fig.2 Correlation between experimental and computed results after 34days (Zircaloy 2)

fuel rod have been taken into consideration as a function of position and time.

The computed results were shown in Fig.5.

Under these temperature gradient conditions, some concentration were observed. But the maximum hydrogen concentration are less than 50ppm.

So, there are no impact to the reliability of our designed fuel rod.

#### 4. Summary

(1) Two dimensional computer code which can analyze the hydrogen migration under temperature gradient have been developed.

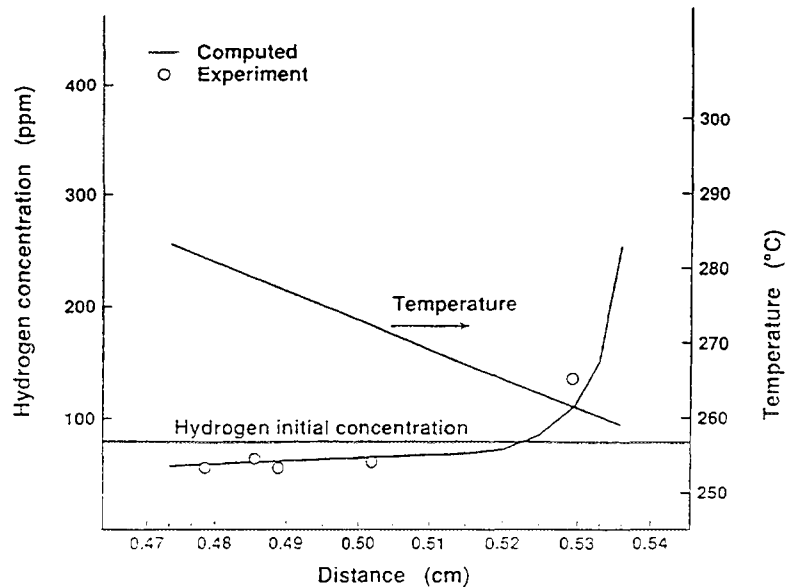


Fig.3 Correlation between experimental and computed results after 72hr (Zircaloy 2)

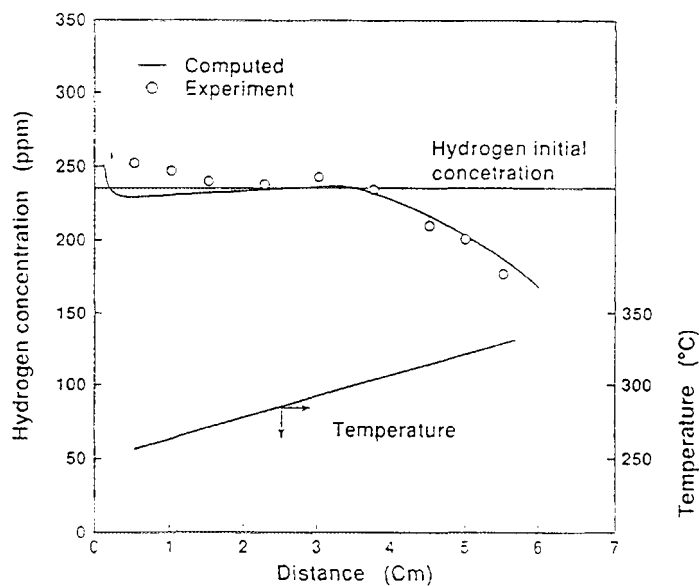
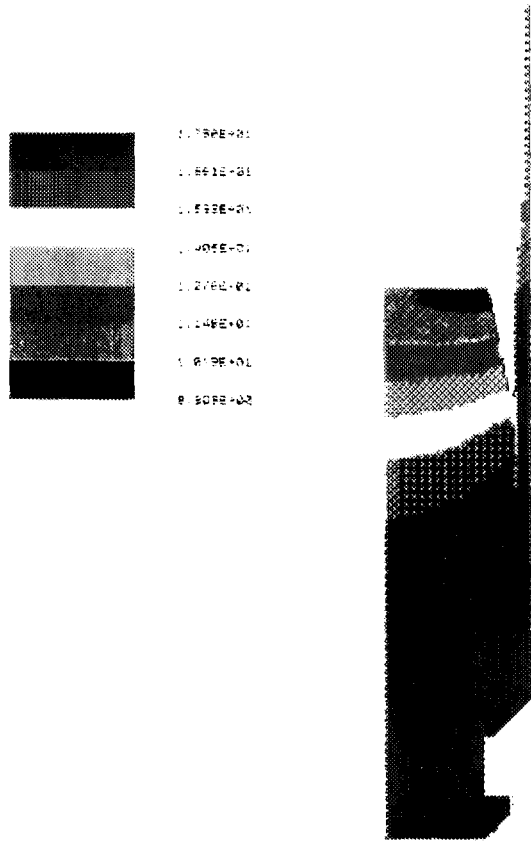


Fig.4 Correlation between experimental and computed results after 24days (Zircaloy 4)

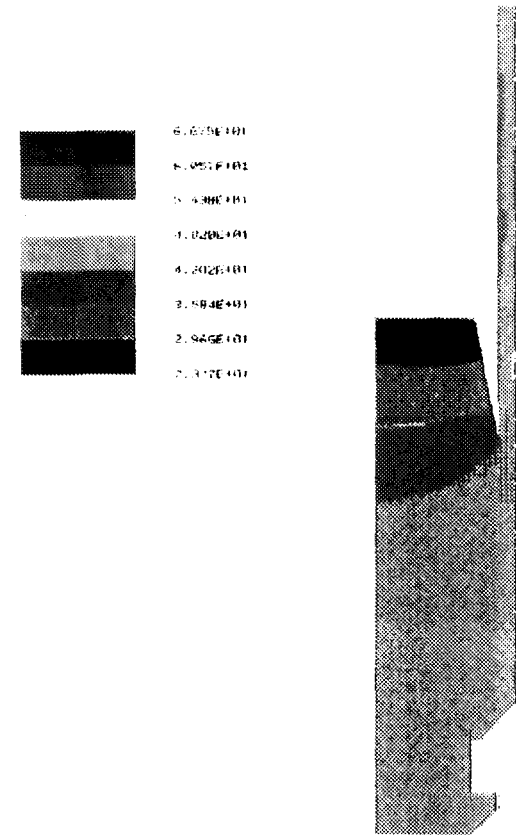
- (2) Using this computer code, we can analyze the hydrogen distribution and hydriding behaviors of materials.
- (3) Good correlation have been observed between test and computed results for Zry-2 and Zry-4 alloys.
- (4) This computer code will be applied to our designing studies to improve the reliability of fuel assemblies.

### **REFERENCES**

- [1] Someno etal ; Trans. Jap. Inst. Met., 24 (1966), p.249
- [2] J. J. Kearns ; J. Nucl. Mater., 43 (1972), p.330
- [3] A. Sawatzky ; J. Nucl. Mater., 9 (1963), p.364
- [4] S. Morozumi ; Trans. Jap. Inst. Met., 6 (1967), p.3
- [5] J. M. Markowitz ; Geneva Conf., paper (1958), p.709
- [6] J. J. Kearns. J. Nucl. Mater., 22 (1967), p.292
- [7] W.H. Erickson, etal ; J. Nucl. Mater., 13 (1964), p.254
- [8] G.F. Slattery ; J. Inst. Metals. 95 (1967), p.43



Temperature distribution



Hydrogen distribution

Fig.5 An example of application to the designing studies of fuel rod

NEXT PAGE(S)  
left BLANK



## THE TERMINAL SOLID SOLUBILITY OF HYDROGEN AND DEUTERIUM IN Zr-2.5Nb ALLOYS

I.G. RITCHIE\*, Z.L. PAN, M.P. PULS  
Materials and Mechanics Branch, AECL Research,  
Whiteshell Laboratories, Pinawa, Manitoba,  
Canada

### Abstract

The presence of hydrides in zirconium based alloys is an important factor in assessing the potential for delayed hydride cracking in pressure tubes and the embrittlement of other in-core components fabricated from these alloys. Consequently, the terminal solid solubility (TSS) of hydrogen in the zirconium alloys used in the Nuclear Industry is an important parameter. However, at the low hydrogen concentrations found in practice, the TSS is difficult to measure accurately and even the measurements of hydrogen concentrations by standard techniques are notoriously difficult to make reproducibly at the nominal levels found in pressure tube materials. The presence of hydrides, their dissolution and nucleation gives rise to a number of internal friction phenomena and changes in Young's modulus that can be useful from the practical point of view. These phenomena can be used to establish expressions for the TSS as a function of temperature, the hysteresis between dissolution and nucleation and hydrogen supercharging from the gas phase. In particular, such studies show that the hysteresis between the TSS measured during heating and cooling is particularly sensitive to the thermal history of the sample. This paper reviews the phenomena involved and presents some recent results on Zr-2.5Nb pressure tube material.

### INTRODUCTION

When the concentration of hydrogen isotopes in a reactor core component exceeds the Terminal Solid Solubility (TSS) at the temperature under consideration, hydrides may be present and embrittle the component. For example, TSS data on hydrogen isotopes in Zr-2.5 Nb pressure tubes are required to assess the potential for delayed hydride cracking (DHC) and hydride blister formation in CANDU pressure tubes. At present, Kearns' TSSD (Dissolution) data for hydrogen in zirconium and the zircalloys [1] is used in the Fitness-for-Service Guidelines for CANDU pressure tubes as one of the threshold criteria that must be met for susceptibility to DHC initiation.

Similarly, embrittlement of zirconium-based alloy components in light water reactor systems (PWRs and BWRs) occurs and can lead to problems during handling and manipulation of the components, both in - and out-of-reactor. For example, difficulty in relocating control rods in a PWR reactor was recently experienced and traced to broken and deformed guide tubes caused by hydride embrittlement [2]. The pick-up of hydrogen caused by radiolysis of the cooling water and corrosion mechanisms, and its subsequent redistribution to cold spots by thermal diffusion, will become more of a problem as fuel assemblies are pushed to higher and higher burn-ups.

---

\* Current address: Nuclear Fuel Cycle and Materials Section, Division of Nuclear Power and the Fuel Cycle, International Atomic Energy Agency, P.O. Box 100, A-1400 Vienna, Austria.

It is well known that there is a large hysteresis between the phase boundaries for precipitation (TSSP) and dissolution (TSSD) of hydrides in Zr [3] and a theoretical model of this hysteresis has been proposed by Puls [4,5]. This has important physical consequences for DHC, hydrogen ingress and blister formation. DHC obviously requires hydride precipitation at the crack tip which is governed by TSSP.

Only limited experimental data is available on TSSP of hydrides in Zr-2.5 Nb, but modeling of DHC, hydrogen ingress and blister formation in this material requires a thorough understanding of TSS hysteresis and accurate TSSP data [6,7].

To address these concerns, round robin measurements of TSS in deuterated Zr-2.5 Nb pressure tube materials were carried out using Calorimetry, Internal Friction techniques, Small Angle Neutron Scattering (SANS) and DHC techniques by the laboratories working in this area in Canada. The differential scanning calorimetry (DSC) technique has been used successfully to measure TSS temperatures (and hence hydrogen concentrations) in both irradiated and unirradiated pressure tube materials. Both internal friction and dynamic elastic modulus techniques have also been used previously to study hydrogen and its TSS in the hydride-forming metals [8-16]. This presentation reviews the Internal Friction results and discusses their interpretation.

## ***PREVIOUS RESULTS***

Figure 1 shows TSSD data for hydrogen and deuterium in Zr-2.5 Nb material obtained by diffusion [17], dilatometry and DHC techniques and compiled by Coleman [18]. It was found that the data was similar to Kearns' TSSD data on zirconium and the Zircalloys. However, there is considerable scatter which was believed to be mainly caused by uncertainties in hydrogen analyses. In addition, it is somewhat surprising that the TSSD data corresponds closely with the solubility limit for DHC since the latter clearly requires hydride precipitation at the crack tip, which is governed by TSSP. Moreover, recent advances in DHC theory [19,20] and experimental results [21] show that DHC can occur without either the presence or, if present, the dissolution of *matrix* hydrides at test temperature.

## ***OBJECTIVES***

The objectives of the internal friction and dynamic elastic modulus measurements can be split into two groups: technological objectives and scientific objectives.

Our technological objectives were to measure both TSSD and TSSP (continuously if possible), the cool-down TSS in the presence of pre-existing hydrides and the thermal hysteresis between TSSD and TSSP.

The scientific objectives were less specific, but we wanted to learn as much as possible about the role of misfit dislocations, the type and stability of hydrides involved, the nucleation and subsequent growth or shrinkage of hydrides, and the effect of stress on the TSS.

In this presentation we concentrate mainly on the technological objectives.

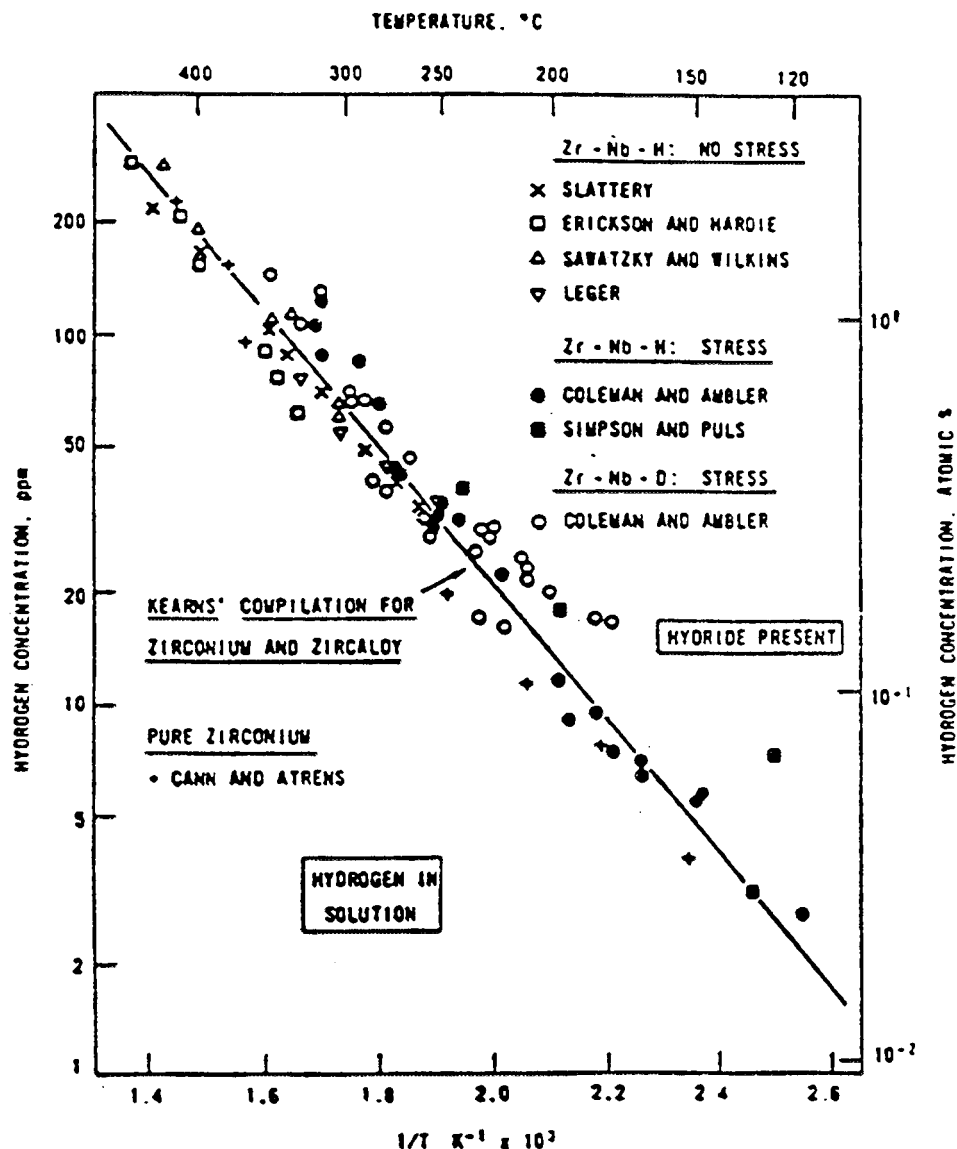


Figure 1 Summary of Terminal Solid Solubility of Hydrogen isotopes in cold worked Zr-2.5 Nb material.

### MATERIAL PREPARATION

#### Source Pressure tube

A Zr-2.5 Nb pressure tube, which was rejected for reactor use due to out-of-specification wall thickness, was selected for the TSS round robin study. Chemical composition was determined from other tubes fabricated from the same ingot as follows:

ELEMENT	SPECIFICATION	ANALYSIS
H	25 µg/g	8.5 µg/g
N	<80 µg/g	23.5 µg/g
O	900-1300 µg/g	1060 µg/g
Nb	2.4-2.8 %	2.73 %

The mechanical properties of the selected tube at 300°C are shown below:

Ultimate Tensile Stress (axial)	529 MPa
Yield Stress	374 MPa
Elongation	17.8%

### *Hydriding*

The hydriding procedure described below was carried out by G. Shek of the Metallurgical Research Department of Ontario Hydro. It was intended to deuteride the source material to six concentration levels (including the as-received concentration) up to a maximum concentration of 100 µg/g H equivalent (0.9 at. wt. %). Deuterium was chosen over hydrogen because it provides a stronger response to neutron scattering and because it is the isotope that is absorbed by the reactor pressure tubes. The source material was deuterated by the electrolytic hydriding (deuteriding)/thermal diffusion technique. In this procedure, a solid deuteride layer was electrolytically deposited onto the outside surface of the tube in a 0.1 M D<sub>2</sub>SO<sub>4</sub> electrolyte at 90°C with a current density of 100-120 mA/cm<sup>2</sup>. The deuterium was diffused into the tube by equilibrating the deuteride layer with the pressure tube matrix at Kearns' TSSD temperatures corresponding to the hydrogen/deuterium concentration required. After a diffusion anneal, the remaining surface deuteride layer was removed by machining. Although it is not critical to achieve the precise target concentrations, it is important that the hydrogen or deuterium isotope in the source material for the round robin be uniformly distributed. Hydrogen<sup>1</sup> homogeneity was mainly controlled by the uniformity of temperature during the diffusion anneal and the quality of the hydride layer that is needed to supply sufficient hydrogen to reach the equilibrium concentration throughout the sample. Three thermocouples, 120° apart, were spot welded to each end face of sections of tube 190 mm long. The temperatures were continuously monitored during the diffusion anneal. The record showed that the variation in temperature among the six thermocouples was less than 2°C. This represents a variation of 2.5 to less than 1 µg/g of H concentration over the temperature range employed.

The hydrided tubes were checked for hydrogen homogeneity by metallographic examination of the hydride distribution on either one or both end faces. In addition, 3 coupons, 120 degrees apart, were taken from each end of the tubes for calorimetric comparison of TSSD. Three coupons were also cut out around the circumference and sent to the Whiteshell Laboratories of AECL Research for hydrogen isotope analysis by the hot vacuum extraction method.

After the diffusion anneal treatment, metallographic examination showed that the hydrides were uniformly distributed around the circumference and through the thickness of the material. Hence, it was not necessary to perform a homogenization treatment. Results of the calorimetric measurements and the hydrogen analyses are shown in Table 1. It should be pointed out that the calorimetric measurements were performed with a high transient rate (30°C/min) by K. Tashiro of the Metallurgical Research Department of Ontario Hydro. The results indicated that the source tubes

---

<sup>1</sup>In the following, both hydrogen and deuterium are referred to as hydrogen for simplicity.

Table 1. Results of Hydrogen Analysis and Calorimetry TSSD Temperatures of Source Tubes

Target H Conc. ( $\mu\text{g/g}$ )	H Conc. (Chem.) ( $\mu\text{g/g}$ )	H Conc.(Chem.) (at. wt%)	TSSD of 5 or 6 coupons ( $^{\circ}\text{C}$ )
100	89.7 (89,90,90)	0.81	331.7 $\pm$ 1.6
75	66.7 (66,67,67)	0.60	306.6 $\pm$ 2.7
55	57.7 (56,57,60)	0.52	287.0 $\pm$ 2.4
40	42.0 (41,42,43)	0.38	258.0 $\pm$ 3.8
25	30.3 (28,30,33)	0.27	244.4 $\pm$ 1.8
As Received	7.3 (7,7,8)	0.06	171.3 $\pm$ 0.6

had fairly uniform hydrogen distribution as indicated by the small standard deviation and that there was sufficient difference in concentration among the source tubes to establish the TSS curve. The hydrogen analyses also indicated that the tubes were slightly off from the target levels. From hereon, the tubes will be designated by the hydrogen equivalent concentration in  $\mu\text{g/g}$  (7, 30, 42, 58, 67 and 90). A section about 90 mm long was subsequently taken from each tube for use in the round robin test program.

### ***EXPERIMENTAL PROCEDURE***

The test procedures for dynamic elastic modulus are described in this section. The general guideline for the round robin tests were as follows:-

Thermal Cycles:- at least  $20^{\circ}\text{C}$  beyond the TSS temperature

Heating rate:-  $2-4^{\circ}\text{C}/\text{min}$

Cooling rate:-  $2-4^{\circ}\text{C}/\text{min}$

Number of cycles:- at least 3.

### ***Internal Friction and Dynamic Elastic Modulus Techniques***

Elastic modulus and internal friction studies [8-13] have been reported previously to map H-TSS boundaries of hydrogen-doped pure Zr. In the past few years, these investigations have been extended to the study of the TSS in Zr-2.5 Nb alloy pressure tube materials [14-16] containing hydrogen or deuterium. Most recently, the same techniques have been used in the preliminary survey of the H-TSS in Excel alloy [22]. It should be noted that internal friction techniques are regarded as standard methods for the determination of the H-TSS in the bcc hydride-formers V, Nb and Ta. Although an internal friction ( $Q^{-1}$ ) peak associated with hydride dissolution on heating and hydride precipitation on cooling, similar to those obtained in V, Nb and Ta, is indeed observed in pure Zr-H alloys as shown in Fig. 2, no such peak is observed in Zr-2.5 Nb-H alloys as shown in Fig. 3. This is attributed to the lack of long misfit dislocations in the pressure tube alloy compared with the copious numbers found in pure Zr-H alloys [23]. Nevertheless, a more or less sharp knee in the dynamic elastic modulus (proportional to  $F^2$ ) is observed at the expected TSS on both heating and cooling. For this reason, we chose the most precise method of determining dynamic elastic modulus as a function of temperature available to us for this study.

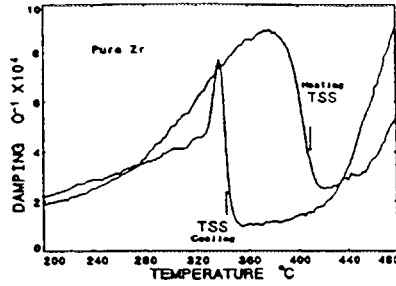


Figure 2(a) Internal friction as a function of temperature measured at  $-2$  Hz in the flexure pendulum on pure zirconium containing  $200 \mu\text{g/g}$  of hydrogen.

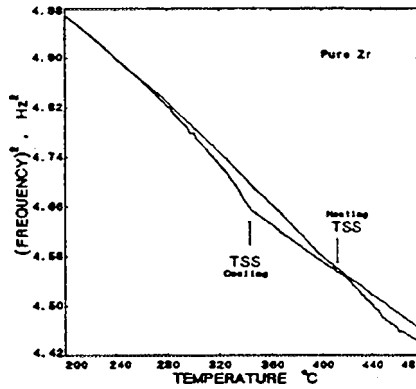


Figure 2(b) Frequency as a function of temperature measured concurrently with the results in Fig. 1.

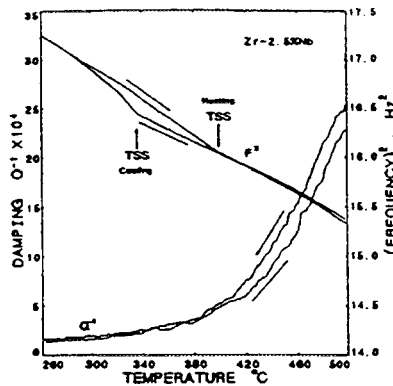


Figure 3 Internal friction and frequency as a function of temperature measured in the flexure pendulum on Zr-2.5 Nb pressure tube material containing  $\sim 200 \mu\text{g/g}$  of hydrogen

## Apparatus

A general overview of the methods used to measure the elastic (Young's) modulus ( $E$ ) and internal friction ( $Q^{-1}$ ) based on the Automatic Piezoelectric Ultrasonic Composite Oscillator (APUCOT) has been given elsewhere [16,24,25]. With the APUCOT (see the schematic diagram in Fig 4), the specimen temperature is measured by a thermocouple inserted in a calibrated dummy specimen of the same material as that being tested. The dummy specimen, of the same dimensions as the actual specimen, is located together with the real specimen so that they are symmetrically situated about the center of the cylindrical cavity of a small, non-inductively wound furnace. The

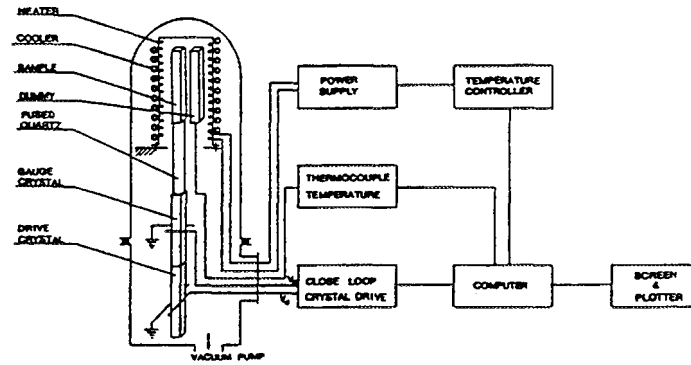


Figure 4 Schematic diagram of APUCOT

furnace is 100 mm in length and 18 mm in internal diameter. A typical Zr-2.5 Nb specimen with dimensions  $3 \times 3 \times 46 \text{ mm}^3$  is located in the center of the uniform temperature region of the furnace. This configuration allows temperature measurements to within an error of  $\pm 0.5^\circ\text{C}$  in the range of  $50\text{--}500^\circ\text{C}$  while the heating rate is less than  $5^\circ\text{C}/\text{min}$ . (Heating rates up to  $100^\circ\text{C}/\text{min}$  are available with the APUCOT for special tests in air.) The test chamber is normally evacuated before a test to prevent substantial oxidation of the specimen. The temperature measuring system was carefully recalibrated at heating and cooling rates of  $2^\circ\text{C}/\text{min}$  for the series of TSS tests described herein. A very stable heating (or cooling) rate is important for the precise determination of the temperature dependence of Young's modulus used to map the H-TSS boundaries.

### *Elastic Modulus vs. Temperature*

It has been shown [14-16] that a sharp "knee" in the elastic modulus vs. temperature plot is associated with the dissolution of hydrides during heating and their precipitation during cooling in Zr-2.5 Nb alloys. The temperature at the knee-point can be used to identify the solvus temperature and, therefore, to map H-TSS boundaries. Young's modulus is proportional to the resonant frequency squared ( $F^2$ ) of the specimen in longitudinal vibration. With the APUCOT, resonant frequency measurements are much more precise than those obtained using other elastic modulus measuring techniques. Consequently, the APUCOT was employed for the round robin series of TSS tests, rather than the low frequency flexure pendulum technique, which we have employed to study hydrogen in pure Zr-H alloys [12,16].

The hysteresis between the hydrogen dissolution (TSSD) and precipitation (TSSP) is easily observed in the  $E$  vs.  $T$  curves obtained on the same specimen during a thermal cycle through the TSS (see Fig. 5). Two methods were used to estimate the knee-point, i.e. the TSS temperature. In the first method, straight lines are drawn through the experimental data points above and below the knee, and their intersection is taken as the TSS temperature, as shown in Fig. 6. This procedure is somewhat subjective. In the second method, curves of the derivative of frequency vs. temperature ( $-dF/dT$  vs.  $T$ ), or the derivative of Young's modulus vs. temperature ( $-dE/dT$  vs.  $T$ ) are calculated and plotted, as shown in Fig. 7. In this case, the TSS temperature is taken to be the point of maximum slope on the sharp peak in this plot. Using blind tests, we have found that both techniques are equivalent within an error of  $0.5^\circ\text{C}$ .

Even though the second method is more objective, the peak can be rather low and ragged, making the point of maximum slope difficult to determine with accuracy for the lowest H concentrations.

### *Relationship between Dynamic Elastic Modulus and H Concentration*

In Zr-2.5 Nb-H, Zr-H and Ti-H, when all the hydrogen is in solution, the E vs. T curve is extremely linear for temperatures below 550°C [8,16]. More importantly for this study, the presence of increased levels of hydrogen depresses the elastic modulus at any given temperature. Consequently, a set of E vs. T curves for different levels of

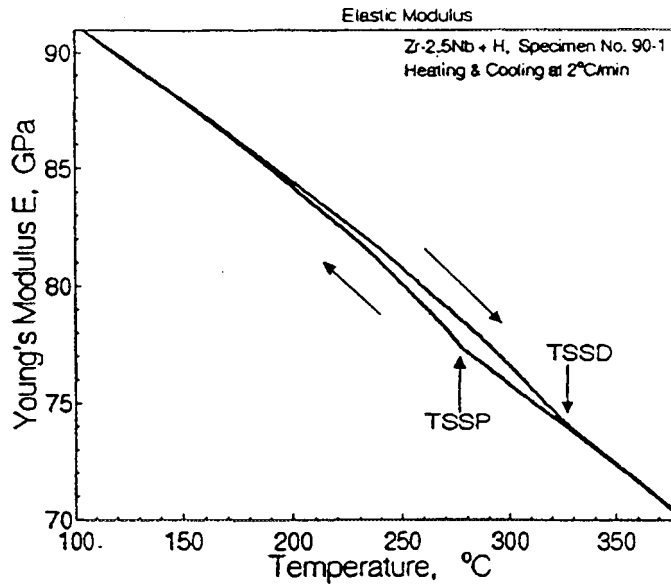


Figure 5 Young's modulus E vs temperature curves showing hysteresis between hydrogen dissolution (TSSD) and precipitation (TSSP).

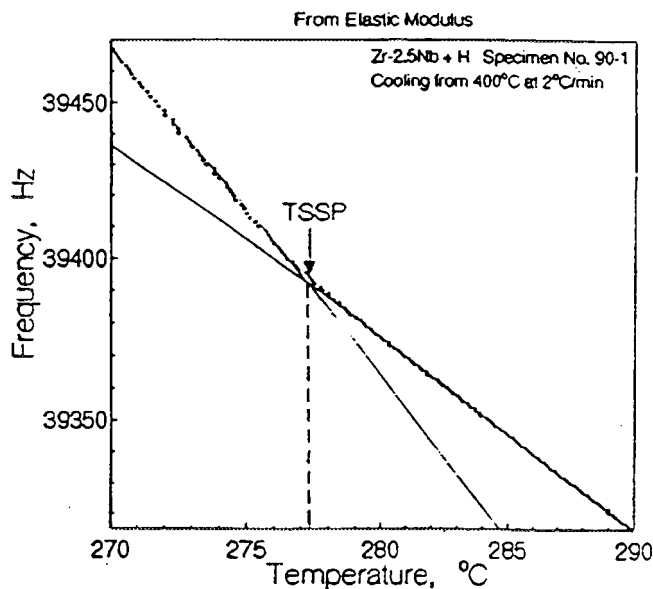


Figure 6 TSS temperatures determined from the interception of straight lines extrapolated from modulus data above and below the "knee".

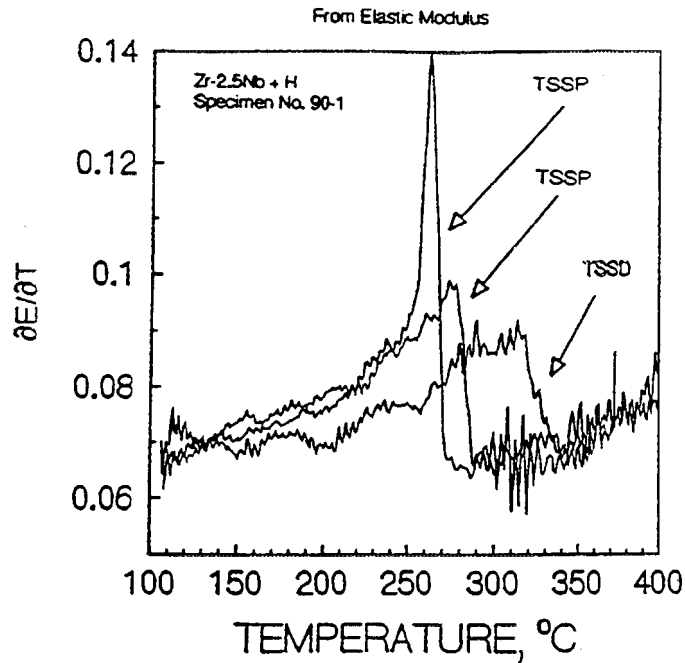


Figure 7 TSS temperatures determined from derivative of frequency vs temperature, or the derivative of Young's modulus vs temperature.

hydrogen are parallel straight lines, when all the hydrogen is in solution. For example, the experimental results for four different nominal levels of hydrogen are shown in Fig. 8. These observations strongly suggest that for a particular E vs. T curve, such as the cooling branch of the 90  $\mu\text{g/g}$  specimen in Fig. 8, the excess of the low temperature curved portion of the curve, over the linear extrapolation of the high temperature region to low temperatures, simply represents the amount of hydrogen present as hydrides. This means that an analysis of this excess yields an estimate of the solubility of hydrogen at any point lower than the TSS in this specimen. Such an analysis has been carried out on the 90  $\mu\text{g/g}$  specimen.

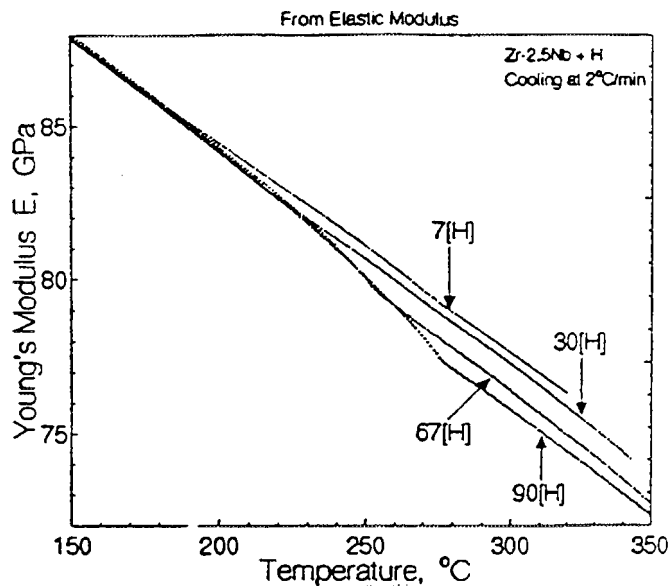


Figure 8 Young's Modulus vs temperature curves for different levels of hydrogen.

The results for TSSD on heat-up and for TSSP on cool-down, using this novel procedure, are shown in Figs. 9 and 10, respectively. In the important range of concentration from 15 to 100  $\mu\text{g/g}$  H (from the point of view of pressure tubes), the analysed curve (concentration vs.  $1/T$ ) does indeed agree with an Arrhenius line calculated from the TSS data of several specimens with different levels of hydrogen. At very low solubilities, the data are scattered because they represent very small differences between two large quantities and because they contain some contribution to the  $E$  vs.  $T$  curve from the modulus defects of relaxation processes at low temperature. In principle, the whole Arrhenius plot for the TSS boundary can be estimated by this analysis technique using the data from only one thermal cycle on a specimen containing a suitably high level of H. This is the primary advantage of the Young's modulus measuring technique in the field of TSS studies.

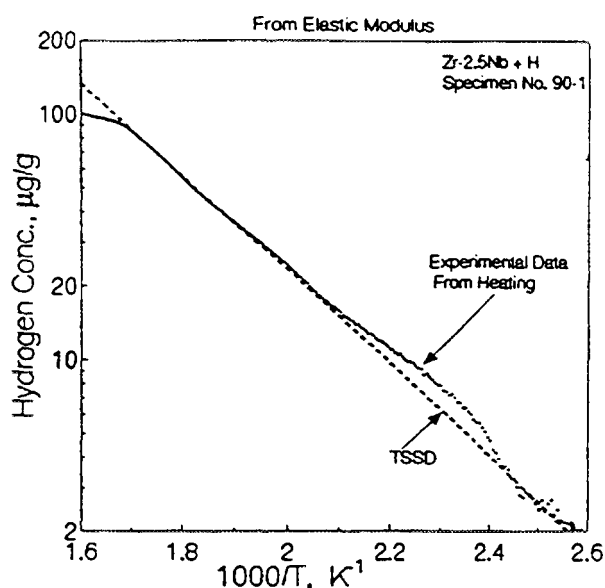


Figure 9 Demonstration that the TSSD curve can be obtained by the dynamic elastic modulus method from a single specimen having sufficient hydrogen.

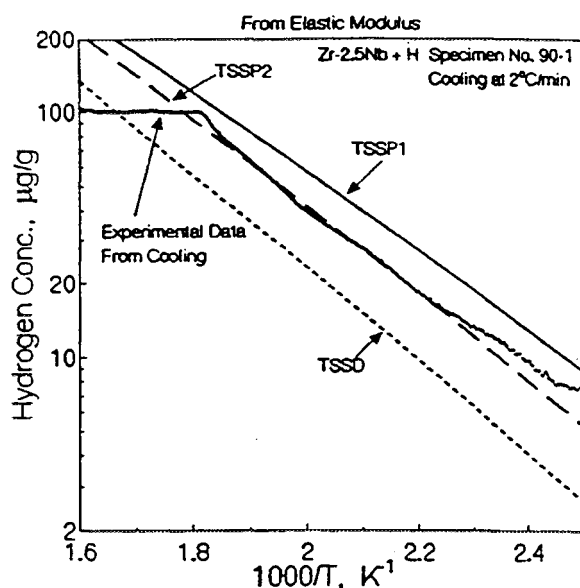


Figure 10 TSSP curve obtained by the dynamic elastic modulus method from a single specimen containing 90  $\mu\text{g/g}$  hydrogen.

## DYNAMIC ELASTIC MODULUS RESULTS

### TSSD

All of the TSSD temperatures obtained by the APUCOT during heating at 2°C/min on the six round robin Zr-2.5 Nb-H pressure tube rings are listed in Table 2. Duplicate specimens, cut from the same pressure tube rings, were also tested to compare with the first set of specimens. For most of the specimens, ten or more thermal cycles were observed to check the repeatability of our technique. No apparent influence of heating rate and/or the maximum temperature reached during a thermal cycle on the TSSD temperatures was detected. Therefore, the average value of multiple measurements on the same specimen is taken as the TSSD temperature of that specimen and listed in Table 2. The standard deviations of the TSSD temperatures for most specimens are less than or close to 1°C. Thus, the reproducibility of our TSSD measurements is satisfactory, except for the "as-received" specimen with the lowest level of hydrogen. The TSSD data of Sample 1 in Table 2 are well represented by the following Arrhenius equation calculated by linear regression ( $R^2 = 0.997$ ):

$$C = 1.35114 \times 10^5 \exp[-36018/RT] \mu\text{g/g}$$

where  $R = 8.3144 \text{ J/molK}$  and  $T$  is in K. This Arrhenius equation is plotted in Fig. 11 and compared with the experimental TSSD data. An analysis as described above from a single 90  $\mu\text{g/g}$  specimen can also be used to derive an Arrhenius plot, as shown in Fig. 9. There is a good agreement between the Arrhenius plot from experimental results on one specimen and the Arrhenius line calculated with TSSD data from six different specimens.

### TSSP

Previous studies [15,16] have confirmed that the processes of nucleation and precipitation of hydrides in Zr-2.5 Nb are very complex, and that the TSSP temperature depends sensitively on the microstructure of the material in question and the maximum temperature ( $T_{\text{max}}$ ) reached during a thermal cycle. Even if  $T_{\text{max}}$  does not reach the dissolution TSS, i.e.  $T_{\text{max}} < \text{TSSD}$ , a TSSP temperature can be still be detected. Therefore, every datum of TSSP should always be associated with a given

Table 2. TSSD Data from Dynamic Elastic Modulus Technique

Specimen No.	H Conc. ( $\mu\text{g/g}$ )	Number of Tests	TSSD Temp. ( $^{\circ}\text{C}$ )
90-1	89.7	25	329.2
67-1	66.7	7	304.2
58-1	57.7	11	274.3
42-1	42.0	8	258.7
30-1	30.3	15	234.3
7-1	7.3	3	173.9
90-2	89.7	6	329.0
67-2	66.7	4	304.3
58-2	57.7	6	278.0
30-2	30.3	11	235.4

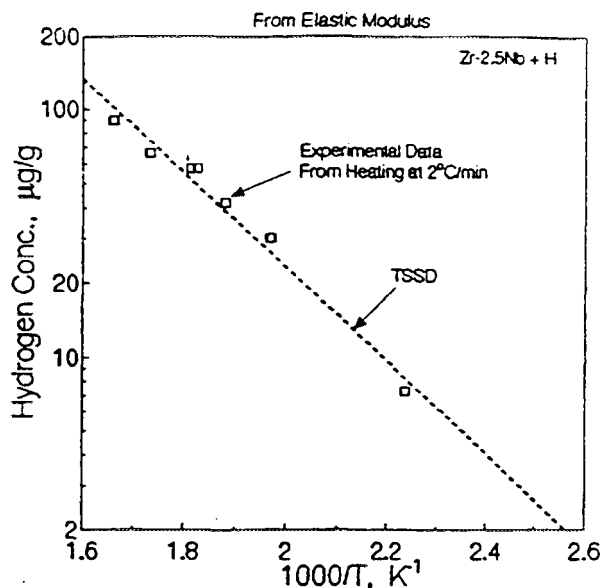


Figure 11 TSSD curve established from elastic modulus on samples with different concentrations.

$T_{\max}$ . In the round robin series of TSS tests, we have defined TSSP1 and TSSP2 as the TSSP temperature obtained after cooling from the highest and lowest  $T_{\max}$  chosen, respectively. In practice, we usually chose both of them to be above the TSSD temperature.

The experimental results for TSSP1 and TSSP2 and their corresponding  $T_{\max}$  values for the six Zr-2.5 Nb materials are listed in Table 3. Observed differences between TSSP1 and TSSP2 varied from 18.4°C for the 90 µg/g specimen to 28.2°C for the 30 µg/g specimen. Both TSSP1 and TSSP2 were also plotted on an Arrhenius diagram as shown in Fig. 12. The corresponding Arrhenius equations are as follows:

$$C = 1.01388 \times 10^5 \exp[-31074/RT] \text{ } \mu\text{g/g, for TSSP1}$$

and

$$C = 0.4433 \times 10^5 \exp[-28868/RT] \text{ } \mu\text{g/g, for TSSP2}$$

If the value of  $T_{\max}$  chosen in a particular test is between the highest and lowest  $T_{\max}$ , then the corresponding TSSP temperature measured in the test will be between the TSSP1 and TSSP2 lines. The experiments on TSSP as a function of  $T_{\max}$  were carried out on the five Zr-2.5 Nb-H materials at a cooling rate of 2°C/min, and the results are shown in Figs. 13 and 14. Similar curves of TSSP vs.  $T_{\max}$  were observed with TSSP decreasing to a minimum flat value at about 400°C in every case. However, at a lower cooling rate of 0.2°C/min the TSSP temperatures for the 58 and 67 µg/g specimens decreased to minimum values at 380°C and 360°C, respectively. These values are significantly lower than those found at a cooling rate of 2°C/min. When the 58 µg/g specimen was held for four days at a particular  $T_{\max}$  and subsequently cooled at 0.2°C/min, then as shown in Fig. 15, the TSSP temperature decreased to a minimum value at a  $T_{\max}$  of 350°C, significantly lower than that found without annealing for four days. In conclusion, it appears that the hysteresis between dissolution and precipitation of hydrides in Zr-2.5 Nb can be extended if the specimen

Table 3. TSSP Data from Dynamic Elastic Modulus Technique

Specimen No.	H Conc. (μg/g)	T <sub>max</sub> (°C)	TSSP1 Temp. (°C)
90-1	89.7	450	267.6
67-1	66.7	383	246.0
58-1	57.7	420	219.2
42-1	42.0	400	200.8
30-1	30.3	420	177.4
7-1	7.3	280	125.5
			TSSP2 Temp.
90-1	89.7	329	286.0
67-1	66.7	301	266.0
58-1	57.7	300	243.2
42-1	42.0	280	222.7
30-1	30.3	260	205.6

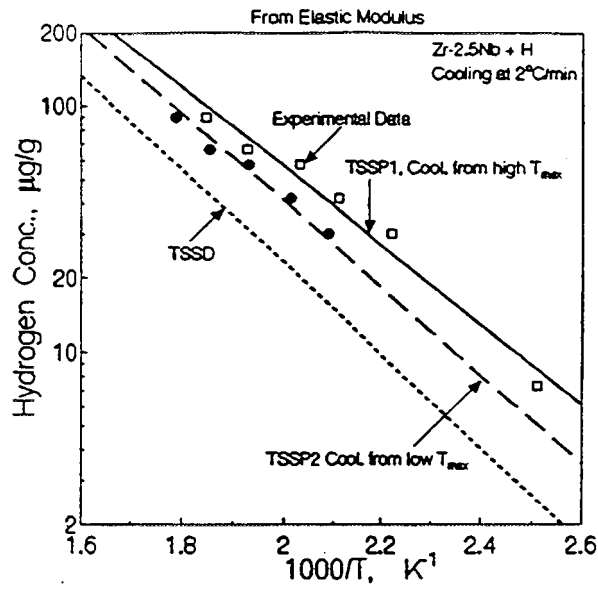


Figure 12 TSSP curves established with different peak temperatures.

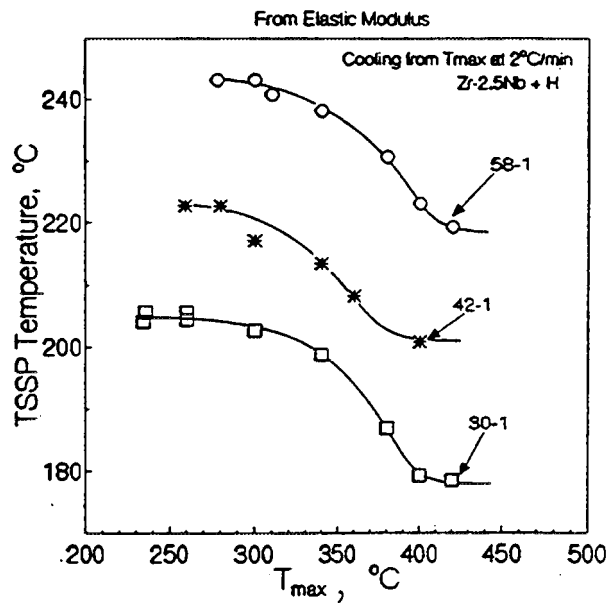


Figure 13 Effects of peak temperatures on TSSP in samples containing nominal hydrogen concentrations of 30, 42 and 58 μg/g.

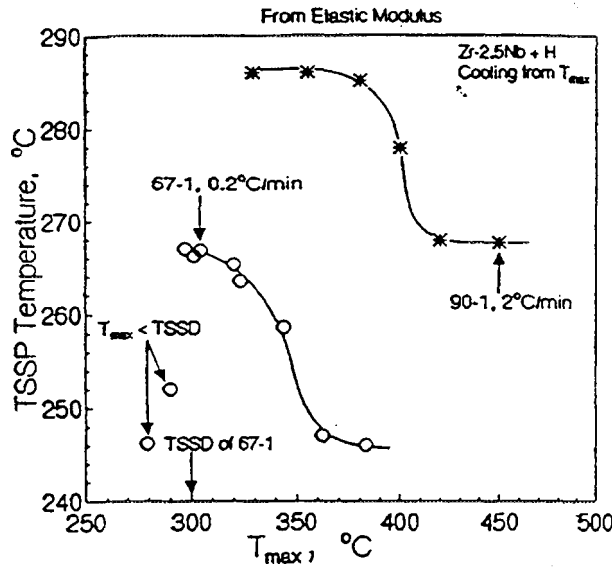


Figure 14 Effects of peak temperatures on TSSP in samples containing nominal hydrogen concentration of 67 and 90  $\mu\text{g/g}$ . Included in the figure are two data points in which the peak temperature is below TSSD.

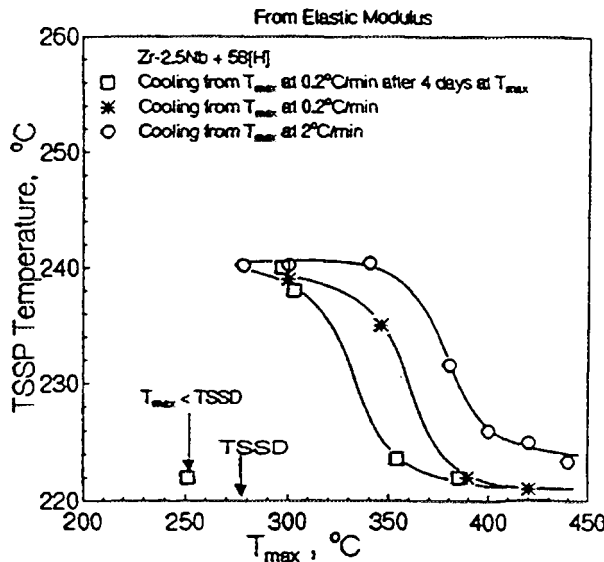


Figure 15 Effects of peak temperatures, cooling rates and holding time on TSSP for the 56  $\mu\text{g/g}$  sample. Included in the figure is one data point in which the peak temperature is below TSSD.

is cooled very slowly or if the specimen is pre-annealed for a long time at a sufficiently high temperature.

In Figs. 14 and 15, three TSSP data were observed in thermal cycles for which  $T_{\text{max}}$  was deliberately chosen to be below TSSD. These data are of interest because they reveal the effective TSSP for the nucleation of "new" hydrides in the presence of pre-existing hydrides. Similar experimental results on Zr-2.5 Nb specimens containing 200  $\mu\text{g/g}$  of hydrogen were reported and discussed in detail elsewhere [15,16]. These results appear to show that the existing hydrides do not grow significantly for the cooling rate used in our tests. Rather, the supersaturation of hydrogen builds up until either nucleation occurs at new sites in the lattice or growth on existing hydrides is

possible. This phenomenon may be important in the specification of the Fitness-for-Service Guidelines of Zr-2.5 Nb pressure tube materials.

## DISCUSSION

### Comparison of Results

#### TSSD

The DSC results obtained by K. Tashiro, DHC results obtained by G. Shek, SANS results obtained by R. Fong of AECL Research, Chalk River Laboratories, together with the results of this study are compared with those from Kearns' compilation (Fig. 1) in Table 4. The least squares fits of the individual sets of data are shown below Table 4 and are plotted in Fig. 16. There is good agreement between the TSSD obtained by calorimetry and dynamic elastic modulus measurements. The uncertainties

Table 4. Comparison of TSSD Temperatures

H conc.	Kearns	Cal.	Dyn.El.Mod	DHC (3 t/c)	SANS
7.3	171.8	168.9	173.9	157	190 ± 5
30.3	248.2	240.5	239.43	228	250 ± 5
42.0	269.6	257.6	258.7	250	-
57.7	292.2	283.9	276.1	273	-
66.7	303.1	303.5	304.2	284	-
89.7	326.8	326.0	329.1	304	-

All temperatures in Celsius.

Least Squares fit to obtain Arrhenius TSSD.

Kearns:  $C = 1.20000 \times 10^6 \exp(-35900/RT)$

Calorimetry:  $C = 1.08489 \times 10^6 \exp(-35095/RT)$

Dynamic Elastic Modulus:  $C = 1.35114 \times 10^6 \exp(-36018/RT)$

DHC (3 t/c)  $C = 1.33733 \times 10^6 \exp(-35142/RT)$

C in  $\mu\text{g/g}$ , R is gas constant and T in Kelvin.

Fitted TSSD Curves: Data from different techniques

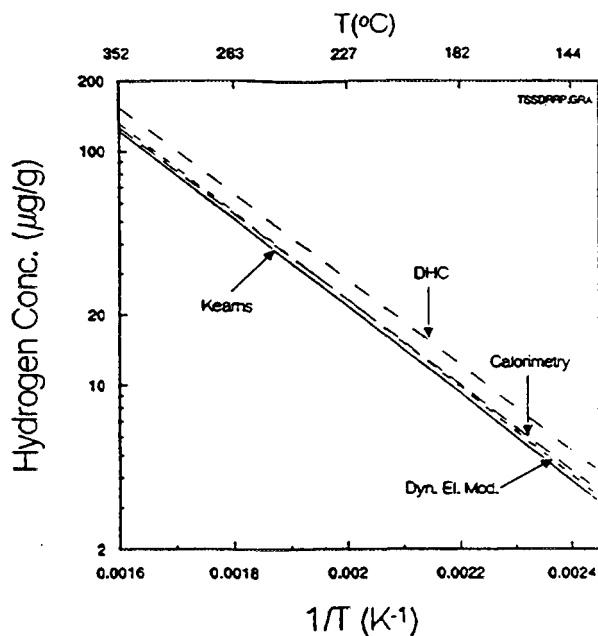


Figure 16 Comparison of TSSD curves by the different techniques.

in the SANS measurements are relatively large, but the TSSD temperatures are in reasonably good agreement with Kearns' data.

Only the maximum DHC cracking temperatures on cool-down after thermal cycling were included in Table 4 and Figure 16 for comparison. The DHC temperatures on cool-down are lower than the TSSD temperatures, but not as low as TSSP.

### TSSP

Table 5 compares the TSSP temperatures determined by dynamic elastic modulus and calorimetry. The comparison also includes TSSP data from Slattery [26]. The least squares fit of the individual sets of data are shown below the Table and plotted in Fig. 17 together with the fits to the TSSD data. The agreement is not as good as that for the TSSD results. However, TSSP depends on thermal history such as the maximum

Table 5. Comparison of TSSP Temperatures by Calorimetry and Dynamic Elastic Modulus (TSSP1)

H Conc.	Calorimetry (2°C/min)	Calorimetry (10°C/min)	Dyn. El. Mod. (2°C/min)	Slattery /26/
7.3	107.3	-	125.5	117
30.3	199.0	168.6	177.4	194
42.0	207.5	189.3	200.8	216.1
57.7	231.7	217.9	219.2	239.7
66.7	260.3	242.4	246.0	251.3
89.7	275.8	264.1	267.6	276.7

Arrhenius fit of TSSP:

Slattery:  $C = 4.1100 \times 10^6 \exp(-28002/RT)$

Calorimetry:  $C = 2.2167 \times 10^6 \exp(-25534/RT)$

Dynamic Elastic Modulus:  $C = 1.01388 \times 10^6 \exp(-31074/RT)$   
(2°C/min; TSSP1)

C in  $\mu\text{g/g}$ , R is gas constant and T in Kelvin.

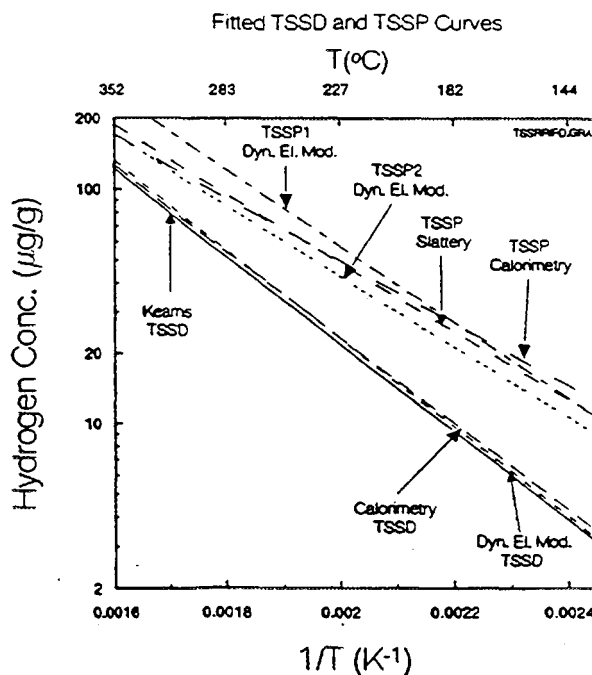


Figure 17 Comparison of TSSD and TSSP curves by the different techniques.

sample temperature and the cooling rate. A possible explanation is that the higher maximum temperature annealed out the dislocations on prior hydride precipitation sites (memory effect [27]) making nucleation more difficult and therefore lowering the precipitation temperatures because the hydride nucleation energy would be larger.

### *Hydrogen Homogeneity*

Comparison of the TSS results would obviously be affected by the homogeneity of hydrogen in the source materials. Since calorimetry has been demonstrated to be an accurate, fast and reproducible method of measuring TSS, some of the tested specimens from the DHC and dynamic elastic modulus experiments were re-analyzed by the calorimetric method. Only TSSD was measured and this was done with a high heat-up rate (30°C/min).

Results of the calorimetric measurements of the DHC specimens are shown in Table 6. The results show that the TSSD in the DHC specimens are all higher than those of the calorimetric round robin samples. There was a spread of 8°C in TSSD temperatures among the three 42 µg/g samples. The other DHC specimens appeared to have uniform concentrations.

The difference in TSSD in the DHC and calorimetric round robin samples is not due to any uncertainty in the calorimetric analyses as some of the original calorimetric round robin samples were re-analysed and the TSSD temperatures are within 0.5°C of previous results. The possible causes for the difference are hydrogen inhomogeneity in the source material and hydrogen pick-up as a result of the DHC tests. Hydrogen inhomogeneity can be caused by non-uniform temperature during diffusion anneal, inconsistent hydride layer quality, metallurgical inhomogeneity such as variations in the beta phase distribution and non-uniform residual stresses. One might suppose that if there are large, local variations in hydride distribution, these might be seen in the calorimetric analyses because of the small coupon size used. However, the evidence, based on the consistently positive deviation of the results, is that sample size is not a problem in the round robin samples.

The DHC specimens were machined from the source material by the electro-discharge method (EDM) using the wire cutting process. Previous study [27] has shown that there was little hydrogen pick-up as a result of the EDM process. Therefore, it is not likely that there was hydrogen pick-up by the specimen from the DHC test.

Another intriguing explanation of the difference between the DHC results and both TSSD and TSSP is that the stress applied in DHC experiment shifts TSSP, which should control DHC, to higher temperatures. This shift is in the expected sense, i. e. a tensile stress at the crack tip favours the presence of hydrides.

Results of the calorimetric measurements on the dynamic elastic modulus samples are shown in Table 6. Using the calorimetric technique, comparison between the calorimetric TSSD temperatures measured on the dynamic elastic modulus samples and the calorimetric round robin samples shows that, except for the 7 µg/g sample, the dynamic elastic modulus samples give higher TSSD temperatures than the original calorimetric (round robin) samples. These results suggest that there was hydrogen inhomogeneity in the source tubes. An inhomogeneity in the much larger dynamic

Table 4. TSSD temperatures (in °C) determined from dynamic elastic modulus samples by calorimetry.

Specimen No. (Nom. [H], $\mu\text{g/g}$ )	Dyn. El. Mod. (RR Samples)	Calorimetry (DEM Samples)	Calorimetry (RR Samples)
D782 (7)	173.9	168.3	168.9
D786 (30)	234.3	243.4	240.5
D785 (42)	258.7	263.1	257.6
D787 (58)	274.3	288.6	283.9
D780 (67)	304.2	315.2	303.5
D784 (90)	329.2	336.3	326.0

elastic modulus specimens could also be implied by these results, but the fact that all the deviations between the dynamic elastic modulus and the calorimetric results have the same sign suggests that this may not be the case. The most likely reason for the systematic differences between the two methods may be due to the different interpretations of the point on the response curve giving the temperatures that correspond to TSSD. Alternately, there could be a difference in the accuracy of the temperature measurements, since the temperature of the dynamic elastic modulus specimen cannot be measured directly, but must be taken from an adjacent dummy specimen.

We should note that the hydrogen inhomogeneity in the source tubes was higher than expected, despite the care put into sample preparation. This supports the belief that scatter in previous TSS data (Fig. 1) may be due to both uncertainties in hydrogen analysis and spatial inhomogeneity.

### *TSS Data and Hysteresis*

The calorimetric and dynamic elastic modulus results confirm previous observations that TSSD is not very sensitive to heat-up rate and previous peak temperatures. In contrast, TSSP is strongly affected by thermal history (peak temperature, hold time, cooling rate etc.). This could have significant effects on DHC behaviour, since TSSP affects the amount of hydrogen supersaturation in the matrix after a cool-down cycle and during ingress. For example, this may explain previous experimental observations [28] that the effectiveness of a temperature maneuver procedure (approaching the hot shut down temperature at 250°C by cooling to 210°C and then heating to 250°C) depended on prior thermal history and hydrogen concentration.

### **CONCLUSIONS**

It is conservative to use TSSD as a threshold criterion for DHC initiation and propagation in unirradiated Zr-2.5 Nb pressure tube.

There is fairly good agreement between the TSSD curves determined by calorimetry and dynamic elastic modulus compared with the curves determined from previous data compiled by Kearns.

There is good agreement between dynamic elastic modulus and calorimetry on observations regarding thermal history effect on TSS hysteresis. Thermal history has a strong effect on TSSP and has little effect on TSSD. There is a significant difference

in slope between the TSSP curves obtained by dynamic elastic modulus and calorimetry even though they were determined at the same cooling rate. This is probably because they were determined using slightly different maximum temperatures.

## REFERENCES

- [1]. Kearns, J.T., *J. Nucl. Mat.* 22,292 (1967).
- [2]. Bjornkvist, L., "Oxidation and Hydriding of Fuel Assembly Guide Tubes", First Meeting of the PWR Working Sub-Group of the European Federation of Corrosion, Sept. 1992.
- [3]. Puls, M.P., *Acta Metall.* 29, 1961 (1981).
- [4]. Puls, M.P., *Acta Metall.* 32,1259 (1984).
- [5]. Puls, M.P., *J. Nucl. Mater.* 165, 128 (1989).
- [6]. Puls, M.P., *Metall. Trans. A*, 21A, 2905 (1990).
- [7]. Leger, M. and Byrne, T. P., "Hydride Blister Growth in Zr-2.5 Nb Pressure Tube Material", Canadian Nuclear Society, 12th Simulation Symposium on Reactor Dynamics and Plant Control", Hamilton, Ontario, April, 1986.
- [8]. Bungardt, K. and Preisendanz, H., "Damping and Modulus of Shear of Zirconium and Zirconium-Hydrogen Alloys", *Zeitschrift für Metallkunde* 51, 280-289 (1960).
- [9]. Provenzano, V., Schiller, P. and Schneiders, A., "Internal Friction Study of Zirconium Alloyed with Hydrogen and Deuterium", *Journal of Nuclear Materials* 52, 75-84 (1974).
- [10]. Mishra, S. and Asundi, M. K., "Determination of Solid Solubility Limit of Hydrogen in Alpha-Zirconium by Internal Friction Measurements", *ASTM STP* 551, 63-71 (1974).
- [11]. Mazzolai, F. M., Ryll-Nardzewski, J. and Spears, C. J., "An Investigation of the Zirconium-Hydrogen System by Internal Friction", *Nuovo Cimento della Societa Italiana di Fisica B* 33B, 251-263 (1976).
- [12]. Ritchie, I. G. and Sprungmann, K.W., "Hydride Precipitation in Zirconium Studied by Low-Frequency Pendulum Techniques", *Journal de Physique* 44, C9-313-318 (1983).
- [13]. Numakura, H., Ito, T. and Koiwa, M., "Low-Frequency Internal Friction Study of Zr-H and Zr-D Alloys", *Journal of the Less-Common Metals* 141,285-294 (1988).

- [14]. Nuttall, K., Dutton, R. and Shillinglaw, A. J., "Terminal Solubility of Hydrogen in Zr-2.5 wt% Nb Determined by the Resonant Bar Technique", *Hydrogene et Materiaux Congres International*, 3eme, Paris,, Vol.1, 167-172 (1982)
- [15]. Ritchie, I. G. and Pan, Z. L., "Internal Friction Study of Zr-2.5Nb-H Alloys" *Philosophical Magazine A63*, 1105-1113 (1991).
- [16]. Ritchie, I.G. and Pan, Z. L., "Internal Friction and Young's Modulus Measurements in Zr-2.5Nb Alloy Doped with Hydrogen" *ASTM STP No.1169*, 385 (1992).
- [17]. Sawatzky, A. and Wilkins, B. J. S., *J. Nucl. Mater.* 22,304 (1967).
- [18]. Coleman, C. E. and Ambler, J. F. R., *CRNL-2259*, 21(1982).
- [19]. Eadie, R. L., Mok, D., Scarth, D. and Leger, M., *Scripta Met.* 25, 497, (1991).
- [20]. Puls, M. P., *Metall. Trans. A*, 21A, 2905 (1990).
- [21]. Shek, G. K. and Graham, D. B., *Zirconium in Nuclear Ind., Eighth Int. Sym.*, ASTM STP 1023, 1989.
- [22]. Pan, Z. L., Puls, M. P. and Ritchie, I. G., "Measurement of Hydrogen Solubility During Isothermal Charging in a Zr Alloy using an Internal Friction Technique", *Tenth International Conference on Internal Friction and Ultrasonic Attenuation in Solids*, Rome, Sept. 1993, to be published.
- [23]. Carpenter, G. J. C. and Watters, J. F., *J. Nucl. Mater.* 73,190 (19978).
- [24]. Marx, J, "Use of the Piezoelectric Gauge for Internal Friction Measurements", *Rev. Sci. Instr.* 22, 503-509 (1951).
- [25]. Robinson, W. H. and Edgar, A., "The Piezoelectric Method of Determining Mechanical Damping at Frequencies of 30 kHz", *IEEE Transaction Sonics & Ultrasonics*, SU-21(2), 98-105 (1974).
- [26]. Slattery, G. F., *J. Inst. Metals* 95, 43-47 (1967).
- [27]. Cameron D. J. and Duncan, R. G., *J. Nucl. Mat.* 68, 340-344 (1977).
- [28]. Coleman C. E., Sagat, S., Shek, G. K., Graham, D. B., and Durand, M. A., *Int.J. Pres. Ves. & Piping* 43, 187 (1990).



## CORROSION RATE TRANSIENTS OBSERVED BY LINEAR POLARIZATION TECHNIQUES AT Zr-1%Nb ALLOY

J. BERAN, K. ČERNÝ  
ZJS SKODA plc., Pelzen,  
Czech Republic

### Abstract

Momentary corrosion rate of Zr-1%Nb alloy during nonisothermal autoclave experiments at temperature up to 328°C in various solutions was determined by  $T/R_p$  values (  $T$  - absolute temperature,  $R_p$  - polarization resistance), multiplied by temperature independent conversion factor. This factor was found by comparison of conventinal corrosion loss evaluation with electrochemical measurements. Corrosion rate transients in boric acid solutions and in lithium hydroxide differed significantly. Great differencies were also found in stabilized corrosion rates at the end of experiments. Temperature irregularities caused considerable changes in corrosion rate.

### Introduction

Application of linear polarization techniques for continuous and remote corrosion monitoring of Zircaloy-2 was previously reported by a number of authors /1/,/2/,/3/. Further, this method was extensively used as well in corrosion test program of Zr-1%Nb alloy. For this purpose it was necessary to clarify some theoretical problems, develop high-pressure, high-temperature, radiation resistant electrochemical probes and carry out many autoclave experiments in various solutions to determine the conversion factor polarization resistance versus corrosion rate.

The main result of the theoretical work consisted in the introduction of criterion  $T/R_p$  instead of usual  $1/R_p$ . This modification provides great advantage for corrosion measurements during nonisothermal experiments. Momentary  $T/R_p$  values are converted into momentary corrosion rate simply by multiplication with temperature independent conversion factor.

Development of electrochemical probes for severe operating conditions resulted in the insulatory sealing based on voluminal increase of solid phase due to suitable chemical reaction between a porous body and a penetrant. Probes of this type with the designation TIV have been reported previously /4/.

Autoclave experiments for the determination of conversion factor by comparison of mean values  $(T/R_p)_s$  with subsequent conven-

tional evaluation of mean corrosion rate were carried out in stagnant solutions without refreshing. Originally, the solutions were not deaerated. Besides the experimental data necessary for determination of conversion factor, autoclave experiments resulted in many interesting  $T/R_p$  transients, which reflected the corrosion aggressivity of test solutions.

### Experimental results

Every point in the conversion diagram Fig.1 represents one corrosion experiment (test period being several hundred hours) with particular solution and indicates the comparison between mean

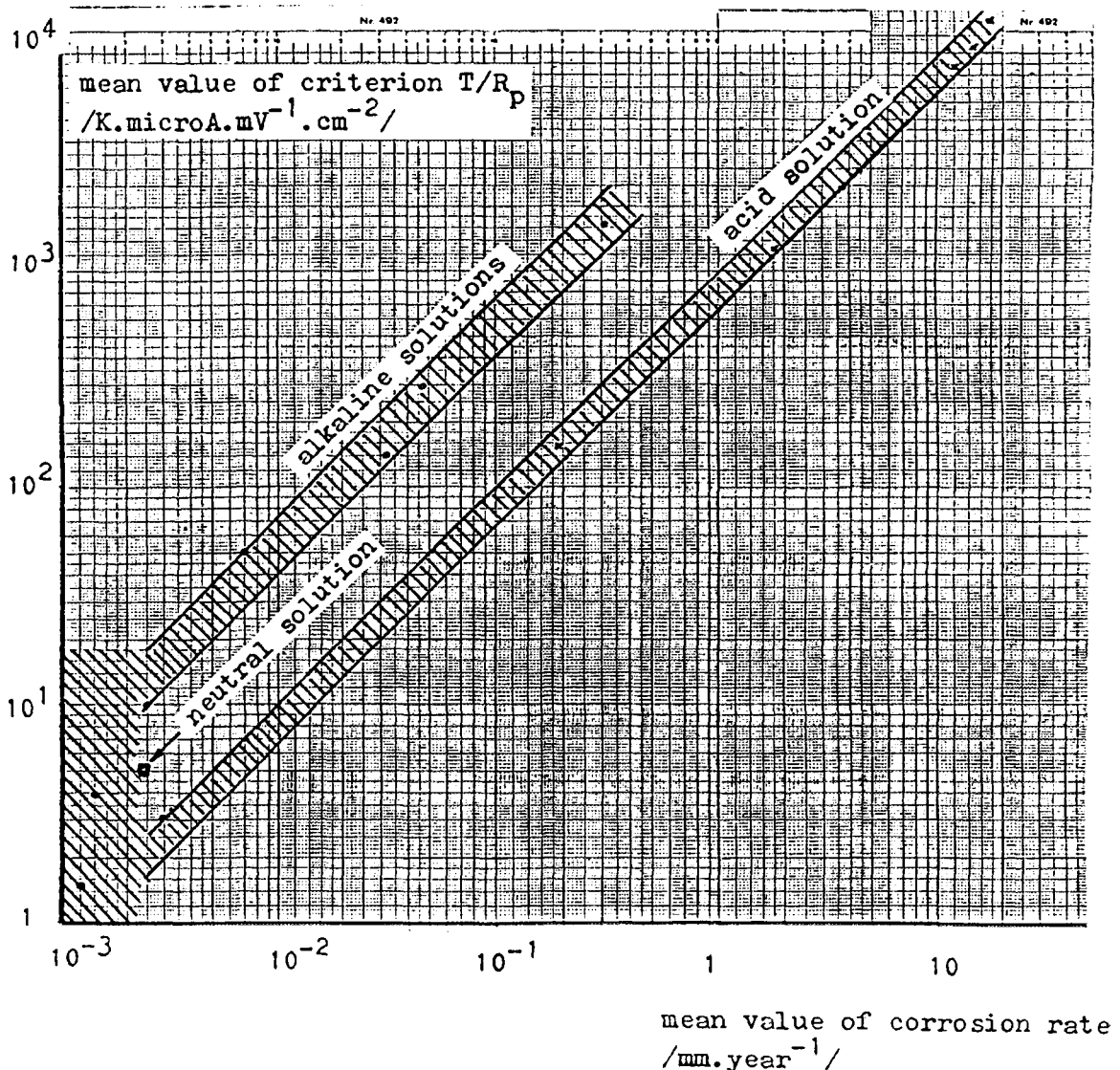


Fig.1

Conversion diagram for Zr-1%Nb and Zr-2.5%Nb alloys

$T/R_p$  value and mean corrosion rate, which was evaluated by gravimetric method. Hatched area marks the individual scatter zones for alkaline and acid solutions. Theoretical treatment /5/ shows that identical conversion diagram is valid for momentary  $T/R_p$  values as well.

Autoclave experiments with typical corrosion rate transients are listed in Tab.1. Intentionally have been chosen solutions with extremely low, medium and extremely high corrosion rates. Temperature in all experiments was predominantly kept near 300°C, occasional temperature irregularities were caused by obligatory restrictions of power consumption. Test period amounted several hundred hours. Experiments with low corrosion rates required longer test periods owing to the necessity of subsequent conventional gravimetric evaluation.

Fig.2 demonstrates temperature- and corrosion rate transients (at very low corrosion attack  $T/R_p$  transients) in boric acid partially neutralized by KOH + NH<sub>3</sub>, pH<sub>20</sub>=10.3. Initial peak of corrosion rate corresponds with temperature increase and reaches maximum value 0.02 mm.year<sup>-1</sup>. Afterwards corrosion rate decreased during 20 hours to negligible values out of the conversion diagram. Nevertheless, it is permanently possible to measure even lowest  $T/R_p$  values. Coincidence of corrosion rate ( $T/R_p$ ) fluctuations with temperature irregularities is observed in a similar way as in other experiments.

Fig.3 shows the transients in analogous solution but without ammonia. Initial peak in corrosion rate is similar to that obser-

TABLE 1. LIST OF AUTOCLAVE EXPERIMENTS

Test solution	Characteristic temperature /°C/	Test period /hours/
boric acid 12 g/l + KOH + NH <sub>3</sub> , pH <sub>20</sub> =10.3	300-318	1285
boric acid 12 g/l + KOH without NH <sub>3</sub> pH=10.3	310-328	840
KOH + NH <sub>3</sub> 40 mg/l pH=10.1	290	565
LiOH 3.5%	300	355

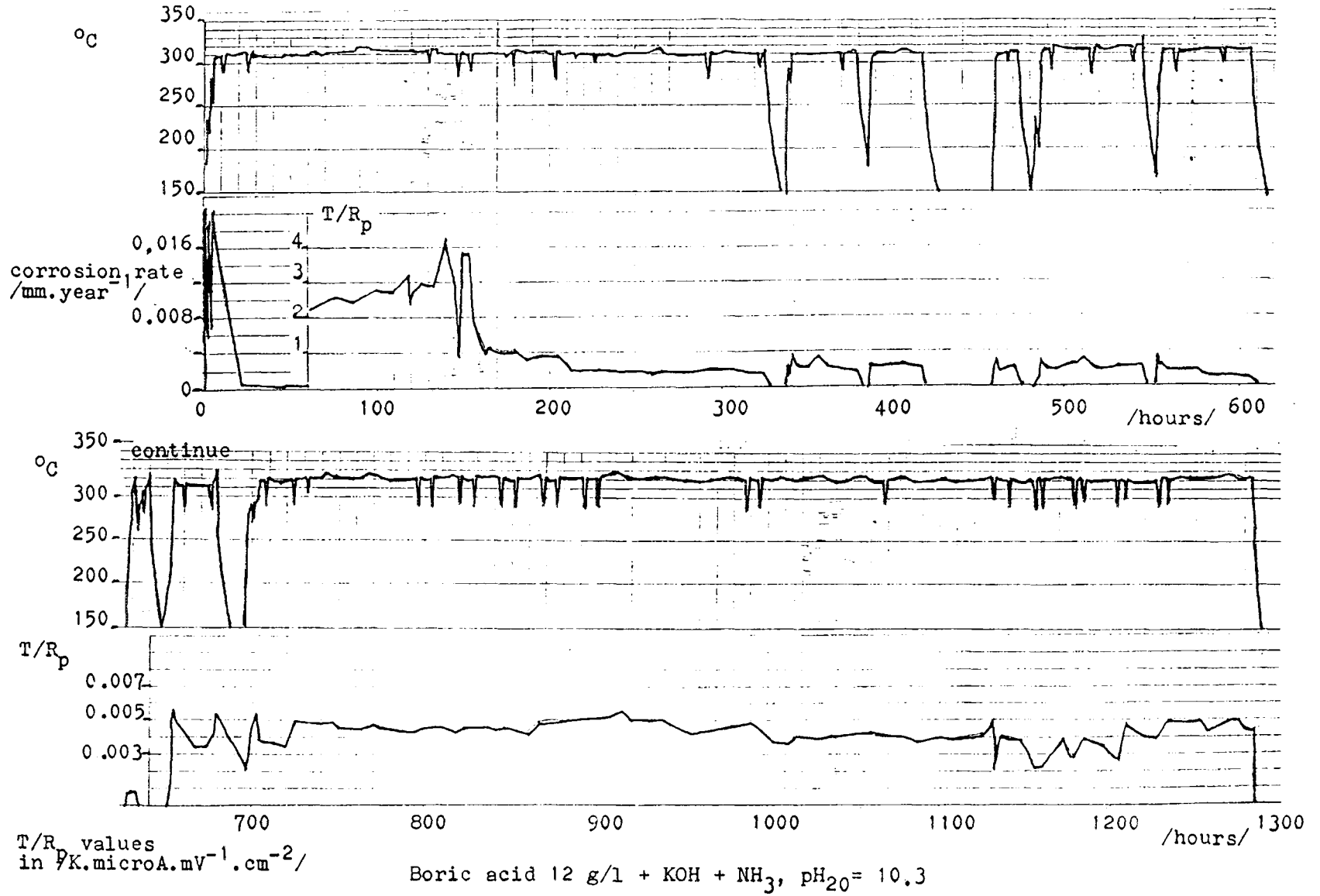
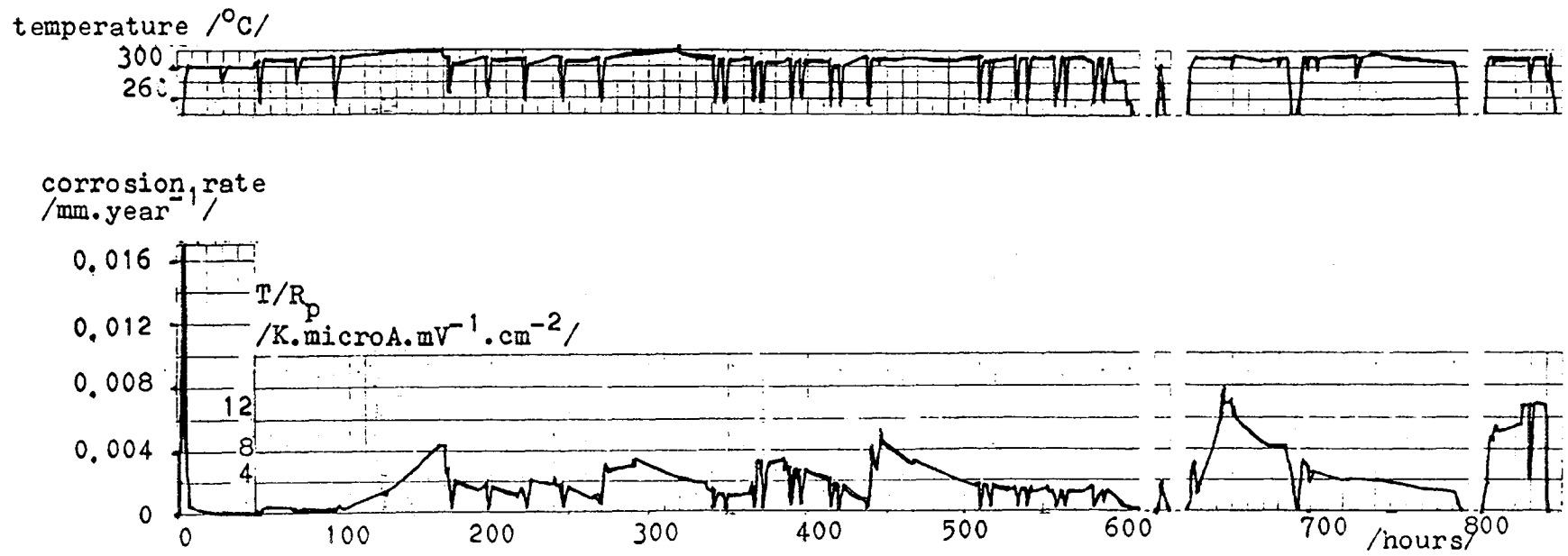


Fig.2



Boric acid 12 g/l + KOH, without ammonia,  $pH_{20} = 10.3$

Fig.3

ved previously. Coincidence of corrosion rate ( $T/R_p$ ) fluctuations with temperature irregularities is also expressed very distinctly. During the first 100 hours corrosion rate is extremely low. Subsequently,  $T/R_p$  values increases, remaining still out of the conversion diagram. Contrary to the experiment with ammonia,  $T/R_p$  values in this period are much higher.

Fig.4 presents corrosion rate transient in solution without boric acid, pH=10.1 being adjusted by KOH + NH<sub>3</sub>. Initial peak of corrosion rate is higher and subsequent decrease follows very slowly. Corrosion rate after 100 hours still amounts about 0.02 mm.year<sup>-1</sup> and after 550 hours 0.004 mm.year<sup>-1</sup>.

Corrosion rate transient during autoclave test in 3.5% LiOH shows Fig.5. Contrary to previous experiments, corrosion rate rapidly increases during initial heating to 0.2 mm.year<sup>-1</sup> and then

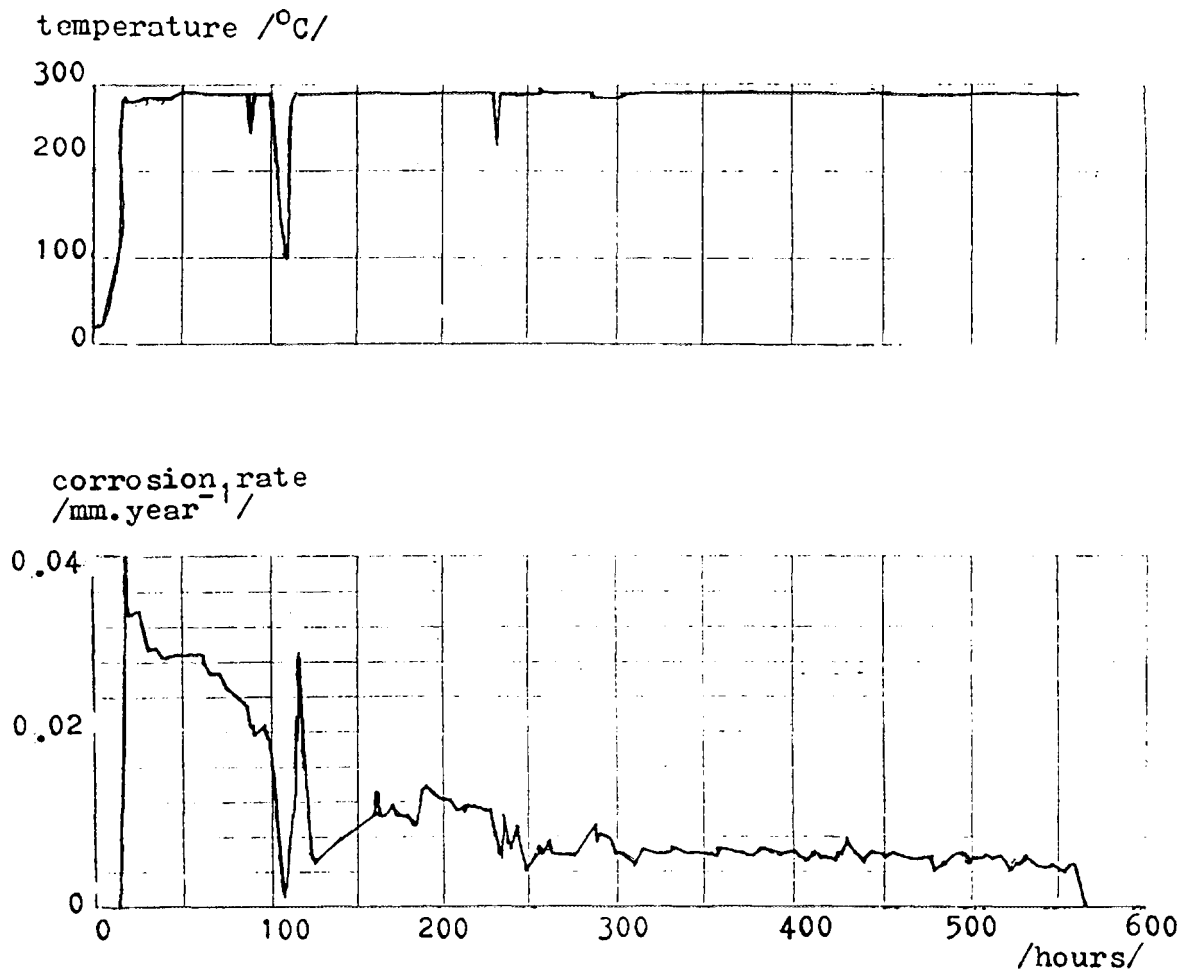


Fig.4

Ammonia 40 mg/l + KOH, pH<sub>20</sub> = 10.1,  
repeated autoclave corrosion test

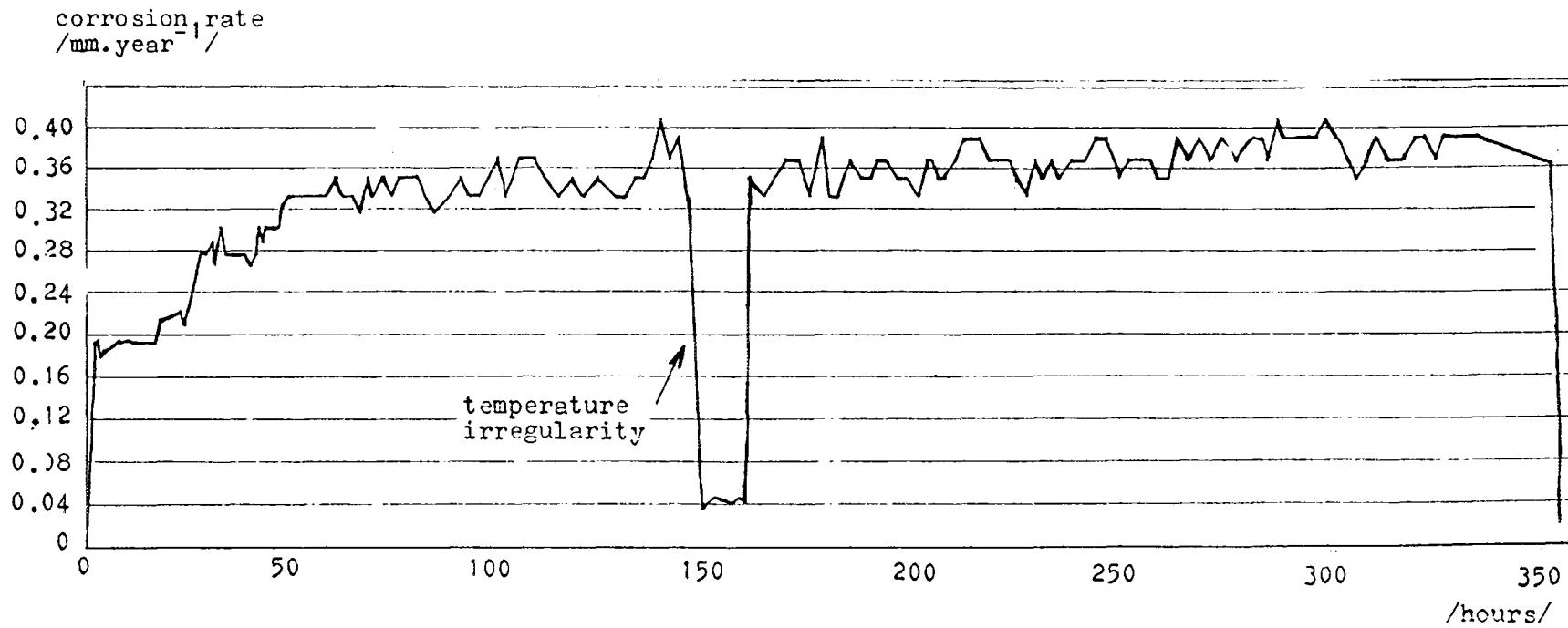


Fig.5

3.5 % LiOH solution, 300°C

follows gradual increase during 50 hours to  $0.3 \text{ mm}\cdot\text{year}^{-1}$ . Typical initial peak of corrosion rate is absent. Slight steady increase of corrosion rate continues till the end of experiment and reaches about  $0.4 \text{ mm}\cdot\text{year}^{-1}$ .

#### Conclusion

Corrosion rate transients of Zr-1%Nb alloy in various solutions obtained by  $T/R_p$  measurements reflected corrosion behaviour in agreement with logical expectation. Interpretation of very low  $T/R_p$  values out of the conversion diagram in terms of corrosion attack requires additional investigation.

#### REFERENCES

1. M.E.Indig and C.Groot: Electrochemical Measurement of Corrosion, Corrosion-NACE, Vol.26, No.5, May 1970
2. Progress Report on Reactor Materials and Fuel Elements, August 1, 1970 to August 31, 1971, AB Atoenergi Studsvik, Sweden
3. G.Östberg, H.P.Myers: Aspects of Swedish Studies of Cladding Materials for Water Cooled Reactors, 3rd United Nations International Conference, A/CONF 28/P/419, May 1964
4. Pressure-Tight Probe for On-Site Electrochemical Measurement, ŠKODA Concern, Nuclear Machinery Plant, Commercial Department, Prospectus
5. J.Beran: Contribution to the Theory of Polarization Resistance Method for Corrosion Testing of Metals, ŠKODA Works Plzeň, ZJE 259, 1982



## **SENSORS FOR ON-LINE MONITORING OF WATER CHEMISTRY PARAMETERS FOR NPP's**

P. AALTONEN, K. MÄKELÄ  
Technical Research Centre of Finland, Espoo,  
Finland

### **Abstract**

The on-line monitoring of the water chemistry parameters of aqueous solutions in nuclear power plants is considered essential to control corrosion phenomena. New sensors and electrodes that can be used under plant operating conditions are key components to the application of this technology. The research and development programs are running to develop practical instruments. The experimental capabilities available to research high temperature and pressure phenomena is growing rapidly. It is now possible to experimentally measure all information needed to make estimations and predictions concerning reactions taking place in the coolant of an operating reactor. However, further development of devices and practical experiences are needed to meet the requirement of power stations.

### **1. INTRODUCTION**

Corrosion phenomena, particularly stress corrosion cracking and corrosion fatigue, are caused by the interaction of environment, materials and stresses. Also general corrosion and erosion corrosion are controlled by the material selection and the chemical environment. Material selection is decided during plant design and thus it is not easily changed in an operating power plant. However, water chemistry can be modified even in operating plants or it can be adjusted to improve the reliability. Successful water chemistry control requires regular and continuous monitoring of such water chemistry parameters as dissolved oxygen content, pH, conductivity and impurity contents. Conventionally the monitoring is carried out at low pressures and temperatures, which, however, has some shortcomings because parameters such as pH, conductivity and redox potential are changing as a function of the temperature.

Electrodes designed for the on-line monitoring of water chemistry parameters at high temperatures and pressures can improve the knowledge of chemical

environment in power plants. This kind of electrodes have existed already several years, but the application in real power plants has not become popular. The plants need commercially available electrodes which are reliable for months and have zero or minimal maintenance.

The present status of electrodes design has improved reliability but at the same time new needs and applications has appeared for on-line monitoring. This paper describes the development and some of the latest applications of the on-line water chemistry monitoring electrodes.

## 2. WATER CHEMISTRY AT ELEVATED TEMPERATURE

In power plants extensive instrumentation and laboratory analysis programs are applied to provide rapid and reliable diagnosis of water chemistry. However, at present chemical monitoring is applied mainly in low temperature, low pressure conditions or by using grab samples. More relevant information concerning the chemical environment could be obtained by using high temperature, high pressure measurements at least for pH, conductivity and electrochemical potentials.

### 2.1 pH at high temperature

Temperature has a great influence on pH, i.e on the activity of hydrogen ions. Owing to the nature of pure water, pH usually shifts towards neutral values at higher temperatures. In general the pH of base solutions is lower and the pH of acidic solutions higher when temperature increases, Fig. 1. This neutralizing effect is caused by the interaction between the water and the dissolved species. The resulting pH of the solution is highly dependent on the buffering capacity of these dissolved species.

### 2.2 Conductivity at high temperature

The conductivity of pure water increases with temperature, Fig. 2. This is due partly to the dissociation of pure water itself and partly to the increase in dissolved impurities at higher temperatures. Additionally the deposition of



dissolved ions changes the conductivity of the solutions in sampling lines if the temperature decreases.

### 2.3 Redox potential and corrosion potentials at high temperature

The electrochemical i.e. corrosion potential of a metal is a measure of the equilibrium reaction obtained between the surface and the environment. Because most metals form some kind of oxide layer on their surface in water-containing solutions, the electrochemical potentials are mainly controlled by the oxygen content and the temperature of the environment, Fig. 3.

Redox potential of the water is a function of the oxidizing and reducing species in the environment and can be measured as a corrosion potential of noble metals which do not have corrosion reactions of their own.

### 3. REFERENCE ELECTRODES

The most important parameters that should be monitored in power plant heat transport circuits are the corrosion potential and pH. This is also because these

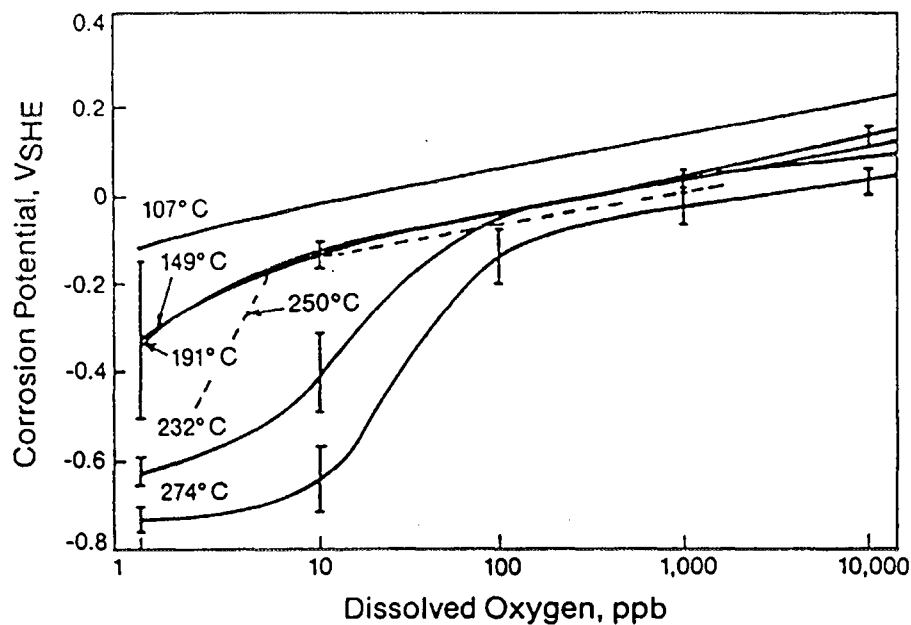


Figure 3. Corrosion potential as a function of oxygen concentrations at high temperatures [8].

two parameters define what corrosion processes are possible and hence provide a basis for interpreting the electrochemical reactions. The reference electrode must provide a potential that is independent of the composition of the environment and which can be placed on a viable thermodynamic scale. The electrode has to withstand the high temperatures and pressures, associated with heat-up and cool-down of the system. The most important characteristics of a reference electrode is that its potential must be related to a rational thermodynamic scale (e.g., the standard hydrogen electrode (SHE) scale), either by calculation or by direct calibration [4]. The reference electrodes that have been used in high temperature aqueous systems are external reference electrodes, or internal reference electrodes.

### **3.1 External Reference Electrodes**

Macdonald, Scott and Wentrcek introduced in 1981 [5] a pressure balanced reference electrode in an attempt to produce a highly stable reference electrode for high temperature aqueous systems. A typical design is shown in Fig. 4. In this type of electrodes some parts fabricated from PTFE (polytetrafluoroethylene) are exposed to the high temperature aqueous environment which limits the maximum operation temperature. However, by employing alternate materials, reference electrodes have been developed that can operate under supercritical conditions ( $T > 374\text{ }^{\circ}\text{C}$ ).

### **3.2 Internal Reference Electrodes**

For highly accurate measurements, internal reference electrodes are preferred. Compared with external reference electrodes the internal reference electrodes are more accurate due to the lack of thermal liquid junction potentials. However, external reference electrodes offer considerable advantages in terms of long term stability and are ideally suited for measuring potentials in the systems where moderate accuracy is acceptable. The drawback of internal electrodes based on the Ag/AgCl electroactive element is thermal hydrolysis of AgCl, which generates a mixed potential rather than an equilibrium potentials as well as changing the chloride activity.

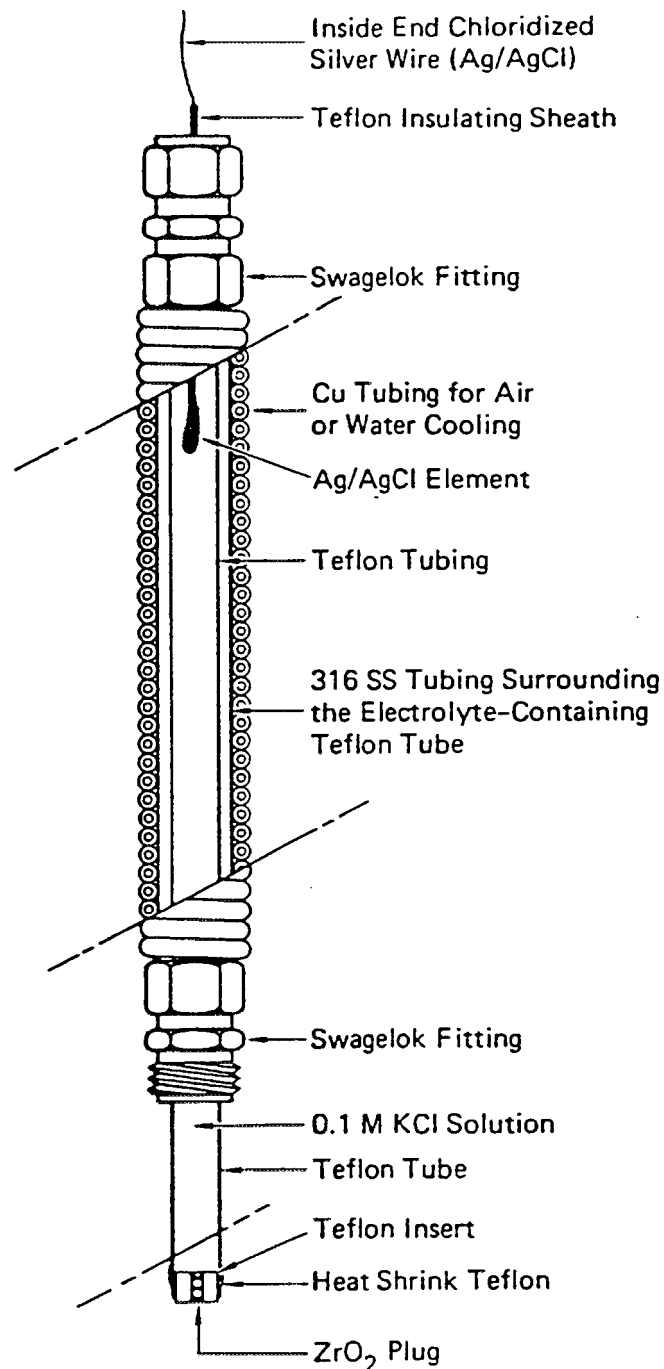


Figure 4. External pressure balanced reference electrode assembly [4].

### 3.3 Cathodically charged Pd electrode

One version of palladium hydrogen electrode is palladium-hydride electrode. The work of Macdonald and co-workers on palladium-hydride electrodes indicated that this system exhibits Nernstian responses up to 275 °C in various boric acid/lithium hydroxide buffer solutions [6]. However, the lifetime of the potential plateau

for palladium-hydride electrode was found to decrease with increasing temperature and therefore the electrode system could not be used for long term measurements. Research conducted at the Technical Research Centre of Finland (VTT) has shown that continuously cathodically charged palladium can operate as a reliable reference electrode for long periods at temperatures up to 360 °C, Fig. 5. The design consisted of a Pd rod which was placed inside of a sintered high purity platinum tube to minimize the effects of flow rate variations. Pd was chosen for hydrogen electrode because Pd potential is less sensitive to oxygen. Porous platinum tube around the Pd was also used to create large surface area for trace oxygen in the solution to react on. The test showed that the electrode was stable and that there was no junction potential at the electrode/water interfaces.

### 3.4 Pd membrane electrodes based on hydrogen diffusion

An other way to overcome the problem of unstable potential plateau is to use a palladium membrane as an electrode with suitable hydrogen partial pressure on the dry side to maintain the Pd/H ratio at the wet surface. In a membrane electrode based on a 75% palladium-25% silver alloy the electrode potential is controlled by the activity of the hydrogen ions and of the dissolved hydrogen in the vicinity of the electrode surface. The dissolved hydrogen activity is a function

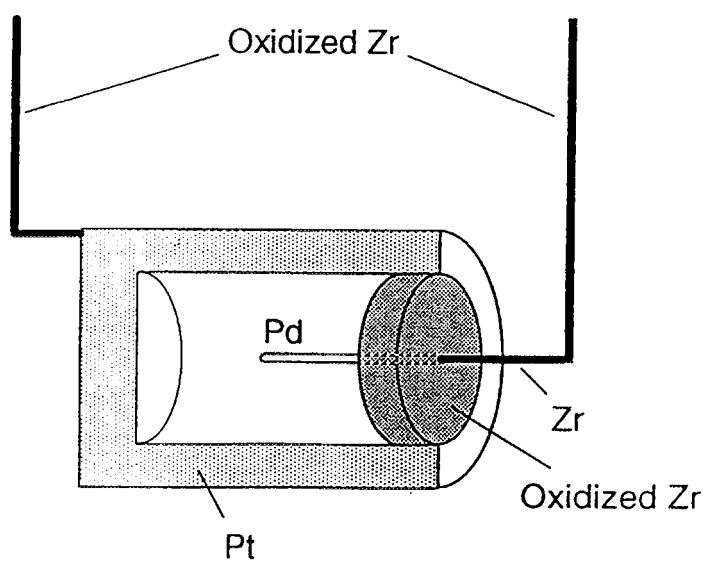


Figure 5. VTT Pd electrode.

of the hydrogen activity in the gas phase on the dry side of the membrane and the diffusion rate of the hydrogen through the membrane and into the solution [7]. For the ideal operation of the electrode, it is required that the diffusion rate through the membrane be much faster than that in the solution. The electrode design is shown in Fig. 6. This type of sensor results in a complex electrode and system design but the electrode is a suitable reference electrode for fast transient measurements.

#### 4. CONDUCTIVITY ELECTRODES

Conductivity can be easily measured at high temperatures by the conventional electrode design based on the impedance measurements. The advantage obtained by measuring conductivity at high temperature is the increased sensitivity. Additionally, the specific conductances of ions are temperature dependent, thus the conductivity is also changing with temperature, Fig. 7. The high temperature conductivities can be estimated by using different mathematical models, but accuracy of these model is a problem. Therefore to have a clear picture of the monitored environment high temperature conductivity sensors should be used.

#### 5. pH ELECTRODES

Over the past decade, considerable interest has arisen in using oxide ion-conducting ceramic membrane electrodes based on yttria stabilized zirconia to

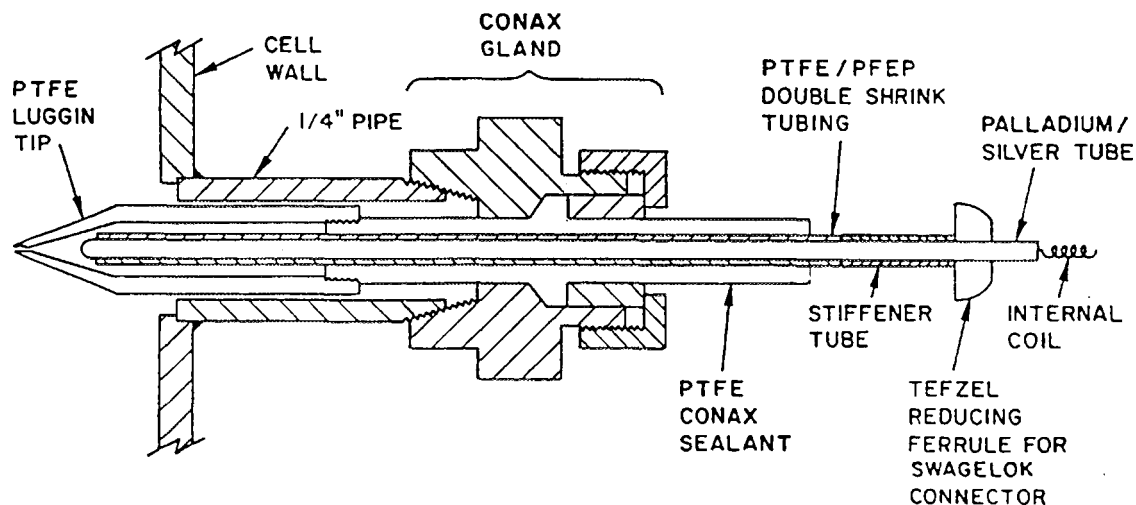


Figure 6. Palladium/Silver membrane electrode [7].

Limiting ionic conductances ( $S\text{ cm}^2\text{ eq}^{-1}$ )

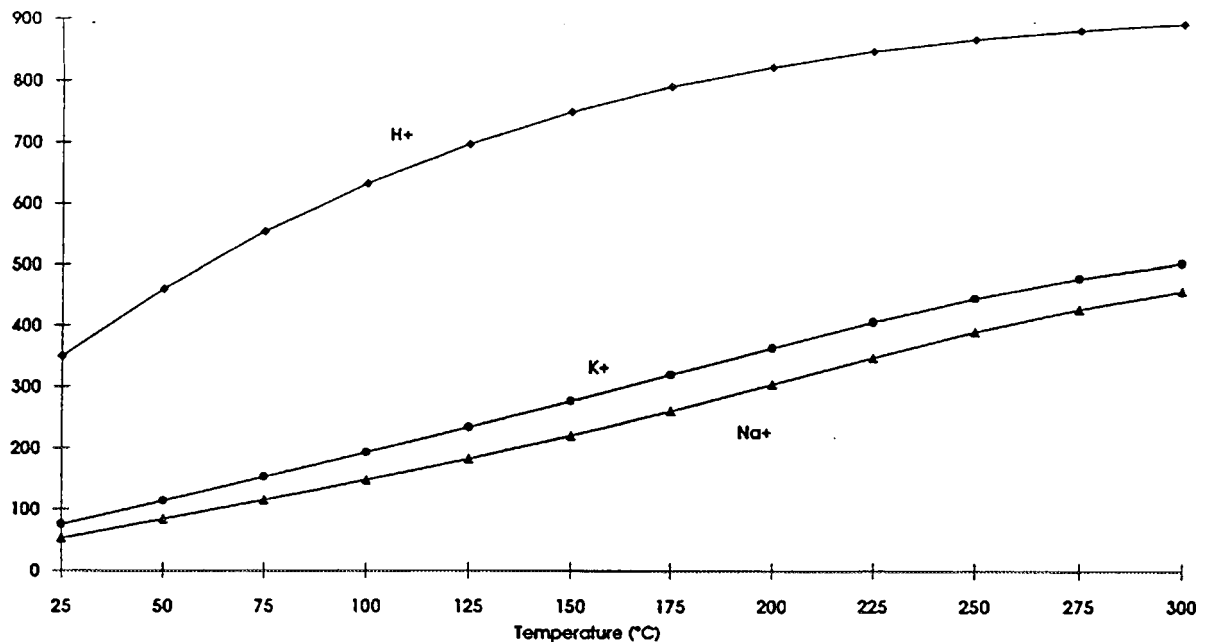


Figure 7. Limiting ionic conductances of the  $H^+$ ,  $Na^+$  and  $K^+$  as a function of temperature [8].

measure pH in high temperature aqueous systems. The most popular of these devices employs a metal/metal oxide internal reference element to fix the activity of oxygen vacancies on the inside surface of the ceramic membrane. The design of the  $Ni/NiO/ZrO_2(Y_2O_3)$  sensor currently being used at VTT is shown in Fig. 8. However, the liquid junction potential of the reference electrode can be significant under certain conditions causing as large as 1 unit of pH error.

## 6. OXYGEN MONITORING

No commercial instrument exists capable of measuring oxygen directly in high temperature water. However, experimental sensors has been used to determine the oxygen concentration in both steam and liquid phases [4]. Also the differences in the kinetics of electrochemical reactions on noble metal electrodes has been used to study the oxidizing power and decomposition of  $H_2O_2$  at high temperatures at VTT.

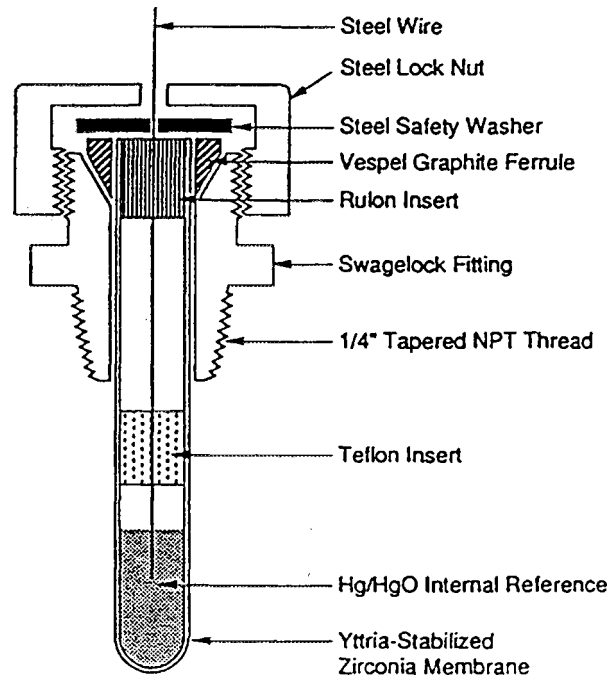


Figure 8. pH electrode design [1].

## 7. SUMMARY AND CONCLUSIONS

This paper described the use and status of reference electrodes, the pH sensor, the conductivity electrodes and an oxygen monitor for the on-line monitoring of water chemistry parameters in high temperature aqueous systems.

- External reference electrodes in present state can be used for monitoring electrochemical potentials over a wide range of temperature and pressure.
- Internal reference electrodes need further testing to provide needed stability for long term in core potential measurements.
- The pH sensors is a convenient and reliable device for measuring pH in both subcritical and supercritical aqueous systems. However, pH measurements requires a stable reference electrode.
- Conductivity electrodes already now fulfill the requirements for plant conductivity measurement.
- The oxygen sensors can be used to measure oxygen concentration, but further development is needed.

## REFERENCES

- [1] MÄKELÄ, K., HETTIARACHCHI, S. and MACDONALD, D. D., The importance of on-line pH measurements to control corrosion of materials in water and steam, p. 3-2. Proceedings of International Conference on Interaction of Iron Based Materials with Water and Steam, June 3 - 5, 1992, Heidelberg, Germany.
- [2] COHEN, P., Water coolant technology of power reactors, p. 57. Gordon and Breach Science Publishers, NY 1969.
- [3] COHEN, P., The ASME Handbook on Water Technology for Thermal Power Systems, p. 872. The American Society of Mechanical Engineers, NY 10017, 1989.
- [4] MACDONALD, D. D. et al., Development of sensors for in-situ monitoring of corrosion and water chemistry parameters for the electric power utility industry. Proceedings of 12th International Corrosion Congress, p. 4274 - 4285, Houston, USA, 1993.
- [5] MACDONALD, D. D., SCOTT, A. C. and WENTRCEK, P. R., J. Electrochem. Soc. 126 (1979), p. 908.
- [6] MACDONALD, D. D., WENTRCEK, P. R. and SCOTT, A. C., The measurement of pH in aqueous systems at elevated temperatures using palladium hydride electrodes. J. Electrochem. Soc., p. 1745-51, 8 (vol. 127), August 1980.
- [7] NAGY, Z. and YONCO, R. M. Environmental Degradation of Materials in Nuclear Power Systems - Water Reactors, p. 157 - 164, The Metallurgical Society, 1988.
- [8] COHEN, P., The ASME Handbook on Water Technology for Thermal Power Systems, p. 582. The American Society of Mechanical Engineers, NY 10017, 1989.



**OPERATIONAL EXPERIENCE OF WATER QUALITY  
IMPROVEMENT ACCOMPANIED BY MONITORING  
WITH ON-LINE ION CHROMATOGRAPH**

M. KOBAYASHI, K. MAEDA  
Toshiba Corporation, Yokohama

H. HASHIMOTO, T. ISHIBE  
Chubu Electric Power Co., Inc.,  
Nagoya

N. USUI  
Hitachi Engineering Co., Ltd,  
Hitachi

K. OSUMI  
Hitachi Limited,  
Hitachi

K. ISHIGURE  
University of Tokyo,  
Tokyo

Japan

**Abstract**

Hamaoka Unit NO.1 (BWR 540 MWe) of Chubu Electric Power Company, Inc. had experienced fuel failures caused by fuel cladding corrosion at the cycle 11 in 1990. This cladding corrosion was considered to be caused by a combination of cladding material susceptibility to corrosion and anomalous reactor water quality. Based on the intensive investigations on the causes of anomalous reactor water quality, several countermeasures were proposed to improve the reactor water quality for the subsequent cycles operation. As the results of countermeasures, reactor water quality of Hamaoka Unit No.1 in the cycle 12 became much better than that of any other previous cycles and neither failure nor accelerated corrosion was found in the subsequent annual inspection. As one of the countermeasures for water quality improvement, an on-line ion chromatograph has been installed on Hamaoka Unit No.1 to reinforce reactor water quality monitoring, that has enabled us to identify ion species in reactor water and to evaluate reactor water behavior in detail.

## 1. Introduction

BWR plant is designed and operated to keep reactor water in high pure quality for plant reliability, that is, to restrain corrosion damage of plant component materials, radiation build-up and so on.

Hamaoka Unit No.1 (BWR 540 MWe) of Chubu Electric Power Company, Inc., however, had experienced fuel failures caused by fuel cladding corrosion at the cycle 11 in 1990. This cladding corrosion was considered to be caused by a combination of cladding material susceptibility to corrosion and such anomalous reactor water quality as described below;

- (1) reactor water conductivity spikes at reactor start-up period, and
- (2) high sodium concentration in reactor water during normal operation resulted in reactor water conductivity spikes at reactor shutdown period.

Generally, ion impurities give impact against reactor water quality and they are usually brought from feedwater. Ion impurities in feedwater, however, are in very low concentration and cannot usually be detected. Therefore, in order to evaluate behavior of reactor water, it is very important that not only ion impurities in reactor water should be directly measured but also organic compounds called TOC in feedwater, which decompose to ion impurities in reactor water, should be measured.

The present report describes operational experience of water quality improvement for Hamaoka Unit No.1 accompanied by monitoring with an on-line ion chromatograph.

## 2. Causes of Anomalous Reactor Water Quality

### 2.1 Reactor Water Conductivity Spikes at Reactor Start-up

Hamaoka Unit No.1 experienced two times of reactor water conductivity spikes reaching 1.0–1.2  $\mu\text{S}/\text{cm}$  at reactor start-ups of the cycles 9 and 11 as shown in Fig.1. It was estimated that these spikes were caused by ionic impurities such as sulfate and nitrate which were produced from decomposition of organic impurities such as benzenesulfonic acid and trimethylamine called TOC in feedwater by heat and radiation.[1][2]

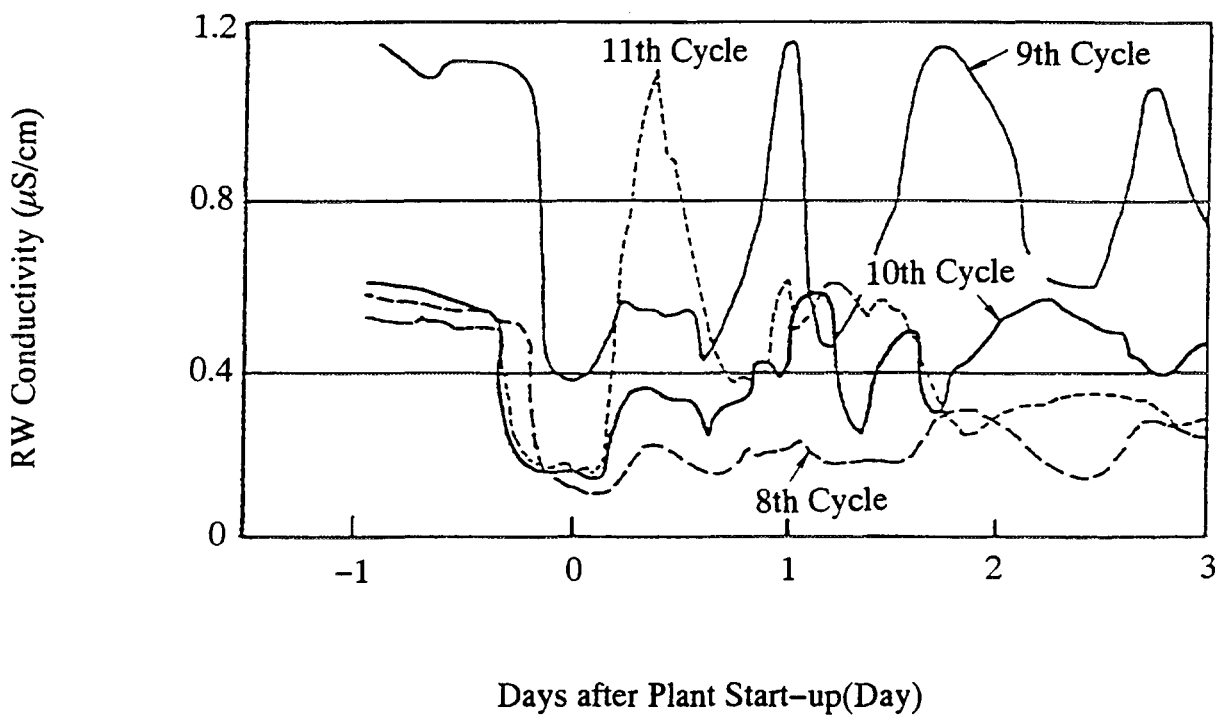
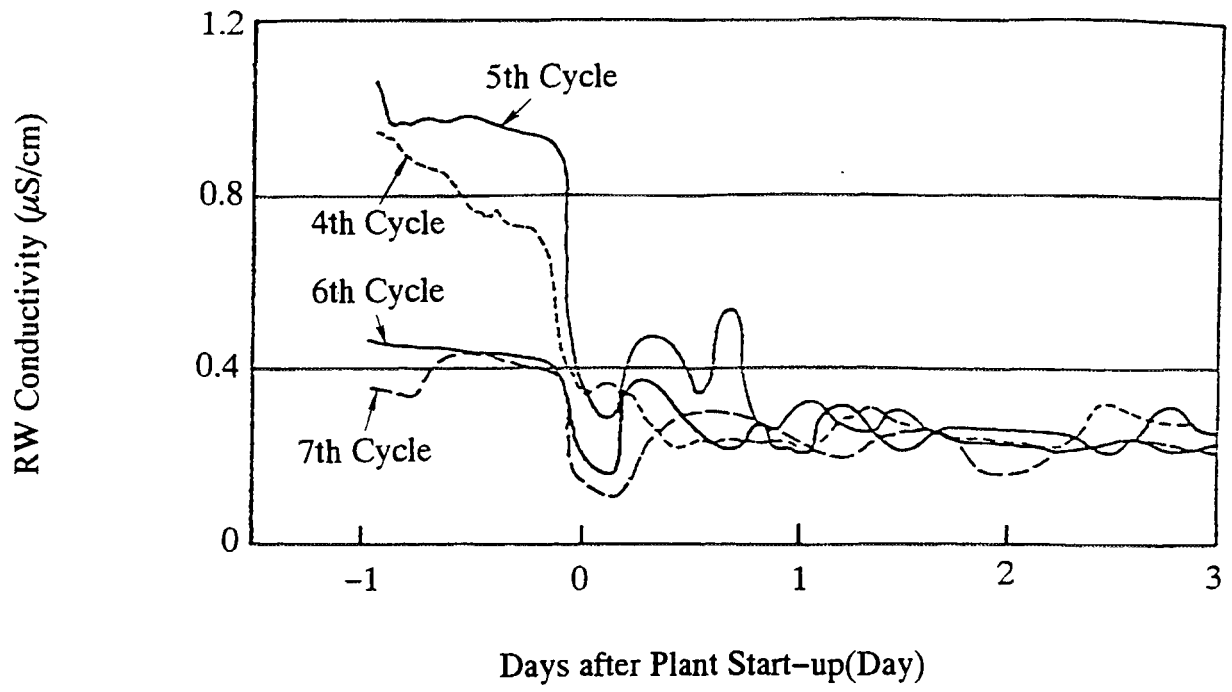


Fig.1 Reactor Water Conductivity at Start-up of Hamaoka Unit No.1

## 2.2 High Sodium (Na<sup>+</sup>) Concentration in Reactor Water during Normal Operation

Concentration of Na<sup>+</sup> in reactor water during normal operation had been about 15 ppb through 4 cycles when the corroded fuels had been loaded. These Na<sup>+</sup> concentrations were higher than that in other Japanese BWRs. Water quality pH had been 7.7 during these cycles, and was also comparatively high because of higher Na<sup>+</sup>. Inflow of Na<sup>+</sup> to reactor was caused from Na<sup>+</sup> dissolution out of condensate demineralizer (CD) resin which had captured Na<sup>+</sup> by reverse chemical regeneration. That is, at the time of chemical regeneration for CD resin, cation resin which was not completely separated from anion resin was regenerated by NaOH instead of proper chemical, H<sub>2</sub>SO<sub>4</sub>.

## 2.3 Reactor Water Conductivity Spikes at Reactor Shutdown

Hamaoka Unit No.1 experienced two times of reactor water conductivity spikes reaching about 0.9 μS/cm at reactor shutdown of the cycles 10 and 11 as shown in Fig.2. Fairly big peaks of Na<sup>+</sup> and SO<sub>4</sub><sup>2-</sup> were detected at reactor shutdown of the cycles 10. These ions were thought to be dissolved from Na<sub>2</sub>SO<sub>4</sub> which had concentrated in the oxide layer on the corroded fuel cladding surface.

# 3. Countermeasures for Reactor Water Quality Improvement

## 3.1 Countermeasures against Reactor Water Conductivity Spikes at Reactor

### Start-up

### 3.1.1 Countermeasures of TOC Reduction in the Primary Water

#### (1) Removal of TOC from the primary water

Usually, CD resin is kept in CD tanks filled up with condensate water until plant start-up from CD isolation at the end of cycle. Therefore, CD tanks result in containing high TOC leached from CD resin, which causes conductivity spikes at reactor start-up. These TOC were drained just before CD inserviced in to condensate system prior to reactor start-up.

#### (2) TOC generation reduction

Furthermore, for reduction of TOC generation and accumulation in CD tanks, CD tanks were inserviced to condensate system during flushing operation after vacuum-up of main condenser prior to reactor start-up.

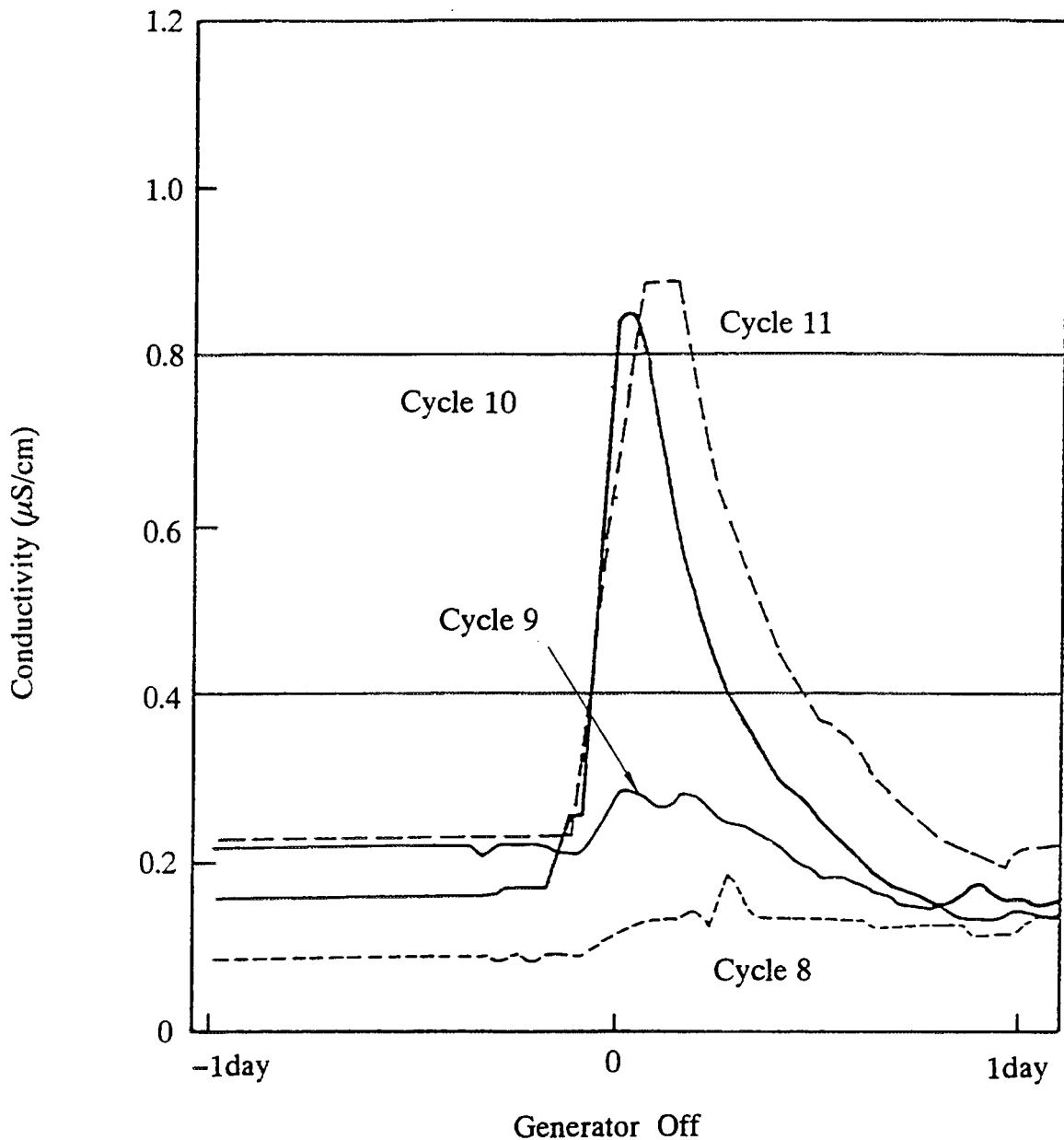


Fig.2 Reactor Water Conductivity at Shutdown of Hamaoka Unit No.1

### (3) TOC decomposition

TOC in feedwater can be decomposed by gamma ray emitted from reloaded fuels even before reactor heat-up, and decomposition products can be removed by reactor clean-up (RWCU) system. Feedwater, therefore, was positively fed into reactor through control rod driving system(CRD) as cooling water before reactor start-up.

### 3.1.2 Countermeasures of TOC Input Reduction to Reactor

For input reduction of a large amount of ion impurities produced from TOC, feedwater flow rate was controlled during start-up period described below.

- a) Keeping reactor power at 10 Kg/cm<sup>2</sup> of reactor pressure for several hours.
- b) Restriction of a degree of opening of turbine bypass valve (T.B.V.).

### 3.1.3 Improvement of Decontamination Factor(DF) of RWCU for Ion Impurities

#### Removal in Reactor Water

For improvement of DF of RWCU for ion impurities removal in reactor water, back-washed RWCU was inserviced after vacuum-up of system to avoid reduction of ion capacity caused from capturing H<sub>2</sub>CO<sub>3</sub>.

### 3.2 Countermeasures against Reactor Water Na<sup>+</sup> Concentration

For Hamaoka Unit No.1, CD resin contaminated with Na<sup>+</sup> was exchanged to new resin.

### 3.3 Reinforcement of Water Quality Control

Based on the observed correlation between feedwater TOC concentration before reactor start-up and reactor water conductivity spikes at reactor start-up, temporary water quality criteria has been established for feedwater TOC concentration before reactor start-up and reactor water conductivity at reactor start-up as shown in Table 1. Furthermore, an on-line ion chromatograph for reactor water and an on-line TOC detector for feedwater have been installed in Hamaoka Unit No.1 to reinforce water quality monitoring for the first time in Japanese BWR plants.

The configuration of the on-line ion chromatograph is shown in Fig.3. Sample water is passed through a sample cooler and a pressure regulator in order to adjust the temperature and the pressure. Then, the sample water is passed through 1 $\mu$ m and 0.2 $\mu$ m filters to remove crud. After ion impurities in the sample water are concentrated in a concentrator column, the sample water is led into a separator column with eluting solution. The ion impurities chromatographically separated from the separator column are measured by a conductivity meter. The

Table 1 Temporary Criteria of Water Chemistry

Item	Temporary Criteria		Current Criteria	
	Target Value	Limit	Limit	Maximum Limit
1. REACTOR WATER				
(1) Normal Operation				
Na <sup>+</sup> (ppb)	7	15	-	-
pH	6.3-7.3	5.6-8.6	5.6-8.6	4.0-10.0
(2) Start-up				
Conductivity ( $\mu$ S/cm)	0.6	1	-	10
(3) Before Start-up				
TOC (ppb)	100	-	-	-
2. FEEDWATER				
(1) Before Start-up				
TOC (ppb)	150	-	-	-

data are recorded as a digital number, trend graph and so on. A waste fluid is disposed after the pH control by an ion exchange column.

#### 4. Water Quality after The Countermeasures

##### 4.1 Water Quality Experiences in Normal Operation

Good experiences of water quality in normal operation after the countermeasures are shown in Table 2 about the recent 3 cycles of Hamaoka Unit No.1 including 1 cycle before the countermeasures. Na<sup>+</sup> concentrations, pH

and conductivities in Hamaoka Unit No.1 reactor water have become less than 1 ppb from 17 ppb, 7.0 from 7.7 and 0.08  $\mu\text{S}/\text{cm}$  from 0.20  $\mu\text{S}/\text{cm}$ , respectively.

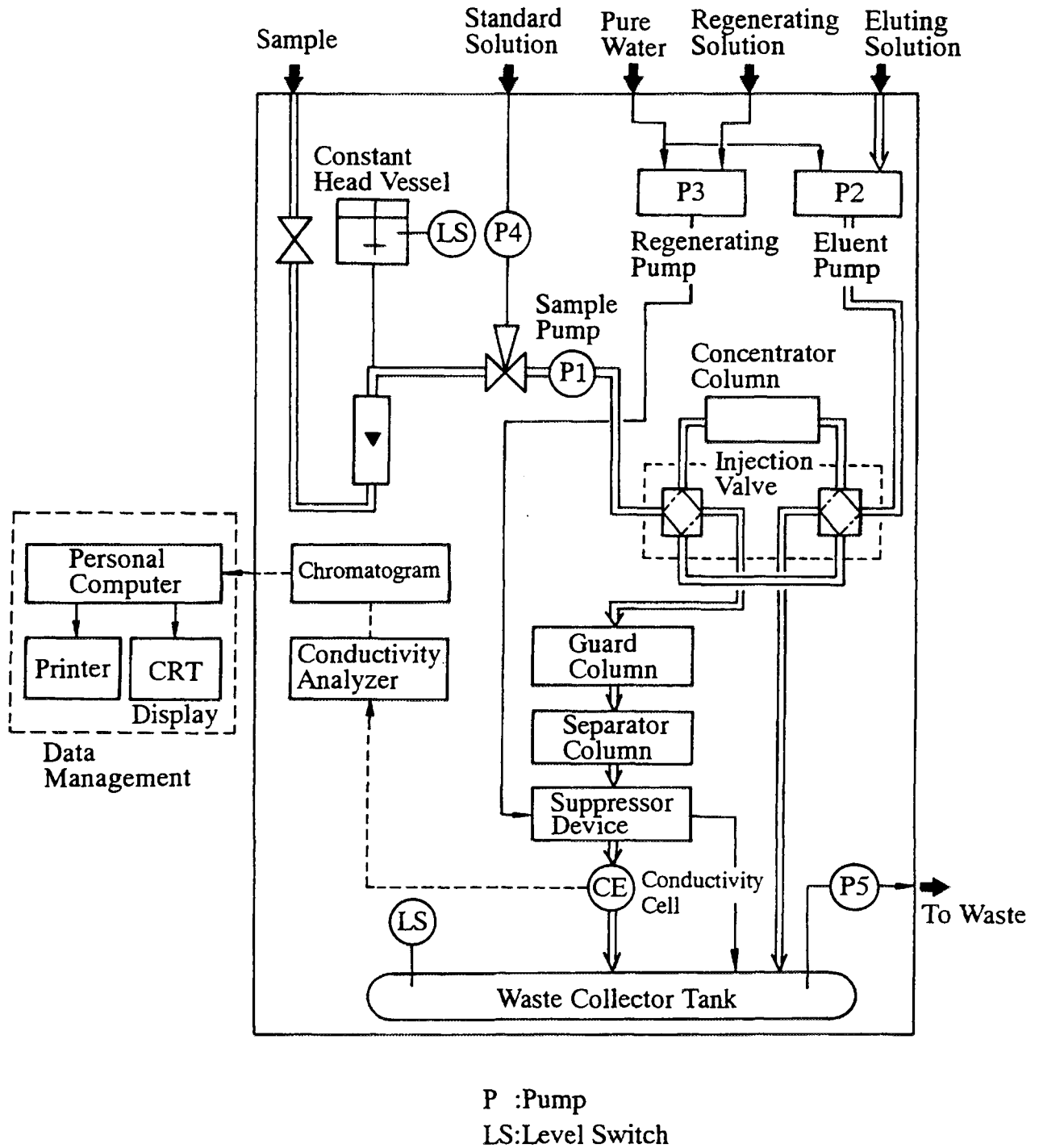


Fig.3 Flow Diagram for On-line Ion Chromatograph System

Table 2 Main Reactor Water Quality of Hamaoka Unit No.1

Item	Cycle	11* (89/9-90/6)	12 (91/7-92/2)	13 (92/7-93/2)
Conductivity( $\mu\text{S}/\text{cm}$ )	(250)	0.20	0.11	0.08
pH	(250)	7.7	6.9	7.0
Sodium ( $\text{Na}^+$ )	(ppb)	17	<1	<1
Chloride ( $\text{Cl}^-$ )	(ppb)	2	2	<1
Nitrate ( $\text{NO}_3^-$ )	(ppb)	6	5	2
Sulfate ( $\text{SO}_4^{2-}$ )	(ppb)	1	1	1

\*: Data Before Countermeasures

## 4.2 Water Experiences at Start-Up Operation

### 4.2.1 TOC Concentration

Countermeasures for TOC reduction before start-up has satisfied temporary criteria for TOC concentrations of feedwater and reactor water, that is 150 ppb and 100 ppb, respectively, as shown in Fig.4. These data show descending curves to verify effectiveness of the countermeasures for TOC reduction.

### 4.2.2 Reactor Water Quality

As another temporary criteria at reactor start-up,  $0.6\mu\text{S}/\text{cm}$  has been established for reactor water conductivity.

Reactor water conductivity is easily changed during reactor start-up.[3] It increases with reactor water temperature and feedwater flow. Hamaoka Unit No.1 has satisfied the temporary conductivity criteria after countermeasures against conductivity spikes in reactor water at start-up. As an example, reactor water conductivity of Hamaoka Unit No.1 during start-up at the cycle 13 is shown in Fig.5.

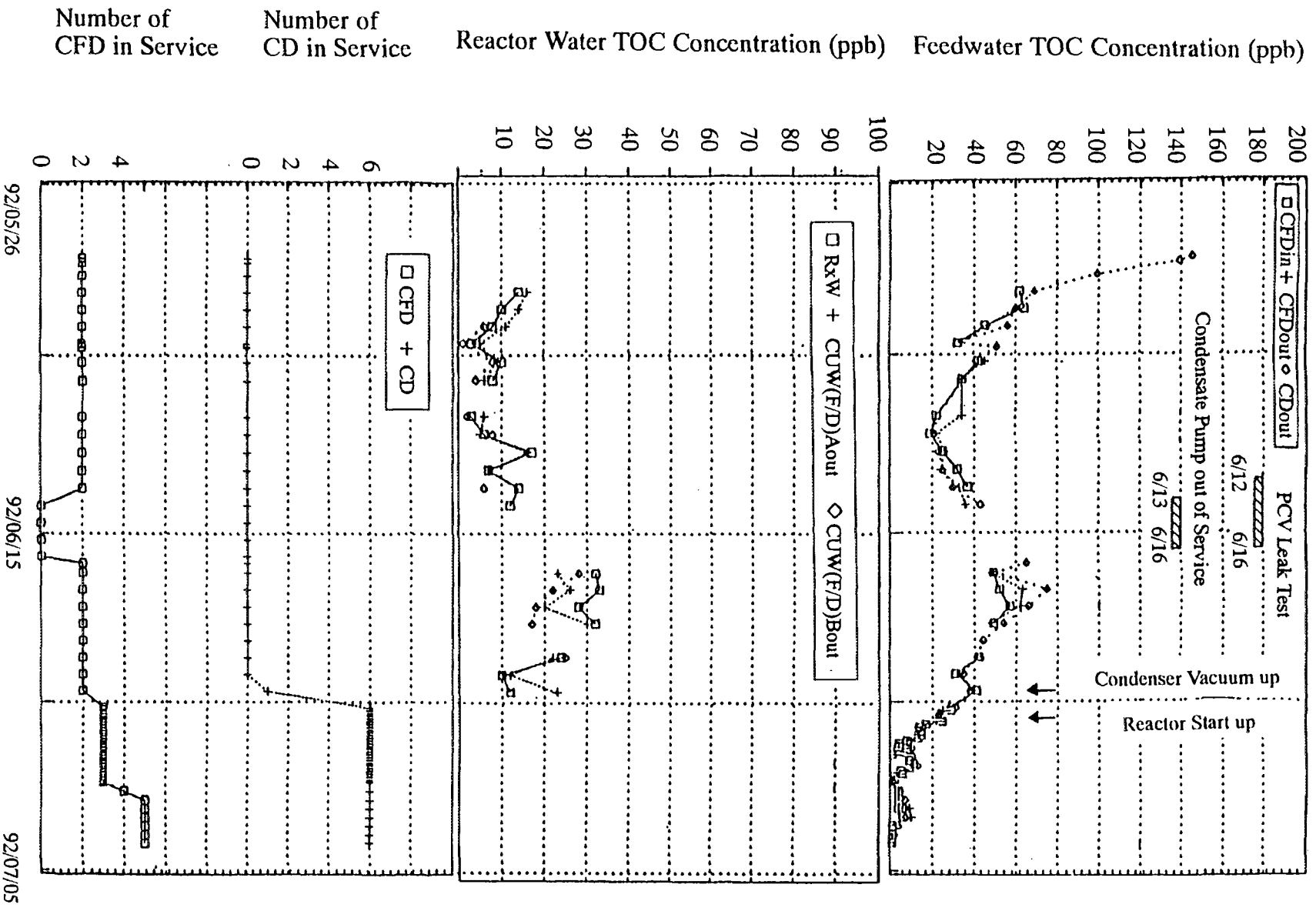


Fig.4 Hamaoka Unit No.1 TOC Concentration in Primary Water  
(before the Cycle 13 Start-up)

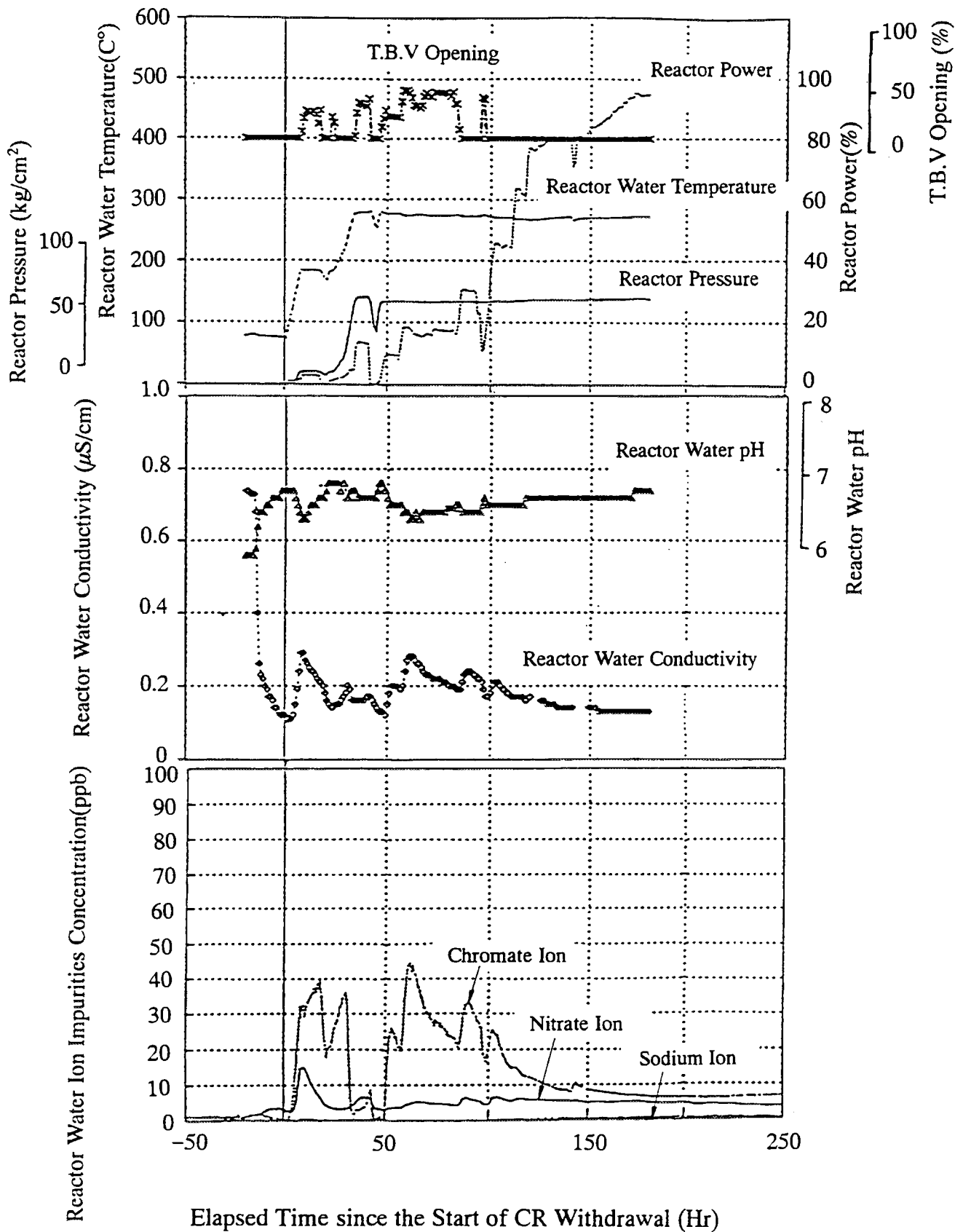


Fig.5 Hamaoka Unit No.1 Reactor Water Chemistry  
(at the Cycle 13 Start-up)

Reactor water has been monitored continuously by on-line ion chromatography since 1991 at Hamaoka Unit No.1. Reactor water conductivities showed small peaks of up to about  $0.3 \mu\text{S}/\text{cm}$  at the beginning of control rod (CR) withdrawal. These small peaks were caused by chromate ion, not by nitrate ion which had caused big peaks of about  $1.0\text{--}1.2\mu\text{S}/\text{cm}$  before countermeasures against conductivity spikes.

As shown in Figs.5 and 6, very detailed data of reactor water quality were obtained during not only reactor normal operation but start-up operation. Fig.5 shows that chromate ion changed rapidly with the start-up of plant operation. But chromate ion decreased gradually with plant power-up. A part of chromate ion must be dissolved from oxide films of stainless steel components. Fig.6 shows that reactor water conductivity decreased gradually from  $0.15\mu\text{S}/\text{cm}$  to  $0.1\mu\text{S}/\text{cm}$  and pH changed from slightly acidic to neutral. It also shows that sulfate, sodium and chloride ions were at the stable and very low level, whereas nitrate and chromate ions decreased gradually.

It was confirmed in Hamaoka Unit No.1 that the values of conductivity calculated from ion species obtained by on-line ion chromatography and actual pH data agreed very closely with measured conductivities by on-line monitor as shown in Figs.7 and 8.

## 5. Conclusion

Our results described below were obtained from the operational experience of water quality improvement for Hamaoka Unit No.1.

- (1) Countermeasures to reduce of TOC concentration in primary water before reactor start-up were effective to suppress reactor water conductivity spikes at reactor start-up.
- (2) Reduction of  $\text{Na}^+$  concentration in reactor water was achieved by exchanging CD resin with new one, and it resulted in high pure reactor water quality during normal operation.
- (3) It became possible to identify ion species in reactor water by monitoring with on-line ion chromatograph, and it was verified that on-line ion chromatograph was very effective to evaluate reactor water behavior in detail.

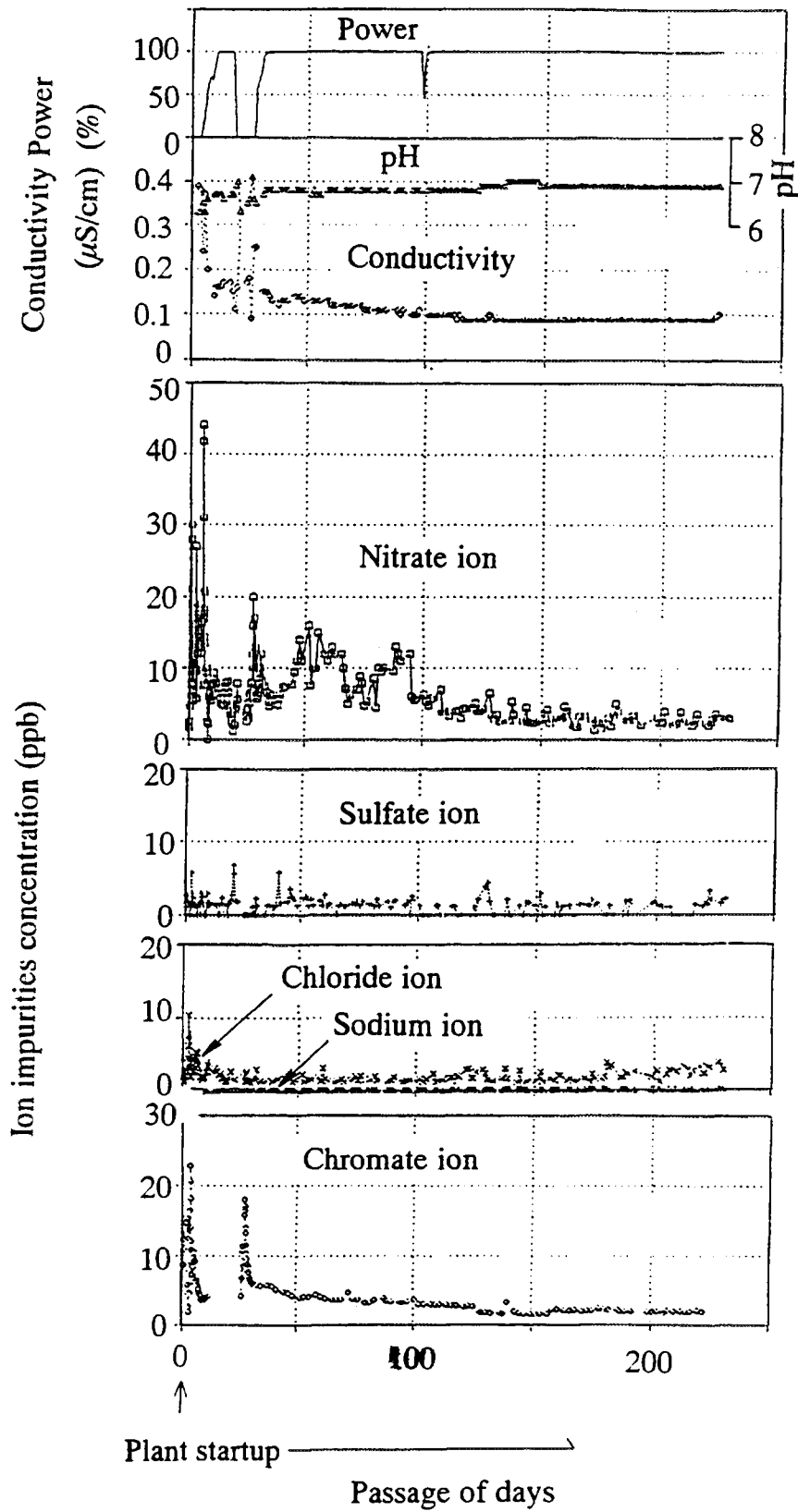


Fig.6 The Reactor Water Quality Trend during the Normal Operation in Hamaoka Unit No.1 (at the cycle 12)

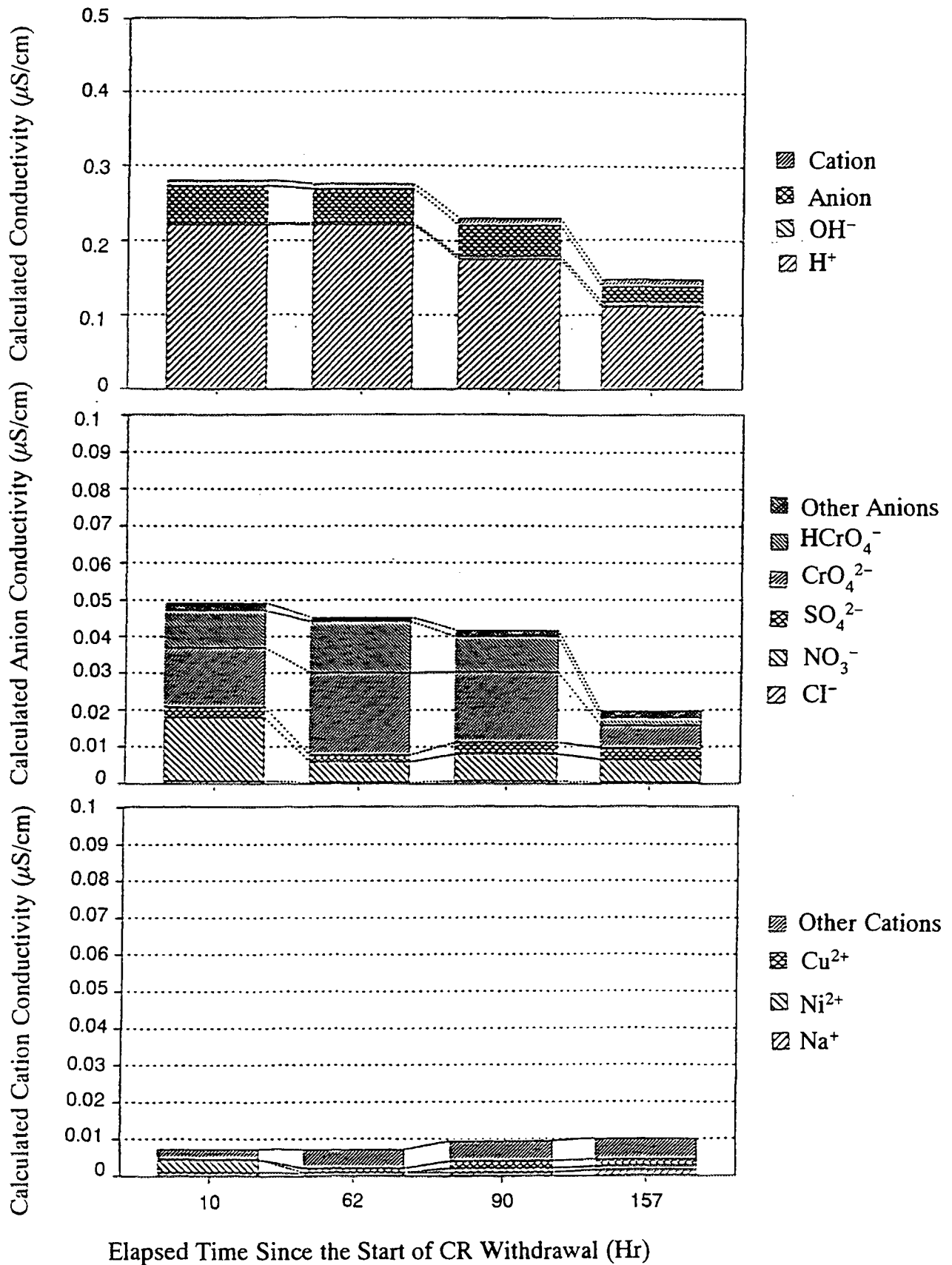
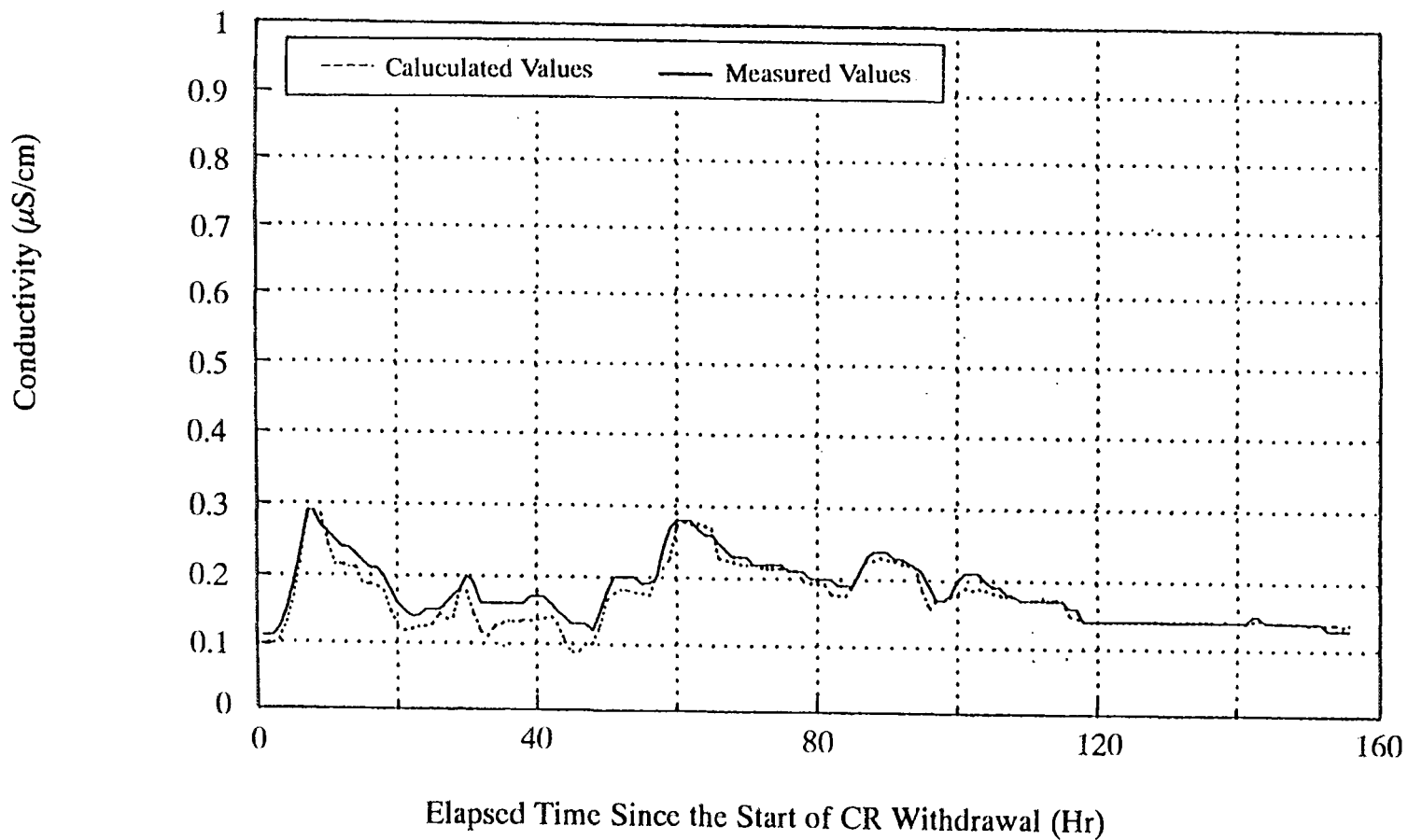


Fig.7 Contribution of Ion Impurities to Reactor Water Calculated Conductivity (at the Cycle 13 Start-up of Hamaoka Unit No.1)



**Fig.8** Comparison of Reactor Water Conductivity between Calculated Values and Measured Values (at the Cycle 13 Start-up of Hamaoka Unit No.1)

## REFERENCES

- [1] AGUI, W. et al., Leachables from Strong Acid Cation exchange Resins, J. Jpn. Oil Chem. Soc. Vol.37, No.12 (1988)
- [2] AGUI, W. et al., Fundamental Study on the Production of Ultrapure Water. VI., Leachables from Strong Base Anion exchange Resins, J. Jpn. Oil Chem. Soc. Vol.39, No.5 (1990)
- [3] MAEDA, K. et al., Experience of Reactor Water Quality Improvement in BWR Plants, 52nd International Water Conference, pp.240–245, IWC–91–30, Pittsburg, U.S.A. October 1991.



## IN PLANT CORROSION POTENTIAL MONITORING

B. ROSBORG, A. MOLANDER  
Studsvik Material AB,  
Niköping, Sweden

### Abstract

Examples of in plant redox and corrosion potential monitoring in light water reactors are given. All examples are from reactors in Sweden. The measurements have either been performed in side-stream autoclaves connected to the reactor systems by sampling lines, or in-situ in the system piping itself.

Potential monitoring can give quite different results depending upon the experimental method. For environments with small concentrations of oxidants sampling lines can introduce large errors. During such circumstances in-situ measurements are necessary.

Electrochemical monitoring is a valuable technique as a complement to conventional water chemistry follow-up in plants. It can be used for water chemistry surveillance and can reveal unintentional and harmful water chemistry transients.

### 1. INTRODUCTION

Electrochemical methods are common tools for corrosion research, corrosion engineering, and in plant monitoring. The measurements are often easy and straightforward in systems working at temperatures close to ambient and at low pressures. However, in high-temperature water experimental problems can arise. In this paper our experiences with redox and corrosion potential monitoring in nuclear power plants are reviewed.

Potential monitoring offers significant advantages compared with conventional water chemistry analysis. It is one of the few ways of obtaining a rapid response from water chemistry changes in a plant. It is also of great value when exposing specimens for corrosion testing in the water circuits of a plant.

In general terms potential measurements are considered a practicable approach for corrosion monitoring when the corrosion behaviour is not very sensitive to small changes

in the corrosion potential. The main disadvantage of the technique is, generally stated, that a fair knowledge about the system studied is needed compared with some other methods for corrosion monitoring.

Real time corrosion measurements by means of electrochemical noise techniques, or other methods, may also be of great value for corrosion monitoring. However, such methods are not treated in this presentation.

## 2. METHODS

In plant potential monitoring is performed in a number of ways. Two principal methods are recognized:

- (a) exposure of electrodes in side-stream autoclaves, and
- (b) using in-situ electrodes.

### 2.1. Side-stream autoclaves

The first method is the commonly used on-line technique using autoclaves connected to the process system to be monitored by means of sampling lines. In the autoclave working and reference electrodes are exposed.

### 2.2. In-situ electrodes

The second method is the in-situ technique where the reference electrode is installed directly in the process system itself. The corrosion potential of the plant material itself is monitored.

In-situ measurements are preferred from a scientific point of view.

### 2.3. Selection of method

It is not always possible to install in-situ electrodes due to safety or other restrictions. Thus, side-stream autoclaves connected to the process system via existing low-flow sampling lines has often to be used.

As the corrosion potential depends on local conditions, variations inside a plant system occur if the environment is not identical in the whole system. When side-stream autoclaves are used, it is strongly recommended to qualify the influence of the sampling system by flow-rate changes, dosage of selected species, or by other means.

It is also wise to remember that an unfilmed electrode behaves differently than a filmed electrode.

#### **2.4. Modelling work**

It is not possible to perform measurements in all locations of a process system. Thus, it is of great value to develop models that can predict potentials between measuring locations and even estimate potentials outside measuring locations. Such work is in progress.

### **3. CORROSION POTENTIAL MONITORING IN BWRs**

In boiling water reactors (BWRs) corrosion potential monitoring is an established technique to follow the effect of hydrogen dosage to the feedwater when applying so-called hydrogen water chemistry (HWC). Results from corrosion potential monitoring in Swedish BWRs are presented to illustrate the different results that can be obtained depending upon the measuring location and the experimental method.

#### **3.1. Hydrogen water chemistry surveillance**

Hydrogen addition to the feedwater of a BWR is used as a remedy for intergranular stress corrosion cracking of weld-sensitized stainless steel piping. The purpose of the addition is to suppress the corrosion potential of the steel below a critical potential where intergranular stress corrosion cracking does not occur, or where the crack growth rate is substantially reduced.

In Fig. 1 an example of installations for corrosion potential monitoring in the residual heat removal system of a BWR is given. The installations were used for hydrogen water chemistry surveillance. The autoclave was installed with sampling lines connected to the

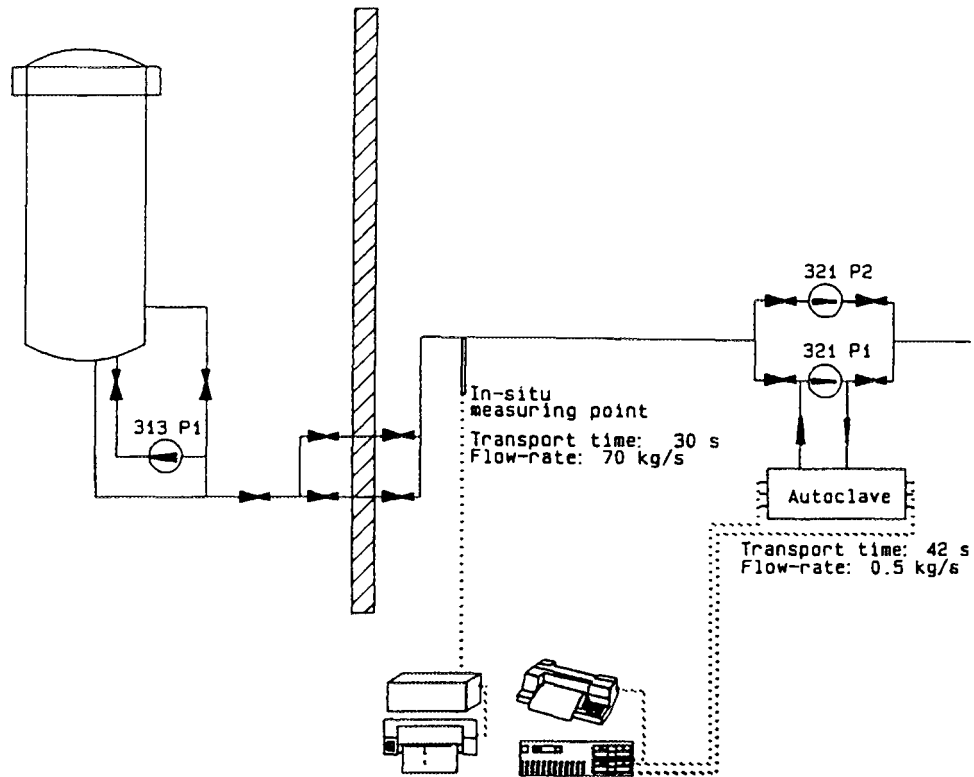


Fig. 1. Corrosion potential monitoring in the Barsebäck 1 BWR using both in-situ reference electrode and side-stream autoclave.

reactor system. For the in-situ measurements a platinum electrode was used as the reference electrode. The design of the platinum electrode is shown in Fig. 2. The platinum electrode was installed with a fitting to a pipe welded to the system pipe. Such electrodes are presently used in several Swedish BWRs.

### 3.2. Results and experiences

A few results from the above hydrogen water chemistry surveillance are shown in Fig. 3 and 4. It is obvious that too low corrosion potentials were measured by conventional corrosion potential monitoring in side-stream autoclaves. From this follows that the hydrogen demand is underestimated and that the relevant system parts will not be protected from intergranular stress corrosion cracking.

The major oxidants in BWR environments are hydrogen peroxide and oxygen, which will be consumed during transport in the high temperature piping. The different corrosion

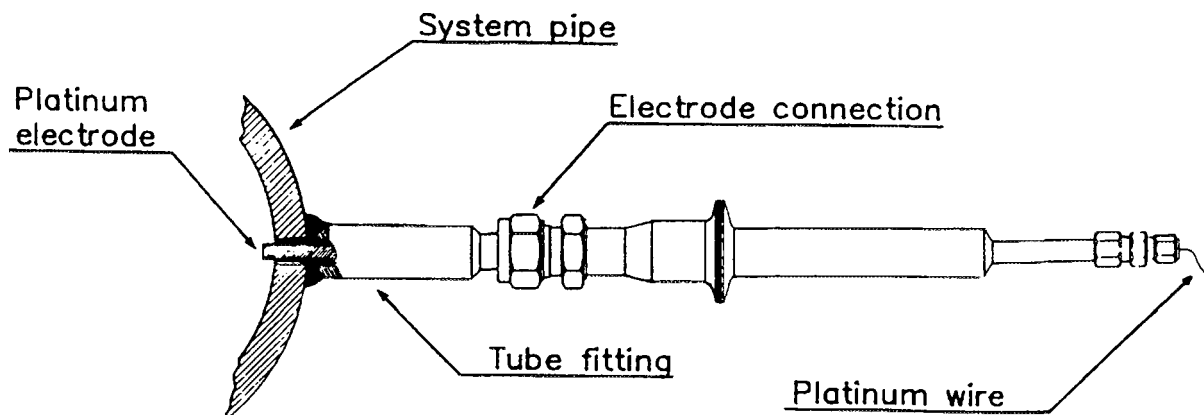


Fig. 2. In-situ platinum electrode.

potentials measured in-situ in the piping itself and in side-stream autoclaves are explained by differences in the environment due to decomposition of hydrogen peroxide and consumption of oxygen in the piping and particularly in the sampling lines. Due to oxidant consumption in low-flow sampling lines, potential monitoring in side-stream autoclaves may give erroneous results. In these cases it is necessary to measure the corrosion potentials in-situ, that is inside the piping itself. Also surface conditions of the working electrodes and mass transfer conditions are important.

The in-situ monitoring is a more sensitive technique: It has a fast response and is much more sensitive to transients in reactor operation. Some transients were only possible to detect by the in-situ monitoring.

Another example of corrosion potential monitoring in a BWR is shown in Fig. 5 through 7.

In summary: Corrosion potential monitoring can give significantly different results depending on experimental methods. In-situ corrosion potential monitoring is considered necessary for hydrogen water chemistry surveillance (in Swedish BWRs).

### 3.3. Recommendations

In-situ corrosion potential monitoring is strongly recommended to follow the effect of hydrogen dosage to BWRs. Significant errors can be introduced by relying on

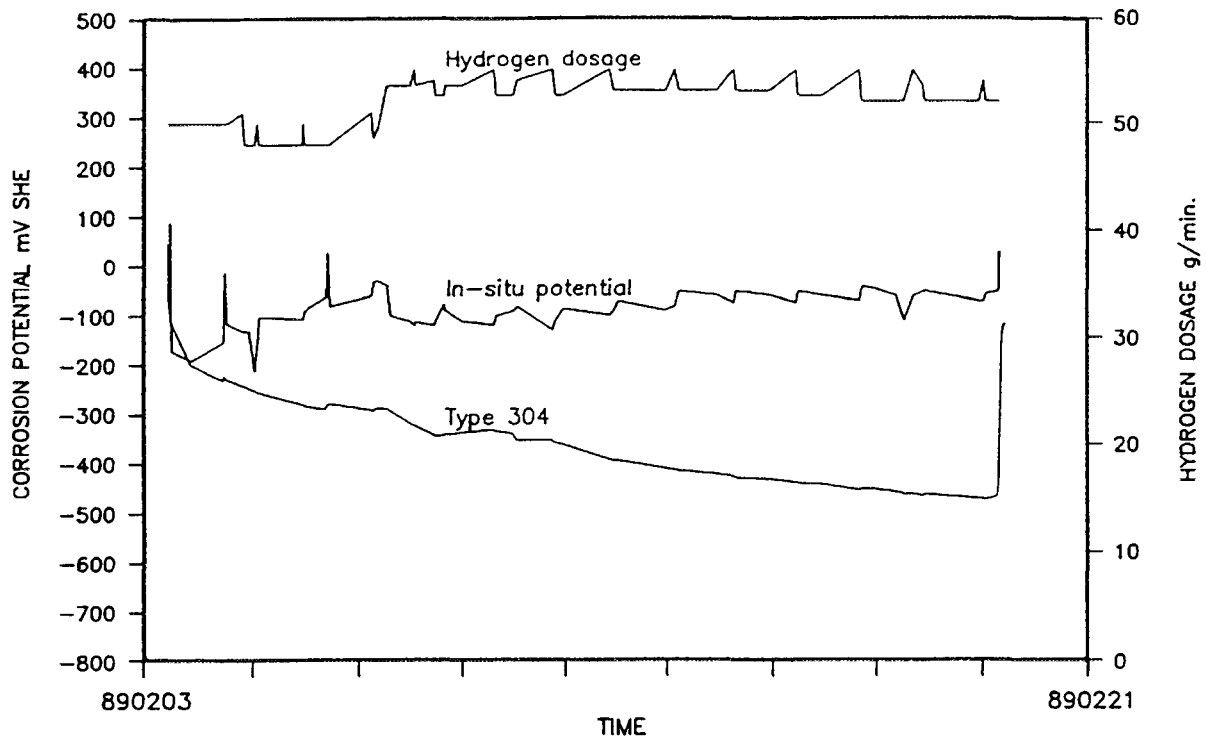


Fig. 3. Corrosion potentials recorded in system piping (In-situ potential) and in side-stream autoclaves (Type 304).

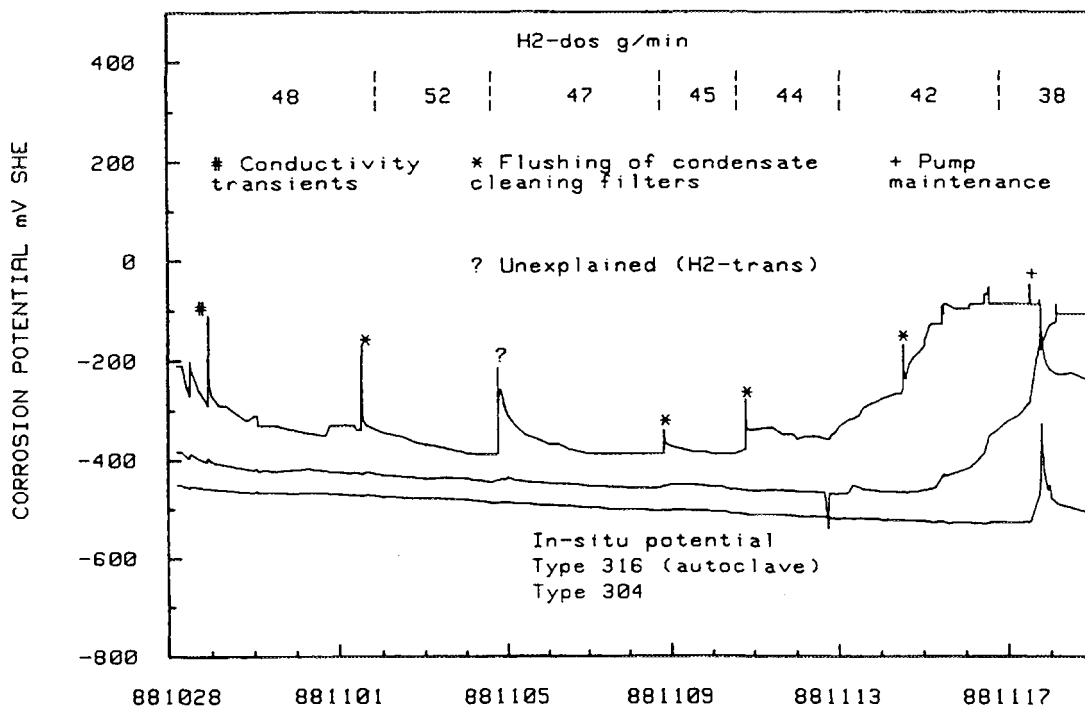


Fig. 4. Influence of variations in reactor operation on the corrosion potentials measured at different locations.

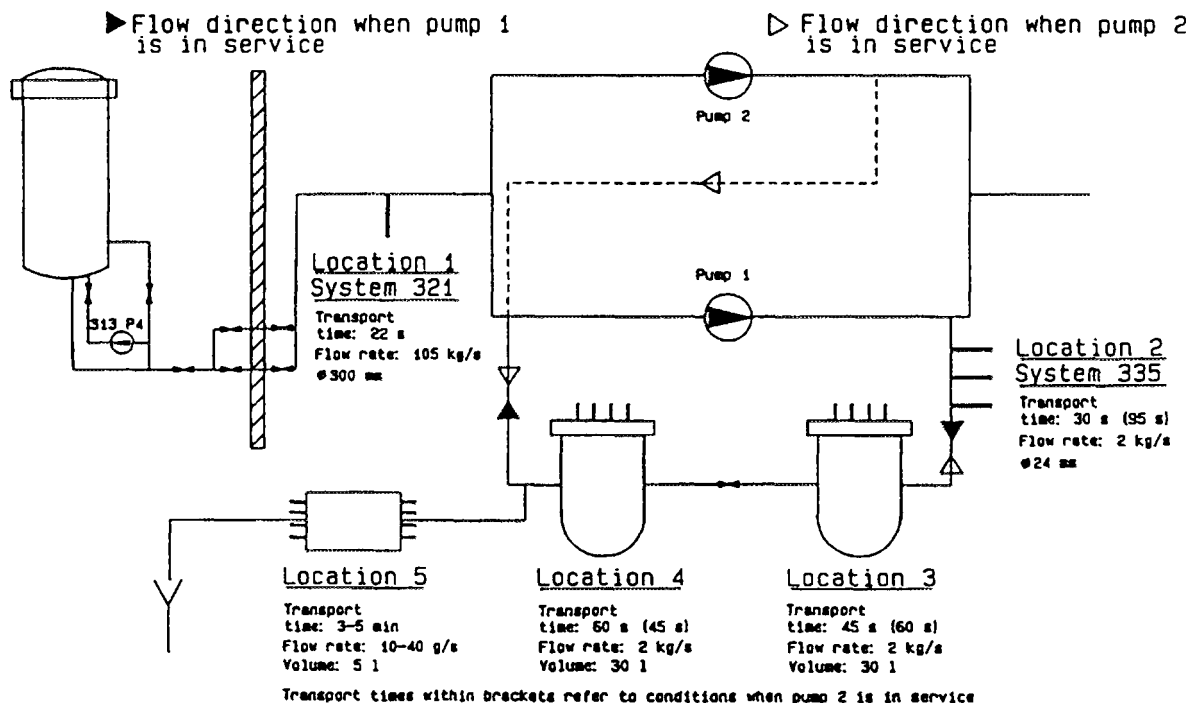


Fig. 5. Principal illustration of the locations of measurements in the Ringhals 1 BWR. Results for the different flow directions are shown in Fig. 6 and 7.

conventional measurements and the required hydrogen dose rate can be underestimated. For the hydrogen dose rates presently applied to establish hydrogen water chemistry conditions in BWRs, the corrosion potential of the stainless steel piping can differ considerably between different locations. The corrosion potential criteria for HWC is therefore without meaning if not the measuring technique and the location of measurement are specified.

#### 4. CORROSION POTENTIALS IN THE REACTOR WATER OF A PWR

In plant measurements have been performed in Ringhals 4, which is a 915 MWe PWR of Westinghouse design. A side-stream autoclave was used; it was installed as a by-pass in the primary coolant sampling system.

Measurements were performed during steady reactor operation, during deliberate pH changes, and during start-ups and shut-downs.

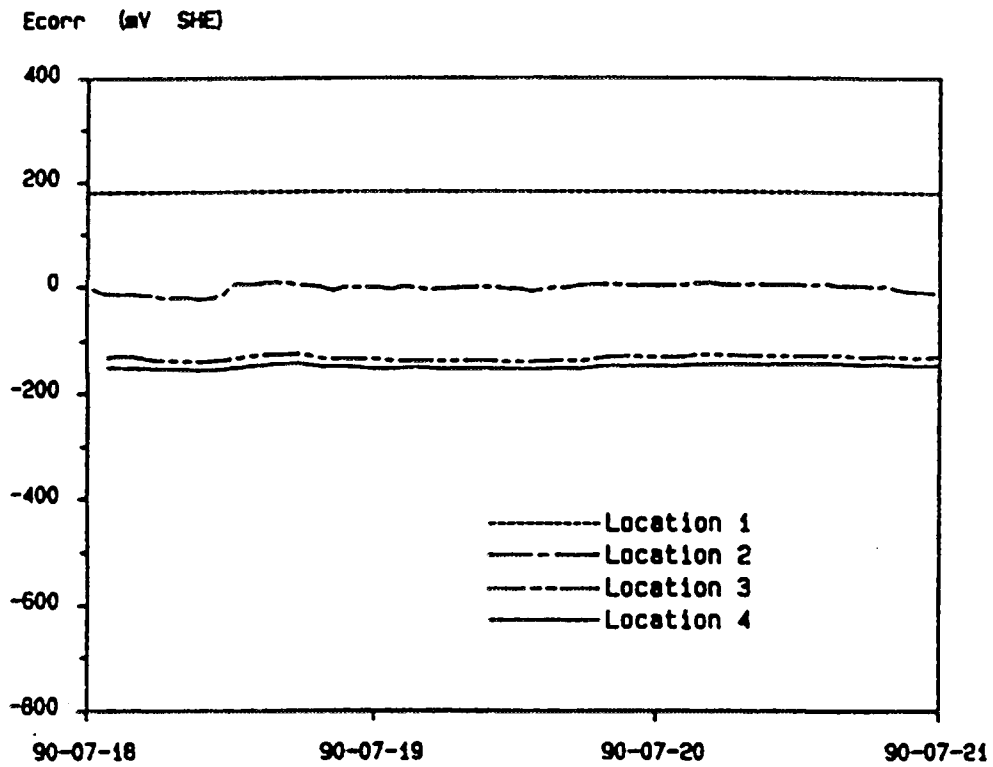


Fig. 6. Corrosion potentials when pump 1 (see Fig. 5) was in service.

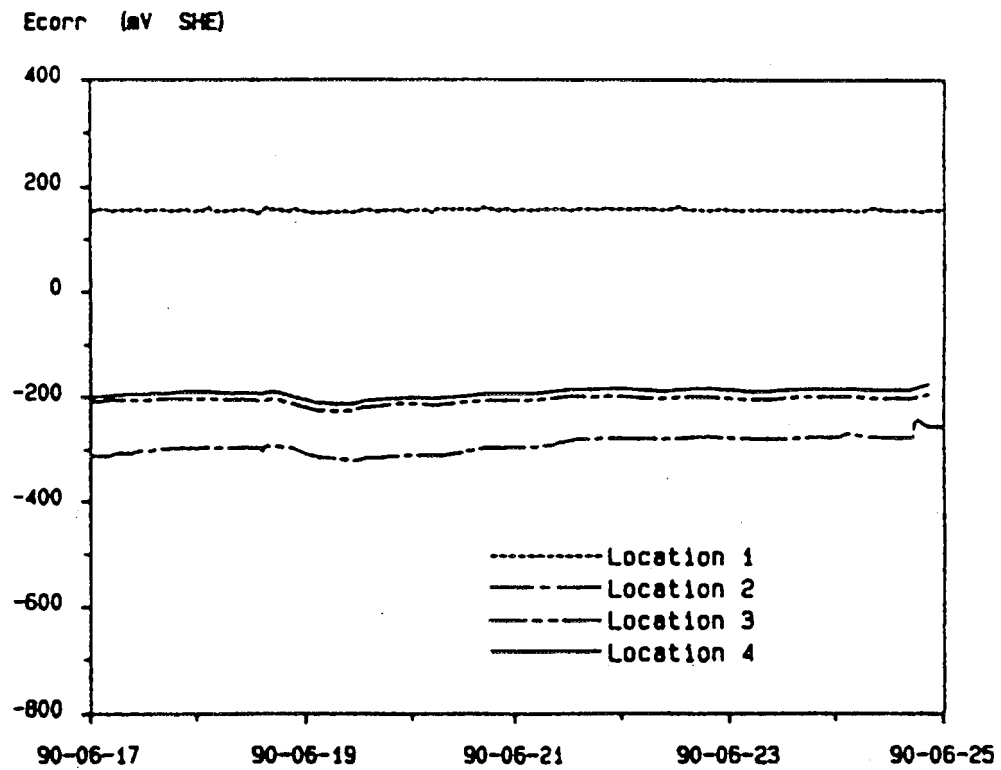


Fig. 7. Corrosion potentials when pump 2 (see Fig. 5) was in service.

#### 4.1. Results and experiences

The results from the measurements at steady reactor operation show that the corrosion potentials of the plant materials exposed, including nickel-base alloys, stainless steels, and a pressure vessel steel all coincide within a few mV with the potential of platinum, that is with the hydrogen equilibrium potential.

During a 24 h period the lithium hydroxide content of the reactor water was kept at four levels. The response of the pH-changes on the electrode potentials was direct and in good agreement with calculated high-temperature pH-values. The results are illustrated in Fig. 8.

During start-ups and shut-downs of the reactor the corrosion potentials differ significantly. The major changes from an electrochemical point of view occurred well below full reactor temperature, see the examples in Fig. 9 and 10.

#### 4.2. Recommendations

With the presently used water chemistry with high hydrogen contents electrochemical monitoring seems to be of limited practical value; the corrosion potentials coincide with

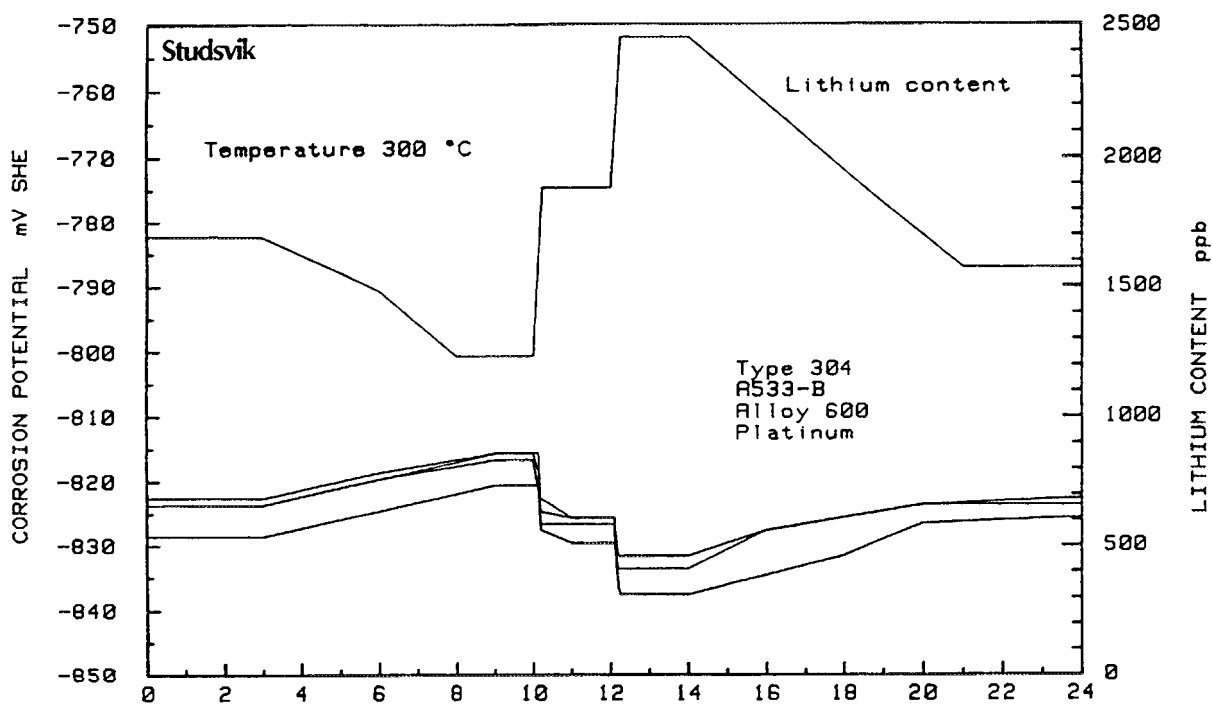


Fig. 8. Corrosion potentials during pH-transient experiments in Ringhals 4 1987-01-23.

the hydrogen equilibrium potentials and can be calculated. If considerably lower hydrogen contents will be used in the future redox and corrosion potential monitoring will be helpful.

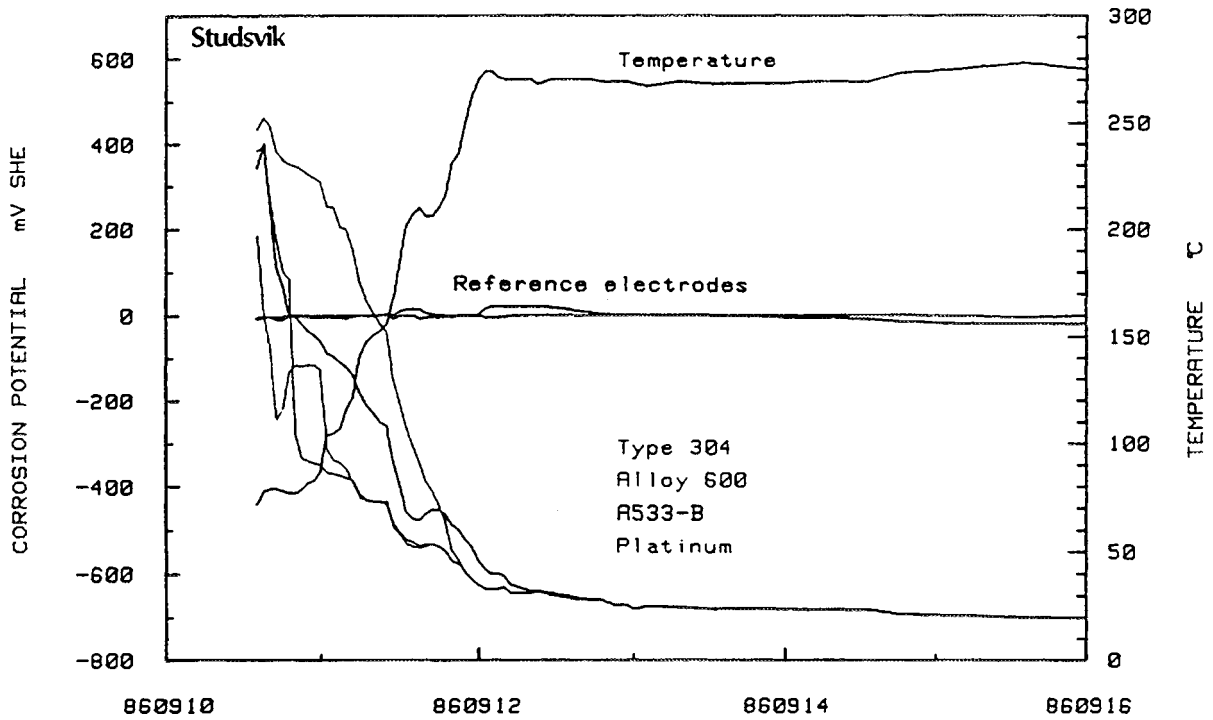


Fig. 9. Corrosion potentials in Ringhals 4 during start-up in 1986.

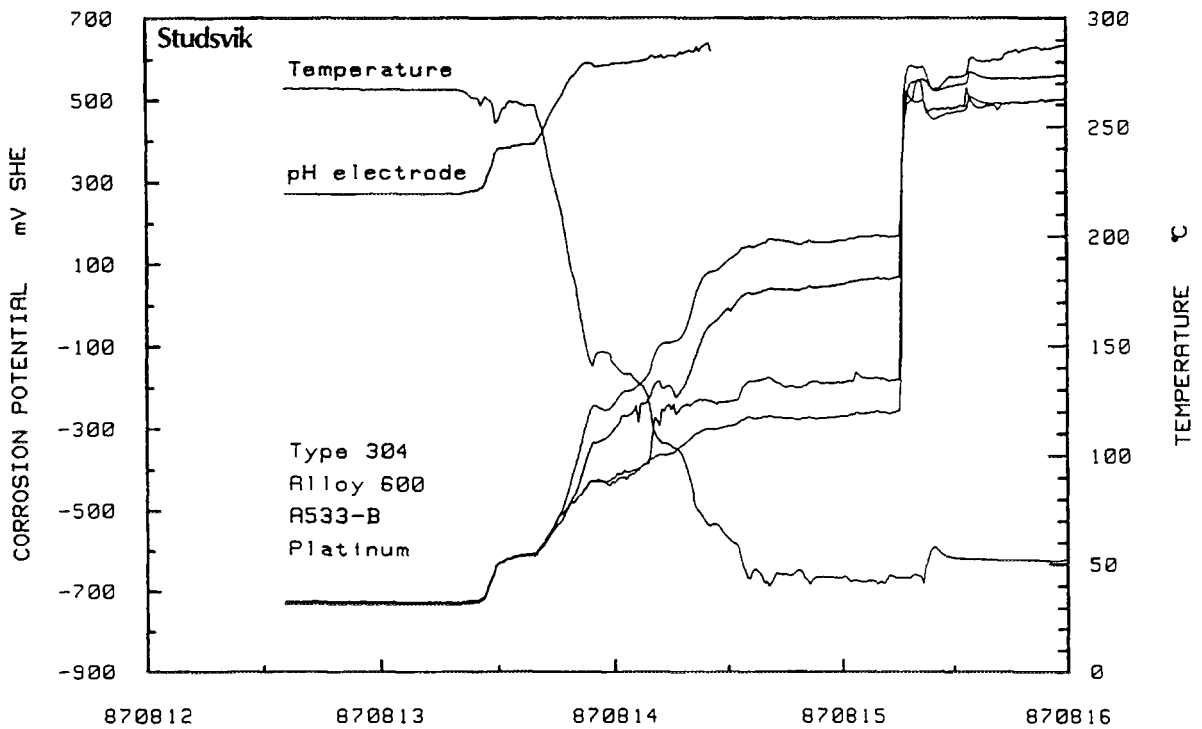


Fig. 10. Corrosion potentials in Ringhals 4 during shut-down in 1987.

## 5. REDOX POTENTIAL MONITORING IN PWR FEEDWATER

The water chemistry in PWR steam generators is of prime importance to prevent corrosion degradation of the tubing. Reducing conditions in the feedwater have to be secured. Redox potential monitoring in condensate and feedwater offers a complement to the conventional water chemistry follow-up.

In plant potential monitoring is presently performed in the Ringhals 3 and 4 PWRs. Side-stream autoclaves are used at different locations in one of the feedwater trains, see Fig. 11. Deliberate dosages to the sampling line and deliberate flow-rate changes have been performed to qualify the potential readings.

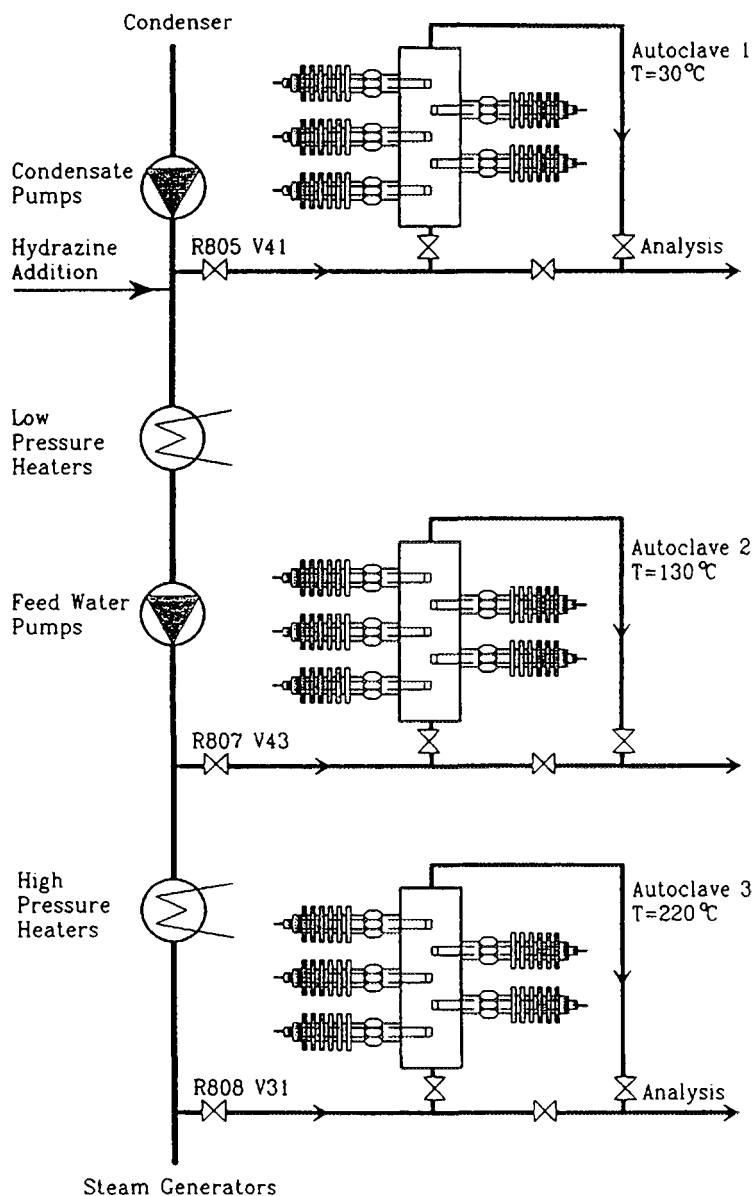


Fig 11. Locations of side-stream autoclaves in one of the Ringhals 3 turbine loops.

### 5.1. Results and experiences

Changes in redox potentials and water chemistry during unintentional oxygen inleakages are exemplified in Fig. 12 and 13. Changes during deliberate oxygen dosages are shown in Fig. 14.

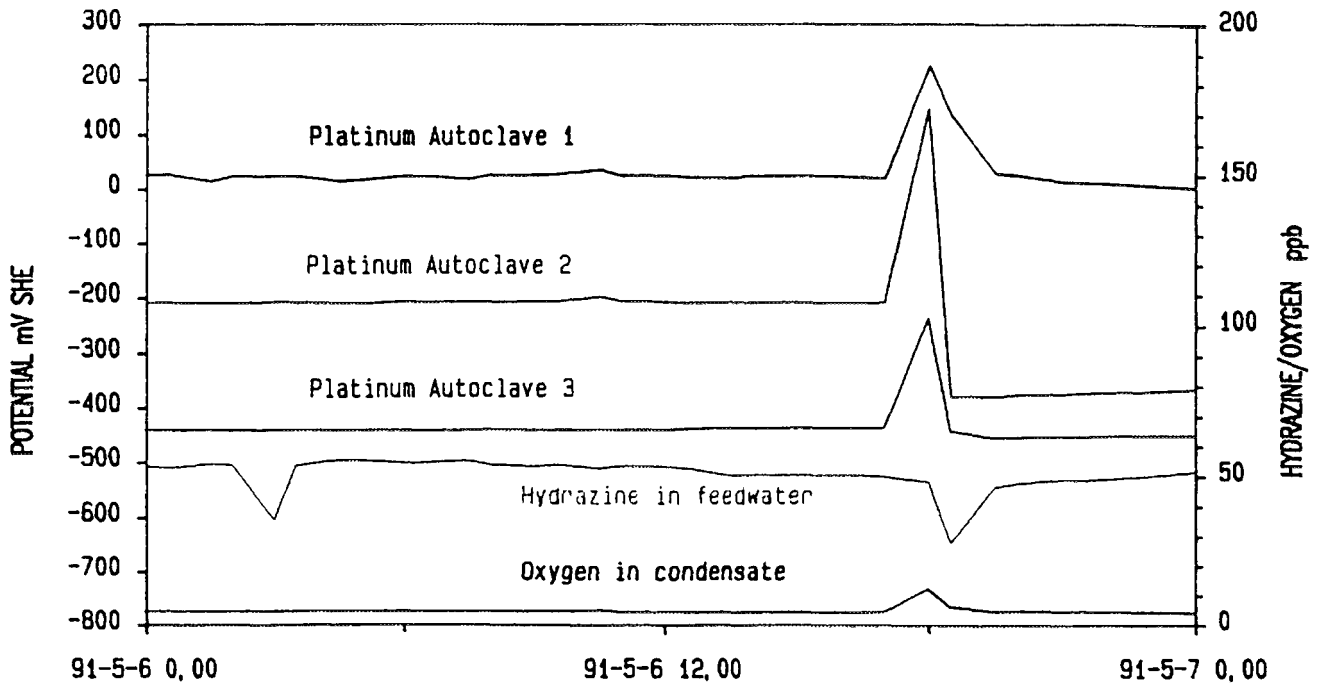


Fig.12. Changes in redox potentials due to an oxygen transient from the shift of a condensate pump.

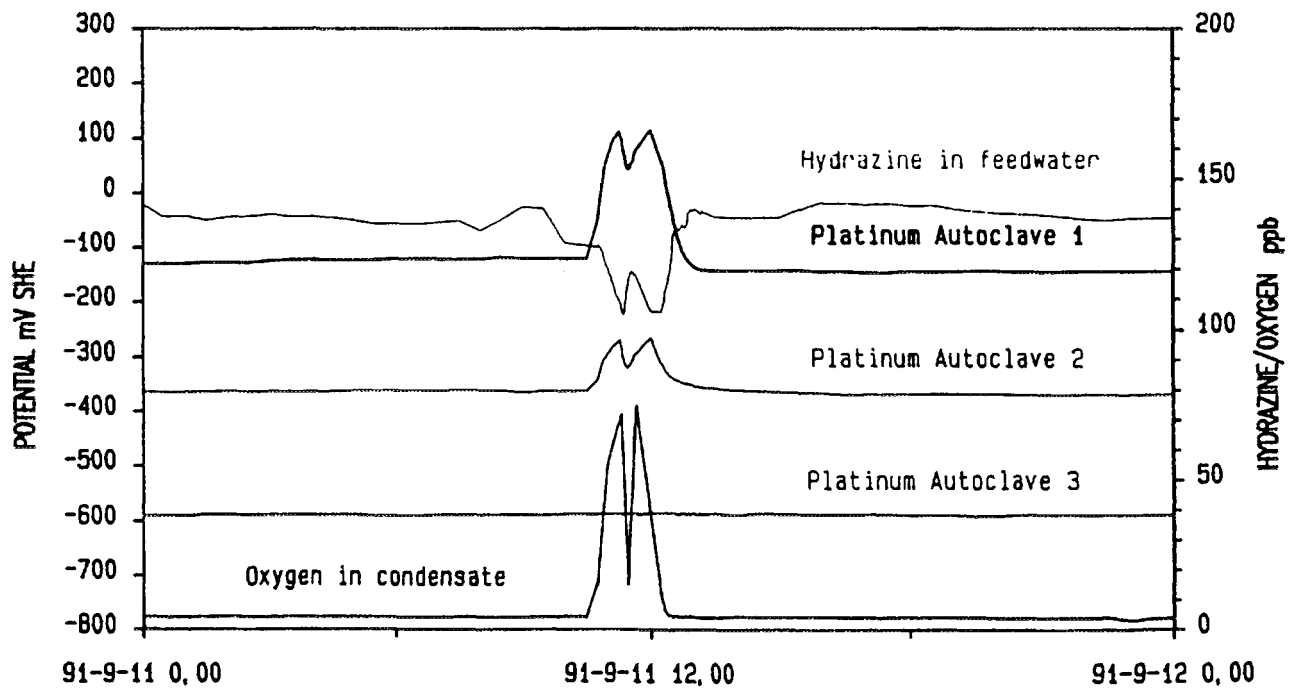


Fig. 13. Changes in redox potentials during air ejector outage.

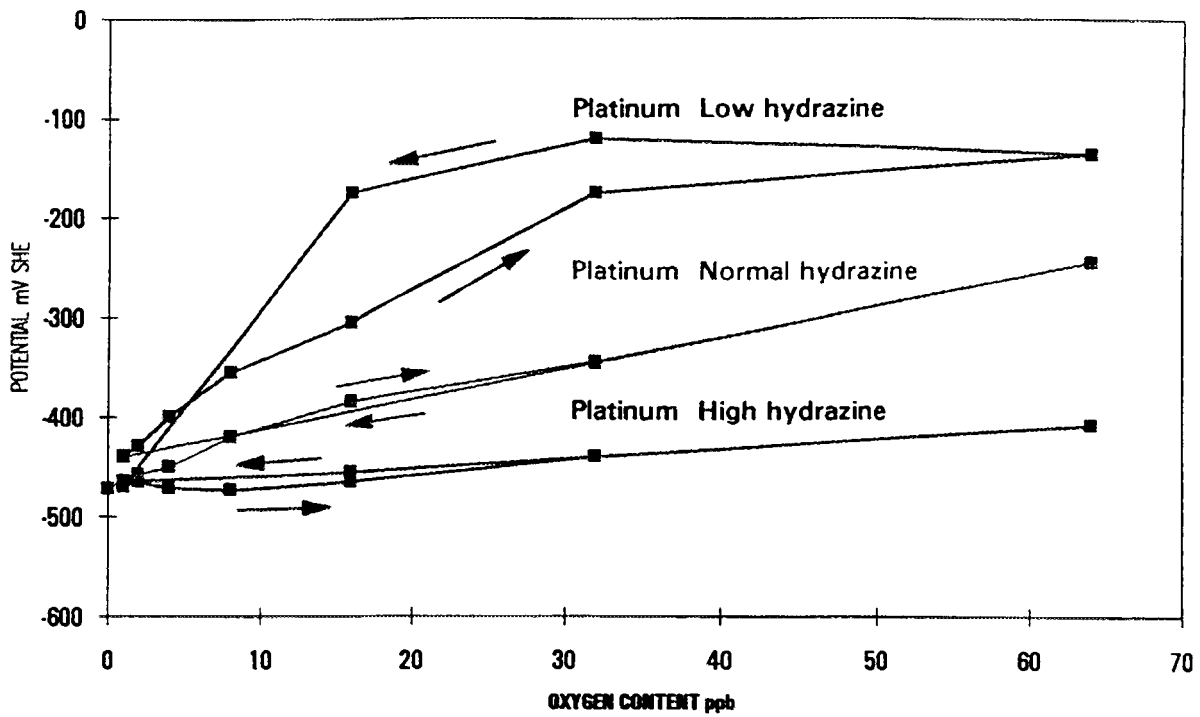


Fig. 14. The redox potential versus oxygen dosage for different hydrazine concentrations.

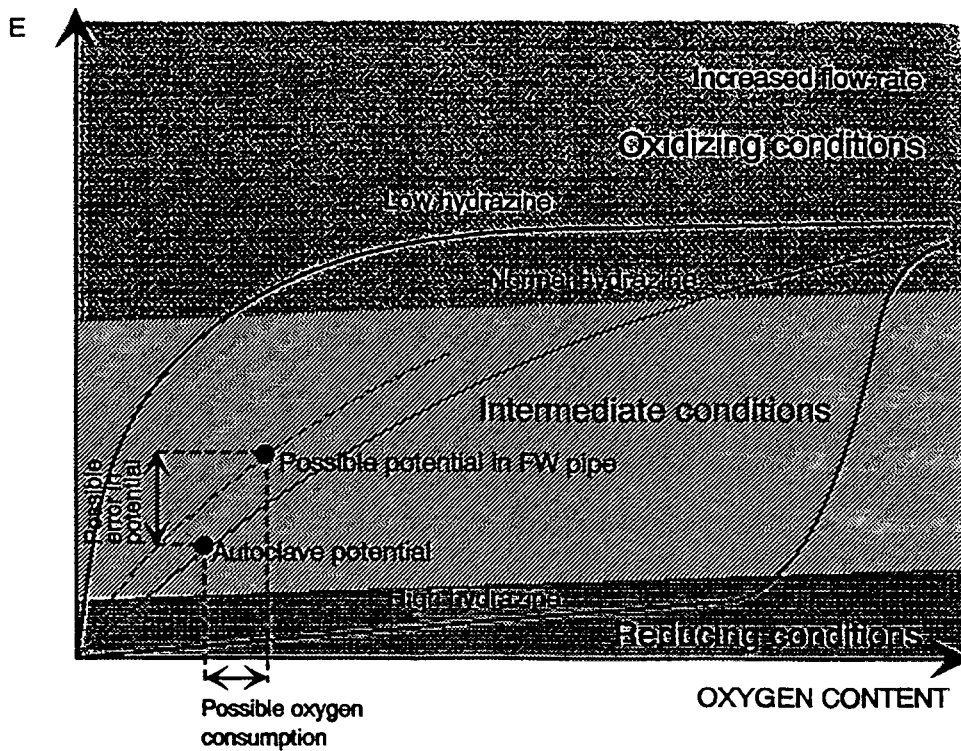


Fig. 15. Redox potential domains in the secondary system of a PWR.

The different redox potential domains in PWR feedwater are visualized in Fig. 15. In this figure an example of a possible error in the potential measured due to the use of a side-stream autoclave is also depicted.

Electrochemical monitoring offers an improved water chemistry surveillance method in PWR secondary systems compared to conventional oxygen and hydrazine analyses. Present monitoring of feedwater redox potential by means of oxygen measurements is not satisfactory: oxygen is partly consumed in the sampling line and the response is slow.

## **5.2. Recommendations**

Electrochemical monitoring should be recognized as a possible future method for routine use in secondary systems of PWRs.

## **6. CORROSION POTENTIAL MONITORING AND CONTROL IN THE LABORATORY**

Corrosion testing in the laboratory is often performed in low-flow systems. For careful environmental control of corrosion experiments it is considered necessary to monitor the corrosion potential of the specimen itself. Electrochemical monitoring on separate electrodes should either be avoided, or carefully demonstrated to be valid.

## **7. SUMMARY**

In plant corrosion potential monitoring offers an important complement to conventional water chemistry measurements.

Corrosion potential monitoring can give quite different results depending upon experimental method. Side-stream autoclaves are most commonly used, but for some applications it is necessary to use in-situ electrodes.

For environments with small concentrations of oxidants sampling can introduce large errors. During such circumstances in-situ measurements are necessary.

It is favourable to measure at several locations. This helps in interpreting and qualifying the obtained data.

However, it is not possible to perform measurements in all locations of a process system. Thus, modelling work is of great interest in predicting potentials in between and outside measuring locations.

In-situ measurements are preferred from a scientific point of view. However, in-situ measurements cannot always be used and one has to rely on measurements in side-stream autoclaves. It is then of utmost importance to validate the measurements.

### **ACKNOWLEDGEMENTS**

This paper is based on work that has been sponsored by the Swedish utilities OKG Aktiebolag, Sydkraft and Vattenfall AB, and by Studsvik AB.



**FIELD EXPERIENCE WITH ADVANCED METHODS OF  
ON-LINE MONITORING OF WATER CHEMISTRY AND  
CORROSION DEGRADATION IN NUCLEAR POWER STATIONS**

B. STELLWAG  
Siemens/KWU,  
Erlangen, Germany

P. AALTONEN  
Technical Research Centre of Finland (VTT),  
Espoo, Finland

J. HICKLING  
CML GmbH,  
Erlangen, Germany

**Abstract**

Retrospective off-line inspections of the cumulative effects of corrosion damage do not hold the key to maximum reliability and availability of nuclear power stations. They cannot provide meaningful control, because "control" implies feedback within a time scale effective in stopping the problem. For maximum control, real-time, on-line feedback is required. Taking account of this fact, advanced methods for on-line, in-situ water chemistry and corrosion monitoring in nuclear power stations have been developed during the past decade. The terms "on-line" and "in-situ" characterise approaches involving continuous measurement of relevant parameters in high temperature water, preferably directly in the systems and components and not in removed samples at room temperature. This paper describes the field experience to-date with such methods in terms of three examples:

- (1) On-line water chemistry monitoring of the primary coolant during shutdown of a Type VVER-440 PWR.
- (2) Redox and corrosion potential measurements in final feedwater preheaters and steam generators of two large KWU PWRs over several cycles of plant operation.
- (3) Real-time, in-situ corrosion surveillance inside the calandria vault of a CANDU reactor.

The way in which water chemistry sensors and corrosion monitoring sensors complement each other is outlined: on-line, in-situ measurement of pH, conductivity and redox potential gives information about the possible corrosivity of the environment. Electrochemical noise techniques display signals of corrosion activity under the actual environmental conditions.

A common experience gained from separate use of these different types of sensors has been that new and additional information about plants and their actual process conditions is obtained. Moreover, they reveal the intimate relationship between the operational situation and its consequences for the quality of the working fluid and the corrosion behaviour of the plant materials. On this basis, the efficiency of the existing chemistry sampling and control system can be checked and corrosion degradation can be minimised. Furthermore, activity buildup in the primary circuit can be studied.

Further significant advantages can be expected from an integration of these various types of sensors into a common water chemistry and corrosion surveillance system. For confirmation, a complete set of sensors will be installed in the near future in a loop of a test reactor operated with PWR primary coolant chemistry. The purpose of these investigations is to obtain a better understanding of activity build-up on materials as a function of the coolant chemistry.

## **1. Introduction**

The quality of the working fluid is of prime importance for the reliability and availability of power stations. Surveillance of the working fluid in steam power stations relies in essence on standard water sampling practice: water samples are withdrawn from relevant plant systems and components, cooled and continuously or discontinuously analysed with respect to certain important parameters, such as pH value, conductivity, concentration of impurities, etc. . Specified water quality levels must be maintained. In case of excursions from the specified values, actions must be taken.

Water sampling and analysis practice has been successfully used for decades. It is an indispensable tool for the plant chemist.

Considered from the viewpoint of chemical engineering, sampling lines represent chemical reactors. Depending on the layout, temperature and operation mode of

these chemical reactors, the chemistry of the water flowing through the tube can be considerably affected:

- (1) At high temperatures, chemically active species in the fluid, such as oxygen, hydrogen peroxide or hydrazine can react with the tube walls of the sampling lines.
- (2) Corrosion products can be deposited and reentrained during sampling.
- (3) The process of cooling the water samples can alter the solubility and valency of dissolved substances. In addition, it is associated with a change in the pH value of the fluid.

As a consequence, the interpretation of water chemistry data requires considerable expertise on the part of the plant chemist even in case of optimum layout and operation of the sampling systems.

Taking account of these facts, advanced methods for on-line, in-situ water chemistry and corrosion monitoring in steam power stations have been developed during the past decade. This paper describes the field experience to-date with such methods in terms of three examples:

- (1) On-line water chemistry monitoring of the primary coolant during shutdown of a Type VVER-440 PWR.
- (2) Redox and corrosion potential measurements in final feedwater preheaters and steam generators of two large KWU PWRs over several cycles of plant operation.
- (3) Real-time, in-situ corrosion surveillance inside the calandria vault of a CANDU reactor.

The measurements have been already described in detail elsewhere [1], [2],[3], [4]. Purpose of this paper is not to summarise their results. Instead, an attempt is made to trace out common features and inherent benefits of on-line, in-situ water chemistry and corrosion monitoring in power stations. The terms "on-line"

and "in-situ" characterise approaches involving continuous measurement of relevant parameters in high temperature water, preferably directly in the systems and components and not in removed samples at room temperature.

## **2. On-line Monitoring of Primary Coolant Chemistry during Shutdown of a Type VVER-440 PWR**

### **2.1 Requirements to PWR Primary Coolant Chemistry**

The chemistry of the primary coolant of PWRs has to fulfil various major requirements:

- Reactivity control. Chemical shim is usually achieved by dosing boric acid into the coolant.
- Minimisation of release, transport and deposition of corrosion products in the primary circuit. These processes are very important for activity build-up in the system. It is effected by an alkaline water treatment and reducing conditions. Lithium or potassium hydroxide are used as alkalisating agents. Hydrogen or ammonia are added to maintain low redox and corrosion potentials. Ammonia decomposes in the radiation field under formation of hydrogen.
- Compatibility of chemistry to structural materials and fuel cladding.

Reactivity control and thus the concentration of boric acid in the coolant is a function of the burnup of the fuel.

Metal release rates depend on the pH value, temperature and corrosion potential and are material specific. Widely used plant materials for nuclear power stations are austenitic stainless steels, nickel base alloys and cobalt base alloys, which are used for hardfacings. Generally, for minimisation of release, transport and deposition of corrosion products, an elevated pH value of the coolant is favourable [5], [6]. The optimum pH value depends on the major construction

materials used in the considered power station. It may thus slightly differ from plant to plant.

In contrast to minimisation of activity build-up which is achieved by high pH values, advanced fuel element concepts (longer cycles, higher burn-up, increased power) impose a limitation on the use of alkalising agents, especially lithium hydroxide. For steam generators tubed with the nickel base alloy I 600, an influence of the lithium concentration of the coolant on primary water stress corrosion cracking is currently being debated.

The primary coolant chemistry in PWRs is therefore subjected to conflicting demands.

On-line water chemistry and corrosion monitoring enables prompt recording of the response of plant systems to variations in water chemistry. Critical parameters can be identified, yielding the clue to an understanding of the underlying mechanisms. Equipment for measurement of high temperature water chemistry parameters and the concentration of corrosion products has been installed in the Loviisa 1 and 2 nuclear power stations. Results obtained with this equipment are described in the following section.

## 2.2 On-line Monitoring of Primary Coolant Chemistry during Shutdown of a PWR

The shutdown of PWRs is characterized by large chemistry and temperature gradients. This section concentrates, therefore, on measurement data obtained during a shutdown of Loviisa 1 nuclear power station. Each of the six primary loops of this Type VVER 440 PWR is equipped with coolant cleaning systems. The continuous coolant cleaning system consists of two independent ion-exchanger lines operating under full system pressure at temperatures below 100°C. One is a mixed-bed filter and the other is a cation-anion filter.

The reactor pressure vessel is weld clad with austenitic stainless steel. Primary coolant piping and steam generator tubing are also made of austenitic stainless steels similar to Type AISI 321. Fuel cladding is a zirconium alloy. Nickel and cobalt base alloys are usually not used in Type 440 VVER PWRs.

The corrosion potential of austenitic stainless steel, the high temperature pH value  $\text{pH}_T$  and the temperature were continuously monitored. Electrodes and sensors were installed in a cell which was connected to a sampling line coming from the RPV core near to the reactor water inlet. The temperature in the cell during power operation was 240°C. The reactor water inlet temperature is 267°C.

Corrosion and redox potential measurements in reactor water of a PWR were also performed by A. Molander et al.[7].

The concentration of soluble corrosion products was measured on-line with ion chromatography using the same sampling line. In addition grab samples were taken at regular intervals from the standard sampling system during shutdown. Conventional water chemistry analyses at room temperature were carried out every two hours during the shutdown.

The variation of the water chemistry parameter during shutdown is shown in Fig. 1. Four operation phases can be distinguished. They are also indicated in Fig. 1:

- (A) Stoppage of ammonia dosage and subsequent start-up of the primary water clean-up system.
- (B) The reactor reaches a subcritical state.
- (C) Boration of the primary water.
- (D) Reactor water temperature decreases below 120°C and degasification is started.

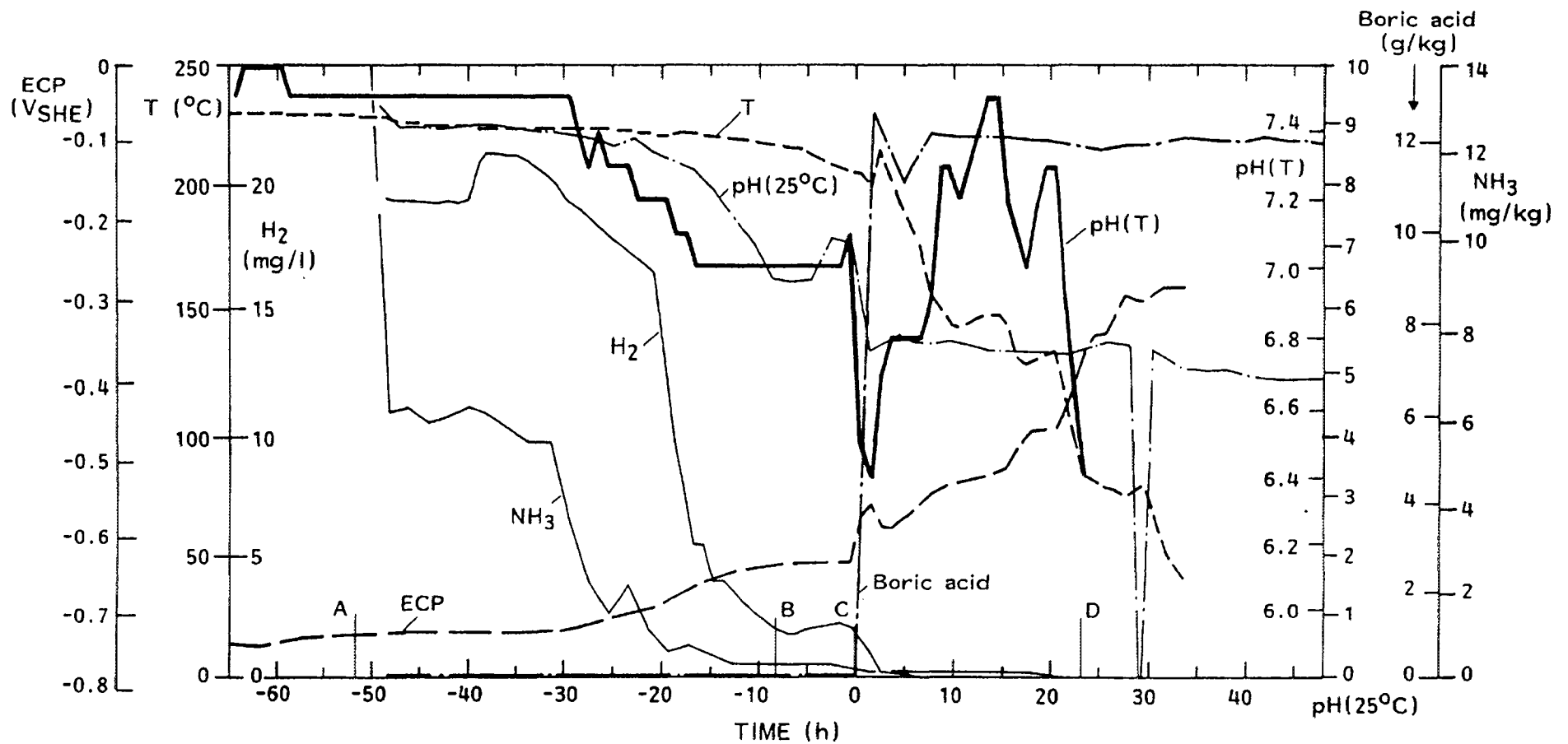


**Figure 1** Variation of water chemistry parameters in the primary system during shutdown of the plant.

- Phase A: Stoppage of NH<sub>3</sub> dosage, subsequent start of clean-up system.
- Phase B: Subcriticality of reactor.
- Phase C: Boration of the primary water.
- Phase D:  $T_{\text{Reactor}} < 120^{\circ}\text{C}$ , start of degasification

The stoppage of ammonia dosage and the subsequent start-up of the clean-up systems is associated with the removal of ammonia and other water treatment chemicals (potassium hydroxide, total alkalinity, i.e.  $K^+ + Na^+ + Li^+$ ).

Therefore, both  $pH_T$  and  $pH_{RT}$  decrease. Since hydrogen is produced through radiolytical decomposition of  $NH_3$ , its concentration decreases in parallel. As a consequence of the decrease in both pH and  $H_2$  concentration the corrosion potential increases from ca. - 740 mV<sub>SHE</sub> to ca. - 640 mV<sub>SHE</sub>.

Phase B (reactor reaches a subcritical state) is characterised by the constancy of water chemistry conditions.

Boration of the system and the following operation period (Phase C) is associated with pronounced fluctuations in the chemistry parameters. The temperature decrease during this phase is ca. 100°C. Upon boration, the high temperature  $pH_T$  value decreases rapidly to 6.4. The room temperature  $pH_{RT}$  value drops simultaneously to 5.5 and then remains more or less constant. However, the high temperature  $pH_T$  value fluctuates significantly between 7.5 max. and 6.4 min.. These fluctuations were associated with simultaneous variations in the coolant temperature and the flow rates in the clean-up systems. The fluctuations in the high temperature  $pH_T$  value are ascribed to the capture of boric acid by the ion exchangers and the simultaneous release of basic anions. The effect apparently depends on the flow rate in the clean-up system.

Boric acid is a weakly dissociating substance. Dissociation thus decreases with temperature. This is not the case for strongly dissociating substances, such as potassium and lithium hydroxide. As a consequence, mixed solutions of these substances with concentrations typical for primary coolant are slightly acidic at room temperature. With increasing temperature, such solutions become alkaline. The measured significant differences between  $pH_T$  and  $pH_{RT}$  are therefore related to the temperature dependent dissociation behaviour of boric acid and

alkalising agents in primary coolant. In addition, actual changes in the coolant composition tend to level out during sampling.

The continuous increase in corrosion potential during this operation period is ascribed to the decreasing coolant temperature.

The final shutdown phase (Phase D, reactor coolant temperature lower than 120°C and degasification) results in a further increase in the corrosion potential. The final value of - 260 mV<sub>SHE</sub> corresponds roughly to the equilibrium value of the hydrogen electrode in boric acid at the given pH<sub>RT</sub> value.

Corrosion product release during shutdown of the plant is shown for nickel and cobalt in Fig. 2. The release characteristics of manganese followed the pattern observed for nickel. The dissolution behaviour of iron was similar to cobalt.

A first dissolution peak of all cations was induced by the boration of the system. During the following temperature decrease and pH<sub>T</sub> fluctuations the various metal cations showed a different response. Release of the various cations always closely followed the variations in the pH<sub>T</sub>. In the case of nickel and manganese, release behaviour was also influenced by variations in the corrosion potential. In the case of cobalt and iron, variations in the corrosion potential were of minor importance. Instead, temperature variations were revealed to be essential for cobalt and iron release.

The results of the simultaneous measurements of high temperature water chemistry parameters and concentrations of corrosion products dissolved in the primary coolant revealed that the release of metal cations is closely linked to pH<sub>T</sub>, temperature and corrosion potential.

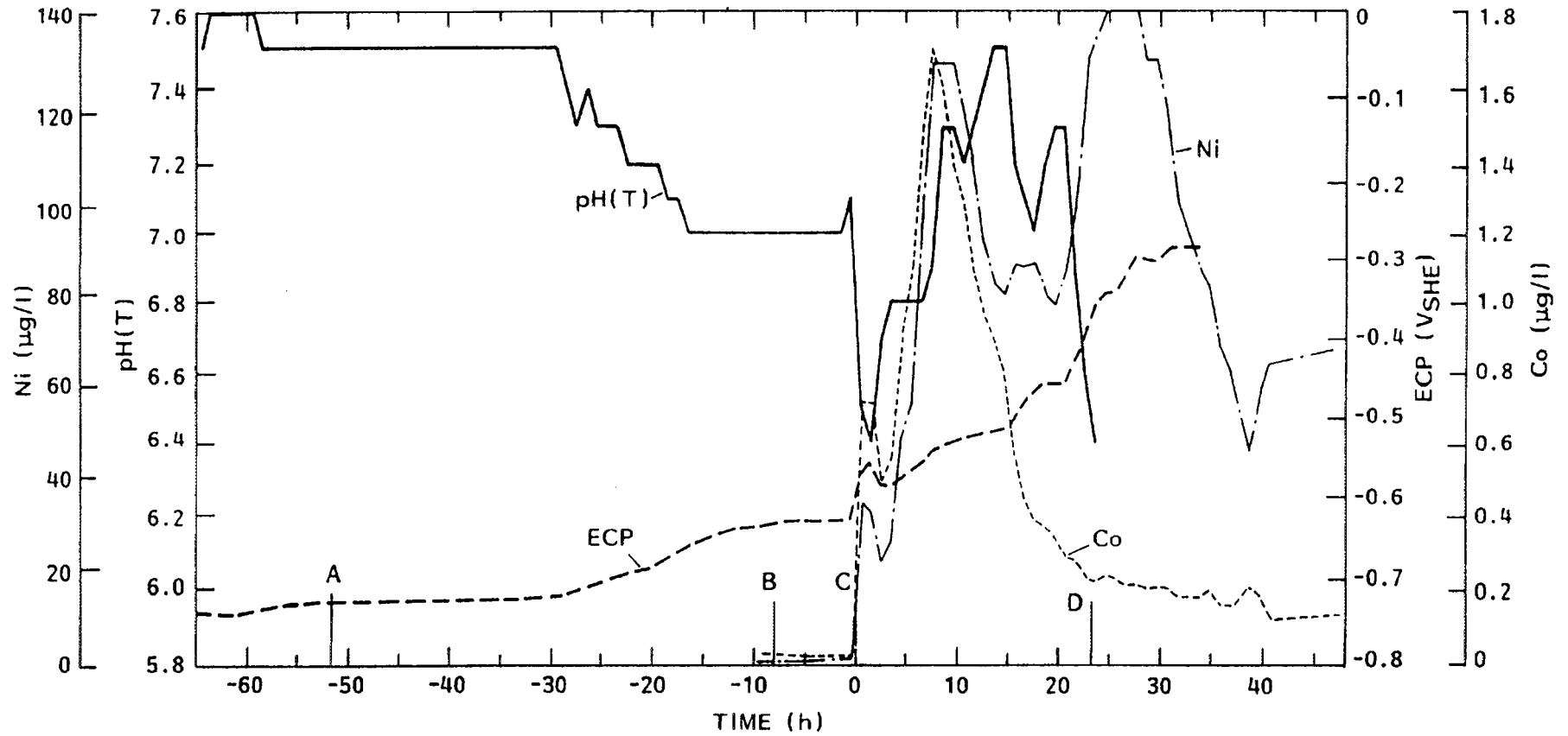


Figure 2 Release of metal cations into the primary coolant during shutdown of the plant.

Moreover, these parameters turned out to be intimately related to plant operation practice. In particular, actual flow rates through the clean-up systems revealed to be of major importance. The induced fluctuations in the high temperature  $\text{pH}_T$  value were not displayed by the room temperature  $\text{pH}_{RT}$  value. In order to understand the causes for the observed  $\text{pH}_T$  fluctuations, the role of the clean-up system and the process taking place during shutdown must be studied in more detail.

### 2.3 Conclusions

Altogether, on-line water chemistry monitoring indeed gave the clue to a better understanding of release of activated corrosion products not only for this particular power station but also in terms of basic processes.

The consequences for improvement of the shutdown practice can be briefly summarised using the term "soft shutdown". Soft shutdown practice has been developed for boiling water reactors and aims at avoiding pronounced gradients in terms of pressure, temperature and water chemistry. The results obtained in Loviisa 1 show that such features must be also taken into account in pressurised water reactors. It is apparent that on-line water chemistry monitoring is an important tool for the study of such practices in PWRs.

On account of the positive experience with the on-line monitoring system in Loviisa 1, such equipment was also installed in Loviisa 2. It has been used since then routinely for evaluation of the water chemistry in both plants.

### **3. On-line, In-Situ Monitoring of Corrosion and Redox Potentials in Steam Generators and Feedwater Heaters of PWRs**

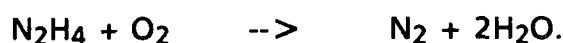
#### **3.1 Requirements to PWR Water/Steam Cycle Chemistry**

In order to protect components of water/steam cycles against corrosion, design and sound materials selection are backed up by suitable chemical feedwater conditioning practices to maintain specified water quality levels. Specifications for steam generator feedwater only permit extremely low levels of impurities. In the event of malfunctions in the condensers, however, salts and oxidants in the feedwater can be entrained into the steam generator and accumulate in pockets of zero flow. The spectrum of water quality which can be encountered in nuclear steam generators can therefore range from extremely pure to heavily contaminated water. Reducing water conditions must prevail if the safety margin with regard to corrosion mechanisms such as pitting and stress corrosion cracking is to be maintained.

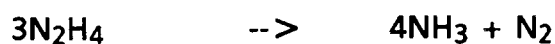
Potential oxidants in steam generator water are dissolved copper species and oxygen. Copper compounds are released from turbine condensers and feedwater heater tubes and transported into the steam generators in stations equipped with copper alloys in these components. As already mentioned, air and thus oxygen may be drawn in by leaking turbine condensers.

Widespread water treatment practice is to add hydrazine  $N_2H_4$  to the fluid.

Hydrazine is a reducing agent. It scavenges oxygen according to



The thermal decomposition of hydrazine to ammonia



provides volatile alkalisation of the fluid in the circuit.

Under oxidizing conditions  $N_2H_4$  is electrochemically oxidized, e. g.



Typically, reactions involving hydrazine under the conditions concerned are irreversible. The kinetics of these reactions are dominated by catalytic effects, being additionally influenced by factors such as temperature, pH value, etc.. Depending on the layout, temperature and operation mode of sampling lines for final feedwater, consumption of hydrazine and oxygen can be considerable. Examples are given in Figs. 3 and 4.

Oxidising conditions in steam generators thus cannot be ruled out on the basis of measurement of the concentration of hydrazine and oxygen concentration in water samples withdrawn from final feedwater. For reliable detection of

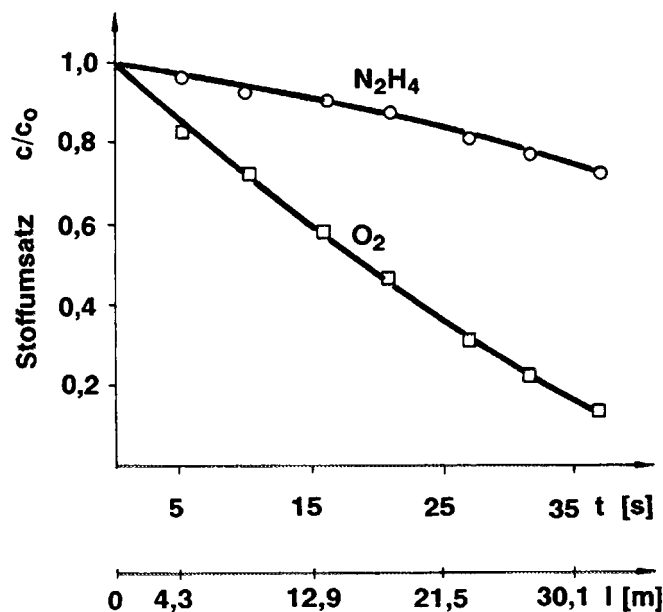


**Figure 3** O<sub>2</sub> and N<sub>2</sub>H<sub>4</sub> concentration in water flowing through a tube as a function of the tube length.

Test conditions: Tube material austenitic stainless steel, inner diameter 4 mm, water flow rate 35l/h, test temperature 170°C, pressure 80 bar,  
 CO<sub>2</sub> ~ 20 ppb; CN<sub>2</sub>H<sub>4</sub> ~ 146 ppb,  
 CNH<sub>3</sub> ~ 1 ppm at inlet.

Prior to the test, the tube was operated with oxygenated water (CO<sub>2</sub> ~ 400 ppb).

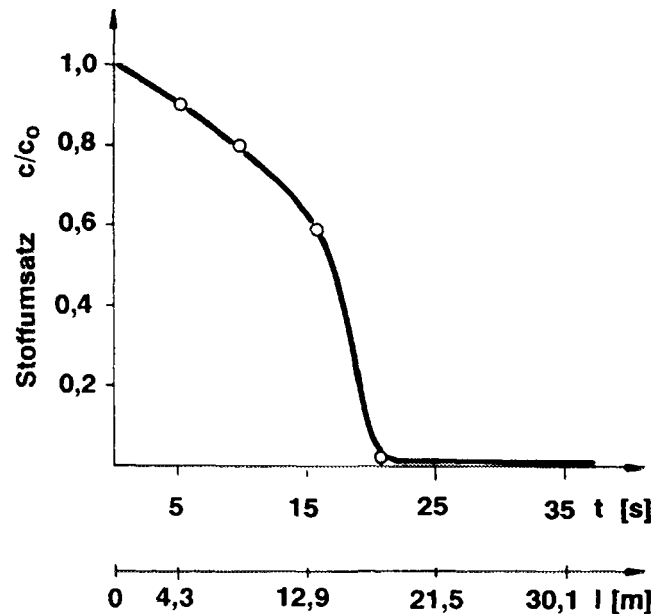


**Figure 4** O<sub>2</sub> concentration in water flowing through a tube as a function of the tube length.

Test conditions as described in Fig. 3 with the following exceptions: Prior to the test the tube was operated with water containing hydrazine ( $C_{N_2H_4} > 100$  ppb,  $C_{O_2} = 0$  ppb). The test was performed with water, containing 40 ppb O<sub>2</sub> and 105 ppb N<sub>2</sub>H<sub>4</sub> at the tube inlet.

oxidising conditions in the steam generator recirculating water, electrode potentials must be measured in-situ.

### 3.2 Corrosion and Redox Potential Measurements in Steam Generator Circulating Water and Final Feedwater

A monitoring unit for measurement of electrode potentials which was installed in the tube bundle of steam generator of the 1204 MW Biblis A PWR is shown in Fig. 5. Its design is described in detail elsewhere [2], [3].

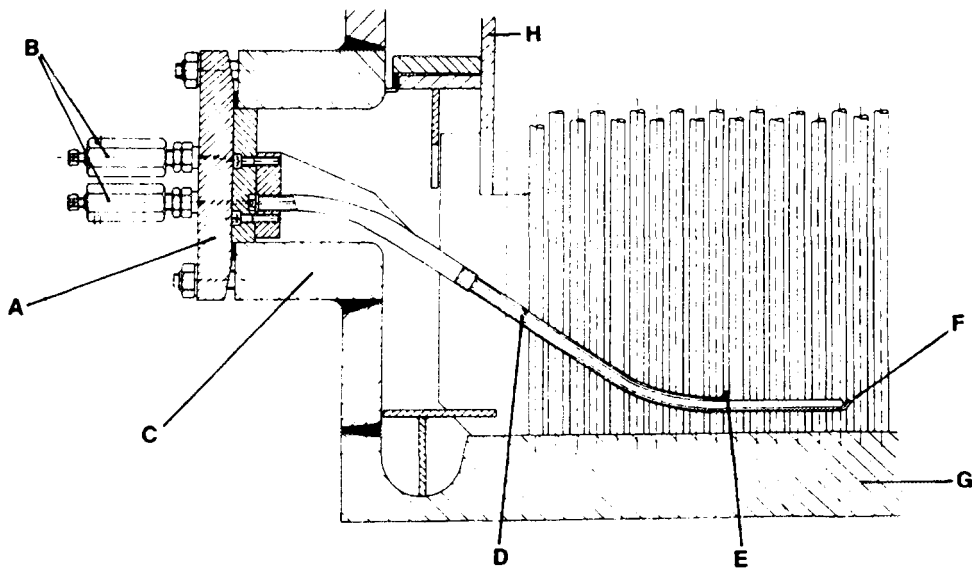


**Figure 5** Monitoring unit A for the measurement of electrode potentials in the tube bundle (side view). The unit consists of a handhole cover preassembled with casings for the electrodes B and probes D for the measurement of potentials at locations E and F ca. 50 mm above the tubesheet G. C denotes the handhole, H the shroud.

In addition, monitoring units of similar design have been installed in final feedwater heaters upstream of the steam generators. Measurements have been taken since 1985. Experience gained from use of these monitoring units is described in terms of various examples.

The response of electrode potentials to stoppage of hydrazine dosing of the fluid and the decrease in hydrazine content is shown as a function of time in Fig. 6.

An increase in electrode potentials is observed during this period.

Changes are pronounced in the feedwater heater (cf. curve 6 in Fig. 6). In steam generator water the effect is less pronounced for various reasons:

- (1) The buffering capacity of the large water reservoir in the steam generator levels out short-term changes in water chemistry.

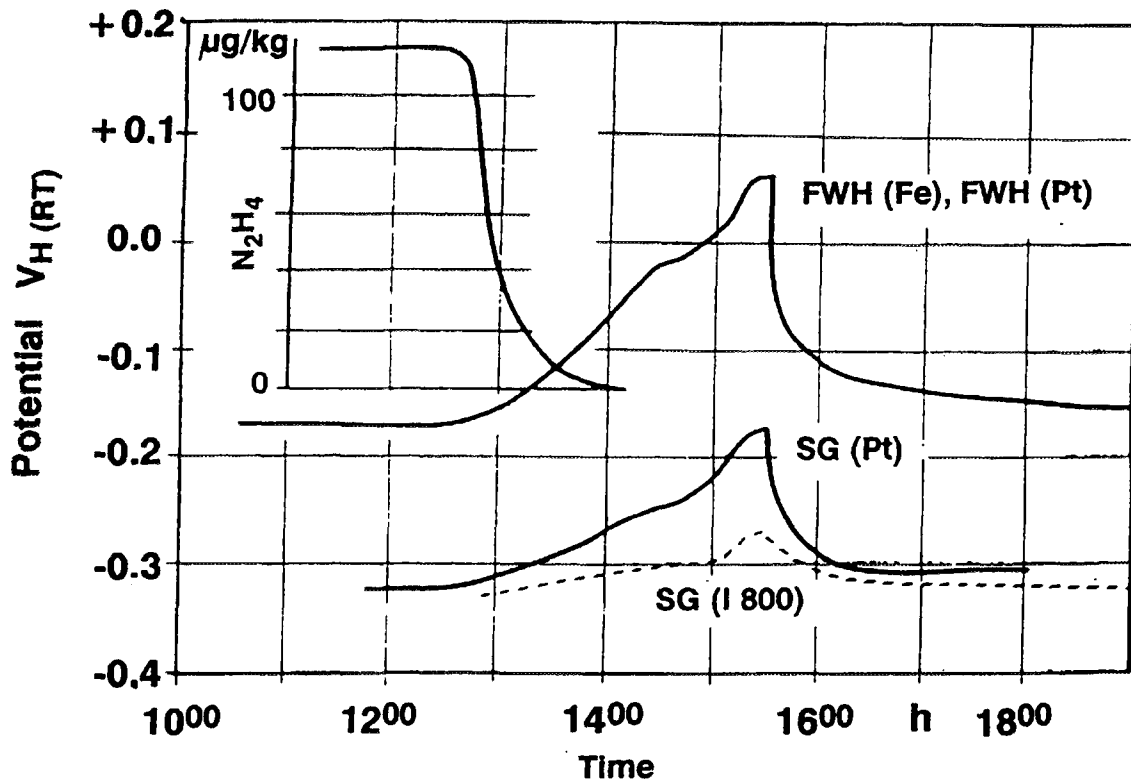


Figure 6 Response of electrode potentials to stoppage of hydrazine dosing of the fluid and decrease in the hydrazine content as a function of time (Insert).

- (2) The rate of reaction of  $O_2$  with  $N_2H_4$  increases significantly with temperature.
- (3) The steam generator acts as a deaerator.  $O_2$  has a significantly higher volatility than  $N_2H_4$  and is therefore preferentially carried into steam. It should be noted that in case of dissolved copper compounds, opposite behaviour must be expected.

The oxygen concentration measured in water sampled from the high pressure heater with the standard plant sampling system was less than 2-3  $\mu\text{g}/\text{kg}$  and constant during this period. The steam-water circuit of this plant is not equipped with copper base alloys. Copper species can be therefore ruled out as oxidants.

In Fig. 7 the response of electrode potentials during cleaning of the turbine condenser water boxes is shown. This results in an increased oxygen content in the steam condensate as displayed. The electrode potentials follow the measured oxygen concentration, although the hydrazine concentration in feedwater was 130  $\mu\text{g}/\text{kg}$  and constant during this time period. The oxygen concentration in the water sampled from the high pressure heater remained constant at 2-3  $\mu\text{g}/\text{kg}$ . This example shows that an abundance of hydrazine does not necessarily exclude anodic excursions of electrode potentials within steam generators.

Steady state corrosion potentials of Alloy 800 steam generator tubes measured as a function of hydrazine concentration in the final feedwater are shown in Fig. 8. A hydrazine concentration  $> 50 \mu\text{g}/\text{kg}$  in the final feedwater is apparently sufficient to maintain reducing water conditions in the associated steam generator.

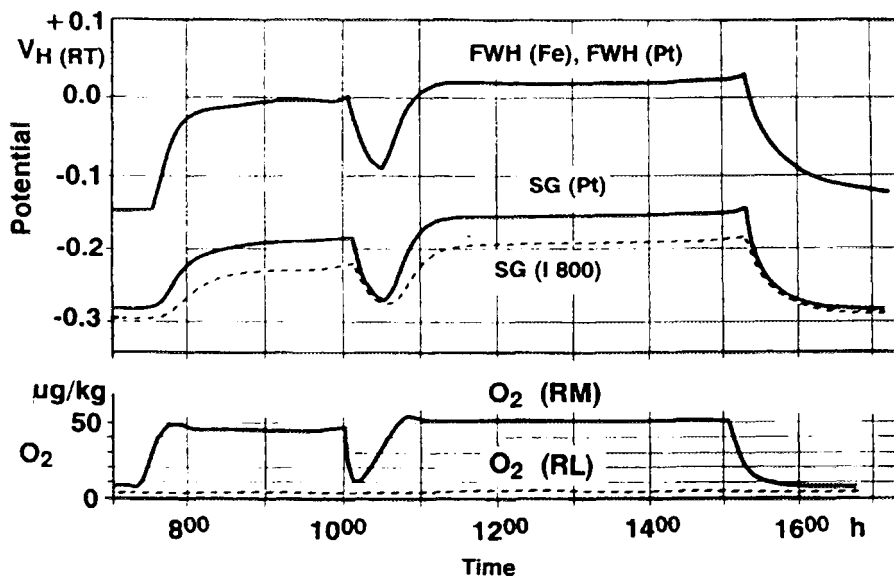


**Figure 7** Electrode potentials measured as a function of time and oxygen concentration in the main condensate (bottom diagram) during successive cleaning of two of the water boxes of the turbine condensers.

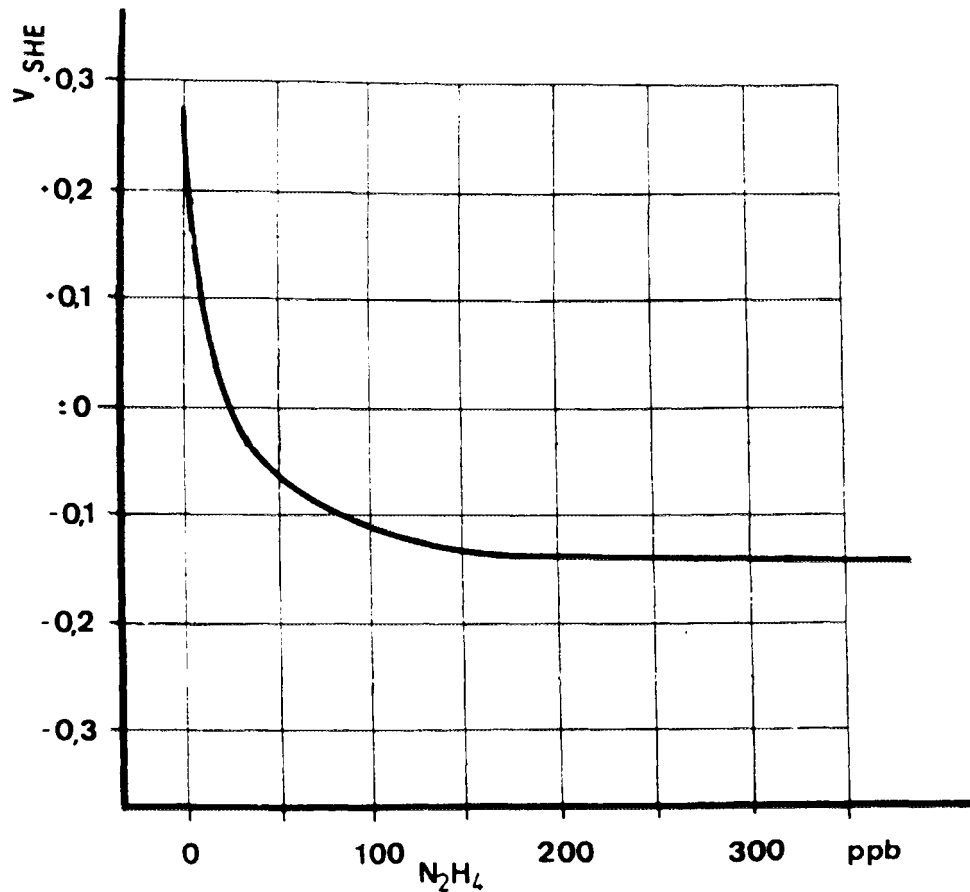


**Figure 8** Steady state potentials of austenitic Alloy 800 steam generator tubes measured as a function of the hydrazine concentration in the final feedwater.

### 3.3 Consequences

The required minimum hydrazine concentration depends on the plant specific situation, i. e. concentration of potential oxidants such as copper compounds and/or oxygen. It can be determined reliably only by on-line electrode potential measurements. Electrode potential measurement units can be further used for detection of the sources of oxidant ingress into the feedwater system. The described examples also show that on-line monitoring can be used to check the efficiency of the normal plant water chemistry sampling system.

With respect to hydrazine dosing it has to be borne in mind that an abundance of hydrazine is associated with high ammonia concentrations in the water-steam

circuit. This may cause increased ammonia corrosion of copper base alloys. In addition, ammonia discharge with waste water has been limited by law. Such conflicting demands can be satisfied with on-line monitoring units: they allow optimisation of the chemistry in water/steam cycles and control with respect to corrosion degradation and environmental requirements.

As in the case of Loviisa 1 and 2, monitoring units have been installed on account of the positive experience gained in Biblis A in the second unit of the Biblis power station (Biblis B PWR with 1300 MW). The monitoring units have been routinely used for evaluation of the quality of the final feedwater by the plant operation personnel.

#### **4. Real-Time, In-Situ Corrosion Surveillance Inside the Calandria Vault of a CANDU Reactor**

##### **4.1 Background**

Corrosion processes in aqueous solutions are normally of an electrochemical nature, i.e. they are associated with the transport of metal ions across the electrically charged metal-solution interface. The resulting charge transfer current is a direct measure of the corrosion rate, which is an indirect function of the corrosion potential. These two parameters, the corrosion current and the corrosion potential, are directly related to the onset of corrosion attack in plant materials and its subsequent intensification.

The use of on-line measurement of corrosion potentials for analysis of corrosion product release and for optimization of water chemistry has been described in Sections 2 and 3. The corrosion potential was measured in these cases using a reference electrode, i.e. on an absolute potential scale.

The anodic corrosion current cannot be directly accessed with simple measuring techniques, since it is balanced by a cathodic reduction current of the same size, i.e. there is no external current flow. However, it has been found that nominally identical electrodes normally have differing balances of anodic and cathodic activity and hence take up slightly different corrosion potentials. The open-circuit voltage between "identical" electrodes can be measured in a non-perturbative way using a high impedance voltmeter. The apparently random fluctuation of the voltage as a function of time is typically in the millivolt range and is described as electrochemical potential noise.

Short-circuiting two such "identical" electrodes with a zero resistance ammeter results in a fluctuating galvanic current, (so-called electrochemical current noise). Current noise signals are typically in the range of 1  $\mu\text{A}$  or less.

Using appropriate equipment, current noise and potential noise can be registered simultaneously as an indication of surface condition. Continuous in-situ measurement of these parameters enables real-time identification of the onset and intensification of corrosion. This is the principle of the electrochemical noise (ECN) techniques. If necessary, the ECN measuring method can be complemented by perturbative techniques, such as electrochemical impedance spectroscopy (EIS) or determination of linear polarisation resistance (LPR). In the case of uniform corrosion, ECN and EIS measuring methods enable determination of actual corrosion rates. Furthermore the initiation of localized corrosion processes, such as pitting or crevice corrosion, stress corrosion cracking, etc., can be monitored. Under favourable conditions, the rate of growth of pits or stress corrosion cracks can also be estimated. Applied together, these techniques provide a comprehensive tool with which to determine the rate and mode of corrosion attack. For brevity, the reader is referred with respect to details to the literature [9], [10].

Two features are essential for successful on-line corrosion surveillance with the described techniques:

- Design of the corrosion sensors (multi-electrode probes).
- Processing and analysis of the measurement signals.

The corrosion sensors must be designed to take account of the corrosion mode which is to be expected. E.g., stressed specimens are required, if the occurrence of stress corrosion cracking is suspected. Creviced specimens enable detection of the onset and growth of crevice corrosion, etc.. The design of the corrosion sensors must also take into account the corrosive environment in the considered plant, which can, e.g., result from a condensate film or deposits on heavily fouled heat exchanger tubes. Last not least, it has to be ensured that variations of the corrosivity of the operating environment are correctly detected by the plant sensors. Considerable experience is therefore necessary to design corrosion sensors adequately and to select an appropriate location for installation.

The random fluctuations of ECN recorded with corrosion sensors are characteristic for the mode of corrosion attack encountered. Different modes of corrosion attack are associated with different signal patterns, which can be therefore used as a "finger-print", indicating, for instance, uniform corrosion, pitting, crevice corrosion or stress corrosion cracking. Moreover, signal patterns of the various modes of corrosion attack vary as a function of the actual status or progress of degradation. In addition to adequate design of corrosion sensors, processing and analysis of recorded data is a key feature of ECN techniques. As a consequence, accurate and effective on-line corrosion surveillance can be achieved only on the basis of modern instrumentation together with sophisticated data processing and analysis techniques.

## 4.2 Application Example

Characteristic features of on-line corrosion surveillance using ECN techniques are now described in terms of measurements in a nuclear power station. The measurements were performed in the calandria of a pressurized heavy water reactor (PHWR) of the pressure tube type [4]. The general features of this type of reactor are shown in Fig. 9. The calandria vault contains the fuel channel assemblies and subsystems of the heavy water moderator system and consists of concrete walls through which all coolant piping must pass. The calandria vault concrete walls, floor and roof, are cooled by a biological shield cooling system. Such cooling is necessary to limit the maximum concrete temperature to 54°C and to minimise thermal movement of the vault concrete. An additional water cooled thermal shield is provided to attenuate the higher flux in certain locations of the calandria. Major construction materials in the calandria include carbon steel and low alloy steels. The calandria vault in the nuclear power station considered has inside dimensions of approximately 6 m width, 10.7 m length, a height of 16.7 m and a free volume of 625.6 m<sup>3</sup> which is filled by nominally dry air. However, as a result of sporadic leaks, for instance through the piping of the biological shield cooling system, the vault air may reach high levels of humidity. The radiolysis of moist air in the calandria vault results in the production of nitric acid by the following reactions:

Nitrogen oxides are produced by radiolysis of nitrogen and oxygen which results in a large number of radicals:



With the addition of water to dry air, nitric acid is produced based on the following reaction step:



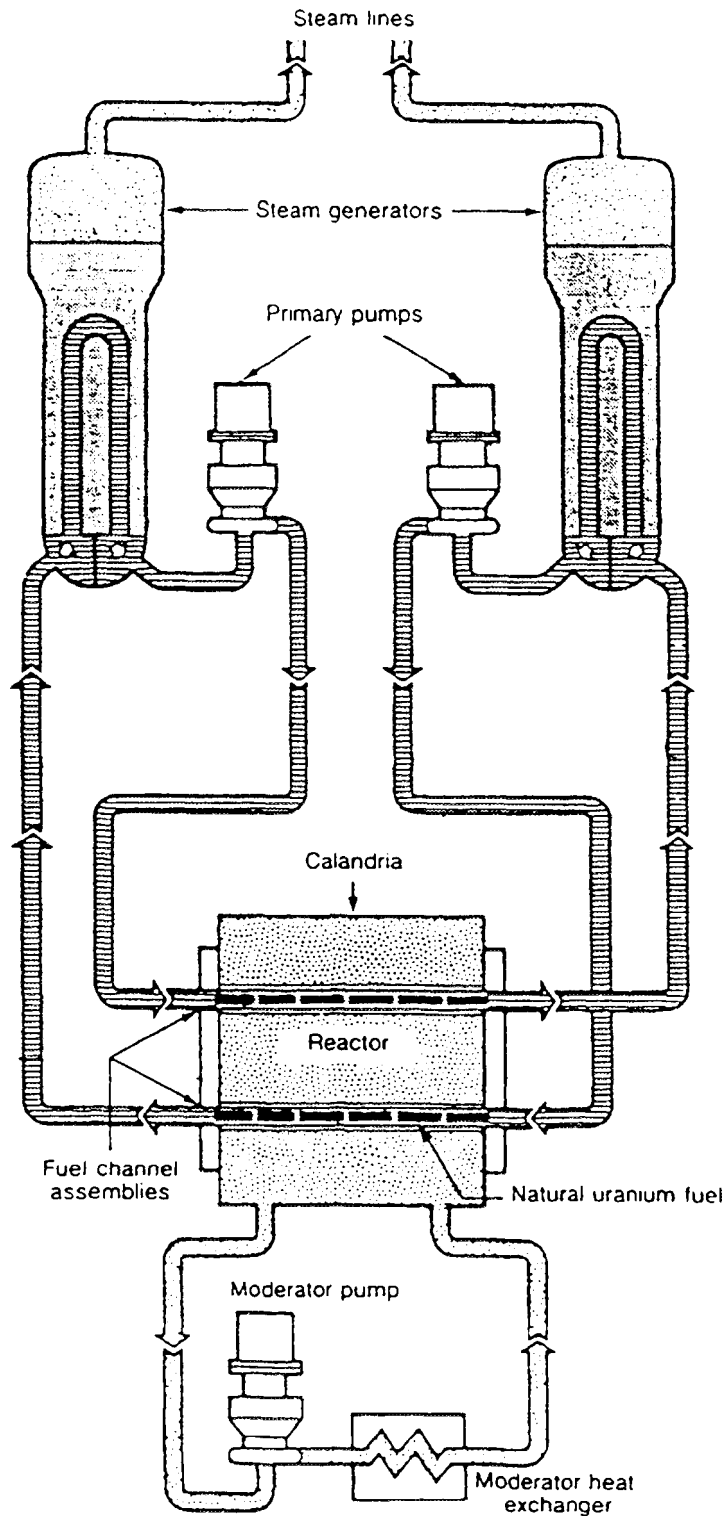


**Figure 9** CANDU nuclear steam supply system. The fluids, represented by different types of shading, are (from top to bottom): light water steam, light water condensate, heavy water coolant, heavy water moderator (from [8]).

The presence of nitric acid has been detected by analysis of vault sump drain samples (measured pH values of 3.2 to 4.8).

In addition, visual inspections of components revealed the local presence of dust-like particles. Samples of dust and loose debris were retrieved, using remotely controlled tooling. Chemical analysis also indicated presence of  $\text{NO}_3^-$  and a minor amount of calcium (2 - 10 wt. pct.). The presence of calcium can be related to release from the concrete walls of the vault. Thus, the possibility of the formation of concentrated aqueous nitrate solutions within a vault with a high relative humidity cannot be totally excluded. Concentrated nitrate solutions can induce stress corrosion cracking in carbon steels, so that concerns were expressed regarding the integrity of all exposed carbon steel components under such conditions.

On-line corrosion surveillance using ECN techniques was implemented in the calandria vault with the following objectives:

- To monitor continuously the corrosion status of carbon and low alloy components.
- To correlate corrosion behaviour with changes in environmental conditions.
- To assess the effects of remedial actions.

Two corrosion sensors were installed in the vault, each consisting of five different materials to be monitored. The top surfaces of the corrosion sensors were covered with a layer of dust and loose debris, which had been retrieved during previous inspections. The deposits favour the absorption of moisture from the environment. In part, stressed sensors were used, since occurrence of stress corrosion cracking in carbon and low alloy steels in the polluted environment could not be completely excluded. Electrical connections were made with radiation resistant sheathed and insulating cables.

The corrosion surveillance system was operated via remote control. The system logged corrosion data 24 hours a day with a data storage capacity for 56 weeks. Data were taken once per hour.

A combination of zero resistance ammetry, impedance spectroscopy and ECN was employed.

In the case of uniform corrosion, the corrosion rate  $i_{corr}$  can be estimated from impedance spectroscopy and ECN measurement data. The charge transfer resistance  $R_{ct}$  obtained from impedance spectroscopy measurements is proportional to the corrosion rate  $i_{corr}$ , i.e.

$$i_{corr} = B'/R_{ct}.$$

The constant  $B'$  is a modified Stern-Geary value.  $i_{corr}$  is converted to a corrosion rate using Faraday's Laws.

In case of ECN measurements, estimates of the rate of uniform corrosion are obtained in an analogous method to that used for impedance. In this case ECN resistance  $R_n$  is calculated by:

$$R_n = V_n/I_n$$

where  $V_n$ ,  $I_n$  are the potential and current standard deviations.

The degree of localisation of corrosion (DoL) provides an indication of the stochastic distribution of microscopic events from current noise ( $I_n$ ) and the root mean square of the current ( $I_{rms}$ ):

$$DoL = I_n/I_{rms}.$$

For uniform corrosion the DoL is typically  $1 \times 10^{-3}$ . In the case of localised corrosion (e.g. pitting, crevice corrosion or stress corrosion cracking) the raw data typically exhibit stochastic transients and the DoL value can approach unity.

Zero resistance ammetry (ZRA) was used for measurement of the galvanic coupling current.

In addition to on-line corrosion measurements with these methods, dewpoint measurements were taken at other locations in the vault.

For brevity, this paper concentrates on measurement data from one of the low alloy steels over a time period of three months (from September to November 1991).

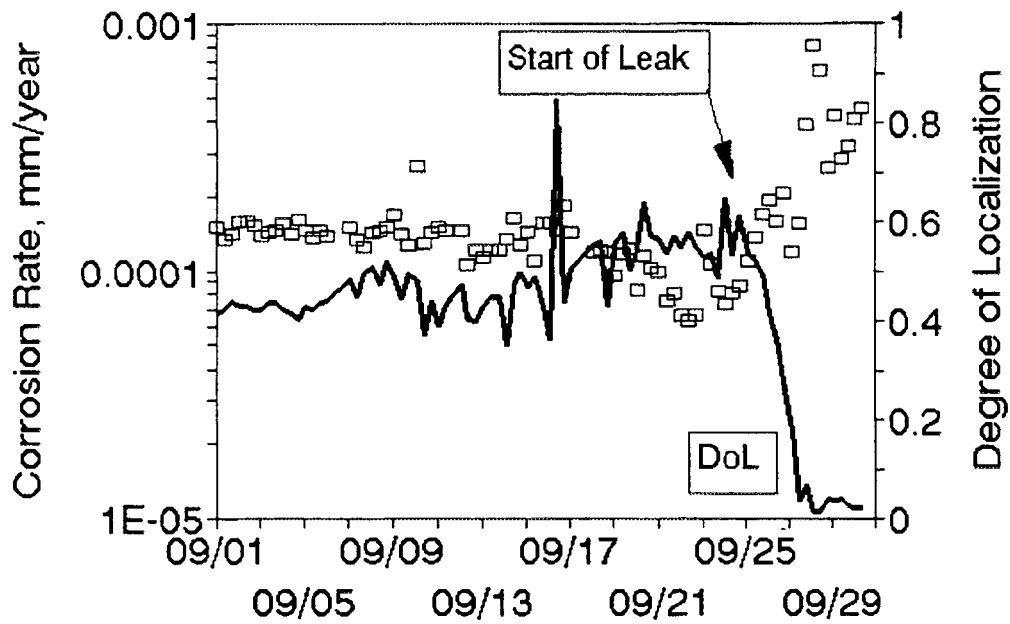
Before the time period considered, the vault environment was dry with negligible corrosion. A significant bioshield cooling supply leak of 10 kg per hour was reported by the staff of the plant on September 30. After a period of about one month, the leak was repaired on November 2.

Figure 10 shows the analysed ECN data measured for September. An increase in corrosion rate and a decrease in DoL is observed in the course of September 26. The mean coupling current, measured with ZRA, increases in parallel (Fig. 11). The data unequivocally signal the onset of increased, uniform corrosion as a consequence of the in-leakage of cooling water into the vault.

The second sensor detected the leak one day later. The delay showed that the location of the leak was closer to the first sensor.

The leak could only be detected with other methods four days later. The equivalent water loss into the vault area during this time was approximately 960 kg.

In October, uniform corrosion continued (Fig. 12). ECN data indicate maximum rate estimates of 0.1 mm per year. Corrosion rate estimates from impedance



**Figure 10** ECN corrosion rates and degree of localisation measured during September, 1991.

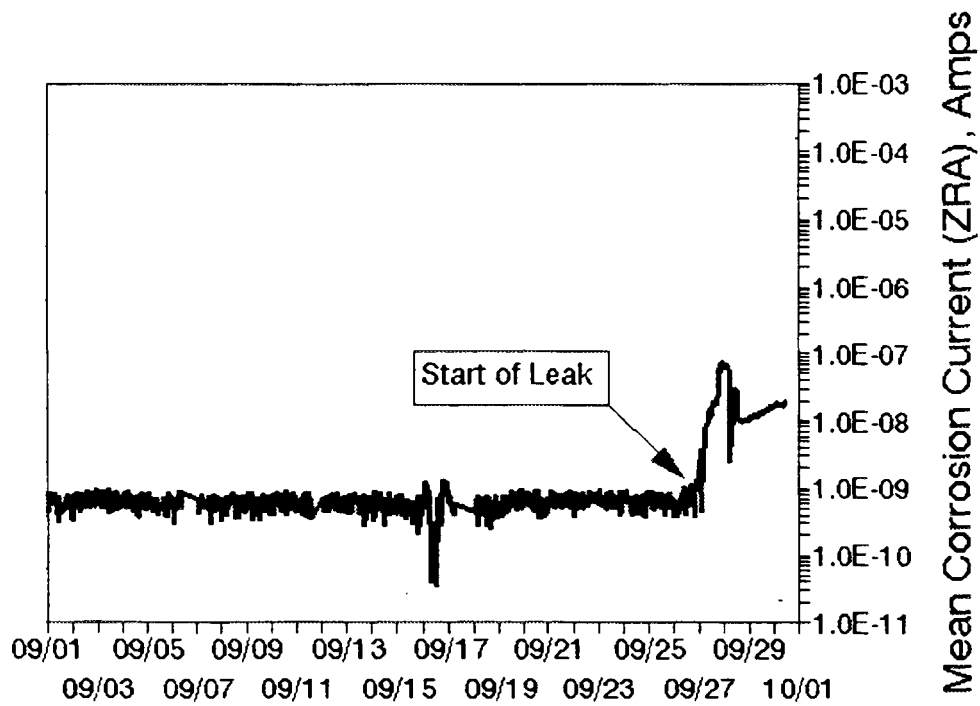


**Figure 11** Increase in the mean coupling current, measured using ZRA, during September 1991.

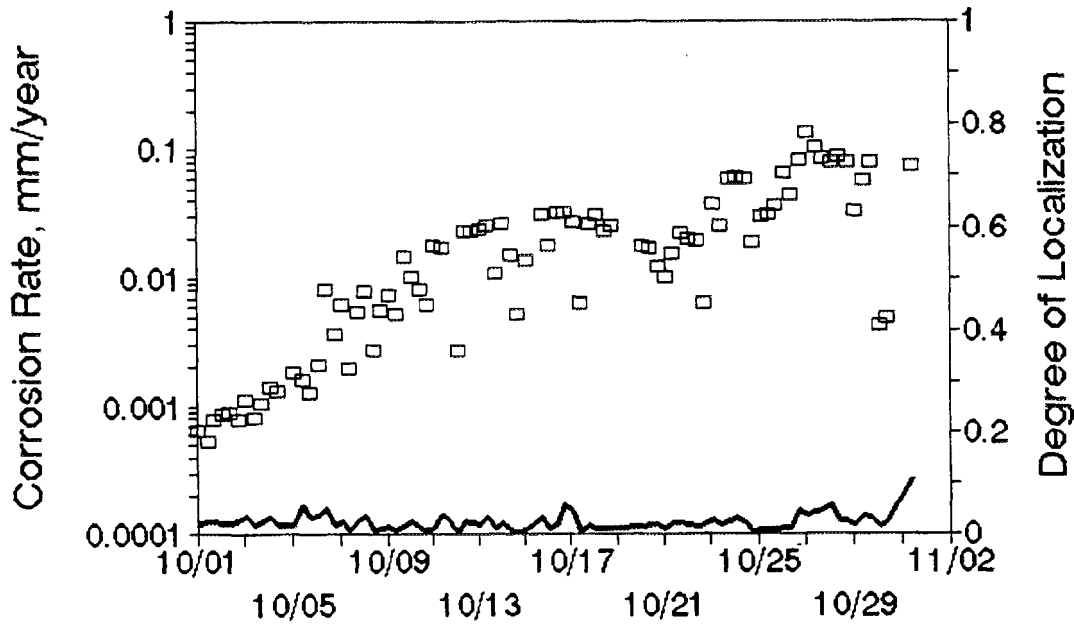


**Figure 12** ECN corrosion rates and degree of localisation measured during October 1991.

spectroscopy were in good agreement with ECN corrosion rate data. Mean coupling currents achieve maximum levels of about  $1 \times 10^{-6}$  A (Fig. 13). These values must be compared to values of  $1 \times 10^{-9}$  A measured during initially "dry" condition levels.

The leak was sealed on November 2. This was associated with an immediate decrease in the mean coupling current to  $1 \times 10^{-7}$  A (Fig. 14). ECN corrosion rate estimates decreased in parallel by one order of magnitude. However, the corrosion activity did not return to the extremely low levels of early September for various reasons:

- Although the leak was sealed, the relative humidity in the vault did not immediately decrease to the initial, very low value.
- The film of corrosion product formed on the surface of the sensor favoured the retention of absorbed moisture.

These effects were expected. However, corrosion activity had been substantially mitigated and continued to decrease subsequently.

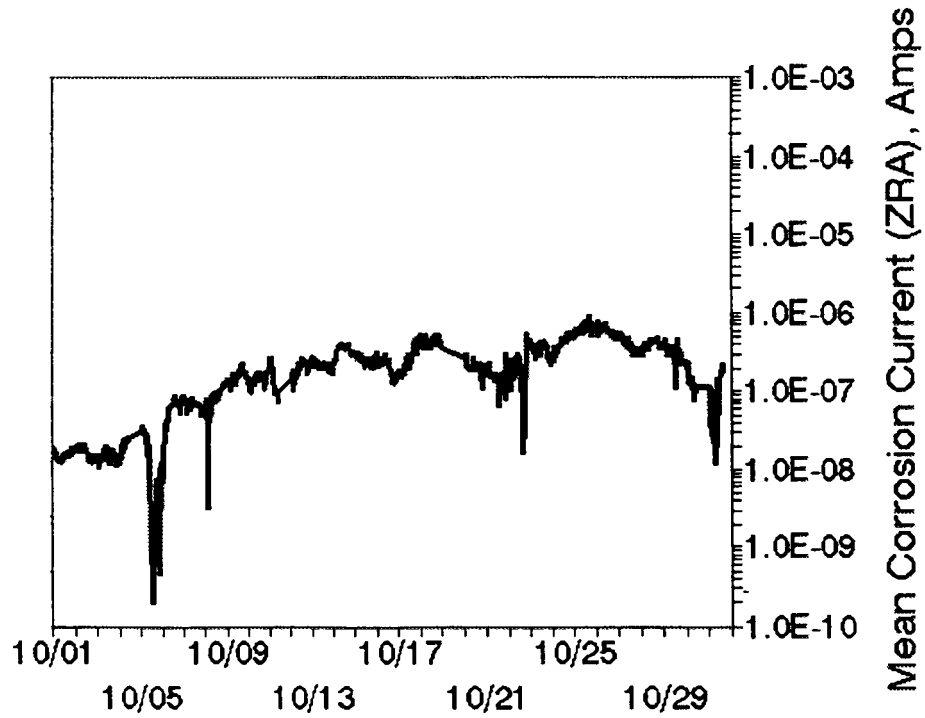


Figure 13 Mean coupling current measured during October 1991.

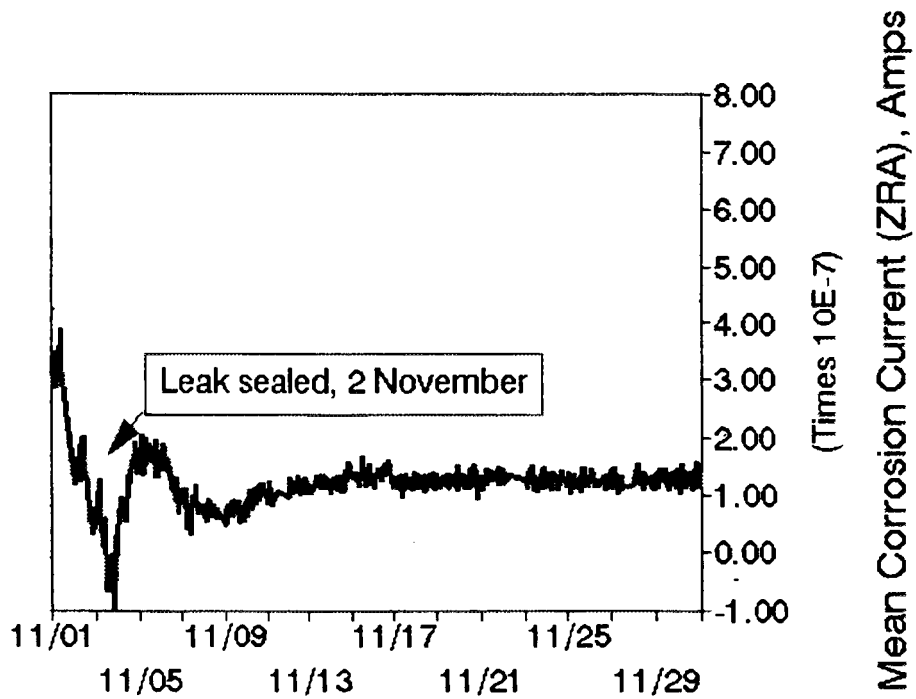


Figure 14 Mean coupling current measured during November 1991.

The analysis of the recorded ECN measurement signals gave no evidence for stress corrosion cracking. Based on these results, the integrity of carbon and low alloy steel components in the vault was clearly maintained.

#### **4.3 Concluding Remark**

In summary, the corrosion surveillance system has proved successful for monitoring variations in low levels of uniform corrosion in acidic humid atmospheres inside the reactor vault. The system had a fast response time for the identification of water leaks and provided corrosion data for the selected materials in real time. The general corrosion behaviour of materials is indeed affected by changes in vault moisture, but no evidence for stress corrosion cracking was observed. The system thus assisted the operator of the nuclear power station to verify the continued safe corrosion status of the facility.

The evident advantages of on-line corrosion surveillance have been outlined using an application case from the nuclear industry. However, the described corrosion surveillance systems have also been used with great success not only in the fossile power industry, as well as in chemical/petrochemical and refining industries and in systems for oil and gas production [11], [12]. Such approaches are now being adopted for permanent plant installation with the ultimate goal of full integration into plant control and measurement systems.

### **5. Discussion and Future Activities**

Sound design and adequate selection of construction materials, in combination with suitable water treatment practices, ensure the reliable operation of nuclear power stations with high availability.

For existing facilities in the nuclear industry, targets such as reduction of radiation exposure levels and higher burn-up of fuel, etc. are gaining in importance. An attempt has been made to outline major advantages in using on-line monitoring sensors in plant systems for water chemistry and corrosion surveillance in order to achieve such targets. Two types of sensors were used:

- (1) Sensors for on-line, in-situ measurement of water chemistry parameters, namely pH value and redox potential. Use of these sensors was backed up in Loviisa 1 by conventional and advanced water chemistry analysis techniques, yielding information about actual concentrations of water treatment chemicals ( $\text{H}_3\text{BO}_3$ ,  $\text{NH}_3$ ,  $\text{H}_2$ ,  $\text{O}_2$ ,  $\text{N}_2\text{H}_4$ ) and various metal cations dissolved in the coolant.
- (2) Sensors for measurement of corrosion parameters, such as corrosion potential, current and potential noise, coupling currents, impedance spectroscopy response.

Both corrosion properties and response of the involved materials and water chemistry parameters must be understood in order to optimise features such as release, transport and deposition of corrosion products and to ensure trouble-free operation of plant systems. Further significant advantages can be expected to accrue from an integration of the various types of sensors described into a common water chemistry and corrosion surveillance system. Experience will be gained in the near future with a complete set of the described sensors. These will be installed in a loop of a test reactor operated with PWR primary coolant chemistry. The goal of these investigations is a better understanding of activity build-up on various materials as a function of the coolant chemistry. For this purpose, the physicochemical properties of the fluid will be recorded concurrently with characterisation of the properties of oxide layers using corrosion surveillance instrumentation. Development of sensors for in-situ  $\text{H}_2$  and

O<sub>2</sub> measurement is also in progress. Depending on the state of development, installation in the loop may be possible.

Notwithstanding these ongoing activities, the experience described from separate use of these different types of sensors with for different purposes shows that new and additional information about plants and their actual process conditions was obtained in each case. Moreover, the intimate relationship between the operational situation and its consequences for the quality of the working fluid and the response of the plant materials was revealed. Advanced on-line, in-situ sensors for water chemistry and corrosion surveillance are clearly very important for a better understanding of plants and their actual process conditions, since in-plant conditions and process control can be optimised. Optimisation of plant operation is, indeed, a prerequisite in order to fulfil the increasing and more stringent demands being made upon existing facilities in the nuclear industry.

## REFERENCES

- [1] Mäkelä, K., Aaltonen, P., Järnström, R.  
"Shutdown water chemistry and dissolution of corrosion products at Loviisa 1 PWR", EPRI-Meeting on PWR Water Chemistry, San Diego, Dec. 1992.
  
- [2] Beyer, W., Stellwag, B., Wieling, N.  
"On-line monitoring of electrode potentials in the steam generator of a PWR", Proc. 3rd Int. Symp. on Env. Deg. of Materials in Nuclear Power Systems - Water Reactors, Eds. Theus, G.J., Weeks, J.R., The Metallurgical Soc., 1988, 173 - 181.

- [3] Haag, J., et al.,  
"On-line Messung von Redox- und Korrosionspotentialen im Wasser für DWR-Dampferzeuger", VGB Kraftwerkstechnik 70 (1990), 236 - 241.
- [4] Quirk, G.P., et al.  
"Corrosion surveillance for reactor materials in the calandria vault of Pickering NGS A Unit 1", 6th Int. Symp, on Env. Deg. of Materials in Nuclear Power Systems - Light Water Reactors, Aug. 1-5 (1993), San Diego.
- [5] Riess, R.  
"Control of water chemistry in operating reactors", this meeting.
- [6] Henzel, N.  
"Alternative water chemistry for the primary coolant of PWRs", this meeting.
- [7] Molander, A., et al.  
"Corrosion potential measurements in reactor water of a PWR, Proc. Conf. on Water Chemistry for Nuclear Reactor Systems 4, BNES, London (1986), 161 - 167.
- [8] Coolant technology of water cooled reactors: an overview, IAEA technical reports series No. 347, IAEA, Vienna, 1993.
- [9] Rothwell, A.N., Eden, D.A.  
"Electrochemical Noise techniques for Determining Corrosion Rates and Mechanisms", NACE Corrosion 92, Nashville, tennessee, 26 April - 1 May 1992.

- [10] Cox, W.M., Syrett, B.C.  
"The Future of On-Line Materials Surveillance for Operating Prozess Plants", NACE Conference - Life Prediction of Corrodible Structures, Cambridge, UK, September 1991.
- [11] Rothwell, A.N., Walsh, T.G., Cox, W.M.  
"On-Line Corrosion Investigation and Surveillance - Chemical Plant Case Studies", NACE Corrosion 91, Cincinnati, Ohio, 11-15 March 1991, Paper 170.
- [12] Illson, T., Eley, C., Mok, W.Y., Cox, W.M., Meadowcroft, D.B.  
"Recent initiatives in the use of modern electrochemical instrumentation for FDG corrosion investigation and surveillance", Werkstoffe und Korrosion 43, 321-328 (1992).



## AN ELECTROCHEMICAL SENSOR FOR MONITORING OXYGEN OR HYDROGEN IN WATER

LEITAI YANG\* , D.R. MORRIS, D.H. LISTER  
Department of Chemical Engineering,  
University of New Brunswick,  
Fredericton, Canada

### Abstract

Preliminary studies have been done on a simple electrochemical sensor which shows promise as a cheap, robust instrument for measuring dissolved oxygen or hydrogen in water. The sensor is based upon the solid-state electrolyte "Nafion" (trade name of perfluorinated sulphonic acid, manufactured by DuPont Inc.).

The Nafion was dissolved in a mixture of aliphatic alcohols, made into a slurry with platinum black, and applied to a ~1 cm-square electrode made of stainless steel gauze. The potential of the electrode was measured relative to a standard calomel electrode (SCE) in acid solutions at room temperature through which mixtures of oxygen and nitrogen or hydrogen and nitrogen were bubbled. The sensor was responsive to the equilibrating gas with good reproducibility. A similar sensor without the Nafion was not at all sensitive to changes in oxygen concentration. The voltage response of the sensor showed non-Nernstian behaviour, which suggests that the electrochemical reactions at the electrode surface are complex. Further testing of the sensor is required to verify its sensitivity and responsiveness in typical reactor coolant chemistries and to demonstrate its durability over a range of temperatures.

---

\* Present Address: Centre for Nuclear Energy Research  
University of New Brunswick,  
Fredericton, Canada

## **2. Introduction**

An important aspect of corrosion control in nuclear reactors is the reduction of dissolved oxygen in coolant systems. In the primary coolant of PWRs and CANDUs, this entails adding hydrogen to promote the radiolytic back-reactions that occur in the core. A similar philosophy is behind the addition of hydrogen to BWR feedwater in the application of Hydrogen Water Chemistry. In secondary coolants, too, control of dissolved oxygen is important to minimize damage to steam generator components.

Effective control of dissolved gases depends upon efficient monitoring techniques. Traditional methods of hydrogen and oxygen measurement involve sampling the coolant and extracting the gases for analysis on a "gas rack" system. Over the last ten years or so, electrochemical instruments have been used more and more - usually with extracted samples. These instruments are expensive and somewhat difficult to operate and maintain. There is clearly a need for a cheap, compact and robust instrument that can measure dissolved oxygen or hydrogen in water.

Solid-state electrolytes are promising materials to form the basis of such instruments. At the University of New Brunswick, studies have been carried out on a sensor consisting of the solid-state electrolyte Nafion, mixed with platinum black and supported on a stainless steel gauze.

## **3. Experimental**

A diagram of the sensor is shown in Fig. 1. It comprises a stainless steel gauze ~1 cm square to which a slurry of platinum black in Nafion solution has been applied. Nafion is a copolymer proton conductor [1] and an excellent catalyst [2]. It is insoluble in water, resistant to oxidizing and reducing environments and can withstand temperatures up to 200°C or so. The

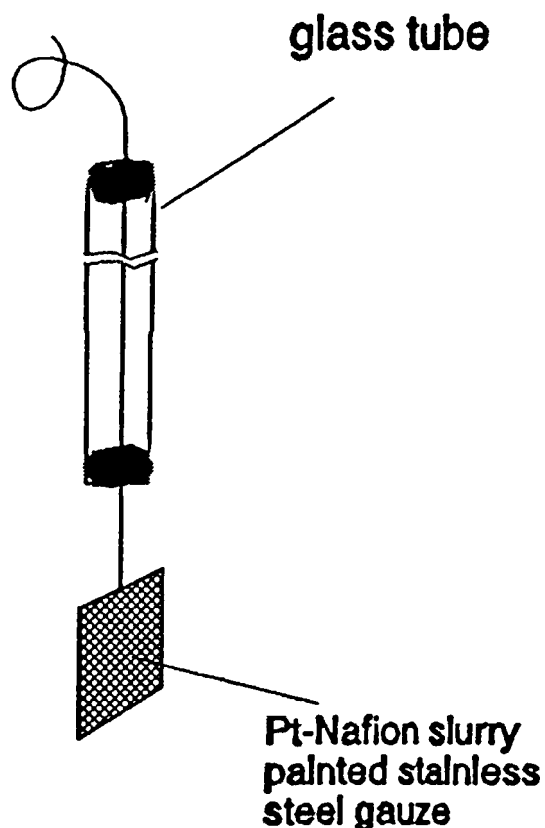
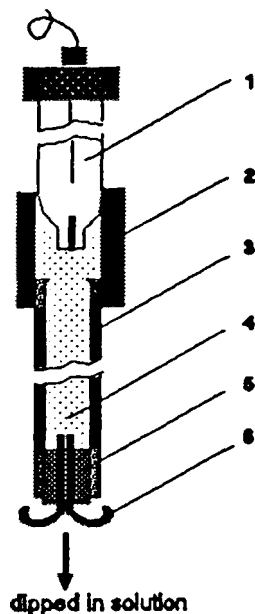


Figure 1 Sensor Electrode for Monitoring Oxygen or Hydrogen in Water.

Nafion solution (which was supplied by Aldrich Chemicals) contains 5%wt of Nafion in the  $H^+$  form, mixed with lower aliphatic alcohols and 10% water. The platinum black was a fuel-cell grade supplied by Johnson Matthey Ltd. (99.9%, surface area  $>20 \text{ m}^2/\text{g}$ ). After the evaporation of the alcohols and water, the platinum black was bonded onto the gauze with a thin film of Nafion.

The electrode potential of the sensor was measured with an electrometer (Keithley 610C) against a calomel reference electrode which was in contact with the test water through a bridge as shown in Fig. 2. The oxygen and hydrogen concentrations in the water were controlled by bubbling a  $H_2-N_2$  or  $O_2-N_2$  gas mixture of known composition at a constant temperature. A stirrer was installed in the air-tight electrochemical cell. In order to have a conducting medium between the sensor electrode and the reference electrode,



- |                      |                  |
|----------------------|------------------|
| 1. Calomel electrode | 4. KCl solution  |
| 2. Seal              | 5. Epoxy seal    |
| 3. Glass tube        | 6. Nafion strips |

**Figure 2 Nafion Membrane Salt Bridge**

the water was slightly acidified by adding a drop of concentrated acid (nitric, acetic or sulphuric).

#### **4. Results and Discussions**

The results of a typical experiment with water that was acidified with acetic acid (pH = 1.3) are shown in Fig. 3. The response of the sensor to the change of oxygen concentration was satisfactory for oxygen concentrations >1.4 mg/kg (the corresponding partial pressures were >0.049 atm). The stability of the sensor potential at constant oxygen concentration for partial pressures >0.049 atm is excellent in comparison with those reported in the literature for a bare metal platinum electrode [3]. When such a bare metal electrode was tested in the same solution as the sensor, its potential was unstable and hardly responded to the change of oxygen concentration. This may be an indication that the catalytic ability of platinum was greatly

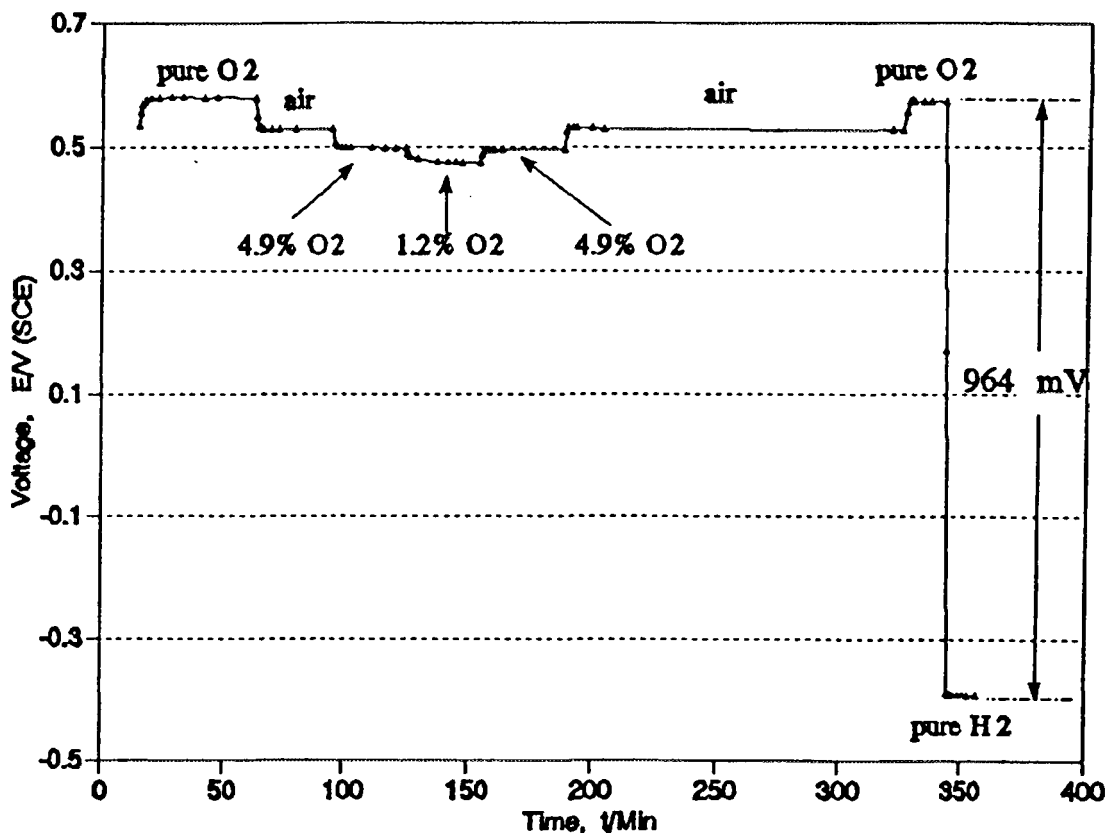


**Figure 3** Sensor Response to Oxygen and Hydrogen in Acidified Water

enhanced by the addition of Nafion. Fig. 3 also shows that the open circuit potential of the sensor for pure oxygen (partial pressure = 1 atm) is 964 mV against that of pure hydrogen. This agrees well with the reported results [3].

The potential of an electrochemical sensor,  $E$ , is related to the concentration or pressure  $P$  of the active species, and is frequently represented in terms of the Nernst equation, of the form:

$$E = E^{\circ} + \frac{2.3RT}{zF} \log P \quad (1)$$

where  $E^{\circ}$  is a constant,  $z$  is the number of electrons involved in the electrochemical reaction and  $R$ ,  $T$ , and  $F$ , have their usual meaning.

The results of the experiments with oxygen/nitrogen gas mixtures shown in Fig. 3 are presented in terms of Equation (1) in Fig. 4. It is seen that the voltage is a curvilinear function of  $\log P$ , which suggests that the electrochemical reaction at the sensor is complex. For oxygen partial pressures  $>0.049$ , the slope in Fig. 4 is 60 mV/decade which indicates, according to Equation 1, that the number of electrons involved in the electrochemical reaction is unity.

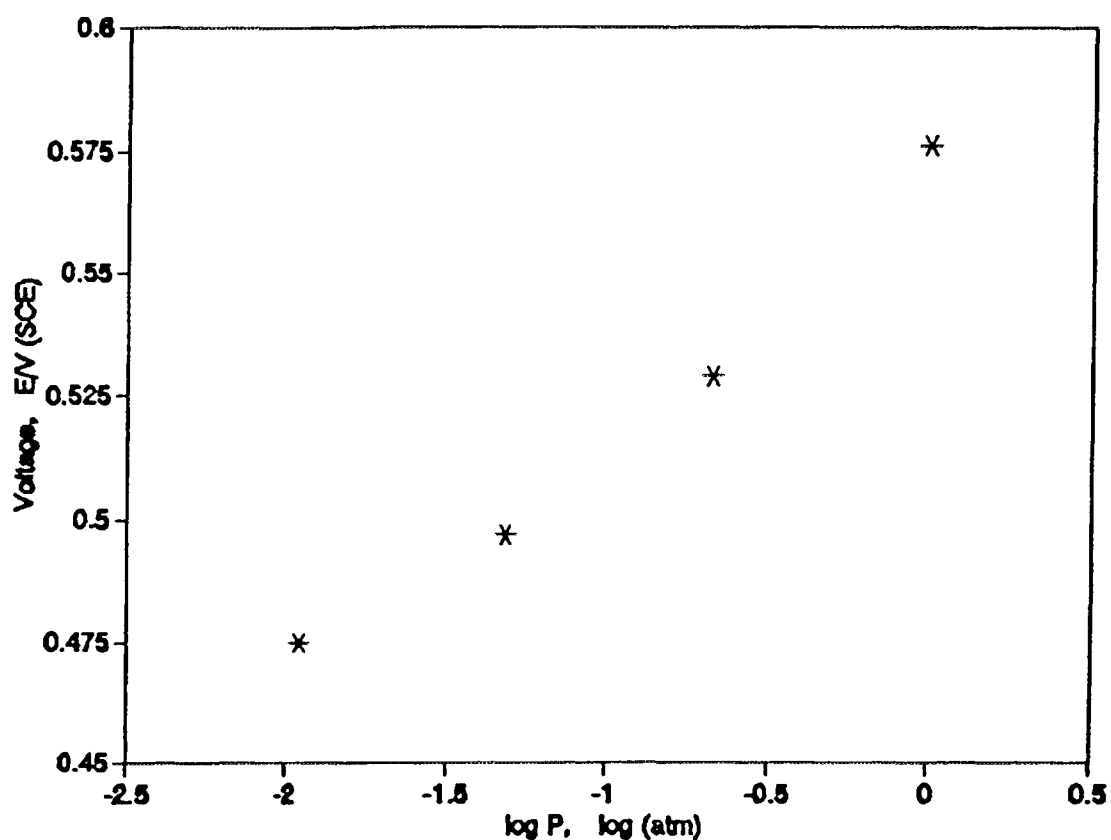


Figure 4 Response of Sensor Potential to Oxygen Pressure

Table I summarizes the relationships between the sensor potential and the logarithm of the partial pressure of oxygen (for the higher values 0.049 to 1 atm) which was equilibrated in water acidified with different acids. All results indicate that the

**Table I SENSOR RESPONSES TO PARTIAL PRESSURE OF OXYGEN BUBBLING IN WATER**

Acid added and pH	Slope (V/decade)	Regression coefficient	z
H <sub>2</sub> SO <sub>4</sub> pH=1.7	0.0573	0.998	1.04
HAC pH=1.3	0.0619	0.993	0.961
HNO <sub>3</sub> pH=2.6	0.0566	0.995	1.05

Temperature: 27°C. Oxygen pressure range: 0.049 to 1 atm.

slopes of the Nernstian plots correspond to a single-electron transfer reaction ( $z=1.017\pm 0.049$ ).

Other observations are summarized as follows:

- For all the solutions tested (i.e., for pH < 3.5), sensor potential was independent of pH. This may be due to the fact that the concentration of H<sup>+</sup> in Nafion is 1.6 M, which is significantly higher than that of the test water. Neutral or alkaline coolants might have to be acidified to give steady results.
- The sensor would not respond to the changes of oxygen partial pressure if the concentration of chloride ion was >70 mg/kg. Such non-responsiveness is due to chloride poisoning of the reactions at the Pt-Nafion electrode, as reported by Paffett et al [4]. This should pose no problems at the low chloride levels experienced in reactor systems.
- It was necessary to maintain a high speed of agitation of the solutions. At low speeds, the electrode potential was not

stable and the responses to changes of oxygen concentration were slow. This behaviour is attributed to mass transfer effects at the electrode/water interface.

## **5. Summary and Conclusions**

The simplicity of the sensor makes it an ideal instrument for routine use, while its cheapness means that it can be replaced frequently if necessary. The tests so far have given promising results, though issues still to be resolved include:

- determining the response at low oxygen and hydrogen concentrations;
- resolving difficulties with interference from hydrogen contamination during oxygen measurement and vice versa (note that such difficulties are common in electrochemical measurements of REDOX conditions);
- characterizing the effects of temperature, high pH and ionic strength; for maximum usefulness, the sensor should work in primary coolant streams (>260°C) with lithium hydroxide to pH ~10.3 (CANDU systems) and high boron and lithium concentrations (PWR systems).

## **ACKNOWLEDGEMENT**

The authors acknowledge financial support provided by the Natural Sciences and Engineering Research Council of Canada.

## **REFERENCES**

- [1] Kipling, B.; in 'Perfluorinated Ionomer Membranes', eds. Eisenberg, A. and Yeager, H.L., American Chemical Society, Washington, D.C., 475-487 (1982).
- [2] Waller, F.J. and Scoyoc, R.W.V.; Chemtech, July, 438 (1987).

- [3] Damjanovic, A.; in 'Modern Aspects of Electrochemistry', eds., J.O'M. Bockris and B.E. Conway, Plenum, New York (1969).
- [4] Paffett, M.T., Redondo, A. and Gotesfeld, S. Proc. Electrochem. Soc., 87-12 (Proc. 2nd Symp. Electrode Materials and Process for Energy Convers. and Storage, 1987), 268-282 (1987).



## ADVANCED ANALYTICAL TECHNIQUES FOR BOILING WATER REACTOR CHEMISTRY CONTROL

H.P. ALDER, E. SCHENKER  
Paul Scherrer Institute,  
Villigen, Switzerland

### Abstract

In the past decade, the recommendations for an optimum water chemistry for boiling water reactors (BWR), have changed drastically. Originally high purity water, characterized mainly by the electrical conductivity, was considered optimum. Now a number of additives are recommended; - hydrogen to prevent stress corrosion cracking (SCC) of primary circuit materials; - to reduce radiological exposure of the personnel: a constant ratio of dissolved Ni/Fe to retain Co-60 on the fuel rods, or Zn to reduce Co-60 deposition on the austenitic surfaces. It is evident that this improved water chemistry requires up-dating of existing and development of new analytical techniques.

The operation of a pilot loop at PSI, simulating the conditions of a BWR external recirculation loop (290°C, 90 bar), provides the opportunity to test advanced analytical techniques for future plant commissioning. The aim being to improve water chemistry control during normal plant operation and transients.

The analytical techniques applied can be divided into 5 classes: OFF-LINE (discontinuous, central lab), AT-LINE (discontinuous, analysis near loop), ON-LINE (continuous, analysis in by-pass). In all cases pressure and temperature of the water sample are reduced. In a strict sense only IN-LINE (continuous, flow disturbance) and NON-INVASIVE (continuous, no flow disturbance) techniques are suitable for direct process control; - the ultimate goal.

An overview of the analytical techniques tested in the pilot loop is given. Apart from process and overall water quality control, standard for BWR operation, the main emphasis is on water impurity characterization (crud particles, hot filtration, organic carbon); on SCC control for materials (corrosion potential, oxygen concentration) and on the characterization of the oxide layer on austenites (impedance spectroscopy, IR-reflection). The above mentioned examples of advanced analytical techniques have the potential of in-line or non-invasive application. They are at different stages of development and will be described in more detail.

## 1. RECENT DEVELOPMENTS IN BWR WATER CHEMISTRY

In the past decade, the recommendations for an optimum water chemistry for boiling water reactors (BWR) with external recirculation loops have changed drastically. Originally high purity water, characterized mainly by the electrical conductivity, was considered optimum. The German VGB-guidelines for the BWR reactor water are shown in TABLE I [1], [2].

TABLE II shows typical values of the reactor water impurities of the two Swiss General Electric (GE) BWR's:

- Mühleberg (KKM, 320 MW, 1972) with a brass condenser and total condensate polishing; iron-addition since January 1991
- Leibstadt (KKL, 942 MW, 1984) with a titanium condenser and partial condensate polishing; zinc-addition since March 1990.

TABLE I: German VGB-Guidelines for the BWR reactor water

		Guide Value	Normal Operation	Limiting Value
Electrical conductivity at 25°C	( $\mu\text{S}/\text{cm}$ )	< 1	0.2	10
Chloride	(ppm)	< 0.100	0.020	0.500
Silicon	(ppm)	< 4	0.500	--

TABLE II: Typical values for reactor water impurities at KKL and KKM

	KKL			KKM		
Cr (tot) [ppb]	1.71	$\pm$	0.81	2.24	$\pm$	0.95
Cu (tot) [ppb]	0.12	$\pm$	0.07	2.25	$\pm$	1.02
Fe (tot) [ppb]	1.65	$\pm$	0.97	0.21	$\pm$	0.05
Ni (tot) [ppb]	0.09	$\pm$	0.03	0.26	$\pm$	0.09
Zn (tot) [ppb]	--			0.76	$\pm$	1.01
SiO <sub>2</sub> [ppb]	117	$\pm$	48	125	$\pm$	51
O <sub>2</sub> [ppb]	--			129	$\pm$	17
<sup>60</sup> Co (tot) [Bq/ml]	13.96	$\pm$	6.50	15.90	$\pm$	8.54

These average values are based on weekly data sets over approximately one year (50 - 70 sets) before reactor water additives were introduced [3].

In recent years a number of additives were recommended with the main purpose:

- to minimize radiological exposure of the staff
- to prevent corrosion of reactor materials
- to achieve high fuel burn-up
- to minimize radioactive waste

### **1.1. Oxygen injection**

Oxygen injection into the feed water prevents the corrosion of the carbon steel piping and reduces the shut-down dose rate [4]. 20 to 60 ppb oxygen injection into the feedwater before the condensate polishing system reduces the corrosion rate of the carbon steel by a factor of 100 and leads to a corrosion product content in the feedwater in the sub-ppb range [5].

Oxygen injection was introduced in Shimane-I in 1974 and subsequently also in other Japanese and US-plants; KKM introduced it in 1981.

### **1.2. Nickel to iron control**

A minimum Co-60 activity in the reactor water can be achieved if cobalt is deposited on the fuel rod cladding in an insoluble form. Dissolved nickel and cobalt, which are chemically similar, form a nickel (cobalt)-iron-spinell ( $\text{NiFe}_2\text{O}_4$ ) on the fuel, provided that the Ni/Fe-ratio is kept at least at the theoretical value of 0.5; in practice 0.2 is recommended. An increase of iron in the feedwater is achieved by by-passing the condensate filter units, by electrolytic dissolution of iron or by addition of iron salts. A reduction of the ionic Co-60 content in the reactor water below 1 Bq/ml was reported [5].

The Ni/Fe-ratio in BWR's is controlled, in particular in Japan and in Sweden. KKM adds 0.65 ppb Fe-III as oxalate to the feedwater since January 1991 to maintain a ratio of 0.24 between II-valent cations ( $\text{Zn} + \text{Ni} + \text{Cu}$  [1/4]) and III-valent Fe [6]. Unfortunately the weekly data sets of the reactor water for the year following the iron addition showed little change in Co-60 activity compared to TABLE II ( $14.8 \pm 5.7$  Bq/ml).

### 1.3. Zinc addition

For GE-BWR's the addition of 5 to 15 ppb zinc to the reactor water is recommended to reduce the local dose rate on austenitic surfaces. Zinc apparently acts as a corrosion inhibitor for stainless steel surfaces and is incorporated into the protective film. Both effects translate into a reduced Co-60 build up. In the plant contact dose rates may be reduced by at least a factor of 3 [5].

Currently 10 US BWR's inject zinc [7]. KKL adds 0.4 ppb zinc to the feedwater by a passive system since March 1990. The weekly data sets for the reactor water for the year following the zinc addition showed a decrease in the Co-60 activity compared to TABLE II ( $7.2 \pm 3.7$  Bq/ml).

The addition of zinc to the reactor water may also reduce the sensibility of materials to stress corrosion cracking (SCC). Fracture mechanic testing of 304 type sensitized stainless steel specimens in autoclaves under simulated BWR-conditions showed that the addition of 5 - 10 ppb zinc reduces the crack growth rate by a factor of 5 [8].

Concerning BWR-zircalloy fuel cladding corrosion, zinc does not appear to have an adverse effect because the concentration of injected zinc does not exceed the level typical for older BWR's with brass condensers [7].

### 1.4. Hydrogen water chemistry

The oxygen concentration in the reactor water is typically 200 - 400 ppb. The high oxygen concentration may cause intergranular stress corrosion cracking (IGSCC) in sensitized steels under tensile stress. To maintain the oxygen level at a few ppb the injection of 0.2 - 2 ppm hydrogen into the reactor water is recommended; hydrogen water chemistry (HWC).

Hydrogen added to the feedwater reacts in the core with radiolytic hydrogen peroxide and oxygen creating a reducing environment; electrochemical potential (ECP)  $< -230$  mV SHE. The main practical problem is monitoring ECP to control the hydrogen addition. Approximately  $1 \text{ m}^3$   $\text{H}_2$  / minute is required [9].

Numerous out-of-reactor and in-reactor tests showed the beneficial effect of HWC in preventing or slowing down IGSCC [10], since it was first introduced in Oskarshamn-2 in 1979. Still, side effects (high dose rates in the turbine building due to N-16; increased dose rates in the

primary system; increased fence dose rates; possible hydrogen pick-up by the fuel cladding; decreased visibility in the reactor water during fuel reloading) have recently led a number of plants, in particular in Sweden, to discontinue HWC.

Due to the new regulation on radiological protection based on ICRP 60 the Swiss BWR operators are concerned about the local fence dose rate and HWC is not planned.

### 1.5. pH adjustment

The pH for the BWR-operation is normally in the neutral region ( $\text{pH}_{20^\circ\text{C}} = 7,0$ ;  $\text{pH}_{300^\circ\text{C}} = 5,5$ ). Increasing the pH leads to a decrease in the corrosion rate and in the solubility of corrosion products. The short timed, controlled addition of potassium hydroxide in a German BWR showed that at  $\text{pH}_{300^\circ\text{C}} = 8$  the dissolved Co-58 and Co-60 activity reached a minimum in the reactor water. Therefore a controlled pH-increase is conceivable to reduce the activity in the reactor water [11].

## 2. OVERVIEW OF ANALYTICAL TECHNIQUES FOR BWR WATER CHEMISTRY CONTROL

To control the BWR reactor water chemistry at KKL, water samples are taken from a line tied to the pressure side of the recirculation pump. This line is cooled to  $30^\circ\text{C}$  and the length of about 30 m causes a delay in sampling of 15 to 30 minutes. The electrical conductivity, the most important parameter, is monitored continuously. Additionally, at regular intervals, oxygen and selected anions, in particular chloride, are determined. Once a week a complete analysis is performed: undissolved impurities ( $> 0.45 \mu\text{m}$  filter) Cr, Fe, Cu, Ti, Ni; dissolved impurities ( $< 0.45 \mu\text{m}$  filter) Cr, Fe, Cu, Ti, Ni, (Zn),  $\text{SiO}_2$ . Further, on the same samples, the  $\gamma$ -activity for selected nuclides, in particular Co-60 (Zn-65), is measured [6].

This procedure has the following disadvantages:

- The reduction in pressure, temperature and the residence time in the sampling line may change the sample composition.
- The time delay in the analytical results retards an intervention.

- The analytical procedure is guided by high purity water chemistry and modern water additives control are only partially taken into consideration.

In recent years analytical techniques in general have progressed stepwise and it may be useful to review modern analytical possibilities for BWR operation. TABLE III divides analytical techniques in different classes [12]:

#### OFF-LINE; AT-LINE; ON-LINE; IN-LINE; NON-INVASIVE

Characteristic features of each class are listed in a general way; examples of analytical methods are given. These methods are either already in use or may be promising for BWR operation. In coming years the tendency will be to move from OFF-LINE to higher classes; the ultimate goal being NON-INVASIVE.

### 3. TESTING OF ADVANCED ANALYTICAL TECHNIQUES IN A PILOT-LOOP

#### 3.1. Description of the pilot loop

At PSI since 1988 a pilot-loop is in operation, simulating the conditions in the external recirculation loops typical for GE-BWR's. The main purpose is the study of the corrosion products behaviour, in particular of Cobalt (liberation, transport and deposition of ionic and particulate material), during steady state operation and transients for different water chemistry parameters. The aim is to reduce the radiological exposure of the staff during operation and maintenance, mainly due to Co-60 deposition on austenitic surfaces. This pilot-loop also offers the opportunity to test analytical techniques.

FIGURE 1 shows a schematic of the pilot-loop. The main parts are water purification (deionization, degassing and adjustment of the oxygen concentration); the high pressure / high temperature loop (high pressure pump, heating tank) with several test sections; the recirculation of high pressure water to the purification system (heat exchanger, depressurisation). For the high pressure / high temperature part austenitic steel 316 nuclear grade (1.4571; DIN X 10 CrNiMoTi 18 10) was used exclusively. TABLE IV shows the physical and thermal hydraulic conditions in the high pressure part of the pilot-loop.

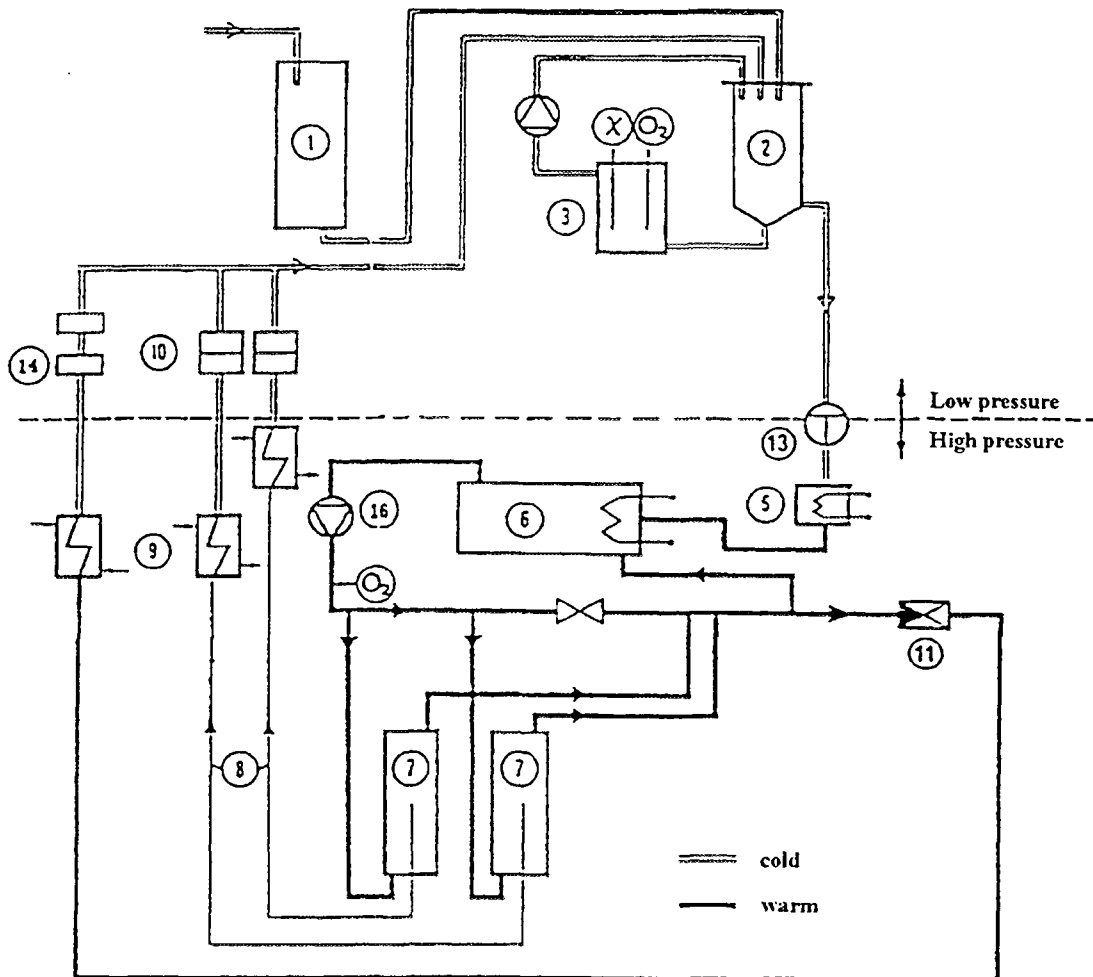
TABLE III: Classification of analytical techniques; Status of water analysis in the present BWR operation; Examples of analytical principles for future applications

	OFF-LINE	AT-LINE	ON-LINE	IN-LINE	NON-INVASIVE
Sampling	Sampling line	By-pass line	By-pass line	Main line Flow disturbance	Main line No disturbance
	Reduced P/T	Reduced P/T	Reduced P/T	Operating P/T	Operating P/T
Analytical equipment	Multi purpose Central lab	Single purpose In plant	Single purpose In loop	Special design In loop	Special design In loop
Sampling interval; Delay in results	Several days Hours	Hours < 1 hour	Continuous In minutes	Continuous Immediate	Continuous Immediate
Typical purpose	Plant balance of corrosion	Consequences of transients	Operation within Tec. Spec.	Automized process control	Automized process control
Typical methods	Spec.rometry (R) (Atom absorption, Mass spectrometry)	Colorimetry (S) (e.g. Peroxide)	Electrochemical (R) (Oxygen, conduc- tivity)	Electrochemical (S), (F)	Nuclide spectro- scopy (S), (F),  Optical (F)
	Ion Chromato- graphy (R)		Ion selective electrodes (S)		

R = Presently used for routine analysis

S = Presently used for special analysis

F = Promising methods for future application



- |   |                     |    |                    |
|---|---------------------|----|--------------------|
| 1 | Water purification  | 8  | Sample lines       |
| 2 | Feed water          | 9  | Cooler             |
| 3 | Feed water analysis | 10 | On-line analysis   |
| 5 | Feed water heater   | 13 | Feed water pump    |
| 6 | Electroboiler       | 14 | Ion exchangers     |
| 7 | Test sections       | 16 | Recirculation pump |

FIGURE 1: Schematic of the pilot-loop for testing advanced analytical techniques

TABLE IV: Physical and thermal hydraulic conditions in the high pressure part of the pilot-loop

Temperature	290°C
Pressure	90 bar
Volume	0.07 m <sup>3</sup>
Recirculation Volume	3 m <sup>3</sup> /h
Feed water	0.05 m <sup>3</sup> /h (1.7 % of recirculation)
Velocity in test lines	0.01 - 10 m/s

## 3.2. Description of analytical techniques

TABLE V summarizes the analytical techniques according to problem areas. The status of implementation in the pilot-loop is indicated. Following some comments to selected problem areas and analytical techniques.

### 3.2.1. Process control

At high temperature / high pressure

- the temperature is measured by Ni / Ni-Cr-thermocouples,
- the pressure is measured by piezoelectric transducers,
- the flow is measured by inductively coupled floating elements or by differential pressure measurements.

### 3.2.2. Overall water quality

The standard method is to measure the electrical conductivity in-line at room temperature. For high purity, salt-free water the conductivity at high temperature can be calculated. For the detection of anomalies in water chemistry an in-line conductivity cell up to 300°C was developed [13].

For high purity, salt-free water the pH can be calculated from the conductivity [14]. For in-line measurements for pressurized water reactors (PWR), yttria stabilized zirconia probes have been applied with success [15], [16], [17].

### 3.2.3. Water impurities

The reactor water contains particulate and dissolved corrosion products, in addition silicate mainly from the initial water supply, as shown in TABLE II, further, organic material mainly from the organic resins used for water purification. **The standard BWR procedure** at KKL is off-line analysis. A certain quantity of water flows through a filter package, consisting of

0,45 µm filter → cation exchange resin → anion exchange resin.

After exposure the filter package is dissolved and the components are determined by ion chromatography and atom absorption spectroscopy. In recent years a very efficient tool for routine

TABLE V: Analytical techniques for testing in the pilot loop

	Ambient Conditions (25°C, 1 bar)	Process Conditions (290°C, 90 bar)
<b>1. Process Control</b>		
a) Temperature	⊙	⊙
b) Pressure	⊙ ⊙	⊙ ⊙
c) Flow	⊙ ⊙	⊙ ⊙
<b>2. Overall Water Quality</b>		
a) El. Conductivity	⊙	⊙ (1)
b) pH	⊙ (2)	⊙ (2)
<b>3. Water Impurities</b>		
a) Standard Procedure		
- Ion Selective Electrodes	⊙ (2)	
- Ion Chromatography	○	
- AAS, ICP-MS	○	
b) Crud Particles		
- Filtration	⊙	⊙ (3)
- Particle Counter	⊙ ⊙	⊙ ⊙ (3)
- AAS, ICP-MS, XRD	○	
c) Activity		
- $\gamma$ -Spectroscopy Loop	⊙ ⊙ (2)	⊙ ⊙ (2)
- $\gamma$ -Spectroscopy Off-Line	○	
d) Organic Carbon		
- UV, VIS, NFIR-Spectroscopy	⊙ ⊙	⊙ ⊙ (4)
- Analysis On-Line	○ ○ ○	
<b>4. Corrosion of Materials</b>		
a) Corrosion Potential		⊙ (4)
b) Oxygen Concentration	⊙	⊙ (4)
c) Hydrogen Concentration	⊙ (1)	
<b>5. Oxide Layer on Austenites</b>		
a) Impedance Spectroscopy		⊙ (4)
b) IR-Reflection		⊙ ⊙ (4)
c) SIMS, SNMS, ICP-MS	○	

TABLE V: Explanation of abbreviations

○ OFF-LINE; ○ ○ AT-LINE; ○ ○ ○ ON-LINE  
⊙ IN-LINE; ⊙ ⊙ NON-INVASIVE

- (1) Commercially available; installation later
- (2) Commercially available; installation not planned
- (3) PSI-development finished; Equipment ready
- (4) PSI-development in progress

AAS = Atom absorption spectroscopy  
ICP-MS = Inductively coupled plasma mass spectroscopy  
XRD = X-ray diffraction  
UV = Ultra violet  
VIS = Visible light  
NFIR = Near field infrared  
IR = Infrared  
SIMS = Secondary ion mass spectroscopy  
SNMS = Sputtering neutral mass spectroscopy

analysis became available: the inductively coupled plasma mass spectroscopy (ICP-MS). ICP-MS allows the direct determination of water impurities in the ppb- and, for selected elements, in the ppt-range, within minutes [18]. It must be noted that the distinction between "undissolved crud" ( $> 0,45 \mu\text{m}$ ) and "dissolved material" ( $< 0,45 \mu\text{m}$ ) is arbitrary. "Dissolved material" consists of particles, colloids and truly dissolved neutral and ionic species.

**Crud particles** play an important role in the transport of Co-60 activity. For older BWR's, it is estimated that 70 % is bound to crud particles. The concentration in the reactor water strongly depends on the plant operating conditions; during transients, in particular power reduction and cool-down, the population increases by a factor of 10 to 100 [6]. In the pilot-loop two new methods for crud characterization are tested:

- A partial stream of the hot loop-water (290°C, 90 bar) flows through a gold foil filter with holes of 0.1, 1, 10  $\mu\text{m}$ ; - in-line crud filtration. The composition of the filter deposit is analyzed. Only very small crud quantities can be collected since the number of filter holes is limited.

- In the hot main stream (290°C, 90 bar) the crud particle number and size between 1 and 100 µm are determined by the reflection of polychromatic (white) light; - non-invasive optical counter [19]. The reliability strongly depends on the long-term transparency of the window. A synthetic sapphire disk of 6 mm thickness was finally selected because of the low corrosion rate (about 1 µm/d). This window has to be replaced after 1 to 2 months of service.

At KKL the **activity in the reactor water** is determined once a day by  $\gamma$ -spectroscopy; - off-line. During the annual shut-down the local dose rate at 8 points of one recirculation loop is measured. The reproducibility for each single point is good, e.g.  $350 \pm 2$  mR/h; between different points are large differences, e.g.  $\pm 150$  mR/h. This means that the activity deposition is only indirectly related to the reactor water activity, but strongly depends on the local (flow) conditions. At KKM the  $\gamma$ -activity is continuously monitored on-line. The measuring cell is kept clean of contamination by adding a trace of sodium silicate.

Initially it was assumed that the **organic carbon (OC)** concentration in the reactor water was high and might play an important role in the transport of inactive and activated corrosion products. Measurements on-line at both plants, KKL and KKM, however showed that the OC-concentration at steady state conditions was only a few ppb and therefore OC could be excluded as a major factor [20]. For non-invasive measurements of the OC-concentration in the test-loop a cell was designed with a light source and a sensing probe, using optical fibres. The transmission loss should provide information on the OC-concentration. Not yet resolved is the selection of the most sensitive optical wave band (UV, VIS, NFIR).

#### 3.2.4. *Corrosion of materials*

The relationship between the **electrochemical potential (ECP)** and stress corrosion cracking of austenitic steels was described before. ECP is a function of the dissolved oxygen concentration in the reactor water or, vice-versa, of the hydrogen addition. Typically an ECP-monitoring cell consists of an austenitic steel working electrode, a platinum counter electrode and a silver/silver-chloride reference electrode. ECP cells haven been used with success at BWR conditions, not only in autoclaves [21], [22] and reactor loops [23], [24] but also in-line in the recirculation loops of Swedish [25] and Japanese reactors [26].

At KKL the **oxygen concentration** is measured on-line by an electrochemical method (ORBISPHERE-Laboratories, Neuchâtel, Switzerland). For in-line application the potential

between two concentric tube electrodes shall be measured. The center tube consists of a palladium alloy with a constant H<sub>2</sub>-pressure, the outer tube of platinum. The electrochemical potential depends on the oxygen concentration in the water.

For the **hydrogen concentration** commercial electrodes for on-line measurements are available.

### 3.2.5. *Oxide layer on austenites*

The behaviour of the oxide layer on austenitic steels at BWR-conditions is quite complex. The oxide formation reduces the corrosion rate, at the same time the oxide layer acts as a scavenger for inactive and activated corrosion products. The chemical composition and the physical structure of the oxide layer depends on several factors: surface pretreatment, conditioning during the start-up period, water chemistry and flow rate. Recent exposure of 316 L samples in our test loop over 290 days, followed by sputtering neutral mass spectroscopy (SNMS) examination, showed a steady corrosion rate of 3 nm/d at 10 m/s flow velocity and 0.3 nm/d at 0.04 m/s [27].

**Impedance spectroscopy** appears to be a promising tool to follow in-line, at BWR-conditions, the behaviour of the austenitic steel surface. A major difficulty presents the low conductivity of the high purity BWR reactor water: 0,05 μS/cm at room temperature, 2,7 μS/cm at 290°C. This fact leads to a cell design with a very narrow gap (a fraction of 1 mm), into which a very thin platinum wire (a fraction of 1/10 mm) is inserted as a reference, between a 316 L steel working electrode and a platinum counter electrode. The resistance measurement and the phase angle shift in the frequency band from 10<sup>-3</sup> to 10<sup>6</sup> Hz should provide the following information:

- Oxide layer thickness (corrosion rate, diffusion coefficient of the rate determining species)
- Electrolyte conductivity
- Total porosity fraction

The same cell can also be used for other electrochemical measurements as current voltage curves and cyclic voltammetry.

For the determination of the oxide layer thickness only, an optical method, diffuse **reflection spectroscopy** (DRS) was investigated off-line on preoxidised steel samples. DRS-spectra were obtained using a guided wave unit and photomultipliers as detectors [28]. Between 200 and 3000 nm wave length iron oxide absorbs strongly, above 8000 nm it becomes transparent.

Therefore only the early corrosion layer build up, up to 100 nm layer thickness, could be determined at about 700 nm and 5500 nm wave length with a beam size of about 1 mm. Independent methods had to be used to correlate light reflection and oxide layer thickness. For an in-line application at BWR-conditions, to monitor the in-situ layer build-up, additional difficulties arise from the window transparency and the light absorption of water above 3000 nm wave length.

#### 4. SUMMARY

Taking the Swiss BWR's with external recirculation loops as examples, the changes in reactor water chemistry in recent years were described. Presently the main aim is to reduce radiological dose rates, in the future also to prevent corrosion, to achieve high fuel burnup and to minimize waste. To achieve these aims the reactor water should be analyzed continuously at operating conditions. Promising techniques for automatized process control are based on electrochemical and optical methods and  $\gamma$ -spectroscopy. Using a pilot-loop for testing advanced analytical techniques the status, experiences and difficulties with these techniques were described. Electrochemical cells were used for reactor water analysis (conductivity, pH, corrosion potential, oxygen concentration) and for the characterization of the corrosion layer on austenites (impedance spectroscopy). Optical methods can provide data on the crud particle population and on the organic carbon concentration in the reactor water, further on the corrosion rate of austenites. By nuclide specific  $\gamma$ -spectroscopy the activity concentration and the deposition on austenites can be followed. These methods have the potential for future plant application to control normal operation and, more important, transients.

#### REFERENCES

- [1] VGB-guidelines for water in light water reactors. VGB-R 401 J, VGB-Kraftwerkstechnik GmbH (1988).
- [2] HICKLING, J. U., REITZNER, U., VGB-Kernkraftwerkstechnik 72 (1992) 359-367.
- [3] LONER, H., PhD Thesis at the Swiss Federal Institute of Technology Zurich (ETHZ), to appear in 1994.
- [4] ASAKURA, Y., et al., Water chemistry of nuclear reactor systems 5, Bournemouth 23 - 27 Oct. 1989, 115 - 122.

- [5] ALDER, H.P., IAEA-TECDOC-667 (Oct. 1992) 124 - 131.
- [6] ALDER, H.P., BRÉLAZ, P., Water chemistry of nuclear reactor systems 6, Volume 1, Bournemouth 12 - 15 Oct. 1992, 45 - 49.
- [7] OCKEN, H., WOOD, C.J., Water chemistry of nuclear reactor systems 6, Volume 2, Bournemouth 12 - 15 Oct. 1992, 1 - 8.
- [8] ANDRESEN, P.L., DIAZ, T.P., Water chemistry of nuclear reactor systems 6, Volume 1, Bournemouth 12 - 15 Oct. 1992, 169 - 175.
- [9] HEMSTRÖM, B., LUNSTRÖM, A., TINOCO, H., ULLBERG, M., Water chemistry of nuclear reactor systems 6, Volume 2, Bournemouth 12 - 15 Oct. 1992, 133 - 139.
- [10] RUIZ, C.P., ROBINSON, R.N., BURNS, W.G., HENSHAW, J., Water chemistry of nuclear reactor systems 6, Volume 2, Bournemouth 12 - 15 Oct. 1992, 141 - 152.
- [11] MARCHL, T.F.J., REITZNER, U., Water chemistry of nuclear reactor systems 6, Volume 1, Bournemouth 12 - 15 Oct. 1992, 33 - 38.
- [12] CALLIS, J.B., ULLMANN, D.L., KOWALSKI, B.R., Analytical Chemistry 59 (1987) 624A - 637A.
- [13] YOKOSE, K., ASAKURA, Y., UCHIDA, S., OHSUMI, K., JAIF int. conf. on water chemistry of nuclear power plants, Fukui City 22 - 25 April 1991, 539 - 542.
- [14] HEITMANN, H.G., Praxis der Kraftwerk-Chemie, Essen (1986).
- [15] TACHIBANA, K., HATTORI, A., HATA, M., YOKOI, M., JAIF int. conf. on water chemistry of nuclear power plants, Fukui City 22 - 25 April 1991, 343 - 348.
- [16] HETTIARACHCHI, S., MAKELA, M., MACDONALD, D., JAIF int. conf. on water chemistry of nuclear power plants, Fukui City 22 - 25 April 1991, 349 - 354.
- [17] AALTONEN, P., JÄRNSTRÖM, R., KWARNSTRÖM, R., CHANFREAU, E., JAIF int. conf. on water chemistry of nuclear power plants, Fukui City 22 - 25 April 1991, 355 - 360.
- [18] BUCKLEY, D., Water chemistry of nuclear reactor systems 6, Volume 1, Bournemouth 12 - 15 Oct. 1992, 202 - 203.
- [19] SCHENKER, E., FRANCONI, W., DEGUELDRE, C., Water chemistry of nuclear reactor systems 6, Volume 1, Bournemouth 12 - 15 Oct. 1992, 133 - 138.
- [20] LONER, H., ALDER, H.P., SCHENKER, E., COVELLI, B., JAIF int. conf. on water chemistry of nuclear power plants, Fukui City 22 - 25 April 1991, 243 - 247.

- [21] KIM, Y.-J., LIN, C.C., PATHANIA, R., Water chemistry of nuclear reactor systems 6, Volume 1, Bournemouth 12 - 15 Oct. 1992, 139 - 143.
- [22] LIN, C.C., SMITH, F.R., JAIF int. conf. on water chemistry of nuclear power plants, Fukui City 22 - 25 April 1991, 277 - 282.
- [23] KARLSEN, T., GUNNERUD, P., VITANZA, C., Water chemistry of nuclear reactor systems 6, Volume 1, Bournemouth 12 - 15 Oct. 1992, 15 - 18.
- [24] KOHSE, G.E., OUTWATER, J.O., ROZIER, M., DRISCOLL, M.J., HARLING, O.K. TAKAHASHI, M., Water chemistry of nuclear reactor systems 6, Volume 1, Bournemouth 12 - 15 Oct. 1992, 190 - 191.
- [25] FEJES, P., Water chemistry of nuclear reactor systems 6, Volume 2, Bournemouth 12 - 15 Oct. 1992, 90 - 95.
- [26] ICHIKAWA, N., HEMMI, Y., TAKAGI, J., Water chemistry of nuclear reactor systems 6, Volume 2, Bournemouth 12 - 15 Oct. 1992, 127 - 132.
- [27] BUCKLEY, D., Chemistry in water reactors, Nice April 24 - 27, 1994, to be published.
- [28] DEGUELDRE, C., DRAN, J.C., SCHENKER, E., J. of Nuclear Materials, to be published.

## CONTROL OF WATER CHEMISTRY IN OPERATING REACTORS

R. RIESS  
Siemens/KWU, Erlangen  
Germany

### Abstract

Water chemistry plays a major role in fuel cladding corrosion and hydriding. Although a full understanding of all mechanisms involved in cladding corrosion does not exist, controlling the water chemistry has achieved quite some progress in recent years. An example, in PWRs the activity transport is controlled by operating the coolant under higher pH-values (i.e. the "modified" B/Li-Chemistry).

On the other hand, the lithium concentration is limited to a maximum value of 2 ppm in order to avoid an acceleration of the fuel cladding corrosion. In BWR plants, for example, the industry has learned on how to limit the copper concentration in the feedwater in order to limit CILC (Copper Induced Localized Corrosion) on the fuel cladding.

However, economic pressures are leading to more rigorous operating conditions in power reactors. Fuel burnups are to be increased, higher efficiencies are to be achieved, by running at higher temperatures, plant lifetimes are to be extended.

In summary, this paper will describe the state of the art in controlling water chemistry in operating reactors and it will give an outlook on potential problems that will arise when going to more severe operating conditions.

### 1. Introduction

The IAEA Technical Reports series No. 347 summarizes the work within the framework of a co-ordinated research programme entitled "Investigations on

**Water Chemistry Control and Coolant Interaction with Fuel and Primary Circuit Materials in Water Cooled Power Reactors (WACOLIN)". This programme was organized by the IAEA and carried out from 1987 to 1991. This reports concludes:**

**"Good reactor coolant chemistry, corrosion control and minimization of activity buildup are indispensable for the optimum performance of nuclear power plants. Without these the systems integrity may be jeopardized, the activity transport may create various problems for heat transfer.**

**The corrosion control and activity buildup depend upon the physicochemical parameters of the coolant. As the nuclear industry has progressed, knowledge of corrosion control and activity buildup through its chemistry has also progressed. With regard to the objectives of the WACOLIN pogramme it can be stated that progress has been made in the following areas:**

**(a) Man-sievert reduction**

- (i) Activity transport is controlled in PWRs and PHWRs by operating the coolant in a narrow range of high pH values.**
- (ii) In BWRs the activity buildup is controlled; for example, by lowering the impurity levels and/or by injecting metal ions (Zn and Fe).**

**(b) Plant life extension**

- (i) In PWRs and PHWRs the selection of an optimized pH contributes to the minimization of primary water SCC phenomena.**
- (ii) Oxidizing conditions that promote SCC in BWRs are being counteracted by low conductivities or by hydrogen dosing.**

**(c) Fuel life extension**

- (i) Limiting the lithium concentration in PWRs is a contribution to limiting the zirconium oxide formation and therefore to extending the fuel life.**

- (ii) The exclusion of copper from the steam-water cycle of BWRs has greatly reduced the copper induced localized corrosion phenomenon.
  - (iii) The hydriding of zirconium alloy components in cores is minimized by the adjustment of the dissolved hydrogen concentrations.
- (d) General safety, materials reliability. For all of the different reactor systems (PWRs, BWRs and PHWRs) there have been no shutdowns in recent years due to violations of chemical parameters in the primary system. This is an excellent indication that with regard to this item (general safety and materials reliability) the coolant chemistry has become mature.

Nevertheless, there is no room for complacency, as corrosion problems and activity buildup continue to occur. Economic pressure are leading to more demanding operating conditions in power reactors. Examples of these conditions are: fuel burnup is to be increased, higher efficiencies are to be achieved by running at higher temperatures, plant lifetime is to be extended, and more and more reactor systems are load following. Therefore, in order to maintain adequate levels of safety and reliability, it is recommended to implement the improvements that are elaborated within this programme."

Possible actions with regard to man-sievert reduction and plant life extension are:

- (1) Avoid the use of cobalt based alloys:
  - as in-core material,
  - as out-of-core RCS material,
  - as material in the CVCS.
- (2) Replace the cobalt based alloys in older plants (if possible).
- (3) Reduce the residual cobalt content of structural materials to a minimum.
- (4) Operate the primary coolant chemistry in the modified lithium-boron version or maintain the co-ordinated potassium-boron chemistry.

- (5) Ensure the smoothest possible surface finish (i.e. electropolishing).
- (6) Carry out prefilming during the first startup.
- (7) Perform system decontamination as and when required (full or partial system decontamination).
- (8) Reduce the corrosion product input in BWR reactor systems.
- (9) Use Inconel 690 or alloy 800 in steam generators of new plants and in replacement steam generators.
- (10) Ensure smooth operation to avoid thermal transients in all systems and components.
- (11) Use HWC in BWR systems.

Despite the fact that all these recommendations are made as a result of this programme, it is felt that in the future several problems will have to be investigated and resolved. These areas are outlined in Table VI of the Technical Reports Series No. 347.

Now, nearly three years later it should be checked what happened to the recommended actions and the areas of future development. With this question in the background, the present paper will handle two areas:

- Review the water chemistry specifications and indicate recent developments.
- Evaluate the recommended actions of 1991.

## 2. Chemistry of Primary Coolant in Water Cooled Reactors

### 2.1 PWRs with LiOH as pH control agent

Typical water chemistry specifications are shown in Table I and Figure 1.

The three options being consistent with the guidelines are:

- Elevated Li-B-Chemistry

- Modified Li-B-Chemistry
- Co-ordinated Li-B-Chemistry.

**TABLE I. EPRI GUIDELINES FOR PRIMARY COOLANT**

Hydrogen (cm <sup>3</sup> (STP)/kg H <sub>2</sub> O) <sup>a</sup>	25 - 50
Chlorides (mg/kg)	< 0.15
Fluorides (mg/kg)	< 0.15
Dissolved oxygen (mg/kg)	< 0.01
Lithium (mg/kg)	Consistent with station lithium programme

a) STP, standard temperature and pressure (0°C, 1 atm).

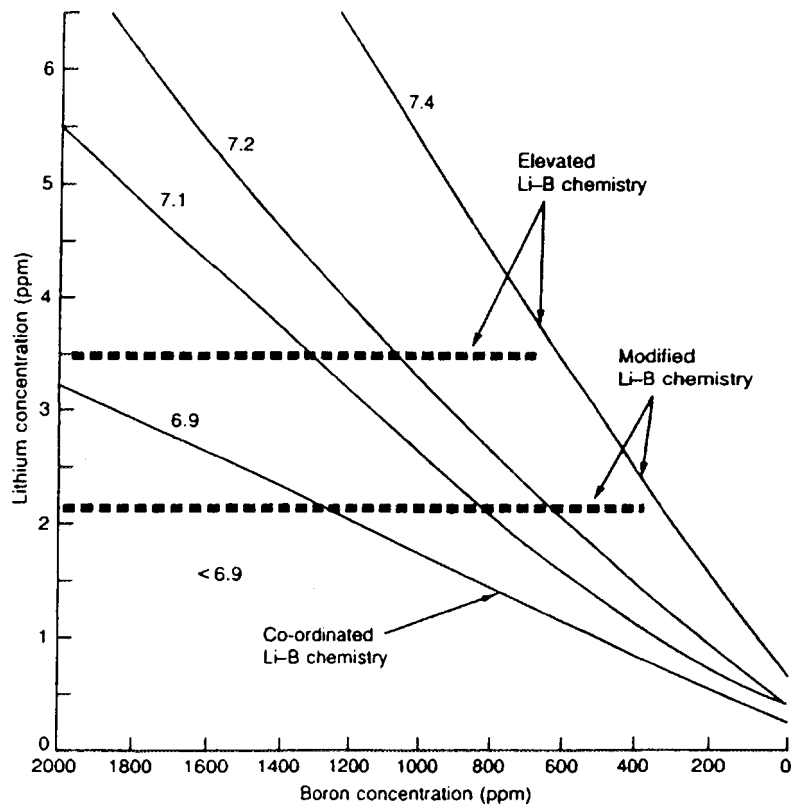


**Fig. 1: Various lithium-boron modes of operation**

Here, the operational experience of the last three years has clearly shown that the modified Li-B-Chemistry should be preferred over the other two options. All trial operations with "Elevated Li-B-Chemistry" were stopped by one reason or the other.

Examples for that are:

- Ringhals: Concerns on Inconel-600 PWSCC
- Millstone-3: } Concerns both on I-600 PWSCC and
- North Anna: } Fuel Corrosion for high burnup

## **2.2 PWRs with KOH as pH Control Agent**

The specifications are shown in Table II.

The only trend that became known recently is to avoid NH<sub>3</sub>-injection for the H<sub>2</sub> production. A direct and continuous hydrogen injection is considered in order to avoid fluctuation of the pH value. All reported fuel cladding corrosion data are extremely low, i.e. there are no concerns.

## **2.3 Pressurized Heavy Water Reactors (PHWRs)**

The specification for this type of reactor is summarized in Table III.

New trends to modify coolant control are not known.

## **2.4 Boiling Water Reactors**

As an example for BWR water chemistry specifications, the EPRI guidelines are listed in Table IV.

**TABLE II. SPECIFICATIONS OF REACTOR WATER QUALITY FOR  
PWRs OF TYPE WWER-440 and WWER-1000**

Indicator (with reactor 'on load')	Values	
	WWER-440	WWER-1000
pH (25°C)	6.0-10.2	5.7-10.2
K <sup>+</sup> , Li <sup>+</sup> , Na <sup>+</sup> (mmol/kg) (depending on H <sub>3</sub> BO <sub>3</sub> concentration)	0.05-0.45	0.05-0.45
NH <sub>3</sub> (mg/kg)	> 5.0	> 5.0
Hydrogen (cm <sup>3</sup> /kg)	30-60	30-60
Chlorides and fluorides (µg/kg)	≤100	≤100
H <sub>3</sub> BO <sub>3</sub> (g/kg)	0-9.0	0-13.5
Oxygen (µ/kg)	≤5	≤5
Copper (ng/kg)	<20	<20
Iron (ng/kg)	<200	<200

**TABLE III. SPECIFICATION OF PRIMARY COOLANT  
QUALITY FOR PHWRs**

PWR	
LiOH (ppm)	1-2
Dissolved deuterium (ppm)	6
Dissolved oxygen (ppm)	0.05
Chloride (ppm)	0.2
pH (25°C)	10.5-10.9
Silica (ppm)	≤4 SiO <sub>2</sub>
Dissolved iron (ppm)	0.5
Crud (ppm)	1
<b>Pressure tube reactor</b>	
pH (25°C, controlled with Li)	10.2-10.8
Dissolved hydrogen ml/kg	3-10
Dissolved oxygen ppb	< 10
Chloride ppm	< 0.2
Fluoride ppm	< 0.1
Crud ppb	< 10

**TABLE IV. EPRI CHEMISTRY GUIDELINES FOR BWRs**

Control parameter	Frequency of measurement	Achievable value	Action levels		
			1	2	3
<b>Reactor water - power operation</b>					
Conductivity (µS/cm at 25°C)	Continuously	≤0.20	>0.30	>1.0	>5.0
Chloride (ppb)	Daily	≤15	>20	>100	>200
Sulphate (ppb)	Daily	≤15	>20	>100	>200
Diagnostic parameter, silica (ppb)	Daily	≤100			
<b>Reactor feedwater / condensate - power operation</b>					
Feedwater conductivity (µS/cm at 25°C)	Continuously	≤0.06	>0.07		
Condensate conductivity (µS/cm)	Continuously	≤0.08	>0.10		>10.0
Feedwater total copper (ppb)	Weekly integrated	≤0.10 ≤0.30	>0.50 >0.50		
Feedwater total iron (ppb)	Weekly integrated	≤2.0	>5.0		
Feedwater dissolved oxygen (ppb)	Continuously	20-50	<10	>200	

These and corresponding guidelines are now worldwide under review. The existing operational problems, specially the IGSCC problem, require more stringent values.

For example, it is currently discussed to fix the chloride and sulphate values for the reactor water and action level 1 at 5 ppb. Also, the iron level for the feedwater seems to be too high. There are even considerations to establish much more stringent chemistry values. Such considerations are made with the following objectives as background:

- ° Avoid IGSCC
- ° Man-Rem < 1 Man-Sievert

- Radwaste volume < 110 m<sup>3</sup>
- No other corrosion problems like fuel cladding corrosion.

These objectives require for example

- Reactor water conditions ( $\mu\text{S/cm}$ ) < 0.08
- Feedwater iron level (ppb) 0.1 - 0.5

To fulfill these requirements the following operational options have to be considered:

- Improve cleanup of the steam water cycle.
- Hydrogen water chemistry (ECP < 230 mV)
- Noble metal coating
- Zinc-injection

### **3. Status of Recommended Actions**

In this section, an update of the recommended actions of the IAEA-Report "Coolant Technology of Water Cooled Reactors" will be given. The number of actions is indicated with ( ) and the current status with "Comment".

- (1) Avoid the use of cobalt base alloys
- as in core material
  - as out-of-core RCS material
  - as material in the CVCS

**Comment:**

EPRI is currently working on Revision 1 of its Cobalt Reduction Guidelines. This guideline contains information that exceeds the current guideline in two aspects:

- a) Test results from various qualification experiments of cobalt replacement materials like NOREM, EB5183 and Everit 50 compared to Sellite 6.

b) Utility Experience with Co-Hardfacing Alloys.

Despite such activities, it became evident at the last EPRI Radiation Control Seminar in Seattle (August 1993) that there is no consensus that the major step forward in reducing radiation fields is the replacement of the cobalt-base alloys.

However, Siemens believes to be in a position to be able to provide the data base for the statement that Stellite-replacement is the key action for reducing occupational radiation exposure. The new standard for occupational radiation exposure in PWRs of western design is < 50 Man-Rem/year and plant (see Figures 2). The surface areas of stellites in older and newer plants designed by Siemens/KWU can be seen in Tables V and VI.

(2) Replace the cobalt based alloys in older plants (if possible).

Comment:

Locations for Stellite in older Siemens-designed plants are shown in Figure 3. The replacement of these components is technically feasible. However, licensing and cost-benefit-aspects are very high barriers to take this action.

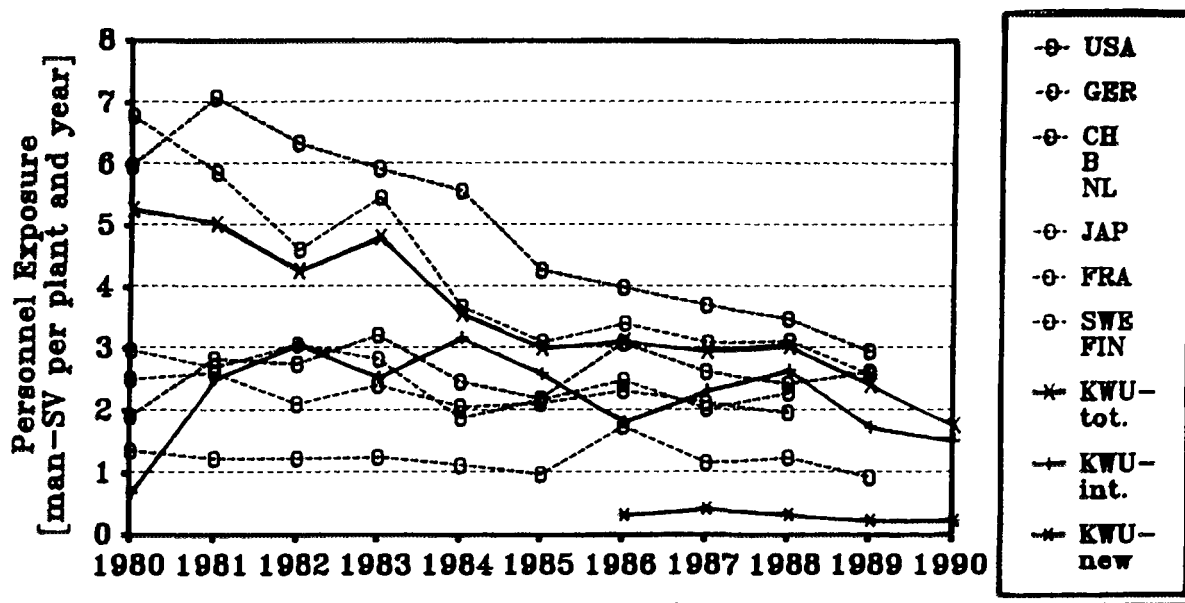


Fig. 2 Average annual personnel radiation exposure of PWRs

**TABLE V: Materials Inventory of "Older" 1300 MWe Siemens-designed PWRs**

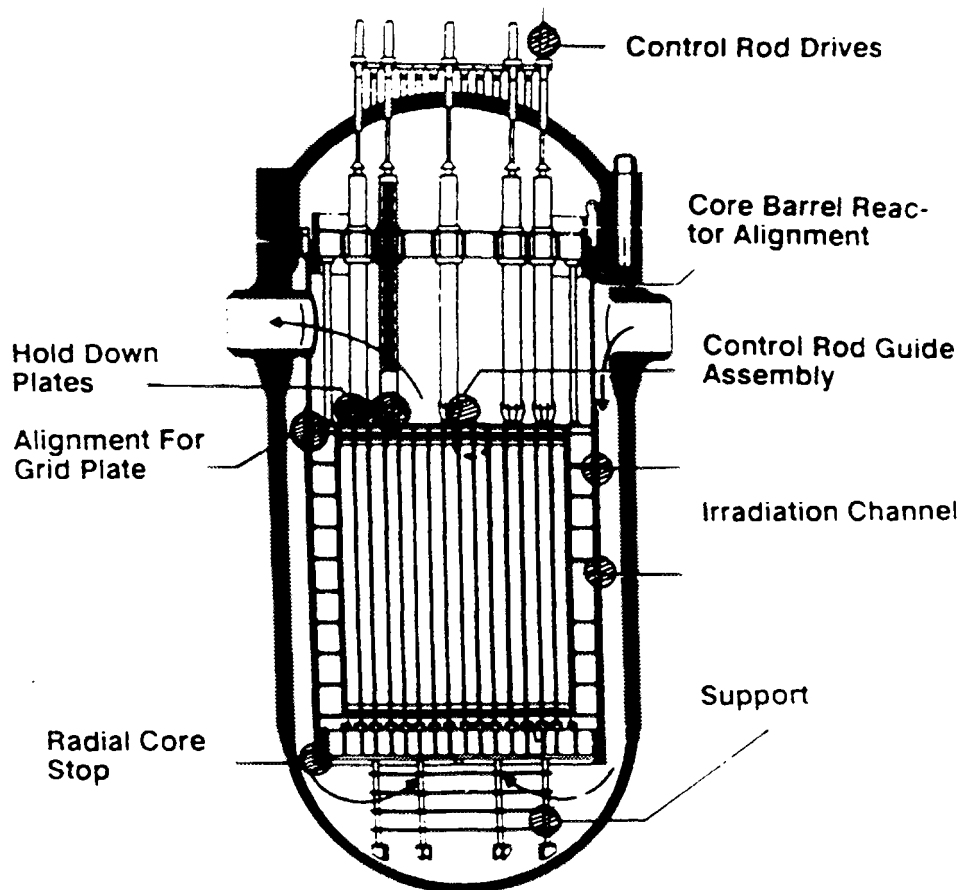
Group	Component	Material	Surface [m <sup>2</sup> ]	Co-59 Specification [%]
1	Fuel*)	Zircaloy 4	9660	~ 0
		Inconel 718	1220	< 0.1
		Stainless steel	220	< 0.1
	RPV-Internals	Stainless steel	1124	< 0.1
		Co-base alloys	1.1	63
2	Control rod assemblies	Stainless steel	340	< 0.1
	Control rod drive	Stainless steel	220	< 0.2
		Co-base alloys	1.54	≤ 67
	Steam generator	Incoloy 800	16276	< 0.1
	RPV, Loops	Stainless steel	719	< 0.2
	Main Coolant Pump	Stainless steel	155	< 0.2
Co-base alloys		1.5	63	
3	Auxiliary systems	Stainless steel	~ 500	< 0.2
		Co-base alloys	6.5	63
	Total	Zircaloy	9660	
		Stainless steel	19554	
		Inconel	1220	
		Co-base alloys	10.64	

\*) Material composition used before 1985, modifications per fuel cycle possible

**TABLE VI: Materials Inventory of "Recent" 1300 MWe Siemens-designed PWRs**

Group	Component	Material	Surface [m <sup>2</sup> ]	Co-59 Specification [%]
1	Fuel*)	Zircaloy 4	~ 10660	~ 0
		Inconel 718	394	< 0.1
		Stainless steel	220	< 0.1
	RPV-Internals	Stainless steel	1126	< 0.1
		Co-base alloys	0.026	63
2	Control rod assemblies	Stainless steel	340	< 0.1
	Control rod drive	Stainless steel	220	< 0.2
		Co-base alloys	1.54	≤ 67
	Steam generator	Incoloy 800	16276	< 0.1
	RPV, Loops	Stainless steel	719	< 0.2
	Main Coolant Pump	Stainless steel	156	< 0.2
Co-base alloys		0	63	
3	Auxiliary systems	Stainless steel	506	< 0.2
		Co-base alloys	0.79	63
	Total	Zircaloy	10660	
		Stainless steel	19563	
		Inconel	394	
		Co-base alloys	2.36	

\*) Modification per fuel cycle possible



ENTIRE HARDFACED AREA	:	Co-BASE ALLOY
Control Rod Drives	:	1.46 m <sup>2</sup>
Core Area	:	1.59 m <sup>2</sup>

**Fig. 3: Stellites in Siemens-designed PWRs**

(3) Reduce the cobalt content of structural materials to a minimum.

**Comment:**

This is an ongoing action item if structural materials are replaced. An example was described at the 1993 EPRI Radiation Control Seminar in Seattle by Niagara Mohawk.

(4) Operate the primary coolant chemistry on the modified lithium-boron version or maintain the co-ordinated potassium-boron chemistry.

**Comment:**

see section 2.1 and 2.2 of this paper.

**(5) Ensure the smoothest possible surface finish (i.e. electropolishing).**

**Comment:**

The enthusiasm existing two or three years ago has gone. Framatome/EdF are doing no electropolishing of the channel heads of new steam generators. This decision was made on cost-benefit considerations. EPRI is still in proposing this surface finish for new steam generators.

**(6) Carry out prefilming during the first startup.**

**Comment:**

Prefilming has been demonstrated to have a beneficial effect on activity buildup. Especially the experiments in Doel have shown that chromating results in lowest radiation fields.

The other chromating technology that should be followed very closely was qualified in Rossendorf and Rez for plant application.

**(7) Perform system decontaminations as and when required (full or partial system decontamination).**

**Comment:**

Decontamination has been accepted by industry as a tool for Man-Rem-Reduction. However, the waste problem is an area of great concern. The most updated status of the decontamination technology can be seen in the Proceedings of the EPRI Decontamination Seminar held in June, 1993, in Charlotte, North Carolina.

**(8) Reduce the corrosion product input in BWR reactor systems.**

**Comment:**

This is an ongoing effort. However, the objective is not to reduce the iron level to the lowest possible values. An optimum range of 0.1 to 0.5 ppb Fe in the feedwater of BWRs seems to be desirable. The cleaning facilities have to be adjusted to meet this objective.

- (9) Use Inconel 690 or alloy 800 in steam generators of new plants and in replacement steam generators.

**Comment:**

This recommended action is fully accepted worldwide in all new projects and used for replacement of steam generators.

- (10) Ensure smooth operation to avoid thermal transients in all systems and components.

**Comment:**

This is recognized by many utilities and it is integrated in their operational procedures. However, this remains an area of future activities.

- (11) Use HWC in BWR systems.

**Comment:**

The benefits of HWC regarding IGSCC are questionable. In addition, HWC has caused a steep increase in the radiation levels in several BWRs. Therefore, OWC (Optimum Water Chemistry) a mixture of HWC and Zinc seems to be the new panacea on the horizon.

#### **4. Conclusion**

The conclusions and recommendations of the WACOLIN programme have been re-evaluated here. Based on this review, it can be stated that:

- All conclusions and recommendations are still valid.
- Priorities have changed in the last three years.
- Fuel life extension is still a major area for future development.
- Alternatives to current water chemistry are still desirable.
- On-line monitoring as a tool for better controlling the corrosion processes is a very reliable recommendation for the continuation of the WACOLIN programme.



# ALTERNATIVE WATER CHEMISTRY FOR THE PRIMARY LOOP OF PWR PLANTS

N. HENZEL  
Siemens/KWU, Erlangen  
Germany

## Abstract

Advanced fuel element concepts (longer cycles, higher burnup, increased rod power) call for more reactivity binding capacity and, moreover, might produce higher void fractions, particularly in the hot channel. Thus, on the one hand, more alcalizing agent is needed to maintain a high coolant pH according to the approved "modified boron-lithium mode of operation" in the presence of more boric acid (chemical shim); on the other hand, increasing enrichment of coolant constituents due to local boiling (higher void fraction), which must not result in accelerated corrosion of fuel cladding and structural materials, imposes enhanced requirements on both, materials technology and water chemistry.

At present, the use of boric acid enriched in B10 (the isotope effective in terms of reactivity control) appears to advantageously compromise in capturing more neutrons with less total boron while maintaining or even slightly reducing lithium concentrations at the same time.

There is no feasible alternative for boric acid used as the chemical shim and for hydrogen gas as the reducing agent used to suppress oxygen formation by water radiolysis.

Systematic screening as performed in phase 1 of a recent project proved potassium hydroxide to be the only potential candidate to favourably replace lithium<sup>7</sup> hydroxide as an alcalizing agent. Unfortunately, the results of pertinent comparative corrosion tests are not unambiguous, and available operational experience with potassium hydroxide in WWER plants is not readily applicable to western world-type PWR plants. Therefore, a switch-over from lithium to potassium can be envisaged only subsequent to a comprehensive qualification program which is planned to be the objective of phase 2 of the project.

This program should also comprise zinc addition tests in order to confirm the alleged positive impact of this element on corrosion rates and activity buildup. Supplementarily, it is recommended to consider amendments to existing water chemistry guidelines with respect to coolant impurities assumed to adversely impact fuel cladding materials.

## 1 Introduction

The tasks of water chemistry in the primary loop of a PWR are manifold: For reactivity control in the primary coolant, homogeneously distributed, i.e. dissolved, boric acid ( $H_3BO_3$ ) is used as a neutron absorbing agent (= chemical shim). In order to establish reducing conditions, the generation of oxygen by water radiolysis is suppressed by hydrogen addition. General corrosion as well as selective attack of fuel element and structural materials is to be counteracted on the one hand by providing for high-purity coolant, on the other hand by alcalizing the coolant with lithium hydroxide highly enriched in the isotope Li<sup>7</sup>. Specific benefit results from alcalization if the coolant pH is adjusted to a value which causes minimum solubi-

lity and maximum fixation of corrosion products at the location where they have been generated, thus minimizing crud formation on heat transfer surfaces, in particular on the fuel rods, and influencing transport and deposition of radioactivity-relevant corrosion products such that the contamination of the primary loop remains low.

The following water chemistry guidelines are aimed at fulfilling these requirements:

Table 1: Water Chemistry Guidelines for the Primary Coolant of KWU-PWR Plants at Continuous Operation

Lithium	$\leq 2 \text{ mg Li}^7/\text{kg} *$
Hydrogen	1 to 4 mg H <sub>2</sub> /kg
Oxygen	< 0.005 mg O <sub>2</sub> /kg
Chloride	< 0.2 mg Cl <sup>-</sup> /kg

In complying with these guidelines, the "modified boron-lithium mode of operation" as shown in Figure 1 has proved to favour the aims discussed above. It is characterized by a BOC (= begin of cycle) boron concentration of 1200 ppm for the first reactor core or 1000 ppm for the equilibrium core, approximately, and a lithium concentration, which starts at 2 ppm, corresponding to an initial pH of 6.9 or 7.0 at 300 °C, respectively, which is maintained at 2 ppm, while the pH continuously increases as a consequence of boric acid withdrawal, and which is then gradually decreased, after achieving the target pH (7.4 in case of Figure 1), such that this pH remains constant until the EOC (= end of cycle). According to experience, the target pH depends on the corrosion product composition, i.e. the material concept, and therefore must be evaluated individually for each plant. This can be done e.g. by using the PC code OPTIMI developed by KWU [1].

---

\*) depending on boron concentration

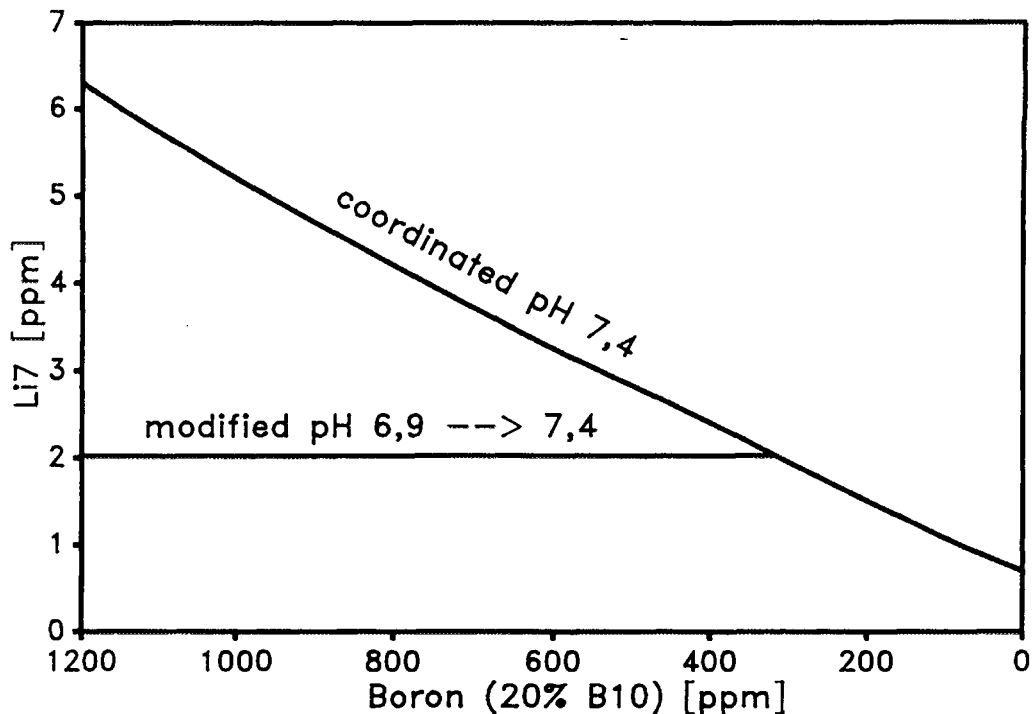


Figure 1: pH(300°C) Diagrams of Different Boron-Lithium Modes of Operation

## 2 Objective

Advanced fuel element concepts aimed at longer cycles, higher burnup and increased rod power call for extended fuel element in-core residence time and higher uranium enrichment, and result in higher void fractions, in particular in the hot channel. As a consequence, thicker zirconium oxide films are accumulated - even if unchanged corrosion behaviour of the fuel rod cladding material (zircaloy-4) is assumed -, the thickness of which has to be limited for safety reasons ("100 µm criterium"), more neutron absorption capacity of the chemical shim, i.e. higher boric acid concentration (initially up to 1800 ppm boron), is required, and higher enrichment of coolant constituents at locations with increased nucleate boiling (causing accelerated zircaloy corrosion) must be envisaged.

As demonstrated by Figure 2 and 3, more boron either means a lower operational pH at BOC, which is undesirable for reasons of radioactivity buildup, or - in order to maintain the high pH(300°C) value - a higher initial Li7OH concentration, which is

known to accelerate the zircaloy corrosion, even if the enrichment effect due to boiling as mentioned above is not considered.

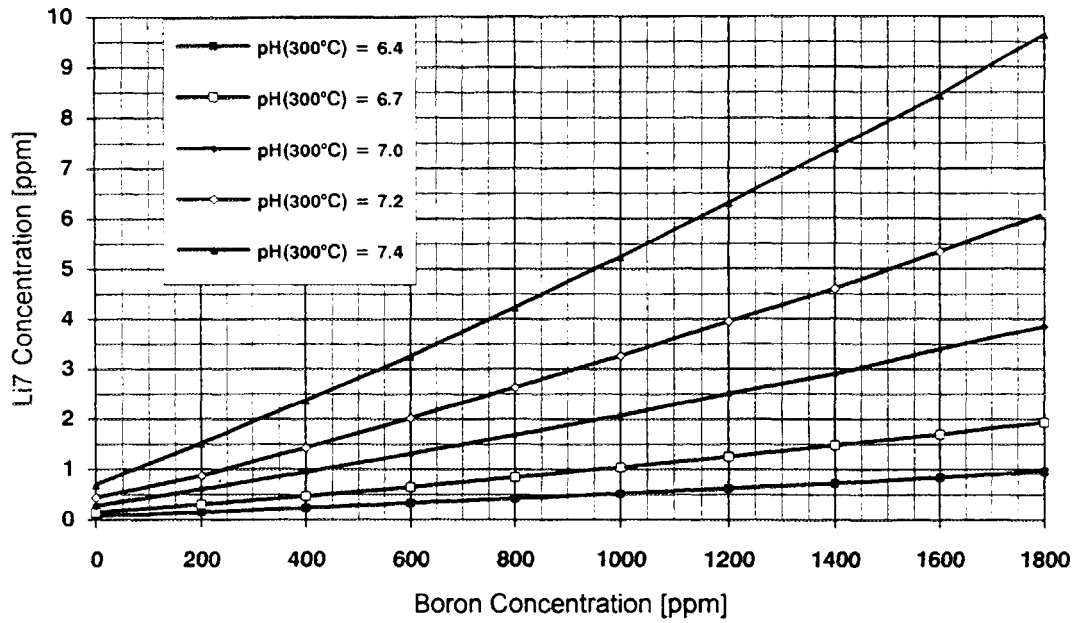


Figure 2: Lithium Concentration as a Function of Boron Concentration Yielding Constant pH Values

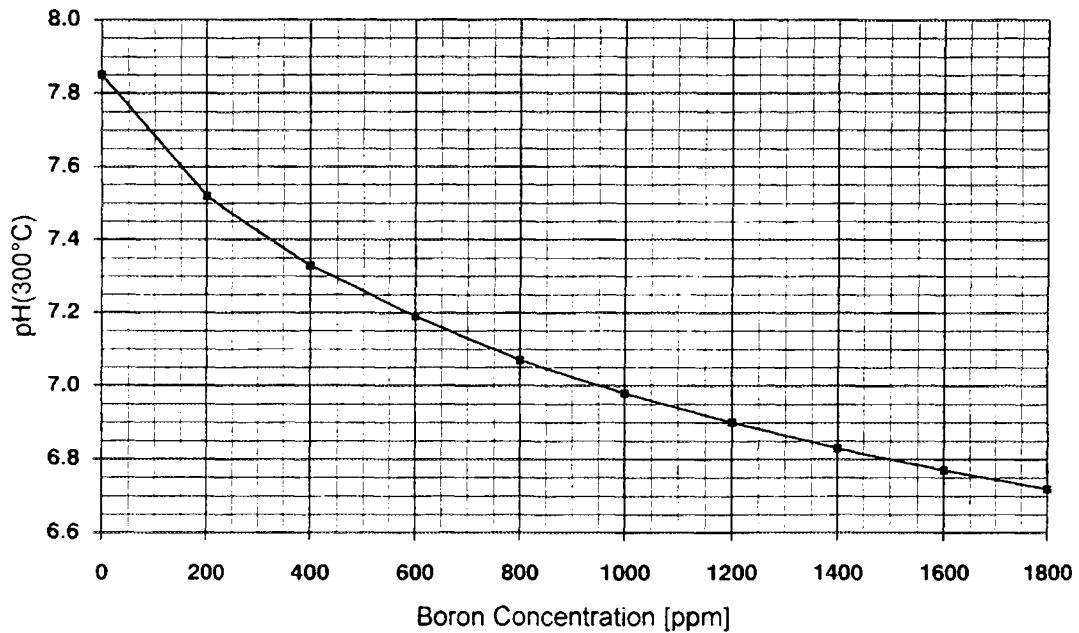


Figure 3: pH(300°C) as a Function of Boron Concentration at Constant 2 ppm Li7

Thus, a conflict of aims exists such that materials development and water chemistry, which have to ensure the overall plant integrity, might set limits to the fuel element exploitation strategy. As a contribution to resolve this conflict, a systematic study was performed, within the scope of the "PWR Planning Contract", entitled "Alternative Water Chemistry, Phase 1". This paper is dealing with the results of that study.

### 3 Options for an Alternative Water Chemistry

#### 3.1 Reactivity Control

As a chemical shim, providing - in addition to the control rods and possibly gadolinium oxide ( $Gd_2O_3$ ) mixed with the fuel which both predominantly are designed for local effectivity - adequate neutron absorption during the entire core life, boric acid has been used worldwide. In principle, elements other than boron could be considered, provided they exhibit a similarly large neutron cross section, e.g. cadmium (Cd), europium (Eu), samarium (Sm), and, in particular, gadolinium (Gd). However, it can be gathered from pertinent handbooks that there are no feasible chemical compounds of these elements which are sufficiently soluble in the coolant and (hydro)thermally stable at the same time.

It might be possible to find, as a result of considerable R&D effort, a "neutron poison" which could substitute boron. In view of the good-natured properties of and the long-term positive operational experience with boric acid, however, no reason can be seen which could justify such effort.

#### 3.2 Suppression of Water Radiolysis

Hydrogen is usually added to the coolant in order to avoid gross oxygen formation due to water radiolysis. According to measurements performed at KWU-PWR plants, 0.5 to 1 ppm  $H_2$  is sufficient to produce reducing conditions in the coolant. In practice, a concentration of 2 to 4 ppm is used. Higher concentrations are

undesirable owing to the risk of enhanced formation of zirconium hydride which would lead to inadmissible embrittlement of the fuel rod cladding material (zircaloy-4).

No other chemical means appears appropriate to interrupt the radical chain reaction associated with water radiolysis and to produce reducing conditions without the disadvantage of hydrogen (see above) or other drawbacks. It could be considered, however, to decrease the operational hydrogen concentration e.g. to between 1 and 2 ppm.

### 3.3 Coolant pH

A pH(300°C) value above 7, as constant as possible, at least not subject to rapid changes, appears to be indispensable. As can be taken from literature, the pH is not critical with respect to the integrity of important structural materials (austenitic stainless steel, I800, I690, stellite) [2], [3]; metal release rates are considerably reduced, however, if the pH is increased [4], [5]. According to present knowledge, the dose rate buildup on material surfaces due to radionuclide deposition is minimized if, on the one hand, the amount of corrosion products which are inevitably generated is small and, on the other hand, these corrosion products are fixed, as far as possible, at the location where they are formed, i.e. are prevented from being transported with the coolant [6]. This means that the temperature coefficient of their solubility is near zero, a condition which is fulfilled, according to calculations referred in [7], [8], at pH(300°C)  $\approx$  6.8 for Fe dissolved from magnetite and at pH(300°C)  $\approx$  7.3 or 7.6, respectively, for Co dissolved from nickel-cobalt spinells.

### 3.4 Alcalizing Agent

The question of an alternative water chemistry therefore is synonymous with the search for an alcalizing agent which could favourably replace Li7OH in exhibiting better corrosion pro-

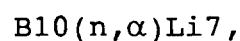
perties with respect to zircaloy-4 and in being compatible with relevant construction materials at the same time.

Volatile alcalizing agents, i.e. some nitrogen-based compounds, although acceptable as to base strength and distribution coefficient between the gas and the liquid phases, are considered inappropriate because of their tendency to (hydro)thermal and radiation-induced decomposition.

A systematic investigation therefore was focussed on solid alcalizing agents. Owing to the requirement of sufficient base strength, only the hydroxides of elements arranged in the groupes one, two, and three of the Periodic System are possible candidates, except H and B which do not form basic hydroxides at all, the radioactive elements Fr, Ra, Ac, and the "noble" elements Cu, Ag, Au, Hg which would be transformed to and precipitated in the metal state in the presence of hydrogen; Cd as a well-known "neutron poison" was not considered either.

The remaining elements were screened by taking in account the solubility of their hydroxides and other relevant compounds, e.g. their borates, and their neutron activation as far as yielding dose rate-relevant radionuclides, again in using pertinent handbooks. The exclusion criteria as applied left potassium (K) and rubidium (Rb) hydroxide as the only feasible candidates to substitute  $\text{Li}^7\text{OH}$ , the agent which has been well established in the western world. From those, KOH is obviously superior for reasons of availability and price. Owing to similar dissociation constants, the same molar concentrations of KOH or  $\text{Li}^7\text{OH}$  would be needed for pH adjustment (because of the higher molar mass of potassium, however, 2 ppm  $\text{Li}^7$  correspond to about 11 ppm K).

It has to be pointed out that, in switching over from  $\text{Li}^7\text{OH}$  to KOH, a fairly appreciable advantage of the present chemistry mode of operation would be sacrificed: As a result of the nuclear reaction



Li7 is permanently formed, during reactor operation, from B10, which is abundant at about 20 atom % in the natural isotopic mixture of boron (and is contained to a corresponding amount in "natural" boric acid). This is the reason why the use of Li7OH is deemed a particularly elegant engineering procedure to meet the alcalization requirement.

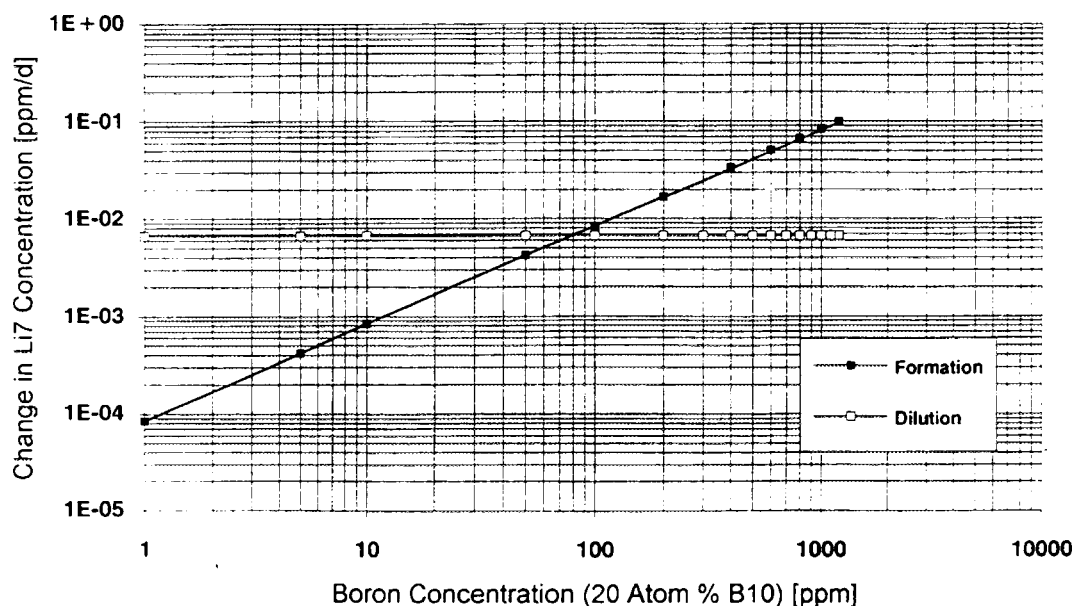


Figure 4: Change in Coolant Li7 Concentration by Simultaneous Formation from B10 and Dilution due to 4 ppm/d Boron Withdrawal (Initially 2 ppm Li7; 300 d Cycle Length; 370 000 kg Coolant)

Figure 4 demonstrates, as an example, how the coolant Li7 concentration, which has to be adjusted to a predetermined value all the time, results from the difference between dilution due to boron withdrawal and formation from B10 (the amount of which is steadily decreasing with time) via the nuclear reaction mentioned above.

Thus, the use of KOH would be a dual-component alcalization anyway requiring increased effort to adjust the desired potassium level and a lithium concentration which preferably is chosen very much lower.

## 4 Discussion

The operational experience gathered from WWER plants with KOH as an alkalization agent cannot readily be transferred to existing KWU-PWR plants or to the future European Pressurized-Water Reactor (EPR) as designed by NPI. Data from literature indicate, though not unambiguously, that KOH is superior to LiOH with respect to the acceleration effect on zircaloy corrosion, but is more aggressive than LiOH with respect to stress corrosion cracking of stainless steel. This is most important if coolant boiling and subsequent enrichment of coolant constituents up to the solubility limits occur not only in extended fuel rod surface areas, but also in limited surface areas of structural materials, e.g. at the core shroud structure, as a consequence of gamma heating.

Against this background, a final assessment of whether KOH is suitable as an alternative alkalizing agent is possible only on the basis of a qualification program comprising plant-specific gamma heating estimates and comprehensive experimental corrosion tests directed towards comparing LiOH and KOH at conditions which include simulation of high void fractions. Siemens/KWU plan to perform such investigation in a phase 2 of their "Alternative Water Chemistry" project. International contributions to this project would highly be appreciated.

## 5 Recommendations

The qualification program as mentioned above could also serve as a suitability test for zinc injection. Zinc hydroxide ( $Zn(OH)_2$ ) or zinc oxide ( $ZnO$ ) are ruled out as alkalizing agents because of insufficient solubility; zinc is discussed, however, as an additional dosing agent, in particular owing to its corrosion inhibiting properties, i.e. its ability to decelerate oxide film growth. Within the scope of such program, it should be checked if zinc exerts the beneficial impact as claimed for stainless steel on zircaloy-4, too, or if, in contrary, zinc tends to densify the zirconium oxide film, i.e. to block the pores of the

film, thus overturning the expected positive effect by deteriorating the heat transfer.

If, later on, zinc injection is applied in PWR practice, a compound should be used in which Zn64 is depleted. BWR plant experience shows that, otherwise, the activation product Zn65 causes an undesirable and avoidable increase in dose rate.

Furthermore, it should be considered to supplement the water chemistry guidelines as presently effective by specifying coolant impurities such as silica ( $\text{SiO}_2$ ), suspended solids or total iron ( $\Sigma\text{Fe}$ ), respectively, and dissolved specie like fluoride ( $\text{F}^-$ ), sulfur - preferably not sulfate ( $\text{SO}_4^{2-}$ ), but sulfide ( $\text{S}^{2-}$ ) - nitrogen/ammonia ( $\text{N}_2/\text{NH}_3$ ), and nickel ( $\text{Ni}^{2+}$ ).

In particular the determination of sulfide or, as an alternative, total sulfur requires the development of new or at least the modification of existing analysis techniques, preferably combined with on-line sampling.

Anyway, i.e. regardless of the alcalizing agent (and as well irrespective of the results of the qualification program as mentioned above), it would be advantageous to use, instead of "natural" boric acid, a product in which B10, the isotope effective in terms of neutron absorption, has been enriched. As indicated by producers, boric acid enriched in B10 is available even in higher chemical purity than the "natural" product. More importantly, B10 enrichment offers the possibility to provide more neutron absorption capacity at lower total boron concentrations and, as a consequence, to achieve the recommended pH without increasing - maybe even while slightly decreasing - the alcalizing agent concentration.

This is illustrated by Figure 5 which shows the "coordinated" and the "modified" boron-lithium modes of operation assuming different B10 enrichment levels.

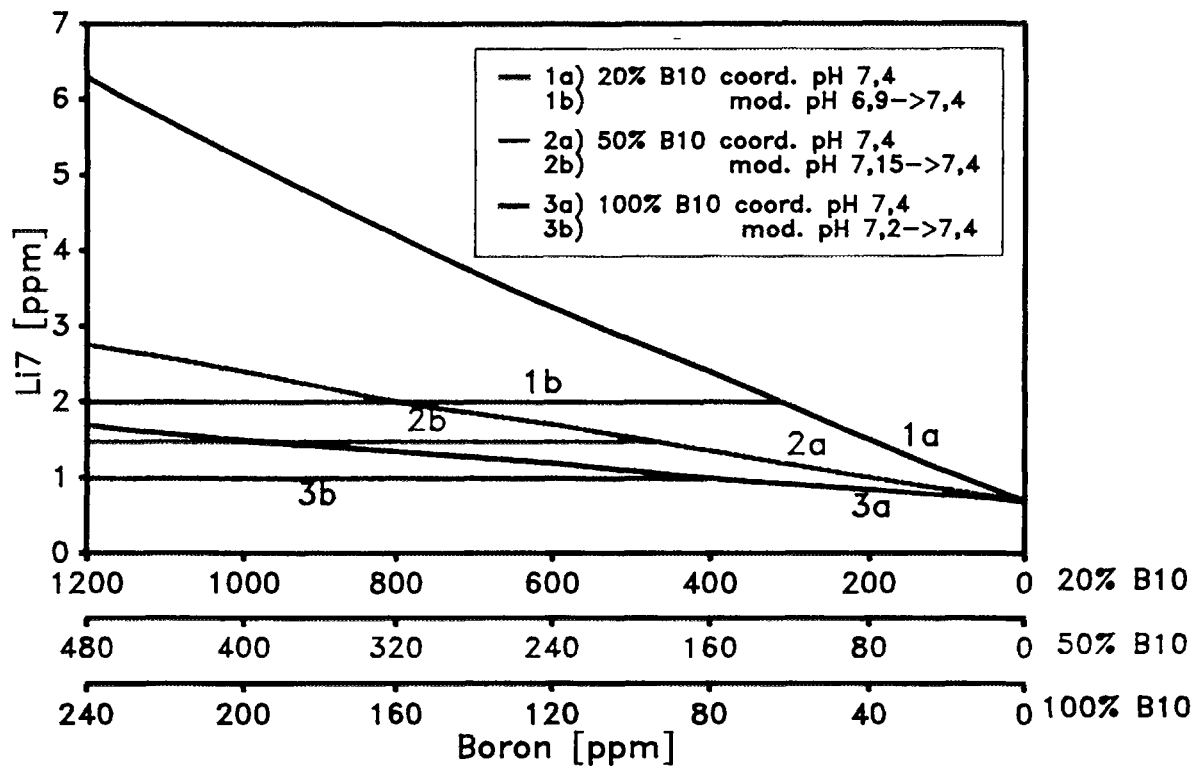


Figure 5: pH(300°C) Diagrams of Different Boron-Lithium Modes of Operation with and without B10 Enrichment

### REFERENCES

- [1] F. Roumiguere, T. Marchl,  
Dose Rate Reduction Strategies in the Field of PWR  
Primary Coolant Chemistry,  
XVII Reunión Anual Sociedad Nuclear Española,  
Madrid, Mai 1992
- [2] C.A. Bergmann et al.,  
Evaluation of Cobalt Sources in Westinghouse-Designed  
Three- and Four-Loop Plants,  
EPRI NP-2681, Final Report, Oct. 1982
- [3] W.E. Berry, R.B. Diegle,  
Survey of Corrosion Product Generation, Transport and  
Deposition in Light Water Nuclear Reactors,  
EPRI NP-522, Final Report, March 1979

- [4] M.J. Driscoll, O. Harling, G.E. Kohse,  
In-Pile Loop Studies of the Effect of PWR Coolant pH on  
Corrosion Product Radionuclide Deposition,  
EPRI TR-100156, Final Report, Febr. 1992
- [5] N.R. Large, D.R. Woodwark,  
Effect of Coolant Chemistry on PWR Radiation Transport  
Processes, Vol. 1-3,  
EPRI NP-6657, Final Report, Dec. 1989
- [6] T. Marchl, R. Rieß, S. Odar,  
Möglichkeiten zur Beeinflussung der Personendosen  
am Beispiel neuerer Druckwasserreaktoren,  
VGB Kraftwerkstechnik 72 (1992), H. 7, S. 611-613
- [7] T. Marchl et al.,  
Optimized Coolant Chemistry with Regard to Dose Rate  
Reduction,  
5th Intern. Conf. on Water Chemistry of Water Reactor  
Systems,  
Bournemouth, Oct. 1989
- [8] S.M. Walker, E.W. Thornton,  
Reanalysis of Oxide Solubility Data: Results for  
Nickel and Cobalt Substituted Ferrites,  
Nuclear Electric Report TD/RPB/REP/0016, Aug. 1990



## WATER CHEMISTRY IN WWER REACTORS

V.A. YURMANOV, V.A. MAMET,  
Yu.M. SHESTAKOV, M.M. AMOSOV  
All-Russian Scientific Research Institute for  
Nuclear Power Plants Operation, Moscow,  
Russian Federation

### Abstract

In this paper "Water Chemistry in WWER Reactors", are briefly described the 30 WWERs in Russia and the Ukraine, and are pointed out the essential differences between the 440s and 1000s. The primary coolant in the six loops of the former type operates at 270 - 290 °C, while the four loops of the latter type are at 290 - 320 °C.

Performance of the fuel has been generally good with some fission product activities emanating from tramp uranium. Incidents causing unusually high fission product levels were overheating of the 16th fuel load at Kola NPP in 1990 by a reduced coolant flow, and fuel defects at Novovoronezh NPP resulting from deposits of carbon and corrosion products. Organic carbon, depositing from the coolant in regions of high turbulence (i.e. at the spacer grids), provokes corrosion product deposition. The source of the organic is not known.

New chemistry guidelines have been implemented since 1992 - 93 for Russian and Ukrainian WWERs. These include higher  $\text{pH}_T$  values (7.0 - 7.1 as opposed to 6.6 - 6.9) and tighter controls on oxygen and impurities. Lower dose rates in steam generator channels are reported. Significant reduction in operator doses are achieved by these methods coupled with a "soft decontamination" involving changing the KOH concentration and, hence, the  $\text{pH}_T$  before shutdown. The benefits of hydrazine treatment for deoxygenating feedwater and coolant prior to start up, for injecting before shutdown and for general chemistry control on radiation fields are described.

At present, 13 WWER-type reactors are in operation in Russia and 12 in Ukraine. In this amount 8 are the WWER-440 reactors and 17 are the WWER-1000 reactors. Recently unit 4 at Balakovo NPS with WWER-1000 reactor was put into operation.

There are some essential differences between parameters of primary circuit NPS with WWER-440 and WWER-1000 reactors. WWER-440 and WWER-1000 primary coolant circuit include 6 and 4 loops respectively. The coolant temperature ranges is about 270-290 C and 290-320 C in WWER-440 and WWER-1000 primary circuits respectively. The coolant pressure is about 12 and 16 MPa in WWER-440 and WWER-1000 primary circuits respectively.

The most essential differences between reactor blowdown cleaning systems include using ion-exchange and high-temperature filters. All NPS with WWER-440 reactor and WWER-1000 reactors at unit 5 New-Voronezh NPS, unit 1 and 2 South-Ukraine NPS, unit 1 and 2 Kalinin NPS are equipped with mixed bed demineralizers. WWER-1000 reactors at units 1-5 Zaporozhe NPS, units 1-4 Balakovo, unit 3 South-Ukraine NPS, unit 3 Rovno NPS and unit 1 Khmel'nitsk NPS are equipped with high-temperature filters. The mixed bed demineralizer flow is 20 and 30 m<sup>3</sup>/h at WWER-440 and WWER-1000 reactors blowdown cleaning systems respectively. The nominal capacity of a high-temperature blowdown cleaning systems is 400 m<sup>3</sup>/h. The high-temperature filter nominal capacity of each main reactor recirculation loop is equal to 100 m<sup>3</sup>/h.

A correct analysis of fuel cladding reliability of different WWER NPS requires certain factors to be taken into account, such as the fuel burnup level, pre-startup thermal-mechanical and startup chemistry treatments for the surface, the operational and the shutdown water chemistry.

No one failed fuel assembly causing exceeding was in Russian NPPs both in 1991 and 1992 life times. I-131 and I-134 maximum activities in Balakovo NPS unit 1, Kalinin NPS unit 2, South Ukraine unit 2 and 3 were lower level which determined by manufacturing uranium dirt on the fuel rod cladding surfaces only. It means failure clads absence in cores.

Inspections of fuel integrity (IFI) for Balakovo NPS unit 3 was performed after reactor shutdown, using container which placed into the cooling pond. This method include fission products activities measurement to detect a leaking assemblies. Only one fuel assembly was found. Fission products specific activities anomaly raised in the next lifetime beginning.

During Kalinin-1 refuelling in December 1991 2 from 66 fuel assemblies were controlled. 2 FA detected as failure and disposed. A burst activity effluent shows some defected assemblies were resided. All kinds of radioactive impurities deposited then at the primary circuit internal surfaces.

In 1990 during the operation of the 16th fuel load of WWER-440 reactor (60 effective days) at Kola NPP, Unit 2, overheating of practically all the fuel assemblies (FA) of the third year of operation was detected. It was caused by coolant flow rate decrease (20-30%) in the FA. When this fact was revealed unit power was reduced up to 90% nominal power. After 90 Effective days of operation reactor was shutdown to refuelling. during the 17th campaign the condition of the mentioned FA has not changed and after operation during 142 effective days at 90% nominal power, reactor was shutdown.

Inspections of fuel integrity of 317 FA after 15 campaigns revealed 5 leaky fuel assemblies, after 17 campaigns - 3 leaky FA. During 16-17 campaigns specific total primary coolant activity (by the sum of iodine radionuclides) fluctuated within the limits of 0.17-0.59 mCi/kg, which is one order of magnitude higher than the coolant activity level of the Kola NPP other units.

Out-of-core inspections of the mentioned fuel assemblies in the Novovoronezh NPP hot cell revealed deposits on the fuel rod surfaces, having filled the gaps between fuel rods and spacer grids. Maximum amount of deposits with the thickness of up to 1mm, is on the peripheral fuel rods (FRs) in the zone of spacer grids 1 and 2 (from the low part of the fuel bundle) with damages in grids 1, 2 and 3. There are through-wall defects in some fuel rods. Chemical and spectral analysis showed that the composition of deposits includes carbon, as well as corrosion products of circuits and fuel rods (Fe, Cr, Ni, Co, Mn, Zr etc.), and also carbon and iron are the main elements (by mass). Inspection results allowed to suggest that the cause of the mentioned event is the deposition of organic compounds from the coolant into the zones with the high flow turbulence (spacer grids). These deposits are the base for structural materials corrosion products precipitation from the coolant flow. The cause of the organic elements appearance in the WWER-440 primary circuit coolant of the Kola NPP is not clear enough.

To evaluate influence of water chemistry on fuel cladding behaviour All-Russian Scientific Research Institute of Nuclear Power Plants has carried out an analysis of data from fuel cladding failures and chemistry monitoring operations on nuclear power-generating units with water-moderated water-cooled (WWER) reactors. Data base include the results of statistical processing of operation data on chemical monitoring of the primary coolant in power-generating units operating with WWER-1000 and WWER-440 reactors. Analysis of the data base obtained makes it possible to compare both the conduct of chemical treatment over a working campaign for power-generating units with WWER reactors on different NPS.

Standard combined ammonia-potassium, hydrazine-potassium and mixed hydrazine-ammonia-potassium water treatment with regulation by boric acid is used in the primary loop of different units NPS with WWER reactors.

The concept of water chemistry ensures that pHt values and hydrogen concentration corresponding to positive values of the temperature gradient of magnetite solubility near its minimum are retained through the working campaign. According to the concept of water chemistry, the fulfilling of this conditions should lead to minimizing of corrosion product deposits in the fuel cladding.

Statistical processing of chemical monitoring data shows that in period before 1992 the mean pHt value was 6.6-6.9 over the whole working campaign. The water chemistry WWER reactor recent guideline ensures that pHt values correspond not to a constant pHt level, but to a variable one, with a monotonic increase over a working campaign constituting on average around 6.7 for WWER-1000 and 6.8 for WWER-440 reactors.

At 1992-1993 in Russian and Ukrainian, NPS with WWER reactors were implemented new the water chemistry guideline. This correction guarantee the possibility of carrying out water treatment with a constant pHt value at level about 7.0-7.1 at in-let reactor temperature (270 and 290 °C at WWER-440 and WWER-1000 respectively).

With revision of primary circuit water chemistry standards:

- controls are in place on Russian and Ukrainian NPS for radiochemical monitoring of radionuclides corrosive origin in the coolant (Cr-51, Co-60, Co-58, Mn-54, Mn-56 and Fe-59),
- maximum admissible concentration of oxygen in the coolant as been reduced from 0.01 to 0.005 ppb,
- the alkali metals (K + Li + Na) - boric acid concentrations mode of operation as been corrected.

As a result of the letter, there has been pHt value increase in the working campaign beginning and reduction at the end.

The alkali metal - boric acid mode of operation for WWER-440 and WWER-1000 before and after revision of standards in 1992-1993 is shown in Fig. 1 and 2. Constant pHt lines correspond calculated ammonia concentration 15 ppm and the in-let reactor coolant temperature (270 and 290 °C at WWER-440 and WWER-1000).

WWER reactors use a mixed ammonia-potassium (NH<sub>3</sub>-K) water chemistry with hydrogen produced by radiolysis of ammonia or hydrazine. The most essential differences between primary water chemistry of WWER reactors include pHt and hydrogen concentration levels of operation.

Mean values and variation ranges in main coolant quality characteristics in first loop of Russian and Ukrainian NPP with WWER-440 and WWER-1000 in 1990-1992 is shown in Table 1-6. Information processing include determination both of standard deviation from mean value and proportion of time norm observed for a hydrogen and a total alkali metal concentrations.

Dosage levels for staff and associate workers on Russian and Ukrainian nuclear power stations with WWER reactors at 1990-1992 is shown in Table 1-6 and Fig. 3-4. Handling data include determination of mean individual dose, collective dose and standardized exposure levels. Operating water chemistry and dosage exposure data of Russian and Ukrainian NPP before 1990 were published earlier.

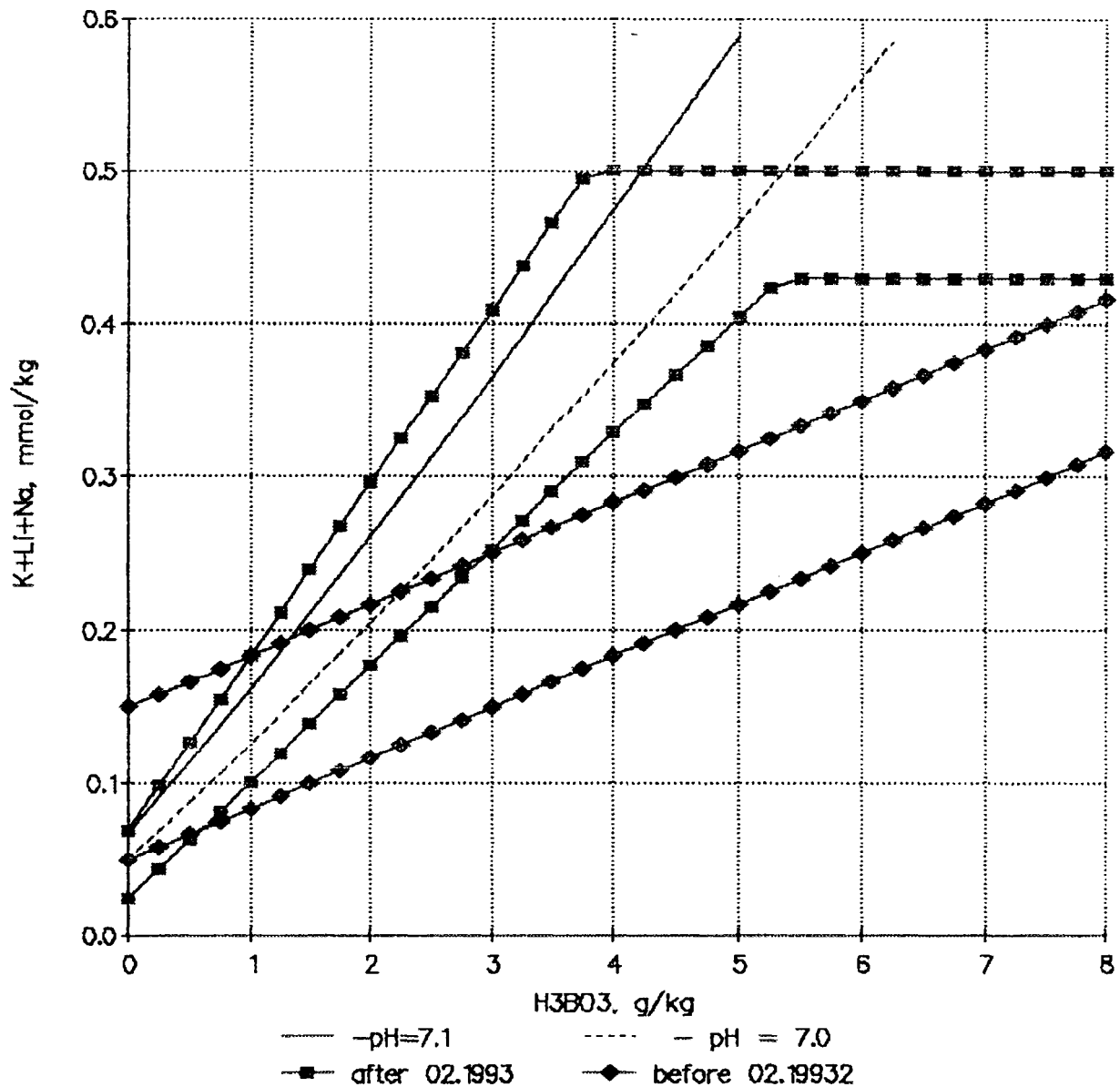


FIG. 1 WWER-440  $pH_{270}$  ( $NH_3=15$  ppm)

Comparison of primary circuit water chemistry during 5th and 6th fuel lifetime at unit 3 Zaporozhe NPS showed both stabilization and increase pH value (see Fig. 5-6). As a result a dose rate reduction in steam generator channel were observed.

Primary circuit water chemistry instability during 5th fuel lifetime at unit 2 Balakovo NPS cause a radiation situation deterioration.

Primary circuit water chemistry was variable from first to seventh fuel lifetime at Kalinin NPS unit 1 and from first to fifth fuel lifetime at unit 2 Kalinin NPS unit 2.

A soft decontamination of primary circuits were realized initially in 1985 at NPS Novovoronez unit 5 (WWER-1000 reactor). In 1993 the primary circuit soft decontaminations were realized at NPS Kalinin unit 2, NPS South Ukraine unit 1 and 2. An experience accumulated allow to propose that correctly manipulated water chemistry during reactor shutdown ensure a significant dose rate reduction

in maintenance and refuelling. Doserates are caused either by radiation of radionuclides carried by the water or by radionuclides deposited at the internal surfaces of primary circuit equipment.

A corrosion radionuclides dynamics in primary coolant during Kalinin NPS unit 2 reactor shutdown 1992 is shown in Fig 7-9. A primary coolant and cleaned water after mixed bed demineralizers and H-cation filters were controlled. Maximum in corrosion product activities corresponds to boric acid increase.

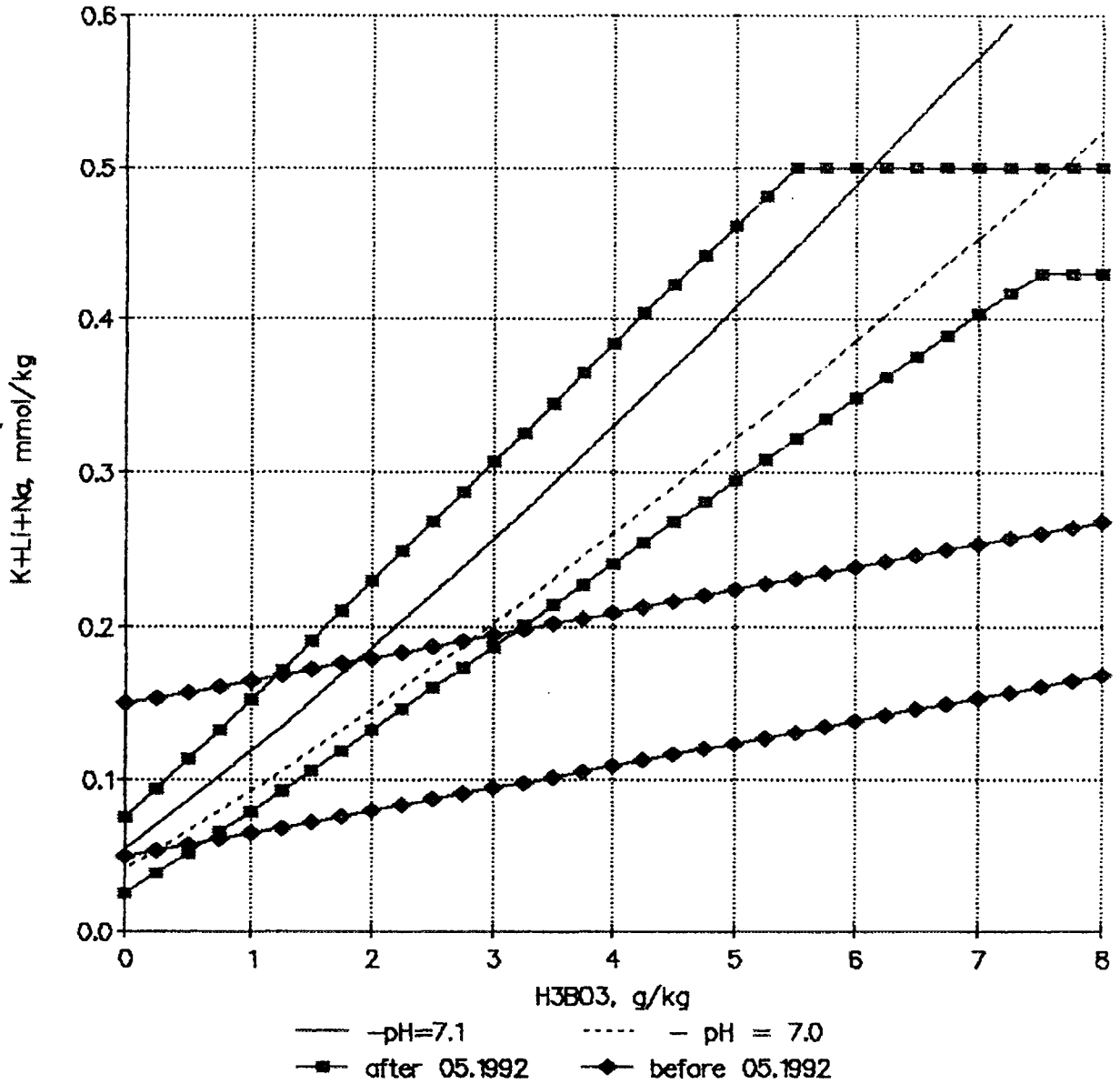


FIG. 2 WWER-1000 pH<sub>290</sub> (NH<sub>3</sub>=15 ppm)

TABLE I Mean Values and Variation Ranges in Main-Coolant Quality Characteristics in First Loop of NPP with WWER-1000 in 1990

NPP	Unit N	Quality characteristics					Proportion of time norm observed, %	
		pH	NH <sub>3</sub> ppm	H <sub>2</sub> nm1/kg	Fe ppb	Cu ppb	K+Li+Na	H <sub>2</sub>
The regulation limit		5.7-10.2	≥ 5	30-60	≤ 200	≤ 20	-	-
New-Voronezh	5	7.84+0.78 7.00-9.40	13+3 8-17	34+2 31-38	22 10-80	≤ 3	100	100
Kalinin	1	7.74+0.34 7.20-8.20	19+3 15-23	37+3 30-40	11+2 10-17	≤ 5	75	100
	2	8.09+0.75 7.30-9.60	19+2 16-22	35+2 32-38	20 10-100	5 ≤ 5-6	100	100
Balakovo	1	7.51+0.30 7.30-7.70	-	38+5 34-41	88+8 80-95	≤ 20	100	100
	2	7.99+0.59 7.10-9.20	-	37+3 32-44	69+51 20-200	19+8 7-37	83	100
	3	7.99+0.63 7.15-8.90	-	35+3 31-41	41+18 20-70	20+12 ≤ 2-50	83	100
Zaporozhe	1	-	13+2 10-15	35+2 31-38	≤ 10	-	92	100
	2	-	13+1 13+14	34	≤ 10	-	100	100
	3	-	13+2 10+16	34+2 32-38	≤ 10	-	100	100
	4	-	12+2 9-16	33+1 32-36	≤ 10	-	92	100
	5	-	14+2 11-17	33+1 31-36	≤ 10	-	100	100
South-Ukraine	1	7.69+0.62 6.80-8.70	29+7 22-40	40+2 35-43	-	-	100	100
	2	7.92+0.56 7.10-8.60	34+6 21-43	41+4 32-44	-	-	100	100
	3	7.79+0.39 7.20-8.70	29+8 17-43	43+1 41-45	-	-	100	100
Hmel'nitsk	1	7.54+0.21 7.30-7.90	17+6 9-23	32+1 31-34	≤ 30	-	100	100
Rovno	3	7.67+0.21 7.30-8.00	19+4 12-23	36+6 31-46	10 5-30	≤ 20	92	100

mean value + standard deviation  
 minimum value - maximum value

TABLE II Mean Values and Variation Ranges in Main Coolant Quality Characteristics in First Loop of NPP with WWER-440 in 1990

NPP	Unit N	Quality characteristics				Proportion of time norm observed, %	
		pH	NH3 ppm	H2 nm1/kg	Fe ppb	K+Li+Na	H2
The regulation limit		5.7-10.2	≥ 5	30-60	≤ 200	-	-
Kola	1	7.76+0.68 7.10-8.87	11+2 10-14	44+3 40-52	≤ 30	100	100
	2	7.5+0.5 7.1-8.6	11+1 10-14	44+4 39-52	≤ 30	70	100
	3	7.7+0.5 7.2-9	29+2 26-33	41+5 35-49	≤ 30	100	100
	4	7.82+0.64 7.15-9.30	27+1 24-29	42+4 35-46	≤ 30	90	100
Novovoronezh	3	8.45+1.01 7.50-10.0	9+2 7-17	36+3 32-43	12+4 ≤10-20	92	100
	4	7.77+0.52 7.30-8.90	8+3 6-16	37+7 32-57	13+5 ≤10-22	70	100
Rovno	1	7.12+0.67 6.20-8.20	15+5 11-23	42+5 35-48	≤ 5	60	100
	2	7.39+0.41 6.75-7.90	18+5 12-23	32+10 5-43	28 ≤10-22	75	92

mean value + standard deviation  
minimum value - maximum value

TABLE III Mean Values and Variation Ranges in Main Coolant Quality Characteristics in First Loop of NPP with WWER-1000 in 1991

NPP	Unit N	Quality characteristics					Proportion of time norm observed, %	
		pH	NH3 ppm	H2 nm1/kg	Fe ppb	Cu ppb	K+Li+Na	H2
The regulation limit		5.7-10.2	≥ 5	30-60	≤ 200	≤ 20	-	-
New-Voronezh	5	7.38+0.50 6.90-8.20	6+2 5-10	39+5 32-45	15+7 10-30	≤ 3	55	100
Kalinin	1	7.81+0.52 7.30-9.00	18+2 15-21	33+2 31-35	10	-	88	100
	2	7.87+0.82 7.28-9.30	17+2 14-19	33+2 31-35	10	-	88	100
Balakovo	1	7.74+0.82 7.10-9.70	19+2 15-21	37+2 34-40	110+90 20-200	19+3 13-20	89	100
	2	7.43+0.31 6.90-7.70	20+2 17-22	38+2 35-40	160+60 60-200	15+3 10-20	79	100
	3	7.89+0.97 7.00-9.70	20+1 18-21	35+3 32-42	120+80 20-200	16+3 13-20	89	100
Zaporozhe	1	7.25+0.22 7.00-7.30	12+1 11-13	33+2 31-36	11+3 10-20	-	90	100
	2	7.15+0.11 7.00-7.30	13+1 11-15	33+2 31-35	≤ 10	-	78	100
	3	7.15+0.10 7.00-7.30	11+2 10-13	32+1 31-34	≤ 10	-	100	100
	4	7.15+0.09 7.00-7.30	12+2 10-15	32+1 31-33	≤ 10	-	75	100
	5	7.20+0.10 7.00-7.30	13+3 9-17	32+1 30-33	≤ 10	-	100	100
South-Ukraine	1	7.43+1.07 5.80-9.20	19+7 6-22	44+2 41-47	≤ 10	-	81	100
	2	7.51+0.77 5.70-8.60	27+8 7-36	38+3 33-42	11+2 10-15	-	79	100
	3	8.29+0.89 7.20-10.2	44+11 27-56	39+4 33-49	14+7 10-30	-	86	100
Hmel'nitsk	1	7.73+0.76 6.90-9.15	17+4 10-21	33+2 32-38	20 10-80	≤ 20	90	100
Rovno	3	7.67+0.81 7.00-9.30	16+4 9-21	40+4 33-45	9+3 3-12	-	86	100

mean value + standard deviation  
minimum value - maximum value

TABLE IV Mean Values and Variation Ranges in Main Coolant Quality Characteristics in First Loop of NPP with WWER-440 in 1991

NPP	Unit N	Quality characteristics				Proportion of time norm observed, %	
		pH	NH3 ppm	H2 nm1/kg	Fe ppb	K+Li+Na	H2
The regulation limit		5.7-10.2	≥ 5	30-60	≤ 200	-	-
Kola	1	7.46+0.33 7.10-8.00	11+2 8-16	46+6 36-55	60+30 30-110	100	100
	2	7.28+0.25 6.90-7.75	14+6 9-25	44+6 37-52	40+30 5-110	70	100
	3	8.15+0.90 7.40-9.20	32+2 29-35	39+13 4-46	≤ 30	100	100
	4	7.83+0.45 7.30-8.55	33+3 29-39	40+4 35-48	≤ 30	90	100
Novovoronezh	3	7.50+0.15 7.30-7.70	8+1 7-9	40+8 34-56	35+20 ≤10-56	85	100
	4	8.10+0.90 7.20-9.80	9+2 7-12	38+9 31-53	10+1 ≤10-12	80	100
Rovno	1	8.15+0.90 7.00-9.80	28+6 20-38	39+6 32-53	12+2 10-15	83	100
	2	8.17+0.73 7.30-9.45	26+3 23-30	38+3 35-45	13+3 10-22	78	92

mean value + standard deviation  
minimum value - maximum value

TABLE V

Mean Values and Variation Ranges in Main Coolant Quality Characteristics in First Loop of NPP with WWER-1000 in 1992

NPP	Unit N	Quality characteristics					Proportion of time norm observed, %	
		pH	NH <sub>3</sub> ppm	H <sub>2</sub> nm1/kg	Fe ppb	Cu ppb	K+Li+Na	H <sub>2</sub>
The regulation limit		5.7-10.2	≥ 5	30-60	≤ 200	≤ 20	-	-
New-Voronezh	5	7.36+0.39 6.80-7.90	11+8 5-30	39+7 30-51	23+10 10-40	≤ 3	75	100
Kalinin	1	7.45+0.43 6.45-8.07	19+2 16-21	33+2 30-35	15+6 10-30	-	64	100
	2	8.01+0.79 7.10-9.48	18+1 17-21	33+2 30-35	13+5 10-22	-	90	100
Balakovo	1	7.92+0.47 6.95-8.60	-	38+4 32-45	165+74 15-200	18+2 15-20	58	100
	2	7.87+0.51 7.40-9.00	-	37+3 32-42	146+77 20-200	17+3 13-20	50	100
	3	8.16+0.84 7.30-9.60	-	39+3 33-45	139+91 15-200	18+3 15-20	40	100
Zaporozhe	1	-	15+2 13-17	33+1 31-34	≤ 10	-	80	100
	2	-	15+1 13-16	33+1 32-34	≤ 10	-	80	100
	3	-	13+1 12-15	33+2 31-37	≤ 10	-	88	100
	4	-	13+1 12-16	32+1 30-33	≤ 10	-	70	100
	5	-	14+1 12-15	33+1 32-34	≤ 10	-	64	100
Rovno	3	7.58+0.68 6.60-8.90	14+5 8-23	42+3 37-48	19+12 5-38	7+3 4-12	55	100
South-Ukraine	1	7.29+0.17 7.05-7.55	29+3 6-15	43+3 40-48	10+3 10-20	-	75	97
	2	7.47+0.61 6.90-8.90	27+9 14-42	40+6 33-54	≤ 10	-	100	100
	3	7.21+0.71 7.30-9.70	44+12 14-57	38+2 36-41	≤ 10	-	81	96

mean value + standard deviation  
minimum value - maximum value

TABLE VI Mean Values and Variation Ranges in Main Coolant Quality Characteristics in First Loop of NPP with WWER-440 in 1992

NPP	Unit N	Quality characteristics				Proportion of time norm observed, %	
		pH	NH3 ppm	H2 nm1/kg	Fe ppb	K+Li+Na	H2
The regulation limit		5.7-10.2	≥ 5	30-60	≤ 200	-	-
Kola	1	8.02+0.55 7.45-8.80	13+2 11-16	42+6 34-52	≤ 30	80	100
	2	7.52+0.66 6.7-8.8	19+11 10-38	38+5 33-46	≤ 30	67	100
	3	7.72+0.34 7.3-8.3	34+13 30-38	43+5 35-52	≤ 30	91	100
	4	8.03+0.52 7.45-9.00	32+2 30-35	42+4 35-46	≤ 30	100	100
New-Voronzh	3	7.69+0.43 7.20-8.5	7+1 6-9	41+8 32-54	35 ≤10-170	70	100
	4	7.96+0.65 7.30-9.00	7+1 6-8	43+4 39-50	16+8 ≤10-31	45	100
Rovno	1	8.16+0.92 7.70-9.90	27+4 22-32	38+2 35-42	14+11 ≤10-47	64	100
	2	7.91+0.79 6.30-9.18	25+4 18-32	39+3 34-44	15+10 ≤10-45	67	100

mean value + standard deviation  
minimum value - maximum value

TABLE VII Dosage levels for staff and associate workers on Russian and Ukrainian nuclear power stations with WWER reactors at 1991/1990

NPS	Unit N	Reactor type	Startup date	Mean individual dose, cSv/year	Collective dose, cSv	standardised exposure levels, cSv/(GWt h)
Kola	1	WWER-440	08.1973	0.46/0.49	895/984	74.6/80.0
	2	WWER-440	12.1974			
	3	WWER-440	03.1981			
	4	WWER-440	11.1984			
New-Voronezh	3	WWER-440	03.1971	0.59/0.46	1809/1269	181/129
	4	WWER-440	12.1971			
	5	WWER-1000	06.1980			
Kalinin	1	WWER-1000	0.5.1984	0.19/0.29	402/649	34.1/51.9
	2	WWER-1000	12.1986			
Balakovo	1	WWER-1000	12.1985	0.47/0.048	127/98	8.17/7.76
	2	WWER-1000	12.1986			
	3	WWER-1000	12.1988			
Zaporozhe	1	WWER-1000	12.1984	0.14/0.08	483/281	17.8/11.3
	2	WWER-1000	10.1985			
	3	WWER-1000	12.1986			
	4	WWER-1000	12.1987			
	5	WWER-1000	08.1989			
South-Ukraine	1	WWER-1000	12.1982	0.67/0.42	1389/1272	83.2/88.3
	2	WWER-1000	12.1985			
	3	WWER-1000	12.1989			
Rovno	1	WWER-440	12.1980	0.27/0.24	538/709	47.2/55.6
	2	WWER-440	12.1981			
	3	WWER-1000	12.1986			
Khmelnitsk	1	WWER-1000	12.1987	0.31/0.43	544/489	90.9/71.0

TABLE VIII Dosage levels for staff and associate workers on Russian and Ukrainian nuclear power stations with WWER reactors at 1991 / 1990

NPS	Unit N	Reactor type	Startup date	Mean individual dose, cSv/year	Collective dose, cSv	standardised exposure levels, cSv/(GWt h)
Kola	1	WWER-440	08.1973	0.46/0.36	895/854	74.6/79.5
	2	WWER-440	12.1974			
	3	WWER-440	03.1981			
	4	WWER-440	11.1984			
New-Voronezh	3	WWER-440	03.1971	0.59/0.48	1809/1347	181/135
	4	WWER-440	12.1971			
	5	WWER-1000	06.1980			
Kalinin	1	WWER-1000	05.1984	0.19/0.16	402/344	34.1/26.7
	2	WWER-1000	12.1986			
Balakovo	1	WWER-1000	12.1985	0.047/0.075	127/189	8.17/10.1
	2	WWER-1000	12.1986			
	3	WWER-1000	12.1988			

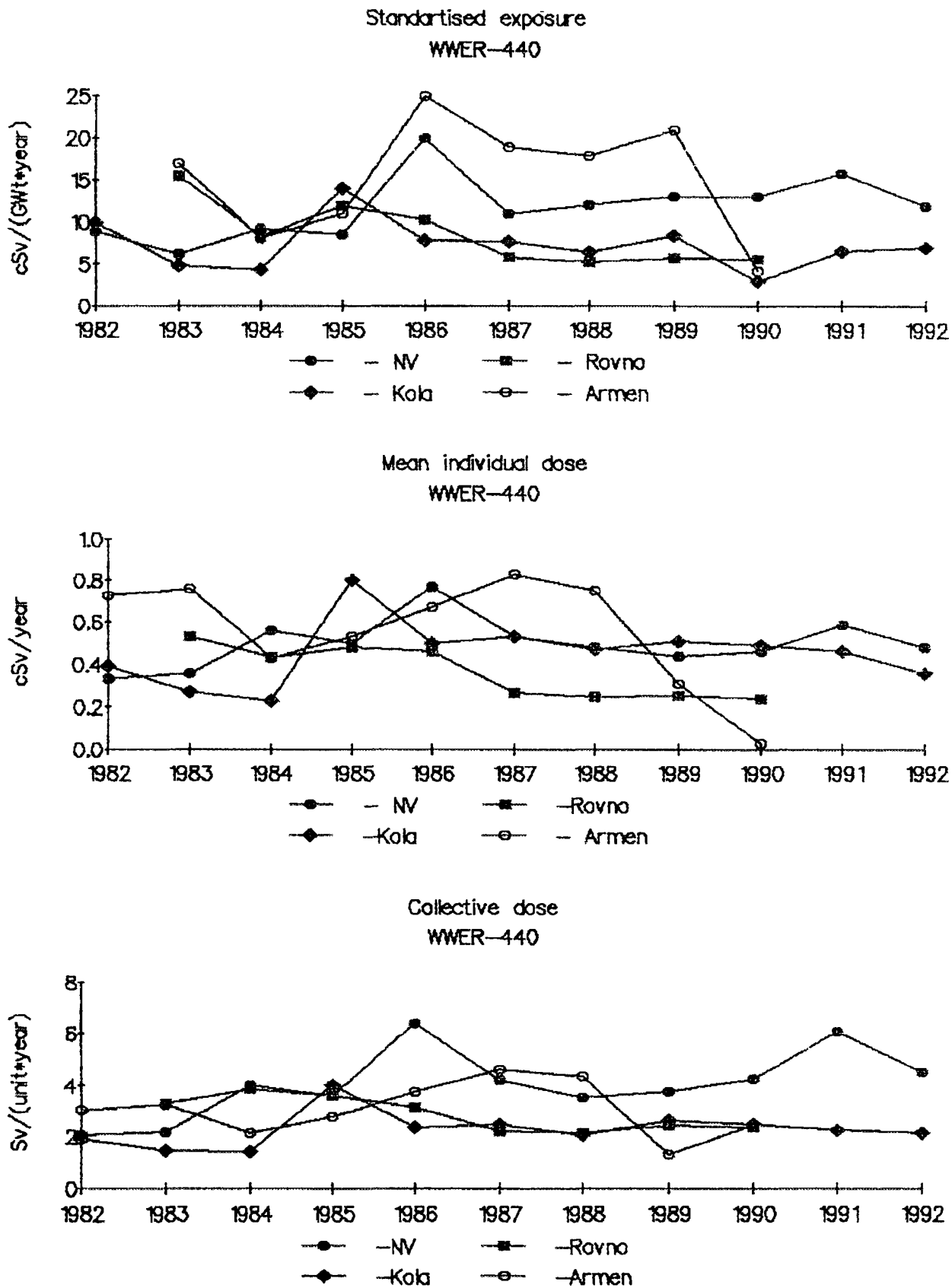


FIG. 3 Radiation exposure in Russian and Ukrainian WWER-400

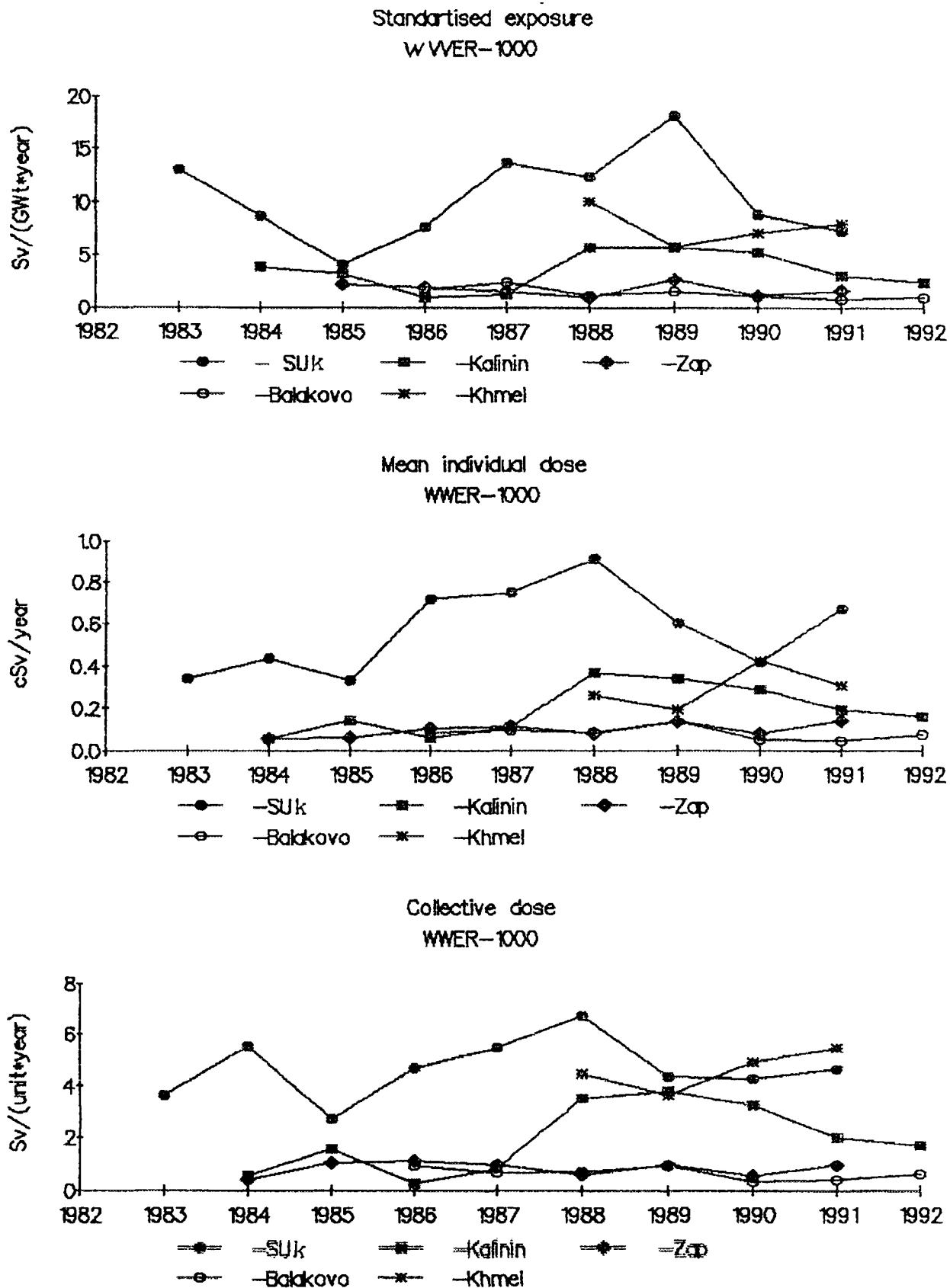


FIG. 4 Radiation exposure in Russian and Ukrainian WVER-1000

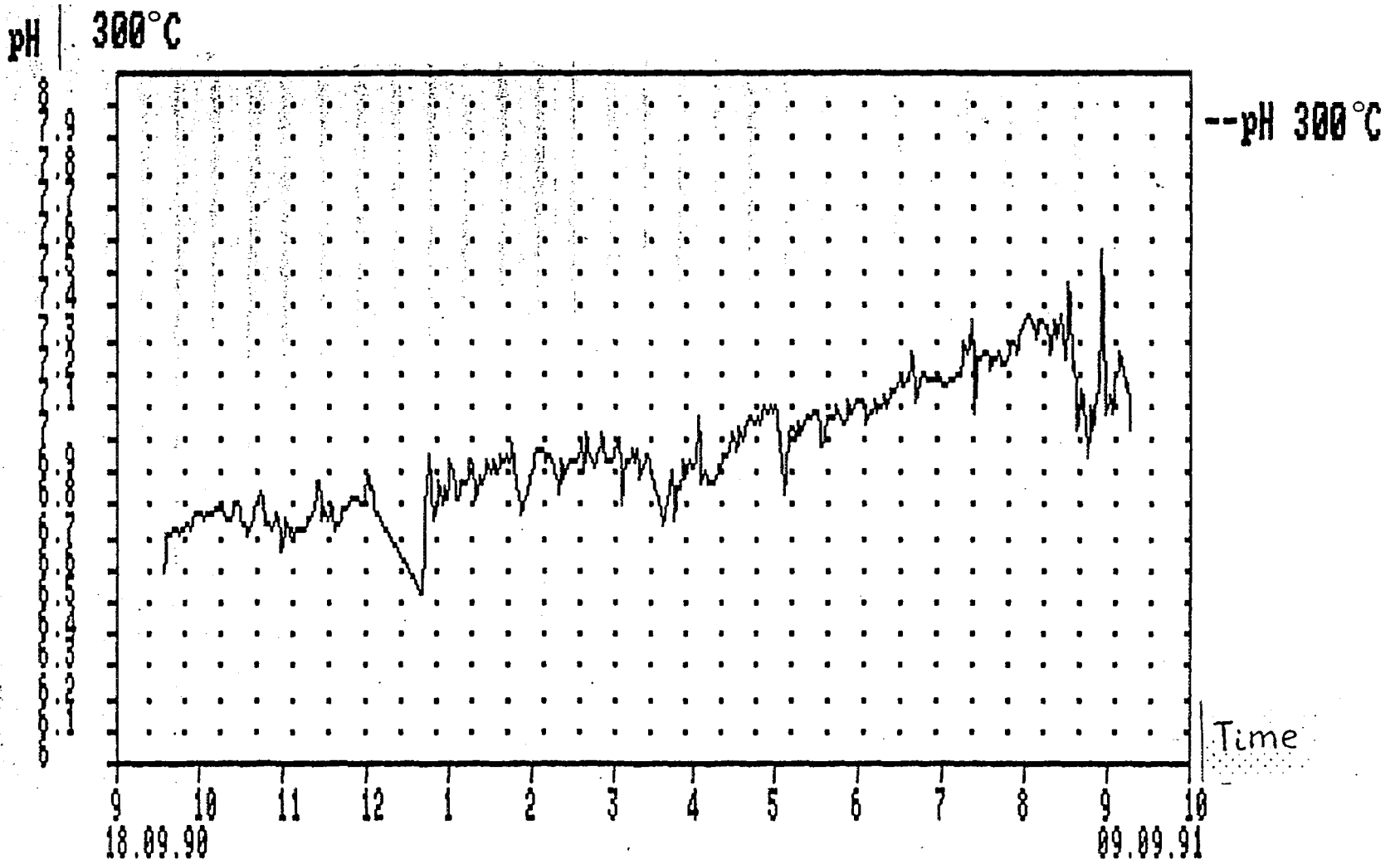


FIG. 5 Zaporozhe Unit 3 pH<sub>300</sub> during cycle 5

pH 300 °C

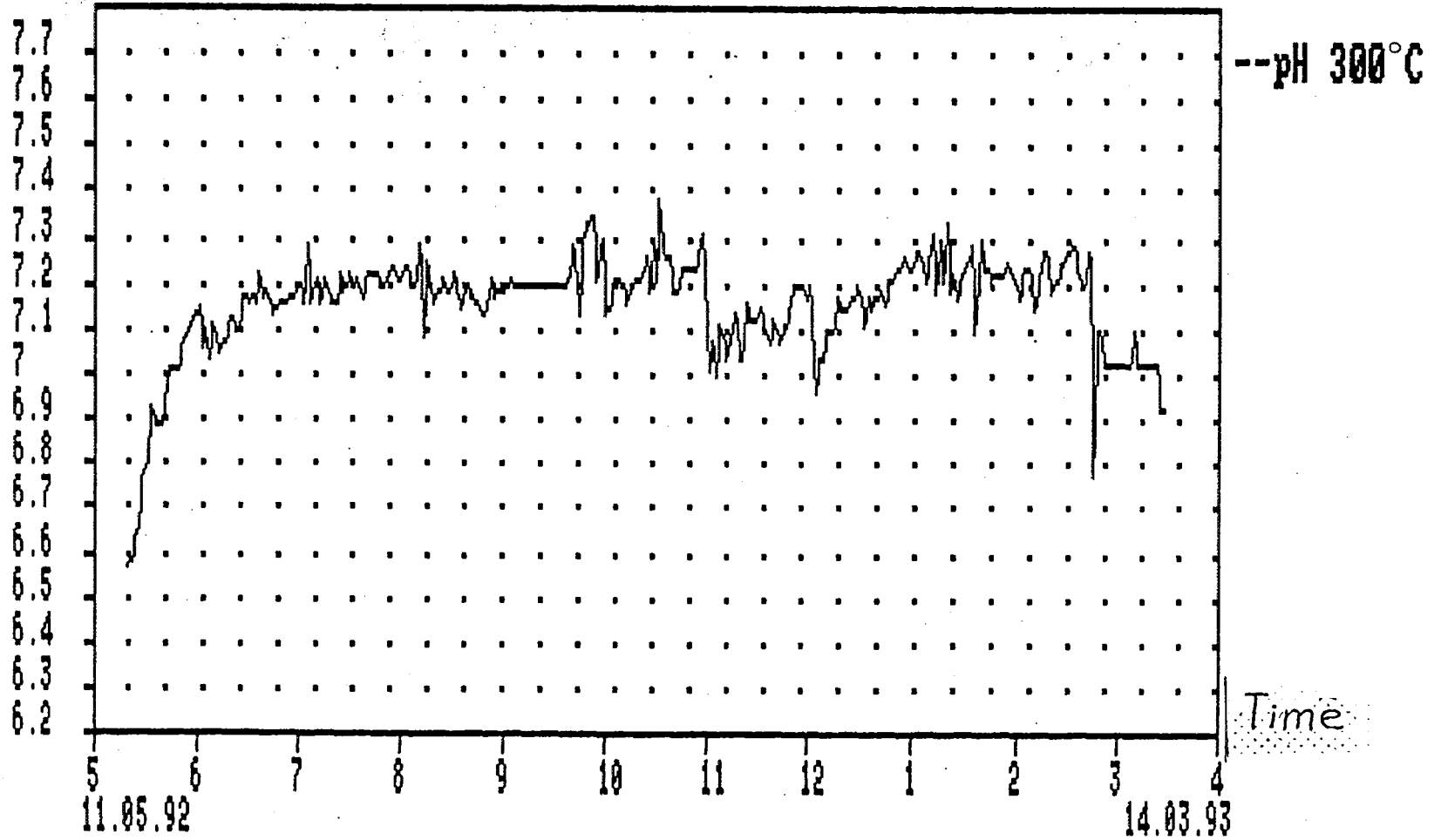
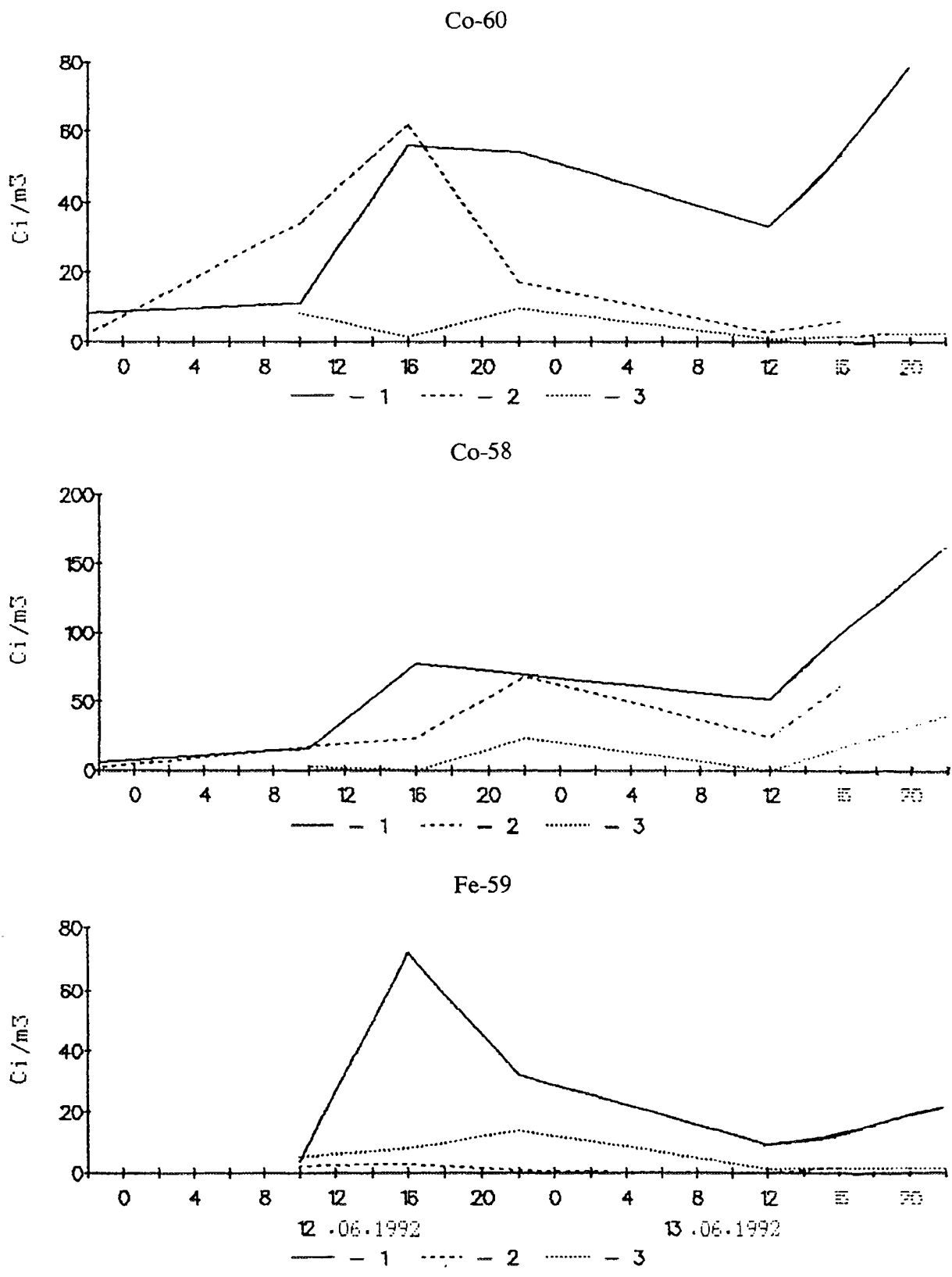


FIG. 6 Zaporozhe Unit 3 pH<sub>300</sub> during cycle 6



1 Primary Coolant    2 After Filter mixed bed demineralizer    3 After H<sup>+</sup> Cation Filter

FIG. 7 Variations of measured activities in primary coolant during "soft" decontamination at Kalinin NPP - 2 before refuelling (1992)

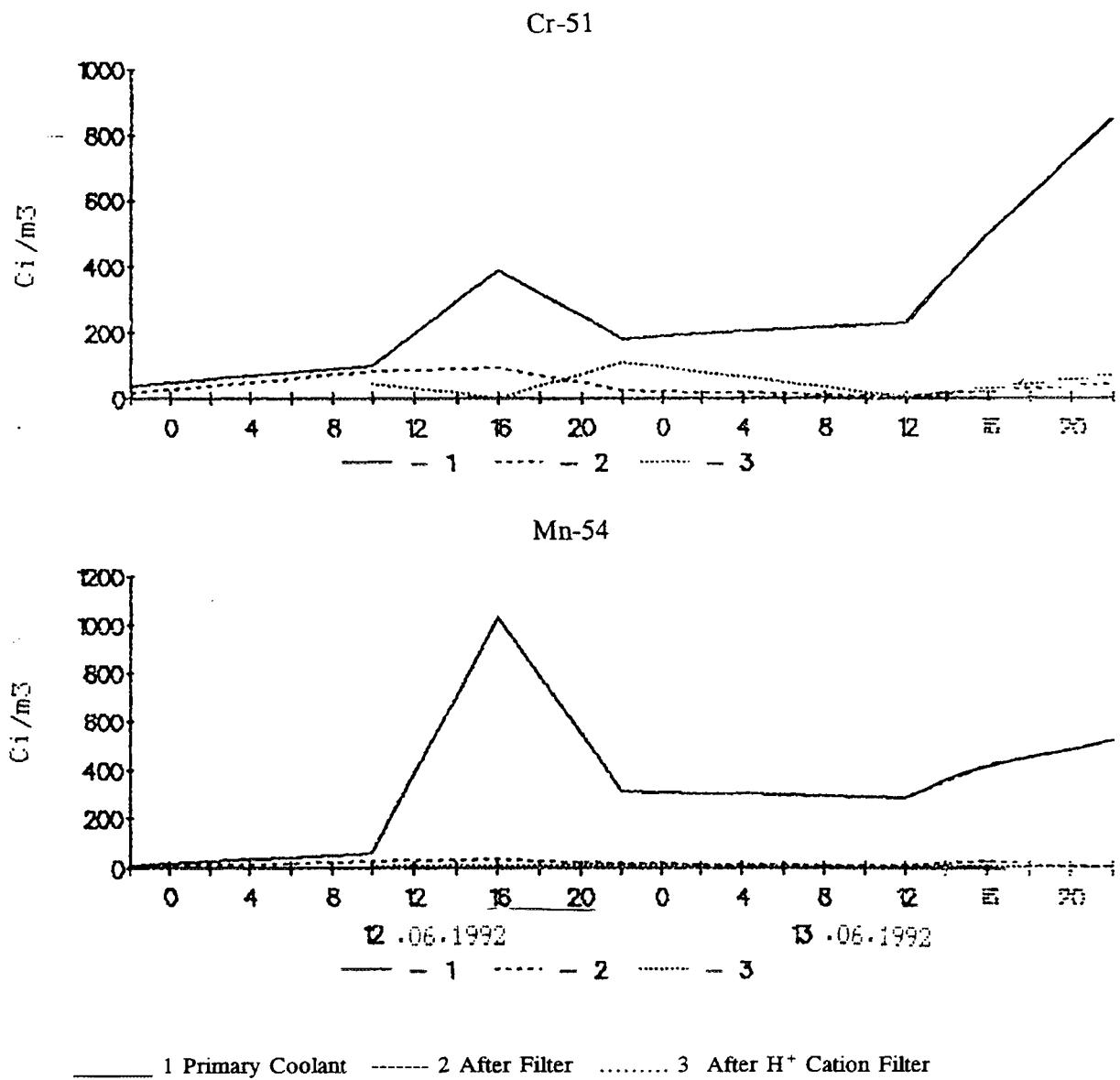


FIG. 8 Variations of measured activities in primary coolant during "soft" decontamination at Kalinin NPP - 2 before refuelling

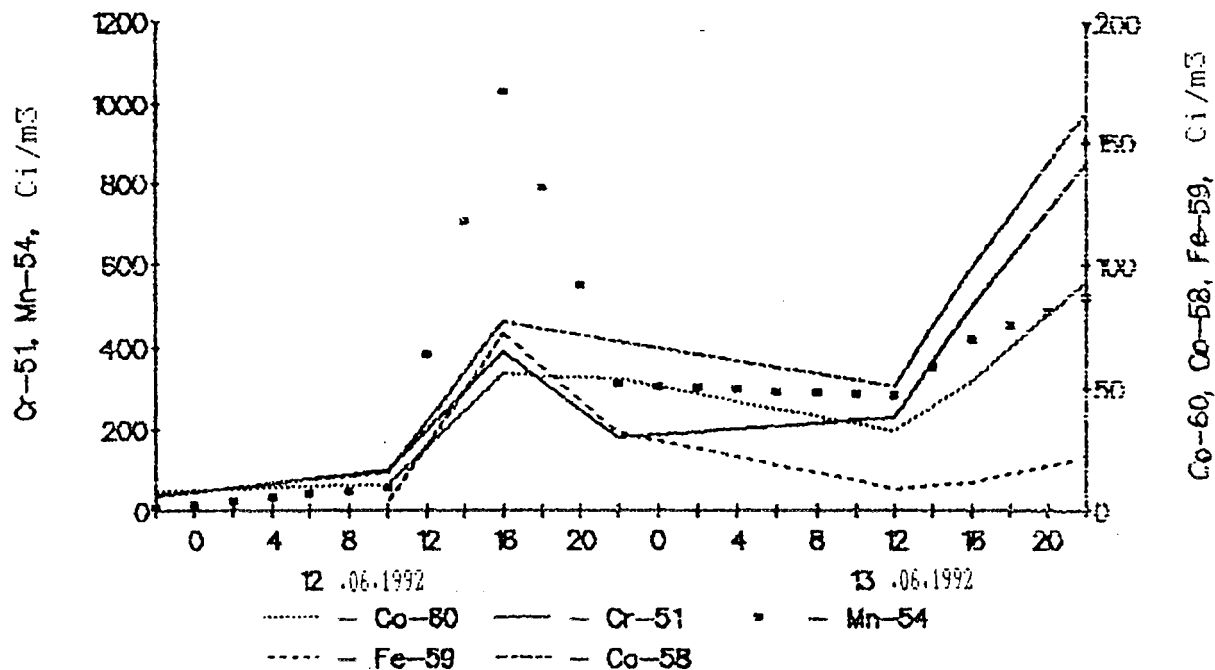


FIG. 9 Variations of measured activities in primary coolant during "soft" decontamination at Kalinin NPP - 2 before refuelling (1992)

## CONCLUSIONS

1. Russian and Ukrainian WWER operating data shows minimal collective doses and radiation fields corresponds:
  - Maximal pHt of Primary coolant
  - Maximal stability of pHt, H<sub>2</sub> and O<sub>2</sub> concentrations
2. New WWER reactors primary water chemistry guidelines (from 1992-1993) involved corrected Boron-alkali metals mode with constant pHt 7.0-7.1 at inlet reactor temperature. Optimal pHt level corresponds positive temperature gradient in zone of magnitude solubility minimum.
3. Organic impurities in primary coolant (ion exchange resins etc.) can cause carbonic deposits on fuel claddings.
4. Primary circuit soft decontamination reduce radioactive deposits on out-of-core equipment.

## SOME CONCLUSIONS ABOUT HYDRAZINE WATER CHEMISTRY

1. A hydrazine water chemistry at KOLA and ROVNO NPP accompanied by optimization and stability main coolant chemical parameters (pHt), hydrogen and oxygen concentration). As a result of both factors radiation situation improved.
2. ROVNO, ZAPOROZHE and NOVovoronezh NPP with WWER reactors use ammonia-hydrazine treatment of feed water with aim of deoxygenation. Hydrazine concentration in primary coolant is negligible.

3. KALININ, BALAKOVO and KHMELNITSK NPP use ammonia-potassium primary water chemistry. Hydrazine treatment used only at start-up with the aim of coolant degazation. At start-up hydrazine treatment of primary coolant produce protective film on stainless steel surfaces.
4. Hydrazine treatment before shut-down cause flush of accumulated corrosion products off deposits because water chemistry monitoring had to use effective reactor blow-down clean-up avoid radiation situation deterioration.
5. During operation REDOX potential of coolant at elevated temperature correlate with hydrogen concentration. The role of hydrazine addition may be connected with hydrazine capacity to accept oxydizing radicals (OH, HO<sub>2</sub>, O<sup>-</sup>) very effectively in comparison with ammonia. Ammonia-hydrazine substitution reduce oxydizing radicals production in core. It cause reduce of corrosion process and increase stability of oxide film on fuel cladding surfaces. Hydrazine radiolytic processes and chemical interaction between hydrazine and coolant impurities in real conditions must be studied.

### ACKNOWLEDGEMENT

Authors express acknowledgement to Russian and Ukrainian NPS workers for their help and operation data.

### REFERENCES

- [1] Peculiarities of operating WWER reactor core containing leaking fuel rods. Velyukhanov, V.P., Voronin, L.M., Ioltukhovsky, A.G., Kanatove, A.I., Chistyakova, V.K. / Int. Conf. Dimitrovgrad, Russia 1992.
- [2] Analysis of trends in fuel rod depressurization and determination of "gas leak" and "pellet-water interaction" type failures using radiation monitoring techniques of fuel rod leak-tightness. Panov, E.A., Shestakov, Yu.M., Miglo, V.N. /Int. Conf. Dimitrovgrad, Russia 1992.
- [3] Peculiarities of operation and radiation monitoring of water-cooled reactors with faulty fuel rods. Shestakov, Yu.M. Panov, E.A. /Int. Conf. Dimitrovgrad, Russia 1992.
- [4] Radiation exposure levels for staff on nuclear power stations with water-moderated water-cooled reactors, and ways of improving the water chemistry of primary loop. Urmanov, V.A., Kham'yanov, L.P., Doroshenko, G.G. / Thermal Engineering 37(7), 1990, 337-342.
- [5] Influence of water chemistry regimes on fuel cladding failure in LWRs. Kritskij, V.G. / Int. Conf. Dimitrovgrad, Russia 1992.
- [6] WWER primary coolant chemistry experience and perspectives. Kysela, J. / water chemistry of nuclear reactor systems, 6, BNES, London 1992, 1-8.
- [7] Standard and hydrazine water chemistry in primary circuit of WWER. Burclova, J. / water chemistry of nuclear reactor systems, 6, BNES, London 1992, 9-14.

## **SOME OBSERVATIONS ON HYDRAZINE AND AMMONIA BASED CHEMISTRIES IN PWRs**

J. BRUNNING, P. CAKE, A. HARPER, H.E. SIMS  
AEA Technology, Oxon,  
United Kingdom

### **Abstract**

This paper presents a comparison of factors related to activated corrosion product transport in pressurised water reactors (PWRs) operating hydrazine and ammonia-based chemistries.

Measurements of the concentrations of corrosion products in the coolant of reactors operating both chemistry regimes are compared under steady operation and during shutdown. These data allow some comparisons to be drawn of corrosion product transport under ammonia and hydrazine based chemistries. Experimental measurements of electrochemical potential under PWR conditions in the presence and absence of radiation fields and under hydrazine and ammonia chemistries are also presented.

### **1. INTRODUCTION**

The transport of activated corrosion products from the reactor core to other parts of the primary circuit via the coolant is an important source of occupational radiation exposure in Pressurised Water Reactors (PWRs) especially at shut-down. A number of approaches to reducing this phenomenon have been applied to operating plants, with varying degrees of success. Identification of those changes which have been effective is complicated by two factors. Often a number of changes have been made simultaneously, thus precluding a simple assessment of effective practices. Furthermore inter comparison of data from different plants is complicated by differences in reactor design. Identification of those measures which have been most effective therefore requires careful assessment of the available evidence.

Experience at PWRs of the VVER type has suggested that minimising the amount of cobalt-containing alloys in the primary circuit together with the use of an ammonia/potassium hydroxide chemistry has achieved low out-of-core doserates at a number of VVER stations [1]. Further reductions in radiation fields have been claimed following trials dosing with hydrazine rather than ammonia [2,3]. This report presents an evaluation of the relative effectiveness of hydrazine and ammonia-based chemistries in reducing the amount of both activated and non activated corrosion products in the primary coolant, and thus the relative propensities for the build-up of out-of-core radiation fields under the two regimes.

As noted above there are significant complications in comparing data from different plants; especially where these plants are of different detailed design. Differences in materials inventory affects the source term, which can have a major effect on measured values; this is extremely

difficult to factor out with any precision. In order to overcome this difficulty it is desirable to compare data from installations where measurements are available spanning a change from ammonia to hydrazine chemistry. This approach has the merit that it removes variability due to materials inventory, although the cycle to cycle variations due to differences in operating conditions remain. A change from ammonia to hydrazine based chemistry has been made at Paks, and a body of data established [4]. This information will be used as the basis for a comparison of the levels of corrosion products in the coolant under steady state conditions and at shutdown under ammonia and hydrazine based chemistry regimes. In addition some experimental measurements of electrochemical potential under PWR conditions in the presence and absence of radiation fields and under hydrazine and ammonia chemistries will be presented.

## 2. PRIMARY COOLANT MEASUREMENTS AT PAKS

The levels of corrosion products have been measured under steady power operation and shutdown at Paks units 1 and 2 during their 8th and 7th cycles [4]. Both units commenced operation following the standard VVER ammonia-potassium hydroxide primary coolant chemistry. Injection of hydrazine in place of ammonia was introduced at Paks 2 shortly after the beginning of the 7th cycle. A concentration of  $40 \mu\text{g kg}^{-1}$  hydrazine was maintained in the primary coolant. Elemental transition metal species and associated radionuclides were determined using high pressure liquid ion chromatography and gamma spectrometry respectively.

The sampling arrangements are shown in Figure 1. Coolant was sampled from the clean-up loop after cooling, but before the flow controlling orifices, upstream of the ion exchange beds (sample point TV20). At this point the coolant is at reactor pressure but at less than  $60^\circ\text{C}$ . This line was resampled under pressure using a capillary line and allowed a continuous representative flow from the primary coolant to be delivered to the analytical equipment. The flow passed through a  $0.45\mu\text{m}$  Millipore filter to collect particulate species and then through a degasser. The sample for the ion chromatograph was extracted from the degasser. Soluble transition metal species were determined using a DIONEX high pressure liquid ion chromatograph following concentration of the species from up to 1 kg of coolant. Insoluble species collected by the Millipore filter, after passage of at least 500 kg coolant, were dissolved after fusion with potassium hydrogen sulphate and analysed using ion chromatography. For selected samples eluent from the chromatograph was collected and analysed by gamma spectrometry.

Tables 1 and 2 present the average values for soluble and insoluble elemental corrosion products and corrosion product activity during steady power operation at Paks 1 and 2. It is apparent that for soluble species only the nickel concentration is significantly different for each plant and is lower by a factor of 3 at Paks 2. Differences in the values for insoluble species are more pronounced between the 2 plants. Concentrations were a factor of 2-3 lower for Cu, Ni, Zn, and Mn, a factor of 5 lower for Co and a factor of 10 lower of Fe at Paks 2. Soluble

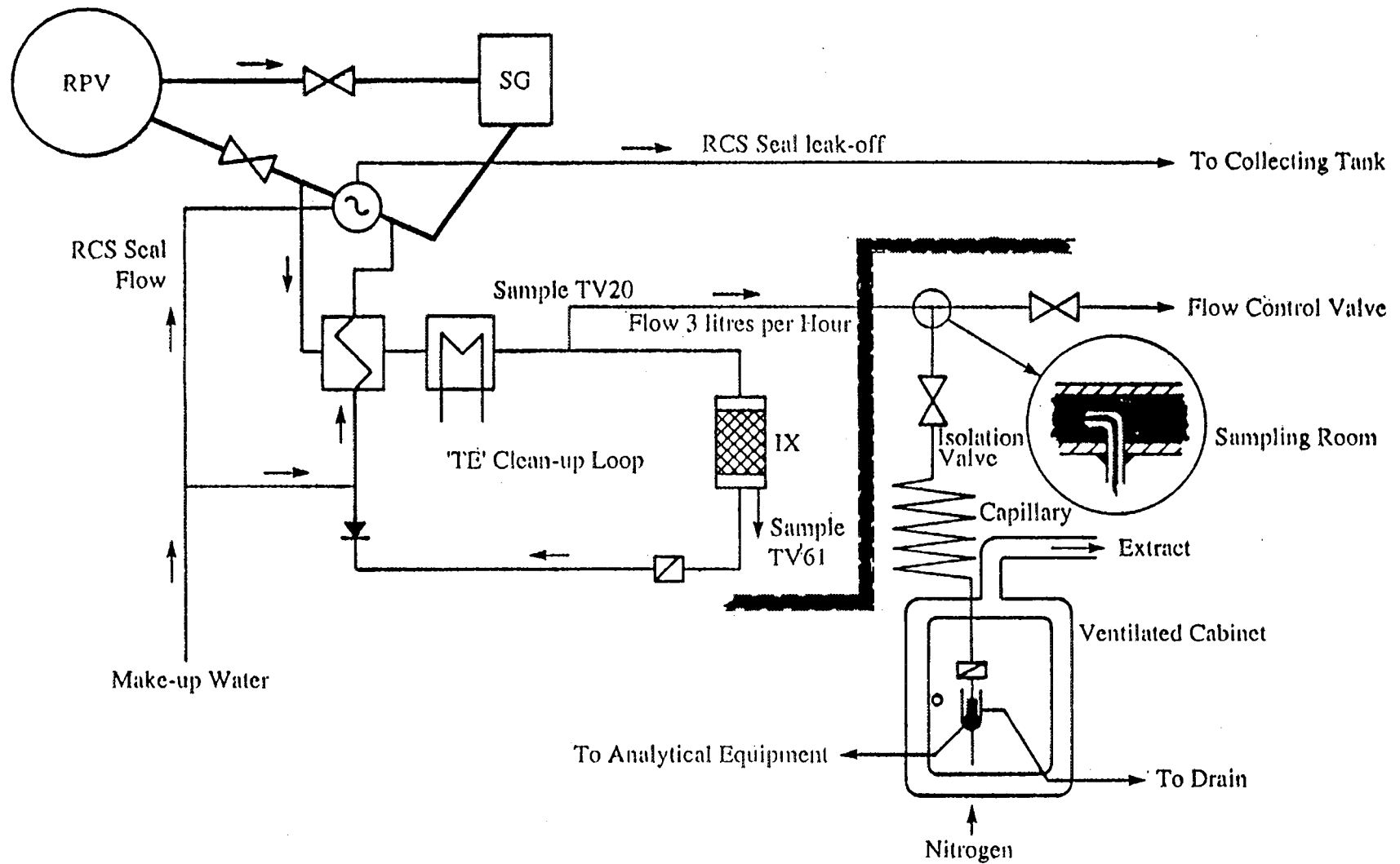
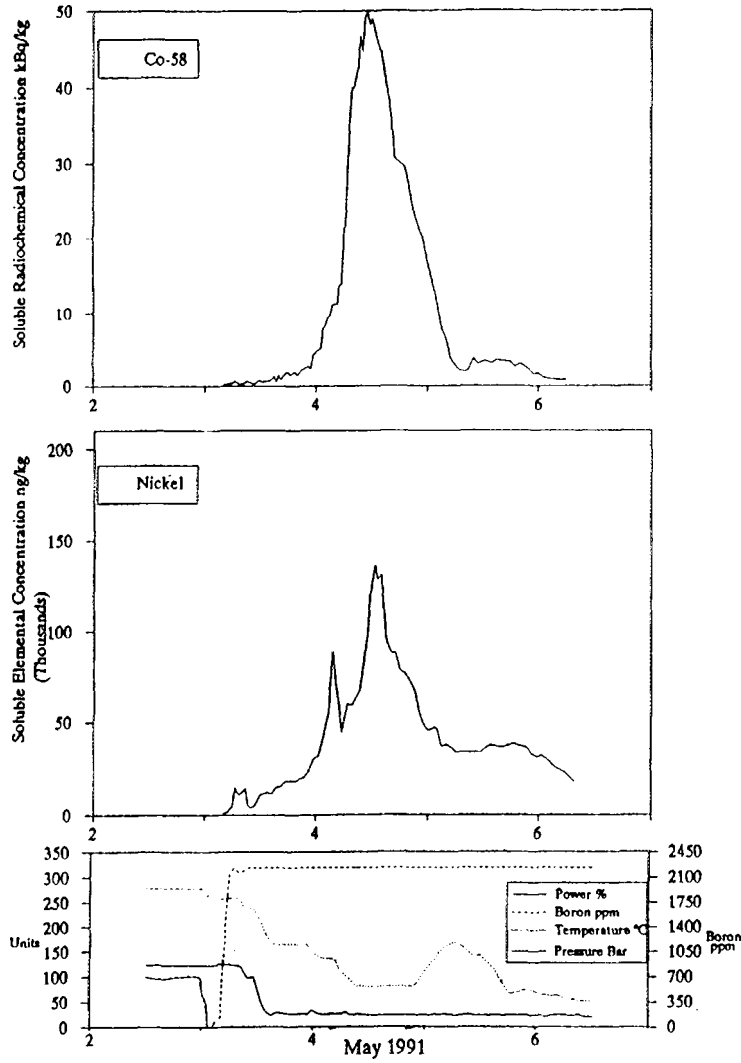
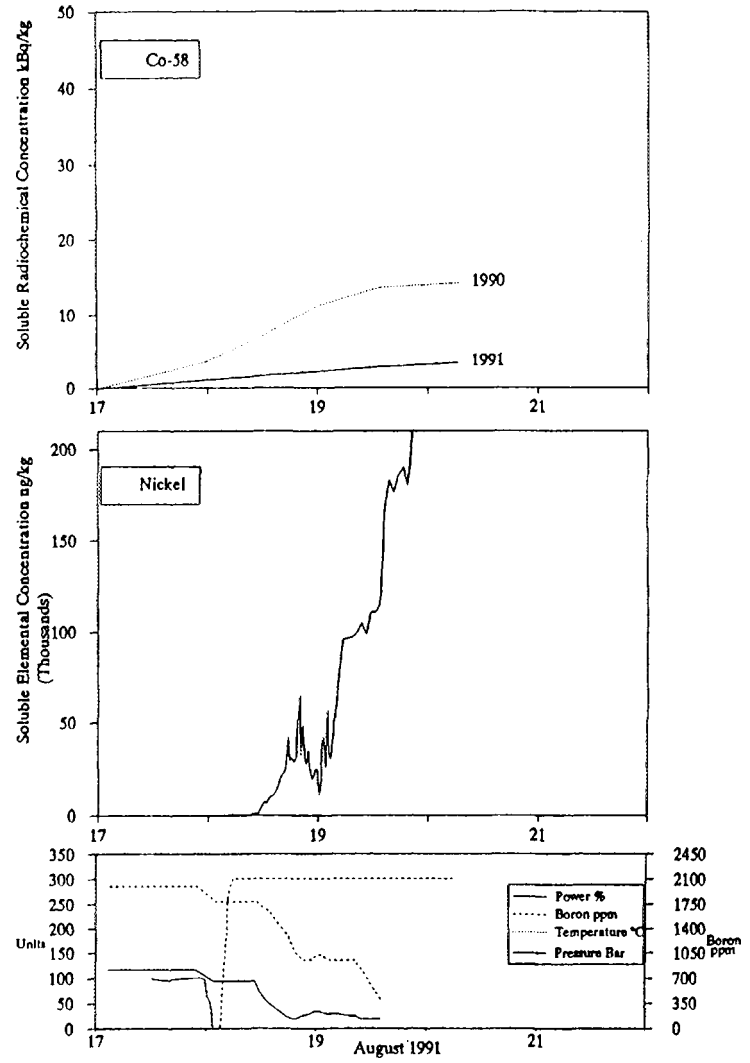


FIG 1 FLOW DIAGRAM OF SAMPLING MODIFICATIONS AT PAKS 1 AND 2.



PAKS 1



PAKS 2

FIG 2 ELEMENTAL NICKEL AND COBALT-58 RELEASE AT SHUTDOWN;  
PAKS 1 MAY 1991 AND PAKS 2 AUGUST 1991.

activity values for Co-58, Co-60 and Mn-54 were about 30% lower at Paks 2, however there is no clear correlation between these reductions and the behaviour of the parental elemental species. Thus specific activities for Co-60 are comparable whilst for Co-58 appeared to be higher at Paks 2. Insoluble activity levels were reduced at Paks 2 but these reductions were less than the corresponding reductions in elemental nickel and cobalt. This resulted in an increase in the specific activity values.

Figure 1 show the release of soluble elemental nickel and cobalt during the shut down. The release of cobalt was similar at each plant, reaching a maximum of  $450 \text{ ng kg}^{-1}$ , the only difference being the initial release at Paks 1 at the time of boration. Release of nickel occurred on a similar timescale and was a factor of 1.5 greater in Paks 2. The release of soluble iron and manganese were similar at each plant. The release of Co-58 and Co-60 closely followed the release of elemental nickel and cobalt. It is clear that the activity released at Paks 2 was less than at Paks 1 for comparable elemental releases. Limited data for Co-58 and Co-60 release during the previous shutdown at Paks 2 are also shown and it is apparent that these values are a factor of 3 greater than for cycle 7.

Comparison of the plant data under steady operation must take account of the different coolant chemistry conditions during the analysis period.(Table 2). Ammonia levels at Paks 2 were twice those at Paks 1 and hydrogen levels were also higher. Likewise potassium and lithium levels were significantly greater at Paks 2. Due to these differences it is not possible to conclude whether the small differences in corrosion product levels under steady operation were as a result of the use of hydrazine at Paks 2 or due to other coolant chemistry considerations. The high ammonia levels at Paks 2 are a direct result of the use of hydrazine and this itself may have a significant effect.

Activity released at shutdown will depend on cycle history but it is clear that the release of activity at Paks 2 after the application of hydrazine during the 7th cycle was significantly less than at Paks 1. It is also apparent that there was a significant reduction in activity release at Paks 2 when compared to the 6th cycle.

### **3. ELECTROCHEMICAL POTENTIALS IN AMMONIA AND AMMONIA-HYDRAZINE SOLUTIONS**

It has been suggested that the presence of hydrazine reduces the electrochemical potential (ECP) of stainless steel in VVERs below the values obtainable with ammonia [2]. The consequent reduction in steel corrosivity is suggested as part of the mechanism by which hydrazine reduces the transport of activated corrosion products and thus the build-up of radiation fields. Measurements of the ECP of 321 stainless steel have been made in ammonia and hydrazine solutions, in the presence and absence of radiation fields, to investigate this possibility.

The experimental arrangement is shown in Fig. 4. Water with controlled chemistry was preheated and pumped at  $280^{\circ}\text{C}$  into an autoclave installed in a Co-60 irradiation cell.

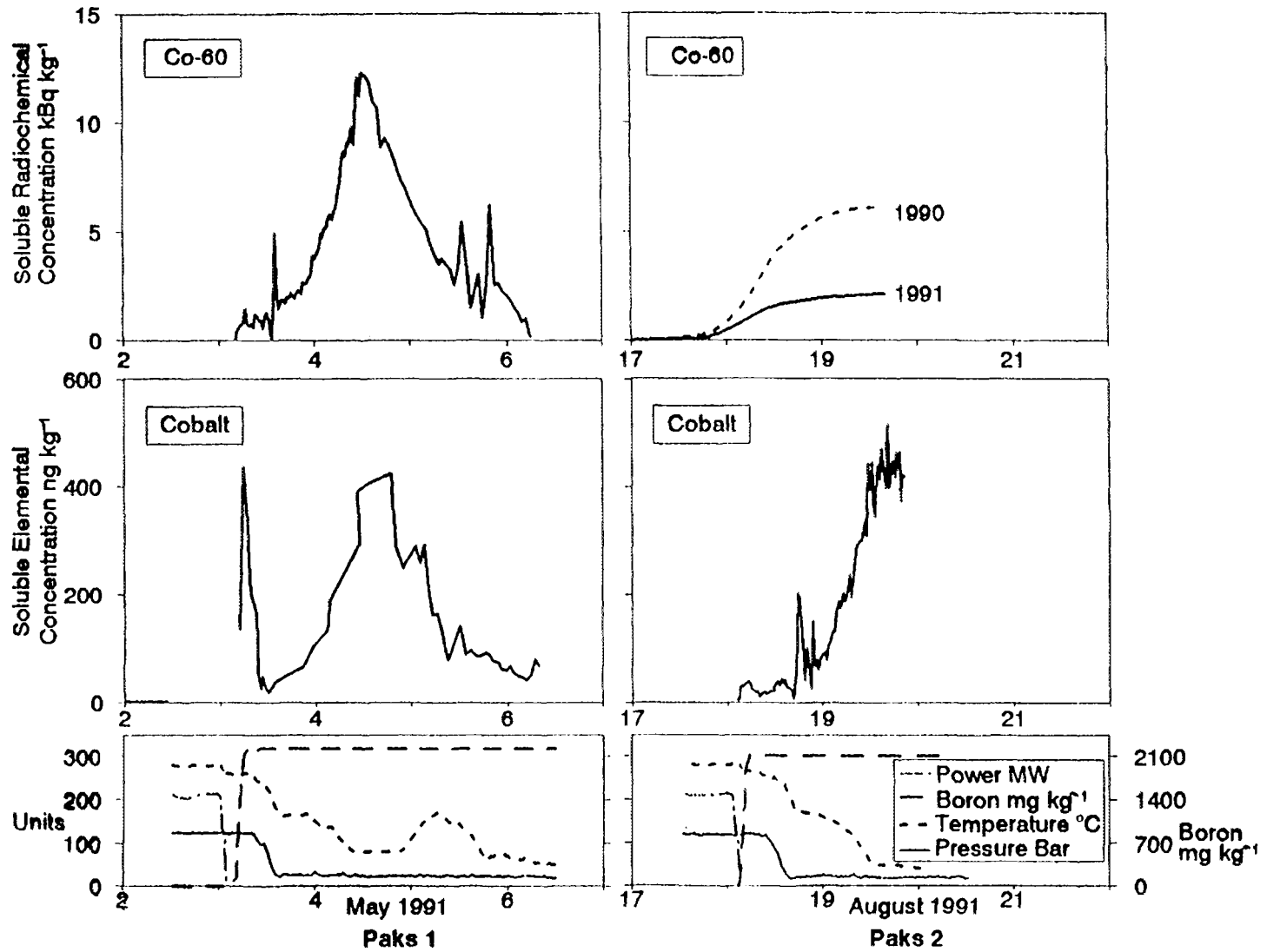


FIG 3 ELEMENTAL COBALT AND COBALT-60 RELEASE AT SHUTDOWN; PAKS 1 MAY 1991 AND PAKS 2 AUGUST 1991.

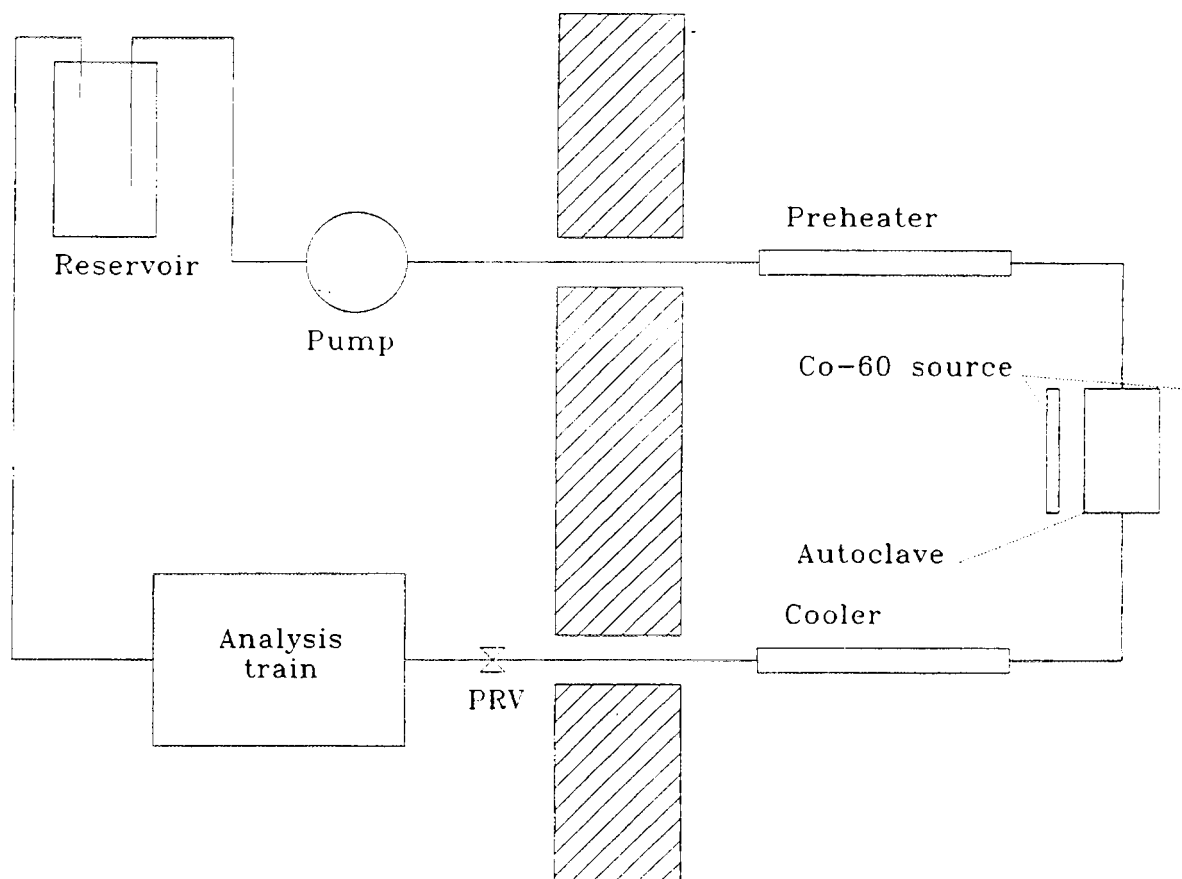


FIG 4 SCHEMATIC DIAGRAM OF EQUIPMENT FOR ECP MEASUREMENTS

Provision was made for the measurement of ECP within the autoclave using electrodes made of Pt and 321 stainless steel. A Ag/AgCl reference electrode was also available. After passage through the autoclave the water was cooled, depressurised, and passed to an analysis train.

Some initial experiments were undertaken to validate the experimental method and to test the operation of the equipment. Introducing the Co-60 source into the g-irradiation cell increased the ECP measured by the 321 stainless steel electrode in contact with water at 280°C containing 250 ppb O<sub>2</sub> from -50 mV to 0 mV. Addition of hydrogen reduced this ECP slightly as a result of the radiolytic recombination of hydrogen and oxygen. These data are consistent with observations reported by other workers, and thus give confidence that the experimental arrangement was behaving satisfactorily.

Figure 5 shows the observed behaviour of ammonia/hydrazine systems. The initial composition of the feedwater was  $1.4 \times 10^{-4}$  mol kg<sup>-1</sup> NH<sub>3</sub> and  $3.3 \times 10^{-5}$  mol kg<sup>-1</sup> hydrogen, with KOH and boric acid added to maintain a pH of 7.0 at 20°C. The temperature of the water in the autoclave was maintained at 280°C throughout the duration of the experiment. This Figure shows that exposing the solution to a radiation field produced a modest increase in hydrogen concentration. There was no change in the potential at the Pt electrode, nor was there any significant change in the rate of drift of the ECP measured by the 321 stainless steel electrode. Removing the radiation source produced no change in the behaviour of either electrode, whilst

**Table 1 Summary of Average Elemental and Radionuclide Values at Paks 1 and 2 During Steady Operation**

Elemental Data

Plant	Element		Copper	Nickel	Zinc	Cobalt	Manganese	Iron
Soluble	Paks 1	1991	1.6	34	19	1.0	185	22
		1992	1.7	20	59	0.4	89	94
	Paks 2	1991	3.1	11	18	0.9	147	26
		1992	3.8	11	28	0.5	116	46
Insoluble	Paks 1	1991	6.3	8.2	4	0.19	5.1	607
	Paks 2	1991	1.7	2.7	2	0.04	3.5	62

Corrosion Product Activity (Bq/kg) and Specific Activity (GBq/g)

Plant		Corrosion Product Activity (Bq/kg)			Specific Activity (GBq/g)		
		Co-58	Co-60	Mn-54	Co-60/Co	Co-58/Ni	
Soluble	Paks 1	1991	12	18	275	17	0.4
		1992	15	18	299	44	0.8
	Paks 2	1991	8.3	14	177	17	0.8
		1992	7.2	9.7	163	25	0.9
Insoluble	Paks 1	1991	2.3	1.4	2.8	16	0.5
	Paks 2	1991	1.9	1.0	0.5	53	0.9

**Table 2 Summary of Primary Circuit Chemistry Parameters During Steady Full Power Measurements at Paks 1 and 2**

	PAKS 1	PAKS 2
Mean Boron Value (mg kg <sup>-1</sup> )	176	381
Ammonia (mg kg <sup>-1</sup> )	25	55
Hydrogen (ml kg <sup>-1</sup> )	44	51
Potassium (mg kg <sup>-1</sup> )	2.63	7.7
Lithium (mg kg <sup>-1</sup> )	0.51	1.3
Sodium (mg kg <sup>-1</sup> )	0.20	0.26
Equivalent Potassium (mg kg <sup>-1</sup> )	6.0	15.0
Equivalent Lithium (mg kg <sup>-1</sup> )	0.98	2.68
Calculated ) 300°C	7.244	7.447
pH at ) 282°C	7.083	7.272
Temperature ) 270°C	7.012	7.190

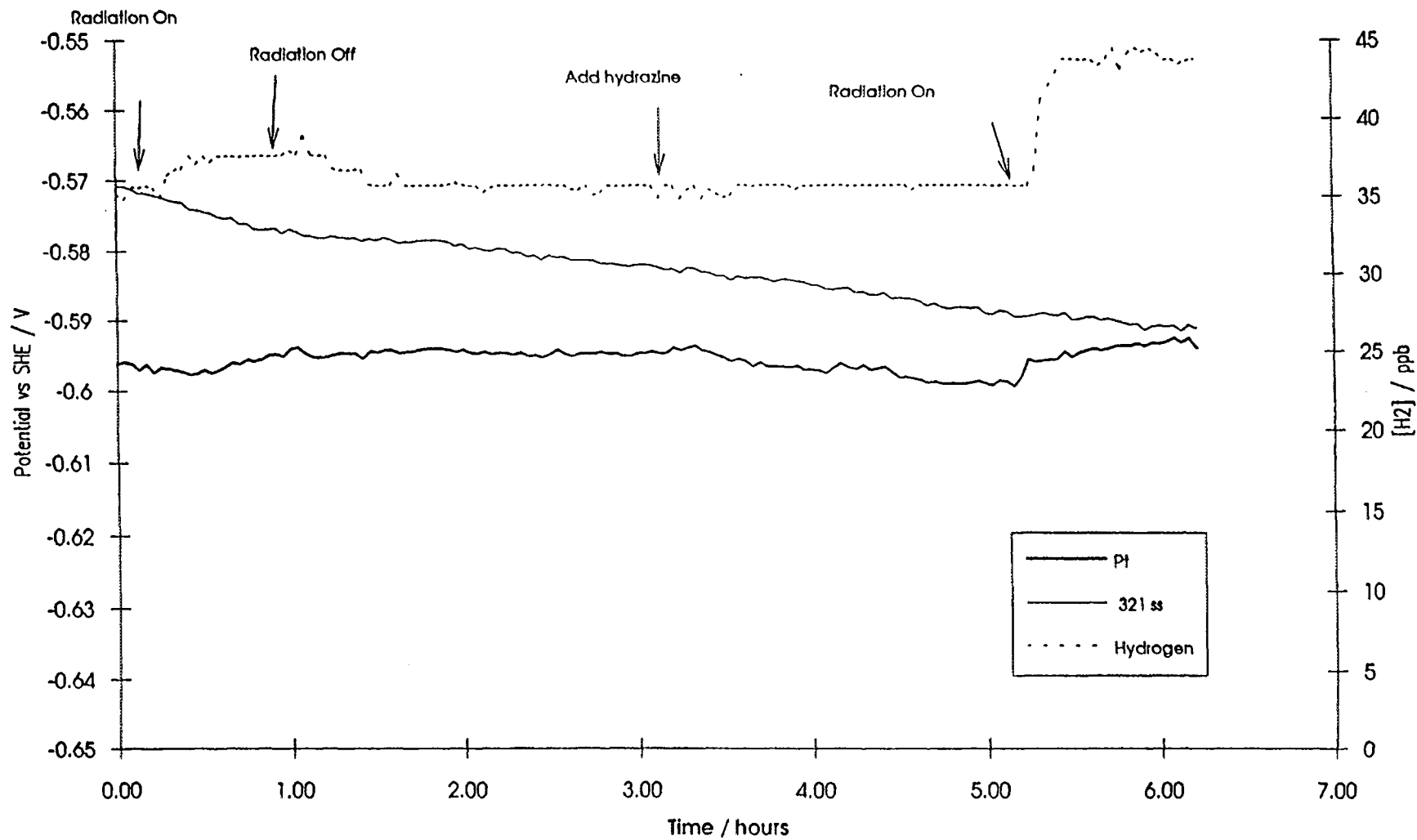


**FIG 5 THE EFFECT OF RADIATION ON THE ECP OF AMMONIA AND HYDRAZINE SOLUTIONS**

the hydrogen concentration returned to its original value. Introducing hydrazine ( $2.5 \times 10^{-5}$  mol  $\text{kg}^{-1}$ ) in addition to the starting level of ammonia produced no change in measured ECP values or the standing level of hydrogen in the absence of irradiation. Introducing a radiation source caused a marked increase in hydrogen concentration; this was greater than that observed for ammonia alone, and may be ascribed to the radiolytic degradation of hydrazine. No change was observed in the potential at either the Pt or the stainless steel electrode.

These results do not support the contention that hydrazine reduces the ECP of stainless steels below those attainable with ammonia. In the context of VVER it should be noted that the hydrazine concentrations used in the present experiments were substantially above those employed in practice, and the hydrogen concentrations substantially below; It might therefore be expected that the effects of hydrazine in the present experiments would be greater than those observed in reactor.

#### 4. CONCLUSIONS

The results of the sampling measurements at Paks indicate that the addition of hydrazine may reduce corrosion product and activity levels in primary coolant, however the laboratory results show that the ECP is unchanged in the presence of ammonia. Thus the hypothesis that hydrazine reduces the corrosivity of steel and thereby reduces the transport of activated corrosion products is not supported. Under a hydrazine chemistry the standing level of ammonia in the coolant for a given hydrogen concentration are double those for direct ammonia injection, whilst the standing level of hydrazine is small. It is therefore entirely possible that any differences in behaviour are due to the different ammonia concentrations.

#### ACKNOWLEDGEMENTS

The work described in the paper was partly funded by the UK Health and Safety Executive.

#### REFERENCES

- [1] KYSELA J., 'VVER primary coolant experience and perspectives', Proc. Int. Conf. on Water Chemistry of Nuclear Reactor Systems, Bournemouth, October 1992, BNES, London
- [2] PASHEVICH V.I., Thermal Engineering, 1984, 31(11), 595
- [3] PASHEVICH V.I., Thermal Engineering, 1985, 32(11), 29
- [4] SCHUNK J., BOGANCS J., TILKY P., BRIDLE D.A., CAKE P., SYMONS W.J., and PASHEVICH V.I., 'Elemental and radiochemical measurements carried out in primary coolant at VVER-440 PWRs Paks 1 and 2 in Hungary during steady full-power operation and at end of cycle shutdown', Proc. Int. Conf. on Water Chemistry of Nuclear Reactor Systems, Bournemouth, October 1992, BNES, London



# PRIMARY WATER CHEMISTRY MONITORING FROM THE POINT OF VIEW OF RADIATION BUILD-UP

G.L. HORVÁTH

Institute for Electrical Power Research,  
Budapest

V. CIVIN

Hungarian Electricity Generating Board

T. PINTÉR

Nuclear Power Plant PAKS

Hungary

## Abstract

Basic operational principles of a computer code system calculating the primary circuit corrosion product activities based on actual measured plant chemistry data are presented. The code system consists of two parts:

- FeSolub.prg: calculates the characteristic iron solubilities based on actual primary water chemistry ( $H_3BO_3$ , KOH, ... etc.) and plant load (MW) data. A developed solubility calculation method has been applied fitted to magnetite solubility data of several authors
- RADTRAN.exe: calculates primary circuit water and surface corrosion product activities based on results of FeSolub.prg or planned water chemistry data up to the next shutdown.

The computer code system is going to be integrated into a general primary water chemistry monitoring and surveillance system.

## 1. INTRODUCTION

During the past several years of operation of the PAKS nuclear power plant there were no serious troubles in the field of primary water chemistry, and the actually measured shutdown dose rates are very favorable compared to other plants. This situation happened among others due to constant attention paid to water chemistry conditions. One of the most important conclusion of several studies in this field [1-7]-- confirmed by actual plant radiation measurements [1-3]-- was that there is an optimal primary water chemistry range where minimal out-core surface activities can be obtained ensuring the minimal personal doses during shutdown and maintenance.

Present day computer techniques provide the possibility to obtain an overall and quick analysis of the water chemistry parameters to qualify it against key parameters ensuring minimal out-core surface activities. A monitoring system could warn about favorable conditions and provide advise how to improve the conditions.

Major parts of such a monitoring system are the followings:

- primary water chemistry data base handling and updating system
- graphical presentation system

- program set for calculating physical parameters and performing predictions:
  - a. code calculating primary circuit corrosion product (magnetite) solubilities at operating temperatures: FeSolub.prg
  - b. code calculating primary circuit corrosion product activities: RADTRAN.exe

One of the central parts of such primary water chemistry monitoring system is a set of computer codes able to calculate and predict out-core corrosion product surface activities.

## 2. CORROSION PRODUCT ACTIVATION ANALYSIS PROCEDURE

The basic flow of data processing during corrosion product activation analyses is given in Fig 2\_1. Some more details of the system are given in Fig. 2\_2.

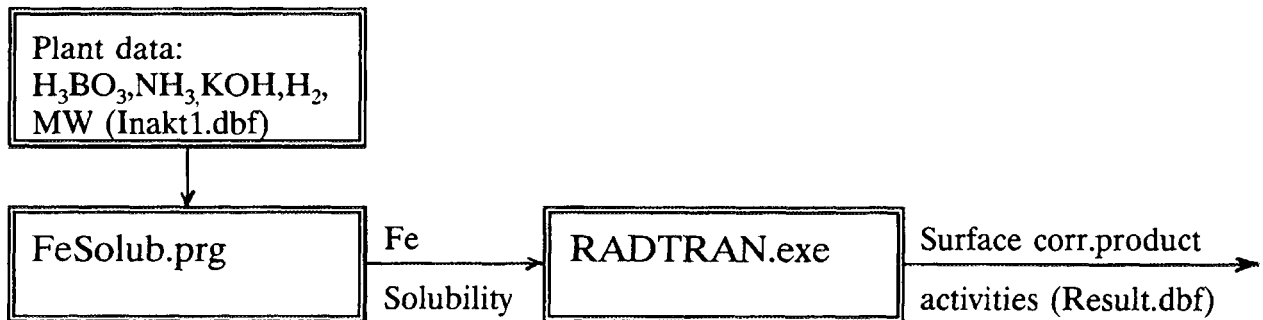


Fig.2\_1 Data flow in case of primary circuit corrosion product activation analysis.

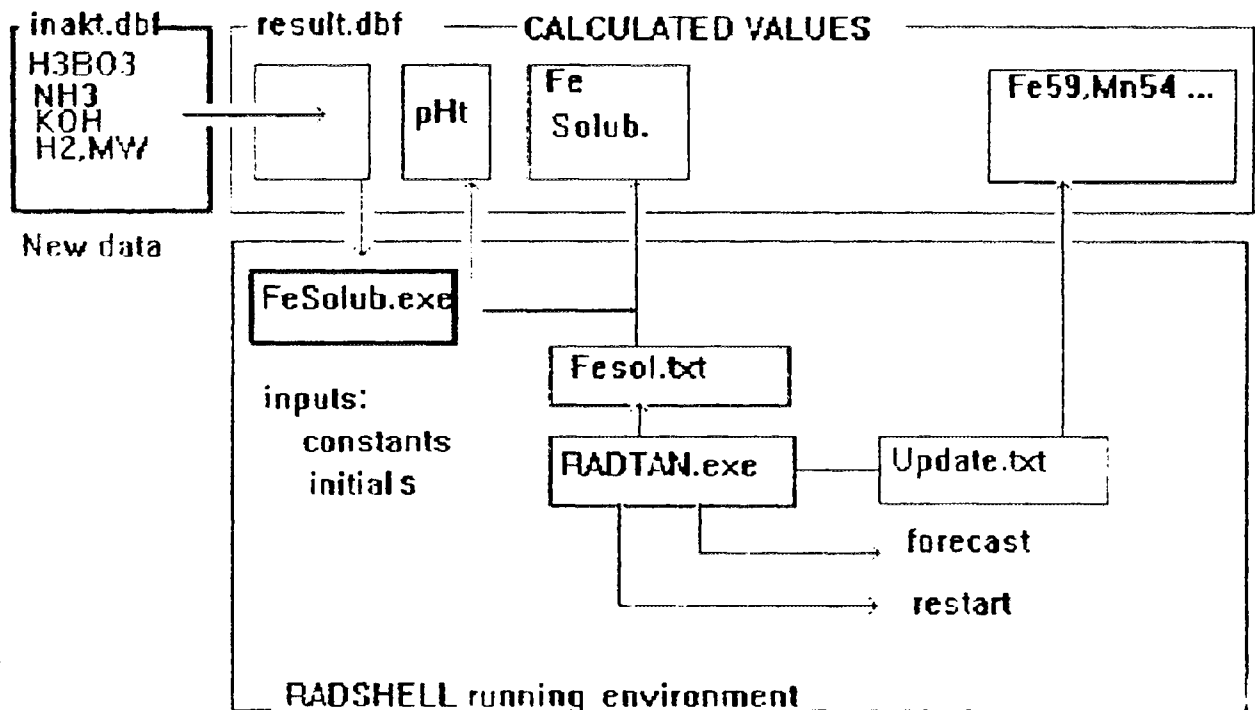


Fig. 2\_2 Data flow in the corrosion product activation monitoring system

Main parts of the system are the followings:

- Inakt1.dbf - database of basic plant data containing the needed data versus time
- Result.dbf - intermediate data base file containing apart from the above mentioned basic data also most of the results
- RadShell - computer shell organizing the operation of the FeSolub.exe (calculating magnetite solubilities) and of the RADTRAN code calculating radiation build-up.

Computer code FeSolub.exe (dbase) calculates Fe solubility and high temperature pH and stores them in Results.dbf file and also in an other transient file (FeSol.txt) for RADTRAN code.

The RADTRAN code calculates primary circuit corrosion product activities using the above mentioned and basic physical and geometry data (RadInp) and places them into the Result.dbf data base file.

### 3. HIGH TEMPERATURE PH AND FE SOLUBILITIES

Fe solubility and high temperature pH calculation method (FeSolub.exe) uses actual plant chemistry and power-rate data and provides Fe solubility data for four characteristic primary circuit temperatures:

- $C_s^{av,Fu}$  - at axial and radial average temperature of the outer surface of the fuel cladding
- $C_s^{av,Ass}$  - at axial and radial average temperature of the outer surface of non heated fuel assembly walls (taken as average temperature of the coolant in the core)
- $C_s^{av,SG}$  - at average temperature of the primary side of the steam generator heat exchange surface
- $C_s^{in,CORE}$  - at average temperature of the coolant at the core entry.

These temperatures depend on the thermal power rate of the reactor. Temperatures have been calculated for 10 different power rates from 10% up to 100 % and a regression line has been fitted to these calculations. RADTRAN code uses this line for power rates different from nominal.

Fe solubilities for the 4 temperatures mentioned are placed into a database file and also into a transient file (FeSol.txt), which is to be used as input by the RADTRAN code.

#### 3.1 PHYSICO-MATHEMATICAL MODEL

Calculational method is based on reference [11], and takes into account boric acid, ammonia and strong base expressed as equivalent Potassium ( $K^+$ ).

Dissociation mechanism of the boric acid has been taken according to Messmer [13,14] which means four dissociation reactions. The ion product of water has been taken into account by one of the mostly used formula by Marshall-Frank [15]. Ion strength of the solution has been included by Debye-Hückel activity coefficients.

A unit fugacity coefficient of hydrogen has been assumed. The partial pressure of hydrogen was calculated from Henry's law.

Equilibrium constants of Iron solubility were calculated with taking into account (II) and (III) valent states of Fe species by an extended version of the Tremain-LeBlanc model using 10 Fe species. According to this model the dissociation constant (at temperature T) can be expressed as

$$(K_b)_z = \exp \left( \frac{((\Delta S_b^\circ)_z (1-T^\circ/T) - (\Delta G_b^\circ)_z/T)}{R} \right)$$

where:

- $(\Delta S_b^\circ)_z$  - change of enthalpy during chemical reaction at standard temperature  $T^\circ$ , J/(mole K)
- $(\Delta G_b^\circ)_z$  - change of free energy during chemical reaction at standard temperature  $T^\circ$ , J/mole
- index<sub>b</sub> - applies to valent state of Fe  $b=2$  or  $3$
- index<sub>z</sub> - applies to charge of Fe species (number of OH<sup>-</sup> radicals in Fe species)
- $T^\circ$  - standard temperature,  $T^\circ=298.15$  K
- R - gas constant

This extended model has been fitted to available Fe (magnetite) solubility data available for us [11]. These were the following:

- Sweeton - Baes
- Tremain-LeBlanc
- Lambert.

As a result of this fitting procedure new and extended values for the Fe equilibrium dissolution constants have been obtained (Table 2\_1). these values represent an accuracy level when difference of two consequent values of the least quadratic deviation was less than 5%.

### 3.2 PROCESSING MEASURED PLANT CHEMISTRY DATA

Physico-mathematical model described in ch. 3.1 was incorporated into a program module reading the primary water chemistry data directly from the plant database files and writing the output Fe solubilities at 4 characteristic temperatures mentioned in ch.3. It may provide also the temperature gradients of Fe solubility to characterize the past periods from point of view of corrosion product transport.

## 4. APPLICATION OF THE RADTRAN CODE TO LOAD & CHEMISTRY FOLLOWING CALCULATIONS

Water chemistry dependent data (Fe solubilities) are obtained from the program module FeSolub.exe (see Fig.2\_2) but the thermal power-rate is used by RADTRAN also directly.

Parameters used by RADTRAN are independent of either power-rate and chemistry or only power-rate dependent.

Table 2\_1: Fe (magnetite) equilibrium dissolution constants obtained as a result of fitting to measured data of Sweeton - Baes, Tremain-LeBlanc and Lambert.

Species	Valent state of Fe (z)	Number of OH <sup>-</sup> radicals (b)	( $\Delta G_b^\circ$ ) <sub>z</sub> J/mole	( $\Delta S_b^\circ$ ) <sub>z</sub> J/(mole K)
Fe <sup>2+</sup>	2	0	-60517	-96.651
FeOH <sup>+</sup>	2	1	14000	-276.63
Fe(OH) <sub>2</sub> <sup>o</sup>	2	2	49000	-100.0
Fe(OH) <sub>3</sub> <sup>-</sup>	2	3	110000	-198.0
Fe(OH) <sub>4</sub> <sup>2-</sup>	2	4	188290	-328.579
Fe <sup>3+</sup>	3	0	3000	-231.0
Fe(OH) <sup>2+</sup>	3	1	21000	-134.0
Fe(OH) <sub>2</sub> <sup>+</sup>	3	2	48000	-128.0
Fe(OH) <sub>3</sub> <sup>o</sup>	3	3	74000	-67.0
Fe(OH) <sub>4</sub> <sup>-</sup>	3	4	129000	-188.0

#### 4.1 Chemistry and power-rate dependent parameters

Influence of chemistry and power-rate appears through the Fe solubilities calculated at 4 characteristic temperatures mentioned above. Parameters of the physical model influenced in this way are given in Table 4\_1.

Table 4\_1 Parameters of the RADTRAN physical model influenced by plant chemistry and power-rate.

PARAMETER in RADTRAN		INFLUENCING FACTOR
NOMINATION	MARKER	
Dissolution rate on fuel cladding surface	$k^{\text{diss,Fu}}$	$C_s^{\text{av,Fu}}, C_s^{\text{in,CORE}}$
Dissolution rate on fuel assembly walls	$k^{\text{diss,Ass}}$	$C_s^{\text{av,Ass}}, C_s^{\text{in,CORE}}$
Incorporation rate of active nuclides into the oxide layer growing on out-core surfaces	$k^{\text{act}}$	$C_s^{\text{av,SG}}, \text{Density of water}$

#### 4.1 Power-rate dependent parameters

Influence of reactor thermal power-rate appears directly through the thermal power rate provided by the file FeSol.txt. Power-rate dependent parameters are calculated inside the RADTRAN code. Parameters of the physical model influenced by the power-rate only are given in Table 4\_2.

In the first two rows of the table influence of the instantaneous neutron flux is valid. In the 3<sup>rd</sup> row the effect of neutron flux averaged up to the current time should be taken into account.

Table 4\_2 Parameters of the RADTRAN physical model influenced by power-rate only.

PARAMETER in RADTRAN		INFLUENCING FACTOR
NOMINATION	MARKER	
Generation of active nuclides	$\sum_{j=\text{fast}}^{\text{fast}} \sigma_j \cdot \Phi_j$ $\sum_{j=\text{therm}}^{\text{therm}}$	$\Phi_j$
Active nuclide burn-out rate	$\sigma^a \Phi_{\text{therm}}$	$\Phi_{\text{therm}}$
Corrosion product release rate of activated construction materials under heavy neutron flux	$(\Sigma \sigma \Phi F)$ $\lambda^* = \lambda + \sigma^a \Phi_{\text{therm}}$	$\Phi_j, \Phi_{\text{therm}}$

Legend to table 4\_2:

- $\sigma$  - microscopic neutron adsorption cross section of target nuclide
- $\sigma^a$  - microscopic neutron adsorption cross section of burn-out of activated nuclide
- $\Phi_j$  - neutron flux in the j-th energy range
- $\Phi_{\text{therm}}$  - neutron flux in the thermal energy range
- F - surface of construction material under heavy neutron flux
- $\lambda$  - decay constant

#### 4.3 ANALYZING AND PREDICTING BY THE RADTRAN CODE

As a new feature of the RADTRAN code it is possible to combine analysis of past plant periods and make predictions for the future practically up to the next fuel reloading periods.

#### 4.4 TESTING OF THE CODE SET WITH PLANT DATA

The code system has been tested with the primary water chemistry data of Unit 1 of PAKS nuclear power plant, using the data of the first two cycles. Results are illustrated by Fig. 4\_1, showing a good agreement of calculated and measured data.

## 5. PROTOTYPE RUNNING ENVIRONMENT FOR ACTIVATION STATE ANALYSIS

The RADShell prototype activation state analyzing system provides at present the following features:

- choosing the radionuclide to be analyzed
- running the parts of the code set FeSolub & RADTRAN.

Planned features of RADShell:

- analysis of the past water chemistry for temperature gradient of corrosion product (Fe) solubilities
- analysis of deviation of the past water chemistry from optimal conditions using different considerations (Fe solubility, high temperature pH, water chemistry specifications) .

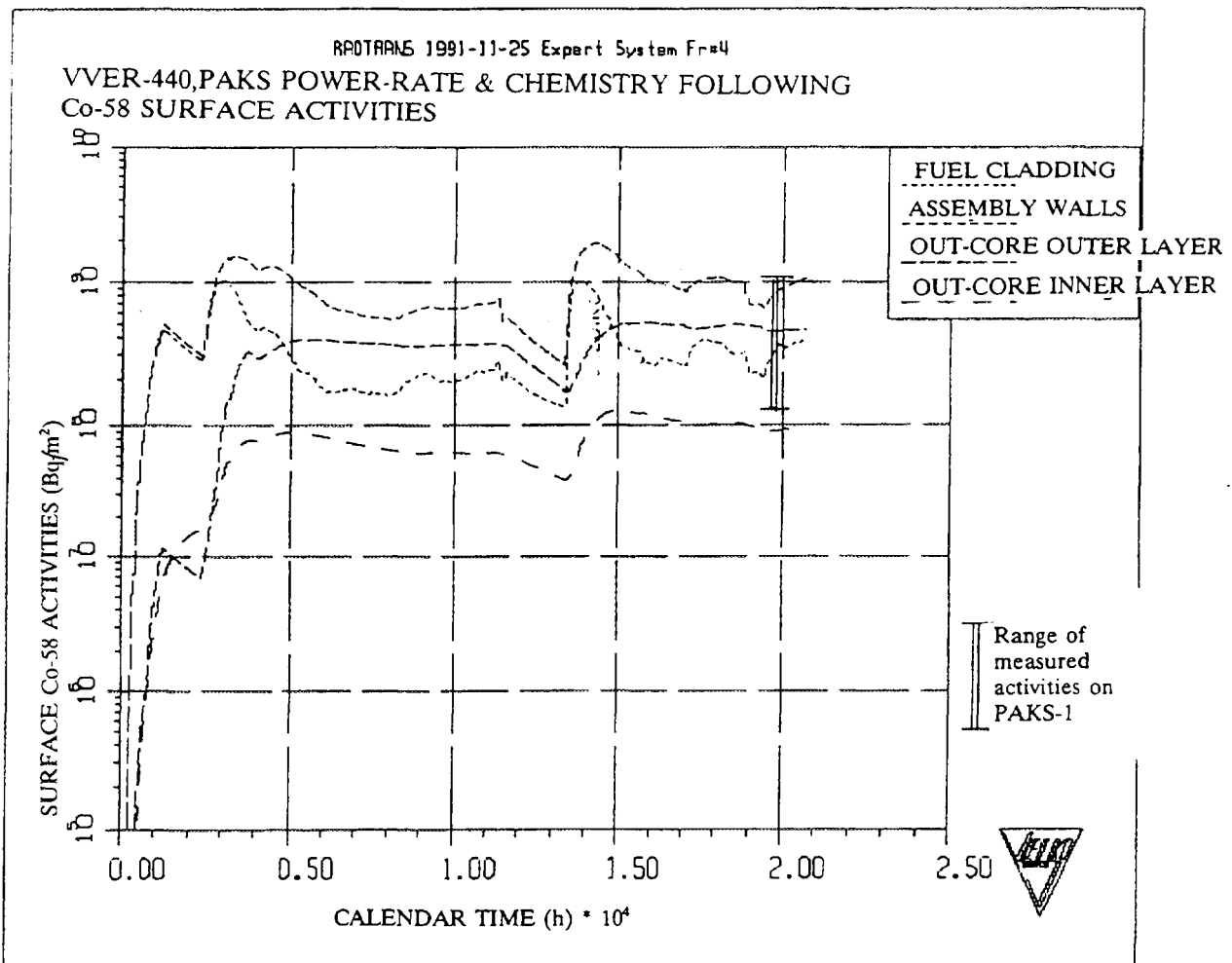


Fig. 4\_1 Measured and calculated Co-58 surface activities of PAKS Unit1 using actual plant chemistry data for the RADTRAN code.

## REFERENCÉS

- [1] HORVÁTH, L.G.: VVER atomerômûvek vízüzemi és aktivitás adatainak összehasonlító elemzése. VEIKI Report, 93.92-320-2, 1988. december
- [2] HORVÁTH, L.G.: Priméerköri korróziótermék aktivitás és a vízüzem összefüggésének vizsgálata. VEIKI Report, 94.92-416-2, 1988. december
- [3] HORVÁTH, L.G.: Radioaktivitás mennyiségének csökkentése atomerômûvek priméerkörében. VEIKI Report, 93.92-058-2. 1989. december
- [4] HORVÁTH, L.G.: Az aktív zónán kívüli felületaktivitások és a priméerköri vízüzem összefüggése. VEIKI Report, 93.92-402-2, AHF, 1987. szeptember
- [5] BODROGINÉ VÁNKAI ANDREA, HORVÁTH, L.G.: A Paksi Atomerômû 1. és 2. blokk priméerköri vegyi méréseinek feldolgozása a felaktiválódott korróziótermékek szempontjából. VEIKI Report 93.93-402, 1986.
- [6] HORVÁTH, L.G., BODROGINÉ VÁNKAI A., ORMAI, P., PINTÉR, T., C.SZABÓ, I.: Paksi Atomerômû 1. és 2. blokk vegyi és dorimetriai mérések értékelése a felaktiválódott korroziótermékek szempontjából. VEIKI Report, 1885. december
- [7] HORVÁTH, L.G., ORMAI, P., PINTÉR, T., C. SZABÓ, I.: Korroziótermékek aktivitása a Paksi Atomerômû 1. blokkján a második üzemév után. VEIKI Report, 93.90-031-2/3.4, 1985. június
- [8] CIVIN, V.: A pH jelentősége és számításának lehetőségei bóros szabályozású VVER-440 atomerômûvi blokkok primer körében. VEIKI Report, 21.90-139-2/1, Vegyészeti Főosztály, 1980
- [9] CIVIN, V.: A priméerköri hõhordozó nagyhõmérsékletû pH-jának szabályozása az ioncserélõ kezelõk figyelembe vételével. VEIKI Report, 22.92-404-2, Vegyészeti Főosztály, 1987
- [10] PATTANTYUS: Gépész és Villamosmérnökök kézikönyve, MK, Budapest, 1959.
- [11] CIVIN, V.: A nagyhõmérsékletû pH és a magnetit oldhatóság számításának egységes rendszere. VEIKI Report, Vegyészeti Főosztály
- [12] SWEETON, F.H., BAES, C.F.: J. Chem. Thermodynamics, 2 p.479 (1970)
- [13] MESMER R.E., BAES C.F., SWEETON F.H.: 32nd Int. Conference on Water, Pittsburg, (1970) 55.
- [14] MESMER, R.E., BAES, C.F., SWEETON, F.H.: Inorg. Chem. 11 (3) p.537 (1972)
- [15] MARCHALL, W.L., FRANCK, E.V.: J. Phys. Chem. Ref. Data 10 (2) p.295 (1981)

# VVER WATER CHEMISTRY RELATED TO FUEL CLADDING BEHAVIOUR



XA9743709

J. KYSELA, M. ZMÍTKO  
Nuclear Research Institute plc.,  
Řež

V. VRTÍLKOVÁ  
Nuclear Fuel Institute,  
Prague

Czech Republic

## Abstract

Operational experience in VVER primary water chemistry and corrosion related to the fuel cladding is reviewed. Insignificant corrosion of fuel cladding was found which is caused by good corrosion resistance of Zr1Nb material and relatively low coolant temperature at VVER-440 reactor units. The differences in water chemistry control is outlined and an attention to the question of compatibility of Zircalloys with VVER water chemistry is given. Some results of research and development in field of zirconium alloy corrosion behaviour are discussed. Experimental facility for in-pile and out-of-pile cladding material corrosion testing is shown.

## INTRODUCTION

At present 44 VVER-type reactors are in operation in seven countries. In this amount, 26 represent the VVER-440 reactors and 18 are the VVER-1000 reactors. The VVER reactors generally exhibit high load factor (>75%) and low occupational radiation exposures. For fuel cladding material Zr1Nb alloy is used. In the near future there is an intend for using other fuel vendors for VVER reactors which use Zircaloy-4 for PWR fuel cladding. So far no experience with Zircaloy-4 in VVER coolant chemistry (involving potassium and ammonia) is available.

## VVER PRIMARY COOLANT TECHNOLOGY

### Standard water chemistry

Water chemistry of VVER's reactors is based on boron/potassium coordination during the fuel cycle and radiolytic decomposition of ammonia is used for hydrogen

# VVER boron/potassium coordination

## Standard water chemistry control

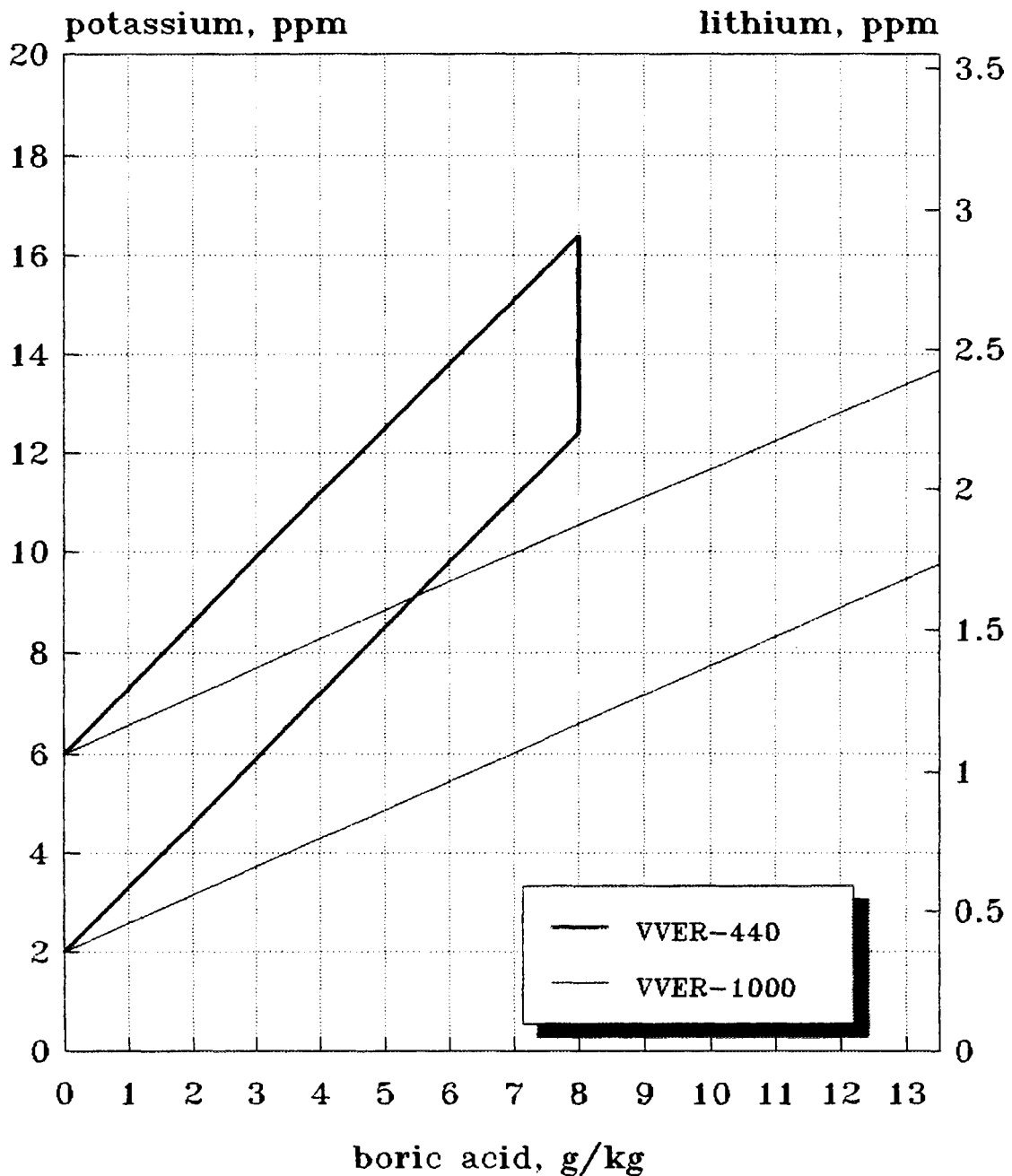


Fig.1 Standard boron/potassium water chemistry coordination during reactor cycle of VVER-440 and VVER-1000

adjustment. The coordination of boron/potassium is shown in Fig.1. Some of the primary coolant parameters are summarized in Table 1.

Alkalinity in Table 1. is given as a total potassium, lithium and sodium concentration recalculated to  $K^+$  equivalent concentration. Lithium concentration varies during the cycle from approximately 50 ppb up to 600 ppb with average values 300-350 ppb (data from NPP Dukovany). Sodium concentration changes from approximately 30 ppb to 350 ppb with average values 200-250 ppb (data from NPP Dukovany). Ratio  $K^+/Li^+$  (concentrations in ppm) changes during the cycle and varies from 10 up to 100 with average values in range of 10-30.

**Table 1. Primary coolant specification for VVER reactor types**

Parameter	VVER-440	VVER-1000
boric acid, g/kg	0 - 8	0 - 13.5
total alkalinity, ppm	2 - 16.4	2 - 13
ammonia, ppm	> 5	> 5
hydrogen, Nml/kg	30 - 60	30 - 60
oxygen, ppb	< 10	< 10

### Hydrazine water chemistry

Except ammonia hydrazine is also used to achieve hydrogen concentration in the primary coolant. As can be seen in Table 2. all VVER reactors which are operated at present use ammonia or hydrazine water chemistry. It means essentially that the needed excess of hydrogen concentration in the primary coolant is maintained by means of radiolytic decomposition of ammonia or hydrazine. Hydrogen concentration is thus maintained in dependence on the reactor power.

In the case of the hydrazine water chemistry, hydrazine is continuously fed; hydrazine is decomposed in the primary circuit to hydrogen, ammonia and nitrogen.

**Table 2. Nuclear power plant units with VVER reactors in operation**

<b>Country/Reactor</b>	<b>Capacity MW<sub>e</sub></b>	<b>Water chemistry</b>
<b>BULGARIA</b>		
Kozloduy 1-4	4 x 440	S
Kozloduy 5,6	2 x 1000	S
<b>CZECH REPUBLIC</b>		
Dukovany 1-4	4 x 440	S&M
<b>FINNLAND</b>		
Loviisa 1,2	2 x 440	S
<b>HUNGARY</b>		
Paks 1-4	4 x 440	S/H
<b>RUSSIA</b>		
Balakovo 1-3	3 x 1000	S
Kalinin 1,2	2 x 1000	S
Kola 1-4	4 x 440	H
Novovoronezh 3,4	2 x 440	S
Novovoronezh 5	1 x 1000	S
<b>SLOVAKIA</b>		
Bohunice 1-4	4 x 440	S
<b>UKRAINE</b>		
Khmelnitski 1	1 x 1000	S
Rovno 1,2	2 x 440	H
Rovno 3	1 x 1000	S
South-Ukraine 1-3	3 x 1000	S
Zaporozhe 1-5	5 x 1000	S

**Note: S - standard, H - hydrazine, M - modified**

The values of ammonia concentration in units with hydrazine water chemistry are in range from 40 to 60 ppm NH<sub>3</sub>. For comparison a difference between ammonia and hydrogen operating levels at hydrazine (Kola and Paks) and standard (Dukovany) water chemistries is shown in Table 3. Considerable higher ammonia and hydrogen level is

also presented in [1,2]. Operational results and differences thus may be attributable to the use of hydrazine either directly or indirectly as a result of higher operating level of ammonia.

At hydrazine water chemistry the tendency of corrosion products to deposit on fuel assembly surfaces could be decreased. Measurements at NPP Rheinsberg (VVER-70 type) have shown no spikes of radioactivity in the primary coolant during the shut-downs following hydrazine water chemistry cycle in distinction from standard water chemistry [3]. This observations are also confirmed by measurements of Co60 and Co58 releases providing at Paks NPP [4]. Nevertheless, reduction of corrosion products

**Table 3. Ammonia and hydrogen concentration in some VVER units with standard and hydrazine water chemistry**

Unit/year	Water chemistry	NH <sub>3</sub> (ppm)	H <sub>2</sub> (Nml/kg)
Kola 3/1986	H	45	56
Kola 3/1987	H	33	51
Kola 4/1987	H	36	52
Paks 2/1991	H	55	51
Paks 1/1991	S	25	44
Dukovany 1/1990	S	15	32
Dukovany 2/1990	S	14	35
Dukovany 3/1990	S	13	37
Dukovany 4/1990	S	13	34

**Note:** Average of ammonia and hydrogen concentrations during steady operation, H - hydrazine, S - standard water chemistry

deposition on the fuel surfaces resulting from the use of hydrazine or ammonia is still open question because no direct oxide thickness measurement on fuel element surface has been provided.

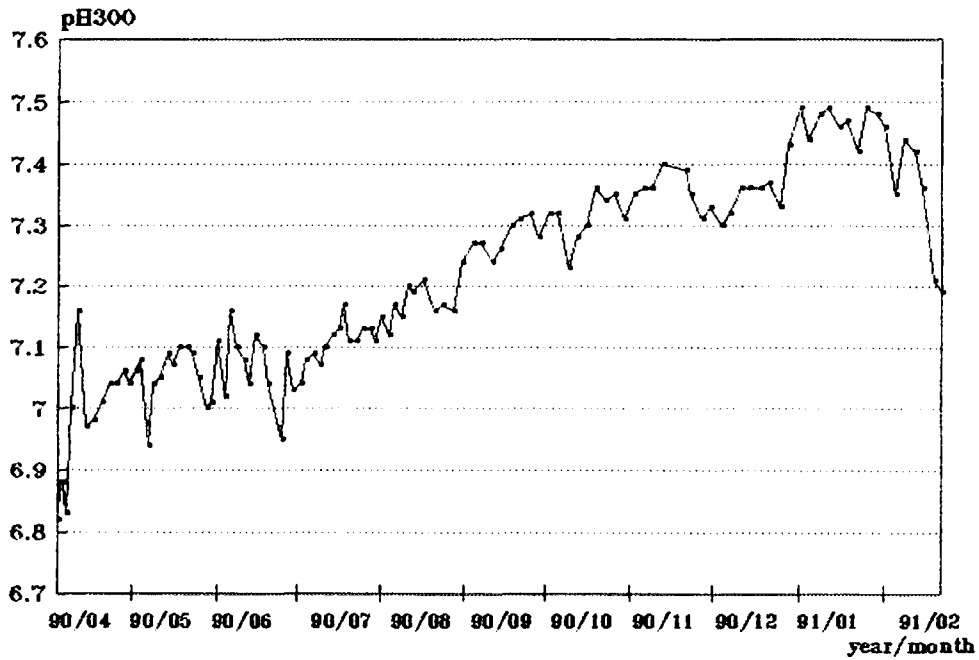
## Modified water chemistry

Coordinated potassium/boron standard water chemistry does not ensure constancy of physical-chemical conditions in the primary coolant during the reactor cycle. Typical change of high-temperature  $\text{pH}_T$  values (referring to  $300^\circ\text{C}$ ) during the reactor cycle of NPP Dukovany is shown in Fig.2. It can be seen that the  $\text{pH}_{300}$  values increase from about 6.8-6.9 at the beginning up to 7.4-7.5 at the end of the reactor cycle. This is the reason why a new proposal for primary water chemistry control was developed. Main idea of the modified water chemistry is to ensure stable physical-chemical conditions in the primary coolant during the whole reactor cycle. The choice of an optimal  $\text{pH}_{300}$  value is based on analysis of plant data [5] and results of mathematical modelling [6]. As the optimal value for VVER-440 was chosen  $\text{pH}_{300}=7.2$ . The modified water chemistry which is used in NPP Dukovany assumes that at the beginning of the cycle total alkalinity concentration (K,Li,Na) is kept on the maximum allowed level 20 ppm of equivalent  $\text{K}^+$  until the reaching of optimal  $\text{pH}_{300}$  value. From this moment till the end of the cycle is followed alkalinity concentration giving the  $\text{pH}_{300}$  values in range of  $7.2 \pm 0.1$  (see Fig.3). The testing of modified water chemistry at NPP Dukovany has begun in December 1991. Duration of the testing is supposed to be two or three reactor cycles.

## **VVER FUEL CLADDING BEHAVIOUR**

During the whole period of about 60 reactor-years operation experience of Czech and Slovak nuclear power plants only 15 defective fuel rods were found, confirming excellent fuel reliability. With the exception of three rods, the detected failures are supposed to be due to PCMI [7]. Insignificant corrosion is caused by good corrosion resistance of the Zr1Nb cladding material and relatively low coolant temperature (max.  $300^\circ\text{C}$  for 440 MW reactor). In cladding tube corrosion studies a compact oxide layer with thickness of 2.5-5 microns (at  $300^\circ\text{C}$ ) and 7.5-9 microns (at  $350^\circ\text{C}$ ) after 16,000 hours was found [8]. These results are confirmed by destructive examinations on selected high burnup fuel rods irradiated in Loviisa NPP carried out at Studsvik Nuclear AB's hot laboratories. Only minimal cladding external corrosion of 1-4 microns was found [9].

Standard water chemistry  
NPP Dukovany, Unit 2, Cycle 5



Modified water chemistry  
NPP Dukovany, Unit 3, Cycle 6

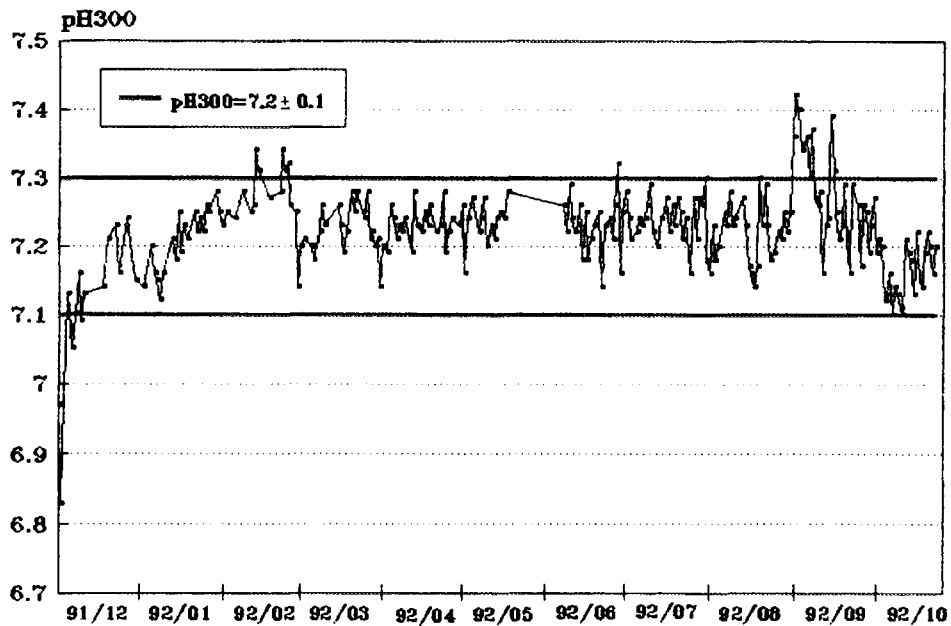


Fig.2 Typical  $\text{pH}_T$  course at standard and modified VVER primary water control

# Modified water chemistry control for VVER-440 units NPP Dukovany

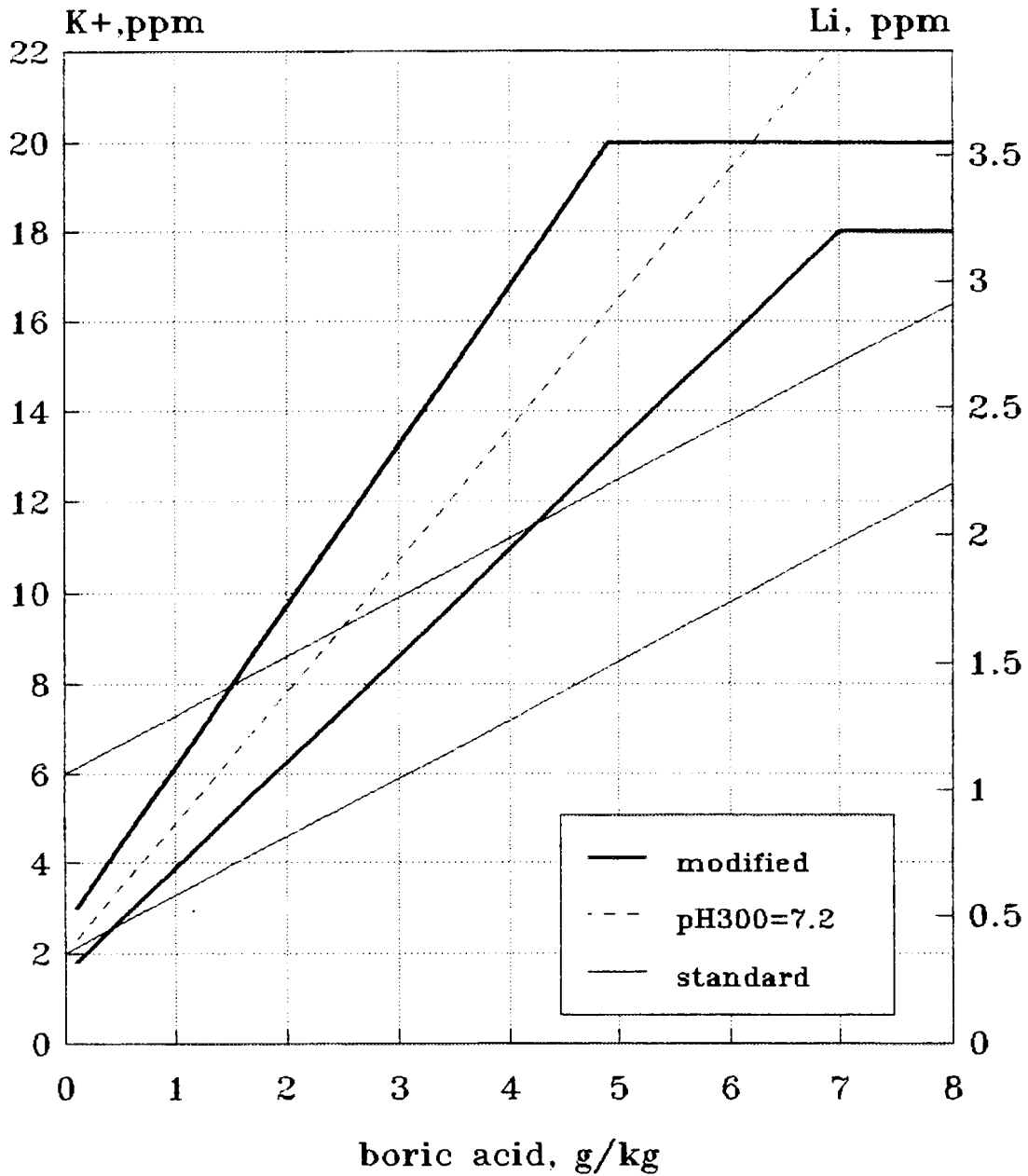


Fig.3 Standard and modified primary water chemistries for VVER-440 units (NPP Dukovany)

The tests of a great number of the fuel assemblies have shown that corrosion and fretting corrosion do not limit the increase in the fuel burnup. The core of the VVER-440 was originally designed for a three year cycles with batch average burnup of 29-31 MWd/kg and maximum linear heat generation rate of 32.5 kW/m. At present these reactors are being changed to four year cycles with 4.4% fuel enrichment. Experience of four-year operation more then 800 VVER-440 fuel assemblies, average burnup of 36 MWd/kg and maximum fuel burnup of 40-50 MWd/kg, has been obtained [10].

## **R&D RELATED TO FUEL CLADDING BEHAVIOUR**

Nuclear Fuel Institute in Zbraslav has been provided an experimental research in the field of fuel cladding behaviour under operational, transient and accident conditions. The research program has been focused on the corrosion and hydriding behaviour in hot water and superheated steam in wide range of temperature and pressure conditions and deformation behaviour, especially mechanical and creep properties and deformations at multiaxial stress. Detailed results are presented at this meeting by special paper [11]. This paper only discusses corrosion behaviour of Zr1Nb cladding material in water environment and summarizes main differences between Zr1Nb and Zircaloy alloys.

The long-term autoclave corrosion tests of Zr1Nb cladding tubes in demineralized water and in water with addition of boric acid (4000 ppm) and potassium hydroxide (11 ppm) at temperatures 300°C and 350°C have been provided. Statistically treated results are shown in Fig.4. These results confirmed that Zr1Nb alloy as compared to Zircaloy does not exhibit any break on the corrosion curves even after 30,000 hours. The oxide layers formed on cladding material had black colour and adhesive character. As seen in Fig.4, the corrosion rate in demineralized water was found to be slightly higher. Weight gains after 30,000 hour exposition achieved approximately 90 mg/dm<sup>2</sup> at 300°C and 180 mg/dm<sup>2</sup> at 350°C. The thickness of compact oxide layers was about 6 resp. 12 microns. Hydrogen concentration did not exceed 30 ppm at 300°C and 200 ppm at 350°C. The amount of absorbed hydrogen was lower than 13% resp. 30% of theoretically generated hydrogen by reaction with water. At 300°C the hydrogen quantity absorbed by the alloy did not practically increase when the oxide layer thickness of 1.5 micron was achieved.

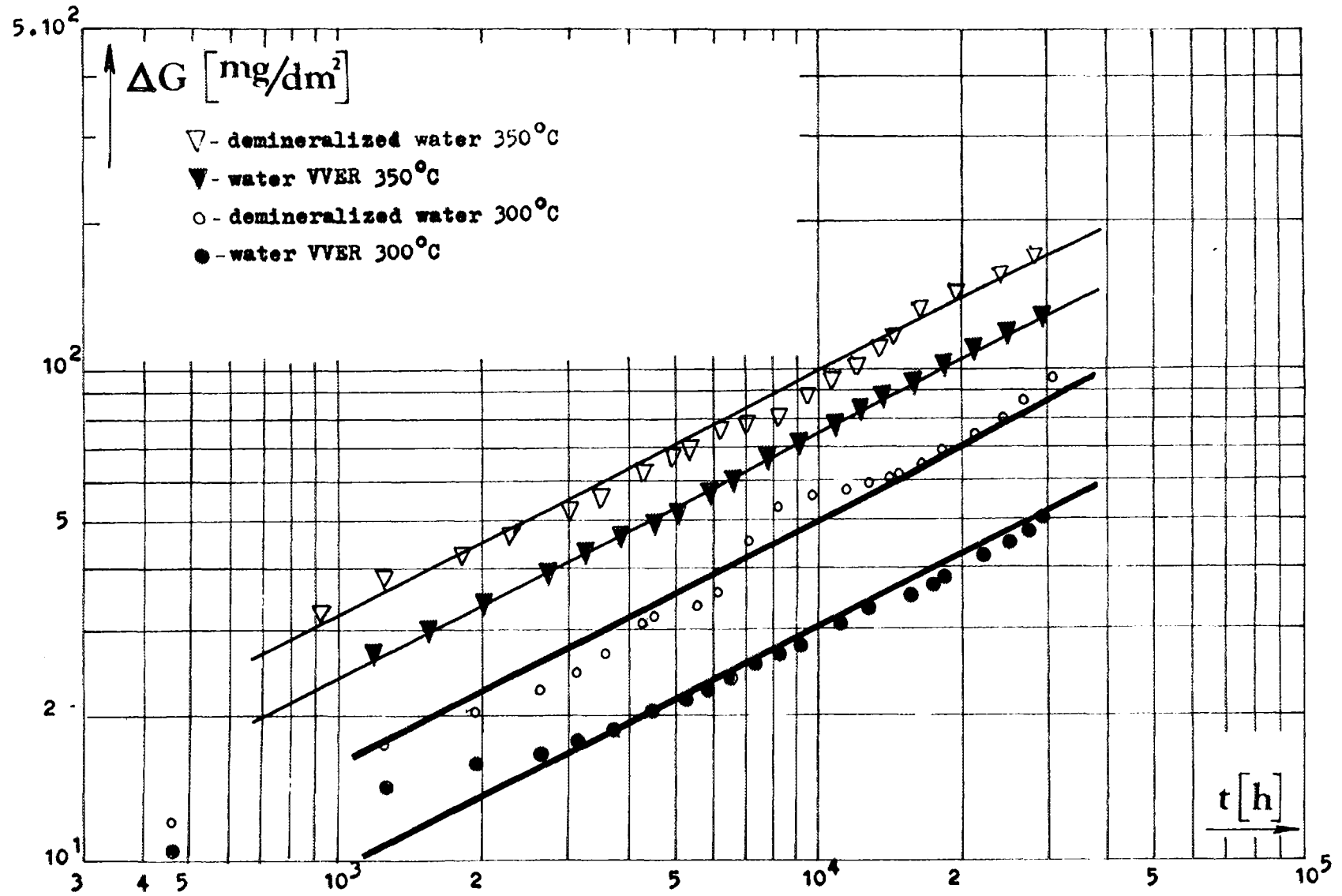


Fig. 4: Corrosion kinetics of Zr1Nb alloy at water 300 and 350°C.

At present, autoclave corrosion tests of Zr1Nb alloy in water environment containing LiOH and H<sub>3</sub>BO<sub>3</sub> are provided. Preliminary results obtained in 250 ppm Li, 500 ppm Li and 500 ppm Li + 1500 ppm H<sub>3</sub>BO<sub>3</sub> solutions indicate a higher sensitivity of Zr1Nb alloy to the high lithium concentrations in comparison with Zircaloy-4. The results also show a corrosion rate moderating effect of boric acid [12]. For the time being the critical concentration of lithium for Zr1Nb alloy enhanced corrosion is not known but it will probably be lower than that for Zircaloy-4.

Based on the performed autoclave experimental testing the main differences in corrosion behaviour of Zr1Nb and Zircaloy-4 alloy can be summarized as follows:

- Zr1Nb has slightly better corrosion resistance in temperature range of existence of the  $\alpha$ -phase (up to 750°C)
- no changes of Zr1Nb oxidation kinetic occurs even after 30,000 hour-exposition in water environment at 300°C and 350°C
- corrosion resistance of Zr1Nb in high-pressure steam is better
- lower susceptibility of Zr1Nb to the nodular corrosion
- radiation does not accelerate corrosion of Zr1Nb alloy
- absorption of hydrogen by Zr1Nb alloy is slightly lower (except high-temperature conditions)
- higher sensitivity of Zr1Nb alloy to the oxygen presence in the coolant
- short-term overheating of Zr1Nb for a few seconds up to region of existence of  $\beta$ -phase (above 900°C) causes the spalling of the oxide layer
- oxidation of Zr1Nb in steam at higher temperatures causes the higher embrittlement as a result of oxidation during the  $\alpha \rightarrow \beta$  transformation.

## **COMPATIBILITY OF ZIRCALOY-4 WITH VVER WATER CHEMISTRY**

Till the present time, Zr1Nb alloy has been used as a cladding material for fuel rods of VVER-type reactors. However, in the near future there is an intent in the Czech Republic and also in Slovakia to use fuel vendors utilizing Zircaloy-4 for PWR fuel cladding material. For instance, Westinghouse is to be the fuel vendor for NPP Temelín which is two units of VVER-1000 (start-up in 1995/1996). Also NPP Dukovany and NPP Mochovce (Slovakia) are going to have other fuel vendor. From this point of view the

question of compatibility of Zircaloy-4 with VVER water chemistry and its corrosion behaviour is arising. This problem can be divided into two areas.

First, using of potassium as a main alkalinity agent in VVER coolant technology instead of lithium used in PWR should not be followed by some unexpected results and essential differences in corrosion behaviour of Zircaloy-4. However, it is necessary to note that the current VVER water chemistry control - which is chosen to ensure a control in radiation field build-up - realizing maximum allowed potassium level up to 20 ppm (equivalent to 3.5 ppm of lithium) is based on experiments performed with Zr1Nb alloy.

Second, using of ammonia for hydrogen generation in VVER coolant technology could - from compatibility point of view - entail unforeseeable results and a different Zircaloy behaviour than under PWR conditions. Main problem here could be ammonia behaviour in high-temperature, irradiation conditions, radiolysis products formation and their possible interaction with fuel cladding [13]. In this connections hydrogen uptake by Zircaloy-4 cladding under VVER coolant conditions could be different from experience in PWRs [14].

Taking into account mentioned above and the fact that till now there are neither operational experience nor experimental results in the field of Zircaloy-4 behaviour under VVER primary coolant conditions an intensive attention to this problem should be given.

## **IN-PILE CORROSION TESTING**

For corrosion behaviour testing of cladding materials in different water chemistries the reactor water loop is intended to use.

Since 1983 reactor water loop RVS-3 is operated in the LVR-15 research reactor at NRI Řež. The loop was designed as a universal facility providing wide experimental possibilities. Its utilization is defined above all by the fact that the loop models thermal hydraulic conditions and water environment of pressurized water reactor primary circuits.

Equipment of the loop enables radiation experiments in wide range of operational parameters limited by following maximum values:

pressure	16.7 MPa
temperature	334°C
flow rate	10 t/h
neutron flux	$1.10^{14}$ 1/cm <sup>2</sup> .s
loop volume	300 dm <sup>3</sup>

Working medium of the loop is the standard water environment of PWR primary circuit with possible modifications according to the requirement of an experiment. The loop is a closed stainless steel pressurized water system with forced circulation (see Fig.5).

The facility for cladding material corrosion testing consists of two experimental sections of electrically heated fuel rods with maximum power of 100 W/cm<sup>2</sup>. One section is situated in the loop outside the reactor core (out-of-pile section), the second section is situated in the irradiation channel (in-pile section). In-pile section serves for research of corrosion under the effects of irradiation.

## CONCLUSIONS

1. Extensive experience in VVER primary coolant chemistry control has been obtained. Water chemistry is one of the main factor responsible for good radiation situation at VVER units. At present, VVER reactors are operated at several different modes, but generally boron/potassium/ammonia coolant technology is used. Standard, hydrazine and modified water chemistry differ in concentration levels of main chemical parameters (hydrogen, ammonia, hydrazine, potassium).

2. In VVER reactors Zr1Nb alloy is used as a fuel rod cladding material. Results of laboratory testing and limited number of operational data show very good corrosion resistance of Zr1Nb alloy under VVER water chemistry. For evaluation of the effect of different modes of VVER water chemistry on fuel cladding behaviour and corrosion products transport in reactor system more operational data are necessary.

## RVS-3 REACTOR WATER LOOP

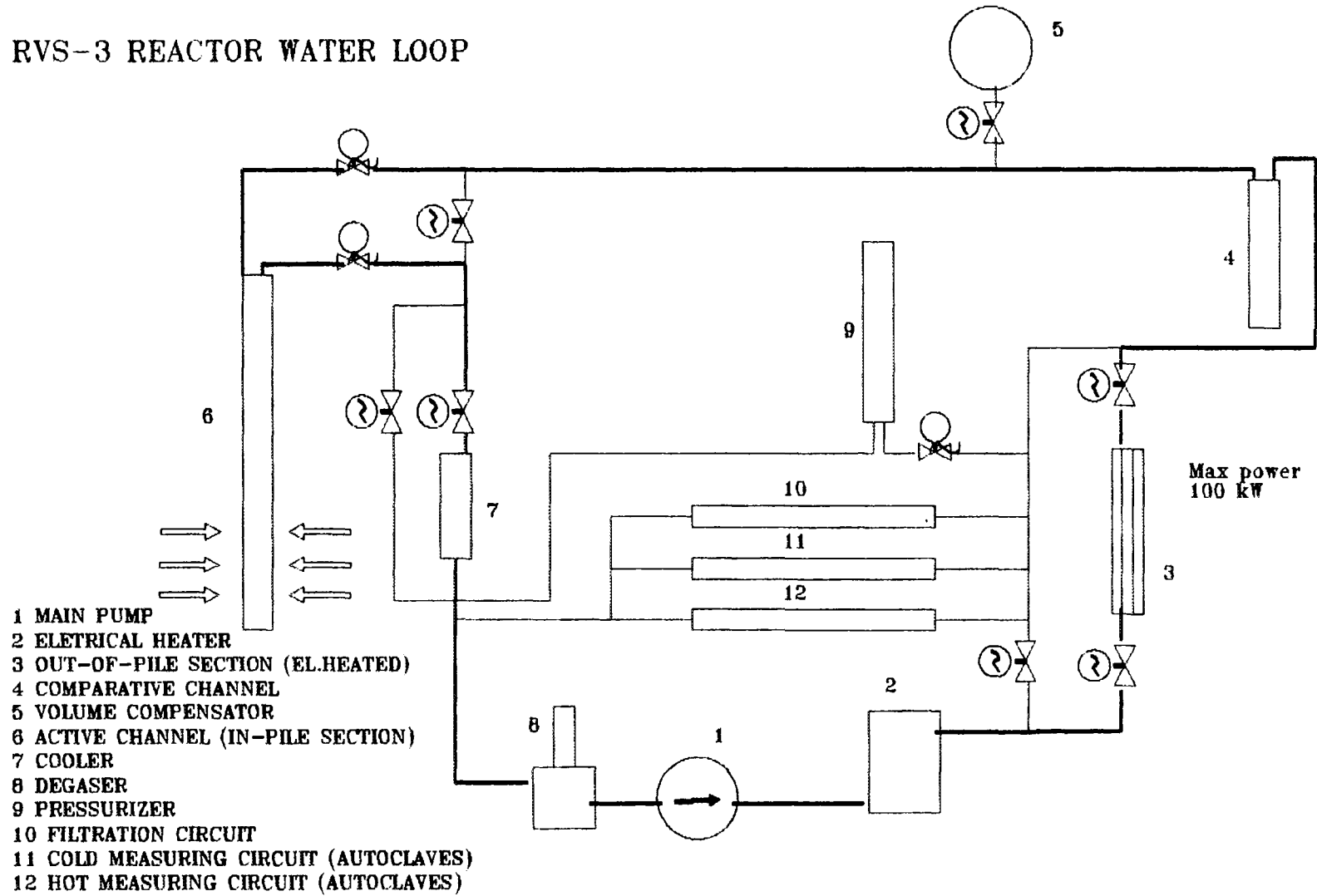


Fig.5 Reactor water loop RVS-3 diagram (NRI Řež)

3. So far there are only very limited data on behaviour of Zircaloy-4 in VVER coolant environment. In relation to the intention to use for VVER plants other fuel vendors using Zircaloy-4 as a fuel rod cladding material an intensive attention to the problem of compatibility of Zircaloy-4 with VVER water chemistry should be given, including the performance of in-pile corrosion testing.

#### REFERENCES

- [1] BOGANCS,J., SCHUNK,J., PASHEVICH,V.I., HVOROSTOV,I.V., ZINCHENKO,V.A., Experience with hydrazine water chemistry in the primary coolant of VVER 440 reactors, Seminar on Primary and Secondary Side Water Chemistry of Nuclear Power Plants, Balatonfüred, May 1992
- [2] BRIDLE,D.A., CAKE,P., SYMONS,W.J., KATONA,J., The measurements of corrosion product levels in the primary coolant at Paks unit 1 and 2 using transition metal ion chromatography, *ibid* 1.
- [3] HEROLD,C., SCHÖNHERR,M. et al., Coolant technology of water reactors, Report of CRP Program on WACOLIN, IAEA, Vienna, to be published
- [4] SCHUNK,J., BOGANCS,J., TILKY,P., BRIDLE,D.A., CAKE,P., SYMONS,W.J., Elemental and radiochemical measurements carried out on the primary coolant at VVER-440 Paks 1 and 2 in Hungary..., 6th Conf. Water Chemistry of Nuclear Reactor Systems, Bournemouth, 12-15 October 1992
- [5] BURCLOVÁ,J., *Jaderná energie*, 1990, v.36,6, p.211-216
- [6] ZMÍTKO,M., PhD.Thesis, Moscow Power Engineering Institute, Moscow, 1991
- [7] PAZDERA,F., BÁRTA,O., Research on VVER fuel rods behaviour and operational experience, IAEA Technical Committee Meeting on Fuel Performance at High Burnup for Water Reactors, Nyköping, Sweden, 5-8 June 1990
- [8] VRTÍLKOVÁ,V., RANSDORFOVÁ,B., HAMOUZ,V., MOLIN,L., Zr1Nb alloy cladding tube corrosion, Report ÚJP Zbraslav 579, 1985

- [9] MOISIO,J., TERÄSVIRA,R., RANTA-PUSKA,K., Experience from examinations of fuel rods irradiated to high burnups in Loviisa reactors, *ibid* 7.
- [10] YAKOVLEV,V., PAZDERA,F., ONUFRIEV,V., PROSYOLKOV,V., VALVODA,Z., BIBILASHVILI,Yu., Incentives for extended burnup for VVER reactors, *ibid* 7.
- [11] VRTÍLKOVÁ,V., VALACH,M., MOLIN,L., Oxidizing and hydriding properties of Zr1Nb cladding material in comparison with Zircalloys, IAEA Technical Committee Meeting on Influence of Water Chemistry on Fuel Cladding Behaviour, Řež near Prague, 4-8 October 1993
- [12] VRTÍLKOVÁ,V., MOLIN,L., Influence of additions in the coolant on the Zr1Nb cladding, Report NFI Zbraslav 720, 1992
- [13] COX,B., What is wrong with current models for in-reactor corrosion, IAEA Technical Committee Meeting on Fuel Failure in Normal Operation of Water Reactors, Mechanisms and Management, 26-29 May 1992, Dimitrovgrad, Russian Federation
- [14] WEIDINGER,H., Situation on Zry alloy corrosion in LWR environment, European Federation of Corrosion PWR Corrosion Sub-Group Meeting, Řež, 16-17 September 1993



## **HYDRAZINE - HYDRATE WATER REGIME AND OPERATION OF FUEL ELEMENTS**

V.I. PASHEVITCH, D.V. PASHEVITCH  
Pand Co.,  
Russian Federation

J. BOGÁNCSS, P. TILKY  
Paks NPP,  
Hungary

### **Abstarct**

Water chemistries currently used in WWER reactors are potassium based water chemistry (KOH) to adjust the pH with ammonia or hydrazine as oxygen scavenger.

Based on the measurement of Zr 95 which is a corrosion product of the zirconium cladding, it is shown in this paper that the amount of corrosion products accompanying the reactor shutdown is smaller when hydrazine is used. This is particularly obvious on PAKS 1 and 2 when Zr 95 measurements are performed before and after switching the water chemistry from ammonia to hydrazine.

It is concluded that the main advantage of using the hydrazine water chemistry is to decrease the thickness of the corrosion product layer formed on the fuel cladding, therefore the fuel temperature can be kept low. It is estimated that the fuel temperature increase due to the layer of corrosion products is 120 deg. C for KOLA 3 which is operated with ammonia water chemistry.

## **HYDRAZINE - HYDRATE WATER REGIME AND OPERATION OF FUEL ELEMENTS**

It is well known, that corrosion products in an operating reactor are situated on the surface of fuel elements. The amount of corrosion products originated directly from constructional material of reactor is less than 15% of the total amount of corrosion products.

As a result of changes in reactor operation (power increase or decrease, hydrodinamical changes, etc.) corrosion products' transport to coolant will increase. The radioactivity of primary coolant will consist of fission products, activated  $^{14}\text{N}$ ,  $^{24}\text{Na}$ ,  $^{42}\text{K}$  and corrosion product, like  $^{60}\text{Co}$ ,  $^{58}\text{Co}$ ,  $^{59}\text{Fe}$ ,  $^{54}\text{Mn}$ ,  $^{56}\text{Mn}$ ,  $^{110m}\text{Ag}$ ,  $^{95}\text{Zr}$ . The latest corrosion products are present in form of dispersed material mainly and they absorb onto the surface of fuel element rods where they will activate and decrease the heat transfer between the coolant and fuel element cladding. As a consequence of deterioration of heat transfer the fuel element cladding temperature -- which consists of Zr-Nb alloy -- will increase and the operation safety will decrease.

As the effect of hydrazine-hydrate the degree of sorption will decrease for all the constructional materials, so for zirconium alloy. The crud coming from the surfaces are caught by CVCS while there is no possibility for the production of new crud because of checked corrosion of constructional materials and of restricted sorption on the surface respectively. Consequently the continuous dosing of hydrazine-hydrate will result in removing of corrosion products from the surface of fuel element cladding.

The analyzes of data from backwashing of CVCS filters (1) makes sure that depending on the time range of effect of hydrazine-hydrate the amount of corrosion products will decrease. The radioactive corrosion products ( $^{60}\text{Co}$ ,  $^{59}\text{Fe}$ ,  $^{54}\text{Mn}$ ,  $^{51}\text{Cr}$ ) will be washed out from fuel element cladding so that their radioactive concentration will increase towards the washing out of deeper corrosion layers. As the result of these processes the amount of corrosion products settled on the fuel element cladding will decrease.

Results make possible the modeling of corrosion products' transport in the close vicinity of fuel element cladding. The supposed model is shown on Fig. 1.

Corrosion products in the coolant pass through the field of fuel element cladding in case of steady power. During this process in case of positive temperature stress ( $+\Delta T$ ) a crud layer will be produced on the surface of the fuel element cladding having uneven density and radioactivity. The layer with the highest density is situated directly on the cladding wall and its radioactivity is the highest as well. As the effect of hydrazine-hydrate the crud will be dissolved gradually into the coolant and will be caught the CVCS.

It is confirmed by a great number of experiments that the increase of average temperature of fuel element as an effect of corrosion layer settled onto the fuel element cladding is between  $60\text{ }^{\circ}\text{C}$  (Connecticut - Yankee, USA) and  $120\text{ }^{\circ}\text{C}$  (Kola NPP).

Experiments have been carried out in Kola and Armenian NPP to determine reactivity change as the consequence of removal of corrosion layer from fuel element cladding. At Unit 1 in Kola NPP there was a continuous hydrazine dosing in January 1980 in sufficient amount to produce  $60\text{ Nml/kg}$  dissolved hydrogen concentration in primary coolant. The flow rate to the CVCS filter was  $30\text{ t/h}$ . The excess amount of hydrogen was incinerated with  $6\text{ t/h}$  flow rate.

The amount of corrosion products removed from the fuel element cladding surfaces determined by the change of radioactive concentration of  $^{56}\text{Mn}$ . In order to determine positive reactivity released the following critical parameters were measured:

- thermal power of reactor,
- average temperature of reactor coolant,
- position of control rod groups,
- boric acid concentration.

The change of reserve reactivity during experiment agrees with that of calculated by BIPR program after making some experimental correction of basic data.

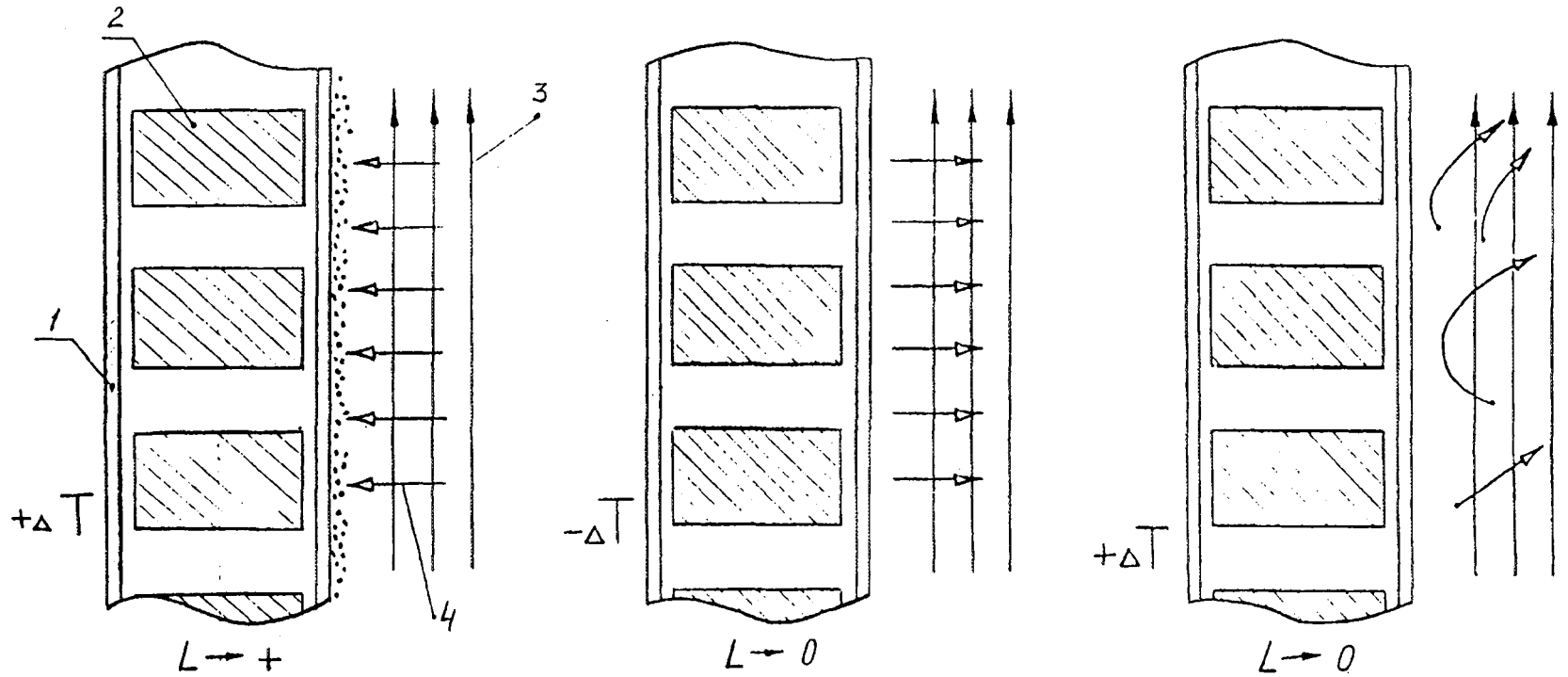
During the 10.8 effective day long experiment there was no change in reserve reactivity, that is only 0.32% reserve reactivity was released.

Taking into consideration the heat transfer coefficient of corrosion layer --  $0.002 \text{ W} \cdot \text{cm}^{-1} \cdot \text{°C}^{-1}$  -- the thickness of this layer according to the calculation was 12-15  $\mu\text{m}$ . On the base of back washing of CVCS filters during the change of water regime of VVER-440 type units to hydrazine addition chemistry the specific activity of corrosion layers could be determined as the function its thickness at steady power and standard boric-ammonia-potassium water regime.

In addition of the above mentioned facts the reduction of fuel element cladding temperature will improve the operational conditions of Zn-Nb alloy.

In order to determine the amount of corrosion products at Paks NPP samples were taken during shut-down periods at given time intervals. After filtration corrosion products on a 0.45  $\mu\text{m}$  pore size filter were measured by gamma spectroscopy. The amount corrosion products from the corrosion of fuel element cladding was determined by the help of  $^{95}\text{Nb}$ . Due to that at Paks NPP Unit 3 and 4 operate with standard boric-ammonia-potassium water chemistry and since 1991 Unit 2 and since 1992 Unit 1 have been operated with hydrazine dosing water chemistry we had the possibility to compare the effects on Zr-Nb alloy fuel element cladding.

The change of  $^{95}\text{Nb}$  radioactive concentration during shut-down of Unit 1, 2, and 3 can be seen on Figs. 3, 4 and 5. It can also be seen that following the change to hydrazine addition water chemistry the amount of  $^{95}\text{Nb}$  has considerably decreased. The measure of decrease can be determined according to the maximum concentration or area under the curves during shut-down periods. For example at Unit 1 -- hydrazine addition water chemistry has been used since 1992 -- the amount of  $^{95}\text{Nb}$  washed out from fuel element cladding surface was 12 times less than during previous shut-down in 1991 (Fig. 3). Figure 4 shows that in case of a long lasting hydrazine addition water regime the amount of  $^{95}\text{Nb}$  continuously decrease and will stabilize on a lower concentration than before. The Figure 5 shows the change of  $^{95}\text{Nb}$  concentration in



a. transport of corrosion products in case of boric acid-ammonia-potassium water regime,  $E_{Pt} \sim -50$  mV SHE.

b. transport of corrosion products from fuel element cladding to the coolant in case of power decrease,  $E_{Pt} \sim -50$  mV SHE.

c. transport of corrosion products in the vicinity of fuel element cladding in case of strongly reducing water regime ( $N_2H_4 \cdot H_2O$ )  $E_{Pt} \sim -350$  mV SHE.

Where:  $\Delta T$  - heat production  
 L - thickness of corrosion product layer  
 1 - fuel element cladding  
 2 - fuel element pellets  
 3 - stream of coolant  
 4 - direction of corrosion products' transport

FIG. 1.

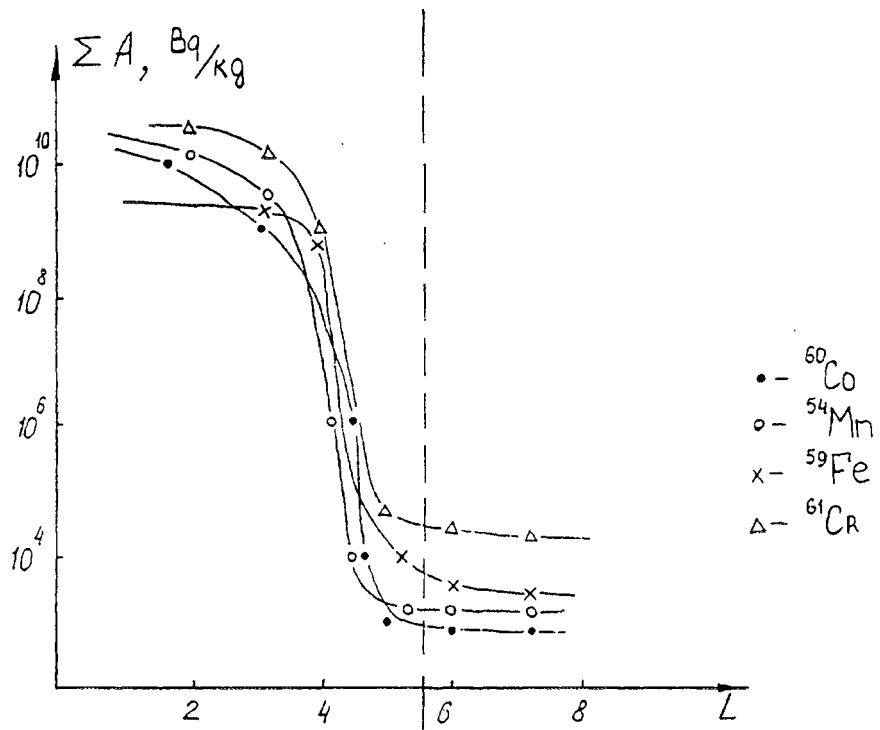


FIG. 2. Distribution of corrosion products on the fuel element cladding surface (+ $\Delta T$ ).

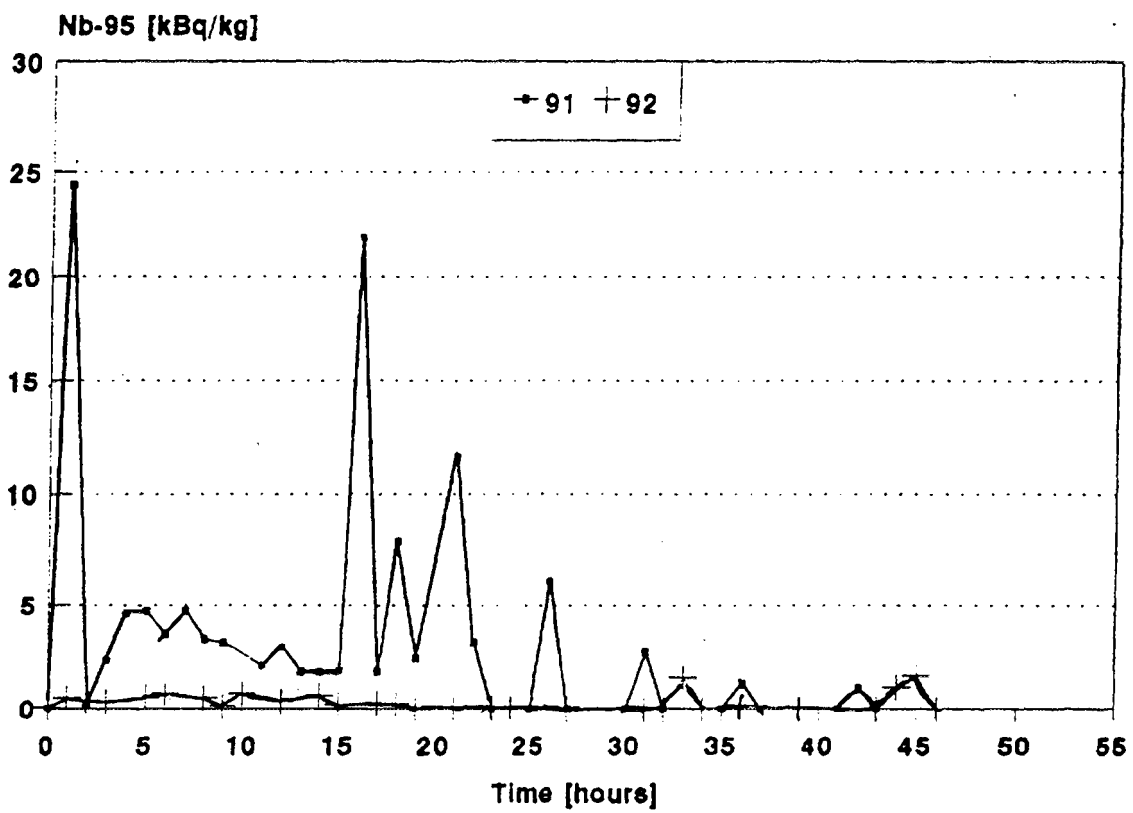


FIG. 3. Unit 1.

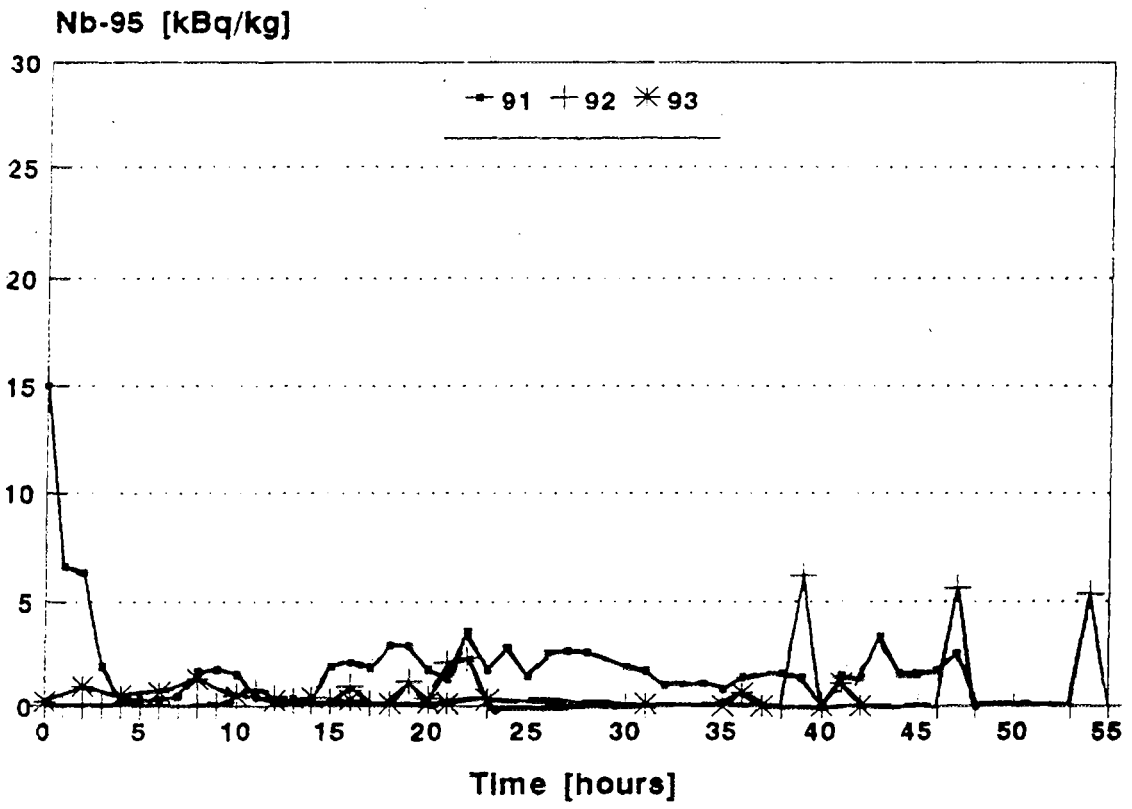


FIG. 4. Unit 2.

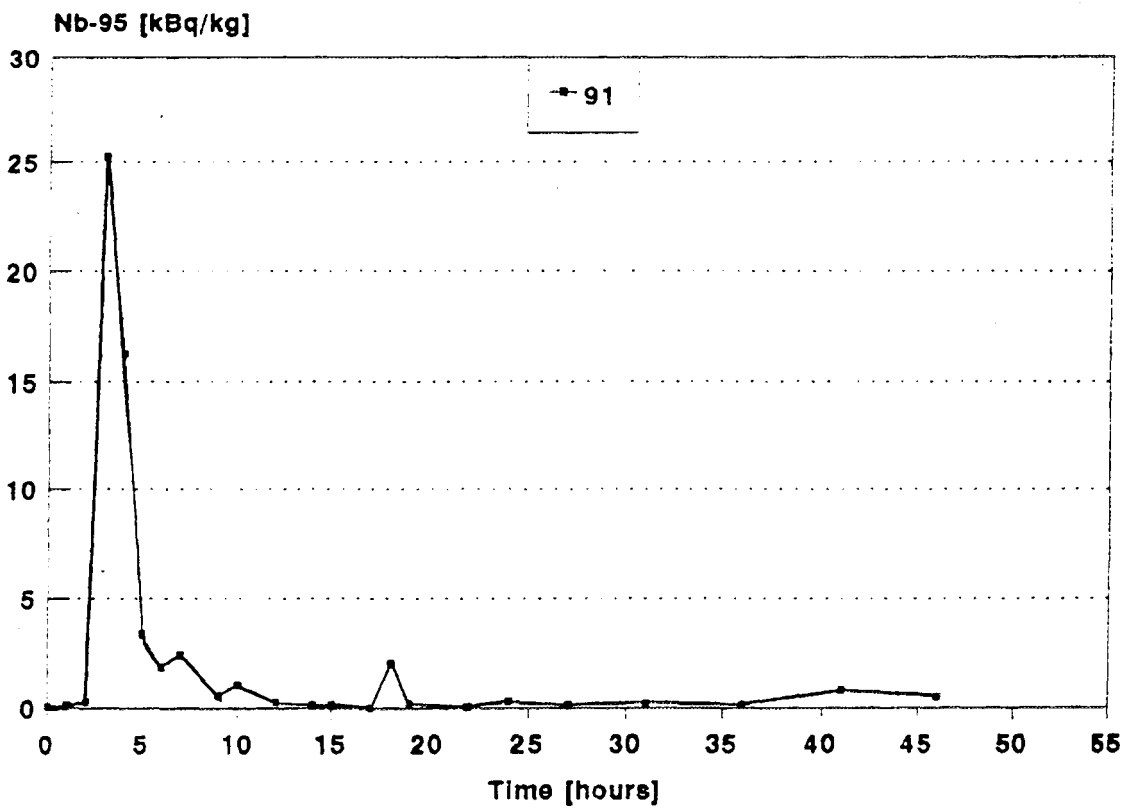


FIG. 5. Unit 3.

the primary coolant of Unit 3 having the standard boric acid-ammonia-potassium water regime. The decrease of  $^{95}\text{Nb}$  concentration is due to the decrease of corrosion rate of fuel element cladding material and of sorption of corrosion products on the fuel element cladding surface.

Basing on these facts the following conclusions can be drawn:

- as the effect of hydrazine addition water chemistry corrosion products will be washed out from the surface of fuel element cladding.
- washing out of corrosion products leads to the decrease of fuel element cladding temperature that results the improvement of operational conditions of Zr-Nb alloy.
- as the effect of hydrazine addition water chemistry the amount of corrosion products from the fuel element cladding material will considerably decrease.

**NEXT PAGE(S)  
left BLANK**

## LIST OF PARTICIPANTS

Aaltonen, P.A.	Technical Research Centre of Finland (VTT), Espoo, Finland
Abram, T.J.	BNFL, Springfields, United Kingdom
Alder, H.P.	Paul Scherrer Institute (PSI), Villigen, Switzerland
Anisimova, Irina A.	Ministry of Atomic Energy of the Russian Federation Committee for International Relations, Russian Federation
Aoki, T.A.	Nuclear Fuel Department, Nuclear Power Engineering Corporation, Tokyo, Japan
Arioka, K.	Takasago R & D Center, Mitsubishi Heavy Industries Ltd., Hyogo-ken, Japan
Beran, J.	ZJS SKODA plc., Pelzen, Czech Republic
Bibilashvili, Yu.K.	Nuclear Fuel Department, Moscow, Russian Federation
Brunning, J.	AEA Technology, Oxon, United Kingdom
Carlo Vitanza	Institutt for Energiteknikk, OECD, Halden, Norway
Chantoin, P. ( <i>Scientific Secretary</i> )	International Atomic Energy Agency
Chekmariov, A.M.	"Pand Co", Russian Federation
Cox, B.	University Of Toronto, Centre for Nuclear Engineering, Canada
de Betou, Jan In	Swedish Nuclear Power Inspectorate, Sweden
Deydier, D.	EDF, Direction de l'Equipement SEPTEN, Villeurbanne, France
Diego Valesco, G.	CIEMAT, Spain
El Sayed, A.A.	Atomic Energy Authority, Cairo, Egypt
Gomez Herrera, R.A.	Laguna Verde Nuclear Power Station Federal Commission of Electricity, Mexico
Hanus, V.	NPP Temelín, Czech Republic
Henzel, N.	Siemens AG KWU, S732, Erlangen, Germany
Horváth, L.G.	VEIKI Institute for Electrical Power Research, Budapest, Hungary
Kobayashi, M.	Applied Metallurgy & Chemistry Dept., Toshiba Corporation, Yokohama, Japan

Kobayashi, Shin-ichi	Nuclear Fuel Industries Ltd., Osaka, Japan
Kritsky, V.G.	VNIPIET, St. Petersburg, Russian Federation
Kysela, J.	Nuclear Research Institute Řež plc, Czech Republic
Lemaignan, C.	CEA/DRN/DTP, CENG-SECC, Grenoble, France
Lister, D.H.	University of New Brunswick, Department of Chemical Engineering, Canada
Maroto, A.	Comision Nacional de Energia Atomica (CNEA), Argentina
Novikov, V.V.	All Union Scientific and Research Institute of Inorganic Materials, Russian Federation
Pashevitch, D.V.	"Pand Co", Russian Federation
Pashevitch, V.I.	"Pand Co", Russian Federation
Pêcheur, D.	CEA/DRN/DEC/SECA/LCC - CEN-Cadarache, France
Petrecky, I.	NPP Dukovany, Czech Republic
Pilar, P.	NPP Temelín, Czech Republic
Polley, V.	Nuclear Electric plc, Berkeley, United Kingdom
Riess, R.W.	Siemens AG KWU, Erlangen, Germany
Ritchie, I.	International Atomic Energy Agency
Rosborg, Bo	STUDSVIK Material AB, Nyköping, Sweden
Ruhmann, H.	Siemens AG KWU, BT 63, Erlangen, Germany
Shejbal, J.	NPP Dukovany, Czech Republic
Shimada, S.	Nippon Nuclear Fuel Development Co., Ltd., Ibaraki-ken, Japan
Splichal, K.	Nuclear Research Institute Řež plc, Czech Republic
Stefov, A.V.	"Pand Co", Russian Federation
Stellwag, B..	Siemens AG KWU, S73, Erlangen, Germany
Thomazet, J.	FRAMATOME Nuclear Fuel Division, Lyon, France
Topalova, Ina Penkova	Laboratory on Corrosion, Chemical Department, NPP Kozloduy, Bulgaria
Urbanic, V.F.	Atomic Energy of Canada, Chalk River Laboratories, Canada

Valach, M.	Nuclear Research Institute Řež plc, Czech Republic
Van Berlo, John P.	Atomic Energy Control Board, Ottawa, Canada
Vanderborck, M.	BELGATOM, Belgium
Venkateswaran, G.	BHABHA Atomic Research Centre, Trombay, Bombay, India
Vrtilkova, V.	DIAMO - Ústav jaderných paliv, Czech Republic
Wikmark, G.	Material Development, Fuel Division, ABB Atom AB, Västerås, Sweden
Yurmanov, V.A.	VNIIAES, Russian Federation
Zmitko, M.	Nuclear Research Institute Řež plc, Czech Republic
Zoczek, J.	CEZ a.s. (Czech Power Board), Czech Republic